Reconstructing the Islet Extracellular Niche

By

Daniel M. Tremmel

A dissertation submitted in partial fulfillment of the requirements for the degree of

Doctor of Philosophy
(Cellular and Molecular Biology)

at the

UNIVERSITY OF WISCONSIN-MADISON

2022

Date of final oral examination: 4/15/2022

The dissertation is approved by the following members of the Final Oral Committee:

Barak Blum, Assistant Professor, Cell and Regenerative Biology
Michelle Kimple, Associate Professor, Medicine
Lingjun Li, Professor, Chemistry & Pharmacy
Wan-ju Li, Associate Professor, Orthopedics & Biomedical Engineering
Jon S. Odorico, Professor, Surgery

Table of Contents

Acknowledgements

Over the course of my time in graduate school, I have accomplished a lot, but there's not a single thing that I did entirely by myself. I have been at the University of Wisconsin for many years, and have benefitted greatly from so many connections here in both academia and outside of the university. I could not have accomplished this without all of those who surround me.

First, thank you to my advisors Dr. Jon Odorico and Dr. Sara Sackett. I have had a very unique grad school experience working in your lab, and I have learned and grown so much. You have provided an atmosphere that allowed me to be myself, follow my ideas, be successful, and feel appreciated without having to make major sacrifices in other aspects of my life. Your open-minded approach to research resulted in the development of many exciting projects and has led us to explore many techniques and approaches – I am very grateful to have learned and experienced as much as I have while working with you both. Thank you for all of your support and guidance over the years!

The other members of my thesis committee, Dr. Lingjun Li, Dr. Michelle Kimple, Dr. Barak Blum and Dr. Wan-ju Li, have provided continuous guidance, insight, support, and encouragement, as well as collaborations that have expanded my expertise and led to fruitful and innovative projects.

To my students – Austin Feeney, Vansh Jain, Rachel Maguire, Andrew Curran, Marina Ignatowski, Jenna Menadue, Jess Suderski, Nick Quirini, Colin Steck, Anna Mikat and Sakar Gupta – I have enjoyed working with you all so much! I learned as much from each of you as I hope you've learned from me, and we accomplished so much together. I am happy to share in our achievements and excited to cheer you all on as you go on to do bigger and better things in the

future. I couldn't be writing this document without all of your help and I can't imagine how lonely lab would have been without all of you there. I also have enjoyed working with the other members of the Odorico lab through the years, especially Sam Mitchell – all of the hours in the tissue culture room and overly complicated experiments went so smoothly while we worked together and I am very grateful for your support, expertise and friendship along the way.

I have been at the University of Wisconsin 15 years. At each level of my career here, I have benefited from the experience and kindness of the people I've worked with. To those in Dr. Cameron Currie's lab who helped me get started as an undergraduate student in my first research lab, especially Dr. Frank Aylward – thank you for teaching me and introducing me to this path that I have become so passionate about. To everyone I worked with in Dr. Jerry Yin's lab, and especially Dr. Cedric Wesley for teaching me the importance of grounding yourself with a strong knowledge of the fundamental science underlying whatever experiment you are performing – thank you all for showing me how exciting and fun research can be, and helping me realize that graduate school was the right next step in my career. Of course, there are too many other scientists I have worked with at UW over the years to name, but I am so grateful for all of the intellectual, supportive, and enjoyable friendships we've had.

I want to thank the students in the CMB program, those in my cohort – especially Sarah Rempel, Becky Reese, Taylor Scott, Lauren Ziemer, and Tamara Chamberlin-Safrit – for being a group of incredible, smart and well-balanced people. We have been though the coursework, exams, prelims and grant applications together, but the parts that have been the most meaningful to me are the paint nights, trivia, and the all-around fun and goofy times we've had. While we are here for the science, you all remind me that the other things we do in our lives

matter and are important, and can still be prioritized as we move forward in our careers. I think you're all amazing people and I'm so lucky to have spent the last few years with you.

I want to thank the UW Russian Folk Orchestra and UW Medical Sciences Orchestra as well for providing an opportunity to continue playing music throughout these demanding years of my life. I have always found rehearsals to be invigorating and inspiring to me, even on days when everything else has drained me. I consider the opportunity to play in both orchestras a unique privilege and one of the highlights of my time in Madison.

Finally, I have to thank my family for a lifetime of support. The years I have been in Madison and so close to home are irreplaceable and invaluable to me. I've enjoyed the ability to come back home whenever I have the time, and having the support of my entire family and the all of the family events has helped to keep me motivated and keep my life balanced during grad school. I have to thank my parents for the support in every aspect of my life over the years, and it's been great to grow closer with my sisters during my time at UW as we've all continued to grow together. I've also had four new nieces and nephews born during my PhD! I have treasured our family time and I'm so lucky to have you all. Most importantly, to Travis McKee (and Gypsy and Jasper), thank you for being my best friend throughout these years, for staying in Madison longer than you probably ever planned, and for helping to make our lives more comfortable and stable while I was focused on school and research. We have had a great time here in Madison and I'm excited for our next steps together!

Abstract

Diabetes mellitus is a chronic metabolic disorder that impacts 10.5% of the US population and hundreds of millions of people worldwide - numbers which are projected to continue increasing. Diabetes is characterized by the inappropriate regulation of blood sugar homeostasis due to altered production of the hormone insulin by β cells, residing in the islets of Langerhans in the pancreas. Primary human islets or stem cell-derived islets (SC-islets) can be transplanted to reverse diabetes, but there are several barriers to the success of these cell therapies. When islets are isolated from the pancreas, damage to islet extracellular matrix (ECM) and changes in cell composition and arrangement affect islet survival and function. Protocols to derive SC-islets have improved the efficiency of differentiation and *in vitro* function, but continue to underperform compared to primary islets both *in vitro* and *in vivo*. The studies in this thesis aim to better define the ECM of the human pancreas, to create a matrisome database on which future ECM-based engineering approaches may be modeled, and to use an ECM scaffold to recreate a more native-like islet microenvironment *in vitro* for improved culture and transplantation outcomes.

In Chapter 2 of this thesis, we report that the matrisome changes dramatically between the fetal and adult pancreas, and define those changes both by overall and islet-specific protein abundance as well as changes in ECM localization through the life cycle. This study also measures changes in non-ECM proteins, and is deposited in an accessible database, providing a resource of proteomic data across human pancreas development.

Chapters 3-5 detail the derivation of a human pancreas ECM scaffold that can be used to study how islets and SC-islets interact with the ECM component of the microenvironment. We

show that when combined with pancreatic ECM during differentiation, SC-islets have improved gene expression profiles and higher rates of endocrine cell fate commitment. More in-depth studies of pancreas ECM co-culture with primary human islets in Chapter 5 reveal that ECM improves islet survival, reduces basal insulin secretion and improves the stimulation index of the cells in response to glucose, and affects the architecture of the cells after isolation. In Chapter 6, endothelial cells are cultured within this scaffold to form 3-D vascularized networks around the islets, which may help to model islet-endothelial interactions and improve vascularization of the cells after transplantation.

Finally, in Chapter 7, we use our resources to explore markers of maturation that may help improve SC-islet differentiation protocols, sort mature cells from immature cells for improved SC-islet outcomes, and better understand the role of some of these maturation-associated genes in postnatal islet development.

Together, these studies create a model of the native islet microenvironment *in vitro*, add to the current knowledge of human islet biology, and contribute to a broader goal of generating and transplanting cells to treat diabetes.

List of Acronyms and Abbreviations

BSA……bovine serum albumin
C-Pep……connecting peptide, C-Peptide
DAPI…… 4’,6-diamidino-2-phenylindole
DE……definitive endoderm
eBC……enriched beta cell clusters
EC……endothelial cell
EP……endocrine progenitor
ECM……extracellular matrix
EDTA……ethylenediaminetetraacetic acid
ELISA……enzyme-linked immunosorbent assay
FACS……fluorescence-activated cell sorting
FFPE……formalin fixed paraffin embedded
HEPES……(4-(2-hydroxyethyl)-1-piperazineethanesulfonic acid)
hESC……human embryonic stem cell
hiPSC……human induced pluripotent stem cell
hK-HG……human kidney extracellular matrix hydrogel
HLA……human leukocyte antigen
hP-ECM……human pancreatic extracellular matrix
hP-HG……human pancreatic extracellular matrix hydrogel
hPSC……human pluripotent stem cell
IBMIR……instant blood mediated response
IEQ……islet equivalents
IM……intramuscular
IP……intraperitoneal
GAG……glycosaminoglycan
GSIS……glucose stimulated insulin secretion
GTT……glucose tolerance test
KSC……kidney sub-capsule
MSC……mesenchymal stem cell
MTS 3-(4,5-Dimethylthiazol-2-yl)-5-(3-carboxymethoxyphenyl)-2-(4-sulfophenyl)-2H-tetrazolium
OCT……optimal cutting temperature
PBS……phosphate buffered saline
PCR……polymerase chain reaction
P-ECM……pancreatic extracellular matrix
PE……pancreatic endoderm
PEG……polyethylene glycol
PFG……posterior foregut
PGT……primitive gut tube
PP1……pancreas progenitor 1
PP2……pancreas progenitor 2
QPCR……quantitative real-time PCR
ROCK……rho-associated protein kinase

SC……stem cell
SCβC……..stem cell-derived beta cell
SC-ILC……stem cell-derived islet like clusters
SDS…….. sodium dodecyl sulfate
sGAG……sulfated glycosaminoglycan
SI……stimulation index
SQ……subcutaneous
T1D……type 1 diabetes mellitus
T2D……type 2 diabetes mellitus

List of Gene Names

ARNTL……aryl hydrocarbon receptor nuclear translocator like
β2M……beta 2 microglobulin
CHGA……chromogranin A
COL1A1……collagen type I alpha 1 chain
COL2A1……collagen type II alpha 1 chain
COL3A1……collagen type III alpha 1 chain
COL4A1……collagen type IV alpha 1 chain
COL5A1……collagen type V alpha 1 chain
COL6A1……collagen type VI alpha 1 chain
COL12A1……collagen type XII alpha 1 chain
COL14A1……collagen type XIV alpha 1 chain
COL16A1……collagen type XVI alpha 1 chain
CRFR2……corticotropin releasing hormone receptor 2
CTLA4……cytotoxic T-lymphocyte-associated protein 4
CXCR4……C-X-C chemokine receptor type 4
EMILIN1……elastin microfibril interfacer 1
FAM159B……family with sequence similarity 159 member B
FBN2……fibrillin 2
FN1……fibronectin
FoxA2……forkhead box protein A2
HNF1B……hepatocyte nuclear factor 1 homeobox B
HNF4A……hepatocyte nuclear factor 4 alpha
HOPX……homeodomain-only protein homeobox
IAPP……islet amyloid polypeptide
Ins……insulin
KLF9……kruppel like factor 9
G6PC2……glucose-6-phosphatase catalytic subunit 2
Gcg……glucagon
GCK……glucokinase
Glut1 (*SLC2A1*)…… solute carrier family 2 member 1, glucose transporter 1
Glut2 (*SLC2A2*)……solute carrier family 2 member 2, glucose transporter 2
LAMA4……laminin subunit alpha 4
LAMA5……laminin subunit alpha 5
MAFA……V-maf musculoaponeurotic fibrosarcoma oncogene homolog A
MAFB……V-maf musculoaponeurotic fibrosarcoma oncogene homolog B
Nanog (*NANOG1*)……homeobox protein NANOG
NeuroD1……neurogenic differentiation 1 / β2
Ngn3……neurogenin3
Nkx2.2 (*NKX2-2*)……homeobox protein Nkx-2.2
Nkx6.1 (*NKX6-1*)……homeobox protein Nkx-6.1
NR1D1……nuclear receptor subfamily 1 group D member 1
NTPDase3 (*ENTPD3*)……ectonucleoside triphosphate diphosphohydrolase 3

Onecut2 (OC2)……one cut homeobox 2
Oct4……octamer-binding transcription factor 4
OGN……osteolgyin/mimecan
PD-L1……programmed death-ligand 1
PECAM1 (CD31)……platelet and endothelial cell adhesion molecule 1
Pdx1……pancreatic and duodenal homeobox 1
Ptf1a……pancreas transcription factor 1 subunit alpha
POSTN……periostin
SIX2……homeobox protein SIX2
SIX3……homeobox protein SIX3
Sox17……(sex determining region Y)-box 17
Sox2……(sex determining region Y)-box 2
Sox9……(sex determining region Y)-box 9
Sst……somatostatin
SYT4……synaptotagmin 4
Ucn3……urocortin-3
ZnT8 (*SLC30A8*)……solute carrier family 30 member 8, zinc transporter 8

List of Figures

Chapter 1

Chapter 2

Chapter 3

Chapter 6

Chapter 7

Chapter 8

Appendix Chapter 1

Appendix Chapter 2

Chapter 1

Introduction

Daniel Tremmel wrote the chapter. Some text in this chapter was adapted from review papers written by Daniel Tremmel [1-3]. Figures 1, 2, 4 and 6 were made by Daniel Tremmel. Figure 3 was made by Daniel Tremmel and modified from the previously published version in Sackett et al. 2020 [3]. Figure 4 was designed by Jon Odorico and Sara Dutton Sackett, originally published in Sackett et al. 2020, made by Karen Lynch and altered by Daniel Tremmel for this chapter [3].

Pancreatic Islets and Diabetes

Diabetes and Treatment

Diabetes mellitus is a chronic metabolic disorder that impacts 10.5% of the US population and 463 million people worldwide - numbers which are projected to continue increasing [4]. Diabetes is characterized by the inappropriate regulation of blood sugar homeostasis due to impaired production of the hormone insulin by β cells, residing in the islets of Langerhans (islets) in the pancreas. There are two major types of diabetes; Type 1 diabetes (T1D) is caused by the autoimmune destruction of insulin-producing β cells by the immune system. Type 2 diabetes (T2D), however, is characterized by insulin resistance and progressive β cell dysfunction, stress, and eventually β cell death [5, 6]. In addition to tremendous social and economic costs, long-term complications, including organ failure, contribute to the early death of those affected.

Exogenous insulin administration is an effective short-term treatment yet is imperfect because, unlike the endogenous β cells, a patient is unable to continuously monitor and prevent hyper- and hypoglycemic episodes. β cell replacement therapies, however, can achieve appropriate glycemic control. Whole pancreas transplantation or the transplantation of isolated islets into the liver through the portal vein are two such examples that utilize cadaveric donor tissues to replace a patient's dysfunctional β cells. These therapies provide a sustainable allogeneic replacement for the patient's β cells but a shortage of donor organs, invasiveness of the surgery, inadequate long-term function, and the need for prolonged immunosuppression therapy have made transplantation unavailable or unsuitable to a majority of the affected population [7, 8]. Islet transplantation is also considered an experimental procedure in the United

States. For these reasons, many have looked to novel strategies for deriving and transplanting insulin-producing cells for clinical application.

Human Islet Biology and Islet Isolation

Animal models have been invaluable to the field of developmental biology to study how cells and tissues form throughout development. Rodent models have provided a means to study the most fundamental mechanisms of islet development and function, but we now realize that many key aspects of rodent islet biology have not translated to the human analogue [9]. A very obvious example is that the endocrine cells in the islet (glucagon-producing α cells, insulin-producing β cells, and somatostatin-producing δ cells) are arranged dramatically differently in the human pancreas, where the different endocrine cells are distributed evenly throughout the islets, compared to the mouse, in which the α and δ cells are at the perimeter of the islets and the β cells localize to the core [10]. Many other islet attributes exhibit dissimilarities between

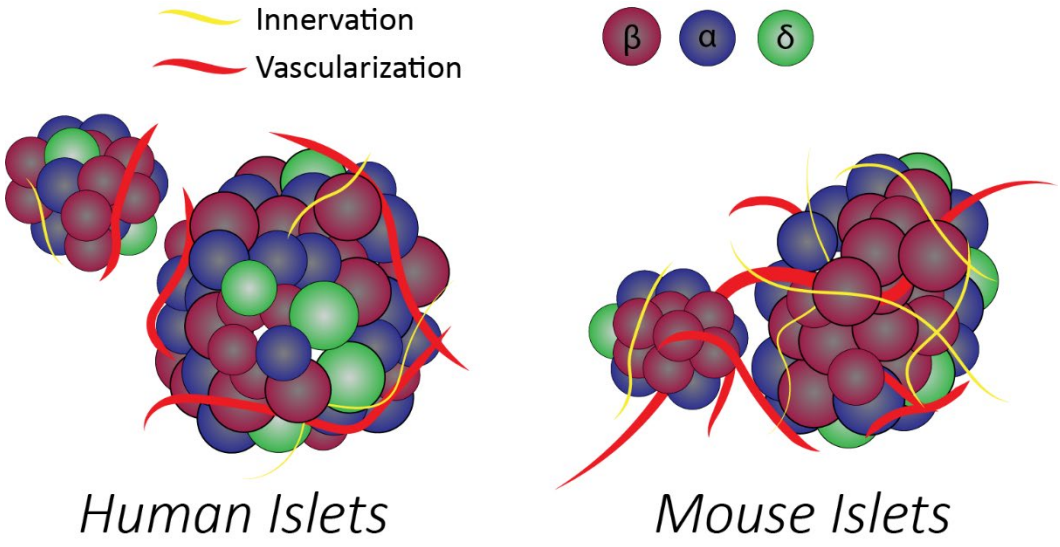

Figure 1. **Anatomical differences in human and mouse islets.** The arrangement of the endocrine cells is evenly distributed throughout human islets, while in mice the β cells localize to the islet core while α and δ cells localize to the mantle. Mouse islets are also more highly innervated and vascularized than human islets.

mice and men; the degree of vascularization [11], the extent of innervation [12], the basement membrane structure [13], as well as differences in the markers of differentiation and maturation of the endocrine cells [14, 15] (Figure 1). Furthermore, there are physiological differences in the resting blood glucose levels and the dynamic insulin secretion between mice and humans.

In order to study human islet function, and because there are limitations to the scope of conclusions that can be made using only preserved human tissues, much that is known about human islet biology has been studied using isolated human islets [16]. The process of islet isolation utilizes enzymatic digestion of the pancreas to free islets from the surrounding tissues, followed by gradient separation of the endocrine clusters from acinar or ductal tissue, and subsequent culture to purify and support the remaining cells [17] (outlined in Figure 2). Enzymes used to free the islets include a blend of collagenase and neutral protease, which are expensive at the concentrations and volumes required for perfusing and digesting the entire human pancreas, making human islet isolation a costly procedure which is not performed routinely at many facilities. For this reason, isolated human islets are often shipped and distributed from isolation labs to research labs, a process that prolongs the time between isolation and experimentation, adds additional transport-related stress and hypoxia that confounds downstream results and data. The isolation itself damages cellular and extracellular components of the native environment, stressing the isolated islets, which are only able to survive for a short period of time in culture [18, 19]. Nevertheless, isolated islets can be used to study human islet function [20, 21], endocrine cell-cell communication and coordination [22], to manipulate gene expression to study the role of various proteins in human islet biology [23], and can be transplanted to study survival, engraftment, and immune responses in translational studies [24].

Unique sequences of insulin and C-peptide (C-pep), the connecting peptide that is cleaved from insulin during processing and co-secreted into circulation, can distinguish human insulin and C-pep from that of rodents or non-human primates when the islets are studied *in vivo*. Although human islet distribution networks have increased the amount of work done using human islets in recent years [16], many functional studies are still done primarily using animal models with unknown translational relevance to the human islet biology.

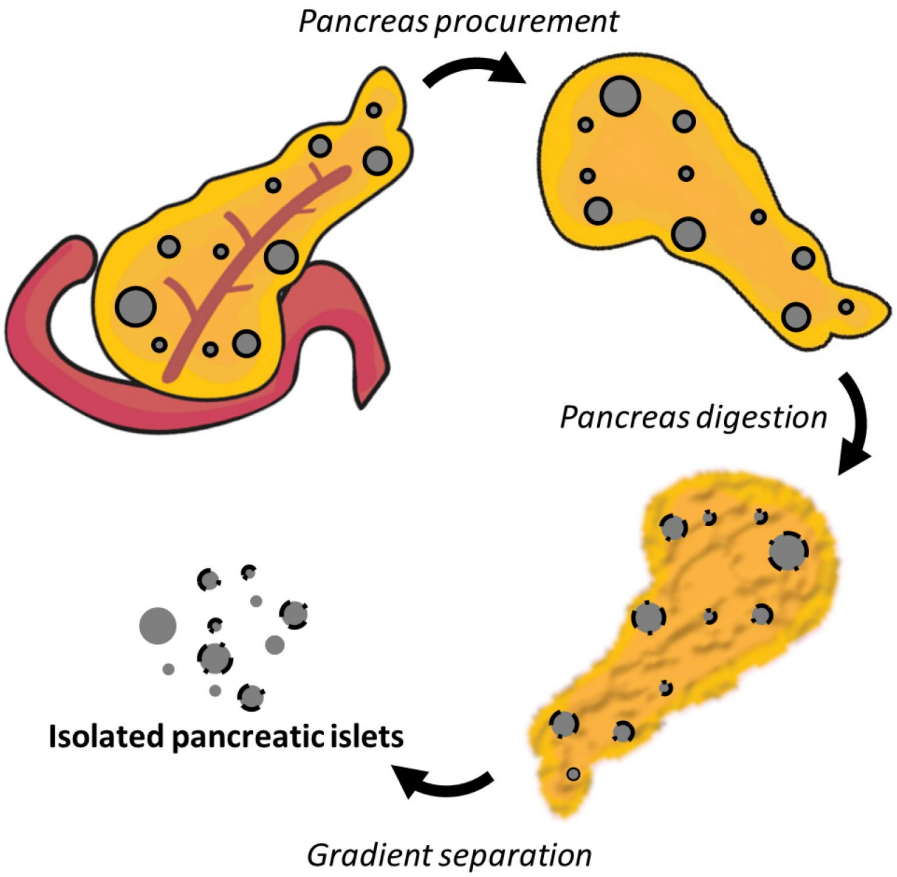

Figure 2. **Islet isolation from the pancreas.** Human islet isolation involves the procurement of the pancreas from a cadaveric donor, the digestion of the pancreas by perfusion of an enzymatic blend through the pancreatic duct, mechanical-assisted disruption of the tissue, and density gradient separation of the resulting cell clusters to isolate a pure or enriched population of islets. Damage to the islet extracellular matrix is indicated in the broken black borders of the islets.

Mimicking Nature-Made β Cells: Stem Cell-Derived Islets

As a method of generating a regenerative source of transplantable human β cells, and to produce better models of human islet development and function *in vitro*, significant effort has been dedicated to the derivation pancreatic islet-like cells from human pluripotent stem cells (hPSCs). The source of hPSCs can be either from human embryos, called human embryonic stem cells (hESCs) or can be reprogrammed from somatic adult human cells, called human induced pluripotent stem cells (hiPSCs). Both cell types have demonstrated the ability to generate insulin-producing and secreting cells, stem cell-derived β cells (SCβCs) or more broadly, stem cell-derived islets (SC-islets) [25]. hESC lines have been derived, banked, and approved by funding agencies for use in research, but importantly are not genetically or immunologically matched to patients to which the cells may be clinically useful [26]. iPSCs, however, could be derived from a patient, differentiated into a therapeutic cell type, and transplanted into the matched patient as a treatment for disease, avoiding unfavorable mismatch-related immune responses. Barriers to such a treatment, however, include the cost and time needed for developing custom-made cell lines for each patient, the variability of differentiating cell lines from different donors which may not respond the same way to the same differentiation media, and the need to correct inherent genetic traits of the patient which may contribute to disease and/or prevent successful derivation of the required therapeutic cell type [26]. For these reasons, both hESCs and hiPSCs are being explored in different approaches to differentiate of SC-islets.

Generation of Insulin-Producing Cells

For decades researchers have investigated the directed differentiation of hPSCs to SC-islets and have published protocols demonstrating progress toward this goal. These protocols

utilize step-wise exposure to growth factors to mimic or closely resemble the temporal and spatial chemical gradients that exist throughout development to stimulate gene expression profiles characteristic of each developmental stage (Figure 3) ([27-30] and reviewed in [3]). Briefly, pluripotent cells are marked by genes such as *OCT4*, *NANOG* and *SOX2*. The expression of these genes is dramatically reduced in the first few days of *in vitro* differentiation. Developmentally, the pancreas, which is comprised of endocrine, exocrine and ductal cell types, is derived from the endoderm layer of the blastocyst; definitive endoderm is marked by co-expression of *FOXA2*, *SOX17*, and *CXCR4* [31]. *FOXA2,* a key regulator in foregut development, continues to be expressed throughout pancreas development and is expressed in mature β cells, while *SOX17* expression turns off as the cells approach a pancreatic fate. *PDX1* is a key transcription factor for the pancreas, is only expressed in pancreatic and duodenal lineage, and is induced in the pancreatic progenitor (PP) stage marking the region of the posterior foregut that will become the pancreas [32]. *PDX1* continues to be expressed in mature β and δ cells, but is not present in mature α cells. Likewise, *NKX6.1* expression is induced at the second PP stage (PP2), and is required for pancreatic endoderm lineage [33]. After this time point a subset of pancreatic endoderm cells begin to transiently express *NGN3* which marks the beginning of the transition of pancreatic endoderm toward an endocrine fate [32]. *NGN3* is rapidly turned off in these cells as genes specific to each endocrine cell type begin to be expressed. For β cells, these genes include *NEUROD1*, *NKX6.1*, *MAFA*, *INS*, and many others. Developmentally, monohormonal pancreatic endocrine cells are present relatively early in human embryos (10 gestational weeks) [34], but functional maturation of these cells (secretion of hormones in response to appropriate physiological cues, such as blood glucose levels) happens postnatally [14, 35]. *UCN3* is thought

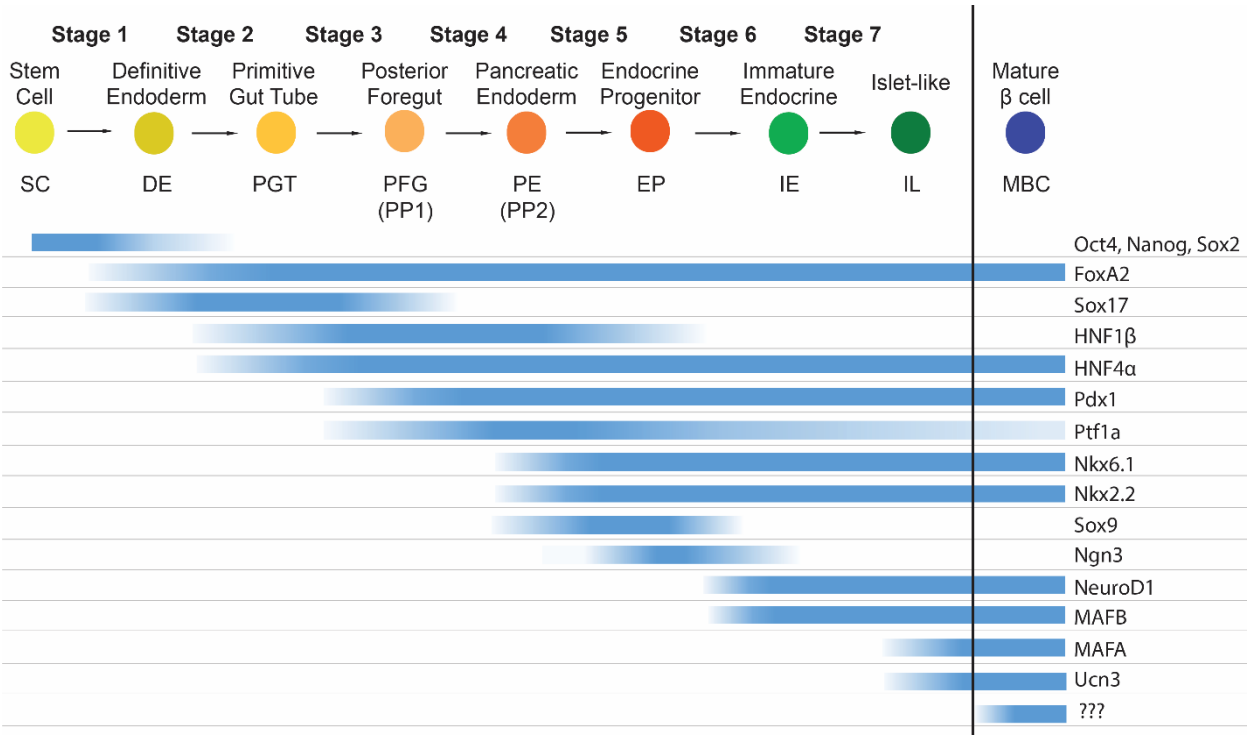

Figure 3. Signature gene expression throughout pancreas and SCβC development. SCβC differentiation protocols assess gene expression at each step of staged differentiation protocols modeled after known pancreas and islets developmental signals and gene expression profiles. Many key genes have been identified at crucial points during development, but less is known about genes that may be expressed or become active at the final stage of β cell maturation. This figure has been modified from the published figure in Sackett et al. 2020 [3]. (SC=stem cell, DE=definitive endoderm, PGT = primitive gut tube, PFG = posterior foregut, PE=pancreatic endoderm, PP=pancreas progenitor, EP=endocrine progenitor, IE=immature endocrine, IL=islet-like, MBC=mature beta cell)

to be one marker of maturation in β cells, but much of the work that has been done to identify such markers is based in rodent models which may not translate to human biology [36, 37]. More work is needed to identify human β cell maturation markers for use in assessing differentiated SCβCs, sorting cells, and to better understand the process of islet maturation and function.

In 2006, D'Amour *et al.* first published the directed differentiation toward a β cell fate, which resulted in a population of cells which were enriched for Chromogranin A (CHGA)-positive cells but only 7% were insulin-positive. Not unexpectedly, these cells were poorly glucose responsive [38]. Successive protocols have since improved the yield and functionality of SC-islets.

In 2014, Pagliuca *et al.* established a scalable protocol, working toward large-scale production which will ultimately be necessary for clinical use, resulting in efficient β cell production with measurable static glucose stimulated insulin secretion (GSIS). These SC-islets had similar gene expression profiles to primary human islets for several key β cell genes [39]. In the same year, Rezania *et al.* published their protocol describing differentiation toward an enriched insulin$^+$ cell population [40]. Both groups achieved approximately 50% insulin$^+$ cells, which when transplanted into diabetic mice resulted in a gradual reduction of hyperglycemic blood glucose levels to normal, non-diabetic levels over the course of several weeks [39, 40]. However, both Rezania *et al.* and Pagliuca *et al.* reported phenotypes of the cells that still suggested immaturity, such as elevated *NGN3* and low *UCN3* transcript levels, blunted dynamic insulin secretory profiles, elevated proinsulin:C-Pep ratio, and overall significantly lower insulin secreted per cell compared to human islets [39, 40]. Moreover, total insulin content per islet equivalent was not reported [39, 40]. Thus, at this point, protocols were able to achieve improved directed β cell differentiation *in vitro*, but cells still appeared phenotypically and functionally immature compared to normal islets.

Whereas many other early protocols led to the development of primarily polyhormonal cells, such as INS$^+$/GCG$^+$ cells, which are poorly functional, several important studies identified a key link between enriching for NKX6.1$^+$ progenitors during differentiation and ultimately achieving improved generation of β-like cells. Rezania *et al.* were the first to identify this link, demonstrating improved *in vivo* maturation and function following *NKX6.1* enrichment prior to transplantation of stem cell-derived pancreatic endoderm cells (PP2) [41]. Nostro *et al.* identified key signaling pathways that contribute to *NKX6.1* enrichment and determine the hormonal fate

of progenitor cells, demonstrating that ineffective induction of *NKX6.1* prior to endocrine hormone production restricted the fate of the progenitor cells such that they could never become monohormonal β-like cells [42]. Russ *et al*. also studied the induction of *NKX6.1* prior to the endocrine progenitor stage and found that increased early *NKX6.1* expression led to a reduced polyhormonal population in the final islet-like clusters, and more glucose-responsive β-like cells [43]. Collectively, these studies significantly advanced our understanding of the complexities of β cell differentiation and the importance of *NKX6.1* expression in *PDX1*$^{+}$ progenitors for generating monohormonal β-like cells.

Acquisition of Mature Phenotypes and Function

Several more recent publications have significantly pushed the boundaries of SC-islet maturation. In 2017, Ghazizadeh *et al.* published the first evidence of *in vitro* expression of the maturation-associated gene, *UCN3* [44]. This was accompanied with an improvement in static GSIS function, however dynamic GSIS was not studied. Velazco-Cruz *et al.* and Nair *et al.* were the first studies to show functional dynamic GSIS, approaching levels comparable to human islet function. Interestingly, these changes were not accompanied by significant improvement in expression of the genes *MAFA* and *UCN3,* thought to be associated with β cell maturation [45, 46].

In their 2017 study, Ghazizadeh *et al.* screened a library of 4000 chemicals and identified five that stimulated at least a 5-fold increase in INS^{+} cell production from PDX1^{+} progenitors. The chemical with the highest efficiency was the molecule H1152, an inhibitor of Rho-associated kinase (ROCK) which inhibits both ROCK I and II. The addition of H1152 into their differentiation protocol increased the efficiency from only 12.2% INS^{+} cells to 29.8% INS^{+} cells. Although the

proportion of INS^+ cells is relatively low, they found that the expression of *MAFA* and *UCN3*, which otherwise had been found to be poorly expressed, were upregulated following culture with H1152. For the first time, *UCN3* mRNA expression was detectable at levels similar to primary islets. *MAFA* expression also increased with H1152 from nearly undetectable to a level approximately 5-fold lower than primary islets. Using their unique differentiation protocol with H1152 in the final stages, they were able to generate glucose-responsive cells with a 3-fold stimulation index (SI) in static GSIS, and total insulin content comparable to human islets [44]. They validated their study with several human stem cell lines and also added H1152 to the differentiation protocol published by Rezania *et al.*, which resulted in SC-islets with improved static GSIS performance and *UCN3* expression. The study did not assess whether H1152 improved the dynamic GSIS of the cells, which was shown to be deficient in Rezania's initial publication. Furthermore, UCN3 is expressed in mature human α and β cells [47]; immunofluorescent staining was not used to demonstrate that the protein was present in the Ins^+ cell population [44].

Key features of normal islet function *in vitro* are (i) rapid first phase insulin release in response to a glucose stimulus followed by a more sustained second phase release, (ii) rapid and complete turn off of insulin release in response to low glucose, and (iii) responses to other chemical secretagogues. Achieving these types of dynamic functional insulin secretory responses of SC-islets is a critical goal. More recently, Velazco-Cruz *et al.* and Nair *et al.* made significant advances toward this goal, describing strategies for improving beta-like cell function [45, 46]. Nair *et al.* implemented a unique strategy utilizing insulin-driven GFP labeling and Ins^+ cell enrichment by fluorescence-activated cell sorting (FACS), followed by reaggregation of clusters from single cells and continuation of *in vitro* culture, thereby attempting to recapitulate the

developmental endocrine clustering process. After an additional 6-8 days of culture, this purification step resulted in highly enriched β cell clusters (eBCs) with 99% endocrine cells, marked by chromogranin A (CHGA), which on average had better gene expression profiles than the unsorted aggregates. The eBC clusters performed successfully in dynamic GSIS, with a stimulation of ~4 in a first phase response, but with a very weak second phase. Compared to human islets, with a first phase stimulation index of ~12, the cells are clearly less potent, but the total C-peptide secreted in response to depolarization (KCl) was similar, ~1.2 pg·min·ng^{-1} DNA for eBCs compared to ~1.8 pg·min·ng^{-1} DNA for islets, suggesting that the potency of the eBCs is close to that of islets. Total insulin content of the eBCs was not reported, although the *INS* mRNA expression level of the eBCs was reported and was nearly 10-fold lower than primary islets. This study is arguably the most complete metabolic study of SC-islets, with an analysis of calcium signaling as well as mitochondrial health and function. eBCs displayed similar levels of mitochondrial energization and increased oxygen consumption in response to high glucose. However, these parameters were only assessed comparing immature cells (day 20) to eBCs (day 26-27), so it is difficult to know whether these mitochondrial properties are unique to eBCs, or are also present in other SC-islets. Finally, this protocol was developed and tested solely with one cell line, dependent on the genetically engineered Ins-GFP cassette [48]. It is difficult to know how well it would work with other non-genetically modified stem cell lines, but based on the unsorted 'non-enriched clusters' in the Nair *et al.* study, the success of the protocol is completely dependent on GFP-labeled cell sorting [45].

Two papers from the same group, Velazco-Cruz *et al.* and Hogrebe *et al.*, have also demonstrated improved dynamic insulin secretion without cell selection and showed that their

protocol could be applied to multiple cell lines [25, 46]. Velasco-Cruz *et al.* convincingly demonstrated that the TGFβR1 inhibitor, Alk5 inhibitor II, has a detrimental effect in the final stage of differentiation. This is significant because Alk5i II has been included in the final stage of many of the leading differentiation protocols [39, 40, 45, 46, 49]. Through the use of a serum-free media, and by removing T3 and Alk5i II in the final stage of differentiation, the protocol derived from Pagliuca *et al.* was significantly improved upon, based on gene expression profiles and insulin secretion patterns. In addition to removing these two components in the final stage of differentiation, they also included a resizing step of the cell aggregates in the final stage and continued the last stage of differentiation for 9-35 days. In the end, their extended culture protocol generated cells with approximately a 10-fold increase in *INS* gene expression and 2-fold higher insulin content, and more importantly displayed improved static and dynamic insulin secretion in response to high glucose compared to Pagliuca *et al.* The SC-islets had a static SI of 3.0, while cadaveric islets SI averaged 3.2. The SI of the first phase of dynamic GSIS was 7.6 for SC-islets, which was lower than an average stimulation of 15.0 for primary islets. The second phase response was also lower for SC-islets. Further, *in vivo* data demonstrated that by 10 days after transplantation into diabetic mice, a glucose-tolerance test was similar to non-transplanted, non-diabetic controls, suggesting early function which is believed to be critical for successful clinical translation of this therapy [46].

Hogrebe *et al.* utilized the protocol improvements established in Velasco-Cruz *et al.* and adapted the protocol to begin in planar adherent culture rather than suspension. Hogrebe *et al.* established that a major reason that differentiation protocols were not broadly applicable to different cell lines was that hPSC lines performed dramatically differently when transitioned into

suspension culture. This is significant because many previous protocols have been developed with specific hESC lines, but have worked less efficiently when implemented using other hESC or hiPSC lines. Therefore, the protocol published by Hogrebe *et al.* is an important step toward developing a universal SC-islet protocol for any hESC line. The protocol starts all cells in planar adherent culture and utilizes latrunculin A treatment during endocrine induction to stimulate actin cytoskeleton rearrangement and facilitate better functional outcomes than had previously been found in planar differentiations [25]. This modified protocol was capable of generating SC-islets from a variety of hESC and hiPSC lines that performed more consistently than if those cell lines were used with other protocols [25]. This is an important step toward deriving a protocol that will work universally on many cell lines for potential use with patient-matched iPSCs.

These recent studies demonstrate an important step toward achieving dynamic β cell function, as compared to realistic and high-functioning islet controls, although SC-islets generated in all three protocols had negligible levels of *MAFA* and *UCN3* mRNA expression [25, 45, 46]. Although both groups cited a 2016 study (Arda *et al.*) revealing that human *MAFA* levels peak during puberty as an explanation for the low SC-islet *MAFA* levels, the Arda *et al.* study does not suggest that human juvenile β cells have zero *MAFA* expression, but rather contain about half that of adult β cells [14]. This suggests that better *MAFA* expression would be expected in β cells even at the juvenile stage of development. Furthermore, the Arda *et al.* study identified several other genes associated with juvenile to adult β cell maturation, such as *SIX2*, *SIX3*, and *ONECUT2*, which have not been assessed in these recent SC-islet differentiation papers [14].

Together, these reports confirm the ability to achieve better gene expression and dynamic function than previously demonstrated in the SC-islet field. The advances presented by

each of these studies have still not achieved a cell population which recapitulates the human islet in every aspect, but each contribute an important piece of this complex puzzle for future investigation. It is now clear that dynamic *in vitro* function can be achieved, even with expression of *MAFA*, *UCN3* and *INS* at levels significantly lower than human islets. Though the reasons for, and implications of, these lower gene expression levels are not clear, it is evident that better insulin secretory function is associated with a more rapid restoration of normoglycemia in diabetic mouse models. A more in-depth understanding of the functional and phenotypic differences in cadaver islet and islet-like clusters at the single cell level will likely pave the way towards generating even more robust function. Increasing the insulin content, and the expression of other candidate maturation genes (*MAFA*, *UCN3* and others) may lead to further improvements in SCβC function. There is also a need to better understand markers of mature β cells and how well those that have been identified in animal models translate to human cells [50]. Methods through which differentiation may be improved are numerous and include further fine-tuning of the chemical components used for differentiation, but could also be expanded to include other signals that cells receive *in vivo*, such as through the extracellular matrix, direct cell-cell contact with neighboring cells, including other endocrine, vascular or per-vascular cells, perfusion and interstitial flow of the nutrient-containing medium mimicking blood flow, or entrainment to a feeding schedule to induce circadian rhythm.

If the dynamics of glucose sensing and insulin secretion are not as precise as native β cells, SCβCs may not be able to fully reverse hyperglycemia in patients, or may overproduce insulin and cause hypoglycemia. It is notable that most GSIS data is derived using high glucose concentrations that are much higher than physiologic non-diabetic levels [51, 52]. Many other signals, like

incretins, are also involved in regulating insulin secretion after eating and are not always included as a component of GSIS data. Prior to clinical use, it may be important to further investigate the maturation of stem cell-derived β cells through both maturation-associated gene and protein expression, as well as functional maturity.

Engineering SC-Islets for Clinical Applications

Since the derivation of hESCs [53], the field of regenerative medicine has envisioned cellular and tissue transplantation therapies based on the numerous differentiated somatic cell types that can be generated from them (reviewed by Wu *et al.* [54]). However, intrinsic to transplantation of stem cell-based therapies, as with organ and tissue transplantation, is the fact that a major obstacle to a successful clinical outcome is the expression of foreign HLA antigens and the recipient's immunological recognition and responses to the cells and tissues bearing these foreign HLA types. Thus, an in depth understanding of the innate and adaptive host immune responses to various cell and tissue types derived from either allogeneic hESCs/iPSCs, or autologous hiPSCs, including SC-islets, will be critical to successful clinical translation. Further, it will be equally important to understand how different routes of administration of cells (i.e. transplant sites) and co-transplantation with other biomaterials or encapsulation technologies may affect immunogenicity and engraftment.

While this aspect of stem cell science is still nascent, strategies to reduce immune responses to stem cell progeny are already being tested. David Russell's team has engineered normal human stem cells using AAV vectors to escape immune rejection by allogeneic $CD8^+$ T cells, B cells and NK cells [55]. While several groups have made PSC lines which are deficient for β2M [56-60] and therefore absent of HLA class I cell surface expression, cells missing Class I

expression may still be vulnerable to attack and elimination by natural killer (NK) cells [61, 62] Hence, they knocked-in HLA-E into the β2M locus in order to overcome the "missing self" response. They showed that these HLA-E expressing, HLA-A, B, C absent ESCs and their progeny are less susceptible to NK cell and CD8+ T cell cytotoxicity. Another strategy for achieving immunoprotection through genetic modification was studied by Rong *et al.* who chose to target co-stimulatory (CTLA4:B7:CD28) and co-inhibitory (PD:PD-L1) pathways, thereby hoping to prevent T cell activation by constitutive expression of these molecules in hESCs [63]. They showed that constitutive dual transgene expression, but not one transgene alone permitted teratomas to survive in humanized allogeneic mice and reduced cellular infiltrates to hESC grafts. Despite efforts to add genetic kill-switch mechanisms to these cells [64, 65], serious concerns still exist about using a cell population that is immune-evasive in clinical applications.

An alternative approach to engineering hESC-based treatments for immune evasion is to physically isolate the cells *in vivo* using a device to prevent the immune system from infiltrating the graft. Devices proposed for this type of work could be microencapsulation devices, in which individual islets are coated with an immunoprotective polymer, or macroencapsulation, in which many islets are housed within a single immune-isolating unit [66]. Both of these strategies require the device to permit exchange of nutrients and hormones bidirectionally across a membrane, but block the movement of immune cells from infiltrating the graft within. While concerns about making cells immune-evasive make these devices appealing, in practice nutrient and gas exchange across the membrane of the device has not been efficient enough to support robust cell survival [67]. Furthermore, isolating the endocrine cells from direct contact with blood vessels and the fibrotic deposits that form around these devices *in vivo* may prevent effective cell

survival and function [66]. Supporting cell health and function within the device will therefore be a key concern if these approaches are to be clinically viable. Strategies for developing SC-islets as a clinical therapy are summarized in Figure 4.

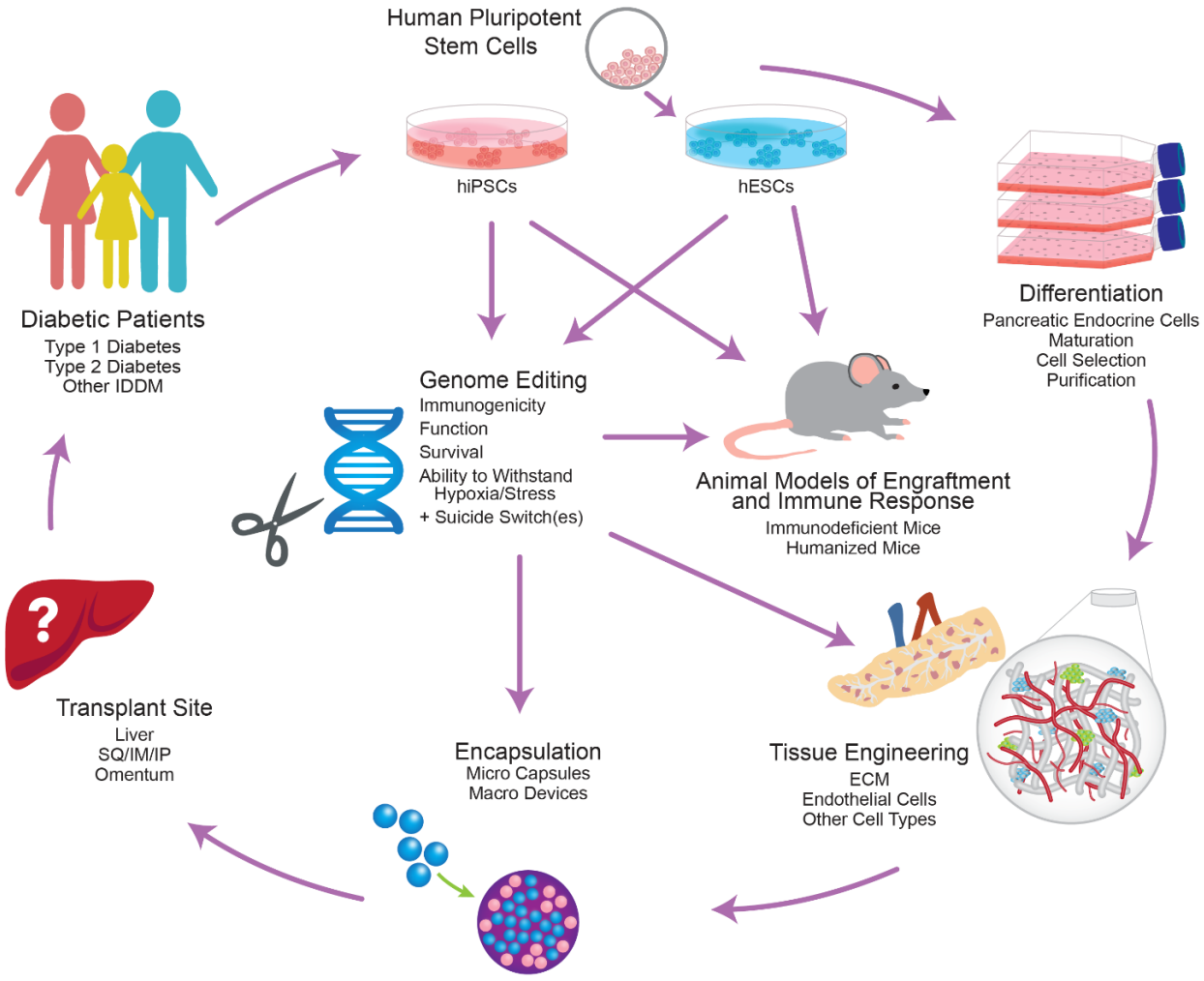

Figure 4: Current strategies for the development of pluripotent stem cell-based therapies for diabetes. Human embryonic stem cells (hESC) and human induced pluripotent stem cells (hiPSC) are being tested as cell sources. Genome editing to confer precise genomic modifications or encapsulation are promising technologies to engineer cells to prevent immune mediated destruction and control potential aberrant cell growth. Tissue engineering could generate insulin-producing tissues that would involve using hPSCs. Encapsulation strategies and the exploration of alternative transplant sites may open new avenues for transplanting hPSC-derived SC-islets. Abbreviations: IDDM, Insulin-dependent Diabetes Mellitus; iPSC, induced pluripotent stem cells; ES, embryonic stem; SQ, subcutaneous; IM, intramuscular; IP, intraperitoneal injection; ECM, extracellular matrix. This figure has been modified from the published figure in Sackett et al. 2020 [3].

Rebuilding a Better Home for Islets

The Extracellular Matrix

The extracellular matrix (ECM) is a network of proteins and polysaccharides which stimulates cells through structural and biochemical interactions. ECM molecules directly bind cell receptors, such as integrins, activating intracellular signaling cascades. The ECM can modulate signaling pathways by sequestering growth factors and affecting growth factor-receptor dynamics [68]. Through these mechanisms, ECM plays a significant role in cell health and identity. The process of isolating islets from the pancreas involves collagenase digestion which destroys much of the native islet ECM, affecting islet health [18, 19, 69]. Since β cell replacement is used as a treatment for diabetic patients, understanding the role of ECM on islet and β cell survival and function could help optimize the treatment. In human islets, ECM has been found to affect β cell proliferation, differentiation, survival, and insulin secretion dynamics [70]. The culture of islets with individual purified matrix components has been shown to positively affect islet-specific gene expression, further underscoring their importance in islet health [71-73].

Anoikis, meaning 'without a home', is an integrin-mediated form of apoptosis due to the absence of ECM in a tissue environment, and is a major contributor to cell death in isolated islets. High purity islet preps have high rates of apoptosis which can be reduced with anoikis inhibitors; impure preps, containing more intact ECM, have exhibited better cell survival [74, 75]. Islets cultured on purified ECM proteins, collagen (COL), laminins (LAM), and fibronectin (FN), have lower apoptosis rates and maintain better β cell function [76, 77]. Soluble integrin-binding ligands, such as fibrinogen, arginine-glycine-aspartate (RGD) peptides and integrin antibodies, also reduce apoptosis in cultured islets [78, 79].

Islet ECM has been previously reported to contain COL I, III, IV, V and VI, as well as LAM and FN. Most studies established this compositional analysis through immunohistochemistry, and data originate from pancreata derived from a variety of different species [70, 80, 81]. Because most native islet ECM is destroyed during isolation, it is difficult to use proteomic methods with isolated islets to further characterize islet-specific ECM [70].

Decellularization

ECM can be isolated from tissues through a process called decellularization (decell), in which detergent-mediated cell lysis and subsequent washing removes cellular material, yielding native ECM (detailed in Figure 5). In this way, ECM has been extracted from many animal and human organs, and has been proposed for use in regenerative medicine for a variety of applications [82-84]. One approach is to use perfusion decell, by delivering detergents through the vasculature with the goal of preserving the macro- and microstructures of the organ [82]. However, seeding cells or islets into a whole perfusion-decelled pancreas has proved challenging [85-90]. Another strategy is to solubilize the ECM with acidic pepsin digestion. The digested ECM can be neutralized and warmed to 37°C to form a hydrogel, or lyophilized to form a sponge [91]. These scaffolds require digestion and reformation of collagen fibrils [92], reorganizing the microstructure and potentially disrupting ECM protein functional domains. On the other hand, a hydrogel can be customized and easily incorporated into cell culture systems and transplantation strategies. The collagenous nature of native ECM hydrogel is advantageous for *in vivo* applications, where the neutralized digest can be injected as a liquid and forms a gel at physiologic temperatures. Due to the potential challenges of seeding intact 3-D scaffolds, a hydrogel's ease of use has practical advantages in tissue culture and transplantation platforms.

The pancreas of many species including mouse, rat, pig and human have been decelled, generating pancreatic ECM (P-ECM). These studies provide clear evidence that pancreatic decell is achievable, resulting in a hypoimmunogenic matrix, free of DNA and cellular debris. The most common decell method utilized has been a perfusion approach, via vasculature or the pancreatic duct. Napierala *et al.* compared perfusion through the portal vein, aorta, or pancreatic duct of a porcine pancreas and found no significant difference in decell efficiency between the three routes [87]. Detergents used have ranged from Triton X-100, to sodium dodecyl sulfate (SDS), to sodium deoxycholate, with no study specifically comparing the efficacy or impact of these detergents on the pancreas, but with all studies having similar decell effectiveness. The length of

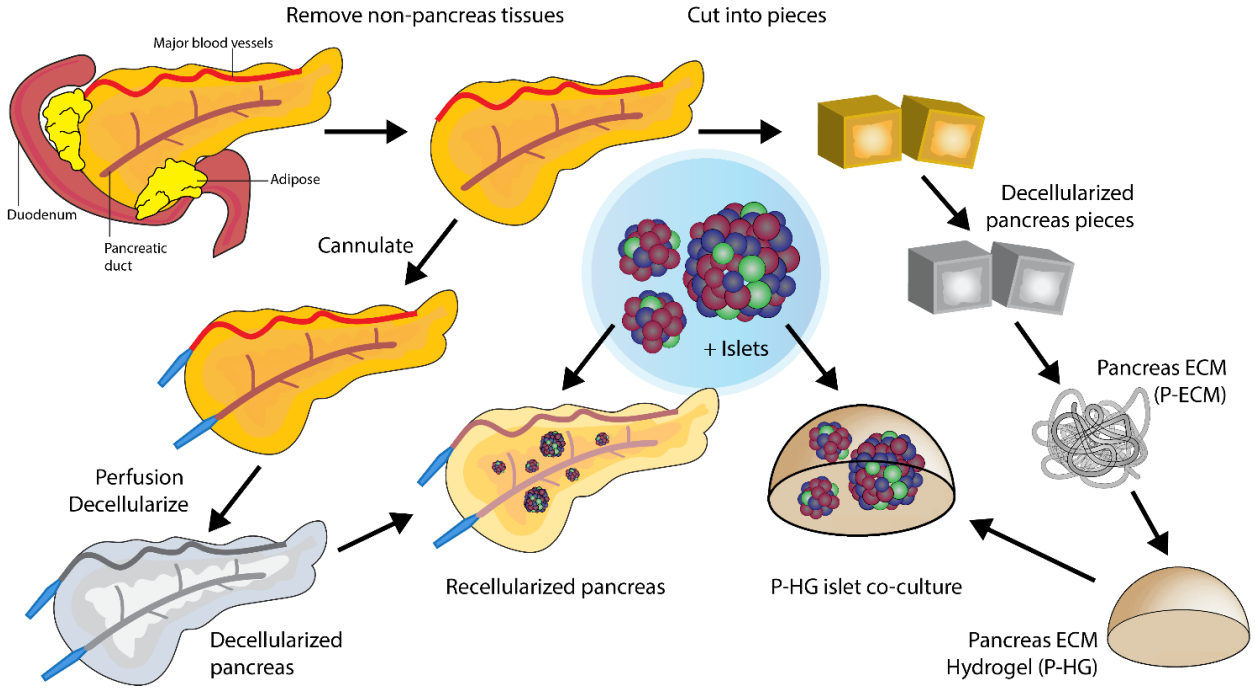

Figure 5. **Schematic representation of pancreas decellularization methods.** The pancreas can be decellularized whole by perfusion of detergents through the vasculature or pancreatic duct, keeping the tissue ultrastructure intact (left side). An alternative approach is to disruption the tissue by cutting or homogenizing, followed by cell lysis, extraction of the pancreas ECM (P-ECM) and reconstitution of the ECM as a hydrogel (P-HG). Either of these scaffolds could be combined with isolated islets or other cell types.

detergent treatment appears to be dependent on species and organ size, with smaller organs (mouse, rat) requiring between 3-5 hours in detergent, and larger organs (pig, human) needing between 8 hours - 3 days [85-87, 89, 93-99]. The detergent used and time exposed to detergent may affect the microstructure and function of retained matrix molecules [83], with one study comparing SDS to Triton-X treatments on porcine pancreas finding that Triton-X paired with a protease inhibitor cocktail had the best retention of the range of ECM components present in the pancreas [100]. A protocol has also been developed for a detergent-free decellularization of the pancreas [101].

Retention of ECM components has been assessed through a variety of methods, however, few in-depth proteomic analyses of P-ECM composition have been previously published. Utilizing mass spectrometry-based proteomics with decellularized mouse pancreas, Goh *et al*. identified 30 ECM-associated proteins in the P-ECM including 17 COL and 7 LAM proteins [95]. It may be important to expand these studies to identify how decell treatments affect the P-ECM composition compared to native tissue, and how the P-ECM proteome varies among species. Utilizing human tissue with these techniques could benefit the understanding of the human pancreatic ECM composition, and create human-specific downstream applications of P-ECM.

The effect of P-ECM on cells and islets has been broadly investigated, but with diverse approaches and results. Cytocompatibility studies testing toxicity of the P-ECM on cell survival have indicated that the decelled matrix is not toxic to cells [85, 86, 95, 97, 99]. When the MIN6 β cell line was perfused into the 3D mouse P-ECM, Goh *et al.* found cell survival and maintenance of insulin gene expression after 5 days [95]. Using SC-islets, Wan *et al*. found that mouse SC-islets on rat P-ECM had a 2-fold increase in insulin gene expression compared to those without P-ECM [89].

Furthermore, Chaimov *et al.* found that hepatocytes transdifferentiated to β cells on P-ECM had more than a 4-fold increase in insulin secretion [93]. When combined with islets, P-ECM has had variable effects. Two studies have found that islets cultured on or within P-ECM survived and functioned equally as well as islets in the absence of matrix over a 4-5 day period [86, 97]. Another group showed that islets within the 3D scaffolds could function, however this was without a comparison to control islets [87]. DeCarlo *et al.* performed a longer study in which rat islets cultured with rat P-ECM maintained insulin secretion up to 6 weeks, while naked islets began declining after 2 weeks [94].

Narayanan *et al.* recently published interesting results with decelled RIN5F (rat insulinoma) β cell cultures. hESCs plated onto acellular RIN5F ECM and treated with RIN5F conditioned medium over 14 days were shown to differentiate into glucose-responsive insulin producing SC-islets, without a staged differentiation protocol or through added growth factors [102]. This study mirrors other work demonstrating the instructive power ECM can have on cells [103], and highlights the potential P-ECM may have on islets and SC-islets.

Few groups have explored the effects that P-ECM may have on transplanted islets. De Carlo *et al.* found that rat islets and rat P-ECM transplanted subcutaneously (SQ) within a polyethylene glycol (PEG) hydrogel reversed hyperglycemia for up to 41 days in diabetic rats, while islets with P-ECM but no PEG only reversed hyperglycemia for a few days before returning to a diabetic state [94]. Chaimov *et al.* also transplanted islets and P-ECM hydrogel SQ within alginate capsules into diabetic mice. They observed a temporary drop in blood glucose, but not a long-term reversal of diabetes [93]. One of the most striking studies has utilized an “islet viability matrix” (IVM) composed mainly of purified collagen 1 to support SQ islet engraftment.

The SQ space is a potential transplant site for islets because it can be easily accessed during transplantation, can be monitored in a non-invasive way, and can accommodate a large volume of cells, but has also been a difficult site into which to transplant cells in animal models due to low levels of vascularization and high levels of cell death after transplant [104], requiring high numbers of islets (2000 IEQ or more) to reverse diabetes. Yu *et al.* transplanted as few as 200 transplanted human islets, successfully lowering the blood glucose of a diabetic mouse when co-transplanted with the IVM material, but the islets were not viable if transplanted alone [105]. These are promising steps toward creating a strategy for SQ islet transplantation, and P-ECM could play a role in enhancing the microenvironment of this space. More studies are required to confirm the potential benefits of P-ECM on transplanted islets or SC-islets, and to better understand the underlying mechanisms.

Alternative Transplantation Approaches

Following intrahepatic islet transplantation, a significant fraction of islet mass is lost after infusion due to instant blood-mediated inflammatory reaction (IBMIR) and microthrombosis, causing damage by a variety of postulated mechanisms [106, 107]. These high levels of islet attrition lead to the need to transplant islets from more than one donor to treat diabetes in a single patient. Even with recent advances, only 44% of patients maintain insulin independence 3 years after infusion [108]. A better islet transplant site is needed to support islet survival and long-term reversal of hyperglycemia [109]. As has been discussed, many advances have been made in differentiating SC-islets [39, 40, 42, 43, 110], however SC-islet transplantation into the liver may encounter similar challenges that have beset cadaver islet transplantation unless a better strategy is identified.

Due to the imperfect islet survival and function when transplanted into the liver, and because the same method of delivery may not be desirable in early trials of SC-islet transplant, alternative approaches are being explored. Recent techniques being tested in clinical and experimental β cell replacement include exploration of novel transplant sites, such as the omentum [111], intramuscular (IM), intraperitoneal (IP) or subcutaneous (SQ) space [112-115], and include encapsulation strategies to protect islets from immune rejection [93, 94, 109]. Many of these approaches have been identified as having microenvironments that limit survival and engraftment of isolated cadaver islets. Recent clinical trials conducted by ViaCyte, in which stem cell-derived pancreas progenitor cells were transplanted into diabetic patients, did not produce sufficient detectable insulin, indicating a critical lack of *in vivo* survival and function [67]. Therefore, an improved microenvironment that supports robust islet survival and function is desirable [109, 116] and could in part be enhanced by providing a matrix substrate such as P-ECM or a P-ECM hydrogel. As SC-islets undergo preclinical testing and enter clinical trials, the same challenges will need to be carefully considered about optimizing the environment of transplanted SC-islets to ensure long-term function and maintenance of β cell identity *in vivo*. These tissue engineering, encapsulation, and transplant site strategies for developing SC-islets as a clinical therapy are also summarized in Figure 4.

Novel Vascularization Methods

To support islet survival during transplantation, many studies have focused on strategies to improve the vascularization of the islet graft following transplantation. Efforts to pre-vascularize a transplant site, such as the SQ space, have demonstrated that rapid revascularization of islets can dramatically improve graft survival and function. Prevascularization

of the SQ space prior to islet transplantation has been shown to enable restoration of glycemic control with fewer transplanted islets that are required for normalization of glycemia if transplanted without prevascularization [104, 114]. Other strategies have involved combining primary endothelial cells (ECs) or mesenchymal stem cells (MSCs) with islets before or during the transplant to improve vascularization [115, 117-120], co-transplanting with adipose-derived microvessels [121], or using vasculogenic biomaterials or soluble factors to improve vascularization of the graft [112, 122, 123] (Figure 6). One approach that has not yet been reported could conceptually involve pre-vascularizing a tissue-like composite of islets and ECs in a scaffold prior to transplantation, which would theoretically provide the components to rapidly vascularize an islet graft in culture and *prior* to transplantation, in order to support faster engraftment (Figure 6E).

Studies using these various approaches have found that islets transplanted alone into the SQ space have poor survival and function and therefore require high islet equivalent (IEQ) counts in order to be even somewhat effective at reversing diabetes in animal models. In contrast, all of the listed vascularization methods have been reported to support islet survival, increase detectable insulin in the blood and improve recipient blood glucose levels [112, 115, 117-123]. These are promising steps employing animal models, but it is yet unknown if these encouraging results will translate to humans in clinical trials. However, it is worth mentioning that each treatment has associated drawbacks. The pre-vascularized SQ space model utilizes the host's foreign body response to create the vascularized pocket for islet transplantation [114], but the fibrosis and inflammation at the site may not be beneficial to the graft. That these reactions are generally stronger in humans than rodent models means the methodology itself may not

translate to the human system. It also requires two separate surgical procedures. The co-transplantation of isolated microvessels with islets is one of the more successful methods of graft vascularization to date, but requires that microvessels be isolated from a donor, which may not immunologically match the recipient, islet donor, or SC-islet cell source [121]. As the field moves toward the clinic with a desire to avoid rejection of the grafts without the use of immunosuppression [3], it is unclear what role microvessels or other primary cell types may be able to play in that future treatment strategies.

ECs are important for connecting the graft to the host vasculature to support graft survival, but EC-islet interactions also play a key role in islet development and function [124]. Most studies establishing the role of ECs in islet development and survival have been performed in animal models, particularly mice and rats. While *in vivo* study of endothelial-islet relationships is ideal for understanding the interplay between cell types, the differences among species in islet structure and biology prevent animal studies from translating directly to human islet biology. Furthermore, many previous studies have incorporated endothelial cells into culture with islets in a physiological way that does not resemble *in vivo* biology. For instance, islets have been coated with ECs, or dissociated and re-aggregated with ECs, without permitting the ECs to form *in vivo*-like 3-D tube structures [125-127]. Recapitulating the 3-D environment in culture is as important as providing the appropriate chemical cues to cells, and in 2D culture cell behavior can be dramatically altered compared to native cells. Few studies have successfully cultured ECs in a 3-D environment with pancreatic endocrine cells. Although several recent reports have made progress on this front [118, 128, 129], the scaffolding used for 3-D culture was not a pancreas-like biomaterial and leaves room for further optimization of these methods.

Overall, a better understanding of the microenvironment of the pancreas and how islets interact with the different constituents of that environment could be a powerful tool for improving islet and SC-islet research and transplantation. If the islet microenvironment could be reconstituted either *in vitro* or alongside transplanted islets *in vivo*, it may facilitate improved islet culture, better modeling of islet interactions with their environment, and improved transplantation outcomes. If applied to SC-islets, there is potential to improve the differentiation, maturation and function of the cells, as well as the possibility of combining SC-islets *in vitro* with various elements of the *in vivo* environment to study disease, drug toxicity and other complex problems that involve multiple cell types. As the foundation of every tissue, and the basis for most *ex vivo* 3-D culture systems, ECM has an important role in these studies. Thus, properly characterizing and recreating a pancreas ECM environment is an important step toward achieving these goals.

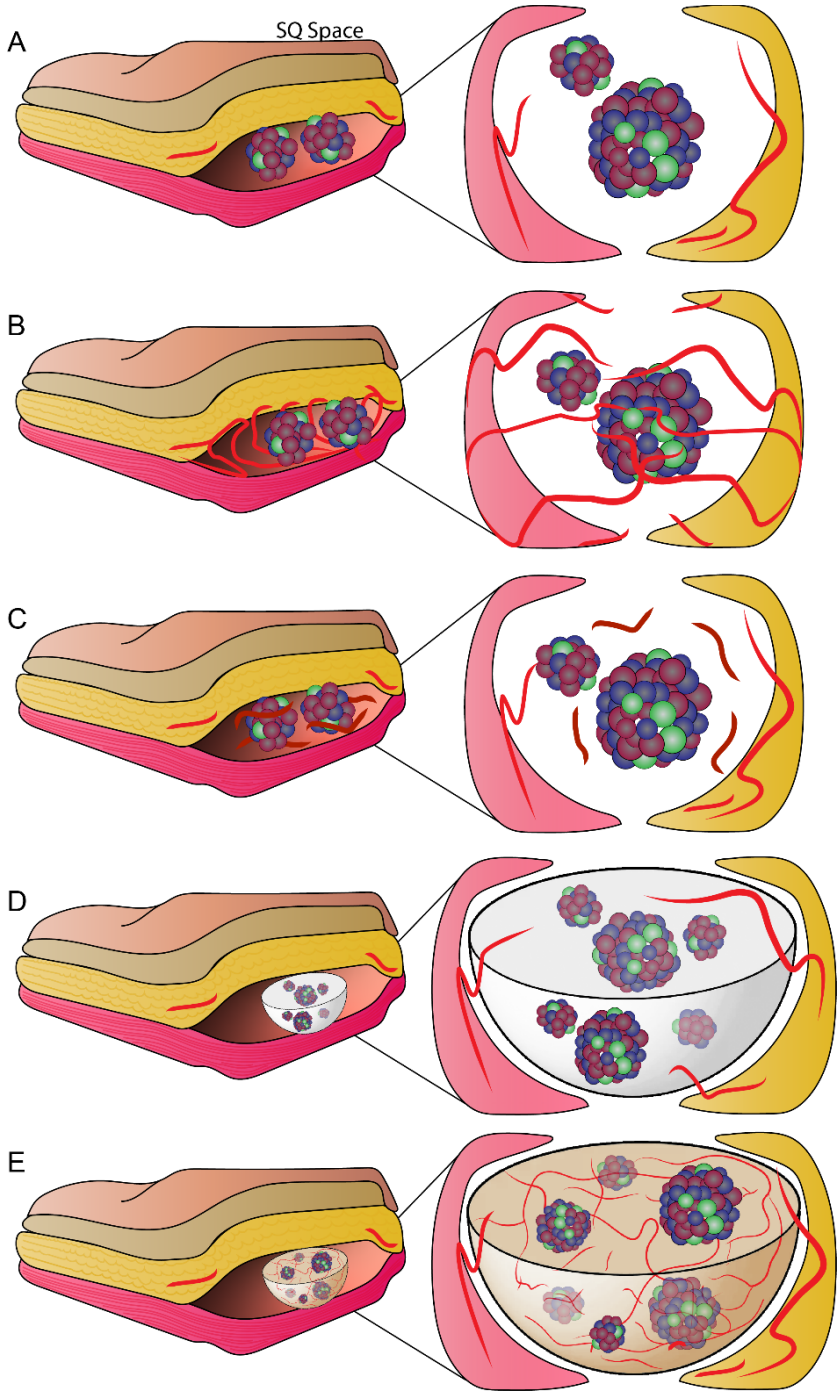

Figure 6. Strategies for improving the vascularization of islets transplanted into the SQ space. A) Islets transplanted alone into the SQ undergo harsh hypoxic conditions and limited vasculature leading to significant cell death. **B)** The SQ space can be pre-vascularized through a variety of strategies creating an environment for rapid islet vascularization and engraftment. **C)** Islets can be co-transplanted with endothelial cells, isolated microvessels, and/or other support cells to improve vascularization. **D)** Islets can be co-transplanted with a vasculogenic scaffold or soluble factors to attract revascularization from the host. **E)** Islets could be pre-vascularized in culture and transplanted in combination with pre-formed endothelial tubes and a supportive ECM hydrogel.

Summary

Prior to the work I present in this thesis, much of the knowledge about pancreas and islet ECM was derived from rodent and other animal models. Protocols to decellularize the pancreas have been established previously, but translating such protocols to scale from small mouse tissues to large human tissues is not comparable or straightforward. Although it is not yet clear whether differences between other species and human pancreas matrisome compositions are significant enough to justify the use of human-specific ECM for applications with human islets or SC-islets, a better understanding of the human pancreas and islet matrisome will undoubtedly help to make future decisions regarding ECM scaffolding to support these cells *in vitro* and *in vivo*. Presented herein we, for the first time, characterize the human pancreas matrisome. Furthermore, we assess how the ECM composition changes in the pancreas throughout development, from early fetal stages to late adulthood. I have developed a protocol to decellularize the human pancreas and generate a human pancreas ECM hydrogel (hP-HG) for use in tissue culture and to support cells during transplantation.

Combining hP-HG with SC-islets, I find that co-culture with pancreatic ECM has beneficial effects on the gene expression profiles and endocrine yield of the differentiated clusters. To optimize my co-culture methodology, hP-HG was combined with primary human islets and yielded surprising and encouraging results. In hP-HG co-culture compared to standard suspension culture, the stimulation index of human islets from low (2.8 mM) to high glucose (28 mM) was dramatically improved. Islet survival was also improved when islets were cultured in hP-HG compared to suspension culture. Further, other aspects of islet biology were altered in hP-HG co-culture. For example, islet mitochondrial maximal respiration was higher in hP-HG embedded

islets compared to islets in suspension. Islet architecture was dramatically altered following islet isolation, but was in hP-HG co-culture architecture was better preserved over 7 days of culture compared to those cultured in suspension, in which the localization of the endocrine cells continued to change over time.

The potential of hP-HG to provide a base scaffold for 3-D modeling studies is perhaps the most promising aspect of this work. As just one example of the role ECM could play in future work, endothelial cells cultured in hP-HG can be stimulated with growth factors to form 3-D tubes within the gel, and can form these tubes when cultured in combination with human islets and an islet-supportive medium. Many current studies aim to model the islet environment *in vitro* as part of larger projects focusing on immune interactions, vascularization, and the roles of other supportive cell types within the context of the natural islet environment. Because so many aspects of islet biology differ from animal models to human islets, model systems to recapitulate human biology will be essential to translate findings from animal models to the clinic. Furthermore, as various approaches are used to evade the response of a patient's immune system to transplanted SC-islets, supporting cell health throughout the process will be essential, especially if enclosed immune-isolating macro-encapsulation devices are a chosen way forward.

Finally, identifying markers of human β maturation and mature function will enable better methods of identifying improvements in SC-islet differentiation. While function itself is a measurable readout, it is time consuming to assess and impractical to scale up for high-throughput screens. If one or more maturation markers correlate strongly with functional maturity, then phenotypic gene markers could be used as a simple endpoint for assessing the impact of interventions (growth factors, matrix, media, agonists, antagonists, etc.) designed to

increase functional maturity. Many maturation markers in the field have been identified using animal models, but have not consistently been validated to reflect normal human islet development. Using the tissues and tools available in our lab, I have screened a list of candidate maturation markers and found that many of these markers are already expressed at early fetal developmental time points in human islets, thus making them unsuitable for predicting functional maturation of SC-islets. Genes that have significant upregulation in islets postnatally compared to their expression in fetal tissue, however, may be better markers of maturation in human development and may help us to better identify environmental cues that signal for developing islets to become functionally mature.

Taken together, I present a collection of data that improve our understanding of islet biology and may translate to the development of novel methods for engineering islet-like tissues *ex vivo*, or for improving islet engraftment, survival and function following transplantation.

References

1. Tremmel, D.M., et al., *Mimicking nature-made beta cells: recent advances towards stem cell-derived islets.* Curr Opin Organ Transplant, 2019. **24**(5): p. 574-581.
2. Tremmel, D.M. and J.S. Odorico, *Rebuilding a better home for transplanted islets.* Organogenesis, 2018. **14**(4): p. 163-168.
3. Sackett, S.D., et al., *Transplantation, bioengineering, and regeneration of the endocrine pancreas*. 2020, Academic Press: London ; San Diego, CA. p. volumes.
4. *IDF Diabetes Atlas*. 2021, Brussels, Belgium: International Diabetes Federation.
5. Leslie, R.D., et al., *Diabetes at the crossroads: relevance of disease classification to pathophysiology and treatment.* Diabetologia, 2016. **59**(1): p. 13-20.
6. Nolan, C.J. and M. Prentki, *Insulin resistance and insulin hypersecretion in the metabolic syndrome and type 2 diabetes: Time for a conceptual framework shift.* Diab Vasc Dis Res, 2019. **16**(2): p. 118-127.
7. Rother, K.I. and D.M. Harlan, *Challenges facing islet transplantation for the treatment of type 1 diabetes mellitus.* J Clin Invest, 2004. **114**(7): p. 877-83.
8. Shapiro, A.M., et al., *Islet transplantation in seven patients with type 1 diabetes mellitus using a glucocorticoid-free immunosuppressive regimen.* N Engl J Med, 2000. **343**(4): p. 230-8.
9. Nair, G. and M. Hebrok, *Islet formation in mice and men: lessons for the generation of functional insulin-producing beta-cells from human pluripotent stem cells.* Curr Opin Genet Dev, 2015. **32**: p. 171-80.
10. Arrojo e Drigo, R., et al., *New insights into the architecture of the islet of Langerhans: a focused cross-species assessment.* Diabetologia, 2015. **58**(10): p. 2218-28.
11. Brissova, M., et al., *Human Islets Have Fewer Blood Vessels than Mouse Islets and the Density of Islet Vascular Structures Is Increased in Type 2 Diabetes.* J Histochem Cytochem, 2015. **63**(8): p. 637-45.
12. Rodriguez-Diaz, R., et al., *Innervation patterns of autonomic axons in the human endocrine pancreas.* Cell Metab, 2011. **14**(1): p. 45-54.
13. Otonkoski, T., et al., *Unique basement membrane structure of human pancreatic islets: implications for beta-cell growth and differentiation.* Diabetes Obes Metab, 2008. **10 Suppl 4**: p. 119-27.
14. Arda, H.E., et al., *Age-Dependent Pancreatic Gene Regulation Reveals Mechanisms Governing Human beta Cell Function.* Cell Metab, 2016. **23**(5): p. 909-20.
15. Benner, C., et al., *The transcriptional landscape of mouse beta cells compared to human beta cells reveals notable species differences in long non-coding RNA and protein-coding gene expression.* BMC Genomics, 2014. **15**: p. 620.

16. Hart, N.J. and A.C. Powers, *Use of human islets to understand islet biology and diabetes: progress, challenges and suggestions.* Diabetologia, 2019. **62**(2): p. 212-222.

17. McCarthy, R.C., M.L. Green, and F.E. Dwulet, *Evolution of Enzyme Requirements for Human Islet Isolation.* OBM Transplantation, 2018. **2**(4): p. 1-1.

18. Cross, S.E., et al., *Key Matrix Proteins Within the Pancreatic Islet Basement Membrane Are Differentially Digested During Human Islet Isolation.* Am J Transplant, 2017. **17**(2): p. 451-461.

19. Meier, R.P.H., et al., *Pancreas collagen digestion during islet of Langerhans isolation-a prospective study.* Transpl Int, 2020. **33**(11): p. 1516-1528.

20. Kayton, N.S., et al., *Human islet preparations distributed for research exhibit a variety of insulin-secretory profiles.* Am J Physiol Endocrinol Metab, 2015. **308**(7): p. E592-602.

21. Camunas-Soler, J., et al., *Patch-Seq Links Single-Cell Transcriptomes to Human Islet Dysfunction in Diabetes.* Cell Metab, 2020. **31**(5): p. 1017-1031 e4.

22. Hodson, D.J., et al., *Lipotoxicity disrupts incretin-regulated human beta cell connectivity.* J Clin Invest, 2013. **123**(10): p. 4182-94.

23. Walker, J.T., et al., *Integrated human pseudoislet system and microfluidic platform demonstrate differences in GPCR signaling in islet cells.* JCI Insight, 2020. **5**(10).

24. Cayabyab, F., L.R. Nih, and E. Yoshihara, *Advances in Pancreatic Islet Transplantation Sites for the Treatment of Diabetes.* Front Endocrinol (Lausanne), 2021. **12**: p. 732431.

25. Hogrebe, N.J., et al., *Targeting the cytoskeleton to direct pancreatic differentiation of human pluripotent stem cells.* Nat Biotechnol, 2020. **38**(4): p. 460-470.

26. Sackett, S.D., et al., *Modulation of human allogeneic and syngeneic pluripotent stem cells and immunological implications for transplantation.* Transplant Rev (Orlando), 2016. **30**(2): p. 61-70.

27. Dai, C., et al., *Islet-enriched gene expression and glucose-induced insulin secretion in human and mouse islets.* Diabetologia, 2012. **55**(3): p. 707-18.

28. Jennings, R.E., et al., *Human pancreas development.* Development, 2015. **142**(18): p. 3126-37.

29. Oliver-Krasinski, J.M. and D.A. Stoffers, *On the origin of the beta cell.* Genes Dev, 2008. **22**(15): p. 1998-2021.

30. van der Meulen, T. and M.O. Huising, *Maturation of Stem Cell-Derived Beta-cells Guided by the Expression of Urocortin 3.* The Review of Diabetic Studies : RDS, 2014. **11**(1): p. 115-132.

31. Zorn, A.M. and J.M. Wells, *Vertebrate endoderm development and organ formation.* Annu Rev Cell Dev Biol, 2009. **25**: p. 221-51.

32. Gu, G., J. Dubauskaite, and D.A. Melton, *Direct evidence for the pancreatic lineage: NGN3+ cells are islet progenitors and are distinct from duct progenitors.* Development, 2002. **129**(10): p. 2447-57.

33. Sander, M., et al., *Homeobox gene Nkx6.1 lies downstream of Nkx2.2 in the major pathway of beta-cell formation in the pancreas.* Development, 2000. **127**(24): p. 5533-40.

34. Jennings, R.E., et al., *Development of the human pancreas from foregut to endocrine commitment.* Diabetes, 2013. **62**(10): p. 3514-22.

35. Otonkoski, T., et al., *Maturation of insulin response to glucose during human fetal and neonatal development. Studies with perifusion of pancreatic isletlike cell clusters.* Diabetes, 1988. **37**(3): p. 286-91.

36. Blum, B., et al., *Functional beta-cell maturation is marked by an increased glucose threshold and by expression of urocortin 3.* Nat Biotechnol, 2012. **30**(3): p. 261-4.

37. van der Meulen, T. and M.O. Huising, *Maturation of stem cell-derived beta-cells guided by the expression of urocortin 3.* Rev Diabet Stud, 2014. **11**(1): p. 115-32.

38. D'Amour, K.A., et al., *Production of pancreatic hormone-expressing endocrine cells from human embryonic stem cells.* Nat Biotechnol, 2006. **24**(11): p. 1392-401.

39. Pagliuca, F.W., et al., *Generation of functional human pancreatic beta cells in vitro.* Cell, 2014. **159**(2): p. 428-39.

40. Rezania, A., et al., *Reversal of diabetes with insulin-producing cells derived in vitro from human pluripotent stem cells.* Nat Biotechnol, 2014. **32**(11): p. 1121-33.

41. Rezania, A., et al., *Enrichment of human embryonic stem cell-derived NKX6.1-expressing pancreatic progenitor cells accelerates the maturation of insulin-secreting cells in vivo.* Stem Cells, 2013. **31**(11): p. 2432-42.

42. Nostro, M.C., et al., *Efficient generation of NKX6-1+ pancreatic progenitors from multiple human pluripotent stem cell lines.* Stem Cell Reports, 2015. **4**(4): p. 591-604.

43. Russ, H.A., et al., *Controlled induction of human pancreatic progenitors produces functional beta-like cells in vitro.* EMBO J, 2015. **34**(13): p. 1759-72.

44. Ghazizadeh, Z., et al., *ROCKII inhibition promotes the maturation of human pancreatic beta-like cells.* Nature Communications, 2017. **8**.

45. Nair, G.G., et al., *Recapitulating endocrine cell clustering in culture promotes maturation of human stem-cell-derived beta cells.* Nat Cell Biol, 2019. **21**(2): p. 263-274.

46. Velazco-Cruz, L., et al., *Acquisition of Dynamic Function in Human Stem Cell-Derived beta Cells.* Stem Cell Reports, 2019. **12**(2): p. 351-365.

47. van der Meulen, T., et al., *Urocortin 3 marks mature human primary and embryonic stem cell-derived pancreatic alpha and beta cells.* PLoS One, 2012. **7**(12): p. e52181.

48. Micallef, S.J., et al., *INS(GFP/w) human embryonic stem cells facilitate isolation of in vitro derived insulin-producing cells.* Diabetologia, 2012. **55**(3): p. 694-706.

49. Millman, J.R., et al., *Generation of stem cell-derived beta-cells from patients with type 1 diabetes.* Nat Commun, 2016. **7**: p. 11463.

50. Barsby, T. and T. Otonkoski, *Maturation of beta cells: lessons from in vivo and in vitro models.* Diabetologia, 2022.

51. Daly, M.E., et al., *Acute effects on insulin sensitivity and diurnal metabolic profiles of a high-sucrose compared with a high-starch diet.* Am J Clin Nutr, 1998. **67**(6): p. 1186-96.

52. *Standards of Medical Care in Diabetes–2006.* Diabetes Care, 2006. **29**(suppl 1): p. s4-s42.

53. Thomson, J.A., et al., *Embryonic stem cell lines derived from human blastocysts.* Science, 1998. **282**(5391): p. 1145-7.

54. Wu, J. and J.C. Izpisua Belmonte, *Dynamic Pluripotent Stem Cell States and Their Applications.* Cell Stem Cell, 2015. **17**(5): p. 509-25.

55. Gornalusse, G.G., et al., *HLA-E-expressing pluripotent stem cells escape allogeneic responses and lysis by NK cells.* Nat Biotechnol, 2017. **35**(8): p. 765-772.

56. Riolobos, L., et al., *HLA engineering of human pluripotent stem cells.* Mol Ther, 2013. **21**(6): p. 1232-41.

57. Lu, P., et al., *Generating hypoimmunogenic human embryonic stem cells by the disruption of beta 2-microglobulin.* Stem Cell Rev, 2013. **9**(6): p. 806-13.

58. Wang, D., et al., *Targeted Disruption of the beta2-Microglobulin Gene Minimizes the Immunogenicity of Human Embryonic Stem Cells.* Stem Cells Transl Med, 2015. **4**(10): p. 1234-45.

59. Feng, Q., et al., *Scalable generation of universal platelets from human induced pluripotent stem cells.* Stem Cell Reports, 2014. **3**(5): p. 817-31.

60. Mandal, P.K., et al., *Efficient ablation of genes in human hematopoietic stem and effector cells using CRISPR/Cas9.* Cell Stem Cell, 2014. **15**(5): p. 643-52.

61. Lanier, L.L., B. Corliss, and J.H. Phillips, *Arousal and inhibition of human NK cells.* Immunol Rev, 1997. **155**: p. 145-54.

62. Liao, N.S., et al., *MHC class I deficiency: susceptibility to natural killer (NK) cells and impaired NK activity.* Science, 1991. **253**(5016): p. 199-202.

63. Rong, Z., et al., *An effective approach to prevent immune rejection of human ESC-derived allografts.* Cell Stem Cell, 2014. **14**(1): p. 121-30.

64. Di Stasi, A., et al., *Inducible apoptosis as a safety switch for adoptive cell therapy.* N Engl J Med, 2011. **365**(18): p. 1673-83.

65. Yagyu, S., et al., *An Inducible Caspase-9 Suicide Gene to Improve the Safety of Therapy Using Human Induced Pluripotent Stem Cells.* Mol Ther, 2015. **23**(9): p. 1475-85.

66. Gamble, A., et al., *The journey of islet cell transplantation and future development.* Islets, 2018. **10**(2): p. 80-94.

67. Shapiro, A.M.J., et al., *Insulin expression and C-peptide in type 1 diabetes subjects implanted with stem cell-derived pancreatic endoderm cells in an encapsulation device.* Cell Rep Med, 2021. **2**(12): p. 100466.

68. Frantz, C., K.M. Stewart, and V.M. Weaver, *The extracellular matrix at a glance.* J Cell Sci, 2010. **123**(Pt 24): p. 4195-200.

69. Wang, R.N. and L. Rosenberg, *Maintenance of beta-cell function and survival following islet isolation requires re-establishment of the islet-matrix relationship.* J Endocrinol, 1999. **163**(2): p. 181-90.

70. Stendahl, J.C., D.B. Kaufman, and S.I. Stupp, *Extracellular matrix in pancreatic islets: relevance to scaffold design and transplantation.* Cell Transplant, 2009. **18**(1): p. 1-12.

71. Daoud, J., et al., *The effect of extracellular matrix components on the preservation of human islet function in vitro.* Biomaterials, 2010. **31**(7): p. 1676-82.

72. Daoud, J.T., et al., *Long-term in vitro human pancreatic islet culture using three-dimensional microfabricated scaffolds.* Biomaterials, 2011. **32**(6): p. 1536-42.

73. Kaido, T., et al., *Impact of defined matrix interactions on insulin production by cultured human beta-cells: effect on insulin content, secretion, and gene transcription.* Diabetes, 2006. **55**(10): p. 2723-9.

74. Thomas, F.T., et al., *Anoikis, extracellular matrix, and apoptosis factors in isolated cell transplantation.* Surgery, 1999. **126**(2): p. 299-304.

75. Thomas, F., et al., *A tripartite anoikis-like mechanism causes early isolated islet apoptosis.* Surgery, 2001. **130**(2): p. 333-8.

76. Weber, L.M. and K.S. Anseth, *Hydrogel encapsulation environments functionalized with extracellular matrix interactions increase islet insulin secretion.* Matrix Biol, 2008. **27**(8): p. 667-73.

77. Zhao, Y., et al., *Preservation of islet survival by upregulating alpha3 integrin signaling: the importance of 3-dimensional islet culture in basement membrane extract.* Transplant Proc, 2010. **42**(10): p. 4638-42.

78. Pinkse, G.G., et al., *Integrin signaling via RGD peptides and anti-beta1 antibodies confers resistance to apoptosis in islets of Langerhans.* Diabetes, 2006. **55**(2): p. 312-7.

79. Wang, R.N., S. Paraskevas, and L. Rosenberg, *Characterization of integrin expression in islets isolated from hamster, canine, porcine, and human pancreas.* J Histochem Cytochem, 1999. **47**(4): p. 499-506.

80. Hughes, S.J., et al., *Characterisation of collagen VI within the islet-exocrine interface of the human pancreas: implications for clinical islet isolation?* Transplantation, 2006. **81**(3): p. 423-6.

81. Wood, G.C., *The formation of fibrils from collagen solutions. 2. A mechanism of collagen-fibril formation.* Biochem J, 1960. **75**: p. 598-605.

82. Crapo, P.M., T.W. Gilbert, and S.F. Badylak, *An overview of tissue and whole organ decellularization processes.* Biomaterials, 2011. **32**(12): p. 3233-43.

83. Gilbert, T.W., T.L. Sellaro, and S.F. Badylak, *Decellularization of tissues and organs.* Biomaterials, 2006. **27**(19): p. 3675-83.

84. Tapias, L.F. and H.C. Ott, *Decellularized scaffolds as a platform for bioengineered organs.* Curr Opin Organ Transplant, 2014. **19**(2): p. 145-52.

85. Elebring, E., et al., *Cold-perfusion decellularization of whole-organ porcine pancreas supports human fetal pancreatic cell attachment and expression of endocrine and exocrine markers.* J Tissue Eng, 2017. **8**: p. 2041731417738145.

86. Katsuki, Y., et al., *Endocrine pancreas engineered using porcine islets and partial pancreatic scaffolds.* Pancreatology, 2016. **16**(5): p. 922-30.

87. Napierala, H., et al., *Engineering an endocrine Neo-Pancreas by repopulation of a decellularized rat pancreas with islets of Langerhans.* Sci Rep, 2017. **7**: p. 41777.

88. Uygun, B.E., et al., *Organ reengineering through development of a transplantable recellularized liver graft using decellularized liver matrix.* Nat Med, 2010. **16**(7): p. 814-20.

89. Wan, J., et al., *Culture of iPSCs Derived Pancreatic beta-Like Cells In Vitro Using Decellularized Pancreatic Scaffolds: A Preliminary Trial.* Biomed Res Int, 2017. **2017**: p. 4276928.

90. Batchelder, C.A., M.L. Martinez, and A.F. Tarantal, *Natural Scaffolds for Renal Differentiation of Human Embryonic Stem Cells for Kidney Tissue Engineering.* PLoS One, 2015. **10**(12): p. e0143849.

91. Freytes, D.O., et al., *Preparation and rheological characterization of a gel form of the porcine urinary bladder matrix.* Biomaterials, 2008. **29**(11): p. 1630-7.

92. Soffer-Tsur, N., D. Peer, and T. Dvir, *ECM-based macroporous sponges release essential factors to support the growth of hematopoietic cells.* J Control Release, 2017. **257**: p. 84-90.

93. Chaimov, D., et al., *Innovative encapsulation platform based on pancreatic extracellular matrix achieve substantial insulin delivery.* J Control Release, 2017. **257**: p. 91-101.

94. De Carlo, E., et al., *Pancreatic acellular matrix supports islet survival and function in a synthetic tubular device: in vitro and in vivo studies.* Int J Mol Med, 2010. **25**(2): p. 195-202.

95. Goh, S.K., et al., *Perfusion-decellularized pancreas as a natural 3D scaffold for pancreatic tissue and whole organ engineering.* Biomaterials, 2013. **34**(28): p. 6760-72.

96. Mirmalek-Sani, S.H., et al., *Porcine pancreas extracellular matrix as a platform for endocrine pancreas bioengineering.* Biomaterials, 2013. **34**(22): p. 5488-95.

97. Peloso, A., et al., *The Human Pancreas as a Source of Protolerogenic Extracellular Matrix Scaffold for a New-generation Bioartificial Endocrine Pancreas.* Ann Surg, 2016. **264**(1): p. 169-79.

98. Wu, D., et al., *3D Culture of MIN-6 Cells on Decellularized Pancreatic Scaffold: In Vitro and In Vivo Study.* Biomed Res Int, 2015. **2015**: p. 432645.

99. Sackett, S.D., et al., *Extracellular matrix scaffold and hydrogel derived from decellularized and delipidized human pancreas.* Sci Rep, 2018. **8**(1): p. 10452.

100. Gaetani, R., et al., *Evaluation of Different Decellularization Protocols on the Generation of Pancreas-Derived Hydrogels.* Tissue Eng Part C Methods, 2018. **24**(12): p. 697-708.

101. Tamburrini, R., et al., *Detergent-Free Decellularization of the Human Pancreas for Soluble Extracellular Matrix (ECM) Production.* J Vis Exp, 2020(163).

102. Narayanan, K., et al., *Extracellular matrix-mediated differentiation of human embryonic stem cells: differentiation to insulin-secreting beta cells.* Tissue Eng Part A, 2014. **20**(1-2): p. 424-33.

103. Hoshiba, T., et al., *Decellularized Extracellular Matrix as an In Vitro Model to Study the Comprehensive Roles of the ECM in Stem Cell Differentiation.* Stem Cells Int, 2016. **2016**: p. 6397820.

104. Pepper, A.R., et al., *Revascularization of transplanted pancreatic islets and role of the transplantation site.* Clin Dev Immunol, 2013. **2013**: p. 352315.

105. Yu, M., et al., *Islet transplantation in the subcutaneous space achieves long-term euglycaemia in preclinical models of type 1 diabetes.* Nat Metab, 2020. **2**(10): p. 1013-1020.

106. Barshes, N.R., et al., *Transaminitis after pancreatic islet transplantation.* J Am Coll Surg, 2005. **200**(3): p. 353-61.

107. Korsgren, O., et al., *Optimising islet engraftment is critical for successful clinical islet transplantation.* Diabetologia, 2008. **51**(2): p. 227-32.

108. Barton, F.B., et al., *Improvement in outcomes of clinical islet transplantation: 1999-2010.* Diabetes Care, 2012. **35**(7): p. 1436-45.

109. Desai, T. and L.D. Shea, *Advances in islet encapsulation technologies.* Nat Rev Drug Discov, 2017. **16**(5): p. 338-350.

110. Kieffer, T.J., *Closing in on Mass Production of Mature Human Beta Cells.* Cell Stem Cell, 2016. **18**(6): p. 699-702.

111. Espes, D., et al., *Rapid Restoration of Vascularity and Oxygenation in Mouse and Human Islets Transplanted to Omentum May Contribute to Their Superior Function Compared to Intraportally Transplanted Islets.* Am J Transplant, 2016. **16**(11): p. 3246-3254.

112. Komatsu, H., et al., *Posttransplant oxygen inhalation improves the outcome of subcutaneous islet transplantation: A promising clinical alternative to the conventional intrahepatic site.* Am J Transplant, 2017: p. Apr;18(4): 832-842.

113. Luan, N.M. and H. Iwata, *Long-term allogeneic islet graft survival in prevascularized subcutaneous sites without immunosuppressive treatment.* Am J Transplant, 2014. **14**(7): p. 1533-42.

114. Pepper, A.R., et al., *A prevascularized subcutaneous device-less site for islet and cellular transplantation.* Nat Biotechnol, 2015. **33**(5): p. 518-23.

115. Vlahos, A.E., N. Cober, and M.V. Sefton, *Modular tissue engineering for the vascularization of subcutaneously transplanted pancreatic islets.* Proc Natl Acad Sci U S A, 2017. **114**(35): p. 9337-9342.

116. Song, S. and S. Roy, *Progress and challenges in macroencapsulation approaches for type 1 diabetes (T1D) treatment: Cells, biomaterials, and devices.* Biotechnol Bioeng, 2016. **113**(7): p. 1381-402.

117. Bowers, D.T., et al., *Engineering the vasculature for islet transplantation.* Acta Biomater, 2019. **95**: p. 131-151.

118. Citro, A., et al., *Biofabrication of a vascularized islet organ for type 1 diabetes.* Biomaterials, 2019. **199**: p. 40-51.

119. Kaufman-Francis, K., et al., *Engineered vascular beds provide key signals to pancreatic hormone-producing cells.* PLoS One, 2012. **7**(7): p. e40741.

120. Takahashi, Y., et al., *Self-Condensation Culture Enables Vascularization of Tissue Fragments for Efficient Therapeutic Transplantation.* Cell Rep, 2018. **23**(6): p. 1620-1629.

121. Aghazadeh, Y., et al., *Microvessels support engraftment and functionality of human islets and hESC-derived pancreatic progenitors in diabetes models.* Cell Stem Cell, 2021. **28**(11): p. 1936-1949 e8.

122. Uzunalli, G., et al., *Improving pancreatic islet in vitro functionality and transplantation efficiency by using heparin mimetic peptide nanofiber gels.* Acta Biomater, 2015. **22**: p. 8-18.

123. Weaver, J.D., et al., *Vasculogenic hydrogel enhances islet survival, engraftment, and function in leading extrahepatic sites.* Sci Adv, 2017. **3**(6): p. e1700184.

124. Hogan, M.F. and R.L. Hull, *The islet endothelial cell: a novel contributor to beta cell secretory dysfunction in diabetes.* Diabetologia, 2017. **60**(6): p. 952-959.

125. Yamada, K.M. and K. Clark, *Cell biology: survival in three dimensions.* Nature, 2002. **419**(6909): p. 790-1.

126. Kirkpatrick, C.J., S. Fuchs, and R.E. Unger, *Co-culture systems for vascularization--learning from nature.* Adv Drug Deliv Rev, 2011. **63**(4-5): p. 291-9.

127. Bakhti, M., A. Bottcher, and H. Lickert, *Modelling the endocrine pancreas in health and disease.* Nat Rev Endocrinol, 2019. **15**(3): p. 155-171.

128. Augsornworawat, P., et al., *A hydrogel platform for in vitro three dimensional assembly of human stem cell-derived islet cells and endothelial cells.* Acta Biomater, 2019. **97**: p. 272-280.

129. Talavera-Adame, D., et al., *Effective endothelial cell and human pluripotent stem cell interactions generate functional insulin-producing beta cells.* Diabetologia, 2016. **59**(11): p. 2378-2386.

Chapter 2

Proteome-wide and matrisome-specific alterations during human pancreas development and maturation.

This chapter was adapted from the paper published as: Li Z* and Tremmel DM*, Ma F, Yu Q, Ma M, Delafield DG, Shi Y, Wang B, Mitchell SM, Feeney AK, Jain VS, Sackett SD, Odorico JS, Li L. Proteome-wide and matrisome-specific alterations during human pancreas development and maturation. Nat Commun. 2021;Feb15;12(1):1020. doi: 10.1038/s41467-021-21261-w. (*Co-first authors) PMID: 33589611

Daniel Tremmel, Zihui Li, Sara Dutton Sackett, Jon Odorico and Lingjun Li designed this study. Daniel Tremmel and Zihui Li performed the experiments and analyzed the data. Daniel Tremmel, Sam Mitchell and Austin Feeney processed and banked human tissues. Fengfei Ma, Yatao Shi, amd Bin Wang were involved in sample preparation and data acquisition. Qinying Yu and Min Ma were involved in data analysis and interpretation. Daniel Delafield helped design the website for database searching. Daniel Tremmel and Vansh Jain performed immunofluorescent staining and quantification. Daniel Tremmel and Zihui wrote the paper under the guidance of Sara Dutton Sackett, Jon Odorico and Lingjun Li. Figure 1 was prepared by Zihui Li and Dniel tremmel, figures 2-3 were prepared by Zihui Li, and Figures 4-5 were prepared by Daniel Tremmel.

Abstract

The extracellular matrix (ECM) is unique to each tissue and capable of guiding cell differentiation, migration, morphology, and function. The ECM proteome of different developmental stages has not been systematically studied in the human pancreas. In this study, we apply mass spectrometry-based quantitative proteomics strategies using N,N-dimethyl leucine isobaric tags to delineate proteome-wide and ECM-specific alterations in four age groups: fetal (18-20 weeks gestation), juvenile (5-16 years old), young adults (21-29 years old) and older adults (50-61 years old). We identify 3,523 proteins, including 185 ECM proteins, and quantify 117 of them. We detect previously unknown proteome and matrisome features during pancreas development and maturation. We also visualize specific ECM proteins of interest using immunofluorescent staining and investigate changes in ECM localization within islet or acinar compartments. This comprehensive proteomics analysis contributes to an improved understanding of the critical roles that ECM plays throughout human pancreas development and maturation.

Introduction

The extracellular matrix (ECM) is the network of proteins and polysaccharides surrounding cells, forming a niche in which cells reside and function. Every tissue has a unique composition and arrangement of ECM components, and ECM is known to be significantly remodeled throughout development, with aging, and during various disease states [1-3]. During development, the ECM changes in both composition and organization, guiding cell migration and influencing cell fate [1]. In cell physiology, ECM plays a multitude of roles, from providing structural and mechanical support, to modifying growth factor diffusion and binding and

providing anchorage-dependent cell survival signals [4, 5]. Modern approaches in regenerative medicine and tissue engineering aim to utilize or recapitulate ECM scaffolding and signaling [6, 7], but only recently have studies been able to extensively define the matrisome of human tissues [8], and studies of ECM composition throughout human development are even more limited. Understanding the complexity of ECM in normal tissue, throughout distinct developmental time points, can provide important context for understanding healthy physiology, identifying and characterizing disease states, improving cell and tissue isolation methods, and recapitulating physiological tissues or development *in vitro*.

The pancreas is a glandular organ which functions in both digestive and endocrine systems. The exocrine cells in the acini secrete digestive enzymes into a ductal system eventually emptying into the duodenum. The islets of Langerhans are clusters of five endocrine cell types in close contact with capillary networks, which secrete hormones into the blood. Pancreatic ECM has been studied in many non-human species and across developmental time frames, and has been found to have significant compositional and structural differences among species and from fetal to adult tissues [9]. The ECM of the pancreas is also known to be heavily altered in states of fibrotic pancreatitis and with the progression of pancreatic cancers [10-12]. Islets are surrounded by a capsule consisting of fibroblasts and ECM [13, 14]; along the vasculature that penetrates the islets, there is a double basement membrane between endocrine cells and islet capillaries, which is unique to human islets [15]. Furthermore, islet and capillary ECM is altered in the progression of both Type 1 and Type 2 diabetes [16-19], and found to play important roles in the survival and function of insulin-secreting beta cells [9, 18, 20]. The role of the ECM in the pancreas, and specifically within islets, is of key interest in the fields of diabetes and beta cell replacement.

To better understand the usefulness of ECM for regenerative medicine and tissue engineering applications, it is essential to have a more complete and comprehensive understanding of the ECM within normal, native tissue. Previous data about the pancreatic matrisome is abundant, but often incomplete and inconsistent. Ample data has been derived from various animal species, but variation among species is well documented [14, 21] and even the architecture of the islets themselves differs dramatically between rodents and primates [15, 22-27]. Until recently, most data on human pancreas and islet ECM has been obtained through immunohistological staining, and thus has not comprehensively identified the compositional profile of ECM proteins. As mass spectrometry (MS) becomes an essential tool for detecting biomolecules, MS-based proteomics shows great potential for the sensitive and large-scale analysis of complex biological systems. Characterization of ECM proteins using MS, however, still faces challenges due to their unique biophysical and biochemical properties. The large dynamic range of the analytes renders it relatively intractable to in-depth analysis, and heavy crosslinking between ECM and other components results in low solubility and therefore decreased identification rates [28]. To overcome these difficulties, various orthogonal separation techniques were utilized prior to liquid chromatography (LC)-MS/MS to decrease sample complexity, including off-gel electrophoresis [29], basic reversed-phase liquid chromatography [30] and strong cation exchange (SCX) [31]. Different protein extraction, ECM enrichment and digestion methods have also been explored to improve ECM coverage [32-38]. As most of these approaches require extensive sample extraction or fractionation, the higher cost of additional sample handling and lengthy LC-MS/MS runs should be considered and balanced against improved proteome coverage [39].

To compare the relative abundance of ECM proteins from different samples, label-free quantification (LFQ), which is based on measuring precursor ion intensities or spectral counting, has been broadly used in related studies [8, 40]. Though easy to perform, LFQ methods demand longer instrument time and the quantification is less accurate due to run-to-run variation [41]. Label-based approaches, on the other hand, allow for accurate and multiplexing quantitative analysis. Among these labeling methods, commercially available isobaric tags such as tandem mass tag (TMT) [11, 42] or isobaric tags for relative and absolute quantitation (iTRAQ) [43-45] have been more widely used recently. Nevertheless, the utility of these commercial isobaric tags in large-scale, discovery proteomics studies is often hampered by the limited multiplexing capacity and the high price of the reagent kits. To address these limitations, we have developed a cost-effective alternative, based on a set of N,N-dimethyl leucine (DiLeu) isobaric tags that can be synthesized in-house at high yield, with three steps using commercially available reagents, at a fraction of the cost. DiLeu isobaric tags were initially demonstrated as a 4-plex set [46], and then expanded to an 8-plex set [47]. The multiplexing capacity was then increased three-fold from 4-plex to 12-plex by taking advantage of the mass-defect feature of stable isotopes to enable simultaneous quantification of 12 samples via 12 reporter ions spanning from 115-118 m/z [48].

Utilizing the aforementioned methods, a few studies have investigated ECM proteins in isolated mouse islets [45], decellularized rat pancreatic tissue [49], and human pancreas with pancreatic ductal adenocarcinoma and pancreatitis [11]. Additionally, we recently reported a MS-proteomic ECM analysis comparing human fetal and adult pancreas using a sample preparation protocol known as the surfactant and chaotropic agent assisted sequential extraction/on pellet

digestion (SCAD) [31, 50]. However, an in-depth quantitative study of pancreatic ECM throughout human development and maturation has not yet been reported. Herein, we present a relatively simple and effective workflow for quantitative ECM analysis with our custom developed 12-plex DiLeu isobaric tags and apply this pipeline to investigating matrisome alterations at various developmental stages of human pancreatic tissue. These results add to the knowledge base in understanding the significant alterations that occur in the ECM and associated extracellular molecules throughout the human life cycle. They also provide valuable information for future regenerative medicine strategies for beta cell replacement.

Results

In-depth proteome-wide and ECM quantification using 12-plex DiLeu isobaric tagging.

We performed quantitative analysis on normal, non-diabetic, non-pancreatitis human pancreatic tissue from four developmental stages including fetal (18-20 weeks gestation), juvenile (5-16 years), young adults (21-29 years) and older adults (50-61 years) (Fig. 1) (Donor Information available in Supplemental Data 1). The SCAD method, which takes advantage of the solubilizing power of both surfactant (SDS) and chaotropic (urea) reagents, together with on-pellet digestion, renders a more comprehensive protein extraction and improves digestion efficiency and recovery of relatively insoluble pellets [31]. We used two sets of 12-plex DiLeu tags to label these samples while a shared sample was involved in each set to allow for better normalization and quantitation. We also replaced the previously utilized SCX [31] with off-line high pH (HpH) fractionation prior to LC-MS/MS which reduced sample complexity, not only improving proteome coverage, but also strengthening detection of low-abundance proteins [51]. In total, we identified 3,523 proteins with high confidence and quantified 2,064 that were present

across all samples (Supplemental Data 2, 3). Among them, 185 proteins were categorized as ECM proteins based on Human Matrisome Database [29, 52, 53] and 117 were quantifiable (Supplemental Data 4, 5), which makes it one of the largest datasets of human pancreas matrisome. The identified proteins show a large dynamic range spanning over six orders of magnitude (Supplemental Fig. 1) that demonstrates the ability of our method to detect low-abundance molecules.

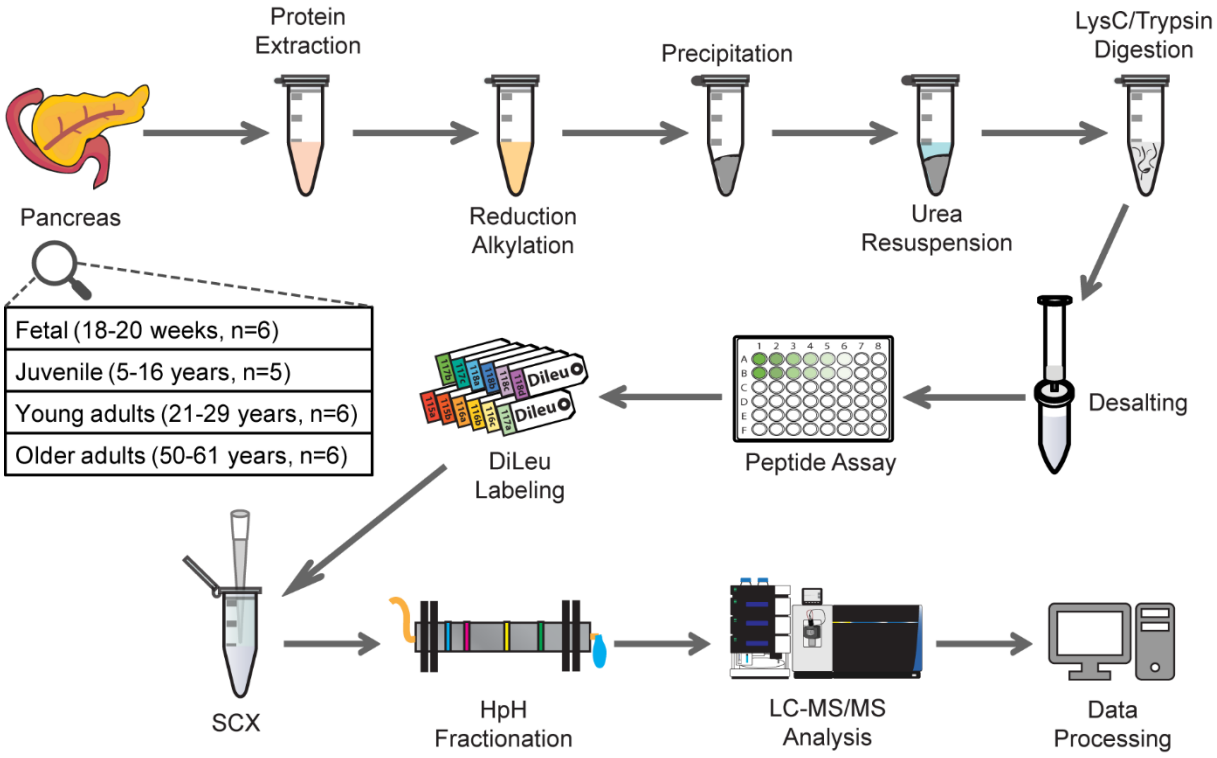

Figure 1. Experimental workflow of quantitative analysis using 12-plex DiLeu isobaric labeling strategy. Pancreas from four age groups were subjected to protein extraction with SDS buffer, precipitation, and digestion according to a slightly modified SCAD method. 12-plex DiLeu isobaric labeling was used to achieve quantitative proteomics analysis. Sample clean-up and fractionation steps were performed prior to LC-MS/MS analysis and data processing was done with commercially available software packages. SCX, strong cation exchange; HpH, high pH.

Proteome-wide alterations at different developmental stages of human pancreas.

We performed hierarchical clustering of all quantified proteins to explore their profiles at different stages (Fig. 2a). This heatmap illustrates column-wise clustering of biological replicates in either the fetal or juvenile group, suggesting larger intergroup differences than intragroup variations. Samples from young adults and older adults, on the other hand, are mixed and

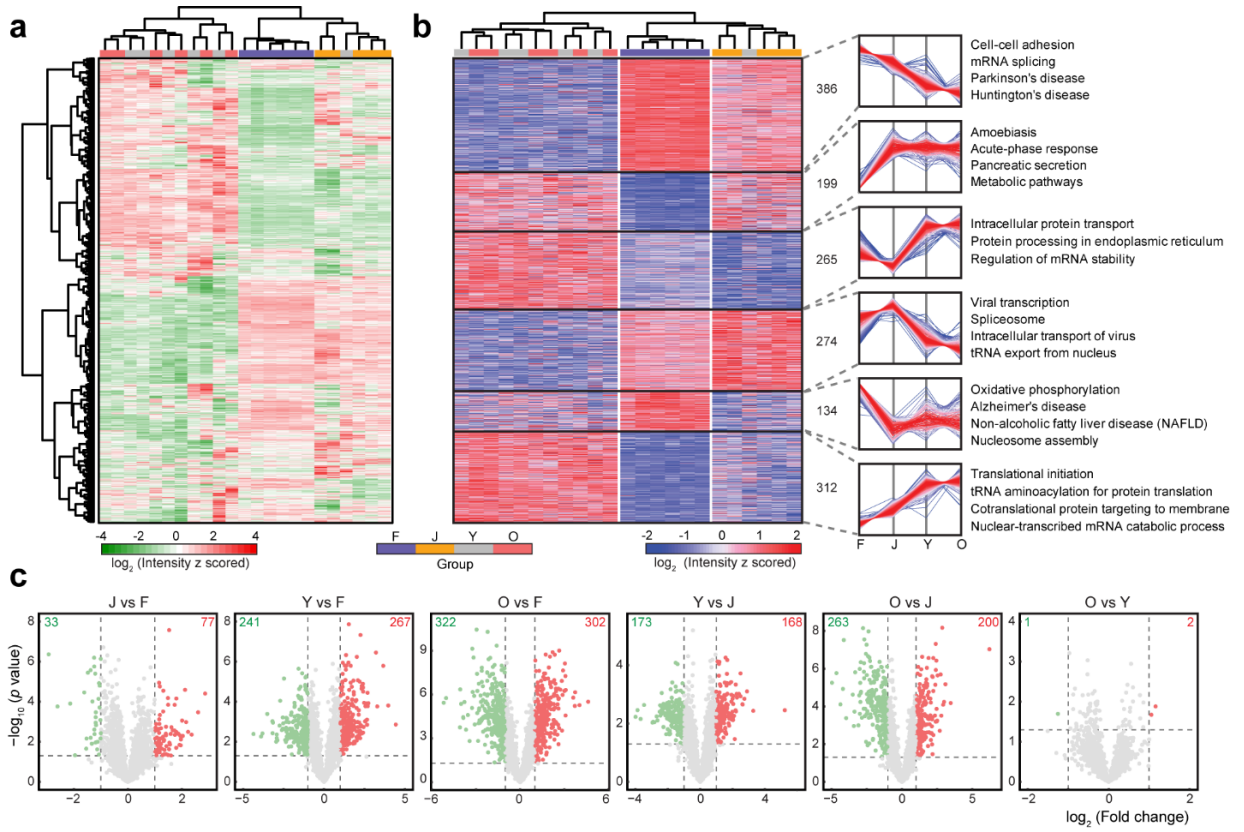

Figure 2. Protein profiles in pancreatic tissue and alterations across multiple developmental stages. **a)** Hierarchical clustering of DiLeu reporter ion intensities of 2064 quantified proteins. **b)** Hierarchical clustering of DiLeu reporter ion intensities of 1570 significantly changed proteins (one-way ANOVA, FDR 0.05). Six clusters of these proteins are depicted based on different intensity profiles across four developmental stages. Color of each line in clusters is based on its distance from the center, red (close) to blue (far). Number of proteins and selected enriched biological processes and pathways are indicated for each cluster. **c)** Volcano plots showing pairwise comparisons of protein expression levels between various stages. Points above horizontal dash lines represent significantly altered proteins (two-sided *t* test, *p* value < 0.05, *p* values were adjusted by Benjamini-Hochberg correction for multiple comparisons). Significantly down-regulated proteins (e.g., lower abundance in J in the first plot) are shown in green (protein fold change < 0.5) and up-regulated ones are shown in red (protein fold change > 2). F, fetal; J, juvenile; Y, young adult; O, older adult.

grouped together, which suggests that the biological environment becomes relatively stable in adulthood. Our workflow shows the capability of accurate protein quantification and our samples are representative of a range of age groups to produce conclusive results. To examine the reproducibility of samples within each group more carefully, we performed pair-wise Pearson correlation analysis and the results were summarized as a heatmap (Supplemental Fig. 2a). Intragroup samples exhibit good correlation with one another, with an average coefficient over 0.9 while shallow-color regions show that samples from different groups are more distinct. We did not observe obvious gender disparities according to dendrograms generated from hierarchical clustering, but a confirmatory conclusion might need verification with larger sample cohorts (Supplemental Fig. 2b). We then conducted one-way ANOVA analysis to compare protein abundance across multiple stages and found 1,570 proteins were significantly changed (FDR 0.05) (Supplemental Data 3). The profiles of these proteins are depicted by hierarchical clustering (Fig. 2b). Six clusters can be further generated based on their changing patterns across the four developmental stages and selected biological processes and pathways are annotated for each cluster. For better pair-wise comparison between groups, we performed Student's t test of all combinations and graphically displayed the results using volcano plots (Fig. 2c). Colored dots refer to significantly changed proteins (p value < 0.05) identified with a fold change greater than two. We examined more closely two pairs of samples: juvenile versus fetal, which reflects postnatal maturation, and young adults versus juvenile, which reflects post-pubertal maturation of the pancreas. Gene set variation analysis (GSVA)[54, 55] was performed to reveal expression changes of functionally related genes or gene sets. Heat maps show the significantly changed cellular components and molecular functions while the color coding indicates normalized

enrichment scores in each sample (Supplemental Fig. 3). Specifically, we found some terms related to the exocrine function of pancreas, such as lipase and exopeptidase activity, were highly expressed in older age groups, which is a clear sign of organ maturation. A full list of enriched cellular components, molecular functions, biological processes, and transcription factor targets in GSVA is also provided (Supplemental Data 6). Biological processes enriched from significantly changed proteins also indicate highly distinct molecular features between each pair (Supplemental Fig. 4a, 4c). Each node refers to an enriched term and different terms are grouped into clusters based on their similarities while the most statistically significant term represents the cluster name [56]. We also generated a chord diagram [57] for each pair to further discern how proteins change within a few processes related to pancreas functions including response to glucose, response to peptide and regulated exocytosis (Supplemental Fig. 4b, 4d). Results indicate the complexity in the regulation of these biological processes with slightly more up-regulated proteins involved. We also found that many previously reported pancreatic cancer biomarkers showed different expression levels at various developmental stages (Supplemental Fig. 5). These findings, along with other interesting correlations not presented, warrant further investigation.

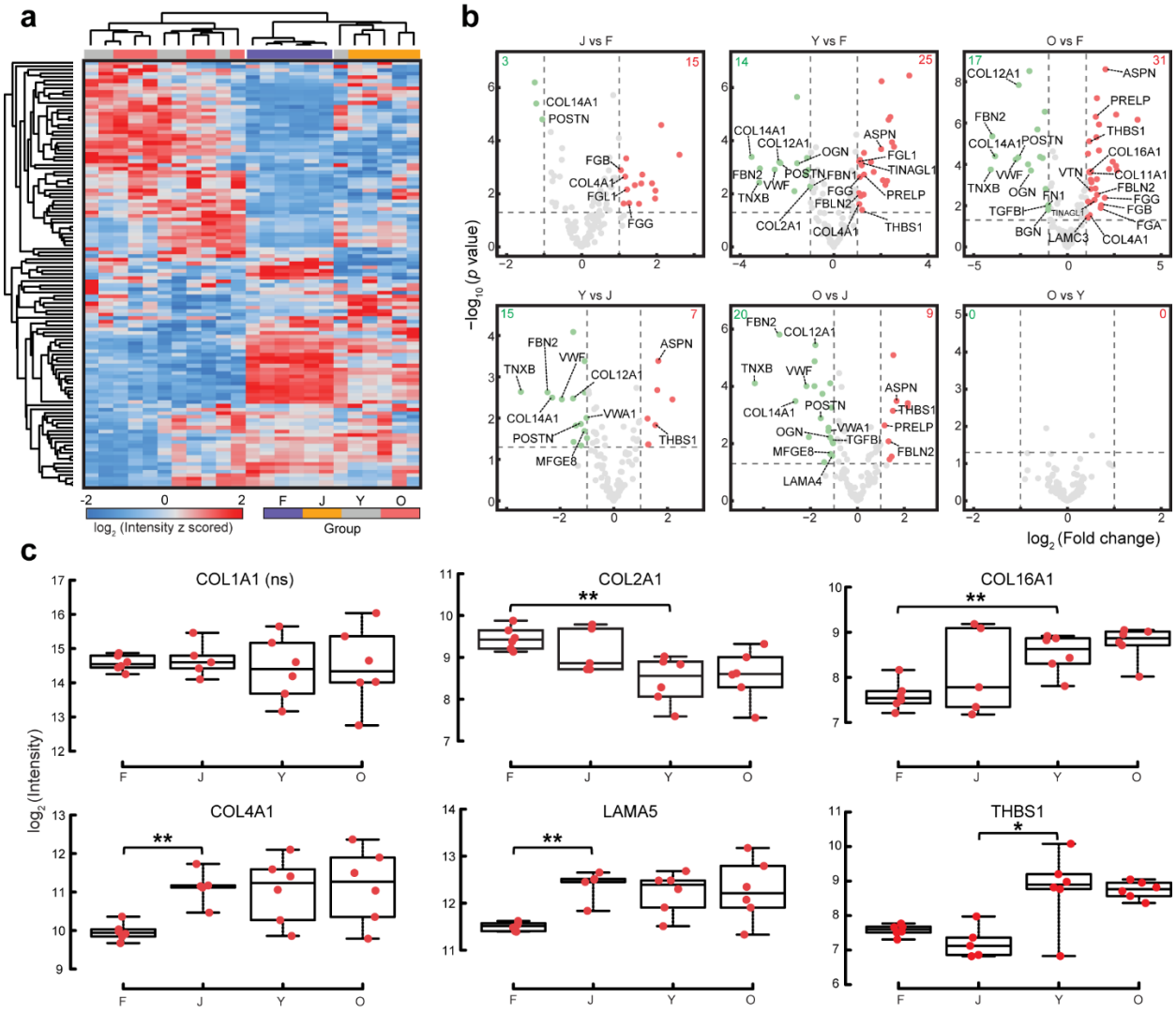

Figure 3. ECM remodeling during fetal and postnatal stages of human pancreas development. a) Hierarchical clustering of DiLeu reporter ion intensities of 117 quantified ECM proteins. **b)** Volcano plots showing pairwise comparisons of ECM protein expression levels between various stages. Points above horizontal dash lines represent significantly altered proteins (two-sided *t* test, *p* value < 0.05, *p* values were adjusted by Benjamini-Hochberg correction for multiple comparisons). Significantly down-regulated proteins are shown in green (protein fold change < 0.5) and up-regulated ones are shown in red (protein fold change > 2). Core matrisome proteins are annotated in each figure. **c)** Box plots showing expression levels of selected proteins at different developmental stages. Red dots indicate replicate data points. All boxplots indicate median (center line), 25th and 75th percentiles (bounds of box), and minimum and maximum (whiskers). Significance level is marked with an asterisk (two-sided *t* test, *p* values were adjusted by Benjamini-Hochberg correction for multiple comparisons, **p* value < 0.05, ***p* value < 0.01; ns, not significant).

ECM remodeling of the human pancreas throughout life.

Hierarchical clustering of all quantified ECM proteins suggested matrisome features unique to different age groups including fetal, juvenile, and adult (Fig. 3a, previous page). Pairwise comparisons showed significant ECM compositional changes throughout the fetal, juvenile, and adult stages, although between young and older adults very few significant differences in ECM were found (Fig. 3b). ANOVA analysis revealed that 84 ECM proteins were significantly changed, accounting for 72% of the 117 quantified ECM proteins (Supplemental Data 5, Supplemental Fig. 6a). Categorical differences of the significantly changed ECM proteins between age groups were also observed. While only 7 of 19 (37%) collagens that were quantified changed in abundance among the developmental groups, the majority of ECM glycoproteins (26/35, 74%), ECM regulators (25/28, 89%) and ECM-affiliated proteins (18/20, 90%) were found to change (Supplemental Fig. 6b, c). The expression levels across developmental stages were compared to select individual ECM proteins that exhibited high abundance in one or more developmental groups, or that showed significant expression changes (Fig. 3c and Supplemental Fig. 7). This analysis highlights at least four patterns of changing expression levels. A subset of collagens shows similar abundance across all stages (e.g., COL1A1, COL3A1, COL5A1, COL6A1). In contrast, a few proteins are expressed at the highest level in the fetal samples and steadily decrease in the juvenile and adult developmental transitions (e.g., COL12A1, COL14A1, FBN2, POSTN, OGN). Others maintain an equal high expression level in the fetal and juvenile stages and only start to decrease at the adult stages (e.g., COL2A1, LAMA4, EMILIN1, FN1). The final group exhibits a lower level in fetal and higher levels in postnatal pancreata (e.g., COL4A1, COL16A1, LAMA5). For four collagen proteins (COL1, COL4, COL5 COL6), multiple isoforms were detected.

COL1, COL4, and COL6 have relatively consistent ratios of the measured isoforms throughout all developmental stages studied. Interestingly, the relative ratio of COL5 isoforms changed; COL5A1 and COL5A2 slightly decreased with age, and COL5A3 became more abundant in the adult groups (Supplemental Fig. 7b).

Visualizing ECM proteins throughout human pancreas development.

To confirm the trends in core ECM protein expression from the MS study (Supplemental Data 7), we performed immunofluorescent staining to visualize a select group of 16 ECM proteins. Representative images are shown in Fig. 4, additional images are included in Supplemental Fig. 8, and higher magnification images in Supplemental Fig. 9 for better visualization of subcellular localization. Proteins found to have non-significant differences in total expression by MS among the four developmental groups (COL1A1, COL3A1, COL5A1, COL6A1) were found to also qualitatively exhibit consistent expression by immunofluorescence across developmental ages. Likewise, proteins expressed at higher relative levels during the fetal stage than postnatal stages (COL2A1, COL12A1, COL14A1, EMILIN1, FBN2, FN1, LAMA4, OGN, POSTN) and proteins expressed at lower relative levels in the fetal stage compared to expression at later stages (COL4A1, COL16A1, LAMA5) consistently displayed similar patterns by immunofluorescence staining as they did by MS. Qualitatively, the immunofluorescence staining correlates well with and validates the matrisome data.

Figure 4. Visualizing ECM proteins across multiple developmental stages. Immunofluorescent images of selected ECM proteins (green) co-stained with insulin (red) in fetal (F), juvenile (J), young adult (Y) and older adult (O) pancreata. Qualitative trends in protein levels corroborate MS data. Representative images are shown, images were taken for N=3 donors per developmental group. An expanded panel of images is available in Supplementary Figure 7. Scale bar = 100 microns. **(Next Page)**

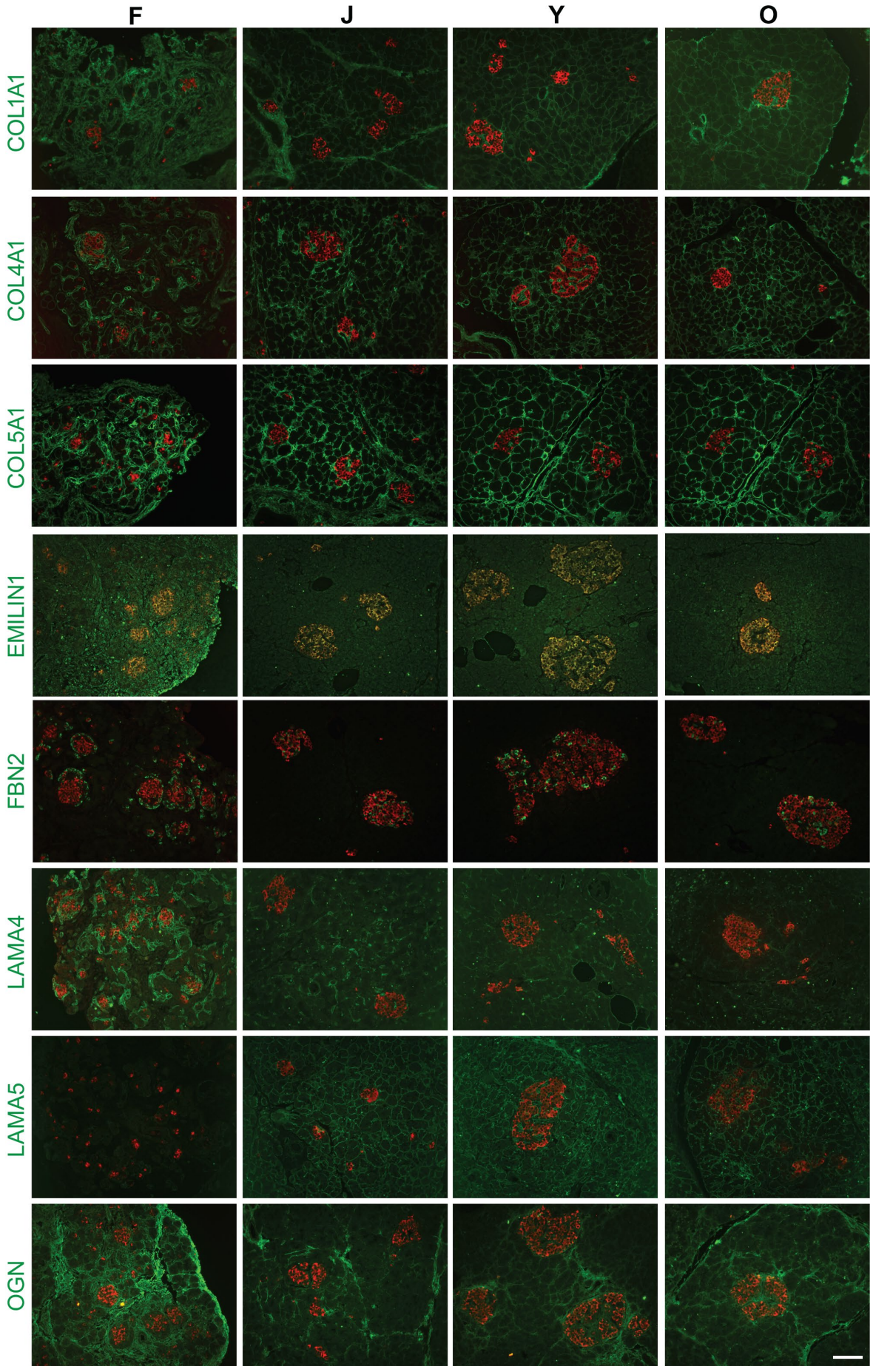
F
J
Y
O
COL1A1
COL4A1
COL5A1
EMILIN1
FBN2
LAMA4
LAMA5
OGN

ECM abundance and localization changes across developmental time points.

The visualization of these proteins within tissue sections provides an opportunity for more precise characterization of ECM localization among the various compartments of the pancreatic tissue. Of specific interest, we quantified the expression of these proteins in the acinar regions, which makes up the majority of the pancreas volume, and the islet regions, which constitute ~1-2% of the pancreas. The ratio of signal in the islet and acinar compartments (islet/acinar) was calculated for each image. This ratio represents the enrichment of each particular ECM protein in islets compared to the acinar for each image, but due to the normalization does not account for the total abundance of the ECM protein itself (Fig. 5a, purple bars). Total abundance as determined by MS is included for side-by-side comparison (Fig. 5a, black bars). Heat maps are included (Fig. 5b) to express overall trends in the data sets.

For many ECM proteins, both abundance and localization were found to change throughout development. Only two of the selected proteins (COL2A1, COL3A1) were expressed at similar ratios in the acinar and islet compartments at all four stages. A subset of ECM proteins studied is generally enriched within the acinar compartment (COL12A1, COL14A1, COL16A1, LAMA5, POSTN). Two proteins (COL12A1, COL14A1) are abundant in fetal acinar tissue, whereas COL16A1 is more strongly expressed within the postnatal acinar compartment. Other ECM proteins are enriched in and around the islets (EMILIN1, FBN2, LAMA4, OGN). Both OGN and EMILIN1 are expressed throughout fetal tissue, but become restricted to the islets in postnatal pancreata; EMILIN1 is concentrated intracellularly in the islets, while OGN is localized to the islet extracellular space and, to a lesser extent, in the nearby acini. FBN2 is intracellularly expressed in delta cells, but not alpha or beta cells (Fig. 4 and Supplemental Fig. 11b). COL4A1 and LAMA4

are both enriched in fetal islets with an islet/acinar ratio of around 2. COL4A1 and LAMA4 proteins are localized around the blood vessels of developing islets; however, beyond the fetal stage, COL4A1 is found to be expressed more evenly throughout acinar regions. LAMA4, on the other hand, becomes more enriched within islets in older adults, as do three other ECM proteins in our study (COL1A1, COL5A1, LAMA5). Although we found no significant changes in the total abundance of those proteins between younger and older adult pancreata, there does appear to be significant accumulation in and around the islets of the older donors. Three proteins (COL14A1, FN1 and POSTN) displayed detectable protein expression in all four groups revealed by MS, but quantifiable staining in islets and acinar was only detectable at the fetal stage. For COL14A1 and POSTN, most expression was found in the fetal mesenchyme (Supplemental Fig. 8). In the adult donors, positive staining for both COL14A1 and POSTN was concentrated around blood vessels and ducts (Supplemental Fig. 11a), with minimal extracellular expression in the islet or acinar compartments, although COL14A1 had faint intracellular staining in the acinar regions. FN1 was found extracellularly in and around the islets in the fetal tissue, but in postnatal tissues was only found faintly and intracellularly in the islets and acinar regions, compared to more robust signal around ducts and vessels, as well as sporadic extracellular staining in the parenchyma, particularly along the boundaries of pancreatic lobules.

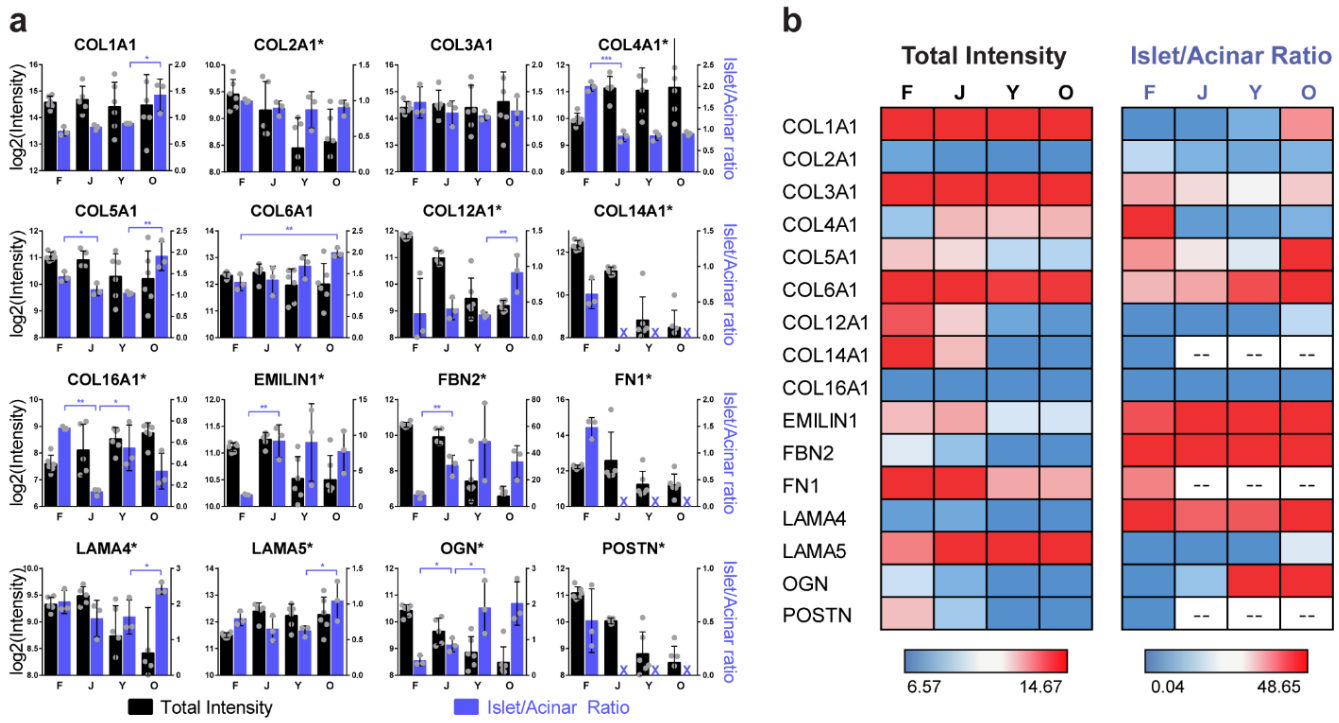

Figure 5. ECM proteins change in abundance and localization across developmental time points. a) Representation of total intensity of selected ECM proteins as measured by MS in the whole pancreas (black bars) (F,Y,O: N=6 donors per group) (J: N=5 donors). Quantification of immunofluorescence (IF) staining in pancreatic acinar and islet regions, depicted as the ratio of islet/acinar (purple bars), in fetal (F), juvenile (J), young adult (Y) and older adult (O) pancreata, graphed as mean ± the standard deviation (purple bars) (N=3 donors per group). Significant difference for islet/acinar ratio was determined by a two-tailed t test (*p < 0.05, **p < 0.01, ***p < 0.001). An asterisk next to¬¬¬ the protein name indicates a significant difference in total protein abundance by ANOVA among the four groups (FDR 0.05). A purple 'X' indicates IF staining was too low in the islets and acinar to calculate the islet/acinar ratio. Source data are provided as a Source Data file; exact p values are included in the Source Data file. **b)** Heat maps depicting the same data as a, with emphasis on relative changes throughout the four groups. Blue color indicates the lower 25th percentile of values, red color indicates the top 75th percentile of values, with a gradient toward white at the 50th percentile.

Discussion

Although dynamic proteome changes are known to occur with aging [2, 3, 58], a comprehensive analysis of the proteome and matrisome across early and late developmental stages of human pancreatic tissue has not been reported. In this study, we present a simple and cost-efficient protocol to achieve in-depth proteome-wide and ECM-specific quantitative analysis which omits labor-intensive extraction or enrichment steps. We utilized this method to systematically examine the dynamics of proteomic composition in human pancreata among four developmental age groups, including fetal, juvenile, young adults, and older adults. We quantified 2,064 proteins and found 1,570 of them were significantly changed across multiple stages which suggests a large degree of proteome remodeling through the human life cycle. The identified yet unquantifiable proteins are the result of differences between two batches of DiLeu labeling, which could reflect the distinct protein profiles between different age groups. In addition, the stochastic nature of data-dependent acquisition (DDA) sampling may also lead to some proteins being below the limit of detection and categorized as undetected across multiple batches [59]. To alleviate this issue, one may consider alternative highly multiplexed labeling strategies such as cPILOT [60] or 27-plex TMT [61]. However, these methods are associated with increased spectra complexity and decreased identification rates which can be emerging concerns. It is also worthwhile to note that we only collected four fractions and ran two technical replicates for each sample but still achieved a relatively deep analysis. Protein coverage can be further improved by simply increasing the number of fractions if instrument resources permit.

Processes or pathways related to the functions of the pancreas are mainly activated with increasing age such as pancreatic secretion and metabolic pathways. On the other hand, some

cancer-related pathways are more often deactivated with age, which is likely a sign of postnatal maturation of the organ. We observed many significant compositional changes from fetal to juvenile and juvenile to young adult pancreata. Young and older adults, on the other hand, are more similar in composition, with very few significantly altered proteins. We examined some interesting targets more closely. As an example, thrombospondin 1 (THBS1) is a glycoprotein that mediates cell-to-cell and cell-to-matrix interactions which is therefore involved in tissue genesis and remodeling [62]. In our study it showed a more than two-fold increase in abundance from juvenile to young adult that is consistent with organ maturation. In addition, THBS1 has been shown to be expressed at high levels during tumor progression [62, 63] and numerous thrombospondin-based therapeutic approaches have been studied [64]. However, our data suggests that conclusions or strategies based on these studies could be further strengthened by taking into consideration the age of the patient. Along this direction we found that many previously reported pancreatic cancer biomarkers showed different expression levels at various developmental stages such as ANXA2 [65], PLG [65], ITGB1 [65], ACTN4 [66], LGALS1 [66] and LAMB1 [66]. ACTN4 and LGALS1, for instance, were reported to show fold changes of 1.85 and 1.75, respectively, in cancerous versus normal tissue. Nevertheless, they also have more than 1.3-fold higher expression in young adults compared to juvenile and this difference is even more dramatic in older adults. Though few studies mentioned an age-dependent effect on biomarker protein expression, our results indicate age-related alterations and the necessity of paying particular attention to patient age in biomarker discovery or disease treatment studies.

In regard to pancreas and islet ECM, previous studies mainly focused on a subset of collagens or laminins, using techniques to quantify specific ECM proteins through gene

expression and immunofluorescent staining [15, 67]. In our study, we have identified 185 ECM proteins and quantified 117 throughout four developmental stages of the human pancreas. 84 of those quantified ECM proteins were significantly changed in total abundance among the four age groups and displayed distinct expression patterns, which revealed the complexity of ECM remodeling during development and maturation. Very few previous studies reported on the changes in ECM abundance or localization among human fetal and adult pancreas tissue. Otonkoski et al. observed the distribution of laminins throughout the acinar and islet regions of fetal and adult human pancreas by immunofluorescent staining [15]. The authors found that the profiles were quite similar between the two age groups, with the major differences being that LAMA1 was expressed in fetal but not in adult islets, and LAMB2 was only expressed in adult islets. Likewise, we found that LAMB2 was expressed at significantly lower levels in the fetal tissue than in adult tissue, but not absent, while LAMA1 was only detected in fetal and juvenile tissues (Supplemental Data 4). Extending these findings to other laminins, our results indicate a general shift in the composition of laminins between fetal and adult stages, with some laminins increasing in abundance from fetal to adult (LAMA2, LAMA5, LAMB2, LAMC3) and only LAMA4 decreasing. LAMB1 and LAMC1 did not significantly change throughout the developmental stages we measured. We further identified ECM proteins only present in some developmental groups, which could reflect the most drastic differences between developmental stages, and these proteins were not quantifiable due to only being detected in a subset of the donors. 59 ECM-related proteins were exclusively detected in the fetal and juvenile groups and 9 were found only in adult samples (Supplemental Data 4). For instance, FMOD, which has critical roles in the extracellular matrix organization as well as the initiation and progression of several malignancies

[68], is present exclusively in the fetal and juvenile groups. On the other hand, MXRA5, which functions in an anti-inflammatory and anti-fibrotic role [69], is only detected in the adult samples. These observations can provide deeper insights into ECM dynamics during pancreas development. Overall, we have found that as a group, collagens change less dramatically throughout development, while glycoproteins and proteoglycans, which contain ECM proteins that contribute to the basement membrane (e.g. laminins, perlecan) exhibit much more dynamic changing patterns throughout development (Supplemental Fig. 6c).

A primary means of studying islet function is to use islets isolated from the pancreas through enzymatic treatment, which destroys much of the native ECM and disrupts islet architecture [70, 71]. This fact has prompted many studies to supplement ECM for improved islet culture, and the limitations to the longevity of islet culture highlight the necessity of ECM for islet survival and function [9, 20, 72, 73]. Studies using human fetal isolated islets have also identified a role for ECM in the differentiation, proliferation, and function of islet endocrine cells during in utero development [67, 74-76]. As many look to use stem cell-derived islets as a future diabetes therapy, some question the role ECM may have in the differentiation, function, and transplantation of these cells [77-82]. To better understand the islet ECM environment, we investigated the localization of selected ECM proteins in addition to total abundance in the pancreatic tissue.

Four of the ECM proteins we studied were enriched in adult islets relative to the exocrine tissue (COL6A1, EMILIN1, FBN2, OGN). Importantly, the relative abundance and distribution of these proteins was found to also change throughout development. OGN for example, is expressed throughout the acinar and islet regions of fetal and juvenile pancreata, whereas in

adult pancreata it is more concentrated in islets. One previous study has found a role for OGN in islet function; whole-body OGN knockout mice have impaired glucose tolerance and reduced beta cell mass, while OGN supplemented in vitro or at a systemic level in vivo, improves beta cell function and glucose tolerance [83]. While this study focused on circulating OGN produced from osteoblastic cells, our finding that OGN is concentrated around human pancreatic islets suggests that OGN may also play a localized role in islet function. Furthermore, FBN2 has been reported as one of 13 methylated genes silenced in human pancreatic cancers [84], but to our knowledge no other studies have reported on the normal function of FBN2 in the pancreas or in islets. Interestingly, somatostatin was another of the 13 genes identified in the study [84]; we now additionally show that FBN2 is exclusively expressed within somatostatin-expressing delta cells of the islet. In addition, a role for EMILIN1 in pancreas or islet physiology has not been reported, but the protein has been identified in previous pancreas and islet matrisome studies [45, 85]. Collagen 6 co-culture has recently been shown to improve human islet survival and function [86], but it is not clear if collagen 6 is more potent than other purified collagens in enhancing islet in vitro function.

Our present study also revealed unexpected differences in the islet ECM between the younger adult (21-29 years) and older adult (50-61 years) groups. Four ECM proteins (COL1A1, COL5A1, LAMA4, LAMA5) were enriched within the islets in the older adults compared to younger adults, while the total abundance of these proteins in the pancreas was insignificantly different between the two groups. This suggests that the adult islet matrisome changes with age, consistent with recent findings that younger and older adult donors have localized differences in

islet ECM, which may impact the effectiveness of enzymatic digestion during islet isolation [87, 88].

Research in animal models has indicated that functional changes in islet maturation occur postnatally [89], but the possible correlation with ECM structural changes in human islets has not been studied. A recent study by Arda et al. comparing gene expression and function of isolated human islets from juvenile and adult donors indicated that there are over 500 genes differentially expressed between the two age groups, with distinct histone-mediated changes in regulation of gene expression. Furthermore, the authors observed that age was correlated with functional changes. Adult islets secreted more insulin than juvenile islets under both basal and glucose-stimulated conditions, while total insulin content did not change between juvenile and adult islets [90]. Our study suggests that the islet ECM environment also changes between childhood and adulthood. Further studies into how maturing islets interact with ECM during this key transition are likely to be informative toward better defining the mechanisms of maturation, and risks of autoimmune diabetes.

Likewise, ECM studies using animal tissues and isolated islets have previously been reported, but whether these findings are relevant to human tissue is uncertain. In their 2017 study, Naba et al. identified 120 ECM proteins in isolated mouse islets, including 66 core ECM proteins [45]. The methodology employed in their study does not appear to translate to the larger and denser human pancreas, as effective efforts to isolate islets from the human pancreas inherently destroy the ECM [91]. In the present study, we have identified 61 core ECM proteins in human pancreas across the four developmental stages. Interestingly, many of the significant proteins highlighted in our study were also identified in the Naba study, indicating previously

unknown similarities of important ECM components between both species. A total of 80 core ECM proteins are identified between the two studies. Though there were similarities between species, 33 proteins, or 41% of all core ECM proteins, only appear in one of the species' datasets. This difference highlights species-specific characteristics in the pancreatic and islet matrisome that may play relevant roles in health and disease. In our separate unpublished study, all 117 ECM-associated genes that were identified in our proteomic study were also detected at the RNA level in isolated adult human islets, which may drive future efforts to quantify the human islet-specific matrisome and investigate islet-specific changes throughout development.

Overall, we present a quantitative proteomic analysis of human pancreas to delineate molecular changes, particularly ECM composition, throughout pancreas development, maturation, and aging. We found that many previously reported pancreas tumor biomarkers displayed significant changes in protein expression across multiple developmental stages and this age-dependent effect could be important knowledge for studies in biomarker identification and clinical implementation. Our study revealed dynamic changes in pancreatic ECM composition and localization throughout life cycle, and have identified specific ECM proteins enriched in pancreatic islets (e.g. COL6A1, EMILIN1, FBN2, OGN) which may provide insight for studying islet development, function and disease. In addition, our protocol can be easily adapted to achieve large-scale and in-depth quantitative analysis of ECM-containing proteome in other biological systems with relatively simple operations and low cost. Our data interpretations are far from exhaustive but instead, we expect our results to serve as a valuable resource for broad audiences with various interests and will provide a foundation for more in-depth investigations.

Methods

Human pancreas tissue preparation

Human fetal pancreas tissue was obtained from secondary sources (Advanced Biosystems Resources, Inc.) under approved Material Transfer Agreements and with protocols approved by the University of Wisconsin's Institutional Animal Care and Use Committee (IACUC) and Institutional Review Board (IRB) (IRB Study #2013-141). ABR, Inc obtains consent in accordance with Uniform Anatomical Gift Act (UAGA) and National Organ Transplant Act (NOTA) guidelines. ABR, Inc warrants that appropriate consent for tissue donation is obtained and adequate records of such consents are maintained. In addition, that tissues are obtained with local, state, and federal laws and regulations governing the procurement of human tissue. Within 24 hours of recovery, the organs were received and cleaned of surrounding connective tissue. Small pieces of tissue were removed and fixed with 4% PFA for histology, and the majority of the pancreas was homogenized in sterile water for 3 seconds. The homogenized tissue was pelleted (16,100 xg, 5 min) and the translucent supernatant was discarded. The pellet was flash frozen and stored at -80 °C prior to further processing for MS analysis.

Juvenile and adult human pancreas tissue was procured by the University of Wisconsin Organ and Tissue Donation Services from donors with no indication of diabetes or pancreatitis, with consent obtained for research from next of kin and authorization by the University of Wisconsin-Madison Health Sciences Institutional Review Board (IRB granted an exempt from protocol approval for studies on post-natal tissue because research on deceased donors is not considered human subjects research). IRB oversight of the project is not required because it does not involve human subjects as recognized by 45 CFR 46.102(f) which defines a 'human subject' as

"a living individual about whom an investigator (whether professional or student) conducting research obtains (1) data through intervention or interaction with the individual, or (2) identifiable private information." Following organ harvest, pancreata were allocated for research if deemed unfit for transplantation due to vascular damage during organ recovery, no suitable recipient, and non-ideal age or BMI. The organs were received within 24 hours of recovery and trimmed of extra-pancreatic connective tissues, including duodenum, large arteries and veins. The parenchyma was cut into 1 cm^3 cubes and frozen at -80 °C for future use, some pieces were also immediately fixed with 4% PFA for histology. One piece of frozen pancreas per donor was thawed and rinsed with 1x PBS followed by sterile water, and then manually chopped into small pieces. The pieces were immersed in sterile water and homogenized for 3 seconds, then pelleted (16,100 x g, 5 min). Any floating lipids were removed, and the translucent supernatant was discarded. The pellet was flash frozen and stored at -80 °C. Donor information can be found in Supplemental Data 1.

Protein extraction and digestion

A slightly modified SCAD method [50] was used to prepare all pancreas samples. Each sample was dissolved in 150 µL of extraction buffer solution (4 % SDS, 50 mM Tris buffer) and sonicated using a probe sonicator (Thermo Fisher Scientific). Protein extracts were reduced with 10 mM dithiothreitol (DTT) for 30 min at room temperature and alkylated with 50 mM iodoacetamide for another 30 min in dark before quenching with DTT. Proteins were then precipitated with 80% (v/v) cold acetone (-20 ℃) overnight. Samples were centrifuged at 14,000 g for 15 min after which supernatant containing SDS (in the extraction buffer) was discarded. Pellets were rinsed with cold acetone again and air-dried at room temperature. 8 M urea was

added to dissolve the pellets and 50 mM Tris buffer was used to dilute the samples to a urea concentration < 1 M. On-pellet digestion was performed with LysC/trypsin (Promega) in a 50:1 ratio (protein:enzyme, w/w) at 37 ℃ overnight. The digestion was quenched with 1% TFA and samples were desalted with Sep-Pak C18 cartridges (Waters). Concentrations of peptide mixture were measured by peptide assay (Thermo Fisher Scientific). 100 µg peptide was aliquoted for each sample, dried in vacuo and reconstituted in 0.5M triethylammonium bicarbonate prior to DiLeu labeling.

12-plex DiLeu labeling

Synthesis of DiLeu tags and labeling process were performed according to protocols previously described [46, 48]. Briefly, L-Leucine or isotopic L-leucine and sodium cyanoborohydride or sodium cyanoborodeuteride (2.5 × molar excess to leucine) were suspended in H2O or D2O, and the mixture was cooled in an ice-water bath. Formaldehyde (CH2O, 37% w/w) or isotopic formaldehyde (CD2O or 13CH2O, 20% w/w) (2.5× molar excess to leucine) was added dropwise, and the mixture was stirred in an ice-water bath for 30 min. The target product was purified by flash column chromatography (MeOH/DCM) and dried in vacuo. Each isotopologue of reporter 115 and 116 requires 18O exchange prior to reductive dimethylation. Leucine or isotopic leucine was dissolved in 1 N HCl H218O solution (pH 1) and stirred on a hot plate at 65 °C for 4 h. Following evaporation of HCl from the solution in vacuo, trace amounts of acid were removed with StratoSpheres PL-HCO3 MP resin (Agilent) to obtain 18O leucine in free base form. The identity and purity of DiLeu tags were confirmed with MS before all experiments. 1 mg of each DiLeu tag was dissolved in 100 µL of anhydrous N,N-dimethylformamide and combined with 4-(4,6-dimethoxy1,3,5-triazin-2-yl)-4-

methylmorpholinium tetrafluoroborate and N-methylmorpholine at 0.7× molar ratios. The activation was performed by vortexing the mixture for 45 min at room temperature and supernatant was added to each sample for peptide labeling. After vortexing at room temperature for 2 h, the labeling reaction was quenched by addition of hydroxylamine to a concentration of 0.25%. The samples were then dried *in vacuo*, combined, and cleaned with SCX SpinTips (PolyLC) according to manufacturer's protocols.

HpH fractionation

HpH fractionation was performed on a Waters Alliance e2695 HPLC using a C18 reverse phase column (2.1 × 150 mm, 5 µm, 100 Å, PolyLC) operating at 0.2 mL/min. Mobile phase A consisted of 10 mM ammonium formate at pH 10 adjusted with ammonium hydroxide and mobile phase B consisted of 90% ACN and 10 mM ammonium format at pH 10. Separation was achieved with a gradient as following: 1 % B (0-5 min), 1-40% B (5-50 min), 40-60% B (50-54 min), 60-70% B (54-58 min), and 70-100 % B (58-59 min). Fractions were collected every 4 min and non-adjacent fractions were concatenated into four samples before being dried *in vacuo* for LC-MS/MS analysis.

LC-MS/MS analysis

Samples were analyzed on an Orbitrap Fusion Lumos Tribrid mass spectrometer (Thermo Fisher Scientific) coupled to a Dionex UltiMate 3000 UPLC system. Each sample was dissolved in 3% ACN, 0.1% formic acid in water before loaded onto a 75 µm inner diameter homemade microcapillary column which is packed with 15 cm of Bridged Ethylene Hybrid C18 particles (1.7 µm, 130 Å, Waters) and fabricated with an integrated emitter tip. Mobile phase A was composed of water and 0.1% formic acid while mobile phase B was composed of ACN and 0.1% formic acid.

LC separation was achieved across a 100-min gradient elution of 3% to 30% mobile phase B at a flow rate of 300 nL/min. Survey scans of peptide precursors from 300 to 1500 m/z were performed at a resolving power of 60k (at m/z 200) with an AGC target of 2×10^5 and maximum injection time of 100 ms. The top 20 precursors were then selected for HCD fragmentation with a normalized collision energy of 30, an isolation width of 1.0 Da, a resolving power of 60k, an AGC target of 5×10^4, a maximum injection time of 118 ms, and a lower mass limit of 110 m/z. Precursors were subject to dynamic exclusion for 45 s with a 10 ppm tolerance. Each sample was acquired in technical duplicates.

Data analysis

Protein identifications and quantifications were performed using Proteome Discoverer (version 2.1, Thermo Scientific). Raw files were searched against the Uniprot H. sapiens reviewed database (September 2018) using Sequest HT algorithm with trypsin selected as the enzyme and three missed cleavages allowed. Precursor mass tolerance of 20 ppm and a fragment mass tolerance of 0.02 Da were set for the searching. DiLeu labeling on peptide N-termini and lysine residue (+145.12801), and carbamidomethylation of cysteine residues (+57.02146 Da) were chosen as static modifications. Dynamic modifications included oxidation of methionine residues (+15.99492 Da), deamidation of asparagine and glutamine residues (+0.98402 Da) and hydroxylation on proline residues (+15.99492 Da). Search results were filtered to 1% false discovery rate (FDR) at both peptide and protein levels. Quantitation was performed in Proteome Discoverer with a reporter ion integration tolerance of 10 ppm for the most confident centroid. Protein quantitative ratios were determined using a minimum of one quantified peptide. Reporter ion intensities were normalized through equal total peptide amount. ECM proteins

were identified and classified by matching the results to Human Matrisome dataset [29]. Missing intensities were replaced using the “replace missing values from normal distribution” feature in Perseus (version 1.6.0.7)[92] prior to further processing. Two-sample Student’s t test with a two-tailed distribution for binary comparison and one-way ANOVA analysis were conducted using Perseus. All p values were further adjusted by Benjamini-Hochberg correction for multiple testing. Bioinformatics analyses including Pearson correlation analysis, hierarchical clustering, protein intensity profiling, volcano plots, GSVA analysis, chord diagram [57] and box plots were achieved using R packages. Biological process network was generated using Metascape (version 3.5)[56] and exported using Cytoscape (version 3.7.1). For protein intensity profiling, biological processes and pathways were enriched using DAVID bioinformatics resources [93] with a FDR cutoff of 0.05. Four selected terms with lower p values were shown for each cluster and the same term was only shown once where it appeared the most significant.

To compare abundance of different proteins, iBAQ method was used embedded in MaxQuant (version 1.5.2.8). Raw files were searched against the Uniprot H. sapiens reviewed database (September 2018) with trypsin/P selected as the enzyme and three missed cleavages allowed. DiLeu labeling on peptide N-termini and lysine residue (+145.12801), and carbamidomethylation of cysteine residues (+57.02146 Da) were chosen as fixed modifications. Variable modifications included oxidation of methionine residues (+15.99492 Da), deamidation of asparagine and glutamine residues (+0.98402 Da) and hydroxylation on proline residues (+15.99492 Da). The iBAQ method was enabled and all other parameters were set as default.

Immunofluorescent staining and quantification

All donor tissue was fixed with 4% paraformaldehyde and embedded in paraffin. 5-micron sections were cut and deparaffinized with xylene and ethanol. Antigen retrieval was performed for 2.5 hours at 80 °C in 10 mM sodium citrate buffer. Following washing with PBS-T (1x PBS/ 0.05% Triton X-100) and blocking for 35 min (1x PBS/ 10% BSA) at room temperature, antibody-specific staining was performed following Supplemental Data 8. Cover slips were mounted with Fluoromount (Sigma, #F4680). Images were taken at 20x magnification using a Zeiss Axiovert 200 M microscope with AxioVision version 4.8.2.0, and analyzed using ImageJ software (ImageJ 1.53c). The color channel representing the ECM protein of interest was converted to a binary image using an auto-threshold adjustment. Images were analyzed by tracing the islets (Ins+ regions, red) and a neighboring acinar section of about the same size and location as each islet (Ins- regions, using nuclear arrangement to define acinar clusters); the ECM protein (green) was quantified for each image and normalized by calculating the ratio of intensity within the islet divided by the acinar compartments (islet/acinar ratio). This method is visually outlined in Supplemental Figure 10. For every combination of antibodies, images were taken for N=3 donors in each developmental group. 1-6 islets were quantified per image, and 4-5 images per donor, for a total of 9-22 islets quantified per donor, per stain. Statistical analysis was performed with Prism 6 for Windows (version 6.07) (GraphPad Software, Inc.). Results were reported as mean values across biological replicates ± the standard deviation of the mean. For immunofluorescent staining, statistical comparisons between two groups were determined using two-tailed unpaired Student's t tests. A p value of less than 0.05 was considered statistically significant, and Prism's recommended classification for significance was followed ($p < 0.0001$ = extremely significant

(****), 0.0001 < p < 0.001 = extremely significant (***), 0.001 < p < 0.01 = very significant (**), and 0.01 < p < 0.05 = significant (*)).

Data availability

The mass spectrometry proteomics data have been deposited to the ProteomeXchange Consortium [94] via the PRIDE [95] partner repository with the dataset identifier PXD020130 (https://www.ebi.ac.uk/pride/archive/projects/PXD020130). Source data are provided with this paper. An online web application "Matrisome and proteome database of human pancreas" is also available at https://nc-webapp.herokuapp.com/, which enables custom searching of all quantified proteins and supports download of all proteomics datasets in this study. Full IF staining results are available from the authors upon reasonable requests. H. sapiens database used for proteomics data searching was downloaded from Uniprot (https://www.uniprot.org/). Human matrisome dataset used for ECM protein matching was downloaded from "the Matrisome Project"(http://matrisomeproject.mit.edu/).

Code availability

All online-available software or R packages to perform data analysis or generate the figures are indicated throughout the manuscript.

Acknowledgements

This study was supported in part by grant funding from the NIH (R21AI126419, R01DK071801, RF1AG052324, P41GM108538, and 1F31DK125021-01), and Juvenile Diabetes Research Foundation (1-PNF-2016-250-S-B and SRA-2016-168-S-B). Data presented here was also in part obtained through support from an NIH/NCATS UL1TR002373 award through the University of Wisconsin Institute for Clinical and Translational Research. The Orbitrap instruments were purchased through the support of an NIH shared instrument grant (NIH-NCRR S10RR029531) and Office of the Vice Chancellor for Research and Graduate Education at the University of Wisconsin-Madison. We would also like to acknowledge the generous support of the University of Wisconsin Organ and Tissue Donation Organization who provided human pancreas for research. Our research team would like to give special thanks to the families who donated tissues for this study. We also acknowledge Sierra Raglin and the University of Wisconsin Department of Surgery Histology Core for help processing and embedding tissues. L.L. acknowledges a Vilas Distinguished Achievement Professorship and the Charles Melbourne Johnson Distinguished Chair Professorship with funding provided by the Wisconsin Alumni Research Foundation and University of Wisconsin-Madison School of Pharmacy.

References

1. Bonnans, C., Chou, J. & Werb, Z. Remodelling the extracellular matrix in development and disease. Nat Rev Mol Cell Biol 15, 786-801 (2014).
2. Kular, J.K., Basu, S. & Sharma, R.I. The extracellular matrix: Structure, composition, age-related differences, tools for analysis and applications for tissue engineering. J Tissue Eng 5, 2041731414557112 (2014).
3. Phillip, J.M., Aifuwa, I., Walston, J. & Wirtz, D. The Mechanobiology of Aging. Annu Rev Biomed Eng 17, 113-141 (2015).
4. Rozario, T. & DeSimone, D.W. The extracellular matrix in development and morphogenesis: a dynamic view. Dev Biol 341, 126-140 (2010).
5. Zvibel, I., Smets, F. & Soriano, H. Anoikis: roadblock to cell transplantation? Cell Transplant 11, 621-630 (2002).
6. Ernst, A.U., et al. Nanotechnology in cell replacement therapies for type 1 diabetes. Adv Drug Deliv Rev 139, 116-138 (2019).
7. Prince, E. & Kumacheva, E. Design and applications of man-made biomimetic fibrillar hydrogels. Nature Reviews Materials 4, 99-115 (2019).
8. Taha, I.N. & Naba, A. Exploring the extracellular matrix in health and disease using proteomics. Essays Biochem 63, 417-432 (2019).
9. Stendahl, J.C., Kaufman, D.B. & Stupp, S.I. Extracellular matrix in pancreatic islets: relevance to scaffold design and transplantation. Cell Transplant 18, 1-12 (2009).
10. Gress, T.M., et al. Role of extracellular matrix in pancreatic diseases. Digestion 59, 625-637 (1998).
11. Tian, C., et al. Proteomic analyses of ECM during pancreatic ductal adenocarcinoma progression reveal different contributions by tumor and stromal cells. Proc Natl Acad Sci U S A 116, 19609-19618 (2019).
12. Weniger, M., Honselmann, K.C. & Liss, A.S. The Extracellular Matrix and Pancreatic Cancer: A Complex Relationship. Cancers (Basel) 10(2018).
13. Nikolova, G., et al. The vascular basement membrane: a niche for insulin gene expression and Beta cell proliferation. Dev Cell 10, 397-405 (2006).
14. van Deijnen, J.H., Hulstaert, C.E., Wolters, G.H. & van Schilfgaarde, R. Significance of the peri-insular extracellular matrix for islet isolation from the pancreas of rat, dog, pig, and man. Cell Tissue Res 267, 139-146 (1992).
15. Otonkoski, T., Banerjee, M., Korsgren, O., Thornell, L.E. & Virtanen, I. Unique basement membrane structure of human pancreatic islets: implications for beta-cell growth and differentiation. Diabetes Obes Metab 10 Suppl 4, 119-127 (2008).
16. Bogdani, M., et al. Extracellular matrix components in the pathogenesis of type 1 diabetes. Curr Diab Rep 14, 552 (2014).

17. Choong, F.J., Freeman, C., Parish, C.R. & Simeonovic, C.J. Islet heparan sulfate but not heparan sulfate proteoglycan core protein is lost during islet isolation and undergoes recovery post-islet transplantation. Am J Transplant 15, 2851-2864 (2015).

18. Lammert, E. & Thorn, P. The Role of the Islet Niche on Beta Cell Structure and Function. J Mol Biol 432, 1407-1418 (2020).

19. Simeonovic, C.J., et al. Loss of intra-islet heparan sulfate is a highly sensitive marker of type 1 diabetes progression in humans. PLoS One 13, e0191360 (2018).

20. Townsend, S.E. & Gannon, M. Extracellular Matrix-Associated Factors Play Critical Roles in Regulating Pancreatic beta-Cell Proliferation and Survival. Endocrinology 160, 1885-1894 (2019).

21. Van Deijnen, J.H., Van Suylichem, P.T., Wolters, G.H. & Van Schilfgaarde, R. Distribution of collagens type I, type III and type V in the pancreas of rat, dog, pig and man. Cell Tissue Res 277, 115-121 (1994).

22. Virtanen, I., et al. Blood vessels of human islets of Langerhans are surrounded by a double basement membrane. Diabetologia 51, 1181-1191 (2008).

23. Kilimnik, G., Jo, J., Periwal, V., Zielinski, M.C. & Hara, M. Quantification of islet size and architecture. Islets 4, 167-172 (2012).

24. Brissova, M., et al. Assessment of human pancreatic islet architecture and composition by laser scanning confocal microscopy. J Histochem Cytochem 53, 1087-1097 (2005).

25. Cabrera, O., et al. The unique cytoarchitecture of human pancreatic islets has implications for islet cell function. Proc Natl Acad Sci U S A 103, 2334-2339 (2006).

26. Dolensek, J., Rupnik, M.S. & Stozer, A. Structural similarities and differences between the human and the mouse pancreas. Islets 7, e1024405 (2015).

27. Steiner, D.J., Kim, A., Miller, K. & Hara, M. Pancreatic islet plasticity: interspecies comparison of islet architecture and composition. Islets 2, 135-145 (2010).

28. Byron, A., Humphries, J.D. & Humphries, M.J. Defining the extracellular matrix using proteomics. Int J Exp Pathol 94, 75-92 (2013).

29. Naba, A., et al. The matrisome: in silico definition and in vivo characterization by proteomics of normal and tumor extracellular matrices. Mol Cell Proteomics 11, M111 014647 (2012).

30. Naba, A., et al. Characterization of the Extracellular Matrix of Normal and Diseased Tissues Using Proteomics. J Proteome Res 16, 3083-3091 (2017).

31. Ma, F., et al. In Depth Quantification of Extracellular Matrix Proteins from Human Pancreas. J Proteome Res 18, 3156-3165 (2019).

32. Schiller, H.B., et al. Deep Proteome Profiling Reveals Common Prevalence of MZB1-Positive Plasma B Cells in Human Lung and Skin Fibrosis. Am J Respir Crit Care Med 196, 1298-1310 (2017).

33. Hill, R.C., Calle, E.A., Dzieciatkowska, M., Niklason, L.E. & Hansen, K.C. Quantification of extracellular matrix proteins from a rat lung scaffold to provide a molecular readout for tissue engineering. Mol Cell Proteomics 14, 961-973 (2015).

34. Schiller, H.B., et al. Time- and compartment-resolved proteome profiling of the extracellular niche in lung injury and repair. Mol Syst Biol 11, 819 (2015).

35. Li, Q., et al. Proteomic analysis of naturally-sourced biological scaffolds. Biomaterials 75, 37-46 (2016).

36. Hansen, K.C., et al. An in-solution ultrasonication-assisted digestion method for improved extracellular matrix proteome coverage. Mol Cell Proteomics 8, 1648-1657 (2009).

37. Onnerfjord, P., Khabut, A., Reinholt, F.P., Svensson, O. & Heinegard, D. Quantitative proteomic analysis of eight cartilaginous tissues reveals characteristic differences as well as similarities between subgroups. J Biol Chem 287, 18913-18924 (2012).

38. Bonvillain, R.W., et al. A nonhuman primate model of lung regeneration: detergent-mediated decellularization and initial in vitro recellularization with mesenchymal stem cells. Tissue Eng Part A 18, 2437-2452 (2012).

39. Wilson, R., et al. Comprehensive profiling of cartilage extracellular matrix formation and maturation using sequential extraction and label-free quantitative proteomics. Mol Cell Proteomics 9, 1296-1313 (2010).

40. Zhu, W., Smith, J.W. & Huang, C.M. Mass spectrometry-based label-free quantitative proteomics. J Biomed Biotechnol 2010, 840518 (2010).

41. Megger, D.A., et al. Comparison of label-free and label-based strategies for proteome analysis of hepatoma cell lines. Biochim Biophys Acta 1844, 967-976 (2014).

42. Gocheva, V., et al. Quantitative proteomics identify Tenascin-C as a promoter of lung cancer progression and contributor to a signature prognostic of patient survival. Proc Natl Acad Sci U S A 114, E5625-E5634 (2017).

43. Tian, Y., et al. Quantitative proteomic characterization of lung tissue in idiopathic pulmonary fibrosis. Clin Proteomics 16, 6 (2019).

44. Caldeira, J., et al. Matrisome Profiling During Intervertebral Disc Development And Ageing. Sci Rep 7, 11629 (2017).

45. Naba, A., Clauser, K.R., Mani, D.R., Carr, S.A. & Hynes, R.O. Quantitative proteomic profiling of the extracellular matrix of pancreatic islets during the angiogenic switch and insulinoma progression. Sci Rep 7, 40495 (2017).

46. Xiang, F., Ye, H., Chen, R., Fu, Q. & Li, L. N,N-dimethyl leucines as novel isobaric tandem mass tags for quantitative proteomics and peptidomics. Analytical chemistry 82, 2817-2825 (2010).

47. Frost, D.C., Greer, T., Xiang, F., Liang, Z. & Li, L. Development and characterization of novel 8-plex DiLeu isobaric labels for quantitative proteomics and peptidomics. Rapid Commun Mass Spectrom 29, 1115-1124 (2015).

48. Acta PaediatrFrost, D.C., Greer, T. & Li, L. High-resolution enabled 12-plex DiLeu isobaric tags for quantitative proteomics. Analytical chemistry 87, 1646-1654 (2015).

49. Bi, H., Ye, K. & Jin, S. Proteomic analysis of decellularized pancreatic matrix identifies collagen V as a critical regulator for islet organogenesis from human pluripotent stem cells. Biomaterials 233, 119673 (2020).

50. Ma, F., Liu, F., Xu, W. & Li, L. Surfactant and Chaotropic Agent Assisted Sequential Extraction/On-Pellet Digestion (SCAD) for Enhanced Proteomics. J Proteome Res 17, 2744-2754 (2018).

51. Yang, F., Shen, Y., Camp, D.G., 2nd & Smith, R.D. High-pH reversed-phase chromatography with fraction concatenation for 2D proteomic analysis. Expert Rev Proteomics 9, 129-134 (2012).

52. Shao, X., Taha, I.N., Clauser, K.R., Gao, Y.T. & Naba, A. MatrisomeDB: the ECM-protein knowledge database. Nucleic Acids Res 48, D1136-D1144 (2020).

53. Naba, A., Hoersch, S. & Hynes, R.O. Towards definition of an ECM parts list: an advance on GO categories. Matrix Biol 31, 371-372 (2012).

54. Hanzelmann, S., Castelo, R. & Guinney, J. GSVA: gene set variation analysis for microarray and RNA-seq data. BMC Bioinformatics 14, 7 (2013).

55. Subramanian, A., et al. Gene set enrichment analysis: a knowledge-based approach for interpreting genome-wide expression profiles. Proc Natl Acad Sci U S A 102, 15545-15550 (2005).

56. Zhou, Y., et al. Metascape provides a biologist-oriented resource for the analysis of systems-level datasets. Nat Commun 10, 1523 (2019).

57. Walter, W., Sanchez-Cabo, F. & Ricote, M. GOplot: an R package for visually combining expression data with functional analysis. Bioinformatics 31, 2912-2914 (2015).

58. Sandovici, I., et al. Ageing is associated with molecular signatures of inflammation and type 2 diabetes in rat pancreatic islets. Diabetologia 59, 502-511 (2016).

59. Koopmans, F., Ho, J.T.C., Smit, A.B. & Li, K.W. Comparative Analyses of Data Independent Acquisition Mass Spectrometric Approaches: DIA, WiSIM-DIA, and Untargeted DIA. Proteomics 18(2018).

60. Frost, D.C., Rust, C.J., Robinson, R.A.S. & Li, L. Increased N,N-Dimethyl Leucine Isobaric Tag Multiplexing by a Combined Precursor Isotopic Labeling and Isobaric Tagging Approach. Anal Chem 90, 10664-10669 (2018).

61. Wang, Z., et al. 27-Plex Tandem Mass Tag Mass Spectrometry for Profiling Brain Proteome in Alzheimer's Disease. Anal Chem (2020).

62. Kazerounian, S., Yee, K.O. & Lawler, J. Thrombospondins in cancer. Cell Mol Life Sci 65, 700-712 (2008).

63. Daubon, T., et al. Deciphering the complex role of thrombospondin-1 in glioblastoma development. Nat Commun 10, 1146 (2019).

64. Zhang, X. & Lawler, J. Thrombospondin-based antiangiogenic therapy. Microvasc Res 74, 90-99 (2007).

65. Chen, R., et al. Quantitative proteomics analysis reveals that proteins differentially expressed in chronic pancreatitis are also frequently involved in pancreatic cancer. Mol Cell Proteomics 6, 1331-1342 (2007).

66. Pan, S., et al. Quantitative proteomics investigation of pancreatic intraepithelial neoplasia. Electrophoresis 30, 1132-1144 (2009).

67. Riopel, M. & Wang, R. Collagen matrix support of pancreatic islet survival and function. Front Biosci (Landmark Ed) 19, 77-90 (2014).

68. Pourhanifeh, M.H., et al. The role of fibromodulin in cancer pathogenesis: implications for diagnosis and therapy. Cancer Cell Int 19, 157 (2019).

69. Poveda, J., et al. MXRA5 is a TGF-beta1-regulated human protein with anti-inflammatory and anti-fibrotic properties. J Cell Mol Med 21, 154-164 (2017).

70. Cross, S.E., et al. Key Matrix Proteins Within the Pancreatic Islet Basement Membrane Are Differentially Digested During Human Islet Isolation. Am J Transplant 17, 451-461 (2017).

71. Lavallard, V., et al. Cell rearrangement in transplanted human islets. FASEB J 30, 748-760 (2016).

72. Jiang, K., et al. 3-D physiomimetic extracellular matrix hydrogels provide a supportive microenvironment for rodent and human islet culture. Biomaterials 198, 37-48 (2019).

73. Stephens, C.H., et al. In situ type I oligomeric collagen macroencapsulation promotes islet longevity and function in vitro and in vivo. Am J Physiol Endocrinol Metab 315, E650-E661 (2018).

74. Beattie, G.M., Rubin, J.S., Mally, M.I., Otonkoski, T. & Hayek, A. Regulation of proliferation and differentiation of human fetal pancreatic islet cells by extracellular matrix, hepatocyte growth factor, and cell-cell contact. Diabetes 45, 1223-1228 (1996).

75. Cirulli, V., et al. Expression and function of alpha(v)beta(3) and alpha(v)beta(5) integrins in the developing pancreas: roles in the adhesion and migration of putative endocrine progenitor cells. J Cell Biol 150, 1445-1460 (2000).

76. Hisaoka, M., Haratake, J. & Hashimoto, H. Pancreatic morphogenesis and extracellular matrix organization during rat development. Differentiation 53, 163-172 (1993).

77. Chaimov, D., et al. Innovative encapsulation platform based on pancreatic extracellular matrix achieve substantial insulin delivery. J Control Release 257, 91-101 (2017).

78. Higuchi, Y., et al. Synthesized basement membranes direct the differentiation of mouse embryonic stem cells into pancreatic lineages. J Cell Sci 123, 2733-2742 (2010).

79. Llacua, L.A., Faas, M.M. & de Vos, P. Extracellular matrix molecules and their potential contribution to the function of transplanted pancreatic islets. Diabetologia 61, 1261-1272 (2018).

80. Narayanan, K., et al. Extracellular matrix-mediated differentiation of human embryonic stem cells: differentiation to insulin-secreting beta cells. Tissue Eng Part A 20, 424-433 (2014).

81. Salvatori, M., et al. Extracellular Matrix Scaffold Technology for Bioartificial Pancreas Engineering: State of the Art and Future Challenges. J Diabetes Sci Technol 8, 159-169 (2014).

82. Tremmel, D.M. & Odorico, J.S. Rebuilding a better home for transplanted islets. Organogenesis 14, 163-168 (2018).

83. Lee, N.J., et al. Osteoglycin, a novel coordinator of bone and glucose homeostasis. Mol Metab 13, 30-44 (2018).

84. Hagihara, A., et al. Identification of 27 5' CpG islands aberrantly methylated and 13 genes silenced in human pancreatic cancers. Oncogene 23, 8705-8710 (2004).

85. Sackett, S.D., et al. Extracellular matrix scaffold and hydrogel derived from decellularized and delipidized human pancreas. Sci Rep 8, 10452 (2018).

86. Llacua, L.A., Hoek, A., de Haan, B.J. & de Vos, P. Collagen type VI interaction improves human islet survival in immunoisolating microcapsules for treatment of diabetes. Islets 10, 60-68 (2018).

87. Spiers, R.M., et al. Development of a Simple In Vitro Assay to Assess Digestion of the Extracellular Matrix of the Human Pancreas by Collagenase Enzyme Blends. Cell Transplant 27, 1039-1046 (2018).

88. Spiers, R.M., et al. Donor age significantly influences the Raman spectroscopic biomolecular fingerprint of human pancreatic extracellular matrix proteins following collagenase-based digestion. Acta Biomater 99, 269-283 (2019).

89. Blum, B., et al. Functional beta-cell maturation is marked by an increased glucose threshold and by expression of urocortin 3. Nat Biotechnol 30, 261-264 (2012).

90. Arda, H.E., et al. Age-Dependent Pancreatic Gene Regulation Reveals Mechanisms Governing Human beta Cell Function. Cell Metab 23, 909-920 (2016).

91. Meier, R.P.H., et al. Pancreas collagen digestion during islet of Langerhans isolation. Transpl Int (2020).

92. Tyanova, S., et al. The Perseus computational platform for comprehensive analysis of (prote)omics data. Nat Methods 13, 731-740 (2016).

93. Huang da, W., Sherman, B.T. & Lempicki, R.A. Systematic and integrative analysis of large gene lists using DAVID bioinformatics resources. Nat Protoc 4, 44-57 (2009).

94. Deutsch, E.W., et al. The ProteomeXchange consortium in 2020: enabling 'big data' approaches in proteomics. Nucleic Acids Res 48, D1145-D1152 (2020).

95. Perez-Riverol, Y., et al. The PRIDE database and related tools and resources in 2019: improving support for quantification data. Nucleic Acids Res 47, D442-D450 (2019).

Chapter 2 Supplemental Information

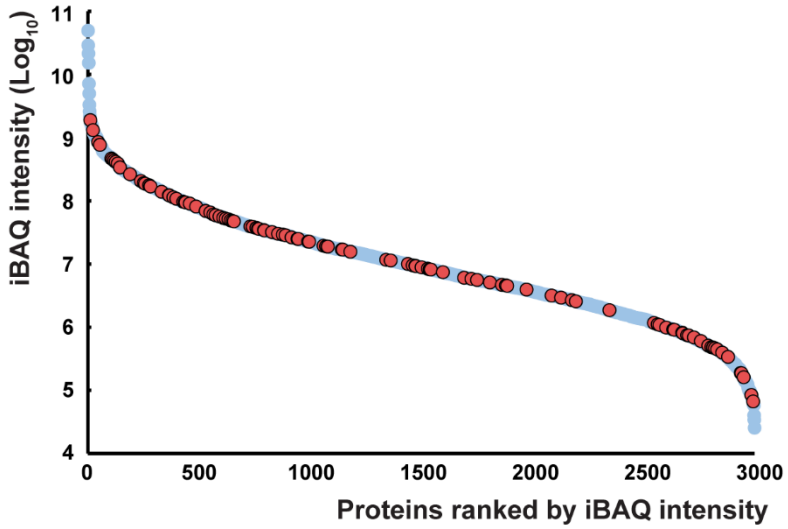

Chapter 2 Supplemental Fig. 1 Dynamic intensity range of identified proteins in adult groups. Proteins identified in young and older adult groups are ranked and plotted from high to low based on iBAQ (Intensity Based Absolute Quantification) intensities. All quantified ECM proteins are highlighted in closed red circles. Detailed information is provided in “Source Data”.

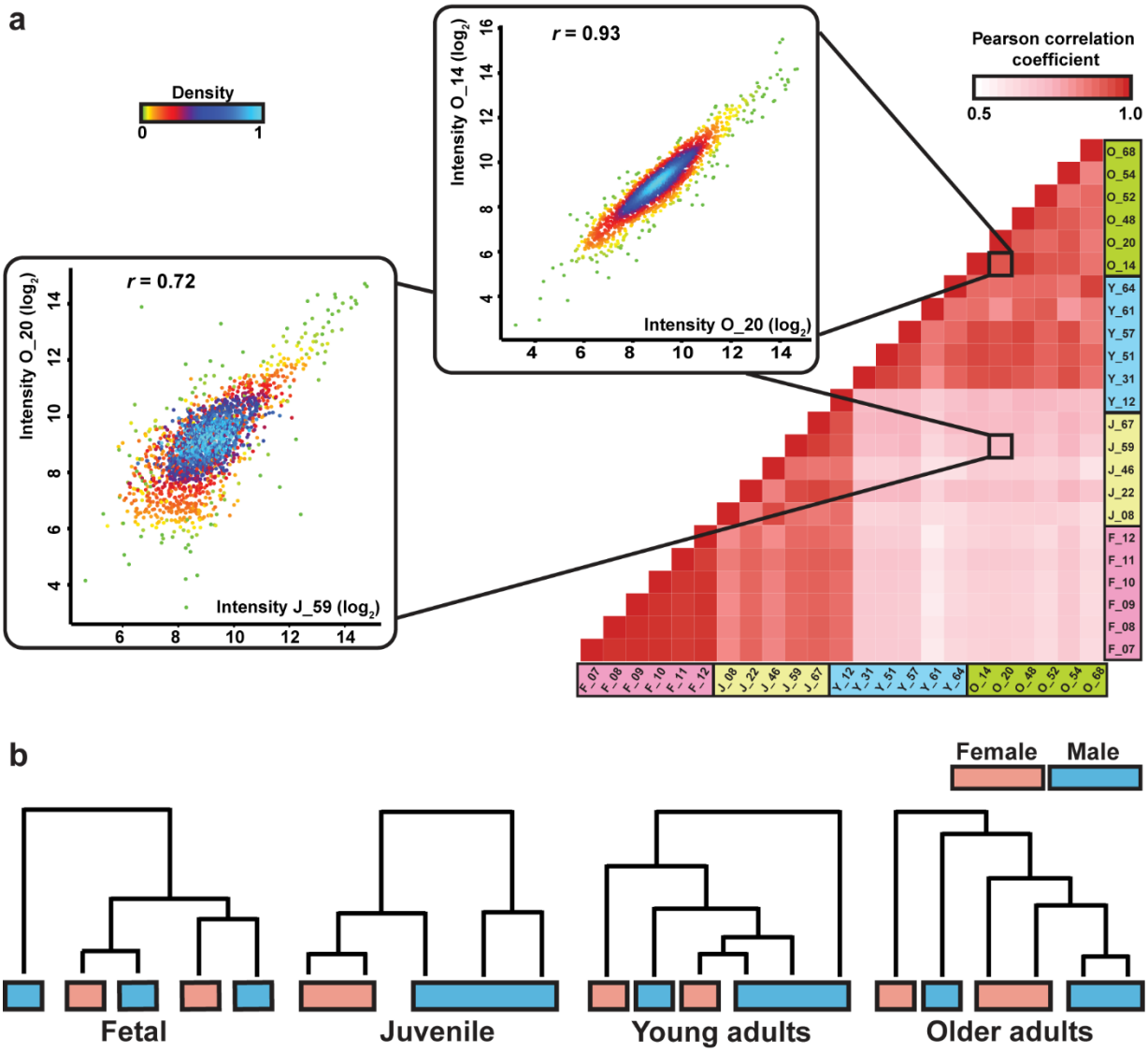

Chapter 2 Supplemental Fig. 2 Correlation between samples and gender differences across developmental groups. a) Pearson correlation analysis of protein intensity in all samples from four age groups. Color coding of each box in the heatmap indicates the Pearson correlation coefficient between the column- and row-indexed samples. Density plots illustrate the intensity correlation of two representative pairs with a good correlated one from two samples in the same age group and a poor correlated one from two samples at different stages. **b)** Dendrograms generated from hierarchical clustering in different groups.

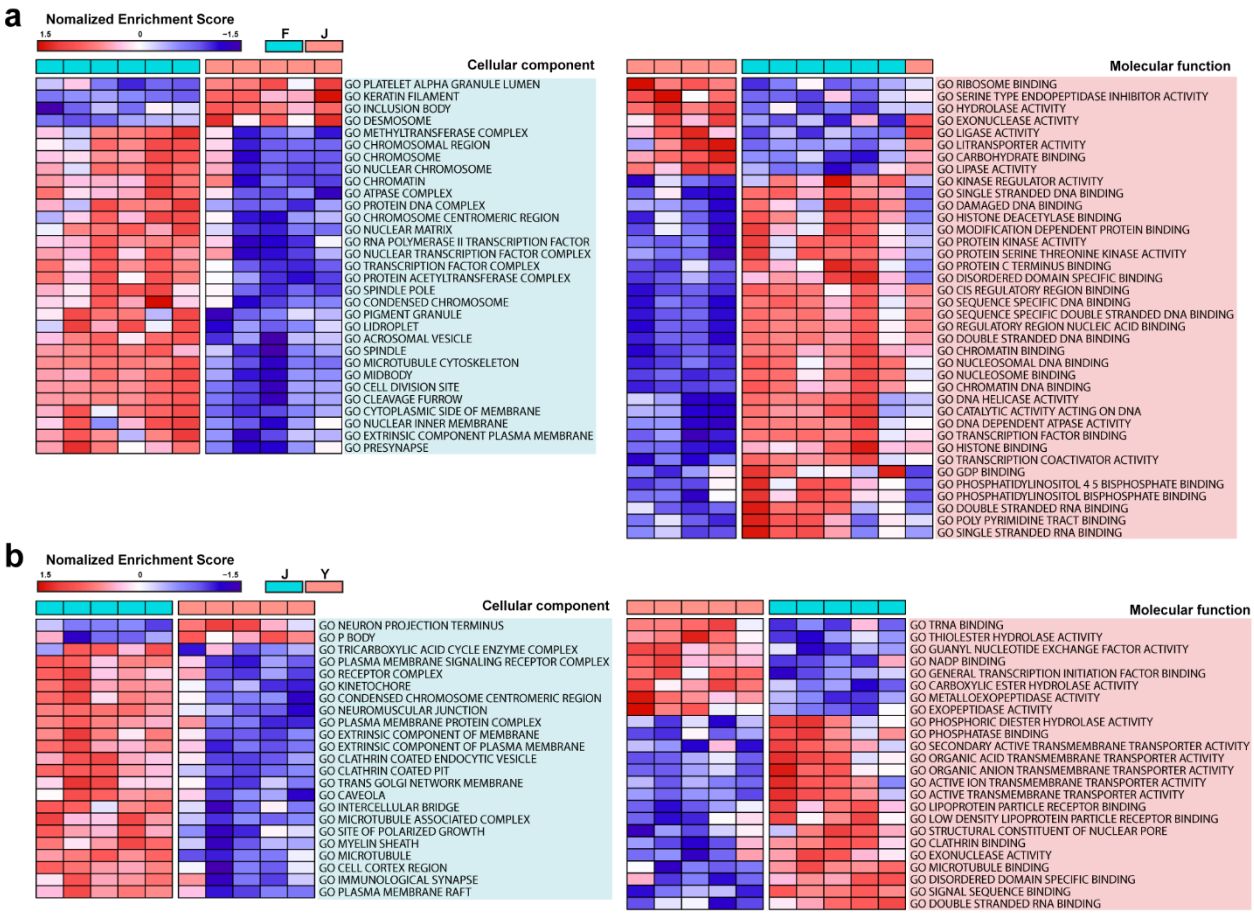

Chapter 2 Supplemental Fig. 3 GSVA analysis in juvenile compared to fetal and young adult compared to juvenile. GSVA analysis showing the significantly changed (two-sided *t* test, *p* value < 0.05, *p* values were adjusted by Benjamini-Hochberg correction for multiple comparisons) cellular components and molecular functions in juvenile versus fetal (**a**) and young adult versus juvenile (**b**). Color coding of the heatmaps indicates normalized enrichment score in each sample. A full list of enriched terms including biological processes and transcription factor targets is available in **Supplementary Table 6**.

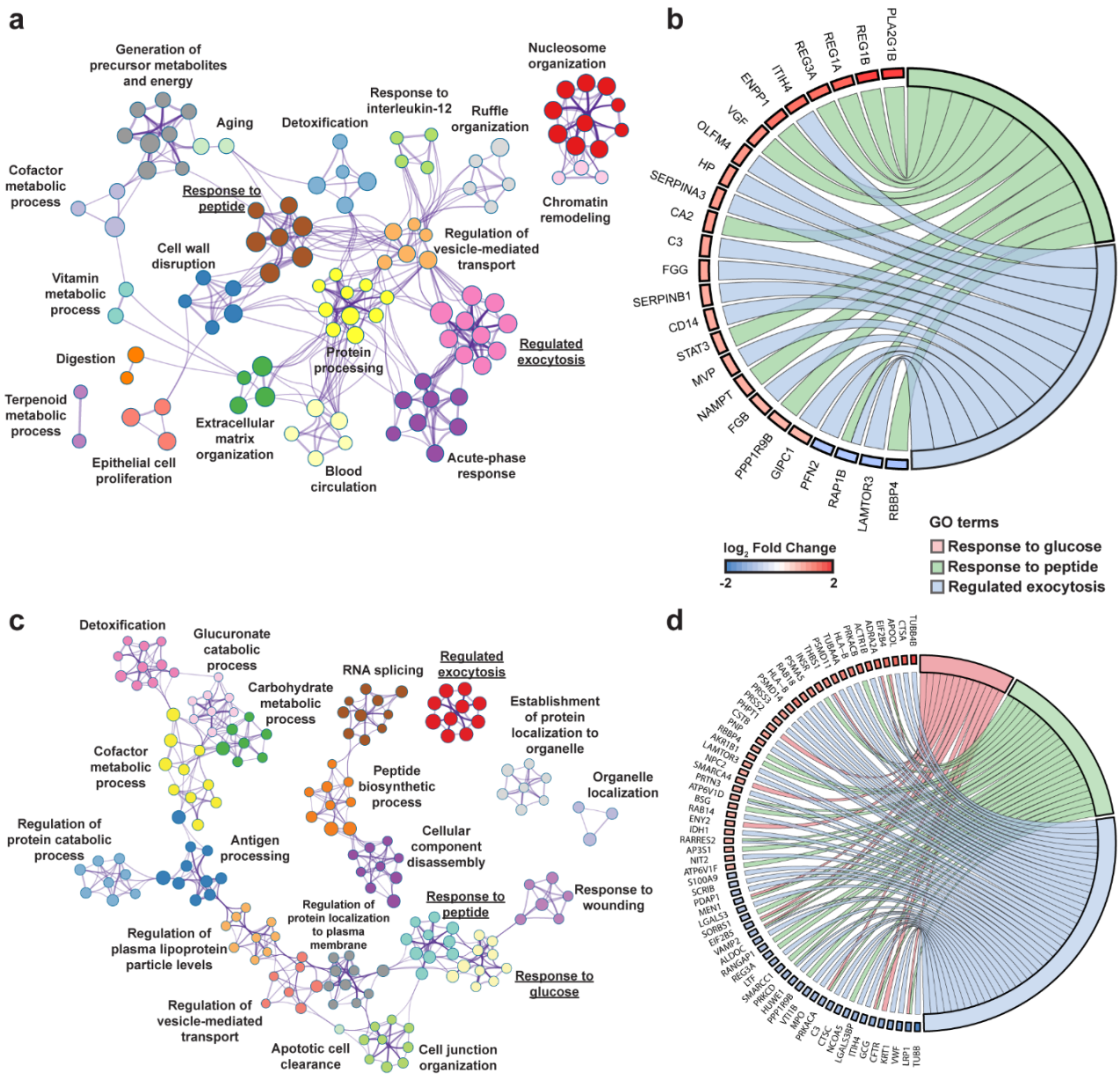

Chapter 2 Supplemental Fig. 4 Profiling differences in juvenile compared to fetal and young adult compared to juvenile. a) Network of biological processes enriched from significantly changed proteins (two-sided *t* test, *p* value < 0.05, *p* values were adjusted by Benjamini-Hochberg correction for multiple comparisons) in juvenile versus fetal. Each node refers to an enriched term and different terms are grouped into clusters based on their similarities while the most statistically significant term represents the cluster name. **b)** Proteins to biological process linkages in juvenile versus fetal. Genes are linked via ribbons to their assigned terms and blue-to-red coding next to the selected genes indicates their fold changes. **c)** Network of biological processes enriched from significantly changed proteins (two-sided *t* test, *p* value < 0.05, *p* values were adjusted by Benjamini-Hochberg correction for multiple comparisons) in young adult versus juvenile. **d)** Proteins to biological process linkages in young adult versus juvenile.

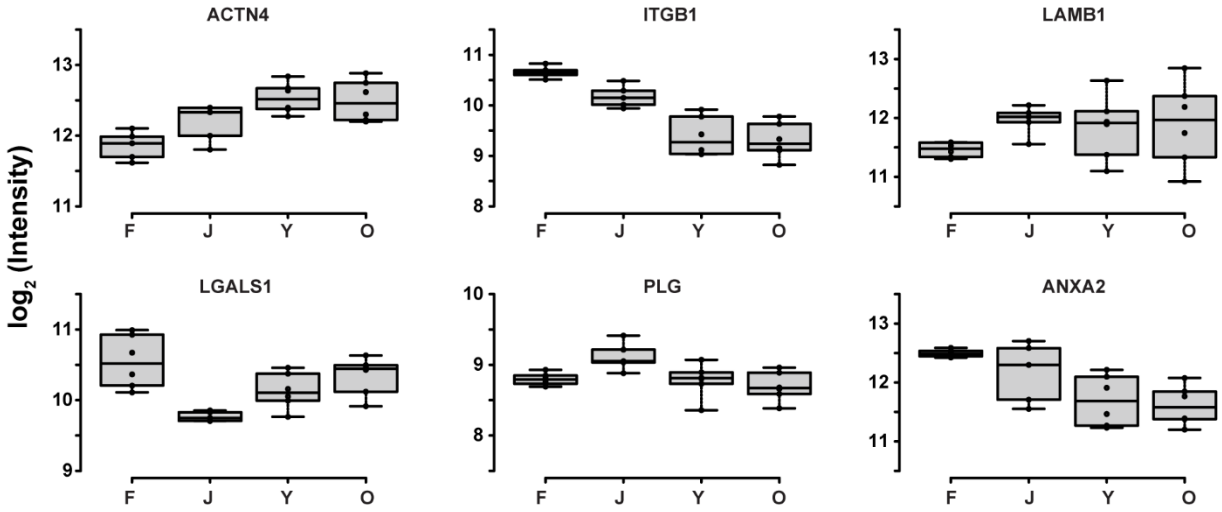

Chapter 2 Supplemental Fig. 5 Protein expression level changes of previously reported pancreatic cancer biomarkers. Box plots showing expression levels of selected proteins at different developmental stages. Dots within boxes indicate replicate data points. All boxplots indicate median (center line), 25th and 75th percentiles (bounds of box), and minimum and maximum (whiskers).

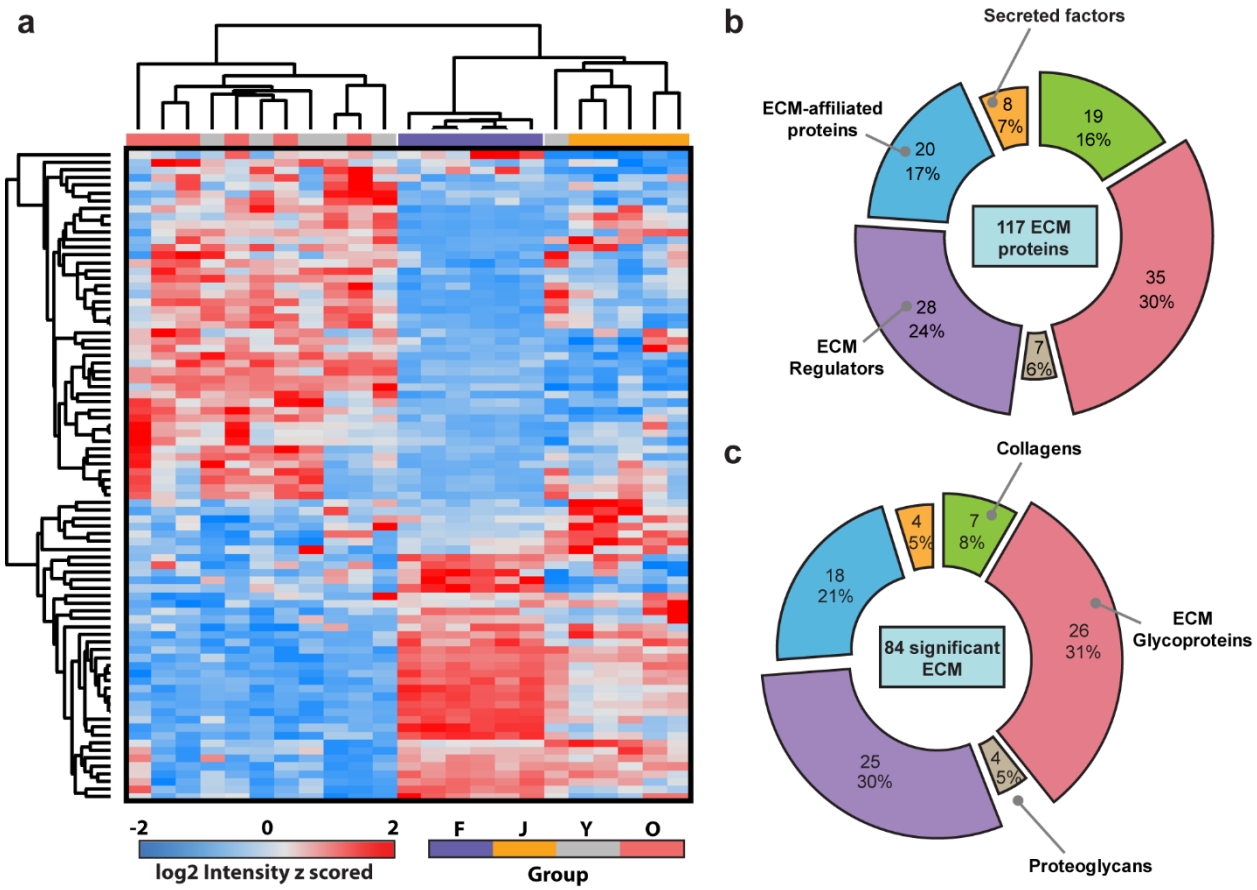

Chapter 2 Supplemental Fig. 6 ECM profile alterations across various developmental stages. a) Hierarchical clustering of DiLeu reporter ion intensities of 84 significantly changed ECM proteins (one-way ANOVA, FDR 0.05). **b)** Pie chart showing the number and proportion of each category of all quantified ECM proteins. **c)** Pie chart showing the number and proportion of each category of significantly changed ECM proteins in **a**.

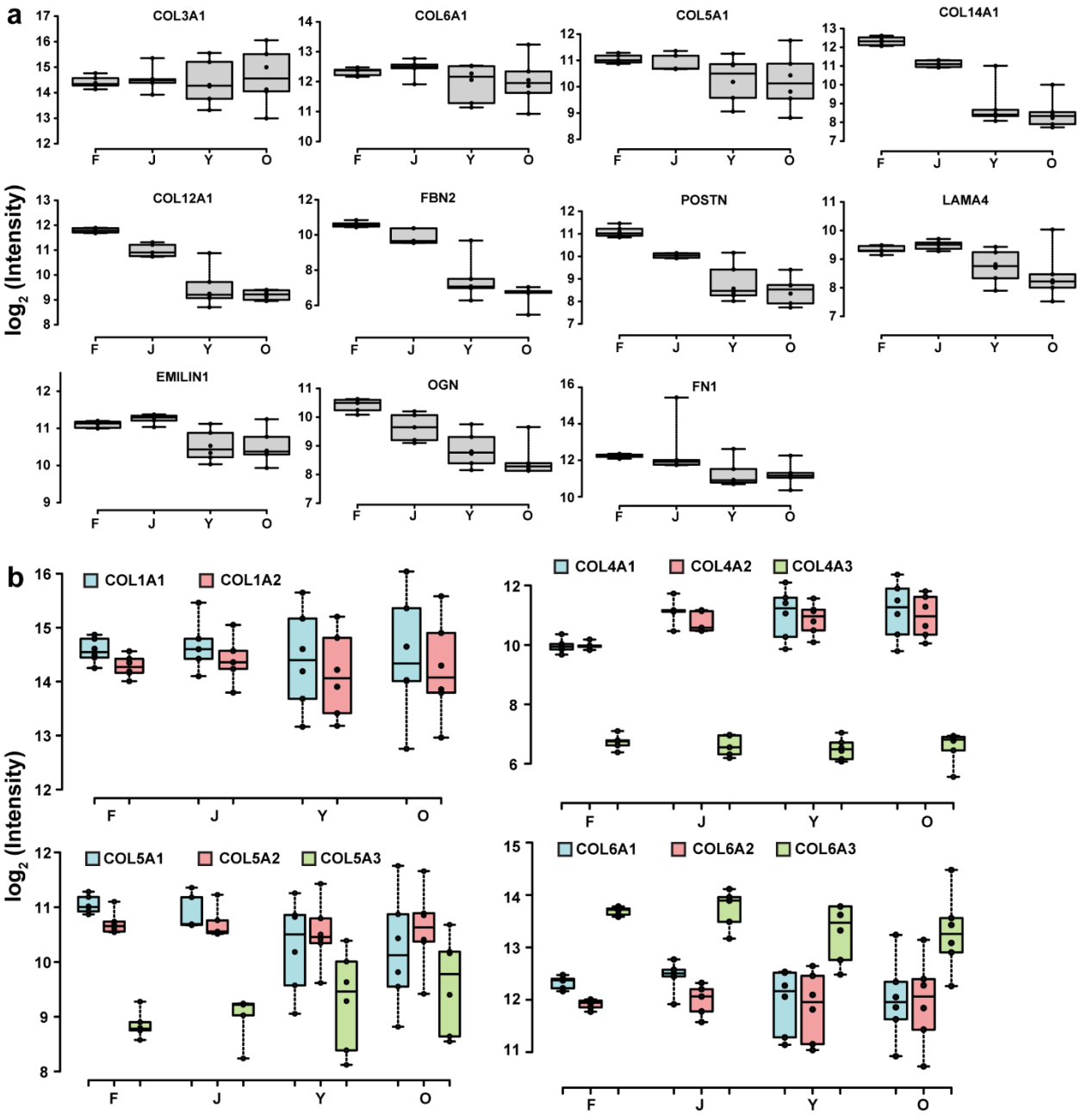

Chapter 2 Supplemental Fig. 7 ECM remodeling of human pancreata across developmental stages. Box plots showing expression levels of selected ECM proteins (**a**) and different chains of the same collagen molecule (**b**) at different developmental stages. Dots within boxes indicate replicate data points. All boxplots indicate median (center line), 25th and 75th percentiles (bounds of box), and minimum and maximum (whiskers).

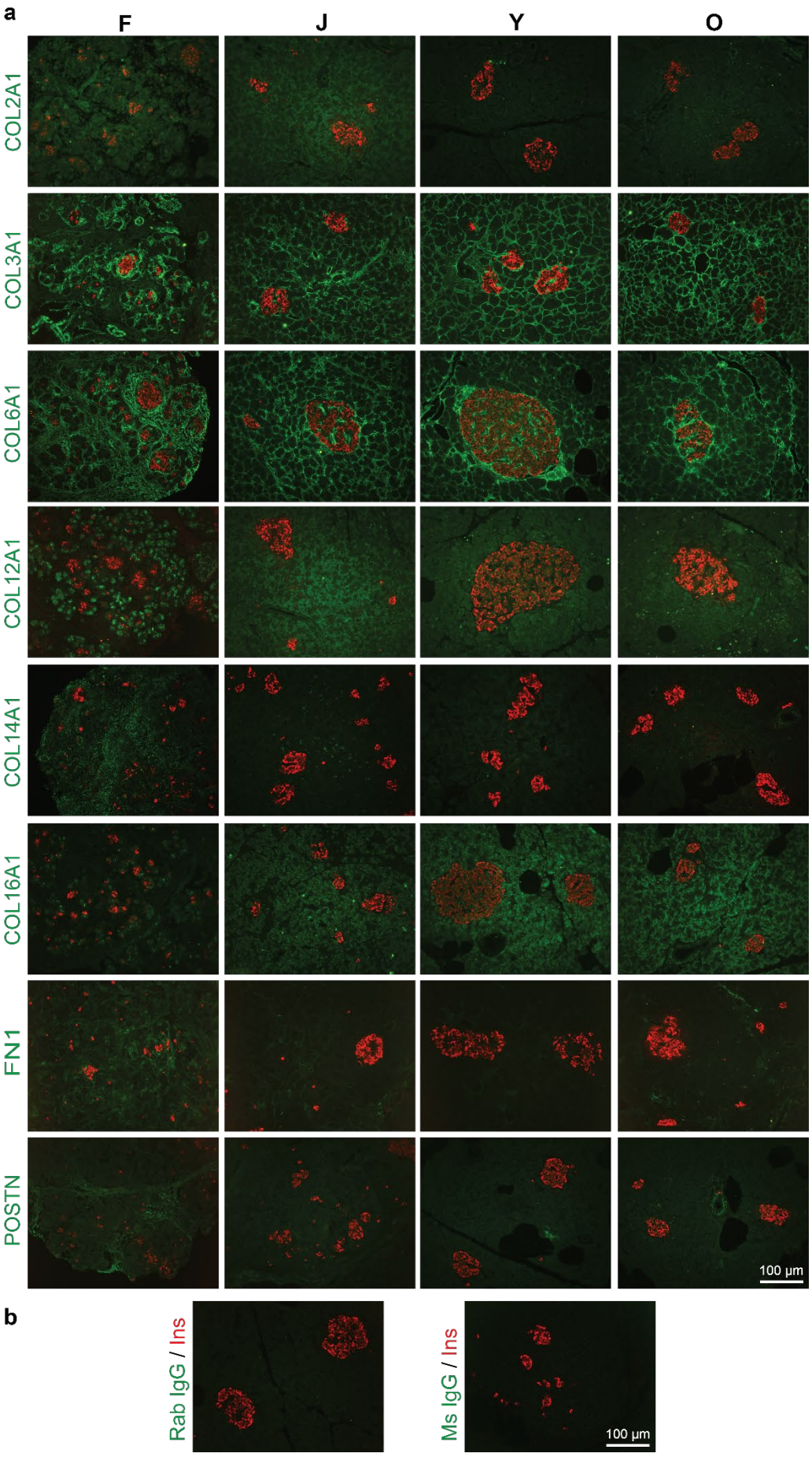
a
F
J
Y
O
COL2A1
COL3A1
COL6A1
COL12A1
COL14A1
COL16A1
FN1
POSTN
100 µm
b
Rab IgG / Ins
Ms IgG / Ins
100 µm

Chapter 2 Supplemental Fig. 8 Visualizing ECM proteins in human pancreata across developmental stages. a) Immunofluorescent images of ECM proteins (green) co-stained with insulin (red) in fetal (F), juvenile (J), young adult (Y) and older adult (O) pancreata. Qualitative trends in protein levels corroborate MS data. Representative images are shown, images were taken for N=3 donors per developmental group. **b)** IgG isotype control images with rabbit or mouse IgG (green) indicate low levels of non-specific signal, N=3 donors. Scale bar = 100 microns. **(Previous Page)**

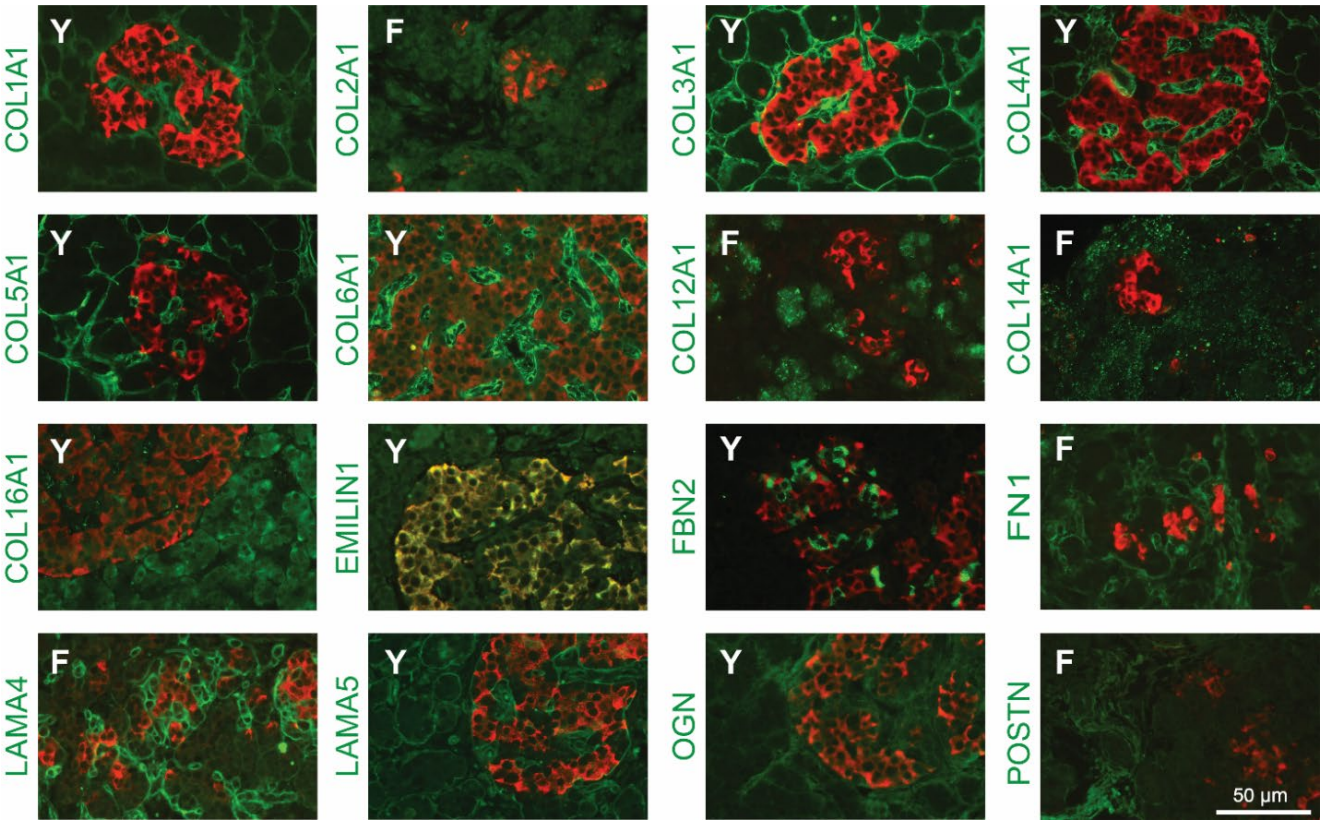

Chapter 2 Supplemental Fig. 9 Cellular localization of ECM proteins in pancreatic islets. Enlarged images of immunofluorescent staining for ECM proteins (green) within human pancreatic islets (insulin = red). Images represent either fetal (F) or young adult (Y) donors as indicated, selected based on which age had higher intensity staining for each protein. Images clearly show differences in subcellular localization; most ECM proteins are expressed extracellularly while some proteins (such as EMILIN1 and FBN2) appear to be expressed intracellularly. Scale bar = 50 microns. Representative images shown, from N=3 donors per developmental group.

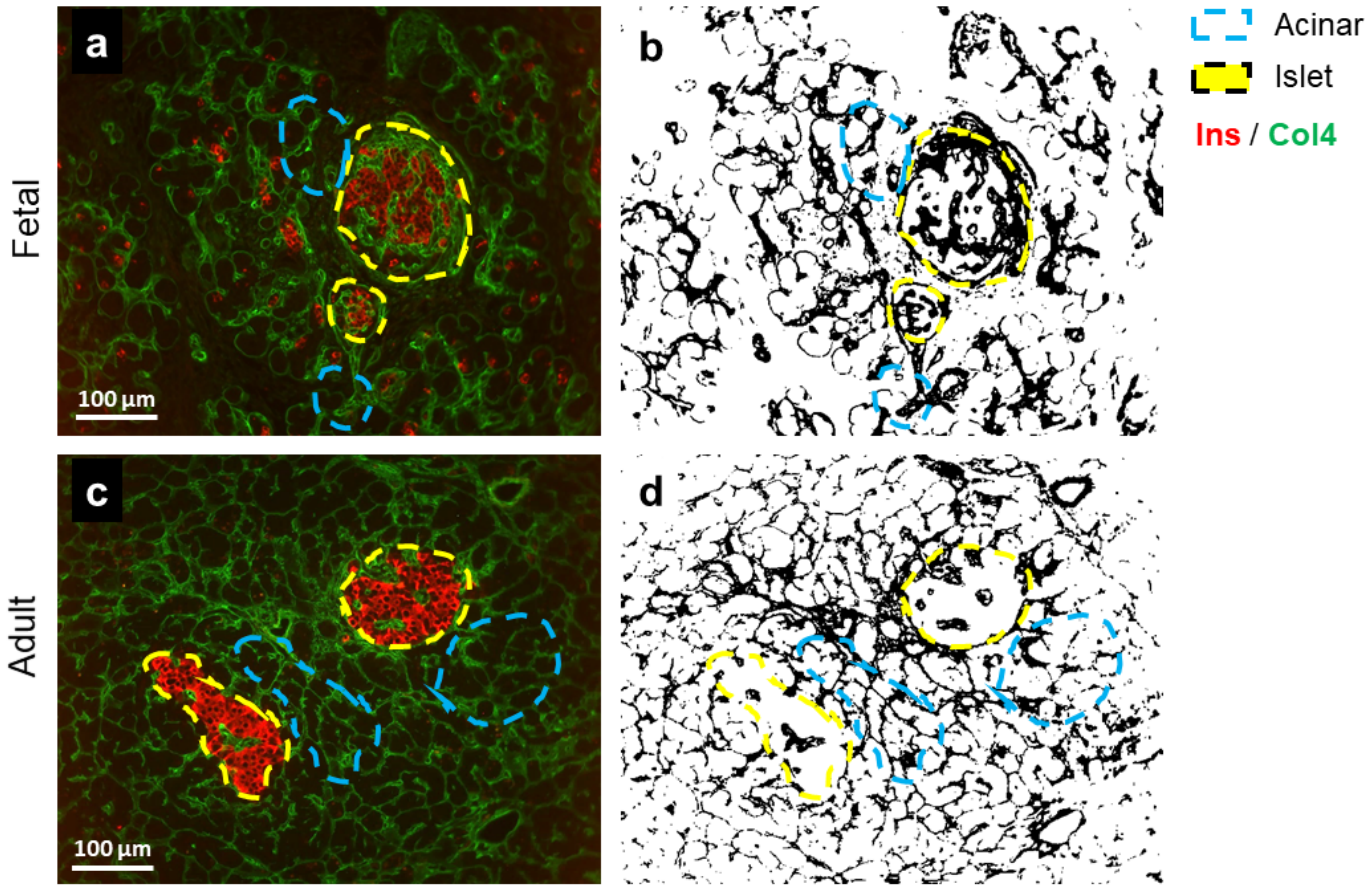

Chapter 2 Supplemental Fig. 10 Method for quantification of Islet/Acinar Ratios. Immunofluorescent images of ECM proteins (green) co-stained with insulin (red) were analyzed using ImageJ software by tracing islets (red stain, yellow dashed line) and acinar (not red, morphologically determined, blue dashed line) in the original images **(a**, **c)**, and measuring the intensity of the ECM signal on adjusted binary images **(b**, **d)**. Representative images of fetal and adult tissue are shown for comparison. Scale = 100 microns. Representative images shown, from N=3 donors per developmental group.

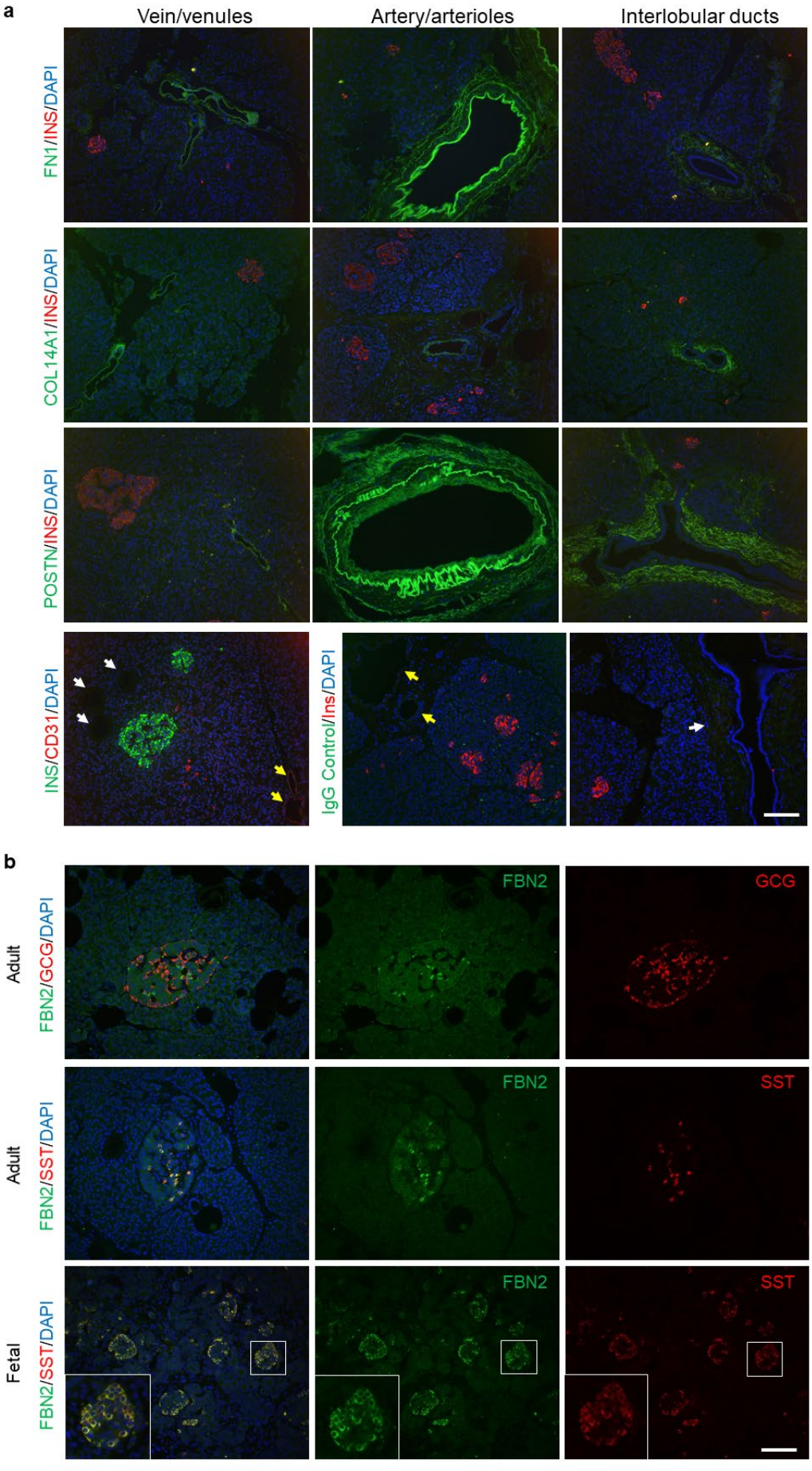
a
Vein/venules
Artery/arterioles
Interlobular ducts
FN1/INS/DAPI
COL14A1/INS/DAPI
POSTN/INS/DAPI
INS/CD31/DAPI
IgG Control/Ins/DAPI
b
Adult
FBN2/GCG/DAPI
FBN2
GCG
Adult
FBN2/SST/DAPI
FBN2
SST
Fetal
FBN2/SST/DAPI
FBN2
SST

Chapter 2 Supplemental Fig. 11 Localization of ECM proteins in specific regions of the pancreas. **a)** Immunofluorescent staining for ECM proteins (FN1, COL14A1, POSTN = green) which had very low levels of signal in islets (Insulin = red) and acinar regions, but relatively high total protein content. These proteins were mainly found to be expressed in vessels and ducts. Control images indicate low levels of autofluorescence in the ducts (white arrows) and vessels (identified in red with positive CD31 staining; yellow arrows) when stained with an insulin antibody in green, or when stained with an IgG isotype control. **b)** Immunofluorescent staining of endocrine markers (GCG, alpha cells = red) (SST, delta cells = red) indicating that FBN2 co-localizes with delta cells, in both fetal and adult islets. Scale bars = 100 microns. Representative images shown, from N=3 donors per developmental group. **(Previous Page)**

Chapter 2 Supplemental Tables can be accessed online:

https://www.nature.com/articles/s41467-021-21261-w#Sec18

Chapter 3

Extracellular matrix scaffold and hydrogel derived from decellularized and delipidized human pancreas.

Chapter 3 Graphical Abstract

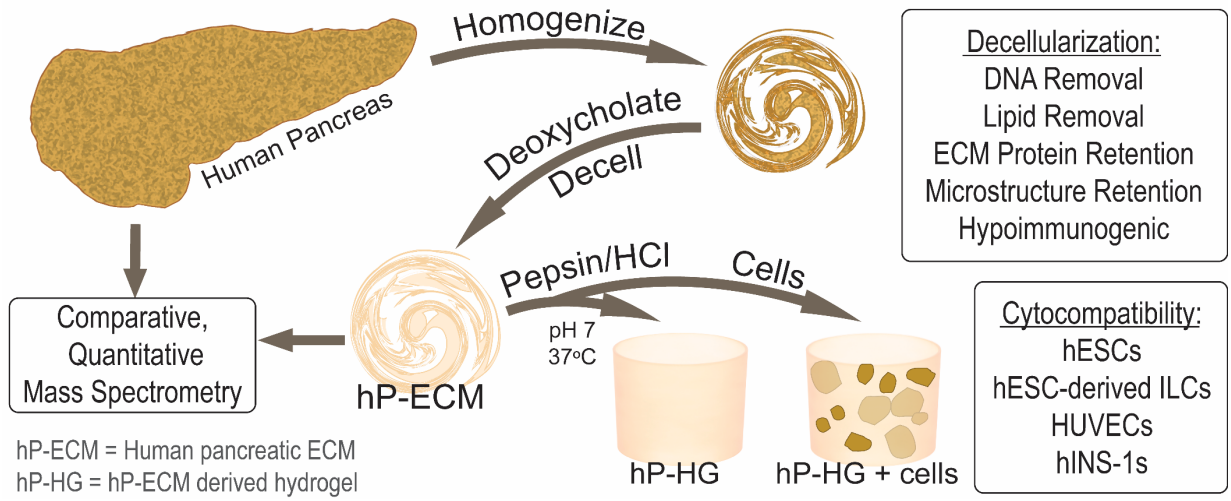

This chapter was adapted from the paper published as: Sackett SD* and Tremmel DM*, Ma F, Feeney A, Maguire R, Brown ME, Zhou Y, Li X, O'Brien C, Li L, Burlingham W, Odorico JS. Extracellular matrix scaffold and hydrogel derived from decellularized and delipidized human pancreas. Scientific Reports. 2018, Jul 11; 8(1):10452. doi: 10.1038/s41598-018-28857-1. (*Co-first authors) PMID: 29993013

Daniel Tremmel, Sara Dutton Sackett and Jon Odorico conceived and designed the study. Daniel Tremmel and Sara Dutton Sackett performed the experiments with the help of Fengfei Ma, Matthew Brown, Ying Zhou, Rachel Maguire, Austin Feeney, Xiang (Grace) Li and Corey O'Brien. Daniel Tremmel and Sara Sackett prepared figures and wrote the manuscript. Jon Odorico and Lingjun Li edited the manuscript. Fengfei Ma and Lingjun Li contributed to the mass spectrometry-based ECM proteomics analysis. William Burlingham contributed to the experimental design for the humanized mouse development. Sara Dutton Sackett and Jon Odorico supervised and directed the research.

Abstract

Extracellular matrix (ECM) plays an important developmental role by regulating cell behaviour through structural and biochemical stimulation. Tissue-specific ECM, attained through decellularization, has been proposed in several strategies for tissue and organ replacement. Decellularization of animal pancreata has been reported, but the same methods applied to human pancreas are less effective due to higher lipid content. Moreover, ECM-derived hydrogels can be obtained from many decellularized tissues, but methods have not been reported to obtain human pancreas-derived hydrogel. Using novel decellularization methods with human pancreas we produced an acellular, 3-D biological scaffold (hP-ECM) and hydrogel (hP-HG) amenable to tissue culture, transplantation and proteomic applications. The inclusion of a homogenization step in the decellularization protocol significantly improved lipid removal and gelation capability of the resulting ECM, which was capable of gelation at 37˚C *in vitro* and *in vivo*, and is cytocompatible with a variety of cell types and islet-like tissues *in vitro*. Overall, this study demonstrates the characterisation of a novel protocol for the decellularization and delipidization of human pancreatic tissue for the production of acellular ECM and ECM hydrogel suitable for cell culture and transplantation applications. We also report a list of 120 proteins present within the human pancreatic matrisome.

Introduction

Biological scaffolds derived from extracellular matrix (ECM) have been widely utilised in regenerative medicine [1-3 and references therein]. The ECM is an essential non-cellular component of the tissue microenvironment, comprised of a network of macromolecules

including polysaccharide glycosaminoglycans (GAGs) and proteins such as collagens, laminins, and fibronectin [2, 4]. In addition to providing structural support to cells, ECM can guide cell migration, proliferation, differentiation and maturation throughout development as well as influence cell function and differentiation *in vitro* [5-9]. Scaffolds designed for tissue engineering ideally include these ECM ligands to mimic cues within the native microenvironment. To obtain natural ECM, various organs and tissues have been decellularized, via a number of techniques utilizing chemical, enzymatic, or mechanical disruption. Decellularization protocols can be designed to address factors such as tissue density, cellularity and lipid content [1, 10]. This is especially important for tissues containing fats such as bone [11], adipose [12], and brain [13], for which decellularization has been combined with a delipidization step, but this process has not been reported for the human pancreas.

Worldwide it is estimated that 387 million people have diabetes and this number is expected to increase by 53% to 592 million by 2035 [14, 15]. Despite continuing advances in insulin delivery technology and recombinant insulins, diabetes and its complications still claim the lives of millions of people, largely due to imperfect long-standing glycemic control resulting in end-organ complications. On the other hand, beta cell replacement therapies including whole vascularized pancreas transplantation or the transplantation of isolated islets of Langerhans are able to fully restore normoglycemia, achieve insulin-independence and can delay end-organ complications [16-18]. However, these therapies suffer from several key limitations: the shortage of organs, inconsistent quality of donor organs, and the need for life-long immunosuppression to prevent allograft rejection [19, 20]. Many envision a tissue engineering solution, via merging a

beta cell source, such as stem cell-derived beta cells, with other cellular and matrix components including natural ECM or biomimetic scaffolds, to address this pressing clinical problem.

The composition and organization of ECM varies from tissue to tissue [21, 22], however the basic function of all ECM is to provide support for the tissue and ligands for cellular attachment. The relationship between cells and ECM in developing organs is a complex and continuous interplay; cells synthesize and deposit macromolecules that influence the growth and remodeling of the organ, and the deposited ECM supports cell survival, function and organization throughout life. For example, data show that cell-matrix interactions are important for mature beta cells to remain functional and avoid apoptosis [23], as well as for maintaining a functional beta cell mass [reviewed in 24]. The ECM in the periphery of the islet has been reported to contain collagen I, III, IV, V and VI, as well as laminin and fibronectin [24]. Convincing data show that islets are often stripped of a large amount of their ECM and dense vascular networks during the isolation process [25-28]. Moreover, islets which retain some of their ECM following isolation exhibit reduced rates of apoptosis and maintain significantly better functional insulin responses than do more aggressively purified islets [29]. Tissue specific ECM sources would provide cellular environments that closely recapitulate the in vivo milieu by harnessing the distinctive properties and therefore provide a potential platform for tissue engineering that can specifically enhance the cells ability to function more similarly to that of the original tissue.

Surprisingly, many human pancreata are discarded after recovery from cadaveric donors, which represents a lost precious resource. Presently in the US, only ~17% of donor pancreata are recovered and transplanted [30-32] and ~25% of those recovered with intent to transplant are discarded [32]. While there are multiple reasons for not recovering pancreata or not

transplanting after recovery, numerous organs are available for research through organ procurement organizations. We suggest that these pancreata be utilized to study the composition of the human pancreatic ECM, and potentially be used for bioengineering and regenerative medicine purposes. Donor selection is very stringent for pancreas transplant, and as a result many are declined based on medical history, fibrosis, fat deposition and other conservative practices [33] even though the pancreas is healthy and functional. These pancreata could be decellularized, processed to construct biomaterials, such as hydrogels, and used for tissue engineering applications rather than be discarded. Hydrogels are versatile materials possessing a number of potential applications, including 2-D and 3-D scaffolds for cell culture, in which cells can be plated on or embedded within the gel. However, the high lipid content of non-transplantable human pancreata has posed a barrier to achieving adequate decellularization and hydrogel formation using methods that are typically sufficient for decellularizing lean organs and tissues.

The objectives of this study were to develop methods for efficient decellularization and delipidization of human pancreata and to produce a hydrogel amenable to tissue culture and transplantation applications. We describe a novel method to effectively decellularize and remove lipids from human pancreata and have characterized the composition and structure of the acellular human pancreatic ECM (hP-ECM). Furthermore, we demonstrate its ability to form a hydrogel (hP-HG) and use as a viable cell culture platform which sustains cell growth/viability in *in vitro* and *in vivo* environments.

Results

Human pancreas decellularization and hydrogel formation

Discarded, non-diabetic human pancreata were decellularized by either a spin-decell or a homogenization-decell protocol, as outlined in Figure 1. The spin-decell protocol, in which 1 cm3 pieces of tissue are incubated in detergent, was compared to the homogenization-decell protocol, in which pancreas is first homogenized and centrifuged to remove extricated insoluble fat, and then incubated in detergent. The resulting human pancreatic ECM (hP-ECM) from both protocols was analyzed for lipid removal (Fig. 2). We found that homogenization prior to deoxycholate treatment resulted in a much more complete lipid removal than was achieved by spin-decell. Lipid content was qualitatively assessed with Oil Red O staining (Fig. 2a-c) and quantified with a modified Folch protocol (Fig. 2b). We found on average that native undecelled donor pancreata contain about 38 ±3.6% lipids by dry weight. hP-ECM derived with the spin protocol contained 13.6 ±3.0% lipids, whereas hP-ECM derived with the homogenization protocol contained 3.9 ±1.1% (Mean ±SD) (Fig. 2-D), significantly lower than without homogenization. An additional 5-hour lipase treatment (150 U/mL) was tested following the deoxycholate, but we found that lipase treatment did not significantly enhance delipidization and in some cases had a negative effect on hydrogel formation (data not shown), so was not pursued further.

Following decellularization, hP-ECM was lyophilized and pepsin digested in the preparation of a human pancreatic hydrogel (hP-HG) (Fig. 1). In addition to the generation of hydrogel, the decellularized hP-ECM material can be fabricated into 3-D scaffolds with a variety of shapes for use in composite cell-matrix applications (Fig. S1).

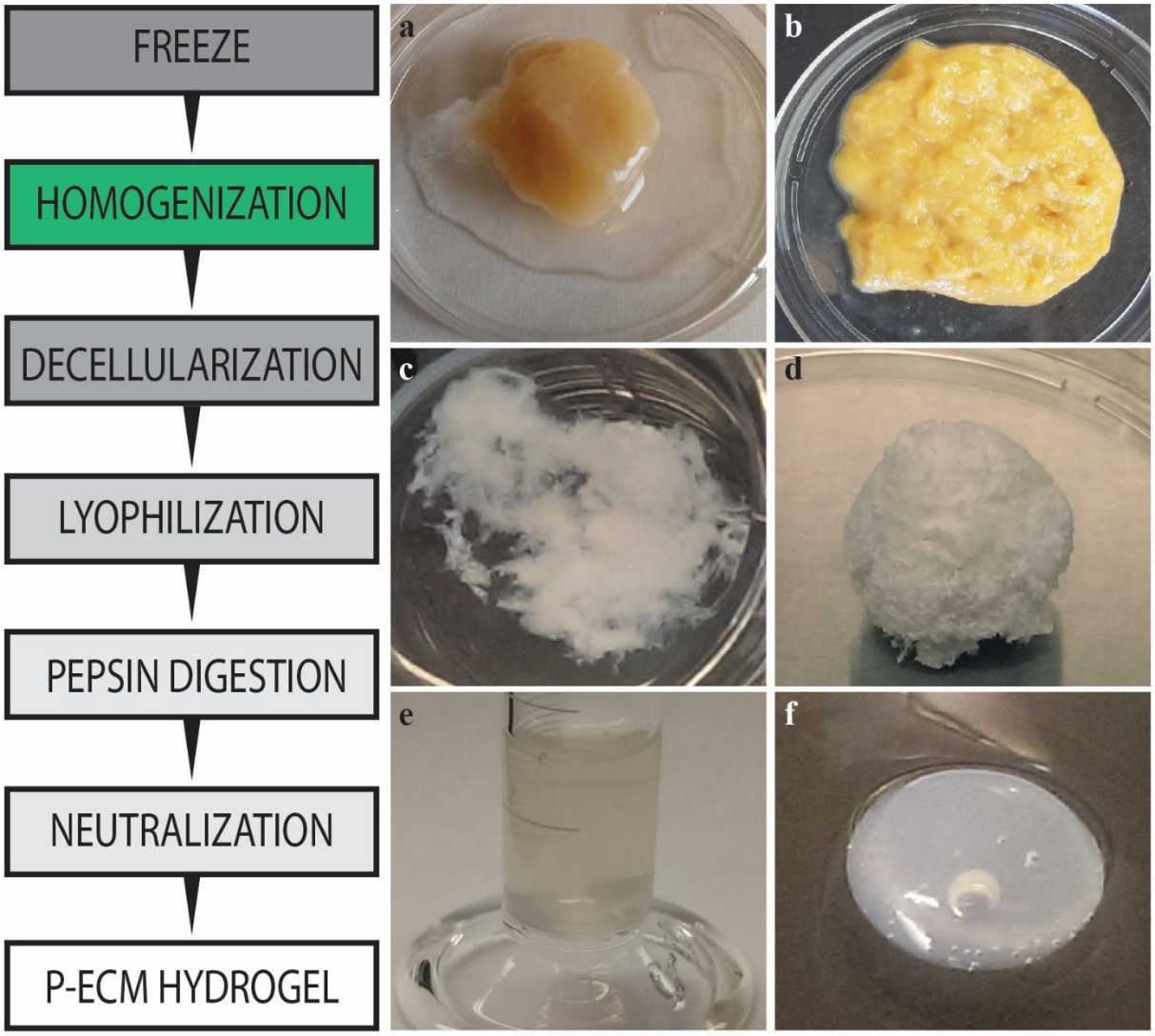

Figure 1. Schematic representation of the preparation of a decellularized ECM hydrogel from pieces of human pancreas. Native tissue is frozen and thawed (**a**), then homogenized (**b**) and decellularized with deoxycholate (**c**). The resulting acellular matrix is lyophilized (**d**) and digested in pepsin/HCl to create a solubilized pancreatic matrix which is liquid at 4°C (**e**). Following neutralization and warming to 37˚C the hydrogel material self-assembles into a fibrous 3D gel (**f**).

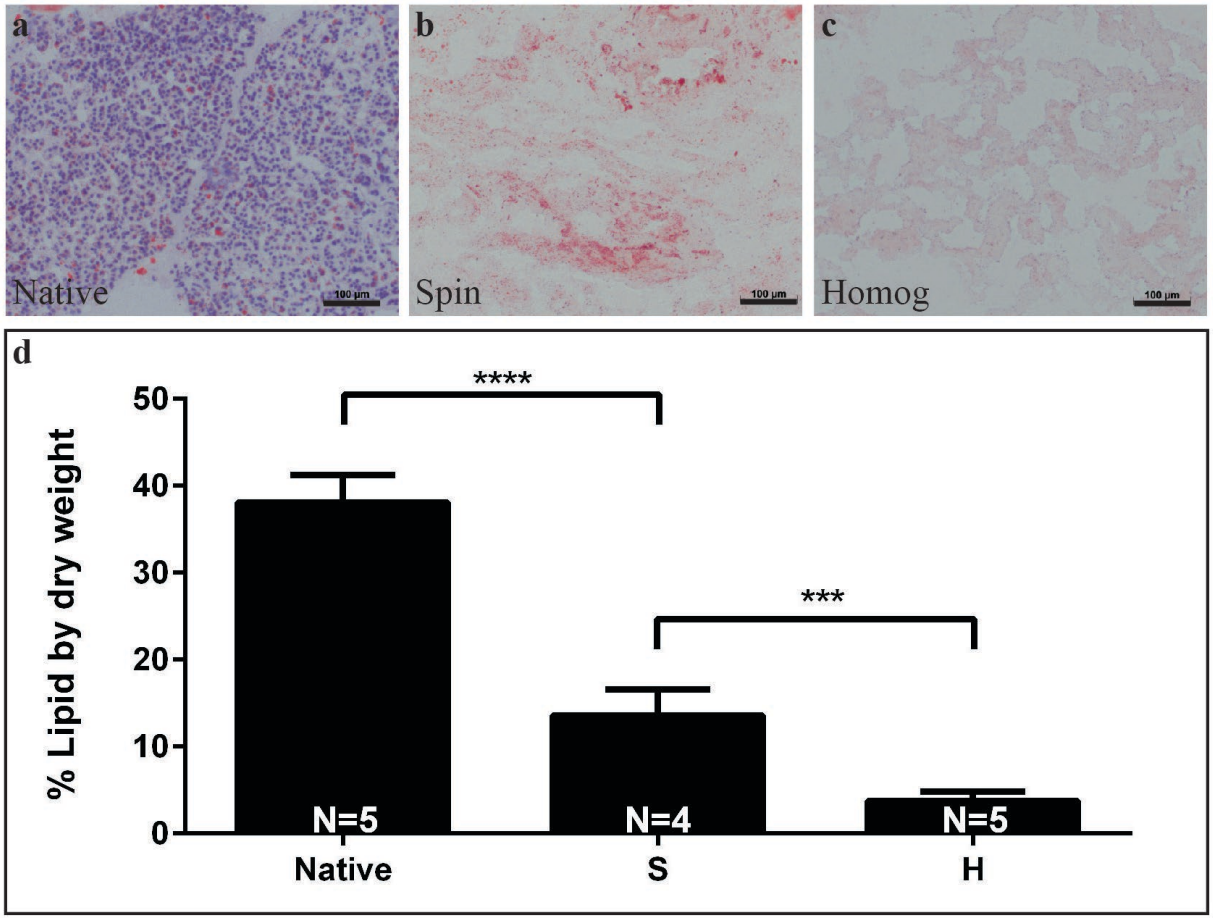

Figure 2. Homogenization improves delipidization. Delipidization was assessed by Oil Red O staining (ORO) on native, and decellularized tissues (**a-c**) and quantification of lipid content per mg dry weight utilizing the Folch method (**d**). (**a**) Native tissue contains a high amount of fat as shown by ORO staining, and tissue decellularized through spin (S) retains much of the fat content (**b**), while tissue decellularized with homogenization (H) has significantly reduced fat content (**c**). Scale bar represents 100µm. N=4-5 biological replicates per group.

Turbidimetric gelation kinetics

Gelation kinetics of hP-HG were characterized through turbidimetric analysis at a 405 nm wavelength and compared to that of purified collagen I hydrogel. hP-HG gels derived from homogenization-decell (Gels 1 and 2) were compared to gels derived from spin-decell (Gels 3 and 4). The normalized absorbance values of hP-HG alongside collagen I hydrogel are shown in Figure 3a, along with the corresponding calculated parameters, shown in Figure 3b. Homogenization-

decelled hP-HG exhibited a sigmoidal curve in the gelation assay, similar to that of collagen I, but with a lag time of about 5-6 minutes, shorter than the 10-15 minute lag time of collagen. Despite the shorter lag time, the gelation speed (S) is slower than collagen gel, while the t1/2 itself was similar between collagen I and hP-HG. This indicates that hP-HG begins to gel more rapidly than collagen when heated to 37˚C, but takes the same overall time to reach complete gelation. In

a

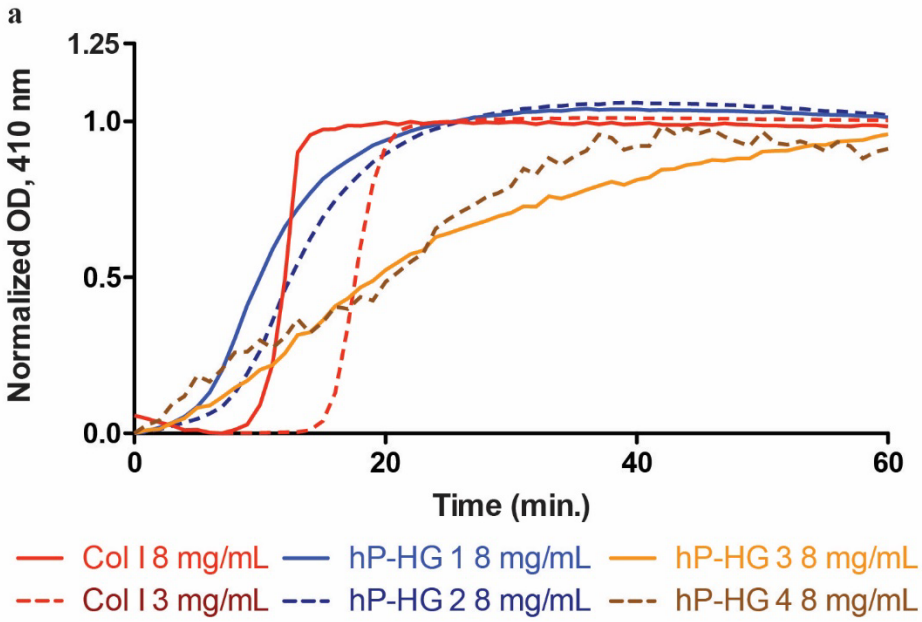

b

Material	S	$T_{1/2}$	T_{lag}
Col I 8 mg/mL	0.340	12	10.5
Col I 3 mg/mL	0.230	18	15.4
hP-HG-1 8 mg/mL	0.089	10	4.6
hP-HG-2 8 mg/mL	0.083	12.5	6.5
hP-HG-3 8 mg/mL	0.036	19.5	5.3
hP-HG-4 8 mg/mL	0.031	20.5	4.3

Figure 3. Homogenization improves gelation. Representative turbidimetric gelation kinetics of collagen I and hP-HG. **a**) Pre-gel solutions of collagen I, homogenization-decell (hP-HG 1&2) and spin-decell (hP-HG 3&4) were neutralized and added to the wells of a cold 96-well plate followed by incubation at 37˚C to induce gelation. **b**) The $T_{1/2}$ (time to 50% maximum absorbance), the speed of gelation (S) at $T_{1/2}$ (indicates gelation rate) and the T_{lag} (time to upslope) calculated from the turbidimetric gelation curves are indicated for each material. N=6 biological replicates for each protocol.

comparing hydrogels derived from the two described decellularization protocols, the spin-decell gels have a significantly slower gelation speed and a significantly longer time to t1/2. Further, these gels took longer to form and, in some instances, would not form gel at all.

Spin-decell hP-ECM generally contained visible fat in the interior of the decelled cubes, and following treatment with pepsin the digest remained cloudy and exhibited poor gelation characteristics (Fig. S2). We concluded from the lipid content and hydrogel turbidimetric data that the homogenization-decell protocol was more effective, demonstrating significant reductions in lipid content with superior hydrogel forming capability; therefore, all subsequent analyses focused on hP-ECM derived with the homogenization protocol, as well as hydrogel produced from this homogenized ECM.

Characterization of hP-ECM and hP-HG

The ECM and hydrogel obtained by the homogenization-decell protocol were analyzed for retention of DNA, sGAG and common ECM proteins. hP-ECM and hP-HG are devoid of nuclei as shown by H&E staining (Fig. 4b and c) compared to native pancreas (Fig. 4a). The DNA content of the decellularized pancreas was reduced to only 3.6% of the DNA content of native tissue, indicating that homogenization and deoxycholate treatment was successful at removing DNA (Fig. 4g). The DNA content of hP-HG was further reduced compared to that of hP-ECM and contained only 3.1% of the native tissue amount.

GAG content for each sample was analyzed using qualitative and quantitative methods to determine GAG retention following decellularization and hydrogel formation. The histochemical stain Alcian blue was used to visualize sGAG, molecules that participate in biochemical signalling, play structural roles within the ECM, and support hydration of ECM and hydrogels. Histological

examination of native pancreas shows positive sGAG staining throughout the parenchyma and more concentrated staining within islets. sGAG content appears to be retained in both hP-ECM and hP-HG as demonstrated by the presence of blue stain in the matrix (Fig. 4d-f). However, the

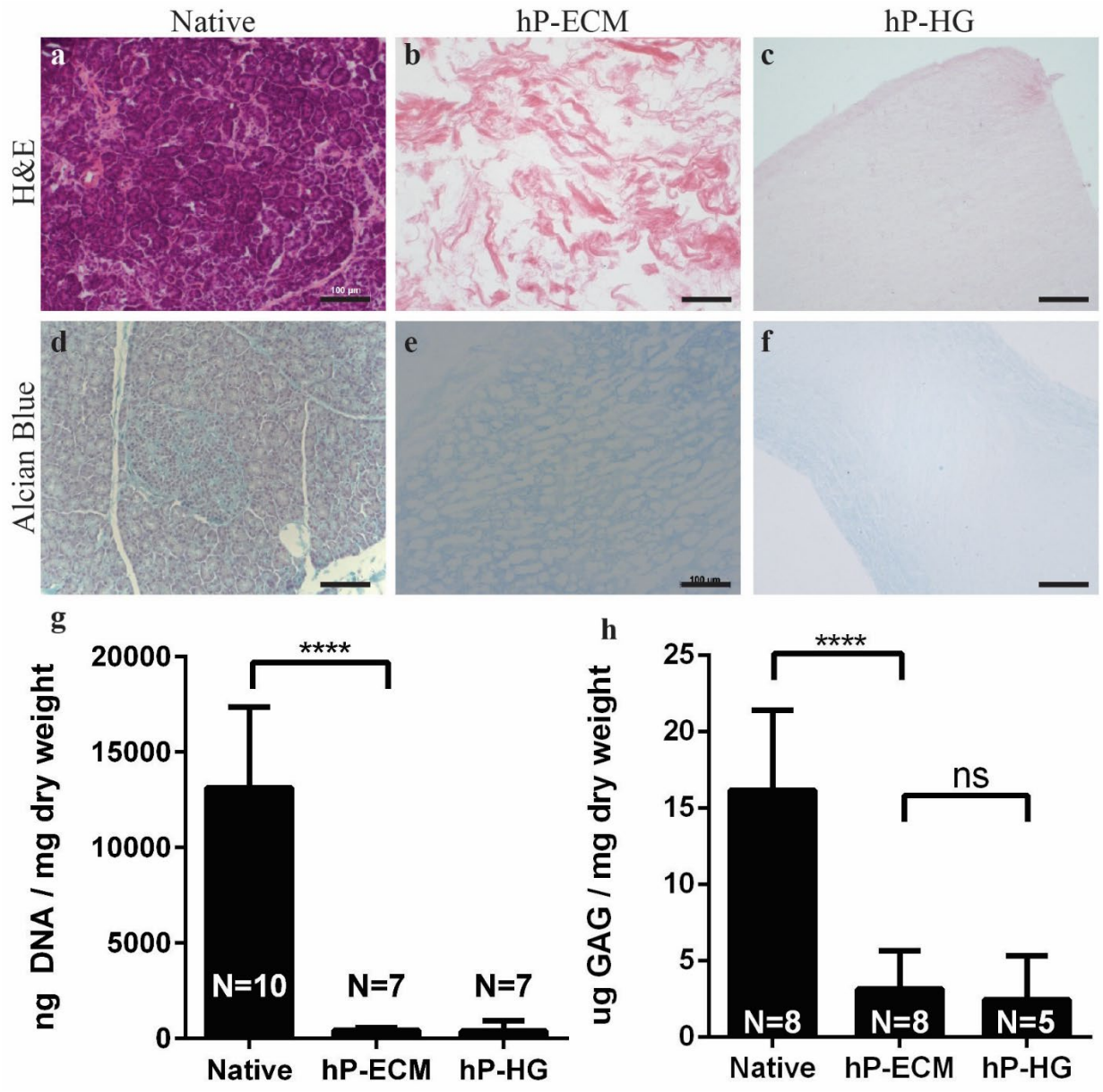

Figure 4. Characterization of pancreas decellularization. Representative images of human pancreas decellularization efficiency assessed qualitatively by H&E before and after decellularization (**a-c**) and quantitatively by PicoGreen Assay (**g**) in ng of DNA / mg dry tissue weight. Histologic evaluation by Alcian Blue (sGAG, blue) staining (**d-f**) and quantitatively (**h**) with biological analysis of ECM sGAG content normalized to ECM dry weight. Scale bar represents 100µm. **** p <0.0001, ***p<0.009

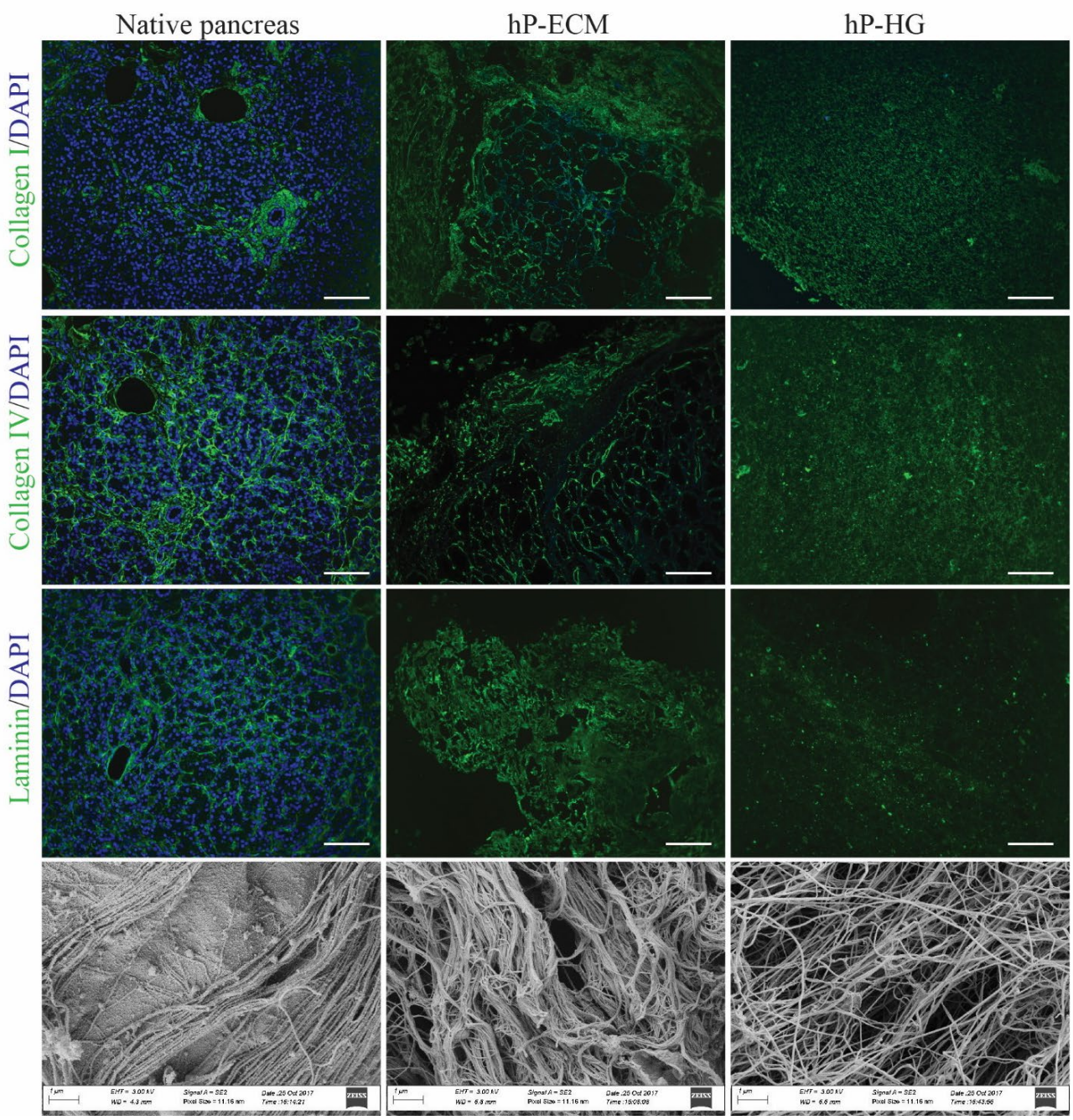

Figure 5. Histological and morphological analysis on native tissue and on decellularized pancreatic hydrogels. ECM protein retention was assessed by IHC in native pancreas (left column), decellularized scaffold (middle column) and hydrogel (right column) for: collagen I (top 3 panels); Collagen IV (upper middle panels) and laminin (lower middle). Scanning electron microscopy (bottom row) of native (left) and hP-ECM (middle) and hP-HG (right). SEM images of scaffold and gel reveal a porous 3D structure composed of intermeshed fibres. Images were obtained at 10,000x magnification. Scale bar represents 100 µm.

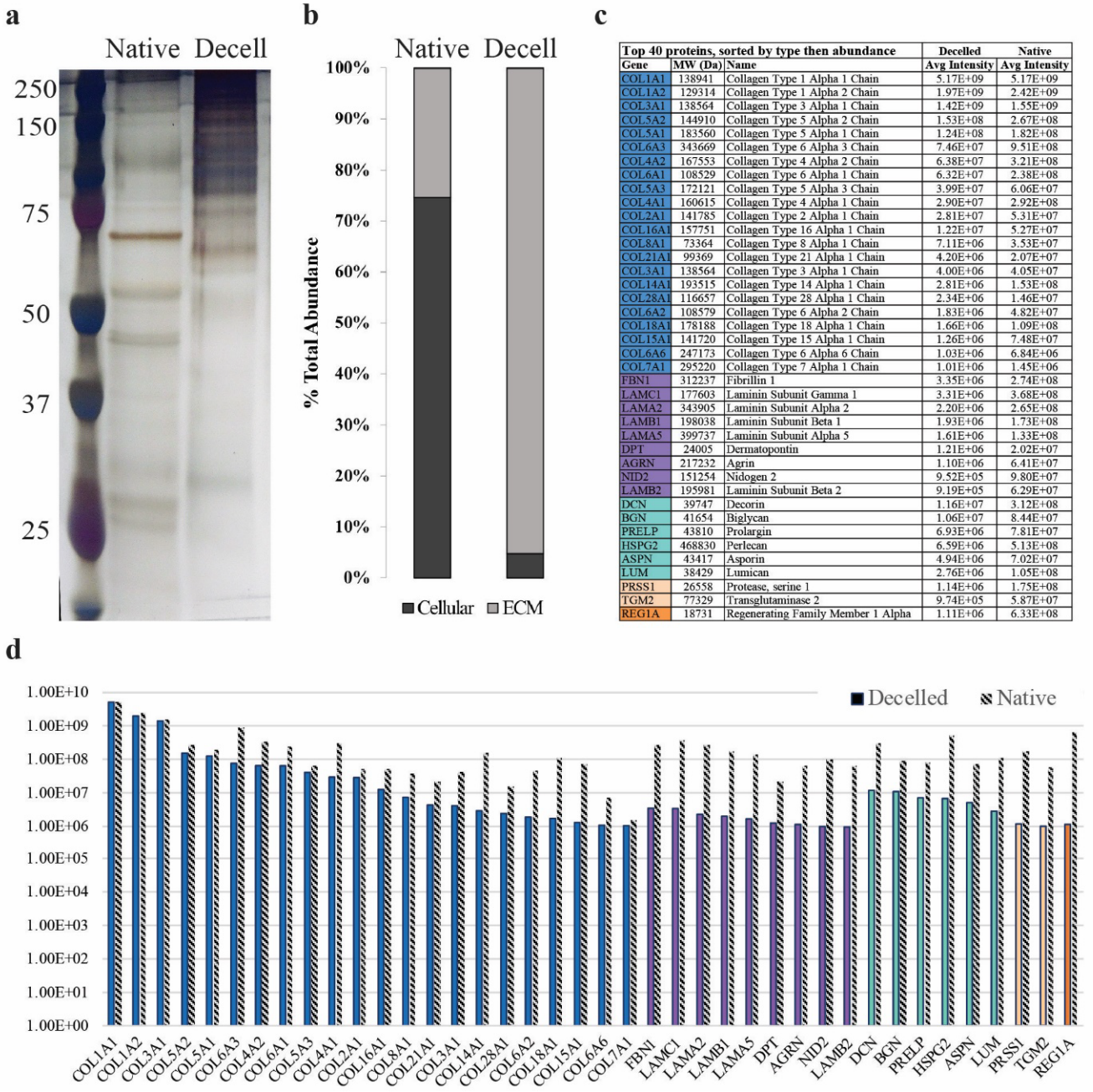

c

Top 40 proteins, sorted by type then abundance			Decelled	Native
Gene	MW (Da)	Name	Avg Intensity	Avg Intensity
COL1A1	138941	Collagen Type 1 Alpha 1 Chain	5.17E+09	5.17E+09
COL1A2	129314	Collagen Type 1 Alpha 2 Chain	1.97E+09	2.42E+09
COL3A1	138564	Collagen Type 3 Alpha 1 Chain	1.42E+09	1.55E+09
COL5A2	144910	Collagen Type 5 Alpha 2 Chain	1.53E+08	2.67E+08
COL5A1	183560	Collagen Type 5 Alpha 1 Chain	1.24E+08	1.82E+08
COL6A3	343669	Collagen Type 6 Alpha 3 Chain	7.46E+07	9.51E+08
COL4A2	167553	Collagen Type 4 Alpha 2 Chain	6.38E+07	3.21E+08
COL6A1	108529	Collagen Type 6 Alpha 1 Chain	6.32E+07	2.38E+08
COL5A3	172121	Collagen Type 5 Alpha 3 Chain	3.99E+07	6.06E+07
COL4A1	160615	Collagen Type 4 Alpha 1 Chain	2.90E+07	2.92E+08
COL2A1	141785	Collagen Type 2 Alpha 1 Chain	2.81E+07	5.31E+07
COL16A1	157751	Collagen Type 16 Alpha 1 Chain	1.22E+07	5.27E+07
COL8A1	73364	Collagen Type 8 Alpha 1 Chain	7.11E+06	3.53E+07
COL21A1	99369	Collagen Type 21 Alpha 1 Chain	4.20E+06	2.07E+07
COL3A1	138564	Collagen Type 3 Alpha 1 Chain	4.00E+06	4.05E+07
COL14A1	193515	Collagen Type 14 Alpha 1 Chain	2.81E+06	1.53E+08
COL28A1	116657	Collagen Type 28 Alpha 1 Chain	2.34E+06	1.46E+07
COL6A2	108579	Collagen Type 6 Alpha 2 Chain	1.83E+06	4.82E+07
COL18A1	178188	Collagen Type 18 Alpha 1 Chain	1.66E+06	1.09E+08
COL15A1	141720	Collagen Type 15 Alpha 1 Chain	1.26E+06	7.48E+07
COL6A6	247173	Collagen Type 6 Alpha 6 Chain	1.03E+06	6.84E+06
COL7A1	295220	Collagen Type 7 Alpha 1 Chain	1.01E+06	1.45E+06
FBN1	312237	Fibrillin 1	3.35E+06	2.74E+08
LAMC1	177603	Laminin Subunit Gamma 1	3.31E+06	3.68E+08
LAMA2	343905	Laminin Subunit Alpha 2	2.20E+06	2.65E+08
LAMB1	198038	Laminin Subunit Beta 1	1.93E+06	1.73E+08
LAMA5	399737	Laminin Subunit Alpha 5	1.61E+06	1.33E+08
DPT	24005	Dermatopontin	1.21E+06	2.02E+07
AGRN	217232	Agrin	1.10E+06	6.41E+07
NID2	151254	Nidogen 2	9.52E+05	9.80E+07
LAMB2	195981	Laminin Subunit Beta 2	9.19E+05	6.29E+07
DCN	39747	Decorin	1.16E+07	3.12E+08
BGN	41654	Biglycan	1.06E+07	8.44E+07
PRELP	43810	Prolargin	6.93E+06	7.81E+07
HSPG2	468830	Perlecan	6.59E+06	5.13E+08
ASPN	43417	Asporin	4.94E+06	7.02E+07
LUM	38429	Lumican	2.76E+06	1.05E+08
PRSS1	26558	Protease, serine 1	1.14E+06	1.75E+08
TGM2	77329	Transglutaminase 2	9.74E+05	5.87E+07
REG1A	18731	Regenerating Family Member 1 Alpha	1.11E+06	6.33E+08

Figure 6. Protein content of native and decellularized pancreata. a) A representative silver stained SDS-PAGE comparing total protein (10 µg) content of native and decellularized pancreas demonstrates enrichment of large molecular weight proteins (80-250kD), and **b**) MS-based analysis of the percent total abundance represented by ECM-associated or cellular proteins in the native and decellularized pancreas. **c**) A list of the top 40 ECM-associated proteins identified in the decellularized material, sorted first by category (blue = collagens, purple = ECM glycoproteins, teal = proteoglycans, beige = ECM regulators, orange = ECM-affiliated proteins) and second by normalized abundance in the decelled sample, **d**) graphed alongside the normalized abundance in the native tissue (grey striped bars). N=3 biological replicates per group analysed for SDS-PAGE/silver stain analysis.

quantitative sGAG assessment demonstrated a significant decrease in content following decellularization procedure. hP-ECM was found to retain 19.6% of the native sGAG content, while hP-HG was found to only retain 15.2% (Fig. 4h).

To further characterize the decellularized pancreatic ECM and the resulting hydrogel, immunofluorescent (IF) detection of ECM proteins was performed. We found that collagen I, collagen IV, and laminins are retained in decellularized materials, and the ECM microarchitecture appears to be preserved within the homogenized hP-ECM (Fig. 5).

To assess matrix ultrastructural morphology, native pancreatic tissue, decellularized hP-ECM and hP-HG were subjected to scanning electron microscopy (SEM). SEM images display retention of 3-D ECM architectural elements as well as preservation of fibrillar structures of the native ECM. These organized fibrillar bundles appear to be preserved through the decellularization and delipidization process which are likely to be the fibrous collagen proteins identified by MS as the top 22 ECM-associated proteins (see Fig. 6). The decellularized ECM material appears to maintain the negative space or “footprint” previously occupied with native cells, providing a physical space for exogenous cells to take up residence and receive direction from the biological components remaining in the ECM scaffold. hP-HG also displays reformed collagen fibrils by SEM. Additional high-magnification images are included in Supplemental Fig. S3.

Having demonstrated the retention of several major ECM proteins after decellularization by IF, we sought to visualize the change in overall protein composition following this procedure. Protein samples from native pancreas and hP-ECM were run on an SDS-PAGE gel and probed with a silver stain to visualize total protein content. With equal total protein loaded for each sample,

the presence of higher molecular weight proteins in the decellularized sample compared to native tissue is apparent, revealing that the large molecular weight ECM proteins [34] have been enriched in the acellular material (Fig. 6a). These bands most likely represent the two main classes of macromolecules, the fibrous proteins such as collagens and the glycoproteins such as laminins, which due to being enriched following dellularization are now detectable, as many other low-abundance proteins are not detectable with this method. To more thoroughly evaluate the retention of the ECM proteins after decellularization, isobaric tagging for multiplexed quantitation using custom-developed dimethylated leucine (DiLeu) labels was employed to enable high-throughput quantitation of relative abundances of all proteins by high-resolution mass spectrometry. All identified proteins were categorized as either 'cellular' or 'ECM' based on the MatrixDB database [35]. Native pancreatic tissue was found to be composed of 74.5% cellular proteins and 25.4% ECM proteins, while decellularized ECM contained only 4.8% cellular proteins and 95.2% ECM proteins (Fig. 6b). The top 40 most abundant ECM-related proteins in the decellularized and delipidized hP-ECM are listed in Fig. 6c, and graphically represented in Fig. 6d. The average signal intensity of each peak is listed in the table, and the intensity of the corresponding protein in the native (i.e. non-decelled) sample is included next to each bar on the graph in grey (Fig. 6d). A complete list of all 120 ECM-related proteins identified in the samples is included in Supplemental Fig. S4.

In vitro cytocompatibility

hP-HG has potential for use as scaffolding or substrate material for in vitro cell culture, where the pancreatic ECM proteins may provide a microenvironmental niche to improve survival of islets or stem cell-derived beta-like cells. We aimed to verify the cytocompatibility of hP-ECM

with a variety of relevant cell types including an insulinoma cell line, stem cell-derived beta-like cells, and endothelial cells, which could ultimately aid in graft vascularization.

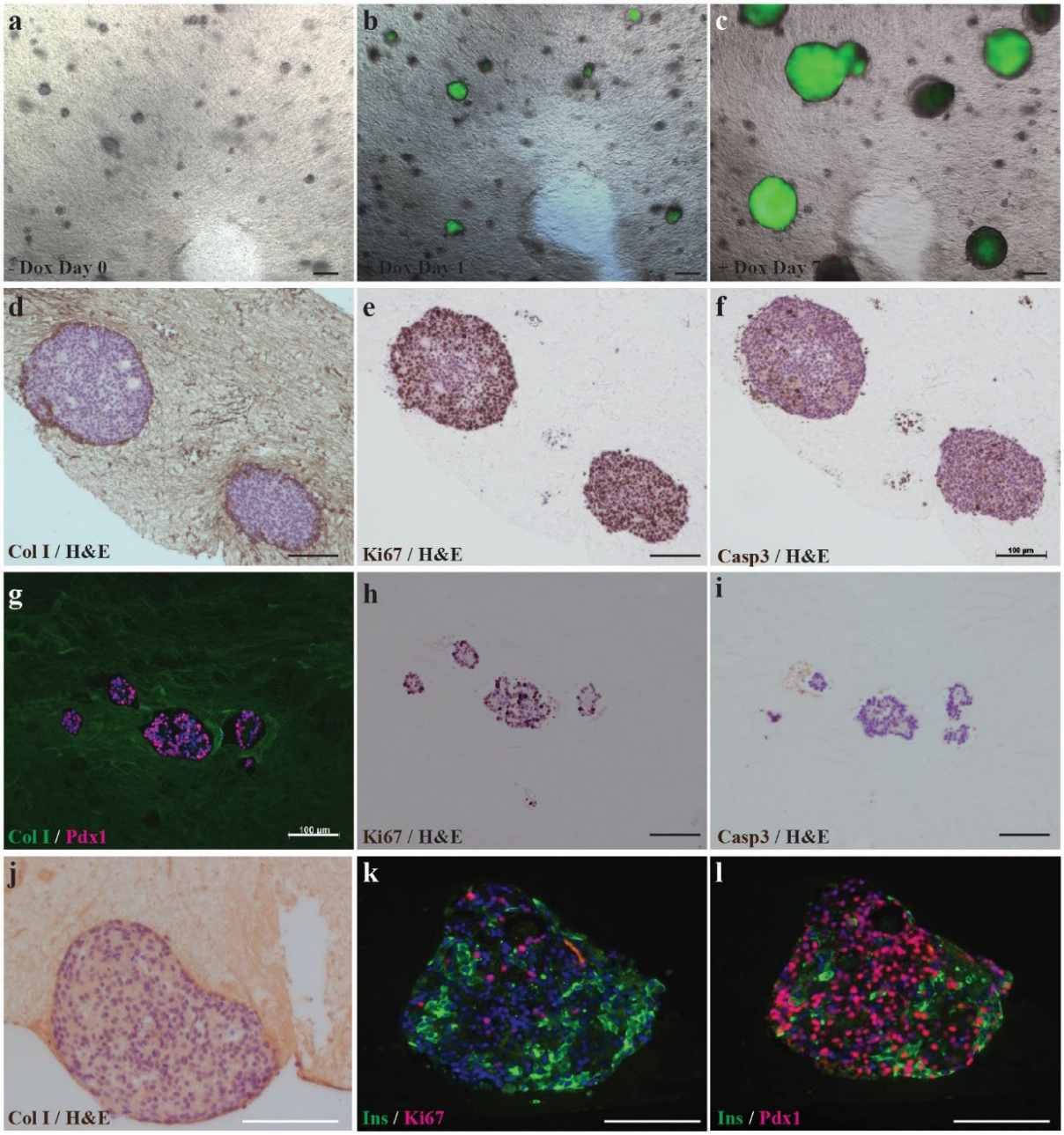

Figure 7. *In vitro* cytocompatibility assessment. Doxycycline inducible GFP H9 hESC clusters were embedded in hp-HG hydrogel. **a-c**) Cells were serially imaged using epifluorescence in live cultures on days 0, 1, and 7 after Dox treatment (1.5 µg/ml in E8 media). Images show progressive expansion of green fluorescing colonies in 3D indicating survival and growth of hESCs. **d-f**) At day 7 of culture, undifferentiated expanded Dox-GFP H9 colonies were fixed, paraffin embedded, and stained with H&E and counterstained for either Col I, Ki67 or Caspase 3 (Casp3). The images show hESC colonies embedded in hP-HG matrix highly express Ki67 proliferation marker and few Casp3 expressing cells. **g-i**) hPSC- derived pancreatic progenitors embedded in hP-HG and cultured for 9 days and fixed, embedded in paraffin, sectioned and stained for Col I (green) and PDX1 (red nuclei). Pancreatic progenitors embedded in hP-HG also express Ki67 indicating expected proliferation, but minimal Caspase 3 positive staining. **j-l**) hPSC-derived ILCs were embedded in hP-HG for 4 days, fixed, embedded, and stained for Col I, Ins (green), Ki67 (red) or PDX1 (red nuclei). Images show healthy cell clusters containing non-proliferative Ins+ cells in the clusters and numerous PDX1+Ins- progenitor cells and Ins^+ $Pdx1^+$ beta-like cells. Scale bar represents 200 µm in **a-c** and **j-l**, and 100 µm in **d-i**. Representative images shown, N=3 biological replicates for all groups. **(Previous page)**

First, we investigated the ability of the hP-HG to support cell adhesion and survival in 2-D cell culture using INS-1 832/13 cells (stably transfected rat insulinoma cells engineered to express human insulin)[36] and human umbilical vein endothelial cells (HUVECs). Each cell line was plated on untreated, hP-HG-coated, and collagen I-coated plates, and interrogated with an MTS metabolic activity assay and live/dead staining on days 1, 2, 3 and 4 after plating. Growth curves were generated for each cell line grown on each substrate. Regardless of substrate, growth curves were indistinguishable from one another for both INS-1 832/13 cells and HUVECs (Fig. S5a-b). In addition, the INS 832/13 cells plated as described above, were subjected to glucose stimulated insulin secretion assays (GSIS) to determine if the glucose responsiveness was maintained in all experimental groups. The stimulation index, a marker for insulin secretion functionality, calculated for all platforms was 2.8 ±1.3, with no group being statistically different from another. This indicates that the cells were functional on all platforms tested. Furthermore, the live/dead staining revealed an insignificant difference in the ratio of live:dead cells for all cells and conditions after 4 days in culture. Importantly, cells grown on hP-HG maintained their cell

fate, as evaluated through IF staining for human insulin and rat NKX6.1 expression in the INS-1 832/13 cells and for vWF and E-Cadherin expression in HUVECs (Fig. S5c-f). Additionally, HUVECs maintained expected expression of CD31 (data not shown). Together, these results demonstrate that cells grow equally as well on hydrogel-coated surfaces as on untreated plastic or Col I in short-term culture, and that hP-HG does not induce significant cell death or inhibit cell growth.

To test 3-D culture compatibility with hESCs, doxycycline-inducible (Dox) GFP-expressing H9 stem cells were embedded as small colonies in hP-HG and maintained in E8 growth medium for 7 days in the presence of Dox, which was initiated 24 hours after plating. After 24 hours of Dox exposure, the cells were imaged and GFP was visible. After 7 days of Dox treatment, GFP expression and expansion of colonies in 3 dimensions was apparent as demonstrated with live imaging (Fig. 7a-c). At the experimental end point the hP-HG embedded cell colonies were fixed and analyzed for Ki67 and Caspase 3 marker expression to assess proliferation and apoptosis, respectively (Fig. 7d-f). These cells were found to be on average 94.0% positive for Ki67 and 3.6% positive for Caspase-3, indicating that undifferentiated H9 cells can expand and grow while embedded in hP-HG. This demonstrates that hP-HG is cytocompatible with the human stem cell line H9, non-toxic and permeable to small molecules such as Dox. Additionally, the H1 hESC line and human iPSC lines derived from CD34+ cells have been combined successfully with hP-HG for short-term undifferentiated expansion (data not shown).

To test for compatibility of hP-HG with hESC-derived cells, pancreatic progenitor cells (differentiated for 11 days), were embedded in hP-HG, cultured in appropriate stage-specific medium, and stained for the stage-specific marker PDX1, as well as Ki67 and Caspase-3 to assess proliferation and apoptosis, respectively, in the embedded cells (Fig. 7g-i). Further, we

investigated cytocompatibility with hESC-derived pancreatic endocrine cells or islet-like clusters (ILCs) (following a stepwise differentiation protocol for 28 days), which were embedded in hP-HG, cultured in end stage differentiation medium for 4 days, and analyzed for insulin, PDX1, Ki67 and Caspase 3 (Fig. 7j-l). Quantification of the differentiated cells co-cultured with hydrogel (H), compared with cells that remained in suspension (S), showed insignificant differences in the percentage of cells which were Ki67+ (H: 36.3%, S: 32.5%), Caspase-3+ (H: 2.7%, S: 2.4%), and PDX1+ (H: 77.5%, S: 74.7%). These studies support the notion that hP-HG supports the growth and maintenance of cell fate of hESC-derived pancreatic progenitors and ILCs and provide a suitable substrate for in vitro culture.

In vivo immunogenicity

In order to utilize this material for biomedical applications such as allograft tissue engineering, it is important to assess whether hP-HG induces an immune response upon transplantation. The major goal of decellularization protocols is to remove the cellular and antigenic material efficiently while maintaining the important ECM molecules, which are themselves inherently hypoimmunogenic [37]. To test the immune response to hP-HG, we employed immunodeficient NSG mice endowed with a humanized immune system using human foetal thymus and CD34+ hematopoietic stem cells. After 12 weeks, allowing for multi-lineage haematopoiesis to occur, the mice exhibited greater than 25% engraftment of human CD45+ cells. The humanized immune system is derived from foetal tissue distinct from the adult donor pancreas with which the hP-HG was derived. Therefore, the humanized immune system should recognise and attack hP-HG if it represents immunogenic material. To test the immunogenicity, a bolus of neutralized hP-HG pre-gel solution was injected subcutaneously into the dorsum of

humanized mice, allowing it to gel in vivo. As a positive control for graft rejection, human foetal pancreas (HFP) tissue from another individual, allogeneic to the foetal tissue used to produce the humanized mouse, was also implanted in the same animal subcutaneously. Grafts were removed after 4 weeks to assess immune response. H&E staining shows strong infiltration of inflammatory cells into the foetal pancreas tissue while the hP-HG shows very little immune cell infiltration. Further immunological evaluations for human CD3 and CD8 were performed and revealed the HFP tissue to be highly infiltrated with cytotoxic T lymphocytes, while hP-HG graft contained little to no infiltration of similar human immune cells (Fig. 8b, d, e).

In the native pancreas, IHC staining indicates expression of HLA class I proteins, while staining of decellularized hP-ECM and hP-HG reveals the absence of HLA class I antigens (Fig. 8j-l). The same trend was seen following interrogation of HLA Class II antigens (HLA-DR) (data not shown). Thus, the in vivo assessment of hP-HG suggests it is hypoimmunogenic in this humanized mouse model consistent with the notion that the cellular and antigenic components of the tissue have been largely removed.

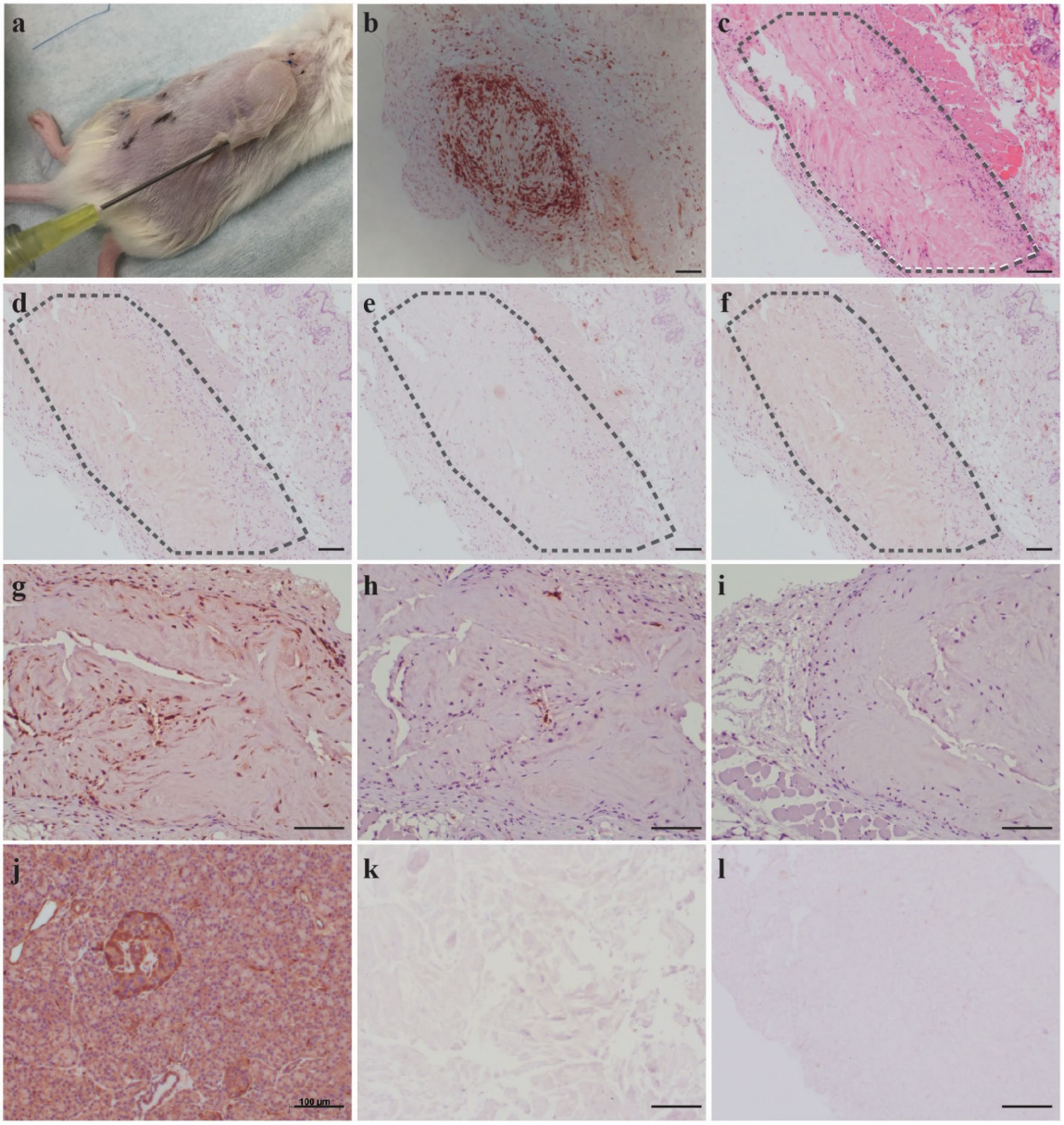

Figure 8. Minimal immune cell responses to decellularized human pancreatic matrix in humanized mice. a) 500µl of hP-HG was injected subcutaneously on one flank and allogeneic human foetal pancreas (HFP) tissue was implanted into the opposite flank of the same humanized mouse. The grafts were collected after 4 weeks and analysed for histology and immune cell infiltration. **b**) HFP showed intense hCD3 immune infiltration suggesting an acute cellular rejection response. **b-l**) The hP-HG hydrogel graft was analysed by: **c**) H&E, and by staining for cellular phenotypes including: **d**) CD3+ T cells, **e**) CD8+ T cells, (**f**) FoxP3+ regulatory cells. The hP-HG graft was also stained for: **g**) mouse specific CD68+ macrophages, **h**) human specific CD68+ macrophages, and **i**) human specific CD20+ B cells. The graft appears to be non-immunogenic as the graft is largely negative for CD3+ and CD8+ T cells and CD20+ B cells. The majority of the infiltrating cells are mouse CD68+ cells with a few scattered human CD68+ cells present (**h**). **j-l**) IHC staining of native (**j**) and decellularized pancreas tissues hP-ECM (**k**) and hP-HG (**l**) for pan human HLA-ABC show that the decellularized ECM and hydrogel are negative for HLA Class I antigen expression. Scale bar represents 100µm.

Discussion

Decellularized tissues from a variety of sources have been utilised in human clinical applications, primarily for soft tissue reconstruction [38]. Natural organ ECM represents an important substrate formed from a complex of highly ordered fibrous proteins which provides many biological properties known to support cell viability and growth. Whole organ decellularized pancreatic ECM has been derived from mice, rats, pigs and humans [39-45] as a potential alternative to traditional organ transplantation where relevant cell types are reseeded into the decellularized matrix with the hope of reconstituting a neo-organ with functional properties. However, recellularizing and rebuilding the vasculature of intact decellularized organ scaffolds can be challenging [39, 41, 43, 45-47]. An alternative approach, which is particularly relevant for an islet endocrine graft, would be to combine cells with ECM-derived hydrogel. Such a strategy is advantageous for tissue engineering applications because of its ease of use.

ECM hydrogels have been the focus of research for a number of years and have been developed from a variety of tissue sources including adipose [12, 22, 48], urinary bladder [49], liver [50], nervous system [51], dermis [52, 53], skeletal muscle [54] and cardiac tissues [55-57]. However, this has not yet been achieved with human pancreas. The human pancreas is an organ that has a relatively high lipid content, which is inhibitory to the production of a hydrogel, as similarly described by Young *et al.* in processing adipose tissue to hydrogel [12]. We found that many human donor pancreata contain a substantially high lipid content, which is due to adipose tissue sequestered throughout the parenchyma of the organ. Notably, we have received some human pancreata which contained up to 70% lipid content by dry weight. This excess lipid prevented successful solubilization and gelation of the hP-ECM. In applying published animal

pancreas decellularization methods to human pancreas, we were not successful in making hydrogel, indicating that further optimization of the protocol was required to remove more lipids. Therefore, to eliminate these lipids from the matrix more effectively, we included a unique homogenization step in the decellularization protocol. This method significantly aided in fat removal from the homogenized matrix, thereby allowing for the efficient generation of hP-ECM scaffolding and hydrogel, with preserved ECM proteins in an arrangement similar in architecture to native pancreas. Following effective delipidization, we demonstrated that a hydrogel can be formed which has similar gelation kinetics to collagen I, as demonstrated by a turbidimetric gelation assay. We also showed that the hP-HG is cytocompatible with a number of cell types in in vitro culture applications and does not elicit an immune response in vivo in humanized mice, supporting its potential in pancreatic endocrine tissue engineering applications.

ECM is comprised of many protein and polysaccharide macromolecules including collagens, laminins, proteoglycans and more. Retention of native ECM proteins is essential in order to reproduce the pancreatic ECM niche and facilitate cell attachment and ECM signaling [58]. We showed through IF staining that collagen I, collagen IV and laminins were retained in the decellularized matrix and that the microstructural organization of these proteins was maintained throughout the decell process, even following homogenization (Fig. 4). Collagen I and collagen IV were retained in the digested hydrogel, while laminin appeared as fragments within the gel. This may be due to the fact that laminins are susceptible to pepsin digestion, and potentially reduced due to the cleaving antibody binding sites. However, results from several studies suggest that following pepsin digestion, laminin fragments still retain growth factor and integrin binding capabilities and therefore may maintain function [59-61].

It is well established that sulphated GAGs are an important component of the ECM, through their involvement in growth factor sequestration and presentation [62-64]. Development of a decellularization/delipidization protocol that maintains these macromolecules is ideal in the production of a material that presents an *in vivo*-like niche. ECM components were expected to be retained in the matrix and hydrogel to varying degrees of efficiency; we found that GAGs were partially retained in the decellularized matrix, and to a lesser extent in the digested hydrogel. It has been established that pancreatic beta cells contain a significant level of intracellular sGAG, which is consistent with our findings that in situ islets are enriched for cellular sGAG [65]. This may contribute to the large reduction in sGAG content, as these molecules would be removed along with the cellular material during decellularization. Furthermore, while pepsin digestion in the process of hydrogel formation may result in an additional, unavoidable, reduction in GAG content, it may be possible to infuse or crosslink the gel with additional GAGs or GAG mimetics to enhance cell signalling and attachment [66]. Further investigation toward delineating the specific roles individual GAGs play within the islet ECM niche will be necessary to fully understand and elucidate the importance of GAGs within this material.

DiLeu isobaric tandem mass tags coupled with high resolution mass spectrometry was employed for high throughput proteomic analysis of the human pancreatic matrisome. This approach has a broad dynamic range, offering accurate and highly sensitive quantitative analysis of protein content. Pooling of labelled native and decelled samples enriches the mixture for ECM proteins and permits detection of low-abundance proteins that may not otherwise been distinguished. 120 ECM and ECM-associated proteins were identified in the hP-ECM, which is four times the number of ECM proteins described in the mouse decelled pancreas [40] and tenfold

greater than what has been identified in the porcine pancreas [67]. Moreover, this is the first reported list of ECM proteins quantitatively measured in the human pancreas by mass spectrometry, enabling assessment of the relative abundance of the various ECM components.

Generally, collagens were observed to have the best retention following the decellularization treatment, with the intensity most closely matching that found in the native tissue. While proteoglycans and glycoproteins have reduced total abundance in the decelled material as compared to the native tissue, many of them increase in rank abundance, meaning that relative to other ECM proteins, they are more enriched following decellularization. We identified proteoglycans of several different families, including those which localize to the pericellular/basement membrane or extracellular space and also including proteins belonging to the heparan sulphate, keratan sulphate, chondroitin sulphate and dermatan sulphate-binding families [68]. The identification of these pancreas-specific ECM proteins and proteoglycans will allow for future testing of their presence and properties within hP-HG scaffold constructs, and their contribution to pancreatic cell fate determination.

To assess the biocompatibility of the hP-HG in vivo, immunogenicity studies were conducted by utilizing humanized mice. When injected subcutaneously, hP-HG did not elicit an immune response, while allogeneic HFP tissue transplanted into the same animals was acutely rejected, as expected. Immune reactions occur with incompatibility between ABO and HLA systems, mainly triggered by the recipient in response to the donor [69]. The IHC performed for HLA class I and II (HLA-ABC/-DR) in native pancreas, hP-ECM and hP-HG clearly demonstrates the removal of these antigens from the decellularized materials, further corroborating the absence of an immune response to the acellular material in the humanized mice. The results suggest this

hypoimmunogenic pancreatic hydrogel, when transplanted with cells or islets, may not illicit immune rejection in an in vivo environment.

hP-HG is a versatile product that can be utilized in a variety of tissue culture and transplantation applications. The pancreatic hydrogel proved to be cytocompatible with a variety of cell types indicating that it permits normal growth of cells and appears to be non-toxic. We observed that INS-1 832/13 cells and HUVECs both grew equally well in 2-D culture on untreated, collagen I-coated, and hP-HG-coated tissue culture plates. These results translated nicely into the use of hP-HG in 3-D culture where we challenged undifferentiated H9 cells, as well as stem cells differentiated toward a beta cell fate, to survive and grow in these matrix modules. When undifferentiated human stem cells were embedded in hP-HG, they expanded in a 3-D spherical pattern. These cells could be induced to express GFP with media containing doxycycline, indicating that the hydrogel is permeable to small molecules and other media components. Likewise, cells differentiated toward a pancreatic endocrine fate survived and retained their identity when embedded in hydrogel, as demonstrated through continued expression of known endocrine markers such as PDX1. Future work will consist of investigating the effect hP-HG may have on differentiating stem cell-derived islet-like cells cultured within the gel, compared to cells differentiated without exposure to hP-HG. We aim to test whether hP-HG has the capacity to improve the differentiation, maturation and function of these cells in vitro.

The results from this study illustrate that discarded human pancreata can be successfully decellularized, delipidized and processed for development of 3-D scaffold casts and hydrogels which maintain their macromolecules, are not toxic to the growth and differentiation of several types of cells and therefore may have value in regenerative medicine applications. In vivo, cells

are in contact with the unique ECM of the tissue they reside within, providing tissue-specific signals which aid in cell fate determination. Therefore, including these tissue-specific cues in an in vitro cell culture system will likely enhance the culture environment in ways that synthetic or purified individual ECM components cannot achieve alone. Studies are ongoing to determine the specific components and properties of the pancreatic ECM in order to establish a useful scaffold for the growth and maintenance of stem cell-derived beta cells and cadaveric islets for transplantation.

Materials and Methods

All experiments were performed using protocols approved by the Animal Care and Use Committee of the University of Wisconsin School of Medicine and Public Health and the Health Sciences Institutional Review Board, and complied with federal and state law.

Pancreas Procurement

Human cadaver pancreata were procured for either research or transplantation. If recovered for transplantation but ultimately deemed unusable, they were earmarked for research. No organs were procured from prisoners. Human pancreata (n = 11, age 13-58 years) were obtained and used in this study through the University of Wisconsin Organ and Tissue Donation with consent obtained for research from next of kin and authorization by the University of Wisconsin-Madison Health Sciences Institutional Review Board and was performed in accordance with federal and state law. A list of donors used in this study and their demographic data are shown in Supplemental Table 1. (More details can be found in Supplementary Methods).

Spin-Decellularization (Spin-decell)

Human pancreata were trimmed of surrounding fat, and the remaining parenchyma was sectioned into approximately 1cm3 pieces, flash frozen and stored at -80˚C. For decellularization, tissue was thawed at 37˚C until soft, rinsed with 1X PBS for 30 minutes, and placed in 2.5 mM sodium deoxycholate/PBS, shaking at RT for 24 hours. The tissue was then rinsed with water and the 24-hour deoxycholate shake was repeated. After a total of 48 hours of agitation in deoxycholate, the tissue was rinsed with water and washed in 1X PBS supplemented with 1X Pen/Strep for 72 hours, with water rinses every 24 hours, and fresh PBS + Pen/Strep replaced each day. The resulting decellularized pancreatic ECM was lyophilized and stored at -80˚C for future use.

Homogenized-Decellularization (Homogenization-decell)

Human pancreata were processed as above until thawed. The tissue was rinsed with 1X PBS for 30 minutes, washed with water and homogenized in water until broken up. The homogenate was centrifuged (4300 rpm, 5 min), floating fat was removed from the surface, and the cloudy supernatant was discarded. The pellet was resuspended in water and centrifuged again (4300 rpm, 5 min). The pellet was then resuspended into 2.5 mM sodium deoxycholate/PBS and incubated for 3 hours (RT, shaker). After this time, the homogenate was strained over a sieve (Sigma, S1145); all collected material was placed back into 2.5 mM sodium deoxycholate/PBS and incubated for an additional 15 hours (RT, shaker). The ECM was strained again, rinsed with water and washed in 1X PBS supplemented with Pen/Strep for 72 hours, with water rinses every 24 hours, and fresh PBS + Pen/Strep replaced each day (RT, shaker). The resulting decellularized pancreatic ECM was lyophilized and stored at -80˚C for future use.

Hydrogel Formation

Lyophilized ECM was digested with an HCl/pepsin solution and then neutralized, as previously described[49]. Controls were made by neutralizing rat-tail collagen type I (Corning, 354249). (More details can be found in Supplementary Methods).

Hydrogel coated plate

Acidic ECM digest was diluted with cold 1X PBS to a concentration of 0.08 mg/ml (a 1:120 dilution) and filtered through a 40 μm filter to remove undigested ECM pieces. 300 μl of diluted digest (pre-gel solution) was added to each well of a chilled 24-well culture plate (Corning, 3527). Plates were incubated at 37˚C for one hour and rinsed with PBS before use.

Matrix characterization

DNA Content. Quantification of DNA was assessed using the Quant-iT™ PicoGreen® dsDNA Assay (Life Technologies, P7589), following manufacturer's protocol. Weighed and lyophilized ECM materials were digested with papain for 3-18 hours at 65˚C prior to the assay.

Sulphated Glycosaminoglycan (sGAG) Content

The sulphated glycosaminoglycan (sGAG) content of native and decellularized pancreata was quantified using the Blyscan GAG Assay Kit (Biocolor, UK), following manufacturer's protocol. Weighed and lyophilized ECM materials were digested with papain for 3-18 hours at 65˚C prior to the assay. The absorbance at 595 nm was measured using a microplate reader (FlexStation 3, Molecular Devices) and compared to standards. Absorbance values were normalized to sample dry weight.

SDS-PAGE analysis

Protein lysates were prepared from native pancreas tissue, decellularized/lyophilized hP-ECM and hP-HG digest solution. Samples were solubilized in 1X RIPA buffer + Halt protease inhibitor cocktail (ThermoFisher, 78430) and total protein content was measured with a DC Protein Assay (BioRad, 5000112). To compare protein distribution, 10 μg of protein from each sample was resolved on a 10% SDS-PAGE gel (Biorad, 3450111) and silver-stained for visualization.

Lipid Content

Samples were embedded in OCT and cut into 5 μm sections. Sections were fixed with 10% neutral buffered formalin for 5 minutes, rinsed with water and then 70% ethanol. Slides were incubated for 10 minutes in Oil Red O (ORO) stain, washed with 70% ethanol and counterstained with haematoxylin. Images were generated with a Zeiss Axiovert 200M microscope for a qualitative evaluation of lipid retention. Quantitative lipid content was assessed using a modified Folch lipid extraction (See Supplementary Methods). The resulting lipid material was weighed to determine lipid content of the original sample.

Histology and Immunofluorescence (IF) Microscopy:

Basic Histology

Native and decellularized samples were fixed in 4% paraformaldehyde (PFA), paraffin embedded, and sectioned (5 μm) for histological examination. Sections were stained with haematoxylin and eosin (H&E). Additional sections were stained with Alcian Blue (AB), following standard protocols.

Immunohistochemistry

Slides were deparaffinized using xylene and rehydrated. Antigen retrieval was performed by treatment with 10mM Citrate Buffer, pH6.0 for 2 hours in an 80˚C water bath. Slides were blocked with 10% BSA/PBS for 1 hour at RT, incubated with primary antibodies overnight at 4˚C, washed, incubated with secondary antibody incubation for 1 hour at RT and cover slipped.

The antibodies and dilutions are listed in Supplementary Table 2. Immunofluorescent secondary antibodies were Alexa Fluor 488 and 568 of anti-goat, anti-mouse, anti-rabbit. Nuclei were counterstained with 40-6-diamidino-2-phenylindole (DAPI). Images were generated with a Zeiss Axiovert 200M microscope. Images were analysed and counted using Image J software. Total Ki67-positive cells were divided by total nuclei to calculate percentage of proliferative cells. Total Casp3-positive cells were divided by total nuclei to calculate the percentage of apoptotic cells. Total Pdx1-positive cells were divided by total DAPI-positive nuclei to calculate the percentage of $Pdx1^{+}$ cells. At least 3000 total nuclei were counted across images in each group.

Turbidimetric-Kinetic Gelation Assay

Turbidimetric gelation kinetics were determined as previously described [49]. 100 µL of cold, neutralized hydrogel (pre-gel) was loaded per well into a flat-bottom 96-well plate, placed in a pre-heated (37˚C) FlexStation 3 (Molecular Devices) plate reader and the OD at 405 nm was recorded in 30-second intervals over the course of 80 minutes. Data was collected using SoftMaxPro software. Two biological replicates were performed in triplicate and averaged. Data was normalized using Equation 1, where A is the absorbance at a given time, A_0 is the lowest absorbance (time zero) and Amax is the maximum absorbance.

Equation 1:
$$Normalized\ Absorbance\ (NA) = \frac{\mathrm{A} - \mathrm{A_0}}{A_{max} - A_0}$$

The time needed to reach 50% of the maximum turbidity absorbance value was defined as $T_{1/2}$; the lag phase (T_{lag}) was calculated by extrapolating the x-intercept of the linear portion of the curve. The speed of gelation (S) was determined by calculating the slope of the curve at $T_{1/2}$ as described in [54].

Scanning Electron Microscopy

Samples were fixed overnight in 4% PFA, washed and stored in 1X PBS. Samples were progressively dehydrated through a series of ethanol washes starting at a 30% solution and ending with 100% ethanol. Samples were dried on a critical point drier and coated with a 40:60 mixture of gold:palladium. Images were taken with a LEO 1530 scanning electron microscope at 1000x, 2500x, 10000x and 40000x.

In Vitro Cytocompatibility

Live/Dead Imaging. HUVECs ($1.6x10^4$ cells/cm2) (Sigma, 200P-05N) and INS-1 832/13 cells ($2.6x10^4$ cells/cm2) [36] were plated on 24-well plates with either no coating, collagen I coating (Corning, 354249) or hP-HG coating, and cultured for 1-3 days. Cells were stained with Calcein-AM (ThermoFisher, C3100MP) and ethidium homodimer (Sigma, 46043-1MG-F) in a live/dead assay: Samples were imaged with a Zeiss Axiovert microscope; 10x images were used to count live cells (green) and dead cells (red) using Image J software. Each cell type was tested with 2 biological replicates of 4 technical replicates each.

MTS Assay

HUVECs ($8.0x10^3$ cells/cm^2) and INS-1 832/13 cells ($25x10^3$ cells/cm^2) were plated onto flat-bottom 96-well tissue culture plates with either no coating, collagen I coating (Corning, 354249) or hP-HG coating, and grown in their respective medium. On days 1, 2, 3 and 4 after

plating, CellTiter-96 (Promega, G3582) reagent was added to the cultures for 3 hours, media absorbance at 490 nm was measured (FlexStation 3, Molecular Devices). Culture media were tested in triplicate for each condition and time point. A growth curve was generated for each cell line and condition tested.

GSIS Assay

INS-1 832/13 cells were plated at a density of $0.5x10^6$ cells per well in a 24-well plate (N=4) (Corning 3527), with either no coating, Col1 coating or hP-HG coating. Cells were expanded for 48 hours in standard medium, and grown until 95% confluent. On the day of the assay each well of cells was washed with Krebs buffer (25 mM HEPES, 115 mM NaCl, 24 mM NaHCO3, 5 mM KCl, 1 mM MgCl2, 2.5 mM CaCl2, 1% BSA) and pre-incubated in a very low glucose Krebs solution (0.5mM) for 2 hours at 37˚C and 5% CO_2. A GSIS was performed using serial low glucose (2.8 mM) and high glucose (28 mM) Krebs solutions with one hour incubations (37˚C, 5% CO_2) for each treatment. At the end of each incubation, supernatant was collected for human C-Peptide content measurement using the Mercodia Ultrasensitive C-Peptide ELISA kit (10-1141-01).

Doxycycline Induction Assay

Undifferentiated H9 cells with a Doxycycline-inducible GFP cassette were passaged with Versene (Life Technologies, 15040066) into small cell clusters, pelleted and mixed into 250 µl of cold 6.0 mg/ml hydrogel. Gel and cells were pipetted into a 12-well Transwell® (Corning 3460), covering the membrane, and incubated at 37˚C for 30 minutes. After 30 minutes, 0.5 mL E8 medium was added over the gels, and 1.0 ml of medium was added to the bottom of the Transwell® compartment. Media was replaced daily for 7 days with E8 media + doxycycline (1.5 µg/ml). GFP was imaged in live cells each day with a Zeiss Axiovert 200M microscope, and gels

were marked with a nick to identify the same spot in each gel every day. On day 7, gels were fixed in 4% PFA for 30 minutes, processed for paraffin embedding, sectioning and staining.

Stem cell differentiation

H1 cells were differentiated toward a pancreatic endocrine fate using a protocol based on Xu et al. (2011) [70], Rezania et al. (2014) [71], and Pagliuca et al. (2014) [72]. After 11 days of differentiation, pancreatic progenitor cells were embedded in hP-HG and cultured for an additional 9 days to test for survival, apoptosis and retention of pancreatic progenitor fate. After 28 days of differentiation, islet-like clusters (ILCs) were embedded in hP-HG for an additional 4 days in end-stage medium, to test for survival, apoptosis and retention of mature beta cell marker proteins. Constructs were fixed in 4% PFA and processed for paraffin embedding and analysis.

Transplantation of ECM into Humanized Mice

Research involving mice was performed in accordance with a protocol that was approved by the University of Wisconsin School of Medicine and Public Health Animal Care and Use Committee, and in accordance with a protocol approved by the University of Wisconsin Institutional Review Board. For immunogenicity studies, 500 µL of hP-HG was injected into the dorsal subcutaneous space of humanized mice (n=2) (See Supplementary Methods). Additionally, human fetal pancreas (HFP) fragments from a donor allogeneic to the donor of the mouse's human immune system was also transplanted subcutaneously into the same animal. The three grafts remained in vivo for a period of four weeks before the animals were sacrificed, and grafts collected for processing and immunohistochemistry.

ECM digestion and proteomics analysis

Protein extraction and DiLeu labelling were performed as previously described [73, 74]. Briefly, same amount of protein was digested with trypsin, labelled with 12plex DiLeu reagents and fractionated by off-line strong cation exchange (SCX) chromatography. Ten fractions were collected to reduce the sample complexity. Peptides were online separated by Dionex UltiMate 3000 LC system before entering the Orbitrap Fusion Lumos tribrid mass spectrometer (San Jose, CA). The descriptions of MS settings have been previously described [73]. (More details can be found in Supplementary Methods).

Quantification was performed using an in-house software called DiLeu tool. For each protein in the native (non-decelled) pancreas, the intensity (I) was normalized using the ratio of Col1A1 intensities of the native and decelled samples, using Equation 2. The normalized native intensity can then be compared to the corresponding experimental intensity for the same protein in the decelled sample. The average intensity for each protein in each group (decelled and native) was calculated using 5 donor pancreata.

Equation 2: $$\mathrm{I}_{norm}(Native, Protein\ X) = \mathrm{I}_{exp}(Native, Protein\ X) * \frac{\mathrm{I}_{exp}(Decell, Col1A1)}{\mathrm{I}_{exp}(Native, Col1A1)}$$

Statistical analysis

Statistical analyses were calculated with Prism 6 for Windows (GraphPad Software, Inc.) and SAS version 9.2 (SAS Institute Inc., Cary, NC). All results are reported as mean values across biological replicates ± the standard deviation of the mean. Statistical comparisons for all samples were made using repeated measures ANOVA testing followed by Tukey's multiple comparison test to determine significance between individual means. A p-value of less than 0.05 was

considered significant, and Prism's recommended classification for significance was followed ($p<0.0001$ = extremely significant (****), $0.0001<p<0.001$ = extremely significant (***), $0.001<p<0.01$ = very significant (**), and $0.01<p<0.05$ = significant (*)).

Acknowledgements

The study was supported through grants from NIH 1R21AI126419-01, JDRF SRA 17_2012_374, JDRF 1-SRA-2016-168-S-B, JDRF 1-PNF-2016-250-S-B, UW VCGRE award #A53-9700 from WARF to JSO and UW SCRMC training award to DT. LL acknowledges funding support from NIH R01DK071801 and P41GM108538. The Orbitrap instruments were purchased through the support of an NIH shared instrument grant (NIH-NCRR S10RR029531) and Office of the Vice Chancellor for Research and Graduate Education at the University of Wisconsin-Madison. The authors would like to thank and acknowledge Dr. Ralph Albrecht and Dr. Rick Noll for their help with processing samples for scanning electron microscopy and Drew Roennenburg and Sierra Raglin for their excellent skills with tissue processing and immunohistochemistry. We would like to thank Dr. Glen Leverson for providing his assistance with the bio-statistical analysis for this study. We would also like to thank Aida Rodriguez for her contributions and scientific conversations. Special thanks to the families who donated tissues for this research.

References

1. Ota, T., et al., Electromechanical characterization of a tissue-engineered myocardial patch derived from extracellular matrix. J Thorac Cardiovasc Surg, 2007. 133(4): p. 979-85.
2. Faulk, D.M., J.D. Wildemann, and S.F. Badylak, Decellularization and cell seeding of whole liver biologic scaffolds composed of extracellular matrix. J Clin Exp Hepatol, 2015. 5(1): p. 69-80.
3. Chen, F.M. and X. Liu, Advancing biomaterials of human origin for tissue engineering. Prog Polym Sci, 2016. 53: p. 86-168.
4. Theocharis, A.D., et al., Extracellular matrix structure. Adv Drug Deliv Rev, 2016. 97: p. 4-27.
5. Cirulli, V., et al., Expression and function of alpha(v)beta(3) and alpha(v)beta(5) integrins in the developing pancreas: roles in the adhesion and migration of putative endocrine progenitor cells. J Cell Biol, 2000. 150(6): p. 1445-60.
6. Kaido, T., et al., Regulation of human beta-cell adhesion, motility, and insulin secretion by collagen IV and its receptor alpha1beta1. J Biol Chem, 2004. 279(51): p. 53762-9.
7. Kaido, T., et al., Impact of defined matrix interactions on insulin production by cultured human beta-cells: effect on insulin content, secretion, and gene transcription. Diabetes, 2006. 55(10): p. 2723-9.
8. Labat-Robert, J., Cell-Matrix interactions, the role of fibronectin and integrins. A survey. Pathol Biol (Paris), 2012. 60(1): p. 15-9.
9. Kim, D.H., et al., Matrix nanotopography as a regulator of cell function. J Cell Biol, 2012. 197(3): p. 351-60.
10. Saldin, L.T., et al., Extracellular matrix hydrogels from decellularized tissues: Structure and function. Acta Biomater, 2017. 49: p. 1-15.
11. Gardin, C., et al., Decellularization and Delipidation Protocols of Bovine Bone and Pericardium for Bone Grafting and Guided Bone Regeneration Procedures. PLoS One, 2015. 10(7): p. e0132344.
12. Young, D.A., et al., Injectable hydrogel scaffold from decellularized human lipoaspirate. Acta Biomater, 2011. 7(3): p. 1040-9.
13. Young, D.A., J.A. DeQuach, and K.L. Christman, Human cardiomyogenesis and the need for systems biology analysis. Wiley Interdiscip Rev Syst Biol Med, 2011. 3(6): p. 666-80.
14. Federation, I.D. IDF Federation Atlas Sixth Edition Update, International Diabetes Federation 2014. 2014.
15. Wild, S., et al., Global prevalence of diabetes: estimates for the year 2000 and projections for 2030. Diabetes Care, 2004. 27(5): p. 1047-53.
16. Hering, B.J., et al., Phase 3 Trial of Transplantation of Human Islets in Type 1 Diabetes Complicated by Severe Hypoglycemia. Diabetes Care, 2016. 39(7): p. 1230-40.

17. Kandaswamy, R., et al., OPTN/SRTR 2015 Annual Data Report: Pancreas. Am J Transplant, 2017. 17 Suppl 1: p. 117-173.

18. Redfield, R.R., et al., Pancreas Transplantation in the Modern Era. Gastroenterol Clin North Am, 2016. 45(1): p. 145-66.

19. Boggi, U., et al., Transplantation of the pancreas. Curr Diab Rep, 2012. 12(5): p. 568-79.

20. Redfield, R.R., J.R. Scalea, and J.S. Odorico, Simultaneous pancreas and kidney transplantation: current trends and future directions. Curr Opin Organ Transplant, 2015. 20(1): p. 94-102.

21. Gilbert, T.W., T.L. Sellaro, and S.F. Badylak, Decellularization of tissues and organs. Biomaterials, 2006. 27(19): p. 3675-83.

22. Uriel, S., et al., Extraction and assembly of tissue-derived gels for cell culture and tissue engineering. Tissue Eng Part C Methods, 2009. 15(3): p. 309-21.

23. Weber, L.M., K.N. Hayda, and K.S. Anseth, Cell-matrix interactions improve beta-cell survival and insulin secretion in three-dimensional culture. Tissue Eng Part A, 2008. 14(12): p. 1959-68.

24. Stendahl, J.C., D.B. Kaufman, and S.I. Stupp, Extracellular matrix in pancreatic islets: relevance to scaffold design and transplantation. Cell Transplant, 2009. 18(1): p. 1-12.

25. Bruni, A., et al., Islet cell transplantation for the treatment of type 1 diabetes: recent advances and future challenges. Diabetes, Metabolic Syndrome and Obesity: Targets and Therapy, 2014. 7: p. 211-223.

26. Cantarelli, E. and L. Piemonti, Alternative transplantation sites for pancreatic islet grafts. Curr Diab Rep, 2011. 11(5): p. 364-74.

27. Carlsson, P.O., et al., Markedly decreased oxygen tension in transplanted rat pancreatic islets irrespective of the implantation site. Diabetes, 2001. 50(3): p. 489-95.

28. Chentoufi, A.A., et al., Type 1 diabetes immunological tolerance and immunotherapy. Clin Dev Immunol, 2011. 2011: p. 103738.

29. Thomas, F., et al., A tripartite anoikis-like mechanism causes early isolated islet apoptosis. Surgery, 2001. 130(2): p. 333-8.

30. Fridell, J.A., J. Rogers, and R.J. Stratta, The pancreas allograft donor: current status, controversies, and challenges for the future. Clin Transplant, 2010. 24(4): p. 433-49.

31. Kandaswamy, R., et al., OPTN/SRTR 2013 Annual Data Report: pancreas. Am J Transplant, 2015. 15 Suppl 2: p. 1-20.

32. Fridell, J.A. and R.J. Stratta, Expanding the Pancreas Donor Pool. Current Transplantation Reports, 2014. 1(2): p. 100-112.

33. Mittal, S., P. Johnson, and P. Friend, Pancreas transplantation: solid organ and islet. Cold Spring Harb Perspect Med, 2014. 4(4): p. a015610.

34. Mecham, R.P., Overview of extracellular matrix. Curr Protoc Cell Biol, 2012. Chapter 10: p. Unit 10 1.

35. Chautard, E., et al., MatrixDB, the extracellular matrix interaction database. Nucleic Acids Res, 2011. 39(Database issue): p. D235-40.

36. Hohmeier, H.E., et al., Isolation of INS-1-derived cell lines with robust ATP-sensitive K+ channel-dependent and -independent glucose-stimulated insulin secretion. Diabetes, 2000. 49(3): p. 424-30.

37. Badylak, S.F., Xenogeneic extracellular matrix as a scaffold for tissue reconstruction. Transpl Immunol, 2004. 12(3-4): p. 367-77.

38. Crapo, P.M., T.W. Gilbert, and S.F. Badylak, An overview of tissue and whole organ decellularization processes. Biomaterials, 2011. 32(12): p. 3233-43.

39. Elebring, E., et al., Cold-perfusion decellularization of whole-organ porcine pancreas supports human fetal pancreatic cell attachment and expression of endocrine and exocrine markers. J Tissue Eng, 2017. 8: p. 2041731417738145.

40. Goh, S.K., et al., Perfusion-decellularized pancreas as a natural 3D scaffold for pancreatic tissue and whole organ engineering. Biomaterials, 2013. 34(28): p. 6760-72.

41. Katsuki, Y., et al., Endocrine pancreas engineered using porcine islets and partial pancreatic scaffolds. Pancreatology, 2016. 16(5): p. 922-30.

42. Mirmalek-Sani, S.H., et al., Porcine pancreas extracellular matrix as a platform for endocrine pancreas bioengineering. Biomaterials, 2013. 34(22): p. 5488-95.

43. Napierala, H., et al., Engineering an endocrine Neo-Pancreas by repopulation of a decellularized rat pancreas with islets of Langerhans. Sci Rep, 2017. 7: p. 41777.

44. Peloso, A., et al., The Human Pancreas as a Source of Protolerogenic Extracellular Matrix Scaffold for a New-generation Bioartificial Endocrine Pancreas. Ann Surg, 2016. 264(1): p. 169-79.

45. Jiang, Z., et al., Laminin-521 Promotes Rat Bone Marrow Mesenchymal Stem Cell Sheet Formation on Light-Induced Cell Sheet Technology. Biomed Res Int, 2017. 2017: p. 9474573.

46. Batchelder, C.A., M.L. Martinez, and A.F. Tarantal, Natural Scaffolds for Renal Differentiation of Human Embryonic Stem Cells for Kidney Tissue Engineering. PLoS One, 2015. 10(12): p. e0143849.

47. Uygun, B.E., et al., Organ reengineering through development of a transplantable recellularized liver graft using decellularized liver matrix. Nat Med, 2010. 16(7): p. 814-20.

48. Kim, B.S., et al., Recellularization of decellularized human adipose-tissue-derived extracellular matrix sheets with other human cell types. Cell Tissue Res, 2012. 348(3): p. 559-67.

49. Freytes, D.O., et al., Preparation and rheological characterization of a gel form of the porcine urinary bladder matrix. Biomaterials, 2008. 29(11): p. 1630-7.

50. Sellaro, T.L., et al., Maintenance of hepatic sinusoidal endothelial cell phenotype in vitro using organ-specific extracellular matrix scaffolds. Tissue Eng, 2007. 13(9): p. 2301-10.

51. DeQuach, J.A., et al., Decellularized porcine brain matrix for cell culture and tissue engineering scaffolds. Tissue Eng Part A, 2011. 17(21-22): p. 2583-92.

52. Wolf, M.T., et al., A hydrogel derived from decellularized dermal extracellular matrix. Biomaterials, 2012. 33(29): p. 7028-38.

53. Cheng, M.H., et al., Dermis-derived hydrogels support adipogenesis in vivo. J Biomed Mater Res A, 2010. 92(3): p. 852-8.

54. Medberry, C.J., et al., Hydrogels derived from central nervous system extracellular matrix. Biomaterials, 2013. 34(4): p. 1033-40.

55. Singelyn, J.M., et al., Catheter-deliverable hydrogel derived from decellularized ventricular extracellular matrix increases endogenous cardiomyocytes and preserves cardiac function post-myocardial infarction. J Am Coll Cardiol, 2012. 59(8): p. 751-63.

56. Singelyn, J.M., et al., Naturally derived myocardial matrix as an injectable scaffold for cardiac tissue engineering. Biomaterials, 2009. 30(29): p. 5409-16.

57. Seif-Naraghi, S.B., et al., Design and characterization of an injectable pericardial matrix gel: a potentially autologous scaffold for cardiac tissue engineering. Tissue Eng Part A, 2010. 16(6): p. 2017-27.

58. Meyer, T., et al., Extracellular matrix proteins in the porcine pancreas: a structural analysis for directed pancreatic islet isolation. Transplant Proc, 1998. 30(2): p. 354.

59. Risteli, L. and R. Timpl, Isolation and characterization of pepsin fragments of laminin from human placental and renal basement membranes. Biochem J, 1981. 193(3): p. 749-55.

60. Sonnenberg, A., et al., Integrin recognition of different cell-binding fragments of laminin (P1, E3, E8) and evidence that alpha 6 beta 1 but not alpha 6 beta 4 functions as a major receptor for fragment E8. J Cell Biol, 1990. 110(6): p. 2145-55.

61. Slade, M.J., et al., Isolation of pepsin-resistant laminin fragments from human placenta: effect on epithelial cells cultured from the kidneys of patients with autosomal dominant polycystic kidney disease (ADPKD). Biochim Biophys Acta, 1996. 1310(1): p. 25-31.

62. Doran, M.R., et al., Surface-bound stem cell factor and the promotion of hematopoietic cell expansion. Biomaterials, 2009. 30(25): p. 4047-52.

63. Mullen, L.M., et al., Binding and release characteristics of insulin-like growth factor-1 from a collagen-glycosaminoglycan scaffold. Tissue Eng Part C Methods, 2010. 16(6): p. 1439-48.

64. Yayon, A., et al., Cell surface, heparin-like molecules are required for binding of basic fibroblast growth factor to its high affinity receptor. Cell, 1991. 64(4): p. 841-8.

65. Choong, F.J., et al., Islet heparan sulfate but not heparan sulfate proteoglycan core protein is lost during islet isolation and undergoes recovery post-islet transplantation. Am J Transplant, 2015. 15(11): p. 2851-64.

66. Claaßen, C., et al., Controlled Release of Vascular Endothelial Growth Factor from Heparin-Functionalized Gelatin Type A and Albumin Hydrogels. Gels, 2017. 3(4): p. 35.

67. Vigier, S., et al., Composition and organization of the pancreatic extracellular matrix by combined methods of immunohistochemistry, proteomics and scanning electron microscopy. Curr Res Transl Med, 2017. 65(1): p. 31-39.

68. Iozzo, R.V. and L. Schaefer, Proteoglycan form and function: A comprehensive nomenclature of proteoglycans. Matrix Biol, 2015. 42: p. 11-55.

69. Christenson, J.T., et al., Blood group incompatibility and accelerated homograft fibrocalcifications. J Thorac Cardiovasc Surg, 2004. 127(1): p. 242-50.

70. Xu, X., V.L. Browning, and J.S. Odorico, Activin, BMP and FGF pathways cooperate to promote endoderm and pancreatic lineage cell differentiation from human embryonic stem cells. Mech Dev, 2011. 128(7-10): p. 412-27.

71. Rezania, A., et al., Reversal of diabetes with insulin-producing cells derived in vitro from human pluripotent stem cells. Nat Biotechnol, 2014. 32(11): p. 1121-33.

72. Pagliuca, F.W., et al., Generation of functional human pancreatic beta cells in vitro. Cell, 2014. 159(2): p. 428-39.

73. Ma, F., et al., Large- scale differentiation and site-specific discrimination of hydroxyproline isomers by electron transfer/higher-energy collision dissociation (EThcD) mass spectrometry. Anal Chem, 2018.

74. Liu, F., et al., PKM2 methylation by CARM1 activates aerobic glycolysis to promote tumorigenesis. Nat Cell Biol, 2017. 19(11): p. 1358-1370.

Chapter 3 Supplemental Information

ID	Sex	Patient Age	Weight (kg)	Height (cm)	BMI	Donor Type	Blood Type	DCD/DBD	CIT (hours)	HbA1c (4.3-6.5)	Lipase (75-390)	Amylase (20-100)
8	Male	13 years	100	177.8	31.63	Head Trauma	O	DCD	7	5.9	196	190
10	Female	53 years	102	170.18	35.22	Anoxia	A	DCD	6	nd	153	35
11	Male	57 years	81.8	177.8	25.88	Cerebrovascular/Stroke	O	DBD	3	5.7	13	37
12	Male	27 years	30	121.92	20.18	Other Specify	O	DCD	20.5	5.8	15	100
13	Male	39 years	97.7	170.18	33.73	Cerebrovascular/Stroke	O	DBD	15.5	nd	390	71
14	Male	55 years	86	177.8	27.2	Head Trauma	A	DBD	8	4.8	12	40
15	Male	31 years	95	182.88	28.4	Head Trauma	A	DBD	9	5	22	43
16	Male	53 years	80	172.72	26.82	Anoxia	A	DBD	19	nd	14	316
23	Male	58 years	81.7	172.72	27.39	Cerebrovascular/Stroke	A	DBD	6.5	nd	19	35
27	Female	45 years	92.8	172.72	31.11	Cerebrovascular/Stroke	A	DBD	13.5	nd	9	55
35	Female	48 years	53	160.02	20.7	Head Trauma	O	DBD	5	5.4	19	31

Chapter 3 Table S1: Characteristics of human cadaver donors providing pancreata for decellularization.

Abbreviations: donor after cardiac death (DCD); donor after brain death (DBD); cold ischemic time (CIT); hemoglobin a1C (HbA1c); Body mass index (BMI).

Antibody	Product Number	Dilution	Manufacturer
Mouse anti-Collagen I	ab88147	1:250	Abcam
Rabbit anti-Pdx1	ab134150	1:1000	Abcam
Mouse anti-Insulin	I2018	1:10000	Sigma-Aldrich
Rabbit anti-Glucagon	ab92517	1:2000	Abcam
Rabbit anti-Ki67	ab16667 clone SP6	1:500	Abcam
Rabbit anti-Caspase3	9662	1:500	Cell Signalling
Mouse anti-Collagen IV	ab6586	1:1000	Abcam
Rabbit anti-Laminin	L9393	1:200	Sigma-Aldrich
Mouse anti-HLA ABC	ab70328	1:100	Abcam
Mouse anti-HLA DR	ab80658	1:1000	Abcam
Mouse anti-Nkx6.1	F55A12-s	1:100	DSHB
Rabbit anti-vWF	A008202-5	1:500	Dako
Mouse anti-VE Cadherin	sc-9989	1:100	Santa Cruz Biotechnology
Anti-human CD3	ab134093	1:500	Abcam
Anti-human CD8	ab108343	1:100	Abcam
Anti-human CD20	555677	1:500	BD Pharmingen
Anti-human CD45	555491	1:20	BD Pharmingen
Anti-human CD68	M0814	1:1000	Dako
Anti-mouse CD68	ab31630	1:100	Abcam
Anti-human FoxP3	ab10563	1:300	Abcam

Chapter 3 Table S2: Antibodies for immunocytochemistry and immunohistochemistry.

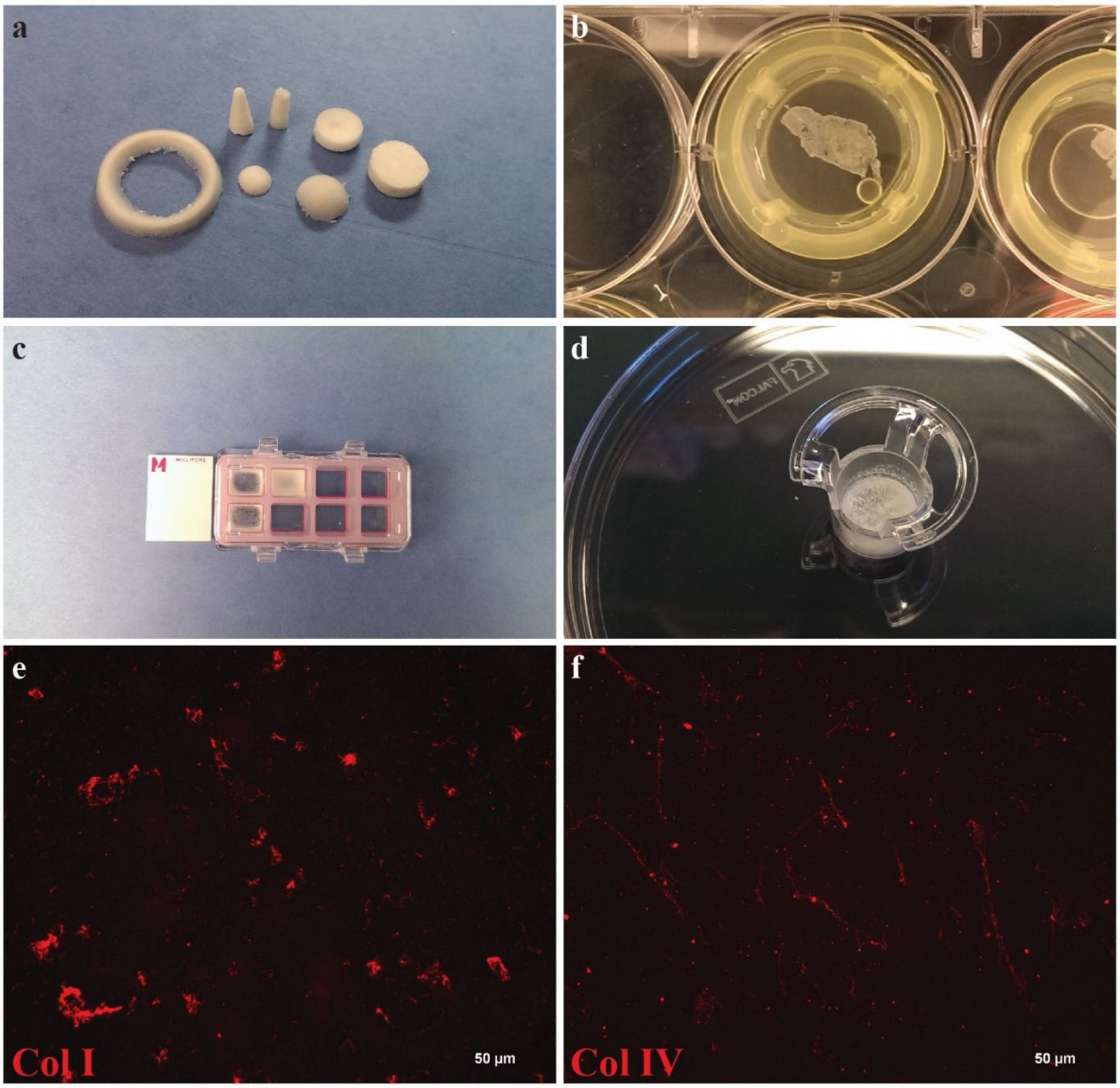

Chapter 3 Fig. S1: Applications for decellularized pancreas ECM. hP-ECM and hP-HG are able to be manipulated to produce several types of acellular natural matrix constructs, including intact 3D matrix (a), cut in thin slices (b), placed in tissue culture vessels such as chamber slides (c) Transwells (d) and applied in thin coatings to tissue culture plate show in e and f stained with collagen I and IV.

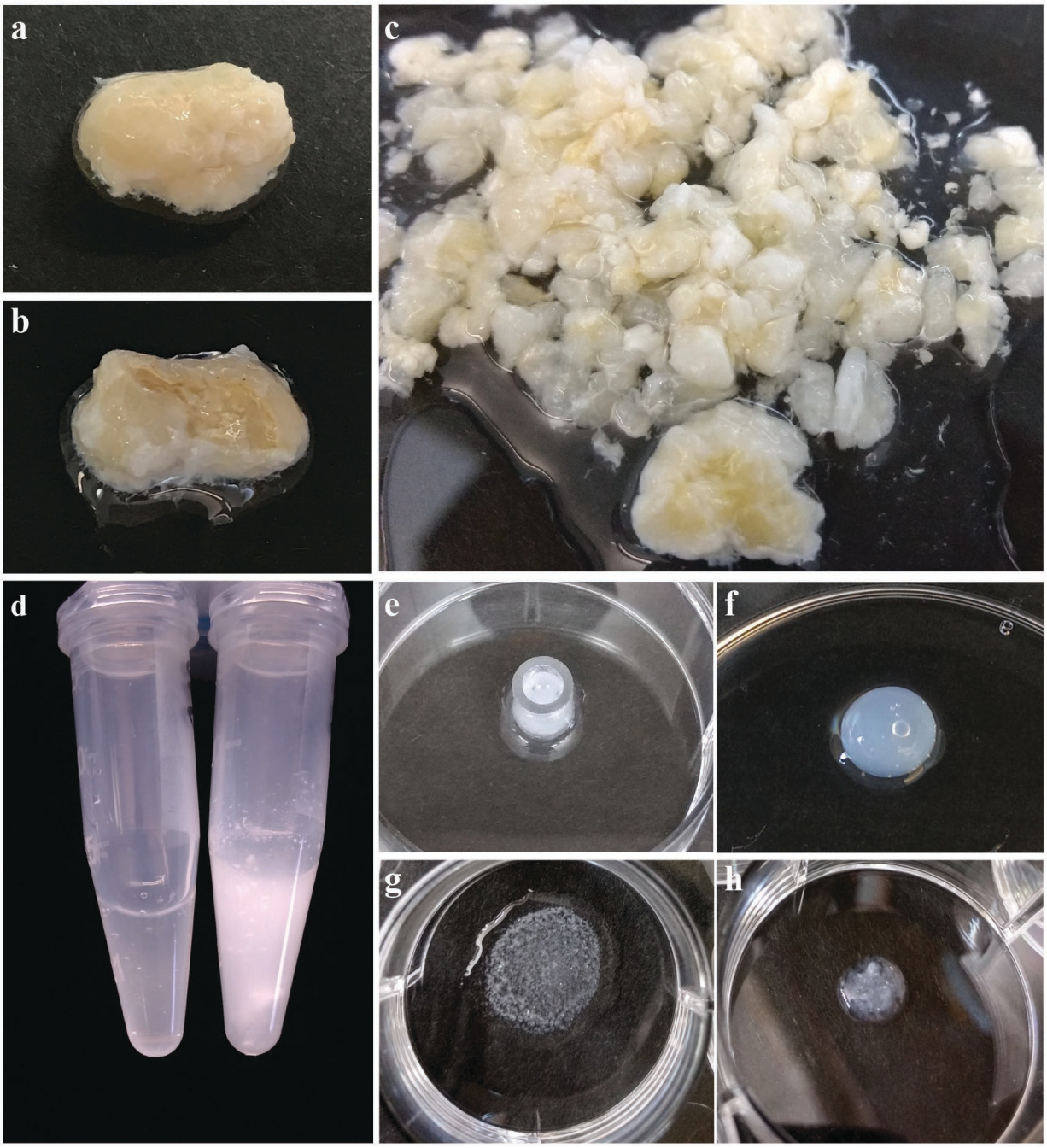

Chapter 3 Fig. S2: High fat content inhibits solubilization and gelation. a) Cube of spin-decellularized pancreas, b) bisected to reveal a yellow interior with higher fat content. c) Several cut up pieces with yellow interiors. Following pepsin digestion, the pre-gel solution is cloudier following spin-decell (d, right) compared to homogenized decell (d, left). When neutralized and gelled in a mold (e) the homogenized-decell consistently yields a sturdy gel (f) while the spin-decell results in no gelation (g) or incomplete gelation (h) - depending on the initial fat content of the donor organ.

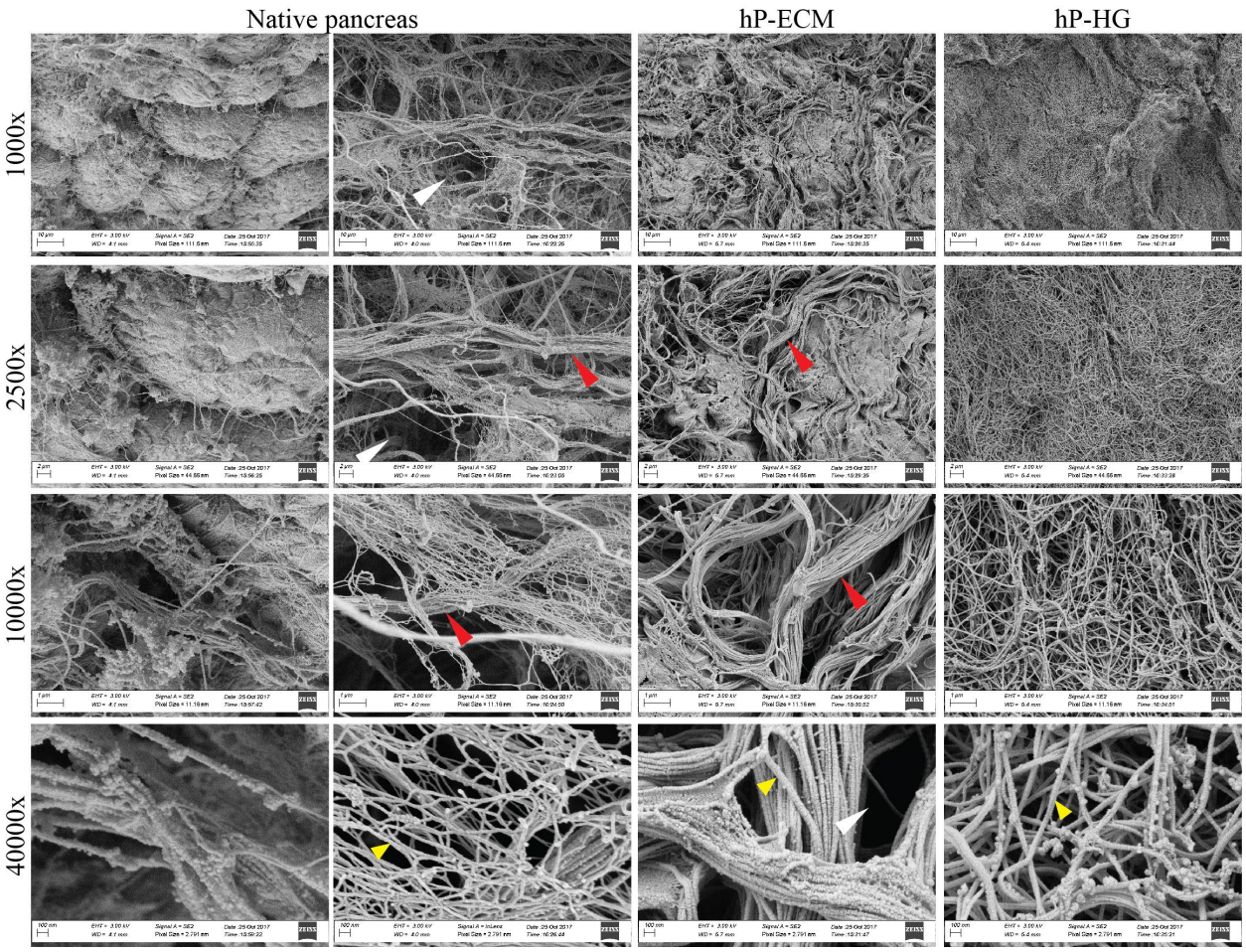

Chapter 3 Fig S3: Organization of native pancreas and decellularized hP-ECM and hP-HG by SEM. Native pancreas demonstrating cells organized in dense clusters and covered by connective tissues of high and low densities. Long white arrows indicate empty space within the ECM, potentially suitable for cell occupation. Long red arrows indicate collagen fibril bundle structures, retained within the hP-ECM. Short yellow arrows indicate collagen fibrils, present in the native tissue, the hP-ECM as well as the hP-HG.

	Protein Group	Type	Gene	Name	Intensity
1	Core matrisome	Collagens	COL1A2	Collagen Type 1 Alpha 1 Chain	1.97E+09
2	Core matrisome	Collagens	COL1A1	Collagen Type 1 Alpha 2 Chain	5.17E+09
3	Core matrisome	Collagens	COL5A2	Collagen Type 5 Alpha 2 Chain	1.53E+08
4	Core matrisome	Collagens	COL5A1	Collagen Type 5 Alpha 1 Chain	1.24E+08
5	Core matrisome	Collagens	COL3A1	Collagen Type 3 Alpha 1 Chain Isoform 1	1.42E+09
6	Core matrisome	Collagens	COL3A1	Collagen Type 3 Alpha 1 Chain Isoform 2	4.00E+06
7	Core matrisome	Collagens	COL6A1	Collagen Type 6 Alpha 1 Chain	6.32E+07
8	Core matrisome	Collagens	COL6A3	Collagen Type 6 Alpha 3 Chain	7.46E+07
9	Core matrisome	Collagens	COL6A2	Collagen Type 6 Alpha 2 Chain Isoform 2C2	1.83E+06
10	Core matrisome	Collagens	COL6A2	Collagen Type 6 Alpha 2 Chain Isoform 2C2A	6.23E+04
11	Core matrisome	Collagens	COL4A2	Collagen Type 4 Alpha 2 Chain	6.38E+07
12	Core matrisome	Collagens	COL14A1	Collagen Type 14 Alpha 1 Chain	2.81E+06
13	Core matrisome	Collagens	COL5A3	Collagen Type 5 Alpha 3 Chain	3.99E+07
14	Core matrisome	Collagens	COL2A1	Collagen Type 2 Alpha 1 Chain	2.81E+07
15	Core matrisome	Collagens	COL16A1	Collagen Type 16 Alpha 1 Chain	1.22E+07
16	Core matrisome	Collagens	COL4A4	Collagen Type 4 Alpha 4 Chain	8.56E+05
17	Core matrisome	Collagens	COL4A1	Collagen Type 4 Alpha 1 Chain	2.90E+07
18	Core matrisome	Collagens	COL18A1	Collagen Type 18 Alpha 1 Chain	1.66E+06
19	Core matrisome	Collagens	COL11A1	Collagen Type 11 Alpha 1 Chain	6.30E+05
20	Core matrisome	Collagens	COL15A1	Collagen Type 15 Alpha 1 Chain	1.26E+06
21	Core matrisome	Collagens	COL8A1	Collagen Type 8 Alpha 1 Chain	7.11E+06
22	Core matrisome	Collagens	COL6A6	Collagen Type 6 Alpha 6 Chain	1.03E+06
23	Core matrisome	Collagens	COL28A1	Collagen Type 28 Alpha 1 Chain	2.34E+06
24	Core matrisome	Collagens	COL4A5	Collagen Type 4 Alpha 5 Chain	1.42E+05
25	Core matrisome	Collagens	COL4A3	Collagen Type 4 Alpha 1 Chain	3.60E+05
26	Core matrisome	Collagens	COL21A1	Collagen Type 21 Alpha 1 Chain	4.20E+06
27	Core matrisome	Collagens	COL11A2	Collagen Type 11 Alpha 2 Chain	3.69E+05
28	Core matrisome	Collagens	COL12A1	Collagen Type 12 Alpha 1 Chain	7.56E+05
29	Core matrisome	Collagens	COL10A1	Collagen Type 10 Alpha 1 Chain	4.20E+05
30	Core matrisome	Collagens	COL13A1	Collagen Type 13 Alpha 1 Chain	5.28E+05
31	Core matrisome	Collagens	COL7A1	Collagen Type 7 Alpha 1 Chain	1.01E+06
32	Core matrisome	Collagens	COL9A3	Collagen Type 9 Alpha 3 Chain	6.77E+05
33	Core matrisome	Collagens	COL8A2	Collagen Type 8 Alpha 2 Chain	4.86E+05
34	Core matrisome	ECM Glycoproteins	LAMA5	Laminin Subunit Alpha 5	1.61E+06
35	Core matrisome	ECM Glycoproteins	LAMC1	Laminin Subunit Gamma 1	3.31E+06
36	Core matrisome	ECM Glycoproteins	LAMB1	Laminin Subunit Beta 1	1.93E+06
37	Core matrisome	ECM Glycoproteins	FBN1	Fibrillin 1	3.35E+06
38	Core matrisome	ECM Glycoproteins	LAMA2	Laminin Subunit Alpha 2	2.20E+06
39	Core matrisome	ECM Glycoproteins	LAMB2	Laminin Subunit Beta 2	9.19E+05
40	Core matrisome	ECM Glycoproteins	AGRN	Agrin	1.10E+06
41	Core matrisome	ECM Glycoproteins	NID2	Nidogen 2	9.52E+05
42	Core matrisome	ECM Glycoproteins	NID1	Nidogen 1	6.23E+05
43	Core matrisome	ECM Glycoproteins	FGA	Fibrinogen Alpha Chain	6.99E+05
44	Core matrisome	ECM Glycoproteins	FN1	Fibronectin 1	7.34E+05
45	Core matrisome	ECM Glycoproteins	TINAGL1	Tubulointerstitial Nephritis Antigen Like 1	4.51E+05
46	Core matrisome	ECM Glycoproteins	FRAS1	Fraser Extracellular Matrix Complex Subunit 1	1.49E+05
47	Core matrisome	ECM Glycoproteins	FGB	Fibrinogen Beta Chain	2.96E+05
48	Core matrisome	ECM Glycoproteins	FGG	Fibrinogen Gamma Chain	3.31E+05
49	Core matrisome	ECM Glycoproteins	VTN	Vitronectin	2.98E+05
50	Core matrisome	ECM Glycoproteins	LAMA4	Laminin Subunit Alpha 4	3.71E+05
51	Core matrisome	ECM Glycoproteins	MFGE8	Milk Fat Globule-EGF Factor 8 Protein	1.98E+05
52	Core matrisome	ECM Glycoproteins	DPT	Dermatopontin	1.21E+06
53	Core matrisome	ECM Glycoproteins	EMILIN1	Elastin Microfibril Interfacer 1	1.54E+05
54	Core matrisome	ECM Glycoproteins	LAMC3	Laminin Subunit Gamma 3	2.81E+05
55	Core matrisome	ECM Glycoproteins	TNXB	Tenascin XB	1.44E+05
56	Core matrisome	ECM Glycoproteins	POSTN	Periostin	8.03E+04
57	Core matrisome	ECM Glycoproteins	TGFBI	Transforming Growth Factor Beta Induced	1.24E+05
58	Core matrisome	ECM Glycoproteins	IGFBP7	Insulin Like Growth Factor Binding Protein 7	1.86E+05
59	Core matrisome	ECM Glycoproteins	VWA5A	Von Willebrand Factor A Domain Containing 5A	5.47E+04
60	Core matrisome	ECM Glycoproteins	THBS1	Thrombospondin 1	2.95E+04

	Protein Group	Type	Gene	Name	Intensity
61	Core matrisome	ECM Glycoproteins	NPNT	Nephronectin	3.68E+04
62	Core matrisome	ECM Glycoproteins	FBLN1	Fibulin 1	2.75E+04
63	Core matrisome	ECM Glycoproteins	IGFBP2	Insulin Like Growth Factor Binding Protein 2	2.38E+04
64	Core matrisome	ECM Glycoproteins	LTBP1	Latent Transforming Growth Factor Beta Binding Protein	1.02E+05
65	Core matrisome	Proteoglycans	HSPG2	Perlecan	6.59E+06
66	Core matrisome	Proteoglycans	BGN	Biglycan	1.06E+07
67	Core matrisome	Proteoglycans	PRELP	Prolargin	6.93E+06
68	Core matrisome	Proteoglycans	DCN	Decorin	1.16E+07
69	Core matrisome	Proteoglycans	ASPN	Asporin	4.94E+06
70	Core matrisome	Proteoglycans	LUM	Lumican	2.76E+06
71	Core matrisome	Proteoglycans	OGN	Osteoglycin	7.76E+05
72	Core matrisome	Proteoglycans	FMOD	Fibromodulin	3.16E+04
73	Matrisome-associated	ECM Regulators	PRSS1	Protease, Serine 1	1.14E+06
74	Matrisome-associated	ECM Regulators	PRSS3	Protease, Serine 3	6.74E+05
75	Matrisome-associated	ECM Regulators	CELA3A	Chymotrypsin Like Elastase Family Member 3A	7.89E+05
76	Matrisome-associated	ECM Regulators	PRSS2	Protease, Serine 2	3.99E+05
77	Matrisome-associated	ECM Regulators	CELA2A	Chymotrypsin Like Elastase Family Member 2A	8.69E+05
78	Matrisome-associated	ECM Regulators	TGM2	Transglutaminase 2	9.74E+05
79	Matrisome-associated	ECM Regulators	CELA3B	Chymotrypsin Like Elastase Family Member 3B	2.78E+05
80	Matrisome-associated	ECM Regulators	CTSD	Cathepsin D	7.98E+05
81	Matrisome-associated	ECM Regulators	CELA2B	Chymotrypsin Like Elastase Family Member 2B	1.52E+05
82	Matrisome-associated	ECM Regulators	AMBP	Alpha-1-Microglobulin/Bikunin Precursor	6.31E+05
83	Matrisome-associated	ECM Regulators	SERPINB1	Serpin Family B Member 1	6.24E+05
84	Matrisome-associated	ECM Regulators	SERPINA3	Serpin Family A Member 3	9.15E+04
85	Matrisome-associated	ECM Regulators	SERPINA1	Serpin Family A Member 1	3.81E+05
86	Matrisome-associated	ECM Regulators	SERPINI2	Serpin Family I Member 2	6.19E+05
87	Matrisome-associated	ECM Regulators	CSTB	Cystatin B	1.25E+05
88	Matrisome-associated	ECM Regulators	CTSB	Cathepsin B	3.34E+05
89	Matrisome-associated	ECM Regulators	SERPINH1	Serpin Family H Member 1	1.05E+04
90	Matrisome-associated	ECM Regulators	A2M	Alpha-2-Macroglobulin	3.57E+04
91	Matrisome-associated	ECM Regulators	ITIH5	Inter-α-Trypsin Inhibitor Heavy Chain Family Member 5	5.27E+04
92	Matrisome-associated	ECM Regulators	CST3	Cystatin C	9.04E+04
93	Matrisome-associated	ECM Regulators	SERPING1	Serpin Family G Member 1	1.67E+04
94	Matrisome-associated	ECM Regulators	KNG1	Kininogen 1	2.71E+04
95	Matrisome-associated	ECM-affiliated Proteins	ANXA4	Annexin A4	7.93E+05
96	Matrisome-associated	ECM-affiliated Proteins	ANXA6	Annexin A6	4.42E+05
97	Matrisome-associated	ECM-affiliated Proteins	ANXA2	Annexin A2	6.07E+05
98	Matrisome-associated	ECM-affiliated Proteins	REG1A	Regenerating Family Member 1 Alpha	1.11E+06
99	Matrisome-associated	ECM-affiliated Proteins	ANXA1	Annexin A1	2.75E+05
100	Matrisome-associated	ECM-affiliated Proteins	REG1B	Regenerating Family Member 1 Beta	1.79E+05
101	Matrisome-associated	ECM-affiliated Proteins	LMAN1	Lectin, Mannose Binding 1	3.77E+05
102	Matrisome-associated	ECM-affiliated Proteins	LGALS4	Galectin 4	4.07E+05
103	Matrisome-associated	ECM-affiliated Proteins	LGALS1	Galectin 1	8.23E+05
104	Matrisome-associated	ECM-affiliated Proteins	ANXA11	Annexin A11	2.71E+05
105	Matrisome-associated	ECM-affiliated Proteins	ANXA3	Annexin A3	9.49E+04
106	Matrisome-associated	ECM-affiliated Proteins	LGALS2	Galectin 2	1.76E+05
107	Matrisome-associated	ECM-affiliated Proteins	ANXA5	Annexin A5	1.08E+04
108	Matrisome-associated	ECM-affiliated Proteins	ANXA7	Annexin A7	1.63E+04
109	Matrisome-associated	ECM-affiliated Proteins	LGALS8	Galectin 8	3.44E+04
110	Matrisome-associated	ECM-affiliated Proteins	LGALS3	Galectin 3	6.71E+03
111	Matrisome-associated	ECM-affiliated Proteins	REG3A	Regenerating Family Member 3 Alpha	7.89E+04
112	Matrisome-associated	ECM-affiliated Proteins	C1QTNF2	C1q And TNF Related 2	6.60E+04
113	Matrisome-associated	ECM-affiliated Proteins	C1QTNF5	C1q And TNF Related 5	2.33E+05
114	Matrisome-associated	ECM-affiliated Proteins	HPX	Hemopexin	4.07E+04
115	Matrisome-associated	Secreted Factors	S100A13	S100 Calcium Binding Protein A13	8.68E+04
116	Matrisome-associated	Secreted Factors	HRNR	Hornerin	1.79E+04
117	Matrisome-associated	Secreted Factors	S100A10	S100 Calcium Binding Protein A10	2.41E+04
118	Matrisome-associated	Secreted Factors	S100A11	S100 Calcium Binding Protein A11	8.73E+03
119	Matrisome-associated	Secreted Factors	CFC1B	CFC1B	2.33E+04
120	Matrisome-associated	Secreted Factors	HCFC1	Host Cell Factor C1	5.72E+04

Chapter 3 Fig. S4: Full list of all 120 matrisome and matrisome-associated proteins identified in the decellularized hP-ECM. Proteins were classified using the MatrixDB database.

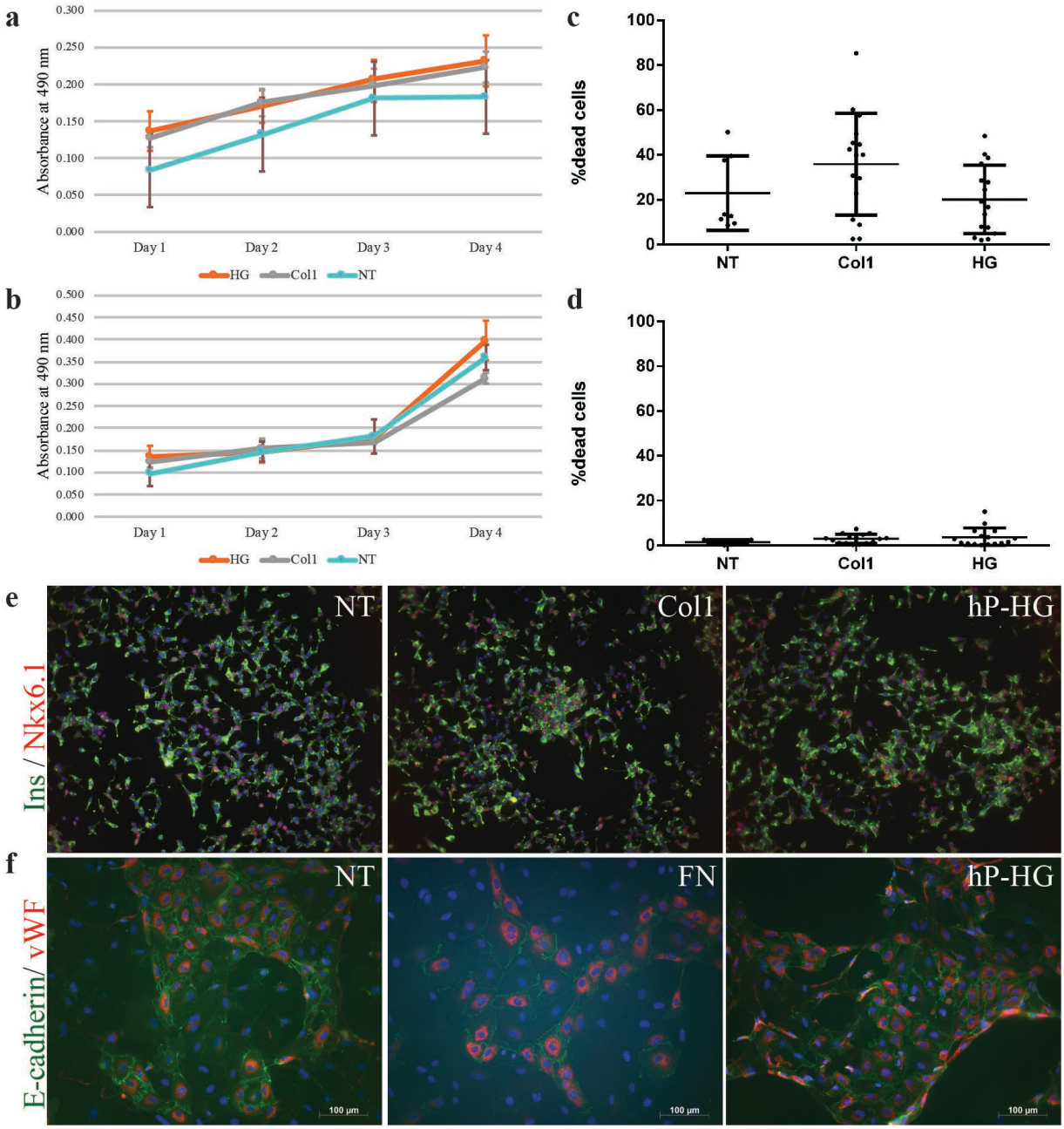

Chapter 3 Fig. S5: *In vitro* cytocompatibility evaluation of hP-HG using HUVECs and INS-1 832/13 cells. Cells were cultured for 4 days on either tissue culture plastic (NT, not treated), collagen I (Col 1), or human pancreatic ECM hydrogel (hP-HG). Cells were analysed daily using the MTS assay, at the end of the culture period by live:dead staining protocol and by specific marker staining. a) HUVEC MTS growth curve. b) INS-1 832/13 cells MTS growth curve. c and d) % dead cells quantified at day 4 of culture for HUVECs and INS-1 832/13 cells, respectively. e) Insulin (green) and Nkx6.1 (red) staining of INS-1 832/13 cells cultured under the 3 different conditions at day 4 of culture. f) E-cadherin (green) and von Willebrand Factor (vWF, red) staining of HUVECS cultured under the 3 different conditions at day 4 of culture.

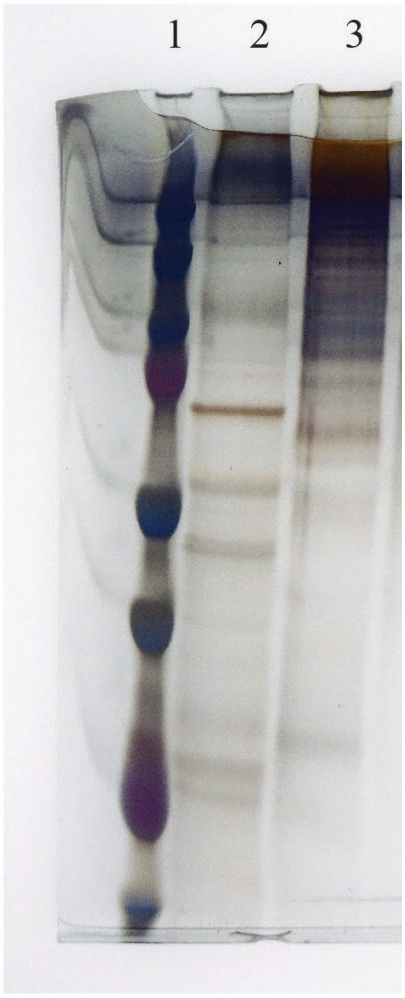

Chapter 3 Fig. S6: Full length image of the SDS-PAGE gel shown in Figure 6. Lane 1 is loaded with the Precision Plus Protein Dual Color Standard. Lane 2 is loaded with 10 µg of the native pancreas from the same donor as Lane 3, loaded with 10 µg of decellularized pancreatic ECM. The remaining lanes of the gel contained samples unrelated to this project. The image shown in Figure 6a was cropped slightly to remove the edges of the gel, and rotated slightly to straighten the lanes.

Chapter 3 Supplementary Methods

Pancreata Procurement

Pancreata are deemed unsuitable for transplantation for some of the following reasons: vascular damage or anomaly, high BMI, or duodenal injury or anomaly after visual inspection. Organs were selected from donors with no history or evidence of pancreatitis, diabetes, pancreatic cancer, hepatitis or HIV infection and were from donation after circulatory death (DCD) or donation after brain death (DBD). Organs were recovered after *in situ* flush with UW Solution [ViaSpan® (TEVA Pharmaceuticals USA, Inc., North Wales, Pennsylvania), SPS-1, (Organ Recovery Systems, Inc. Itasca, Illinois), or UW Belzer® Cold Storage Solution (Bridge to Life, Ltd. Columbia, South Carolina)], and stored in the same solution at 4˚C until tissues were processed within 24 hours of recovery. No organs/tissue were procured from prisoners.

Modified Folch Method

30 mg of lyophilized ECM was weighed; 2 ml of 1:3 (v:v) chloroform:methanol solution was added to each sample. Samples were incubated for 30 minutes shaking at RT, centrifuged (4300 rpm, 5 min), and the supernatant was decanted into a new tube. 800 µl of water and 2.5 ml of chloroform was added to the supernatant, and tubes were vigorously shaken. Samples were centrifuged (2200 rpm, 5 min) and the upper phase was removed. The lower phase was allowed to air dry in a fume hood for 4-7 days until dry; the resulting lipid material was weighed to determine lipid content of the original sample.

Hydrogel Formation

Pepsin was used at a ratio of 0.1 mg pepsin per 1 mg ECM and solubilized in 0.01 M HCl prior to being added to the ECM. The digestion was prepared such that the final gel would have

a density of 8 mg ECM/ml gel. This required a volume of 818 µl of 0.01 M HCl per 1 mg of lyophilized ECM. ECM was digested for 72-96 hours at RT until the solution was transparent and free of undigested pieces. If a significant amount of undigested matrix was still present after 48 hours of digestion, the solution was homogenized and digested for another 48 hours at RT. Neutralization of the acidic digest solution was achieved by mixing ice cold 0.1 M NaOH (equal to 1/10 the volume of acidic digest) and 10X PBS (equal to 1/9 the total volume of digest + NaOH used) and adding this mixed solution to the digested ECM at 4˚C. Mixed pre-gel solution is then placed at 37˚C for 30 minutes for gelation to occur. If not used immediately, the gel was lyophilized and stored at -80˚C.

Generation of Humanized Mice.

Research involving mice was performed in accordance with a protocol that was approved by the University of Wisconsin School of Medicine and Public Health Animal Care and Use Committee, and in accordance with a protocol approved by the University of Wisconsin Institutional Review Board. Humanized mice were generated similarly to previously published reports [65-67]. Briefly, NOD-*SCID IL2rγ*^{null} (NSG) mice aged 7–8 weeks, obtained from Jackson Laboratories (stock #005557), were conditioned with sub-lethal total body irradiation with 250 RAD via an X-RAD 320ix irradiator (Precision X-Ray, North Branford, CT) and within 4 hours transplanted with 1mm^3 human foetal thymus fragments (14-20 weeks gestation and obtained from Advanced Bioscience Resource (Alameda, CA)) into the kidney subcapsular space. Immediately following surgery, mice were intravenously injected with 40,000 purified CD34+ cells, which were isolated from autologous liver tissue. The CD34+ cells were isolated via magnetically activated cell sorter (MACS) separation system (Militenyi Biotec, Auburn, CA). Mice

were monitored for engraftment of human white blood cells (hCD45+) at 8 and 12 weeks and are considered successfully humanized with presence of greater than 25% hCD45+ cells. Further details are available in supplementary materials.

Proteomics analysis.

The OMSSA proteomic Analysis Software Suite (COMPASS) was used for peptide identification and searched against Homo sapiens Uniprot database. Trypsin was selected as the enzyme and maximum of two missed cleavages were allowed. Precursor and fragment ion tolerance was set to 25 ppm and 0.02 Da. DiLeu labelling on N-termini, lysine residue (+145.1267748 Da), and carbamidomethylation of cysteine residues (+57.02146 Da) were chosen as static modifications. Variable modifications included methionine oxidation (+15.99492 Da) and DiLeu labelling on tyrosine residue (+145.1267748). Results were filtered at 1% false discovery rate (FDR) for both peptide and protein.

Chapter 4

Human pancreas ECM hydrogel improves yield and expression profiles of stem cell-derived β cells.

This study was designed by Daniel Tremmel, Sara Dutton Sacket and Jon Odorico. Daniel Tremmel, Austin Feeney, Andrew Curran, and Sam Mitchell performed the experiments. Sara Dutton Sacket and Jon Odorico provided guidance and expertise. Daniel Tremmel prepared the figures and wrote the paper.

Abstract

Stem cell-derived β cells (SCβCs) do not fully recapitulate the functional and phenotypic profiles of primary, mature β cells. While many approaches are being used to improve the differentiation of these cells, the majority of the effort lies in deriving a better chemically-induced protocol for differentiating the cells. We recently developed a human pancreas extracellular matrix (ECM) hydrogel (hP-HG) that recapitulates the ECM environment of the adult human pancreas. Because the ECM is known to play an important role in primary islet health and function, we hypothesize the hP-HG may have a beneficial role in SCβC differentiation. By culturing SCβCs with hP-HG, we show that in the later stages of differentiation, hP-HG may stimulate better endocrine commitment and gene expression, but in its current composition in the context of the protocols tested may not be able to rescue deficiencies in SCβC function.

Introduction

Despite consistent research in diabetes treatment technology, millions of people die every year from diabetes-related complications. Non-invasive treatment options, like insulin injections or pumps, manage symptoms but do not result in consistently stable blood glucose levels, leading to potential long-term complications due to periods of hyper- and hypoglycemia. Surgical β cell-replacement treatment, such as pancreas or islet transplantation, supply functional β cells to effectively regulate blood glucose, but are limited by donor tissue availability and require a lifetime of immunosuppressive treatments for the patient, which adds additional complications and restrictions to a patient's standard of living [1, 2].

Significant research effort has focused on deriving functional SCβCs as an alternate and more sustainable treatment for diabetes. Conceptually, patient-specific induced pluripotent

stem cells (iPSCs) could be derived and re-differentiated into functional insulin-producing cells that immunologically match the patient thereby eliminating or drastically reducing the immuno-suppression therapy requirement [3]. While advances have been made in β cell differentiation from stem cells, a fundamental barrier to this treatment includes a deficit in the ability to produce mature, functional β cells from stem cells *in vitro* [4-6]. The most recent and impressive protocols generate β-like cells capable of dynamic insulin secretion assessed by perifusion glucose stimulated insulin secretion (GSIS), but with significantly lower total insulin content and lower stimulation indices than those of native islets [7, 8]. Glucose stimulated insulin secretion (GSIS) assays test insulin secretion in response to glucose or other secretagogues. Cells are exposed to low (2.8 mM) and high (28 mM) glucose, and results are reported as a stimulation index (SI), defined as the ratio of insulin secreted under high glucose conditions over low glucose conditions, which is a readout for glucose-responsive functionality. An improved dynamic GSIS response is the key next step in SCβC generation.

The development of *in vitro* SCβC differentiation protocols relies on recapitulating step-wise gene expression patterns that have been established from rodent and human islet and pancreas studies. SCβCs express key β cell genes such as insulin (Ins), Pdx1, Nkx6.1 and Nkx2.2, but to varying degrees of similarity to human islets. Gene expression profiling is preformed throughout the step-wise protocols to confirm proper differentiation; for example *PDX1* is expressed in pancreas progenitor 1 (PP1) cells during Stage 3, and continues to be expressed throughout the remainder of the differentiation, following the expression pattern of this gene during development. The endocrine progenitor gene Neurogenin 3 (*NGN3*), a transiently expressed TF during development, is expressed during Stage 5 of differentiation, but continues

to have detectable expression beyond Stage 5. In the pancreas, *NGN3* is not expressed in adult mature β cells [5], and therefore this is indicative of incomplete maturation *in vitro*, in at least a subset of cells. On the other hand, two markers of β cell maturation, the peptide hormone urocortin-3 (*UCN3*), and the critical transcription factor *MAFA*, have been absent, or detected at very low expression levels in SCβCs in most published protocols [5-9]. These gene expression profiles suggest that β-like cells derived *in vitro* are not fully mature.

A hypothesis concerning the barriers to *in vitro* β cell differentiation is that the lack of ECM throughout the differentiation process provides a microenvironment which is insufficient to support the generation of *bona fide* β cells. The ECM is a network of proteins and polysaccharides that regulate cell signaling in a variety of ways: by directly binding cell receptors such as integrins; by sequestering growth factors, affecting diffusion and growth factor-receptor interaction dynamics; and by providing mechanical support to cells [10]. ECM composition is unique to each tissue, and changes dynamically during development [11, 12]. In adult human islets, ECM has been associated with β cell survival and improved insulin secretion dynamics, and in fetal islets, ECM has also been associated with proliferation and differentiation [13]. Furthermore, the process of isolating islets from the pancreas involves collagenase digestion, which destroys much of the native ECM, resulting in reduced islet survival and function post-isolation [14]. Co-culture of islets with individual purified ECM proteins has been shown to affect islet-specific gene expression [15-17]. Islet ECM composition has also been shown to change with the progression of both T1d and T2D [18]. Importantly, ECM expression in SCβCs appears dysregulated and blunted compared to native *in situ* islets (Figure 1). Together these data suggest that pancreatic ECM plays an important role in β cell development, maturation, and survival.

Natural ECM can be isolated from tissues through a process called decellularization, in which cellular material is removed from the native ECM following cell lysis and subsequent washing. In this way, ECM has been extracted from many animal and human organs, and has been proposed for use in regenerative medicine for a variety of applications [19, 20]. Decelled ECM has been successfully used to induce differentiation of stem cells toward liver, kidney and lung lineages [21], providing evidence that ECM can enhance and direct stem cell differentiation.

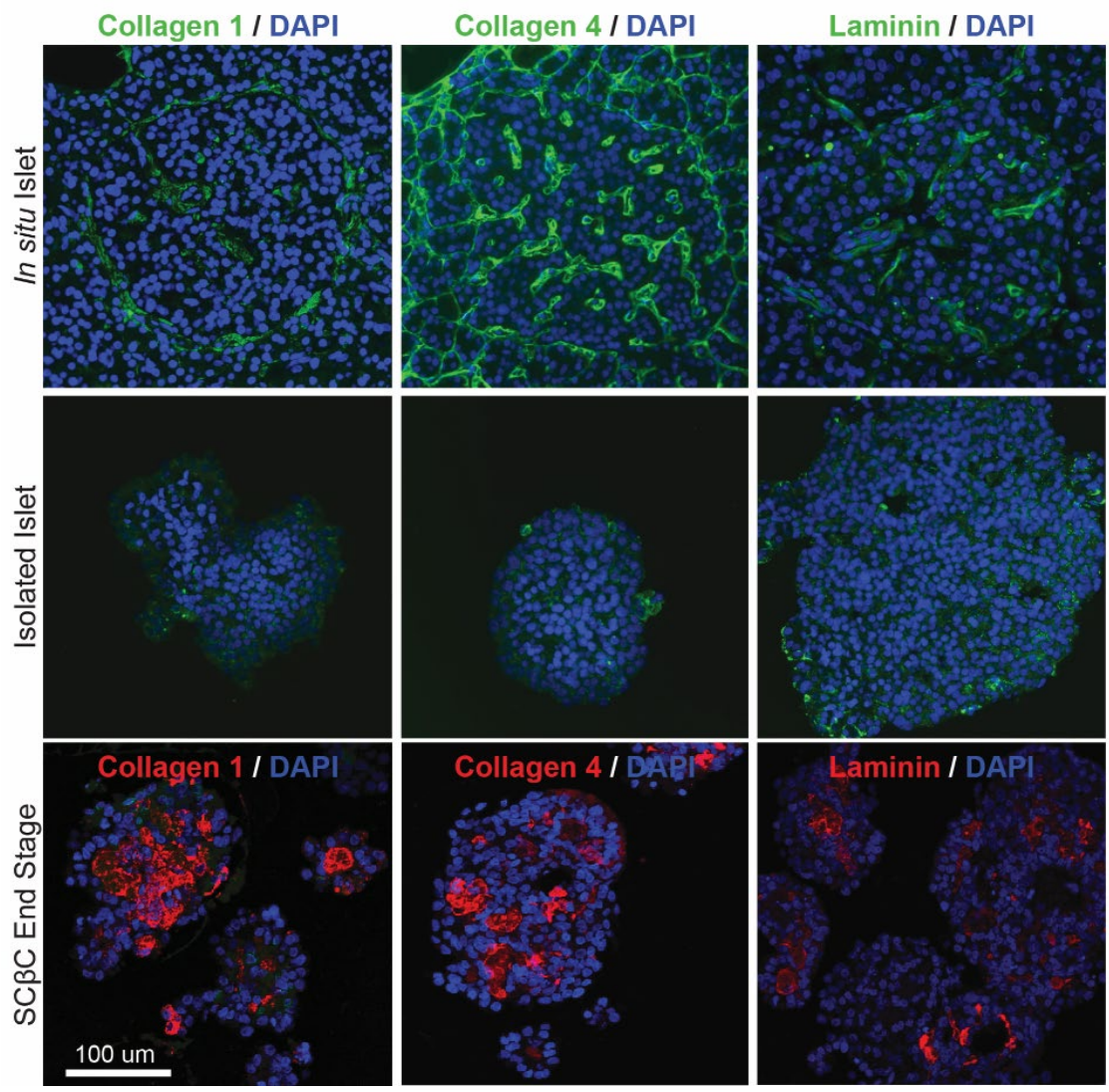

Figure 1. ECM expression in islets and SCβCs. Expression of ECM proteins Collagen 1, Collagen 4 and laminins (detected by a pan-laminin antibody) is dramatically different between islets *in situ*, islets shortly after isolation, and SCβCs at the end point of differentiation.

Decelled ECM can be implemented as a scaffold for cell culture in different ways. Some studies aim to decell an intact organ, generally through perfusion of vasculature, to preserve the macro- and microstructures of the organ [19], however seeding cells into these matrices has proven to be a challenge [22, 23]. Others aim to reconstitute the ECM in a new form, as a hydrogel or sponge [24, 25]. The acellular and purified ECM is digested with acidic pepsin to solubilize the ECM proteins in order to "reform" the ECM. The digested ECM solution can then be neutralized and warmed to form a hydrogel, or lyophilized to form a sponge. This requires digestion and re-formation of collagen fibrils [26], and therefore reorganizes the ECM microstructure.

Our group recently published the first protocol for generating a hydrogel from human pancreatic ECM (hP-ECM) [27]. We demonstrate delipidization, decellularization and digestion of the tissue to generate a hydrogel that retains many of the ECM components of the native tissue. Additionally, we utilized the purified hP-ECM to report the first quantitative mass spectrometry-based characterization of the human pancreatic matrisome. Using the enriched ECM and our highly sensitive DiLeu labeling method, we identified 120 ECM-associated proteins in the decellularized adult pancreas, 4-fold higher than the previously published mouse pancreatic matrisome [28]. In this study, we demonstrated the ability to generate hP-ECM and hP-HG from human tissue as well as the power to characterize the matrisome of these tissues with high sensitivity and consistency, despite complex sample composition. Additionally, we demonstrated that hP-HG is compatible with stem cells and stem cell-derived pancreatic progenitors, indicating that this material is a suitable scaffold for differentiation studies [27].

Several groups have tested the use of ECM products in culture with islets and stem cells. Many early studies utilizing purified ECM proteins in islet culture demonstrated that adding

individual ECM proteins back to islets following isolation has beneficial effects on survival and function [13, 15, 16, 29, 30]; the exact pathways through which ECM enhances these phenotypes is not fully understood. Despite work on islet encapsulation with ECM proteins or synthetic polymers, the application of these materials in β cell differentiation has been very limited. It has been shown that basement membrane-like material containing laminin 511 was able to enhance differentiation of mouse embryonic stem cells (ESCs) toward a pancreatic fate [31]. Another study combined decelled rat pancreas with mouse ESCs and found that the differentiating cells were compatible with the ECM and expressed insulin earlier in differentiation than without the ECM. However the group encountered difficulty with effectively distributing the ESCs into their intact pancreas ECM platform [23]. A recent study using ECM extracted from a rat β cell line was able to induce human ESCs to express β cell markers (Pdx1, Glut2 and Ins) *in vitro*, and restore normoglycemia following transplantation into diabetic mice. However, this study did not assess the maturation and function of the cells and appears to have produced cells of similar quality to other differentiation protocols [32].

While these studies suggest that ECM plays a role in both β cell differentiation and function, none have yet demonstrated sufficient improvements to *in vitro* β cell differentiation, i.e. improved maturation. The ease of incorporating hP-HG into cell culture, and the pancreas-specific composition of the material give promise to the success of our approach and warrant further investigation. This study will assess the effect that hP-HG has on each stage of β cell differentiation to determine the optimal timing and method of hP-HG co-culture. Following optimization of culture conditions, the effect that hP-HG has on SCβC gene expression and function will be assessed.

Results

Our group generates SCβC clusters containing all of the major endocrine cell types of a native islet using a protocol based on our previously published endoderm enrichment and improved upon based on recently published protocols in the field and our own empirically tested modifications [4-6, 33, 34]. The result is a 7-stage, 28-day protocol (Figure 2A) that generates mono-hormonal Ins-positive, glucagon (Gcg)-positive and somatostatin (Sst)-positive cells and can secrete insulin in response to glucose with a low to moderate SI in static GSIS. The protocol has two phases: hESCs are plated on a Matrigel (MG)-coated surface and the first four stages are maintained in adherent culture; at the end of Stage 4, the cells are removed from the plate, gently pipetted to form small masses of cells, and then cultured in suspension where the cell masses form rounded clusters, similar in shape and size to human islets.

*hP-HG treatment in adherent SC*β*C culture*

To incorporate hP-HG into this differentiation protocol, we first assessed whether there was a beneficial effect of culturing on an hP-HG-coated surface in place of MG at each of the first four stages (Figure 2B). The standard protocol for these four stages would be to start the hESCs on MG and not remove them from the plate until the end of Stage 4; this treatment was used as a control (S0→MG).

Bright field microscopy images from cells cultured under each condition reveal similar morphologic patterns at the end of Stage 4 for all cells except for those moved onto hP-HG at the end of Stage 1 (S1→hP-HG) (Figure 2C). Cells moved onto hP-HG at the end of Stage 1 adhered to the plate, but over the next few days the sheet of cells peeled and aggregated into a large mass, which did not generate enough material to quantify gene expression by the end of Stage

4. Furthermore, although there were morphologic similarities in the differentiated cells at the end of Stage 4, none of the cells that were moved onto MG or hP-HG at any stage had higher expression of the desired genes by the end of Stage 4 (Figure 2D). This indicates that in the first 4 stages of culture, dispersing and moving the cells onto a new plate is disruptive to the differentiation, and hP-HG does not have a benefit that overcomes that disruption.

Figure 2. hP-HG treatment in adherent SCβC culture.

A) Schematic diagram of the 7-stage differentiation protocol to generate insulin-producing SCβCs from hESCs.

B) To test hP-HG in adherent culture (Stages 1-4) hESCs were plated onto MG on Day 0 of the protocol, and then either kept on MG through Stage 4, or at each stage a subset of wells were dispersed and re-plated onto either a MG or hP-HG-coated surface.

C) Bright field microscopy images of cells at the end of Stage 4, cultured under each condition. Cells moved at the end of Stage 1 onto MG are indicated S1→MG, and so on. The scale bar in the bottom right corner of each picture is 200 microns.

D) Gene expression data from cells collected at the end of Stage 4, after culturing under each condition. All gene expression is normalized to undifferentiated H1 hESCs. N=2 replicates per treatment.

(Next page)

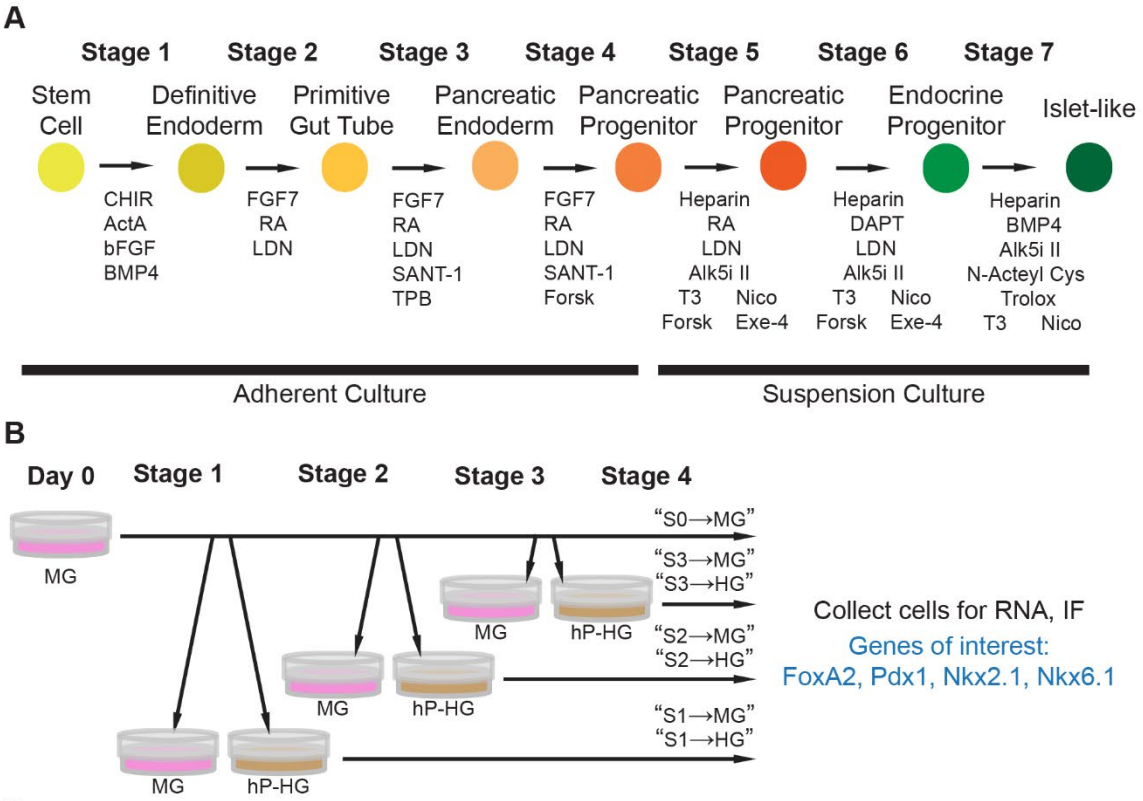
A
Stage 1
Stage 2
Stage 3
Stage 4
Stage 5
Stage 6
Stage 7
Stem Cell
Definitive Endoderm
Primitive Gut Tube
Pancreatic Endoderm
Pancreatic Progenitor
Pancreatic Progenitor
Endocrine Progenitor
Islet-like
CHIR ActA bFGF BMP4
FGF7 RA LDN
FGF7 RA LDN SANT-1 TPB
FGF7 RA LDN SANT-1 Forsk
Heparin RA LDN Alk5i II T3 Forsk Nico Exe-4
Heparin DAPT LDN Alk5i II T3 Forsk Nico Exe-4
Heparin BMP4 Alk5i II N-Acteyl Cys Trolox T3 Nico
Adherent Culture
Suspension Culture
B
Day 0
Stage 1
Stage 2
Stage 3
Stage 4
MG
"S0→MG"
"S3→MG"
"S3→HG"
"S2→MG"
"S2→HG"
"S1→MG"
"S1→HG"
hP-HG
Collect cells for RNA, IF
Genes of interest:
FoxA2, Pdx1, Nkx2.1, Nkx6.1
C
S0→MG
S1→MG
S2→MG
S3→MG
End of Stage 4
Bright field
200μm
S1→hP-HG
S2→hP-HG
S3→hP-HG
D
End Stage 4
NKX2.2
NKX6.1
PDX1
FOXA2
Relative Gene Expression
25000
20000
15000
10000
5000
500
400
300
200
100
0
H1
S0-M
S1-M
S2-M
S3-M
S2-H
S3-H

hP-HG treatment in 3-D SCβC suspension culture

To test the effect that hP-HG co-culture may have on the differentiating cells at the later stages in the protocol, cells were embedded into hP-HG in liquid form (neutralized, cold), pipetted to form 10 µL hemi-spherical droplets, and warmed to 37˚C to induce gelation. Cells were embedded in the gel at the end of Stage 4 ("S4-HG"), immediately following removal of cells from adherent culture, or embedded later, at the end of Stage 6 ("S6-HG"). In parallel, cells were cultured in suspension culture for the entire second half of the protocol as a control ("Suspension", "Susp") (Figure 3A). Fragmented sheets of cells at the end of Stage 4 form rounded clusters over the next few days in suspension culture. When embedded in hP-HG, the cells follow a similar pattern and become larger and rounder clusters as the gel contracts over the final stages of differentiation (Figure 3B). At the end of Stage 7, suspension clusters or gels were either fixed and sectioned for immunofluorescent (IF) staining or lysed in TRIzol and used for RNA extraction and QPCR analysis. IF staining was performed to assess the percentage of each cell cluster that was Ins-positive; the amount of insulin detected in the SCβC clusters was increased in both S4-HG and S6-HG conditions compared to suspension culture. The cells were co-stained for Collagen 1 (Col1) to indicate the hydrogel, and this stain also revealed that the SCβC clusters in suspension expressed high levels of Col1 within the central region of the cell clusters, while this was not seen to as high of an extent in the hydrogel-embedded clusters. Nuclear staining was also performed and quantified for Pdx1 and Nkx6.1, which are co-expressed in β cells (Figure 3C). Co-localization of these markers in the nuclei was increased in SCβC clusters that were cultured with hP-HG as endocrine progenitors, from Stage 6 onward (S6-HG) but there was no difference seen with the earlier S4-HG pancreatic progenitor cells.

To further determine the impacts of the hP-HG, bulk RNA preps were analyzed with QPCR for each treatment. To improve the power of the analysis, all hP-HG co-culture treatments (S4-HG and S6-HG) were averaged together as one hP-HG treated group. The analysis revealed that several pancreatic endocrine genes (Ins, Gcg, Sst, Ucn3, Glut2, IAPP) had a trend of increased expression in the hP-HG treated group (hP-HG) compared to suspension culture (Susp). As an additional control, the relative amount of each gene compared to primary human islet (Islets) was calculated (Figure 3D). Primary human islets have significant donor-to-donor differences in gene expression, insulin content and function; to consider these variations, the islet data represented an average of 10 different islet donor preparations. This reveals that although there are minor increases in gene expression of some important genes, there remains a major deficit in the relative expression compared to the primary tissue. The preparations of SCβC that were used for these experiments were assessed for function in static GSIS, but none of the cells derived at this time had an average stimulation index (insulin secreted in high glucose over insulin secreted in low glucose) above 1.0, indicating that the functional response in these batches of differentiated cells was poor. The hP-HG treatment therefore did not have a beneficial effect on GSIS function in this study, but this could have been due to overall poor differentiation.

Figure 3. hP-HG treatment in 3-D SCβC suspension culture.

A) Schematic diagram of incorporation of hP-HG into the suspension culture phase of the differentiation protocol. At the end of Stage 4, the adherent sheets of cells are broken up to form small clusters. These clusters were embedded into droplets of hP-HG at the end of Stage 4, or the end of Stage 6 to test the effect of hP-HG on the end stages of the differentiation. **B)** Bright field microscopy images of cells embedded in the gel at the end of Stage 4, showing how the cells change morphology over time in 3-D co-culture. The scale bar indicates 500 microns. **C)** Immunofluorescent staining of cells collected at the end of the protocol (end Stage 7) cultured with our without hP-HG. Images were quantified for each of the conditions. Scale = 100 microns. **D)** Gene expression data from cells collected at the end of Stage 7, after culture with or without hP-HG. Data from cells combined with hP-HG at Stages 4 or 6 were pooled in these graphs ("hP-HG"). All gene expression is normalized to differentiated H1 cells in normal suspension culture for the second half of the protocol ("Susp") and compared to the fold-change in primary human islets ("Islets"). N=4 differentiations. **(Next page)**

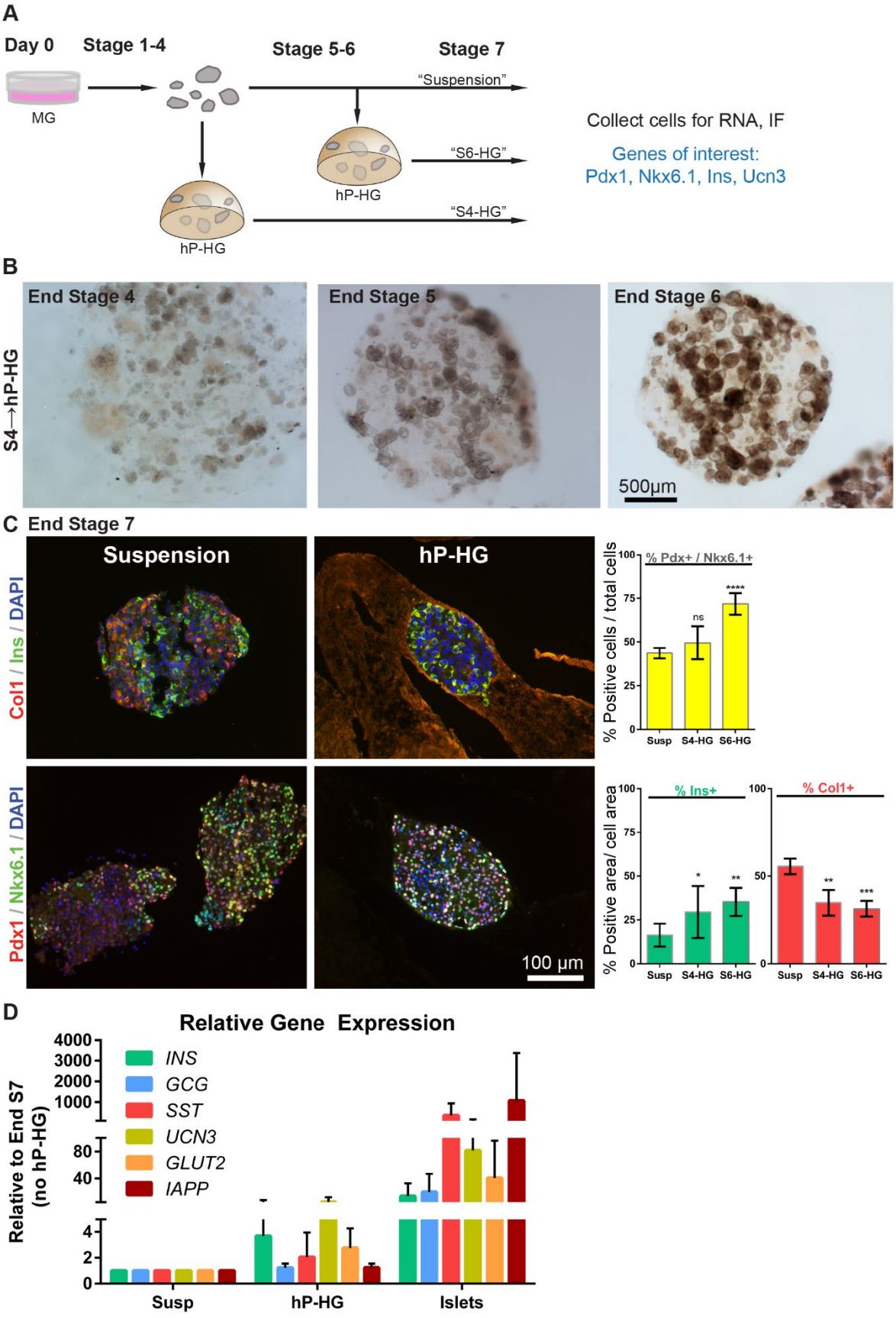
A
Day 0
Stage 1-4
Stage 5-6
Stage 7
MG
"Suspension"
"S6-HG"
hP-HG
"S4-HG"
hP-HG
Collect cells for RNA, IF
Genes of interest:
Pdx1, Nkx6.1, Ins, Ucn3
B
S4→hP-HG
End Stage 4
End Stage 5
End Stage 6
500µm
C
End Stage 7
Suspension
hP-HG
Col1 / Ins / DAPI
Pdx1 / Nkx6.1 / DAPI
100 µm
% Pdx+ / Nkx6.1+
% Positive cells / total cells
ns
****
Susp
S4-HG
S6-HG
% Ins+
% Col1+
% Positive area/ cell area
*
**
***
D
Relative Gene Expression
Relative to End S7 (no hP-HG)
INS
GCG
SST
UCN3
GLUT2
IAPP
Susp
hP-HG
Islets

Discussion

SCβCs hold the potential to be a major life-changing treatment for all people with diabetes rather than the few fortunate enough to receive transplantation [35]. Before the cells can be clinically useful, however, the protocols used to generate SCβCs need to be fine-tuned until the cells consistently phenotypically and functionally resemble native islets. It is important for these protocols to achieve similarity to primary islets for several reasons. If the cells are not fully or terminally differentiated prior to transplantation, there is risk that they may become off-target cell types *in vivo* which would be undesirable or even dangerous to the recipient. If the SCβCs maintain their fate but do not properly function, they may simply not be useful for reducing the patient's blood glucose, or worse, could dysregulate the body's response to glucose if SCβC hormone secretion is not properly controlled.

In order to improve the outcomes of our differentiation, we assessed whether adding hP-HG to the differentiation protocol at various time points had a beneficial effect on SCβC gene expression, protein expression, or function. Perhaps not surprisingly, we found that the introduction of hP-HG in the early stages of the protocol did not have a beneficial effect. This could have a logical basis, because hP-HG is derived from adult human pancreas, which may not resemble the matrisome of the early embryo enough to be supportive at these stages. Indeed, our study of the human pancreatic matrisome across development reveals dramatic differences in the ECM composition of the fetal tissue compared to the adult [36], and presumably the fetal pancreas itself is different from earlier stages in development prior to the formation of distinct organs [37]. Despite limitations in perfectly replicating the developmental process, the beginning of the differentiation protocol is modeled after very early stages of development, with the first

stage being the formation of endoderm; an adult pancreas-specific ECM is out of place both spatially and temporally with regard to the environment of definitive endoderm cells. This may be part of the reason that the cells did not respond well to being plated on hP-HG at the end of Stage 1. Even the transfer of the cells onto fresh Matrigel-coated surfaces after any of the first three stages was detrimental, rather than beneficial, to the differentiation outcomes at the end of Stage 4. This may indicate that the cells are responding to more than just exogenous chemical cues during the differentiation, and the arrangement and cell-cell contacts in the well are important to maintaining their trajectory towards the desired fate.

The addition of hP-HG at later stages in the protocol had more of a beneficial effect on the outcomes. After Stage 4, the cells are lifted out of adherent culture and placed into suspension. Pancreatic progenitor 2 (PP2) differentiated cells were directly combined with hP-HG following detachment from adherent culture or at the endocrine progenitor stage (Stage 6), and cultured through the remainder of the protocol while embedded in the ECM gel. Compared to cells that had been differentiated directly in suspension, the cells in hP-HG co-culture increased the number of cells that were insulin-positive, and decreased the number of cells that were collagen 1-positive. This indicates that more cells were able to take on an endocrine identity (insulin-producing) in the hP-HG co-culture, and fewer cells took an alternative fate (collagen 1-producing). The presence of ECM, through integrin signaling or other ECM-responsive pathways, could be providing ECM-mediated cues that the cells require, relieving a burden for the clusters to make their own ECM and permitting a higher fraction of the cells to take on an endocrine identity. In the standard suspension culture, however, it appears that a high number of cells are making collagen 1, which is not known to be made by any of the endocrine cells of the pancreas

and is probably deposited by endothelial and other support cells *in vivo* [38]. Therefore, a shift toward fewer cells producing collagen in the SCβCs is a desirable outcome. Furthermore, the number of cells co-expressing Pdx1 and Nkx6.1 was significantly increased in SCβCs cultured with hP-HG from Stage 6 onward. Pdx1 and Nkx6.1 are co-expressed in early pancreas progenitor cells, but in islets are only co-expressed in the β cells. An increase in Pdx1+/Nkx6.1+ paired with higher levels of insulin+ area is indicative of a higher number of cells committing to a β cell fate.

Gene expression profiles are routinely used to assess outcomes of hPSC differentiation. Bulk RNA can be extracted from the clusters of cells and compared to primary human islets to assess whether the expression of individual genes is similar to primary islets, or to what magnitude a gene may be deficient in SCβCs, as readouts for proper differentiation. Expression of genes such as *GCG*, *INS*, and *SST* which are essential and unique to α, β, and δ delta cells respectively, help to understand the relative ratio of the different cells in the differentiation end product [37, 39]. Other genes, such as *UCN3*, *GLUT2*, or *IAPP*, may be useful as markers of maturation in the SCβCs Analysis of many of these genes showed trends toward increased expression in the hP-HG-treated SCβCs, but there remains a major gap in gene expression between the hP-HG cultured SCβCs and primary islets. Therefore, hP-HG may have some benefit toward improving the differentiation protocol, but other changes, such as modifications to the chemical cues to stimulate differentiation, or changes to the platforms in which we culture the cells, may need to accompany the inclusion of ECM in order to achieve gene expression levels that are more consistent with human islets.

In this study, the SCβCs did not have significant levels of insulin secretion when exposed to either low glucose (2.8 mM) or high glucose (28 mM) conditions. The hP-HG embedded cells

did not perform differently, and therefore there was no observed glucose-sensitive insulin-secretion function in SCβCs under any of the conditions. Importantly, these protocols were developed prior to robust function being common in the newer and more promising differentiation protocols, which have now demonstrated dynamic insulin secretion in response to glucose [7, 8, 40]. The use of these updated protocols in similar future studies will have more potential for functional improvement in response to the hP-HG environment.

While the hP-HG used in this study was sturdy enough to endure 17 days in culture with embedded cells, one barrier to this project was that the protocol for deriving hP-HG has some inconsistent results based on the condition of the donated pancreas from which the material is derived. In our hands, ECM from only a small number of pancreata that we have decelled could form stable enough gels to perform this type of experiment with. Further, if these hydrogel-SCβC constructs were to be tested in a transplantation setting, the gels would need to be handled without breaking. An improvement in the gelation properties of this material would be desirable to perform larger studies in this field.

Conclusion

ECM is ubiquitously present throughout the body, albeit with unique composition and structure in each tissue, and is essential for the health and function of each organ's resident cells. For this reason, incorporating ECM into the culture of cells *in vitro* is vital to support cell behavior that is reflective of normal, healthy cells *in vivo*. In this study we found that the addition of a pancreas-specific ECM to the differentiation of SCβCs had beneficial effects, but the temporal timing of the introduction of ECM was more advantageous at the later stages of the protocol, once the cells have taken on a pancreatic identity. Gene expression profiles along with protein

expression and localization of Insulin, Pdx1, Nkx6.1 and Col1 showed improvements when SCβCs were embedded in hP-HG. However, major deficiencies in gene expression compared to primary islets and a general lack of glucose-responsive function in these cells was not able to be rescued by the ECM environment, highlighting the limitations of the hP-HG treatment, as well as deficiencies in the differentiation protocol employed in this study. Further improvements to the chemical stimulation provided during differentiation in combination with ECM and possibly other components of the *in vivo* niche should be explored in future studies.

Materials and Methods

*SC*β*C Differentiation*

H1 cells were differentiated toward a pancreatic endocrine fate using a protocol based on Xu et al. (2011) [34], Rezania et al. (2014) [5], and Pagliuca et al. (2014) [4]. Media components for each stage of differentiation are included in detail in Table 1. To initiate the differentiation on "Day 0", H1 colonies were treated with ROCK Inhibitor for 4 h (Y-27632) and plated as single cells onto Matrigel-coated 12-well or 6-well transwell plates (Corning, 3460 and 3450) at a density of $1.5x10^5$ cells per cm^2 surface area. Standard E8 medium (ThermoFisher, A1517001) was added to both sides of the transwell to expand the cells before differentiation was initiated. When the cells covered the transwell membranes at near 100% confluence, Stage 1 was initiated, this was considered "Day 1". Medium was changed every day thereafter in accordance with Table 1. On the first day of Stage 5 (end of Stage 4), Rock Inhibitor (Y-27632) was added to the Stage 4 medium at a concentration of 10 μM and the cells were incubated for 4 h at 37˚C. Following the 4 h incubation, the cells were treated with Versene for 5 min at room temperature to gently break up the sheet of cells that formed on the transwell membrane; the sheet of cells was then

triturated gently in stage 5 medium to recover all cells from the well. The sheet of cells was broken into fragments of about 100 to 200 microns in diameter and diluted into Stage 5 medium for plating in 10 cm ultra low attachment (ULA) plates (Corning, 3261). Clusters from approximately one entire plate of cells were placed into 12 mL of Stage 5 medium and plated into one 10 cm ULA plate. Cells were not fully dissociated or counted at this stage. During Stage 5, media was changed 50% (6 mL per 10 cm plate) each day. For Stages 6 and 7, media was fully changed every other day as detailed in Table 1. At the end of the 28th day of the protocol, cells were collected for downstream analysis. Cluseters were fixed in 4% PFA for 1 h at room temperature and embedded in paraffin for immunostaining. Clusters were lysed in TRIzol (ThermoFisher, 15596026) and RNA was extracted using the QIAprep Spin Miniprep kit (QIAGEN, 27104). Images were taken at various point during the differentiation using a Zeiss Axiovert 200M.

Preparation of hP-HG Scaffolds

hP-HG was prepared as previously described [27]. To coat plates with hP-HG, Acidic ECM digest was diluted with cold 1X PBS to a concentration of 0.08 mg/ml (a 1:120 dilution) and filtered through a 40 µm filter to remove undigested ECM pieces. 600 µl of diluted digest (pre-gel solution) was added to each well of a chilled 12-well transwell culture plate (Corning, 3460). Plates were incubated at 37˚C for one hour and rinsed with PBS before use. To embed clusters of cells into droplets of gel, cells were mixed into the cold neutralized ECM digest solution, pipetted into 10 uL droplets and warmed to 37˚C for 30 minutes. Following gelation, media was added to cover the droplets and gently nudged until the droplets floated in suspension.

Quantitative Real-Time PCR (QPCR)

cDNA was prepared from extracted RNA using the Omniscript RT kit (QIAGEN, 205113). Quantitative Real-Time Polymerase Chain Reaction (QPCR) was performed using the TaqMan Real-Time PCR Master Mix (ThermoFisher, 4304437) and Taqman Gene Expression Assay Primers (ThermoFisher) listed in Table 2.

Immunostaining

5 micron paraffin sections were deparaffinized using xylene and rehydrated. Antigen retrieval was performed by treatment with 10mM Citrate Buffer, pH6.0 for 2 hours in an 80˚C water bath. Slides were blocked with 10% BSA/1x PBS for 1 h at room temperature, incubated with primary antibodies overnight at 4˚C, washed, incubated with secondary antibody for 1 h at room temperature and cover slipped.

The antibodies and dilutions are listed in Table 3. Immunofluorescent (IF) secondary antibodies were Alexa Fluor 488 and 568 of anti-mouse or anti-rabbit reactivity. Nuclei were counterstained with 40-6-diamidino-2-phenylindole (DAPI). Images were generated with a Zeiss Axiovert 200M microscope.

Image Analysis

Images were analyzed and counted using Image J software. Cell area was traced on synchronized windows to permit quantification of signal-positive area in only the cell clusters. Pdx1/Nkx6.1 co-expression was assessed by counting total nuclei on the DAPI channel, and generating an overlapping image of the Pdx1 (red) and Nkx6.1 (green) channels and counting only the double-positive (yellow) nuclei.

Table 1:

hPSC	Day 0	
	MCDB131	--
	Y-27632	10.0 uM

Definitive Endoderm	Stage 1.1	
	MCDB131	--
	BSA	0.5%
	GlutaMAX	1 x
	45% Glucose	4.7 mM
	$NaHCO_3$	1.50 g/L
	Activin A	0.10 ug/mL
	CHIR99	2.0 uM
	BMP4	0.01 ug/mL
	bFGF	0.10 ug/mL
	Stage 1.2 (Day 2)	
	MCDB131	--
	BSA	0.5%
	GlutaMAX	1 x
	45% Glucose	4.7 mM
	$NaHCO_3$	1.50 g/L
	Activin A	0.10 ug/mL
	CHIR99	0.2 uM
	BMP4	0.01 ug/mL
	bFGF	0.10 ug/mL
	Stage 1.3 (Day 3)	
	MCDB131	--
	BSA	0.5%
	GlutaMAX	1 x
	45% Glucose	4.7 mM
	$NaHCO_3$	1.50 g/L
	Activin A	0.10 ug/mL
	BMP4	0.01 ug/mL
	bFGF	0.10 ug/mL

Primitive Gut Tube	Stage 2.1 (Day 4)	
	MCDB131	--
	BSA	0.5%
	GlutaMAX	1 x
	45% Glucose	4.7 mM
	$NaHCO_3$	1.50 g/L
	Ascorbic Acid	0.25 mM
	FGF7	0.05 ug/mL
	Retinoic Acid	0.5 uM
	SB-431542	2.5 uM
	LDN	0.1 uM
	Stage 2.2 (Day 5)	
	MCDB131	--
	BSA	0.5%
	GlutaMAX	1 x
	45% Glucose	4.7 mM
	$NaHCO_3$	1.50 g/L
	Ascorbic Acid	0.25 mM
	FGF7	0.05 ug/mL
	Retinoic Acid	0.5 uM
	LDN	0.1 uM

Progenitor Foregut	Stage 3 (Days 6-8)	
	MCDB131	--
	BSA	2.0%
	GlutaMAX	1 x
	45% Glucose	4.7 mM
	$NaHCO_3$	2.50 g/L
	Ascorbic Acid	0.25 mM
	ITS-X	0.5 x
	Retinoic Acid	1 uM
	LDN	0.2 uM
	SANT-1	0.25 uM
	FGF7	0.05 ug/mL
	TPB	0.2 uM

Pancreatic Progenitors	Stage 4 (Days 9-11)	
	MCDB131	--
	BSA	2.0%
	GlutaMAX	1 x
	45% Glucose	4.7 mM
	$NaHCO_3$	2.50 g/L
	Ascorbic Acid	0.25 mM
	ITS-X	0.5 x
	Retinoic Acid	0.1 uM
	LDN	0.1 uM
	FGF7	0.002 ug/mL
	SANT-1	0.25 uM
	Forskolin	10.0 uM

Endocrine Pancreatic Progenitors	Stage 5 (Days 12-14)	
	MCDB131	--
	BSA	2.0%
	GlutaMAX	1 x
	45% Glucose	14.7 mM
	$NaHCO_3$	1.50 g/L
	ITS-X	0.5 x
	Heparin	10 ug/mL
	LDN	0.1 uM
	Exendin-4	0.01 uM
	Forskolin	10. uM
	Nicotinamide	10 mM
	T3	1 uM
	Retinoic Acid	0.025 uM
	Alk5i II	0.01 mM
	Pen/Strep	1.0 x

Immature Beta Cells	Stage 6 (Days 15-21)	
	MCDB131	--
	BSA	2.0%
	GlutaMAX	1 x
	45% Glucose	14.7 mM
	$NaHCO_3$	1.50 g/L
	ITS-X	0.5 x
	Heparin	10 ug/mL
	LDN	0.1 uM
	DAPT	1.0 uM
	Exendin-4	0.01 uM
	Forskolin	10. uM
	Nicotinamide	10 mM
	T3	1 uM
	Alk5i II	0.01 mM
	Pen/Strep	1.0 x
	Stage 7 (Days 22-28)	
	MCDB131	--
	BSA	2.0%
	GlutaMAX	1 x
	45% Glucose	14.7 mM
	$NaHCO_3$	1.50 g/L
	ITS-X	0.5 x
	Heparin	10 ug/mL
	Nicotinamide	10 mM
	T3	1 uM
	Alk5i II	0.01 mM
	R428	2.0 uM
	Trolox	10.0 uM
	N-Acetyl Cys	1 mM
	BMP4	0.01 ug/mL
	Pen/Strep	1.0 x

Table 2:

Primers used for QPCR

Gene	Product Number
FOXA2	Hs00232764_m1
PDX1	Hs00236830_m1
NKX6.1	Hs00232355_m1
NXK2.2	Hs00159616_m1
INS	Hs02741908_m1
GCG	Hs01031536_m1
SST	Hs00356144_m1
UCN3	Hs00846499_s1
GLUT2	Hs01096908_m1
IAPP	Hs00169095_m1

Table 3:

Antibodies used for IF

Target	Species	Dilution	Product
Ins	Mouse	1:5000	I2018 (Sigma)
Col1	Rabbit	1:500	ab34710 (Abcam)
Col4	Rabbit	1:1000	ab6586 (Abcam)
Laminin	Mouse	1:200	ab49726 (Abcam)
Pdx1	Rabbit	1:1000	ab134150 (Abcam)
Nkx6.1	Mouse	1:100	F55A12-s (DSHB)

Acknowledgements

We would like to offer a special thanks to the families who donated pancreas tissues, without which this study would not be possible. We acknowledge Drew Roenneberg with the University of Wisconsin Department of Surgery Histology Core for help with sample processing.

References

1. Bruni, A., et al., *Islet cell transplantation for the treatment of type 1 diabetes: recent advances and future challenges.* Diabetes, Metabolic Syndrome and Obesity: Targets and Therapy, 2014. **7**: p. 211-223.
2. Miller, K.M., et al., *Current state of type 1 diabetes treatment in the U.S.: updated data from the T1D Exchange clinic registry.* Diabetes Care, 2015. **38**(6): p. 971-8.
3. Sackett, S.D., et al., *Modulation of human allogeneic and syngeneic pluripotent stem cells and immunological implications for transplantation.* Transplant Rev (Orlando), 2016. **30**(2): p. 61-70.
4. Pagliuca, F.W., et al., *Generation of functional human pancreatic beta cells in vitro.* Cell, 2014. **159**(2): p. 428-39.
5. Rezania, A., et al., *Reversal of diabetes with insulin-producing cells derived in vitro from human pluripotent stem cells.* Nat Biotechnol, 2014. **32**(11): p. 1121-33.
6. Russ, H.A., et al., *Controlled induction of human pancreatic progenitors produces functional beta-like cells in vitro.* EMBO J, 2015. **34**(13): p. 1759-72.
7. Nair, G.G., et al., *Recapitulating endocrine cell clustering in culture promotes maturation of human stem-cell-derived beta cells.* Nat Cell Biol, 2019. **21**(2): p. 263-274.
8. Velazco-Cruz, L., et al., *Acquisition of Dynamic Function in Human Stem Cell-Derived beta Cells.* Stem Cell Reports, 2019. **12**(2): p. 351-365.
9. van der Meulen, T., et al., *Urocortin 3 marks mature human primary and embryonic stem cell-derived pancreatic alpha and beta cells.* PLoS One, 2012. **7**(12): p. e52181.
10. Frantz, C., K.M. Stewart, and V.M. Weaver, *The extracellular matrix at a glance.* J Cell Sci, 2010. **123**(Pt 24): p. 4195-200.
11. Bonnans, C., J. Chou, and Z. Werb, *Remodelling the extracellular matrix in development and disease.* Nat Rev Mol Cell Biol, 2014. **15**(12): p. 786-801.
12. Rozario, T. and D.W. DeSimone, *The extracellular matrix in development and morphogenesis: a dynamic view.* Dev Biol, 2010. **341**(1): p. 126-40.
13. Stendahl, J.C., D.B. Kaufman, and S.I. Stupp, *Extracellular matrix in pancreatic islets: relevance to scaffold design and transplantation.* Cell Transplant, 2009. **18**(1): p. 1-12.
14. Wang, R.N., S. Paraskevas, and L. Rosenberg, *Characterization of integrin expression in islets isolated from hamster, canine, porcine, and human pancreas.* J Histochem Cytochem, 1999. **47**(4): p. 499-506.
15. Daoud, J., et al., *The effect of extracellular matrix components on the preservation of human islet function in vitro.* Biomaterials, 2010. **31**(7): p. 1676-82.
16. Daoud, J.T., et al., *Long-term in vitro human pancreatic islet culture using three-dimensional microfabricated scaffolds.* Biomaterials, 2011. **32**(6): p. 1536-42.

17. Kaido, T., et al., *Impact of defined matrix interactions on insulin production by cultured human beta-cells: effect on insulin content, secretion, and gene transcription.* Diabetes, 2006. **55**(10): p. 2723-9.

18. Bogdani, M., et al., *Extracellular matrix components in the pathogenesis of type 1 diabetes.* Curr Diab Rep, 2014. **14**(12): p. 552.

19. Crapo, P.M., T.W. Gilbert, and S.F. Badylak, *An overview of tissue and whole organ decellularization processes.* Biomaterials, 2011. **32**(12): p. 3233-43.

20. Gilbert, T.W., T.L. Sellaro, and S.F. Badylak, *Decellularization of tissues and organs.* Biomaterials, 2006. **27**(19): p. 3675-83.

21. Hoshiba, T., et al., *Decellularized Extracellular Matrix as an In Vitro Model to Study the Comprehensive Roles of the ECM in Stem Cell Differentiation.* Stem Cells Int, 2016. **2016**: p. 6397820.

22. Uygun, B.E., et al., *Organ reengineering through development of a transplantable recellularized liver graft using decellularized liver matrix.* Nat Med, 2010. **16**(7): p. 814-20.

23. Wan, J., et al., *Culture of iPSCs Derived Pancreatic beta-Like Cells In Vitro Using Decellularized Pancreatic Scaffolds: A Preliminary Trial.* Biomed Res Int, 2017. **2017**: p. 4276928.

24. Freytes, D.O., et al., *Preparation and rheological characterization of a gel form of the porcine urinary bladder matrix.* Biomaterials, 2008. **29**(11): p. 1630-7.

25. Soffer-Tsur, N., D. Peer, and T. Dvir, *ECM-based macroporous sponges release essential factors to support the growth of hematopoietic cells.* J Control Release, 2017. **257**: p. 84-90.

26. Wood, G.C., *The formation of fibrils from collagen solutions. 2. A mechanism of collagen-fibril formation.* Biochem J, 1960. **75**: p. 598-605.

27. Sackett, S.D., et al., *Extracellular matrix scaffold and hydrogel derived from decellularized and delipidized human pancreas.* Sci Rep, 2018. **8**(1): p. 10452.

28. Goh, S.K., et al., *Perfusion-decellularized pancreas as a natural 3D scaffold for pancreatic tissue and whole organ engineering.* Biomaterials, 2013. **34**(28): p. 6760-72.

29. Beattie, G.M., et al., *A novel approach to increase human islet cell mass while preserving beta-cell function.* Diabetes, 2002. **51**(12): p. 3435-9.

30. Kim, M.J. and D.Y. Lee, *Pancreas-like extracellular matrix scaffold for successful pancreatic islet transplantation.* Macromolecular Research, 2014. **22**(6): p. 575-582.

31. Higuchi, Y., et al., *Synthesized basement membranes direct the differentiation of mouse embryonic stem cells into pancreatic lineages.* J Cell Sci, 2010. **123**(Pt 16): p. 2733-42.

32. Narayanan, K., et al., *Extracellular matrix-mediated differentiation of human embryonic stem cells: differentiation to insulin-secreting beta cells.* Tissue Eng Part A, 2014. **20**(1-2): p. 424-33.

33. Nostro, M.C., et al., *Efficient generation of NKX6-1+ pancreatic progenitors from multiple human pluripotent stem cell lines.* Stem Cell Reports, 2015. **4**(4): p. 591-604.

34. Xu, X., V.L. Browning, and J.S. Odorico, *Activin, BMP and FGF pathways cooperate to promote endoderm and pancreatic lineage cell differentiation from human embryonic stem cells.* Mech Dev, 2011. **128**(7-10): p. 412-27.

35. Bahar, S.G. and P. Devulapally, *Pancreas Transplantation*, in *StatPearls*. 2022: Treasure Island (FL).

36. Li, Z., et al., *Proteome-wide and matrisome-specific alterations during human pancreas development and maturation.* Nat Commun, 2021. **12**(1): p. 1020.

37. Pan, F.C. and M. Brissova, *Pancreas development in humans.* Curr Opin Endocrinol Diabetes Obes, 2014. **21**(2): p. 77-82.

38. Townsend, S.E. and M. Gannon, *Extracellular Matrix-Associated Factors Play Critical Roles in Regulating Pancreatic beta-Cell Proliferation and Survival.* Endocrinology, 2019. **160**(8): p. 1885-1894.

39. Gregg, B.E., et al., *Formation of a human beta-cell population within pancreatic islets is set early in life.* J Clin Endocrinol Metab, 2012. **97**(9): p. 3197-206.

40. Hogrebe, N.J., et al., *Targeting the cytoskeleton to direct pancreatic differentiation of human pluripotent stem cells.* Nat Biotechnol, 2020. **38**(4): p. 460-470.

Chapter 5

A human pancreatic ECM hydrogel optimized for 3-D modeling of the islet microenvironment

Chapter 5 Graphical Abstract

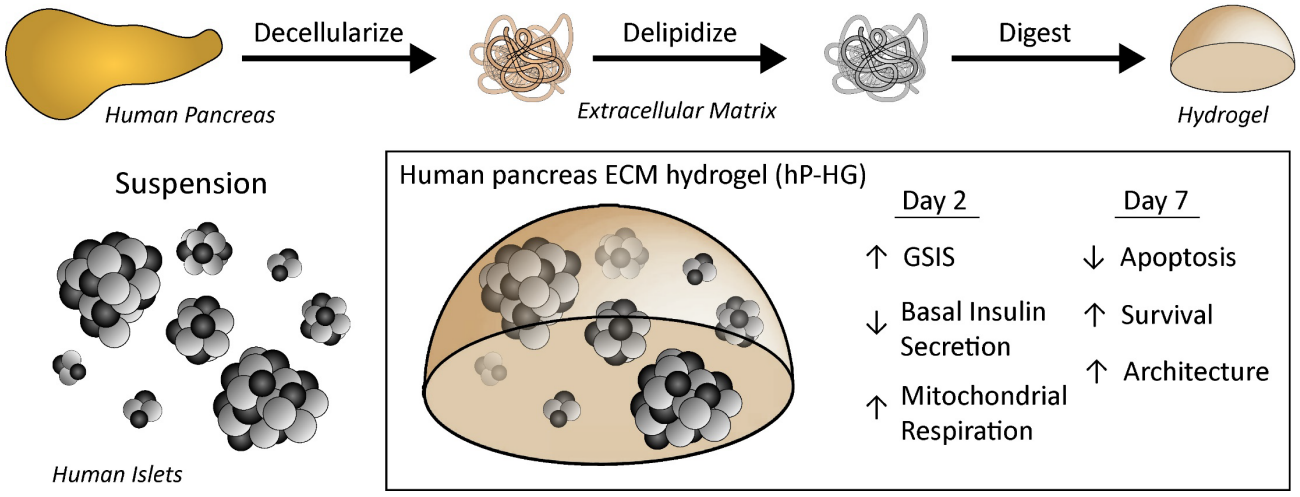

This chapter is published as: Tremmel DM, Sackett SD, Feeney AK, Mitchell SA, Schaid M, Polyak E, Chlebeck PJ, Gupta S, Kimple M, Fernandez LA, Odorico JS. A human pancreatic ECM hydrogel optimized for 3-D modeling of the islet microenvironment. Sci Rep. 2022 May 3;12(1):7188. doi: 10.1038/s41598-022-11085-z. PMID: 35504932

Daniel Tremmel, Sara Dutton Sackett and Jon Odorico designed the study. Daniel Tremmel, Austin Feeney, Sakar Gupta, Sam Mitchell, Michael Schaid and Zsoka Polyak performed the experiments and analyzed the data. Daniel Tremmel, Sam Mitchell and Austin Feeney processed and banked human tissues. Peter Chlebeck and Luis Fernandez provided isolated human islets and guidance on experimental design. Daniel Tremmel prepared all figures and wrote the manuscript with guidance from Michelle Kimple, Luis Fernanadez Sara Dutton Sackett and Jon Odorico.

Abstract

Extracellular matrix (ECM) plays a multitude of roles, including supporting cells through structural and biochemical interactions. ECM is damaged in the process of isolating human islets for clinical transplantation and basic research. A platform in which islets can be cultured in contact with natural pancreatic ECM is desirable to better understand and support islet health, and to recapitulate the native islet environment. Our study demonstrates the derivation of a practical and durable hydrogel from decellularized human pancreas that supports human islet survival and function. Islets embedded in this hydrogel show increased glucose- and KCl-stimulated insulin secretion, and improved mitochondrial function compared to islets cultured without pancreatic matrix. In extended culture, hydrogel co-culture significantly reduced levels of apoptosis compared to suspension culture and preserved controlled glucose-responsive function. Isolated islets displayed altered endocrine and non-endocrine cell arrangement compared to in situ islets, hydrogel preserved an islet architecture more similar to that observed in situ. RNA sequencing confirmed that gene expression differences between islets cultured in suspension and hydrogel largely fell within gene ontology terms related to extracellular signaling and adhesion. Natural pancreatic ECM improves the survival and physiology of isolated human islets.

Introduction

The extracellular matrix (ECM) is an intricate network of proteins and polysaccharides that provides structure and biological signaling to the cells residing in each tissue of the body. In 2-D cell culture, generic ECM is sometimes supplemented to support cell growth, but in 3-D cultures and engineered tissues, ECM is often tailored to the cell or tissue type [1]. Isolated

human pancreatic islets are used in vitro to study the characteristic physiology and function of islet endocrine cells, for diabetes drug discovery research, and for testing new drugs for potential β cell toxicity [2, 3]. Isolated islets are also used clinically as a β cell-replacement therapy for diabetes [4, 5]. Significant cell death throughout the process of isolation, culture, transplantation and engraftment prevent the therapy from achieving long-term euglycemia in many patients. Non-ECM platforms that recapitulate physiological conditions in 3-D culture have recently been reported to enhance islet health and function *in vitro* [6, 7].

It is well established that the process of isolating islets from the pancreas, which requires the use of collagenase and neutral protease, significantly damages the islet ECM [8-10]. The lack of ECM in islets is known to induce anoikis-mediated apoptosis, and has been shown to negatively affect islet function [11, 12]. Several studies have supplemented isolated islets with purified ECM molecules in culture in a variety of ways, demonstrating improved islet health and function with restored ECM contact (reviewed in Stendahl et al., 2009)[13]. Due to the complexity of the native matrisome [14], it has been postulated that decellularized tissue may be a superior scaffold compared to artificial and incomplete ECM environments [15-17], and that pancreas-specific ECM may have a beneficial effect on islets[18]. Furthermore, co-transplanted ECM may have a beneficial effect on the engraftment and survival of transplanted islets [19].

Murine, porcine, and human pancreata have been decellularized in previous studies with the intention of incorporating pancreatic ECM into 3-D cell culture models, or the recellularization of an intact decellularized organ [18, 20-27]. While relatively short protocols efficiently decellularize mouse and rat pancreata, much longer treatments are necessary for larger pig and human organs. Due to species-specific differences in pancreas and islet biology

[28], potential variance in ECM composition by species [13, 29, 30], and structural differences in the basement membrane architecture surrounding the islets [31], a human pancreas ECM scaffold may be more desirable for use with human cells. In previous work, we produced a hydrogel from human pancreas ECM [26], but high lipid content of the human pancreas prevented this protocol from being applied universally to all pancreata, and the hydrogel generated required molding into tissue culture wells and were not stable enough to maintain their shape and structure independently. For practical in vitro applications and for ease of transplantation studies, a durable and pliable gel which doesn't lose its shape in the absence of a mold is desirable.

In this study, we have optimized the decellularization (decell) of human pancreas for improved lipid removal, which resulted in the formation of a durable human pancreas ECM hydrogel (hP-HG). The resulting gel can easily be combined with β cells or islets for in vitro culture. Human islets cultured in hP-HG exhibit a significant improvement in stimulation index as well as improved survival compared to islets maintained in suspension culture. This natural matrix provides for improved islet health, architecture and physiology and may help overcome some of the long-term culture challenges that befall isolated islets due to the loss of native ECM.

Results

Protocol for the decellularization and gelation of human pancreas ECM

Retained lipid content following decell is a barrier to robust gelation of solubilized ECM. We designed an optimized decell protocol to isolate ECM from the human pancreas with minimal lipid and DNA retention, while retaining native ECM proteins and sulfated glycosaminoglycans (sGAG). We revised our previously published protocol by adding an organic solvent wash step to

enhance lipid removal, and Benzonase treatment to improve nucleic acid removal. The optimized human pancreas decell protocol resulted in isolated ECM that was capable of forming a stable hydrogel following pepsin digestion, neutralization and warming to 37 ^{o}C (Fig. 1).

Optimized decell protocol removes lipids and DNA, resulting in an improved hydrogel

The optimized protocol ("Optimized") was compared to the previously published homogenization decell protocol ("Homog") through the quantification of retained DNA and lipid in the isolated human pancreas ECM (hP-ECM). The lipid content derived from the optimized protocol (0.63% lipid by dry weight) was significantly lower than that of the Homog protocol (9.83% lipid by dry weight) (Fig. 2A). On an individual donor basis, the Homog protocol was less effective at removing lipids from pancreata with higher initial lipid content, while the Optimized protocol removed lipids equally well from any donor pancreas (Fig. 2B). Delipidization of lipid-laden pancreata correlated with successful stable hydrogel formation. The DNA content following implementation of the Optimized protocol (0.16±0.06) was significantly lower than the Homog protocol (0.43±0.07) (Fig. 2C). The addition of hexane, acetone and Benzonase treatment did not reduce the sGAG content of the hP-ECM compared to the Homog protocol (Supplemental Fig. 1A). Furthermore, the decelled material retained many of the structural ECM proteins found in the human pancreas (Supplemental Fig. 1B).

When hP-ECM was pepsin-digested to form a hydrogel, the Optimized protocol resulted in gels with more consistent rheologic properties compared to the Homog protocol. This was evident through more uniform clustering of the sigmoidal storage and loss moduli curves (G' and G") in the Optimized hydrogel (Fig. 2D), compared to the broader range of these curves from the Homog protocol (Fig. 2E). Purified collagen 1 (Col1) hydrogel and temperature plots are included

for reference (Fig. 2F). Additionally, the curve of complex viscosity vs. angular frequency was shifted higher for the Optimized compared to the Homog protocol (Fig. 2G), with an increased Young's Modulus (Supplemental Fig. 2C), indicating that the Optimized protocol produced a firmer gel with more consistent and reproducible rheological results than the previous protocol. These rheological properties corresponded with rigid gels that held shape better when pipetted into droplets (Supplemental Fig. 2A-B), similar to Col1 gels. The resulting gels can easily be picked up with forceps (Supplemental Video 1), enabling use in cell culture, functional assays, and transplantation (Supplemental Fig. 2D-E). Similar to other ECM hydrogels, the acellular hP-HG scaffold is capable of gelation in vivo and was found to be highly compatible with minimal immune infiltration when tested in a humanized mouse model (Supplemental Fig. 3).

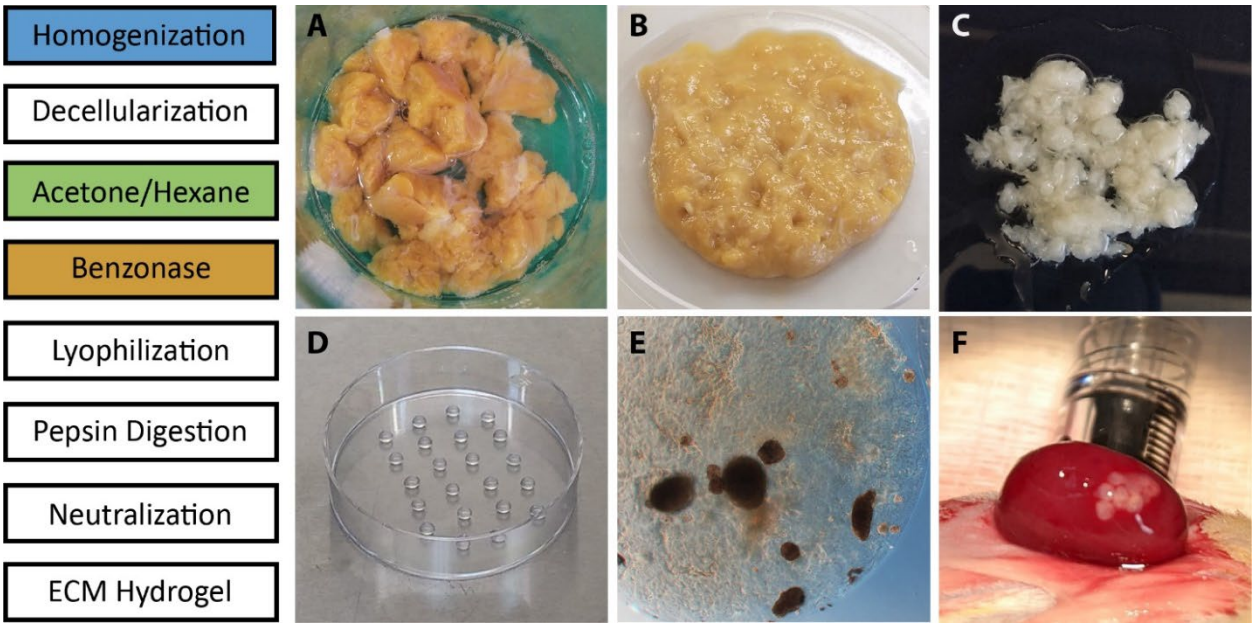

Figure 1: Protocol for the decellularization and gelation of human pancreas ECM. A schematic representation for the protocol to decell, digest and form a hydrogel from human pancreas ECM (left side). Images of the native tissue **(A)**, homogenized tissue **(B)**, decellularized and delipidized ECM **(C)** and multiple 5 µL hydrogel droplets in a 6 cm dish **(D)**. Human islets can be embedded in the hydrogel prior to gelation to form stable droplets for *in vitro* culture **(E)**; the droplets are durable enough to maintain shape and consistency throughout the transplantation process **(F)**.

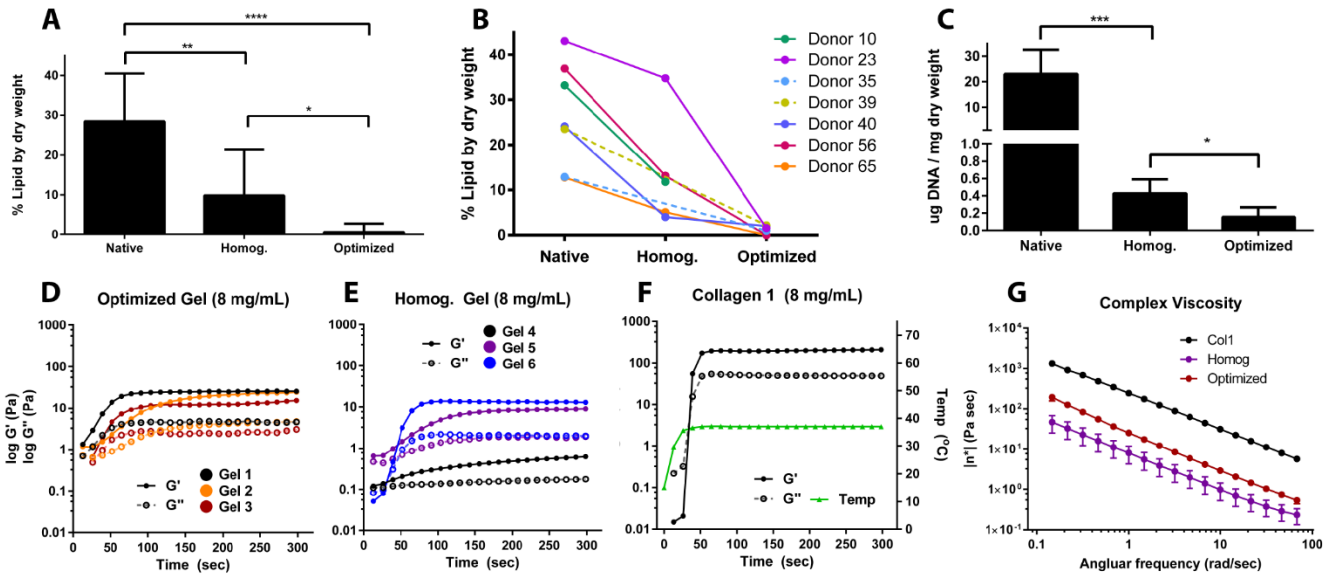

Figure 2: Optimized decell protocol removes lipids and DNA, resulting in an improved hydrogel.

(A-B) Total lipid content by dry weight of the native and decellularized hP-ECM from the Homog and Optimized protocols, determined using a modified Folch method **(A)**, also displayed on a donor-by-donor basis, in which donors with higher lipid content retain significantly more lipids in the Homog protocol **(B)**.

(C) Total DNA content of the native and decellularized hP-ECM from the Homog and Optimized protocols.

(D-F) The storage (G') and loss (G'') moduli of the optimized hydrogels were less variable than the Homog hP-HG hydrogels, and compared to Col1 controls; temperature is plotted in green **(F)**. **(G)** The complex viscosity curves of the Optimized protocol are less variable than the Homog protocol, and all hP-HG gels were less firm than Col1 hydrogel of the same concentration.

(* p<0.05, ** p<0.01, *** p<0.001, **** p<0.0001)

hP-HG co-culture improves islet function after 2 days of culture

The generation of a stable hydrogel using the Optimized decell protocol enabled 3-D studies combining hydrogel and human islets which were not possible with the more fragile Homog protocol. The Optimized protocol was also employed for use in kidney decellularization to generate a human kidney ECM hydrogel (hK-HG) as a control for initial experiments. Isolated islets were cultured in suspension (“S”) (Fig. 3A-a), embedded in hP-HG (“P”) (Fig. 3A-b), alginate

("A") (Fig. 3A-c), purified Col1 ("C") (Fig. 3A-d) and in hK-HG ("K") (Fig. 3A-e) for 2 days. Alginate was included as a control because this material is commonly used to embed and transplant islets as a micro-encapsulation strategy [32-34]; it also provides a non-ECM-based control hydrogel environment for our study. Purified Col1 was used as a non-pancreas specific, simple ECM control, and hK-HG was included as a non-pancreas specific, complex ECM control.

After two days of culture in each condition, a static glucose stimulated insulin secretion (GSIS) assay was performed to assess islet function. Islets in each treatment group were sequentially exposed to low glucose (2.8 mM), high glucose (28 mM), low glucose, and high KCl (30 mM); secreted C-peptide is plotted as a percentage of the total C-Pep content. Alginate encapsulation did not affect islet secretion under any of the four conditions compared to suspension culture (S). All ECM-treated groups (P,C,K) displayed a reduced basal insulin secretion compared to suspension. Furthermore, islets embedded in hK-HG, and Col1 had significantly reduced stimulated C-peptide secretion in high glucose compared to S,P, or A. Islets in hP-HG, however did not have significantly lower stimulated secretion in either high glucose or KCl compared to suspension. Therefore, islets in hP-HG culture had a significantly higher stimulation index (mean SI=9.34) in static GSIS compared to islets in suspension (SI=2.12) and alginate (SI=2.40), and improved compared to Col1 (SI=6.28) and hK-HG (SI=7.78) (Fig. 3D). The stimulation from low glucose to KCl followed the same trend among the treatment groups (Fig. 3E). Total C-peptide content was not significantly different among the five treatments (Fig. 3C). All groups reverted to a lower C-peptide secretion in the second low glucose step, indicating that hydrogel does not impair the return to basal secretion following stimulation (Fig. 3B). Because Col1 and hK-HG had significantly reduced basal and stimulated insulin secretion compared to

suspension and hP-HG cultures, these treatments were considered less desirable for islet function, despite having good stimulation. An alternative representation of these data relative to the basal C-Pep secretion in suspension culture normalized to each individual islet donor are included in Supp. Fig 4G.

hP-HG culture enables proper dynamic function and enhances maximum respiration

To further characterize the effect hP-HG had on islet health and function, additional studies were performed comparing only suspension (S) and hP-HG (P). To assess the dynamic insulin secretion profile of the islets in the hydrogel, perifusion GSIS was performed on human islets after 2 days of culture either in suspension or in hP-HG (Fig. 4A) (Supplemental Fig. 4E-F). The perifusion assay revealed that islets in hP-HG had only a minor delay (1-2 minutes) in response to increased glucose concentration and properly suppressed insulin secretion upon return to low glucose. As with the static GSIS, the stimulation index was higher in hP-HG cultured islets (Fig. 4B). Among the islet donors assayed in static or perifusion GSIS, all but one islet prep had an increased SI when cultured in hP-HG compared to suspension (Supplemental Fig. 4H).

As further confirmation of the protective role of hP-HG culture on β cell function, INS1 832/13 rat insulinoma cells were aggregated as pseudoislets and embedded in hP-HG droplets for 2 days of culture. INS1 cells showed a significantly improved static GSIS stimulation index from low to high glucose, (Supplemental Fig. 4A), an increased SI with KCl (Supplemental Fig. 4B), as well as an increased total C-peptide content compared to suspension clusters (Supplemental Fig. 4C). Like human islets, the increase in SI in hP-HG co-culture was due to significantly lower insulin secretion under low glucose conditions, while the insulin secreted in high glucose was not significantly different (Supplemental Fig. 4D).

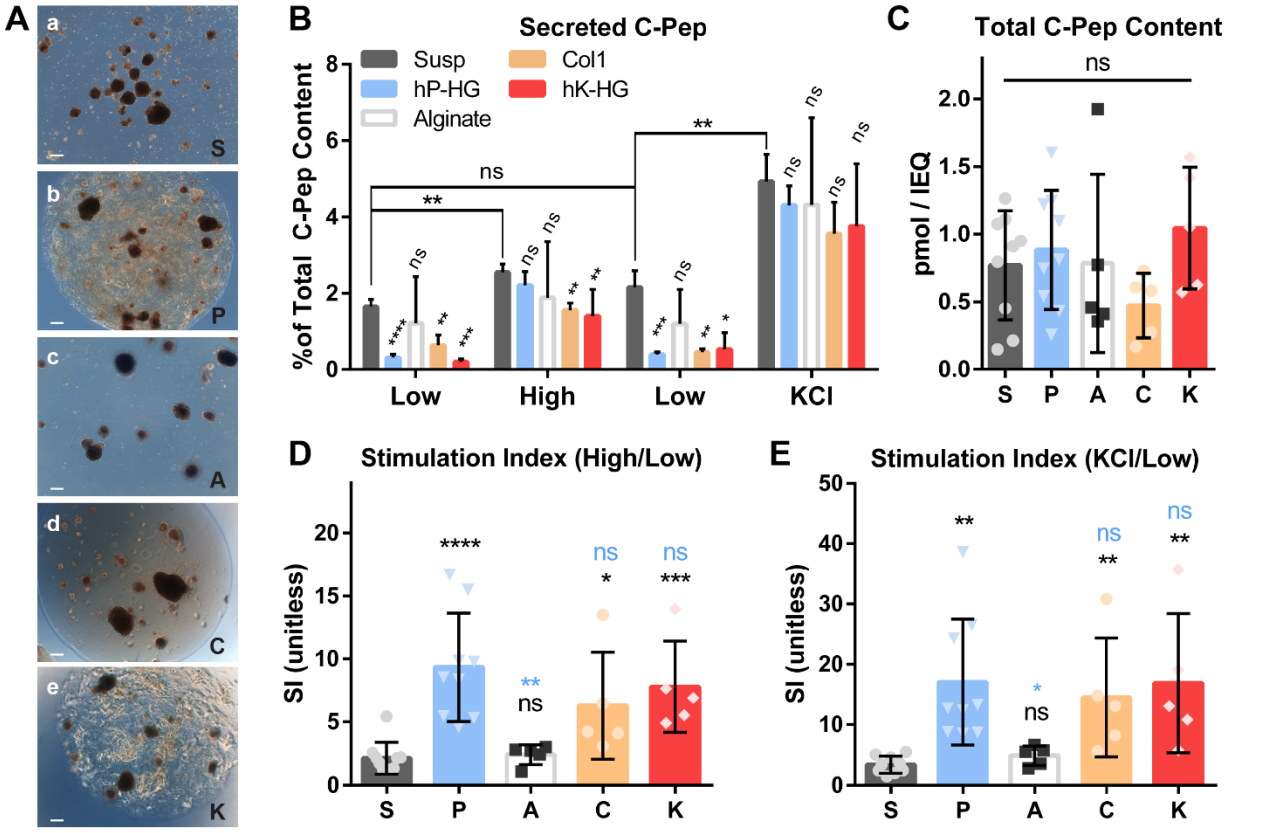

Figure 3: hP-HG co-culture improves islet function after 2 days of culture

(A) Representative phase contrast images of islets cultured in suspension (S) **(a)**, hP-HG (P) **(b)**, alginate (A) **(c)**, Col1 (C) **(d)**, or hK-HG (K) **(e)** were assessed for function on Day 2 of culture (scale = 200 microns).

(B) A static glucose stimulated insulin secretion (GSIS) assay was performed using sequential low glucose (2.8 mM, "Low"), high glucose (28 mM, "High"), a return to low glucose, followed by low glucose + KCl (30 mM KCl, "KCl"); basal and stimulated C-peptide (C-Pep) secreted during the static GSIS with human islets are shown as a percentage of total C-pep content. Statistics indicated above each bar are relative to the "S" control for the same treatment.

(C) Total C-Pep content of islets undergoing the indicated treatments. S

(D and E) Stimulation index **(D**, high/low glucose**) (E**, KCl/low glucose**)** of human islets cultured in all five conditions, determined by static GSIS. Statistical comparisons indicated in black are relative to "S", and indicated in blue are relative to "P".

(S,P: n=9; A,C,K: n=5 islet donors) (ns = not significant, * p<0.05, ** p<0.01, *** p<0.001, **** p<0.0001)

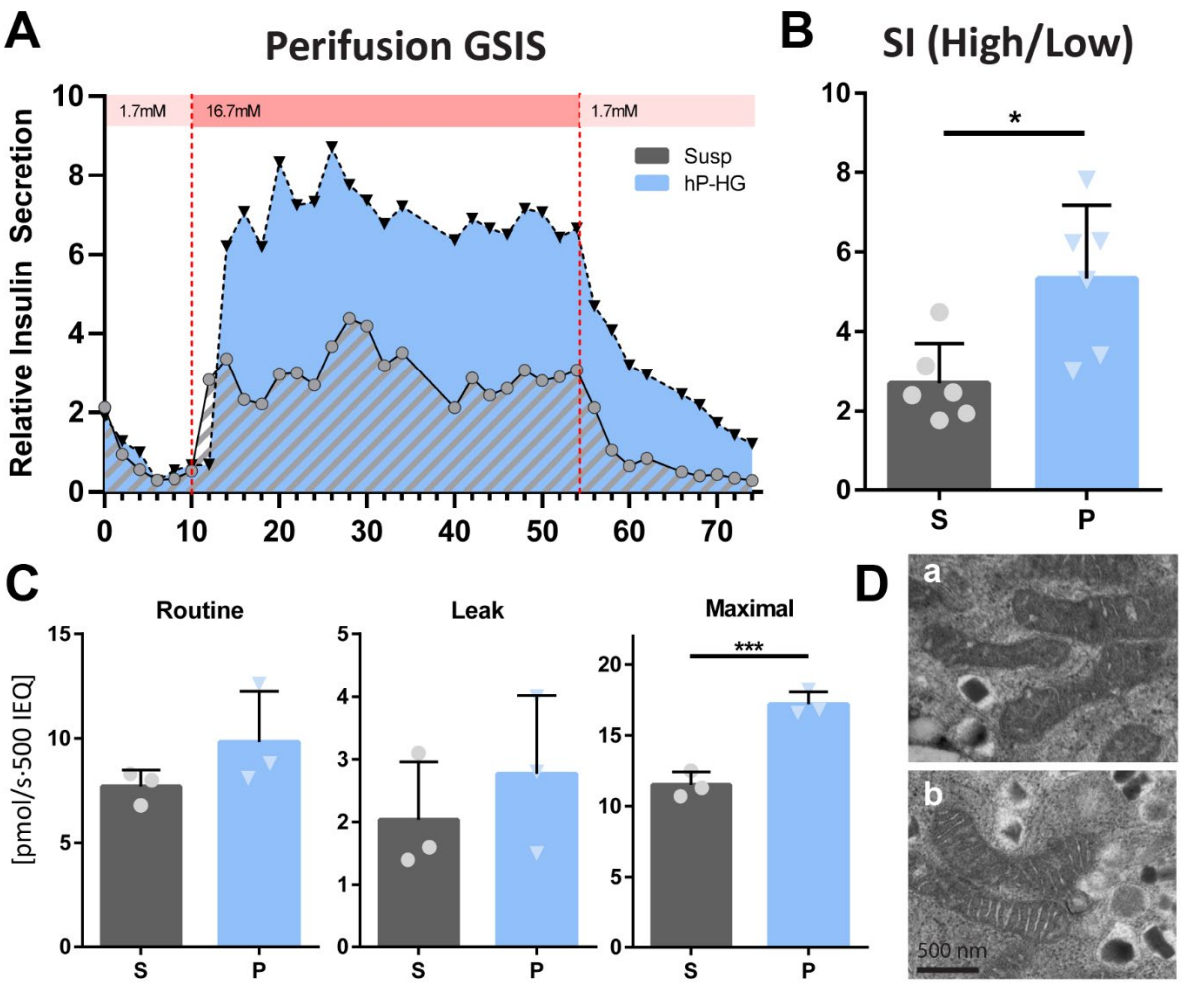

Figure 4: hP-HG culture enables proper dynamic function and enhances maximum respiration

(A) Perifusion GSIS was performed on human islets after 2 days of culture in either suspension (S) or embedded in hP-HG (P), from low glucose (1.7 mM) to high glucose (16.7 mM) and back to low glucose; representative plots shown were generated from 2 technical replicates per treatment, from one islet donor. Insulin secretion is normalized to first low glucose response (unitless). One representative donor is shown, data from additional donors can be found in Supplemental Fig. 4D-E. **(B)** Average stimulation index **(SI,** high/low glucose**)** is reported, N=3 islet donors.

(C) Islets were assessed for mitochondrial respiration after 2 days of culture in either suspension (S) or hP-HG (P); Routine (normal media), Leak (Complex V inhibition), and Maximal (uncoupled) respiration were measured. **(D)** β cell mitochondrial pathology in suspension (a) and hP-HG (b) culture was assessed with transmission electron microscopy. N=3 islet donors. Scale = 500 nm.

(ns = not significant, * p<0.05, *** p<0.001)

To assess whether differences in mitochondrial function may underlie glucose-responsive insulin secretion between islets cultured in hP-HG and suspension, high resolution respirometry was performed. We tested the physiological function of mitochondria by measuring the mitochondrial oxidative phosphorylation (OXPHOS) by detecting oxygen consumption and calculating the rate of oxygen consumption at different respiratory stages in intact cells. Human islets cultured in hP-HG had 27.7% higher, but not significantly different, levels of basal mitochondrial respiration compared to suspension culture (Fig. 4C, Routine), and similarly a 36.5% increase following inhibition of ATP synthase (Complex V) to stop ATP generation (Fig. 4C, Leak). However, after uncoupling the phosphorylation system with FCCP, mimicking a physiological energy demand, islets cultured in hP-HG had a 44.1% significantly increased maximal respiratory capacity of the mitochondria compared to those cultured in suspension (Fig. 4C, Maximal). The change in maximal mitochondrial respiration was not found to be accompanied by a measurable change in mitochondria size or shape, as visualized through TEM (Fig. 4D, Supp Fig. 5).

hP-HG co-culture improves islet survival and function in extended culture

To assess the effect of hP-HG on islet survival in extended culture, islets were kept in suspension or hP-HG for 7 days. Islets were counted and plated on “day 0” and measured on days 1, 3, 5, and 7 using an MTS assay to assess survival. The same number of starting islets were used at all time points, so islet attrition is reflected in a reduction in MTS response as time progresses. As expected, islets in suspension displayed a steady decline in MTS activity over the 7-day period, suggesting cell death. Islets cultured in hP-HG, however, had stable metabolic activity in the first few days, and somewhat greater than 100% metabolic activity by day 7 (Fig. 5A). The MTS

measurements on days 3 and 5 were not significantly different, however by day 7 there was significantly higher MTS response in the hydrogel-cultured compared to suspension-cultured islets (Fig. 5B). Islets cultured in hP-HG had noticeable outgrowth into the gel by day 7 (Supplemental Fig. 6), a potential reason for the increased metabolic activity. Islet function was also assessed on days 2 and 7 through static GSIS. hP-HG co-cultured islets maintained a significantly higher stimulation index from low to high glucose at day 7 (Fig. 5C), and displayed stable secretion levels after one week of culture in both low and high glucose (Fig. 5D). Islets cultured in suspension, however, secreted a significantly higher amount of their stored C-peptide on day 7 compared to day 2, with significant increases in percent secretion under both low and high glucose. Of note, under suspension conditions, the percentage of C-peptide secreted in low glucose (basal) at day 7 (average=3.2% of total C-pep) was consistently equal to or higher than that in high glucose (stimulated) at day 2 (average=2.5% of total C-pep). This level of leaky insulin secretion after a week of culture is indicative of islet dysfunction, and was not observed in hP-HG islet cultures. Total C-pep per IEQ was not significantly different among the two treatments at the two time points (Fig. 5E).

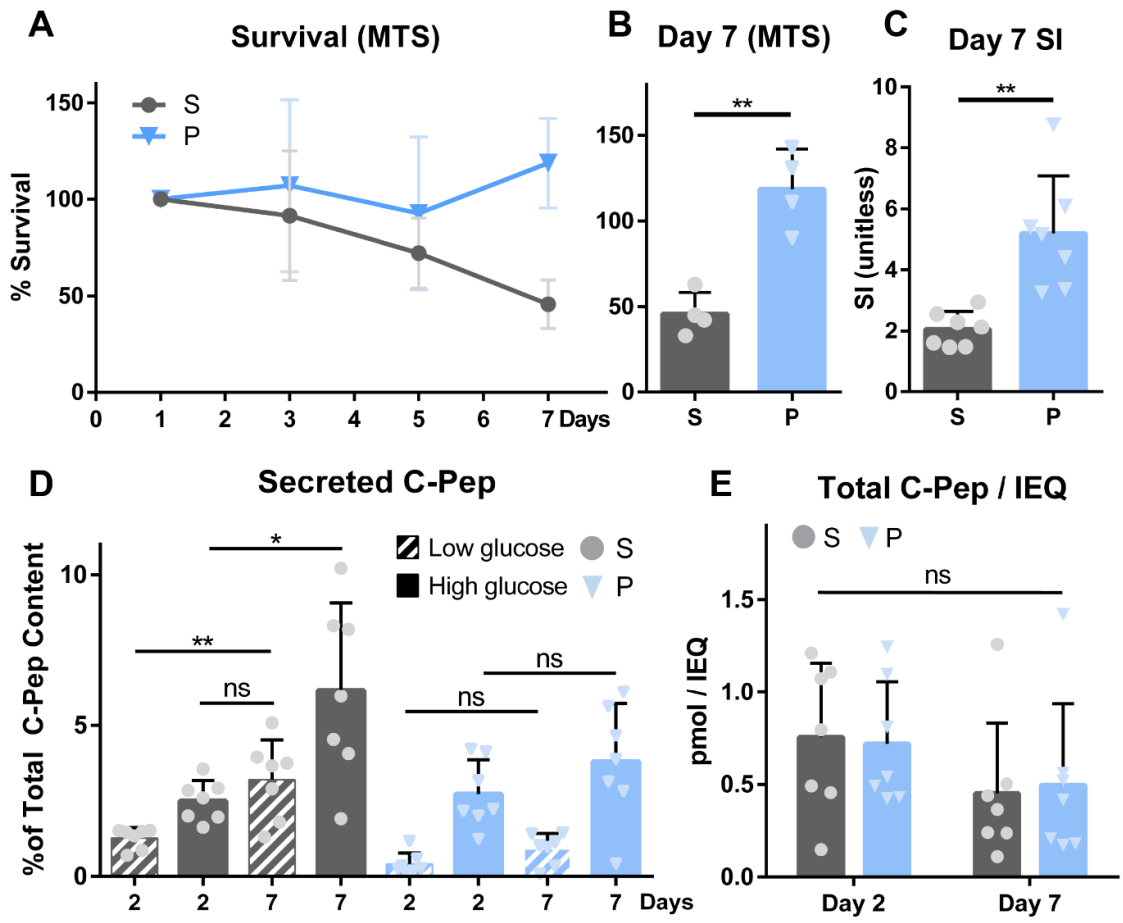

Figure 5: hP-HG co-culture improves islet survival and function in extended culture

(A-B) Metabolic activity of islets cultured in suspension (S) or hP-HG (P) over a 7 day period was assessed by MTS assay, reflecting islet survival over time (presented as a percentage of the Day 1 value). No significant difference in survival was apparent on day 3 or 5 **(A)**, but a significant difference was found on day 7 **(B)**. N=4 islet donors per treatment.

(C-E) Islet function changed over the 7 day period, as assessed through static GSIS. Islets maintained a significantly higher stimulation index (ratio of C-peptide secreted under high/low glucose) at day 7 **(C)**. The percentage of total C-pep content secreted under low and high glucose is plotted for day 2 and day 7 under both suspension and hP-HG culture conditions **(D)**. Total C-pep content was not significantly different among the two treatments at the two time points **(E)**. N=7 islet donors.

(ns = not significant, * $p<0.05$, ** $p<0.01$)

Apoptosis rates and islet architecture are altered in suspension culture and partially preserved in hP-HG

Immunofluorescent (IF) staining was performed to investigate cell health in suspension and hP-HG culture. TUNEL staining was used to assess apoptosis in the islets over time (Fig. 6A, a-c). Consistent with the MTS survival curves, there were significantly higher rates of apoptosis in islets in suspension compared to islets embedded in hP-HG after 7 days of culture (Fig. 6B, red bars). Ki67 staining was assessed to determine relative levels of cell proliferation under the two conditions (Fig. 6A, d-f). Rates of proliferation were low in all samples, but significantly higher in hydrogel-embedded islets after 7 days of culture (Fig. 6B, blue bars). $Ki67^{+}$ staining, although only quantified within islets, does not appear to co-localize with $insulin^{+}$ cells.

Markers for each major endocrine cell type were visualized with IF staining, revealing a change in endocrine architecture following isolation (Fig. 6A, g-l; Supplemental Fig. 7F). Islet sections were quantified for numbers of each endocrine cell type (α, β, δ), interactions of each cell with neighboring cells (α-α, α-β, etc.) and localization of each cell at the mantle or core of the islets. Total cell type composition (Supplemental Fig. 7A), cell-cell interactions (Supplemental Fig. 7B-C), and the ratio of non-endocrine cells (Supplemental Fig. 7G) were not found to be significantly different over 7 days in culture, or in suspension versus hP-HG treatment. In contrast, the mantle-core arrangement of endocrine cells was significantly altered in isolated islets compared to native islets (Fig. 6C). After isolation, islet β cells were more likely to localize to the mantle than the core, while the native islets consistently have about equal distribution of the three endocrine cell types throughout the entire islet, as previously described [35]. By day 7, the distribution of endocrine cell populations in the mantle and core was partially preserved in

hP-HG, with a significantly higher fraction of β cells remaining in the center of the islets (47%), compared to suspension (31%) (Supplemental Fig. 7D). Despite a significant difference in β cell localization between suspension and hydrogel-embedded islets, α cells localized in the core at a very high rate (75%) on day 0 of culture, and did not significantly change over the course of the experiment regardless of treatment (Supplemental Fig. 7E, representative images in Supplemental Fig.7F, Fig. 6A).

Interestingly, the localization of resident non-endocrine cells in the isolated islets also changed dramatically following isolation (Fig. 6A, j-l; Supplemental Fig. 7H), with the majority of TEK tyrosine kinase (Tie2)-positive cells and alpha smooth muscle actin (αSMA)-positive cells localizing toward the center of the islets post-isolation, and throughout culture in suspension. After 7 days in hP-HG, the majority of the $Tie2^+$ and αSMA^+ cells localized at the islet mantle and expanded into the gel. The arrangement of these cells in hP-HG culture was significantly more similar to that of the native in situ islets than in suspension culture (Fig. 6D).

Extracellular signaling-related pathways are significantly influenced by hP-HG culture

To identify whether the biological mechanisms through which hP-HG co-culture improves islet survival and function are related to ECM signaling, we performed bulk RNA sequencing. Following 2 days of culture in either suspension or hP-HG, islets were lysed to collect RNA, and assessed for differentially expressed genes (DEGs). Out of 17,975 total transcripts identified, 1,633 were found to be significantly different between the suspension and hP-HG cultures. Of these, 1,078 genes were expressed at higher levels in hP-HG culture and 555 genes were expressed at higher levels in suspension culture. Gene Ontology (GO) analysis of the DEGs resulted in the identification of 30 GO terms in the Molecular Function (MF) aspect, 191 GO terms

in the in the Biological Processes (BP) aspect, and 27 GO terms in the Cellular Component (CC) aspect (Supplement Fig. 8A). The most significant terms in each aspect related to the extracellular space, cell adhesion, receptor signaling, vesicles/exocytosis, and cytokines/inflammation (Supplement Fig. 8B). Gene expression for key endocrine markers, including insulin, were not significantly different between the two groups (Supplemental Table 3).

Figure 6: Apoptosis rates and islet architecture are altered in suspension culture and partially preserved in hP-HG

(A) Immunofluorescent staining images for native (*in situ*) islets, and islets cultured in suspension or hP-HG for 7 days. Islets are stained for TUNEL/Insulin (a-c), Ki67/Insulin (d-f), Insulin/Glucagon/Somatostatin (g-i), and Insulin/Tie2/αSMA (j-l). White arrowheads indicate projections of $Tie2^+$ and αSMA^+ cells into the hydrogel. All scale bars = 50 microns.

(B) Quantification of cells positive for Ki67 (blue bars, significance indicated by blue stars) and TUNEL (red bars, significance indicated by red stars) in native islets, and on day (d) 0, 2 and 7 in suspension (S) and hP-HG (P) culture. N=4 islet donors.

(C) Assessment of islet architecture by counting α (Gcg^+), β (Ins^+), and δ (Sst^+) cells in the islet mantle (checkered) and core (solid). Data is represented as a percentage of total endocrine cells. N=5 islet donors. (Statistical analyses presented in Supplemental Fig. 7D-E.)

(D) Localization of positive staining for Tie2 (light gray) and αSMA (dark gray) in the islet mantle (checkered) and core (solid). N=5 islet donors. p-values depicted in italics and with the † symbol are relative to the native tissue.

(ns = not significant, */*† p<0.05, **/*†† p<0.01, ****/*†††† p<0.0001)

(Next page)

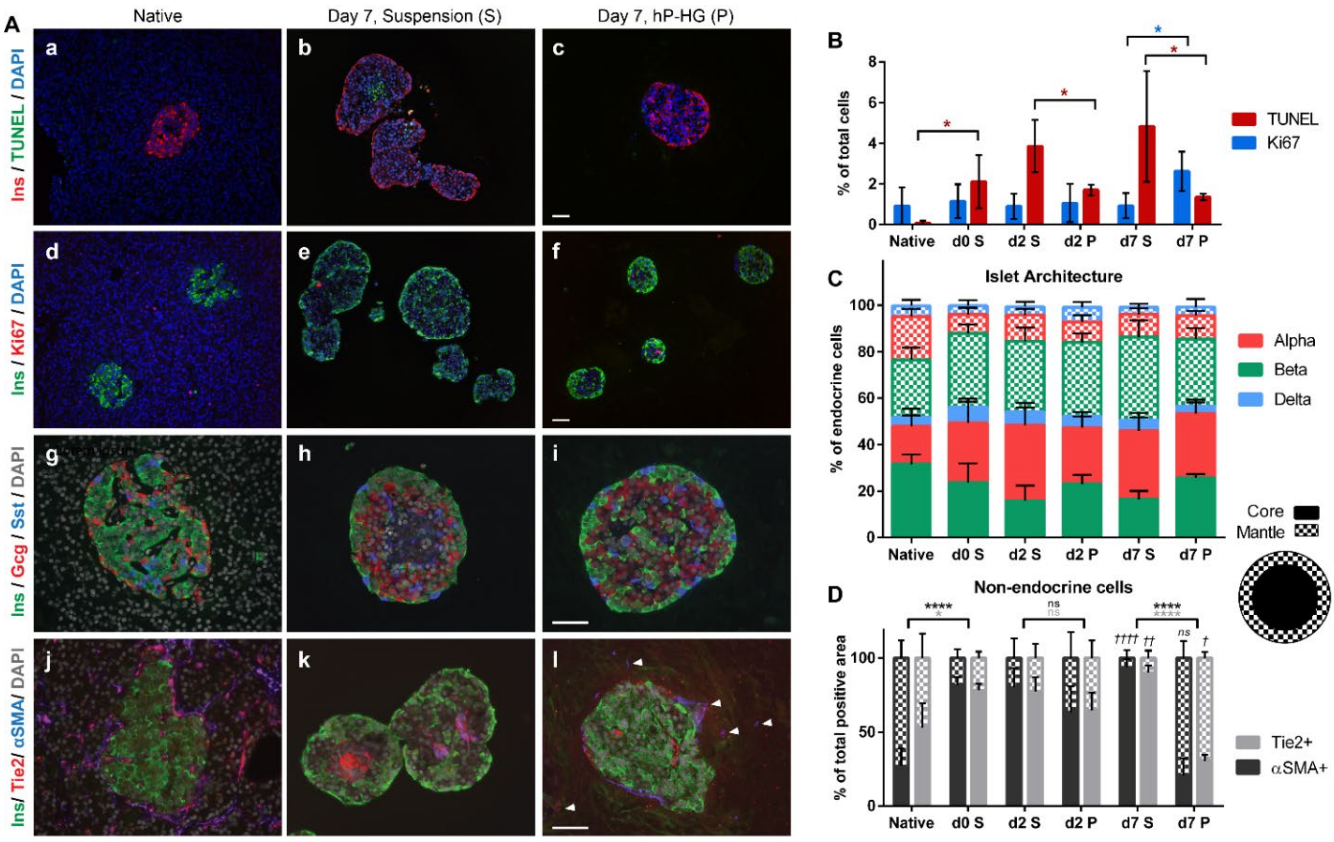

Discussion

Our study aimed to rebuild the 3-D ECM microenvironment of the human pancreas as a hydrogel that can easily be integrated into in vitro culture and is compatible with transplantation. Due to differences in cell behavior between 2-D and 3-D environments, a 3-D islet microenvironment model could be useful for creating better microphysiological islet systems [36]; such may be useful for drug discovery and toxicity testing [37]. We have demonstrated a new protocol for decellularization that removes lipids and DNA from human pancreatic tissue and forms a more stable gel derived from pancreata with substantial lipid content. The decell and gelation process retains collagens well, but there is some reduction in glycoproteins and other ECM components, including a reduction in sGAG content, consistent with previous publications [23, 26, 27]. This enrichment for collagens and reduction of other ECM components has also been

shown in several other pancreas decell studies [18, 21, 22, 26, 27, 38, 39]. Recent work characterizing the human pancreatic matrisome indicates that collagens are the most abundant ECM proteins in the pancreas, and are relatively evenly distributed between the acinar and islet compartments [14], therefore a whole-pancreas hydrogel consisting of mainly pancreatic collagens may be a representative of the native islet ECM environment. This is also an efficient method of constructing a hydrogel made up of these basic ECM components, which individually in purified form are very expensive.

Islets undergo significant injury throughout the process of isolation from the pancreas, and in particular the ECM is heavily damaged leading to anoikis-mediated apoptosis. We hypothesized that replacing the ECM component of the islet microenvironment would help improve islet survival and function in vitro. We found that INS1 cells and primary human islets exhibited positive changes in GSIS when embedded in hP-HG. Consistently, the insulin secreted under basal (low glucose) conditions was significantly reduced compared to suspension cultures, while stimulated insulin secretion was unchanged, resulting in an increased stimulation index. Interestingly, a similar trend of increased stimulation index, due to reduced basal insulin secretion, was recently reported with human islets entrained to daily feeding/fasting rhythms using various stimuli (glucose, arginine, forskolin, and insulin) in culture [6]. Together, this suggests that an improved stimulation index and reduced basal insulin secretion may better reflect the function of in situ islets compared to isolated islets in suspension. Similarly, Singh et al. recently found that the culture of stem cell-derived beta cells with various ECM molecules reduced the basal insulin secretion, and improved GSIS[40]. Several other studies have presented an improved stimulation index in islets cultured with ECM without reporting the raw insulin

secretion values under low and high glucose treatment [41-43], which makes comparison of our study to others unclear. However, other studies have demonstrated that ECM treatment promotes an increase in the stimulated insulin secretion without affecting the basal level [18, 44]. These disparities in response to glucose may be due to differences in ECM composition, co-culture method, or GSIS assays performed using different concentrations of low and high glucose solutions, and warrant further investigation.

After 7 days of culture, islets in suspension secreted more insulin under basal conditions compared to day 2, so much so that the basal insulin secretion on day 7 was higher than the stimulated insulin secretion on day 2 of culture. This trend was not observed in islets cultured in hP-HG, suggesting better maintenance of controlled function throughout the culture period. Islets in hP-HG also had significantly improved survival over 7 days of culture compared to suspension, as assessed through an MTS assay. Immunofluorescent staining corroborated these findings, indicating that islets in suspension have greater levels of apoptosis ($TUNEL^+$ cells) and reduced levels of proliferation ($Ki67^+$ cells) compared to islets cultured in hP-HG. Furthermore, on day 2 of culture, islets in hP-HG had higher maximal mitochondrial function compared to suspension-cultured islets. Mitochondria are crucial in the generation of ATP in response to glucose, affecting both the closure of ATP-sensitive K^+ channels and $Ca2^+$ influx [45-47], which are necessary for insulin secretion. The mitochondria of islets cultured in hP-HG are better equipped to respond to a metabolic challenge, possibly due to maintenance of healthier mitochondrial dynamics compared to islets cultured without hP-HG.

ECM scaffolds have both mechanical and biochemical roles in the cell environment. After two days of culture, islet function was assessed in five different environments: suspension (S),

hP-HG (P), alginate (A), Col1 (C) and hK-HG (K), with a trend in stimulation from low to high glucose: SIS< SIA< SIC< SIK< SIP. This suggests that the mechanical environment of a hydrogel (P, A, C, K) compared to suspension culture may contribute to better islet function. It is also possible that ECM-signaling (P, C, K) may contribute more to islet function than the mechanical environment alone (A), and potentially reveals the importance of a complex mixture of natural ECM proteins (P, K), compared to a singular ECM component like Col1 (C). Finally, the pancreas-specific ECM (P) outperformed the kidney-specific ECM (K) in regard stimulated C-peptide secretion levels, suggesting that the ECM composition of the pancreas itself may have a beneficial effect on islet health and function. Importantly, the generation of these scaffolds for our study was focused on controlling for ECM protein content, and not matching the gel stiffness which has previously been shown itself to have an effect on β cell function [34, 48]. However, a recent study by Enck et al. has also elucidated that ECM has a profound effect on islet function independent of gel stiffness [34]. The RNA-seq GO analyses do indicate that hP-HG co-culture activates significant enrichment in ECM-signaling and adherence-related ontologies, suggesting that islet-ECM signaling helps maintain endocrine cell health.

Our study identified that islet architecture is altered in culture compared to in situ. As has previously been observed [49, 50], a higher fraction of β cells are found at the periphery of the islet in suspension culture compared to in the native pancreas. In hP-HG co-culture, β cell mantle-core arrangement is more similar to native islets, although the α cells are significantly more enriched in the core than in situ. We find that islets in situ have a roughly equal distribution of α, β, and δ cells between the core and mantle; this is consistent with recent conclusions that human islets do not have a mantle-core arrangement, or subunit domains similar to rodents [35]. Islets

embedded in hP-HG on day 0 preserve endocrine architecture on days 2 and 7 that is insignificantly different than freshly isolated (day 0) islets; this indicates that in hP-HG, islet architecture is preserved over time relative to the day islets were embedded. Islets in suspension, however, continue to change endocrine architecture over the 7 day period. This observation is of consequence, because islet architecture is thought to affect cross-talk within the endocrine cell populations, and influence islet function [51, 52]. Interestingly, resident non-endocrine cells, such as endothelial cells ($Tie2^+$), vascular mural cells (pericytes, smooth muscle cells; αSMA^+) or fibroblasts (αSMA^+), display an even more dramatic rearrangement following isolation. Some human islets are surrounded by a capsule of αSMA^+ cells in situ (Fig. 6A-j) and the arrangement of these cells in islets cultured in hP-HG significantly resembles this "capsule" morphology (Fig. 6A-l), while the αSMA^+ and $Tie2^+$ cells in suspension-cultured islets appear to form abnormal internal nodules (Fig. 6A-i). The mechanism through which the cells rearrange could reflect migration of the different cell types in a balance between cell-cell adhesion and cell-ECM adhesion, as has been described in other culture systems [53], but the cellular complexity of isolated islets and affinities for each cell type with one another has not been well established. Importantly, in the present study, only the outer perimeter of the islets is in contact with the ECM hydrogel. Further studies are necessary to explore the potential mechanisms of islet cell arrangement.

Islet transplantation into the liver through the portal vein has been associated with significant islet death following transplantation [54]. Alternative strategies have been suggested for islet and stem cell-derived islet like cluster (SC-ILC) transplantation, including transplantation into the omentum, a vascularized subcutaneous space, or within a device that can protect the

cells from immune rejection [55]. A re-evaluation of transplant site and strategy invites the opportunity for the inclusion of ECM into islet culture and transplantation, particularly to support islet health during the period prior to vascularization and ECM remodeling. A recent study utilizing a collagen-based "islet viability matrix" has demonstrated that indeed, subcutaneous co-transplantation of islets with the matrix improves engraftment, function and provides immune protection [19]. Due to the conserved nature of ECM proteins, decelled ECM is hypoimmunogenic [16, 26, 56] and is therefore compatible with transplantation. A first-in-human clinical trial using decelled ECM hydrogel to treat myocardial infarction has already been completed without serious adverse effects related to the hydrogel [57]. Combined, these results strongly suggest that the inclusion of ECM into islet culture and transplantation could improve the engraftment, survival, and function of the islets; future studies utilizing these materials in transplantation are underway.

Human pancreatic hydrogel may also be useful for accelerating, enhancing, or stabilizing the maturation of SC-ILCs. Due to limited availability of primary donor islets for clinical treatment, efforts have been made to differentiate SC-ILCs with the intention of transplanting functional cells to cure diabetes. Despite significant strides in the field of β cell differentiation, deficits in the maturation and function of the SC-ILCs still exist, including efficiency of β cell yield, total insulin content and secretion, and gene expression for markers of islet maturation [58]. It is thought that ECM signaling may play beneficial roles toward the determination of cell fate, and therefore may be valuable in SC-ILC differentiation [40, 59, 60]. Overall, hP-HG could provide a substrate for improved in vitro islet and SC-ILC culture, a material to support transplanted islets and SC-ILCs, and a scaffold for in vitro 3-D modeling of human pancreas and islet development.

The combination of islets with hP-HG as a liquid prior to gelation allows for alteration of the platform, in which many other components could be added. This could include supplemented ECM components, such as GAGs or glycoproteins that are reduced in abundance through the decellularization and digestion process. Decelled hP-ECM is composed of structural ECM proteins from the whole pancreas, which is mainly exocrine tissue; hP-HG could therefore serve as a base scaffold to which more islet-enriched ECM components could be added for future studies. It would also facilitate the inclusion of other cell types in islet cultures, such as endothelial cells, neurons or immune cells, all of which have important roles in islet health and function. In current culture systems, non-endocrine cells have been combined with islet endocrine cells following single cell dispersion which does not recapitulate the in situ arrangement and sub-structures of the various cell types [61-63]. Finally, future studies using hP-HG could incorporate oxygen generating materials, drug carriers, or immune-modulatory particles, which could all be used to support and protect islets in culture or in vivo. An added feature is that the droplets of gel can be picked up, transferred and transplanted more easily than individual islets.

Conclusion

We have generated a hydrogel from human pancreas ECM that is easy to combine with human islets in culture and which takes advantage of material from discarded organs. The hydrogel co-culture system improves the survival and function of human islets after extended culture, and reduces the level of apoptosis. As early as 2 days in hydrogel co-culture, islets display an improved GSIS stimulation index, through a reduction in basal insulin secretion, as well as improved maximal mitochondrial function. The scaffold appears to better preserve islet architecture during culture, and stimulates gene expression changes through ECM- and adhesion-

mediated pathways. This islet culture platform mimics the native pancreatic niche and may provide a mechanism for better modeling islet biology and physiology in vitro.

Methods

Tissue Procurement and Ethics

Adult human pancreata (n = 10, age 21–61 years) and kidneys were obtained through the University of Wisconsin Organ and Tissue Donation with informed consent obtained for research from next of kin and authorization by the University of Wisconsin-Madison Health Sciences Institutional Review Board (IRB granted an exempt from protocol approval for studies on postnatal tissue because research on deceased donors is not considered human subjects research). IRB oversight of the project is not required because it does not involve human subjects as recognized by 45 CFR 46.102(f), which defines a "human subject" as "a living individual about whom an investigator (whether professional or student) conducting research obtains (1) data through intervention or interaction with the individual, or (2) identifiable private information." Research was performed in accordance with federal and state law and the relevant institutional ethical committee guidelines and regulations. No organs or tissues were procured from prisoners. A list of donors used in this study and demographic data are included in Supplemental Table 1.

Decellularization and Hydrogel Formation

Pancreata were trimmed of extraparenchymal fat, sectioned into 1 cm^3 pieces, flash frozen and stored at -80 °C. For decellularization, pieces were thawed, rinsed with 1x PBS, rinsed with water and homogenized in water until broken up. The homogenate was centrifuged (4300

rpm, 5 min), floating fat removed, and supernatant discarded; the pellet was washed and centrifuged again (4300 rpm, 5 min). The pellet was resuspended into 2.5 mM sodium deoxycholate/PBS and incubated, with shaking, for 3 hours at room temperature (RT). After this time, the homogenate was strained over a sieve (MilliporeSigma, St. Louis, MO); all collected material was placed into fresh 2.5 mM sodium deoxycholate/PBS and incubated for an additional 15 hours (RT, shaker). The ECM was strained, rinsed with water and washed in 1x PBS supplemented with Pen/Strep for 24 hours. Further lipid removal was achieved with additional steps modified from Soffer-Tsur et al. [64]. The ECM from above was strained and dehydrated with 70% ethanol for 30 minutes, followed by 3 washes with 100% ethanol for 30 minutes each. The matrix was washed with acetone 3 times, for 30 minutes each. The dehydrated ECM was washed with 40:60 (v:v) acetone:hexane for 24 hours, with changes into fresh solution approximately every 8 hours. The matrix was washed with 100% ethanol for 30 minutes and rehydrated with 70% ethanol overnight, followed by two washes with 1x PBS supplemented with Pen/Strep for 24 hours each. To remove nucleic acids, the ECM was treated with Benzonase (MilliporeSigma, St. Louis, MO) (500 mU/mL in 50 mM Tris, 1 mM $MgCl_2$, 0.1% BSA, pH=8.0) for 18 hours at 37^{o}C, washed with 50 mM Tris for 2 hours, followed by two 24-hour washes with sterile water. The resulting decellularized pancreatic ECM was lyophilized and stored at -80^{o}C.

Homogenization decellularization (Homog) without acetone:hexane and Benzonase treatment was performed for comparison, as previously described in Sackett and Tremmel et al. [26].

The lyophilized ECM from each decell protocol was pepsin digested for hydrogel formation as previously described [26, 65]. If necessary, the ECM was homogenized after a day

in the pepsin solution to facilitate digestion. Collagen controls were prepared from rat-tail collagen type I (Corning, Corning, NY).

Human kidneys were processed in a similar timeline and manner as human pancreas, and the protocol for decellularization and hydrogel formation was the same as the Optimized protocol for pancreas.

Lipid, DNA and GAG Content

Lyophilized material was weighed to record the whole tissue dry weight. Lipids were extracted from each sample using a modified Folch method as previously described [26, 66]. The lipid phase was dried and weighed to measure the lipid content as a percentage of the initial dry weight.

The delipidized tissue was used for DNA and GAG content analysis. Weighed and lyophilized ECM was digested with papain for 18 hours at 65^{o}C prior to the assays. Quantification of DNA was assessed using the Quant-iT™ PicoGreen® dsDNA Assay (Life Technologies, Carlsbad, CA), following manufacturer's protocol.

Rheology

To compare the rheologic properties of the optimized hydrogel to the previously published hydrogel, a TA Instruments AR-G2 rheometer was used. A 40 mm parallel plate geometry was used with a 500 micron gap distance; a Peltier unit was used to control temperature. First, a time sweep was performed over 10 minutes; the temperature was set to 15^{o}C for loading the samples and warmed to 37^{o}C to induce gelation while measuring oscillatory moduli (storage modulus (G') and loss modulus (G")) at the fixed angular frequency of 1 rad/sec

and strain of 5%. Following gelation, a frequency sweep was performed at 37°C, from 100 rad/sec to 0.1 rad/sec at fixed 5% strain; G' and G" were measured to calculate complex viscosity for each gel. Three different batches of gels were tested from each decellularization protocol (homogenized and optimized), rat-tail collagen type I (Corning, Corning, NY) was used as a control for comparison. All gels were prepared at a concentration of 8 mg/mL. Data was collected and analyzed with Rheology Advantage software (TA Instruments, New Castle, DE), and graphs were created with Prism 6 for Windows (GraphPad Software, Inc.). Each protocol was assessed using three biological replicates, each of a different batch of gel from a different donor.

Cell Culture

Human islets were received through the Integrated Islet Distribution Program (IIDP) and experiments were initiated within 24 hours of receipt. On day 0, islets were counted and plated in suspension or in hydrogel co-culture. Islets were combined with hP-HG (8 mg/mL) at a density of 100 IEQ/10µL of hydrogel. The mixture was pipetted into 5 µL droplets in the bottom of an untreated petri dish, inverted, and incubated at 37^{o}C and 5% CO_2 for 30 minutes. The polymerized droplets were moved into 24-well ULA plates (Corning, Corning, NY) for culture for 1-7 days in PIM(R) medium (Prodo Labs, Aliso Viejo, CA), at which point they were collected for MTS, GSIS, or total insulin content. In parallel, islets were cultured in suspension in 24-well plates for the same period of time. Islets embedded in collagen 1 (8 mg/mL) (Corning, Corning, NY) followed the same protocol as hP-HG. Islets were embedded in alginate following methodology adapted from Alagpulinsa et al. [32]. Briefly, islets were mixed with 1.6% w/v sodium alginate in 150 mM NaCl, at 100 IEQ/10µL, and manually dropped into a 100 mM $CaCl_2$ bath 5 µL at a time to form droplets.

Glucose Stimulated Insulin Secretion and Total Insulin Content

Static GSIS Assays were performed in series, in 24-well plates with cell filter inserts (MilliporeSigma, St. Louis, MO). Cells were added to the filters and moved from low glucose (2.8 mM) to high glucose (28 mM) to low glucose (2.8 mM) to a depolarization solution (30 mM KCl, 2.8 mM glucose). All solutions for GSIS were made in Krebs buffer (25 mM HEPES, 115 mM NaCl, 24 mM $NaHCO_3$, 5 mM KCl, 1 mM $MgCl_2$, 2.5 mM $CaCl_2$, 1% BSA). The supernatant was collected following 1 hour in each step of the GSIS for secreted C-pep measurement. For human islets, 100 IEQ were used per well. Supernatants collected from each treatment were frozen in aliquots. Following GSIS, cells were lysed in 1 mL of lysis buffer (20 mM Tris-HCl, pH 7.5, 150 mM NaCl, 1 mM EDTA, 1% Triton) and homogenized with a PowerGen 500 homogenizer (ThermoFisher, Waltham, MA); these lysates were used to measure total C-peptide content. C-peptide content for all lysates and supernatants were determined with an ultra-sensitive human C-pep ELISA (Mercodia, Uppsala, Sweden). Stimulation index (SI) for the static GSIS was calculated by dividing the average secreted C-Peptide concentration under high glucose by the average C-Peptide secreted under the first low glucose period.

Islets were prepared as described above, and assessed with perifusion GSIS on day 2 of culture. Perifusion was performed using a BioRep 4.0 semi-automated perifusion system (Biorep, Miami, FL) for 30 minutes of low glucose treatment (1.6 mM) followed by 45 minutes of high glucose treatment (16.7 mM) and return to low glucose. Flow-through samples were collected every minute from each chamber, and values from every two minutes were averaged together for graphing. For comparison, graphed values are normalized to the average low glucose response for each curve (unitless measure). The SI for the perifusion GSIS was calculated using

the area under the curve (AUC) of the high glucose period per minute, divided by the AUC of the first low glucose period per minute.

Mitochondrial Respiration

Human islets were assessed for mitochondrial respiratory capacity analysis by high resolution respirometry using an Oxygraph-2k (Oroboros Instruments, Innsbruck, Austria). Islets cultured in suspension or hP-HG for 2 days, were simultaneously analyzed in two separate chambers, in 2 mL volume containing 800 IEQ each. Experiments were performed as previously described [67, 68]. Briefly, mitochondrial respiration was measured by detecting mitochondrial oxygen consumption at 37^{o}C in standard PIM(R) medium. After establishing a basal respiration (Routine), inhibitors for the different mitochondrial respiratory complexes were added to the cells in the following order: oligomycin (2ug/ml) (MilliporeSigma, St. Louis, MO) to inhibit ATP-synthase (complex V) to measure leak respiration (Leak), carbonyl cyanide-p-trifluoromethoxyphenylhydrazone (FCCP) (MilliporeSigma, St. Louis, MO) uncoupler with step-wise titration in 0.5 to 1.5 µM increments to measure the maximal respiratory capacity of the electron transport system (ETS) (Maximal), rotenone (MilliporeSigma, St. Louis, MO) 0.5 µM final concentration to inhibit complex I, and antimycin A (MilliporeSigma, St. Louis, MO) to inhibit complex III in 2.5 µM final concentration. Data was analyzed using DatLab7 (version 7.3.0.3) (Oroboros Instruments, Innsbruck, Austria) software. The use of chambers for the 2 treatments (S and H) was switched between 3 biological replicates to avoid any possible bias due to chamber differences.

MTS Assay

100 IEQ of human islets were plated per well of 24-well ULA plates (Corning, Corning, NY). Islets were embedded in hP-HG or Col1 (50 IEQ / 5 µL gel) as described above, and two 5 µL gels were placed in each well of a 24-well plate (100 IEQ/well); wells were fed fresh medium every 3 days. On days 1, 3, 5 and 7 after plating, the remaining cells or gels from each pre-counted well were transferred to 1.5 mL Eppendorf tubes with 300 µL of medium containing CellTiter-96 reagent (Promega, Madison, WI). The IEQ was not recounted each day, whatever number of islets remained in the well were used to assess survival compared to day 0. The tubes were incubated with shaking and open caps for 3 hours, at 5% CO_2 and 37^{o}C. After incubation, the absorbance of the supernatant was measured on a spectrophotometer at 490 nm (FlexStation 3, Molecular Devices). Each treatment was tested in technical triplicate for each condition and time point.

Histology and Immunofluorescent Staining

Samples were fixed in 4% paraformaldehyde (PFA), paraffin embedded, and sectioned (5 µm) for immunofluorescent staining. Slides were deparaffinized using xylene and rehydrated. Antigen retrieval was performed by incubation in 10 mM Citrate Buffer, pH 6.0 for 2.5 hours at 80°C. Slides were blocked with 10% BSA/PBS for 40 minutes at RT, incubated with primary antibodies overnight at 4^{o}C, washed, incubated with secondary antibody incubation for 40 minutes at RT and cover slipped. All antibodies and dilutions are listed in Supplemental Table 2. Nuclei were labeled with 40–6-diamidino-2-phenylindole (DAPI) (Life Technologies, Carlsbad, CA). Images were generated with a Zeiss Axiovert 200 M microscope or a Nikon A1R confocal microscope. TUNEL staining (ApopTag® Fluorescein In Situ Apoptosis Detection Kit)

(MilliporeSigma, St. Louis, MO) was performed following manufacturer protocol, with the insulin immunostaining performed immediately afterward.

IF staining was quantified in ImageJ by tracing the Ins-positive (islet) clusters. Nuclear stains were quantified by counting the number of total nuclei (DAPI) within the islet regions and the number of TUNEL-positive and Ki67-positive nuclei in the same regions to determine the percentage of positive cells. Cellular stains were quantified by converting the images to binary and measured as percentage of islet area.

For islet architecture analysis, Ins/Gcg/Sst triple stained images were taken as z-stacks of 7 slices and quantified using the 3D Tissue Organization Toolbox plugin to determine cell type, counts and cell-cell interactions[69]. Cells were manually counted as part of the mantle if they were at the outermost edge of the islet, all other cells were counted as part of the core, as previously described [70]. To measure Tie2 and αSMA localization, whole islet clusters and islet mantles (5-10 micron width surrounding the outermost layer of islet nuclei) were manually traced in synchronized windows; positive area within each traced region was measured in all relevant channels.

For each IF analysis, 5 islet donors were assessed for each time point and condition, at least 9 islets were counted per donor and treatment.

Quantification and Statistical Analysis

Data are reported as average ± standard deviation unless otherwise indicated. All p-values were calculated with a Student's two-tailed t-test using Prism 6 for Windows (GraphPad). Prism's suggested significance classification scheme was followed (*p < .05), (**p < .01), (***p< 0.001), (****p<0.0001).

All composite figures were prepared in Adobe Illustrator 24.0 (Adobe Inc.).

Materials Availability

Unique reagents generated in this study, including hP-HG and hK-HG, are listed in the key resources table and available from the lead contact with a completed Materials Transfer Agreement.

Data and Code Availability

All data are available in the manuscript, Supplementary Information, or available from the corresponding author upon request. Raw and processed RNA sequencing data have been deposited in the NCBI Gene Expression Omnibus (GEO) repository, with the accession identifier GSE166505.

Acknowledgements

We would like to offer a special thanks to the families who donated tissues, without which this study would not be possible. We acknowledge Sierra Raglin and the University of Wisconsin Department of Surgery Histology Core for help with sample processing. We would like to thank Dr. Melanie Graham and David Giles and the University of Minnesota Chemical Engineering and

Materials Science Department for use of the Polymer Characterization Facility to perform rheological measurements. We thank Randall Massey at the UW Electron Microscope Core for help with TEM imaging. We thank the University of Wisconsin-Madison Biotechnology Center Gene Expression Center & DNA Sequencing Facility for providing library preparation and next generation sequencing services, and the University of Wisconsin Bioinformatics Resource Center, specifically Mark Berres, for analysis of results. We would also like to thank Dr. Matthew Brown for the generation of humanized mice used in this study, and Melissa Adams for help implementing the 3D Tissue Organization Toolbox and analysis.

Funding

This study was supported in part by grant funding from the NIH (R21AI126419 and 1F31DK125021-01), and Juvenile Diabetes Research Foundation (1-SRA-2016-168-S-B, 1-PNF-2016-250-S-B and 3-SRA-2017-364-S-B). Data presented here was also in part obtained through support from an NIH/NCATS UL1TR002373 award through the University of Wisconsin Institute for Clinical and Translational Research. Support for this research was also provided by the University of Wisconsin-Madison, Office of the Vice Chancellor for Research and Graduate Education with funding from the Wisconsin Alumni Research Foundation. This work was supported in part by Merit Review Award I01 BX003700 (to MEK) from the United States (U.S.) Department of Veterans Affairs Biomedical Laboratory Research and Development (BLR&D) Service and NIH grant R01 DK102598 (to MEK). Data presented here was also supported by the Integrated Islet Distribution Program (IIDP) (National Institutes of Health Grant 2UC4DK098085).

References:

1. Prince, E. and E. Kumacheva, Design and applications of man-made biomimetic fibrillar hydrogels. Nature Reviews Materials, 2019. 4(2): p. 99-115.
2. Amin, J., et al., A simple, reliable method for high-throughput screening for diabetes drugs using 3D beta-cell spheroids. J Pharmacol Toxicol Methods, 2016. 82: p. 83-89.
3. Walpita, D., et al., A human islet cell culture system for high-throughput screening. J Biomol Screen, 2012. 17(4): p. 509-18.
4. Foster, E.D., et al., Improved Health-Related Quality of Life in a Phase 3 Islet Transplantation Trial in Type 1 Diabetes Complicated by Severe Hypoglycemia. Diabetes Care, 2018. 41(5): p. 1001-1008.
5. Shapiro, A.M., et al., Islet transplantation in seven patients with type 1 diabetes mellitus using a glucocorticoid-free immunosuppressive regimen. N Engl J Med, 2000. 343(4): p. 230-8.
6. Alvarez-Dominguez, J.R., et al., Circadian Entrainment Triggers Maturation of Human In Vitro Islets. Cell Stem Cell, 2020. 26(1): p. 108-122 e10.
7. Jun, Y., et al., In vivo-mimicking microfluidic perfusion culture of pancreatic islet spheroids. Sci Adv, 2019. 5(11): p. eaax4520.
8. Rosenberg, L., et al., Structural and functional changes resulting from islet isolation lead to islet cell death. Surgery, 1999. 126(2): p. 393-8.
9. Wang, R.N., S. Paraskevas, and L. Rosenberg, Characterization of integrin expression in islets isolated from hamster, canine, porcine, and human pancreas. J Histochem Cytochem, 1999. 47(4): p. 499-506.
10. Cross, S.E., et al., Key Matrix Proteins Within the Pancreatic Islet Basement Membrane Are Differentially Digested During Human Islet Isolation. Am J Transplant, 2017. 17(2): p. 451-461.
11. Thomas, F., et al., A tripartite anoikis-like mechanism causes early isolated islet apoptosis. Surgery, 2001. 130(2): p. 333-8.
12. Thomas, F.T., et al., Anoikis, extracellular matrix, and apoptosis factors in isolated cell transplantation. Surgery, 1999. 126(2): p. 299-304.
13. Stendahl, J.C., D.B. Kaufman, and S.I. Stupp, Extracellular matrix in pancreatic islets: relevance to scaffold design and transplantation. Cell Transplant, 2009. 18(1): p. 1-12.
14. Li, Z., et al., Proteome-wide and matrisome-specific alterations during human pancreas development and maturation. Nat Commun, 2021. 12(1): p. 1020.
15. Citro, A., et al., Anti-Inflammatory Strategies in Intrahepatic Islet Transplantation: A Comparative Study in Preclinical Models. Transplantation, 2018. 102(2): p. 240-248.

16. Crapo, P.M., T.W. Gilbert, and S.F. Badylak, An overview of tissue and whole organ decellularization processes. Biomaterials, 2011. 32(12): p. 3233-43.

17. Tremmel, D.M. and J.S. Odorico, Rebuilding a better home for transplanted islets. Organogenesis, 2018. 14(4): p. 163-168.

18. Jiang, K., et al., 3-D physiomimetic extracellular matrix hydrogels provide a supportive microenvironment for rodent and human islet culture. Biomaterials, 2019. 198: p. 37-48.

19. Yu, M., et al., Islet transplantation in the subcutaneous space achieves long-term euglycaemia in preclinical models of type 1 diabetes. Nat Metab, 2020. 2(10): p. 1013-1020.

20. Chaimov, D., et al., Innovative encapsulation platform based on pancreatic extracellular matrix achieve substantial insulin delivery. J Control Release, 2017. 257: p. 91-101.

21. Elebring, E., et al., Cold-perfusion decellularization of whole-organ porcine pancreas supports human fetal pancreatic cell attachment and expression of endocrine and exocrine markers. J Tissue Eng, 2017. 8: p. 2041731417738145.

22. Gaetani, R., et al., Evaluation of Different Decellularization Protocols on the Generation of Pancreas-Derived Hydrogels. Tissue Eng Part C Methods, 2018. 24(12): p. 697-708.

23. Goh, S.K., et al., Perfusion-decellularized pancreas as a natural 3D scaffold for pancreatic tissue and whole organ engineering. Biomaterials, 2013. 34(28): p. 6760-72.

24. Napierala, H., et al., Engineering an endocrine Neo-Pancreas by repopulation of a decellularized rat pancreas with islets of Langerhans. Sci Rep, 2017. 7: p. 41777.

25. Peloso, A., et al., The Human Pancreas as a Source of Protolerogenic Extracellular Matrix Scaffold for a New-generation Bioartificial Endocrine Pancreas. Ann Surg, 2016. 264(1): p. 169-79.

26. Sackett, S.D., et al., Extracellular matrix scaffold and hydrogel derived from decellularized and delipidized human pancreas. Sci Rep, 2018. 8(1): p. 10452.

27. Tamburrini, R., et al., Detergent-Free Decellularization of the Human Pancreas for Soluble Extracellular Matrix (ECM) Production. J Vis Exp, 2020(163).

28. Noguchi, G.M. and M.O. Huising, Integrating the inputs that shape pancreatic islet hormone release. Nature Metabolism, 2019. 1(12): p. 1189-1201.

29. van Deijnen, J.H., et al., Significance of the peri-insular extracellular matrix for islet isolation from the pancreas of rat, dog, pig, and man. Cell Tissue Res, 1992. 267(1): p. 139-46.

30. Van Deijnen, J.H., et al., Distribution of collagens type I, type III and type V in the pancreas of rat, dog, pig and man. Cell Tissue Res, 1994. 277(1): p. 115-21.

31. Otonkoski, T., et al., Unique basement membrane structure of human pancreatic islets: implications for beta-cell growth and differentiation. Diabetes Obes Metab, 2008. 10 Suppl 4: p. 119-27.

32. Alagpulinsa, D.A., et al., Alginate-microencapsulation of human stem cell-derived beta cells with CXCL12 prolongs their survival and function in immunocompetent mice without systemic immunosuppression. Am J Transplant, 2019. 19(7): p. 1930-1940.

33. Fuchs, S., et al., Hydrogels in Emerging Technologies for Type 1 Diabetes. Chem Rev, 2021. 121(18): p. 11458-11526.

34. Enck, K., et al., Effect of alginate matrix engineered to mimic the pancreatic microenvironment on encapsulated islet function. Biotechnol Bioeng, 2021. 118(3): p. 1177-1185.

35. Dybala, M.P. and M. Hara, Heterogeneity of the Human Pancreatic Islet. Diabetes, 2019. 68(6): p. 1230-1239.

36. Ernst, A.U., et al., Nanotechnology in cell replacement therapies for type 1 diabetes. Adv Drug Deliv Rev, 2019. 139: p. 116-138.

37. Langhans, S.A., Three-Dimensional in Vitro Cell Culture Models in Drug Discovery and Drug Repositioning. Front Pharmacol, 2018. 9: p. 6.

38. Asthana, A., et al., Comprehensive characterization of the human pancreatic proteome for bioengineering applications. Biomaterials, 2021. 270: p. 120613.

39. Ma, F., et al., In Depth Quantification of Extracellular Matrix Proteins from Human Pancreas. J Proteome Res, 2019. 18(8): p. 3156-3165.

40. Singh, R., et al., Enhanced structure and function of human pluripotent stem cell-derived beta-cells cultured on extracellular matrix. Stem Cells Transl Med, 2020.

41. Beenken-Rothkopf, L.N., et al., The incorporation of extracellular matrix proteins in protein polymer hydrogels to improve encapsulated beta-cell function. Ann Clin Lab Sci, 2013. 43(2): p. 111-21.

42. Davis, N.E., et al., Enhanced function of pancreatic islets co-encapsulated with ECM proteins and mesenchymal stromal cells in a silk hydrogel. Biomaterials, 2012. 33(28): p. 6691-7.

43. Stephens, C.H., et al., In situ type I oligomeric collagen macroencapsulation promotes islet longevity and function in vitro and in vivo. Am J Physiol Endocrinol Metab, 2018. 315(4): p. E650-E661.

44. Llacua, A., et al., Extracellular matrix components supporting human islet function in alginate-based immunoprotective microcapsules for treatment of diabetes. J Biomed Mater Res A, 2016. 104(7): p. 1788-96.

45. Tarasov, A., J. Dusonchet, and F. Ashcroft, Metabolic regulation of the pancreatic beta-cell ATP-sensitive K+ channel: a pas de deux. Diabetes, 2004. 53 Suppl 3: p. S113-22.

46. Antinozzi, P.A., et al., Mitochondrial metabolism sets the maximal limit of fuel-stimulated insulin secretion in a model pancreatic beta cell: a survey of four fuel secretagogues. J Biol Chem, 2002. 277(14): p. 11746-55.

47. Ortsater, H., et al., Contribution of glycolytic and mitochondrial pathways in glucose-induced changes in islet respiration and insulin secretion. Pflugers Arch, 2002. 444(4): p. 506-12.

48. Nyitray, C.E., M.G. Chavez, and T.A. Desai, Compliant 3D microenvironment improves beta-cell cluster insulin expression through mechanosensing and beta-catenin signaling. Tissue Eng Part A, 2014. 20(13-14): p. 1888-95.

49. Lavallard, V., et al., Cell rearrangement in transplanted human islets. FASEB J, 2016. 30(2): p. 748-60.

50. Walker, J.T., et al., Integrated human pseudoislet system and microfluidic platform demonstrate differences in GPCR signaling in islet cells. JCI Insight, 2020. 5(10).

51. Benninger, R.K.P. and D.J. Hodson, New Understanding of beta-Cell Heterogeneity and In Situ Islet Function. Diabetes, 2018. 67(4): p. 537-547.

52. Cabrera, O., et al., The unique cytoarchitecture of human pancreatic islets has implications for islet cell function. Proc Natl Acad Sci U S A, 2006. 103(7): p. 2334-9.

53. Cerchiari, A.E., et al., A strategy for tissue self-organization that is robust to cellular heterogeneity and plasticity. Proc Natl Acad Sci U S A, 2015. 112(7): p. 2287-92.

54. Bennet, W., et al., Isolated human islets trigger an instant blood mediated inflammatory reaction: implications for intraportal islet transplantation as a treatment for patients with type 1 diabetes. Ups J Med Sci, 2000. 105(2): p. 125-33.

55. Pepper, A.R., et al., Revascularization of transplanted pancreatic islets and role of the transplantation site. Clin Dev Immunol, 2013. 2013: p. 352315.

56. Mirmalek-Sani, S.H., et al., Immunogenicity of decellularized porcine liver for bioengineered hepatic tissue. Am J Pathol, 2013. 183(2): p. 558-65.

57. Traverse, J.H., et al., First-in-Man Study of a Cardiac Extracellular Matrix Hydrogel in Early and Late Myocardial Infarction Patients. JACC Basic Transl Sci, 2019. 4(6): p. 659-669.

58. Tremmel, D.M., et al., Mimicking nature-made beta cells: recent advances towards stem cell-derived islets. Curr Opin Organ Transplant, 2019. 24(5): p. 574-581.

59. Mamidi, A., et al., Mechanosignalling via integrins directs fate decisions of pancreatic progenitors. Nature, 2018. 564(7734): p. 114-118.

60. Rozario, T. and D.W. DeSimone, The extracellular matrix in development and morphogenesis: a dynamic view. Dev Biol, 2010. 341(1): p. 126-40.

61. Augsornworawat, P., et al., A hydrogel platform for in vitro three dimensional assembly of human stem cell-derived islet cells and endothelial cells. Acta Biomater, 2019. 97: p. 272-280.

62. Skrzypek, K., et al., Endothelial and beta cell composite aggregates for improved function of a bioartificial pancreas encapsulation device. Int J Artif Organs, 2018. 41(3): p. 152-159.

63. Takahashi, Y., et al., Self-Condensation Culture Enables Vascularization of Tissue Fragments for Efficient Therapeutic Transplantation. Cell Rep, 2018. 23(6): p. 1620-1629.

64. Soffer-Tsur, N., et al., Optimizing the biofabrication process of omentum-based scaffolds for engineering autologous tissues. Biofabrication, 2014. 6(3): p. 035023.

65. Freytes, D.O., et al., Preparation and rheological characterization of a gel form of the porcine urinary bladder matrix. Biomaterials, 2008. 29(11): p. 1630-7.

66. Tremmel, D.M., et al., Hypertension, but not body mass index, is predictive of increased pancreatic lipid content and islet dysfunction. Am J Transplant, 2020. 20(4): p. 1105-1115.

67. Bansal, A., et al., Sex- and Dose-Specific Effects of Maternal Bisphenol A Exposure on Pancreatic Islets of First- and Second-Generation Adult Mice Offspring. Environ Health Perspect, 2017. 125(9): p. 097022.

68. Hutter, E., et al., Biphasic oxygen kinetics of cellular respiration and linear oxygen dependence of antimycin A inhibited oxygen consumption. Mol Biol Rep, 2002. 29(1-2): p. 83-7.

69. Tran Thi Nhu, H., et al., A novel toolbox to investigate tissue spatial organization applied to the study of the islets of Langerhans. Sci Rep, 2017. 7: p. 44261.

70. Adams, M.T., et al., Endocrine cell type sorting and mature architecture in the islets of Langerhans require expression of Roundabout receptors in beta cells. Sci Rep, 2018. 8(1): p. 10876.

Chapter 5 Supplementary Information

Supplementary Methods

Cell Culture

INS-1 832/13 were plated in a single cell suspension into 10 cm ultra-low attachment (ULA) dishes (Corning, 3262) and cultured for 3 days to form INS1 pseudoislets. On day 3, pseudoislets were counted, combined with hP-HG at a density of 200 IEQ/10µL of hydrogel and evenly distributed within the gel. The mixture was pipetted into 5 µL droplets in the bottom of an untreated petri dish, inverted, and incubated at 37 ^{o}C and 5% CO_2 for 30 minutes. The polymerized droplets were moved into 24-well ULA plates (Corning, 3473) for culture for 2 days until the GSIS was performed. For static GSIS with INS1 832/13 pseudoislets, clusters were counted using the human islet IEQ counting mechanism and 800 IEQ were used per well. (N=4 biological replicates)

Rheology

To assess droplet shape retention following gelation, 10 µL droplets of cold, neutralized liquid hydrogel were pipetted onto a tissue culture plate and incubated at 37 C for 30 minutes. Following gelation, droplets were imaged and droplet diameter was measured relative to the standard diameter of the tissue culture well.

Young's Modulus was calculated using Equation 1 and Equation 2, with G' and G" values at last time point of the time sweep (after full gelation) of the gels.

Equation 1: Complex Modulus (G) $$G = \sqrt{(G')^2 + (G'')^2}$$

Equation 2: Young's Modulus (E), with Poisson's ratio, v = 0.5 for hydrogels.

$$E = 2 \times G(1 + v)$$

Bulk RNA Sequencing

RNA was isolated from human islets after 2 days of culture in suspension or hydrogel conditions. cDNA libraries were prepared using Takara SMARTer Total RNA Seq Kit v2 Pico Input kit (Takara Bio USA, Mountain View, CA) and purified with AMPure XP Beads (Beckman Coulter, Brea, CA); RNA-Seq was performed with the Illumina NovaSeq6000 sequencing system with 200 million reads. 3 islet donors were used for each condition. Gene Ontology (GO) was performed using a list of differentially expressed genes with g:Profiler (version e99_eg46_p14_f929183) with g:SCS multiple testing correction method applying significance threshold of 0.05 [1].

Transplantation

5 µL hP-HG droplets derived using the optimized protocol and embedded with human islets (50 IEQ per 5 µL gel) were transplanted into NOD-scid IL2rγnull (NSG) mice. 20 gels were transplanted within the center of a 3 mm-internal diameter silicone O-ring (Hooper, UK, OR3X1.5) in the lateral subcutaneous (SQ) space. 10 gels were transplanted into the right kidney sub-capsule (KSC) space. Images were taken at the time of surgery.

Humanized Mice

Research involving mice was performed in accordance with a protocol that was approved by the University of Wisconsin School of Medicine and Public Health Animal Care and Use

Committee, and in accordance with a protocol approved by the University of Wisconsin Institutional Review Board. Humanized mouse models were generated using NSG mice aged 7–8 weeks, as previously described (Sackett et al., 2018). A small piece of decellularized hP-ECM was transplanted into the left dorsal subcutaneous space, and 500 µL of 10 mg/mL hP-HG was injected into the right dorsal subcutaneous space of humanized mice (N = 3 mice). Additionally, human fetal pancreas (HFP) fragments from a donor allogeneic to the donor of the mouse's human immune system were also transplanted subcutaneously into the same animals. The three grafts remained in vivo for a period of four weeks before the animals were sacrificed, and grafts were collected for processing and immunohistochemistry. Upon collection of the grafts, the hP-HG graft was noticeably smaller after four weeks in vivo, but the large volume of the original injection and the high concentration of ECM (10 mg/mL) ensured reliable recovery of the material within this timeframe. Smaller volumes of the gel were not able to be found after this period of time *in vivo*.

Transmission Electron Microscopy (TEM)

Islets cultured in suspension or hP-HG for two days were fixed overnight with glutaraldehyde-based fixative (2.5% glutaraldehyde, 2.0% paraformaldehyde buffered in 0.1M sodium phosphate buffer (PB)) at 4˚C. The samples were rinsed 5 x 5 minutes in PB, and post-fixed in 1% osmium tetroxide, 1% potassium ferrocyanide in 0.1M PB for 1 hour at room temperature (RT), and rinsed in PB as before.

Dehydration was performed in a graded ethanol series (35, 50, 70, 80, 90% for 10 minutes each step, 95% for 20 minutes, 100% for 2 x 10 minutes) at RT and 100% EtOH at 4˚C overnight (ON) then transitioned in propylene oxide (PO) 2 x 7 minutes at RT. Fully dehydrated samples

were infiltrated in increasing concentrations of PolyBed 812 (Polysciences Inc. Warrington, PA) and Propylene Oxide (PO) mixtures in the following order (RT mixtures with shaker table agitation):

PolyBed 812	PO	Time	Temp.
10%	90%	3 hrs	RT
25%	75%	ON	RT
50%	50%	ON	RT
75%	25%	2 hrs	RT
100%	0%	45 min.	60°C

Embedding and polymerization took place in fresh PolyBed 812 for 24 hours at 60˚C. The samples were sectioned on a Leica EM UC6 ultramicrotome at 100nm. The sections were collected on formvar coated 2x1mm slot Cu grids (EMS Hatfield, PA), and post-stained with uranyl acetate and lead citrate. The sectioned samples were viewed at 80kV on a Philips CM120 transmission electron microscope, equipped with AMT BioSprint12 digital camera (AMT Imaging Systems, Woburn, MA).

sGAG Content

The sulfated glycosaminoglycan (sGAG) content was quantified using Papain-digested tissue or ECM, using the Blyscan GAG Assay Kit (Biocolor, UK), following manufacturer's protocol.

Resources and Reagents

Reagent or Resource	Source	Identifier
Antibodies		
Anti-Insulin (guinea pig)	MilliporeSigma	I8510
Anti-Glucagon (rabbit)	Abcam	Ab 92517
Anti-Somatostatin (mouse)	Proteintech	17512-1-AP
Anti-Ki67 (rabbit)	Abcam	ab16667
Anti-Insulin (mouse)	MilliporeSigma	I2018
Anti-Collagen 1 (rabbit)	Abcam	ab34710
Anti-Collagen 4 (rabbit)	Abcam	ab6586
Anti-Collagen 3 (mouse)	Abcam	ab6310
Anti-Collagen 6 (rabbit)	Abcam	ab6588
Anti-Laminin (rabbit)	MilliporeSigma	L9393
Anti-FN1 (rabbit)	Abcam	ab2413
Anti-OGN (rabbit)	Proteintech	12755-1-AP
Anti-Tie2 (rabbit)	Abcam	ab221154
Anti-αSMA (mouse)	MilliporeSigma	A2547
Anti-CD3 (rabbit)	Abcam	ab134096
Anti-CD45 (mouse)	BD Pharmingen	555491
Chemicals and Reagents		
Sodium deoxycholate	MilliporeSigma	D6750-25G
PIM(R) medium	Prodo Labs	PIM-CR001GMP
DAPI	ThermoFisher	D3571
Sodium alginate	MilliporeSigma	PHR1471-1G
Rat-tail Collagen 1	Corning	354249
Pepsin	MilliporeSigma	P7012-250MG
HCl	MilliporeSigma	NC9894356
Benzonase	MilliporeSigma	E8263
Oligomycin	MilliporeSigma	
FCCP	MilliporeSigma	
Rotenone	MilliporeSigma	
Antimycin A	MilliporeSigma	
AMPure XP Beads	Beckman Coulter	A63880
Materials		
Sieve	MilliporeSigma	S1145
Cell filter inserts	MilliporeSigma	PIXP01250
24-well ULA plates	Corning	3473
Commercial Assays		
ApopTag® Fluorescein In Situ Apoptosis Detection Kit	MilliporeSigma	S7110
Quant-iT™ PicoGreen® dsDNA Assay	Life Technologies	P7589
Blyscan GAG Assay Kit	Biocolor	B1000
Ultra-sensitive human C-pep ELISA	Mercodia	10-1141-01
SMARTer Total RNA Seq Kit v2 Pico Input kit	Takara Bio	634411
CellTiter-96 reagent	Promega	G3582

Cell Lines		
INS-1 832/13	Hohmeier et al 2000	
Computer Software		
Fiji	https://imagej.net/Fiji	
DatLab7 (version 7.3.0.3)	Oroboros Instruments	
Prism 6 for Windows	GraphPad Software	
Unique Materials		
Human pancreatic hydrogel (hP-HG)	University of Wisconsin	

Supplemental Table 1: Pancreas donor information

Donor	Sex	Age	BMI (kg/m^2)	DCD/DBD	CIT (hrs)
Donor 10	F	53	35.2	DCD	6
Donor 23	M	58	27.4	DBD	6.5
Donor 27	F	45	31.1	DBD	13.5
Donor 31	M	21	27.6	DBD	14.5
Donor 32	M	35	30.8	DCD	25
Donor 35	F	48	20.7	DBD	5
Donor 39	M	31	27.1	DBD	16
Donor 40	M	41	29.3	DBD	8.5
Donor 56	M	61	34.6	DBD	17
Donor 65	M	21	28.8	DBD	7

Pancreas donor information. (M = male, F = female, BMI = body mass index, DCD = donation by cardiac death, DBD = donation by brain death, CIT = cold ischemia time)

Supplemental Table 2: Immunohistochemistry information

Target	**Blocking** Blocking buffer; dilution; supplier (catalogue #)	**Primary** antibody; host, dilution, supplier (catalogue #)	**Secondary** antibody; host, dilution, supplier (catalogue #)
Ins	Bovine Serum Albumin; 10%; Fisher Scientific (BP1600)	Insulin polyclonal; Raised in guinea pig; 1:2000; Sigma-Aldrich (I8510)	Goat anti-guinea pig A488; 1:800; Life Technologies (A11073)
Gcg	Bovine Serum Albumin; 10%; Fisher Scientific (BP1600)	Glucagon monoclonal; Raised in rabbit; 1:2000; abcam (ab92517)	Goat anti-rabbit A568; 1:800; Life Technologies (A11036)
Sst	Bovine Serum Albumin; 10%; Fisher Scientific (BP1600)	Tie2 monoclonal; Raised in rabbit; 1:4000; abcam (ab221154)	Goat anti-rabbit A568; 1:800; Life Technologies (A11036)
Tie2	Bovine Serum Albumin; 10%; Fisher Scientific (BP1600)	Somatostatin monoclonal; Raised in mouse; 1:200; Proteintech (17512-1-AP)	Goat anti-mouse A647; 1:800; Life Technologies (A21235)
αSMA	Bovine Serum Albumin; 10%; Fisher Scientific (BP1600)	αSMA monoclonal; Raised in mouse; 1:25,000; Sigma-Aldrich (A2547)	Goat anti-mouse A647; 1:800; Life Technologies (A21235)
Collagen I	Bovine Serum Albumin; 10%; Fisher Scientific (BP1600)	Collagen I polyclonal; Raised in rabbit; 1:500; Abcam (ab34710)	Donkey anti-rabbit A488; 1:800; Life Technologies (A21206)
Collagen III	Bovine Serum Albumin; 10%; Fisher Scientific (BP1600)	Collagen III monoclonal; Raised in mouse; 1:100; Abcam (ab6310)	Donkey anti-rabbit A488; 1:800; Life Technologies (A21206)
Collagen IV	Bovine Serum Albumin; 10%; Fisher Scientific (BP1600)	Collagen IV polyclonal; Raised in rabbit; 1:300; Abcam (ab6586)	Donkey anti-rabbit A488; 1:800; Life Technologies (A21206)
Collagen V	Bovine Serum Albumin; 10%; Fisher Scientific (BP1600)	Collagen V polyclonal; Raised in rabbit; 1:100; Abcam (ab7046)	Donkey anti-rabbit A488; 1:800; Life Technologies (A21206)
Collagen VI	Bovine Serum Albumin; 10%; Fisher Scientific (BP1600)	Collagen VI polyclonal; Raised in rabbit; 1:100; Abcam (ab6588)	Donkey anti-rabbit A488; 1:800; Life Technologies (A21206)
Fibronectin	Bovine Serum Albumin; 10%; Fisher Scientific (BP1600)	Fibronectin polyclonal; Raised in rabbit; 1:200; Abcam (ab2413)	Donkey anti-rabbit A488; 1:800; Life Technologies (A21206)
Laminin	Bovine Serum Albumin; 10%; Fisher Scientific (BP1600)	Laminin polyclonal; Raised in rabbit; 1:200; Sigma-Aldrich (L9393)	Donkey anti-rabbit A488; 1:800; Life Technologies (A21206)
Mimecan (OGN)	Bovine Serum Albumin; 10%; Fisher Scientific (BP1600)	Mimecan polyclonal; Raised in rabbit; 1:50; Proteintech (12755-1-AP)	Donkey anti-rabbit A488; 1:800; Life Technologies (A21206)
CD45	Bovine Serum Albumin; 10%; Fisher Scientific (BP1600)	CD45RO monoclonal; Raised in mouse; 1:2000; BD Pharmingen (555491)	ImmPRESS® HRP Horse Anti-Mouse IgG Polymer Detection Kit, Peroxidase (MP-7402); DAB substrate (SK-4105)
CD3	Bovine Serum Albumin; 10%; Fisher Scientific (BP1600)	CD3G monoclonal; Raised in rabbit; 1:500; Abcam (ab134096)	ImmPRESS® HRP Goat Anti-Rabbit IgG Polymer Detection Kit, Peroxidase (MP-7451); DAB substrate (SK-4105)

Supplemental Table 3: Gene Expression in Islets Cultured in Suspension or hP-HG for 2 Days

Symbol	Fold Change	FDR	Significance	Protein
INS	1.261	0.67	NS	insulin
GCG	1.254	0.65	NS	glucagon
SST	1.043	0.94	NS	somatostatin
CHGA	0.846	0.63	NS	chromogranin A
NKX6-1	1.214	0.23	NS	NK6 homeobox 1
UCN3	1.166	0.27	NS	urocortin 3
ARX	0.854	0.26	NS	aristaless related homeobox

Chapter 5 Supplemental Figure 1: Composition of the hP-ECM and hP-HG.

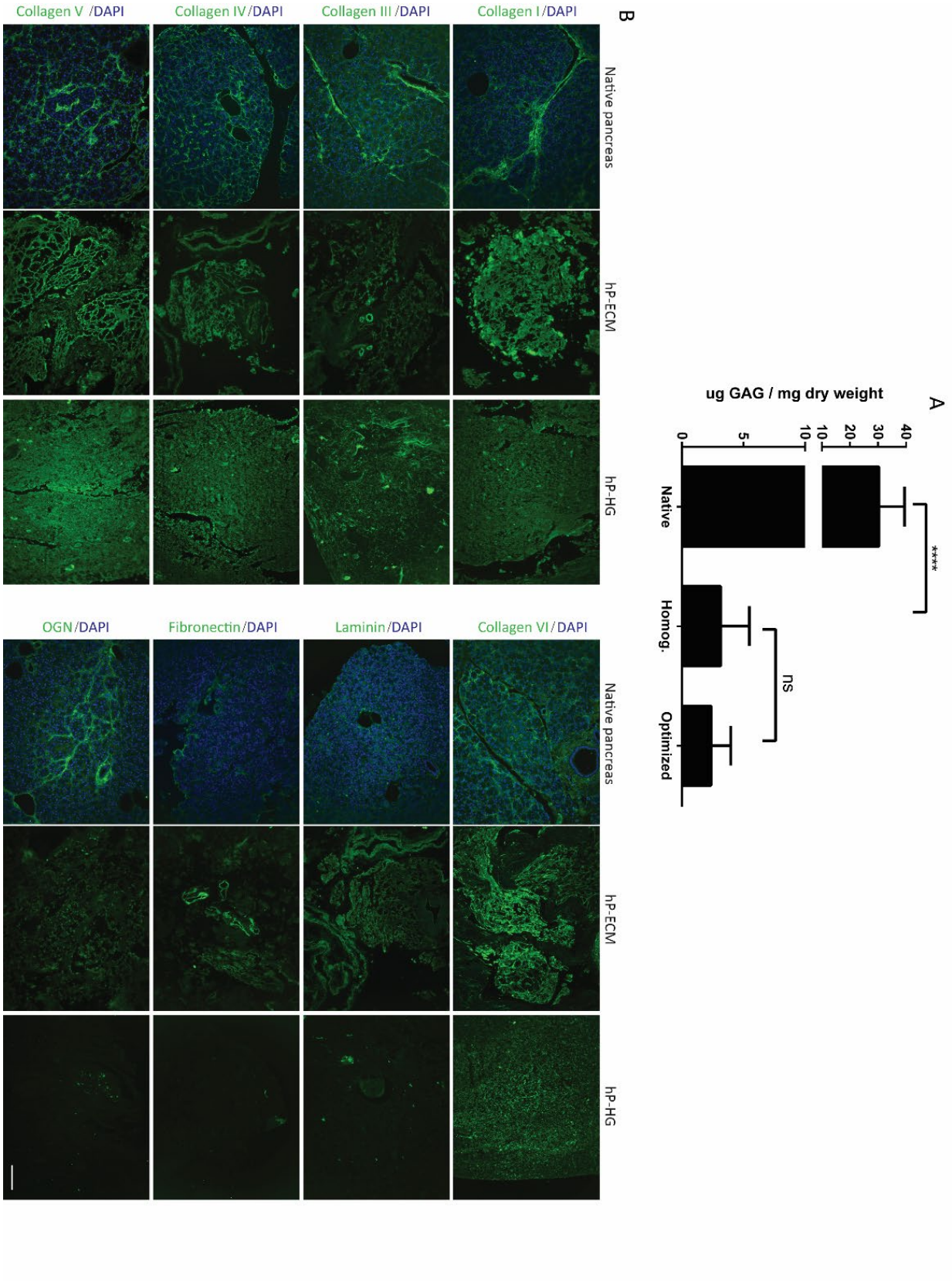

Chapter 5 Supplemental Figure 1: Composition of the hP-ECM and hP-HG.

(A) Sulfated glycosaminoglycan (sGAG) content of native human pancreas compared to decellularized ECM generated with the Homog and Optimized protocols. **(B)** Immunofluorescent staining of native human pancreas, decellularized ECM and hP-HG for various ECM proteins (green), counterstained with DAPI (blue) to also indicate the removal of DNA through decellularization. Scale bar = 100 microns.

(Previous Page)

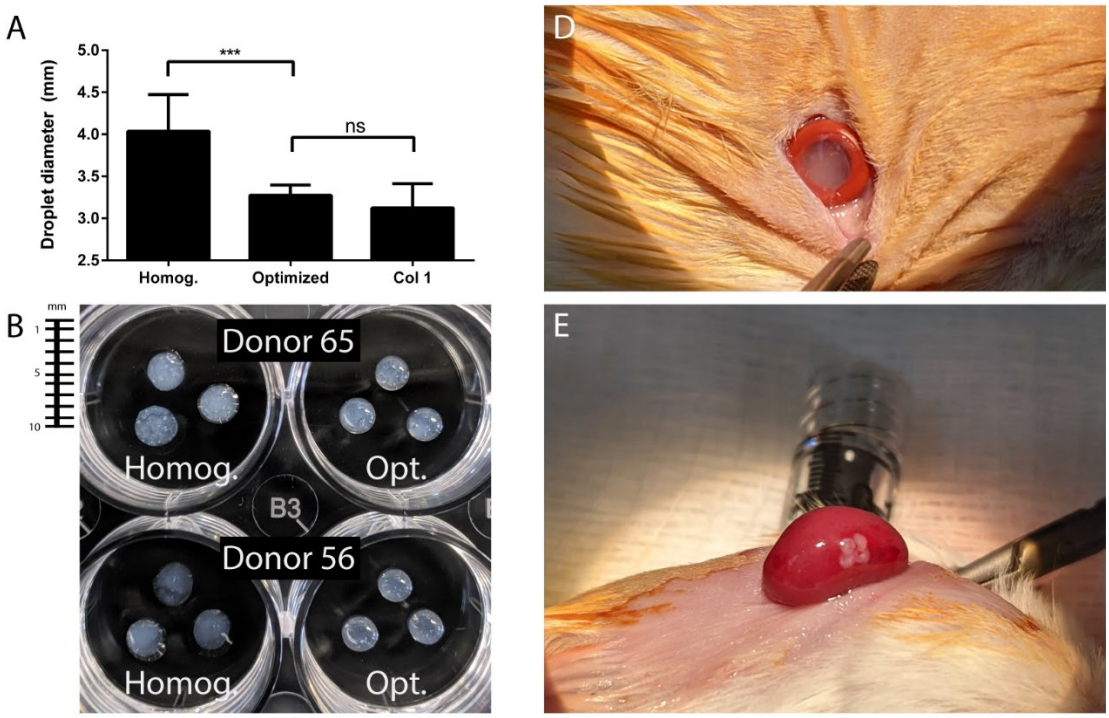

C

	Protein Concentration	Complex Modulus (G)	Young's Modulus (E)
Homogenized Protocol	8 mg/mL	7.66 Pa	22.99 Pa
Optimized Protocol	8 mg/mL	22.15 Pa	66.45 Pa
Purified Rat-tail Collagen I	8 mg/mL	213.91 Pa	641.72 Pa

Chapter 5 Supplemental Figure 2: Optimized-protocol hP-HG holds shape and is transplantable

(A) The diameter of 10 µL gels made from the homogenized protocol (Homog), optimized protocol (Opt) and purified Col1; N=7 donors per treatment. **(B)** Representative images of gels made from two pancreas donors, each processed with the Homog and Optimized (Opt.) protocols. For both donors, the diameters of the gels are noticeably larger following the Homog protocol compared to the Optimized protocol, indicating a lack of firmness and pliability, and a flatter gel. **(C)** Calculated Complex Modulus (G) and Young's Modulus (E) for each measured material at 8 mg/mL protein concentration. The optimized hP-HG gels hold shape well enough that they can easily be transplanted subcutaneously (SQ) **(D)** and into the kidney sub-capsule (KSC) **(E)** without breaking or losing shape.

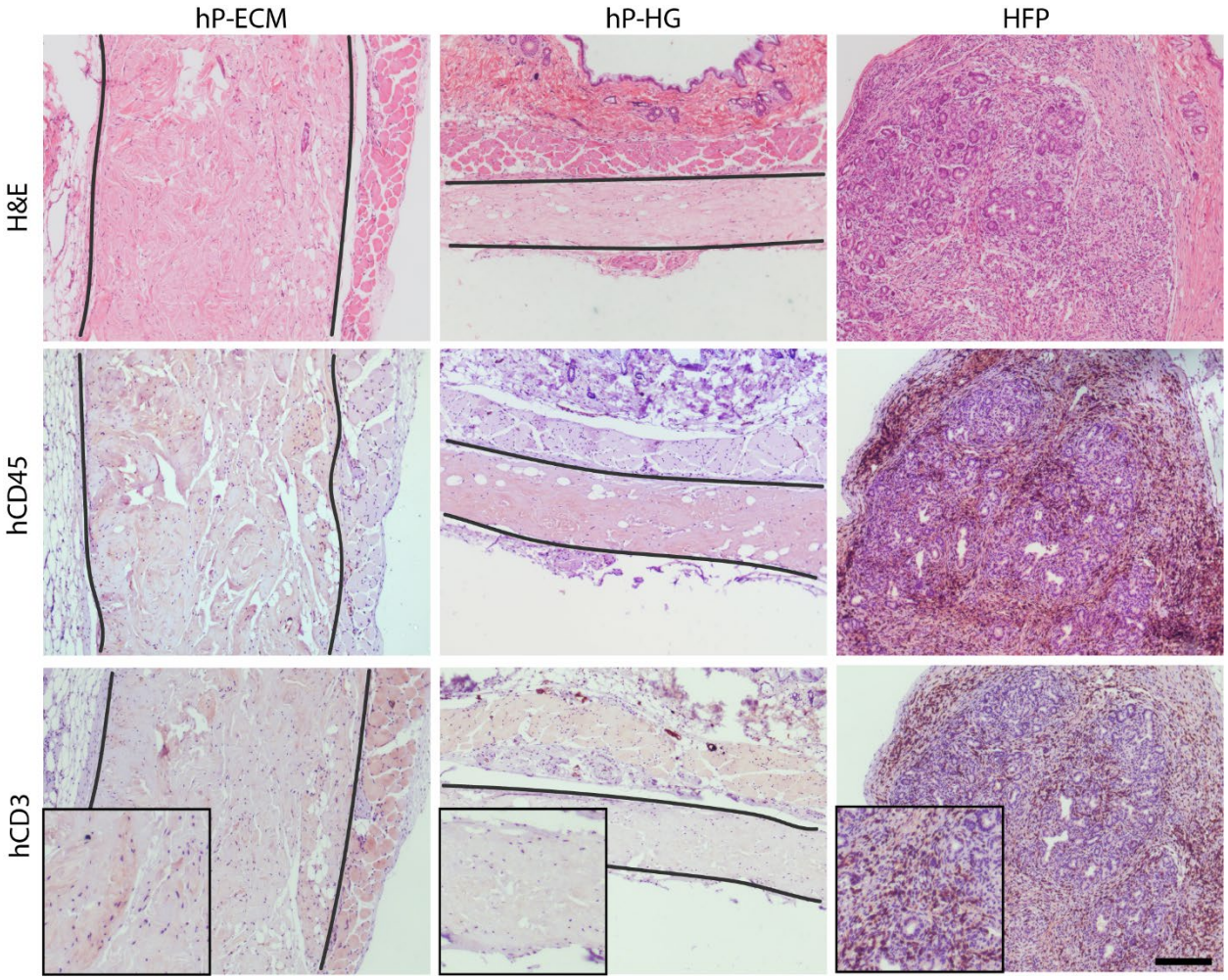

Chapter 5 Supplemental Figure 3: Minimal immune cell infiltration in acellular hP-ECM and hP-HG in humanized mice.

Representative images of Optimized protocol-derived hP-ECM, hP-HG and allogeneic human fetal pancreas (HFP) grafts transplanted subcutaneously into humanized mice and collected after 4 weeks. Decellularizerd gels and ECM scaffolds were transplanted as acellular materials (without cultured cells) to test immunogenicity of the scaffolds themselves. Each mouse was transplanted with all three materials (N=3 mice). Grafts were stained with H&E to examine general immune infiltration, human CD45 (hCD45) to assess infiltration of human immune cells, and human CD3 (hCD3) to assess infiltration of cytotoxic T cells. hP-ECM and hP-HG had extremely low levels of any human immune cell infiltration, while allogeneic HFP in the same animal was heavily infiltrated with both hCD45+ and hCD3+ cells. Insets show more closely the positive (brown) or negative (only purple nucleus) staining for human CD3 within the different explants. Scale bar = 200 microns.

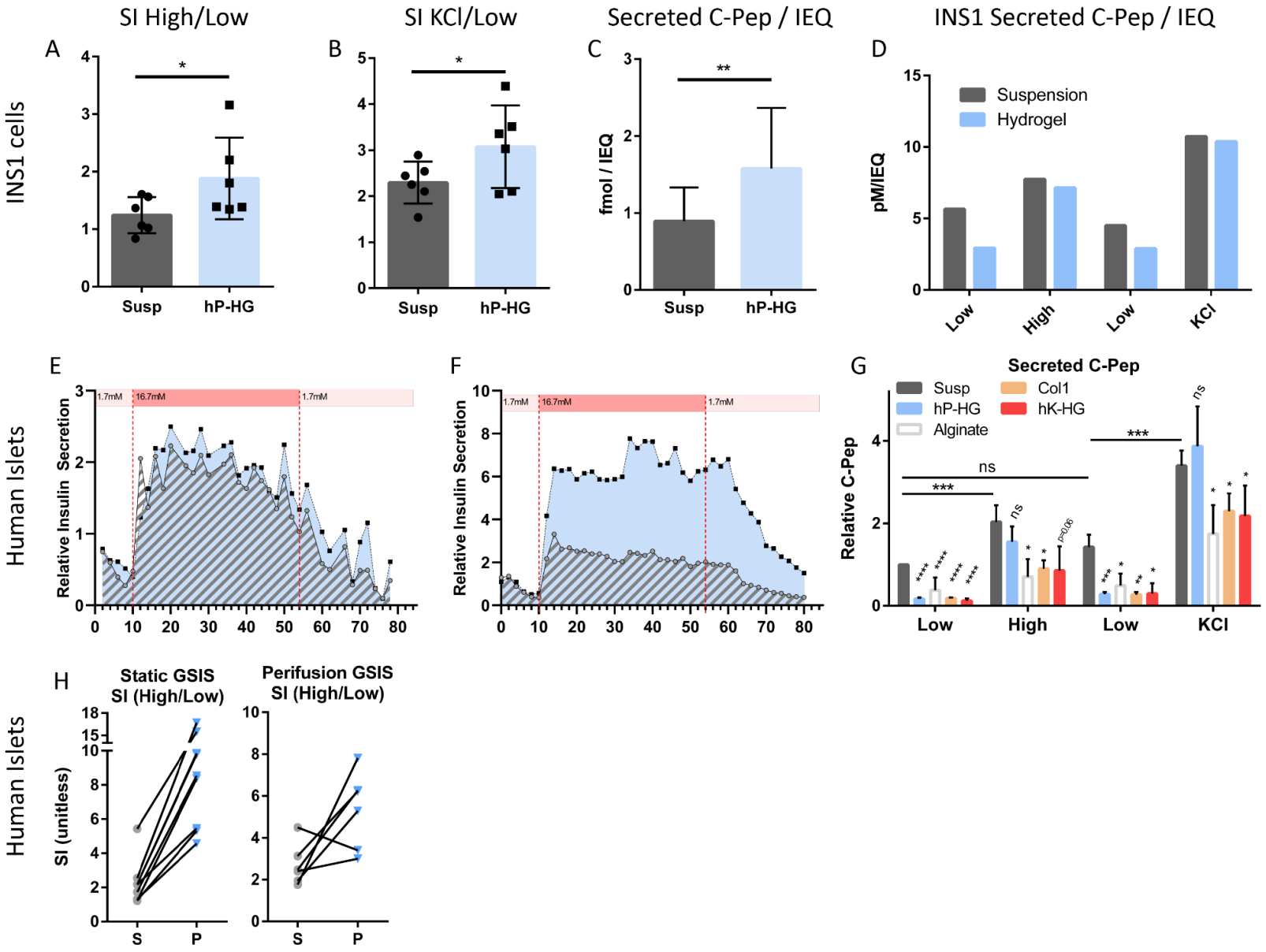
INS1 cells
Human Islets
Human Islets
SI High/Low
SI KCl/Low
Secreted C-Pep / IEQ
INS1 Secreted C-Pep / IEQ
A
B
C
D
Susp
hP-HG
fmol / IEQ
pM/IEQ
Suspension
Hydrogel
Low
High
Low
KCl
E
F
G
Relative Insulin Secretion
1.7mM
16.7mM
1.7mM
Secreted C-Pep
Susp
hP-HG
Alginate
Col1
hK-HG
Relative C-Pep
ns
***
H
Static GSIS
SI (High/Low)
Perifusion GSIS
SI (High/Low)
SI (unitless)
S
P

Chapter 5 Supplemental Figure 4: Additional GSIS data after 2 days of culture.

Stimulation index **(A**, high/low glucose**) (B**, KCl/low glucose**)** of INS1 cells cultured as pseudo-islets in suspension or hP-HG, after 2 days of culture, determined by static GSIS. **(C)** Total C-Pep content, and **(D)** Insulin secretion (pM per IEQ) from INS1 cells cultured in suspension (gray) and hP-HG (blue) and exposed to low glucose (2.8 mM), high glucose (28 mM), low glucose and then KCl (30 mM). N=4 biological replicates. **(E-F)** Perifusion GSIS curves for two additional human islet donors; insulin secretion is normalized to first low glucose response (unitless). **(G)** Human islet static GSIS data presented with an alternative normalization, where all measurements for each islet donor and condition are normalized to the C-Pep level secreted under the first low glucose step. This method of analysis reveals that when not normalized as a percentage of total C-Pep content (as in Fig. 3B) the stimulated C-Pep secretion levels (High and KCl) of A,C, and K are significantly lower than those of S and P. **(H)** Stimulation index (high/low) of islets in suspension (S) or hP-HG (P) under static or perifusion GSIS, tracing the SI between islets from the same donor in each treatment group.

(Previous Page)

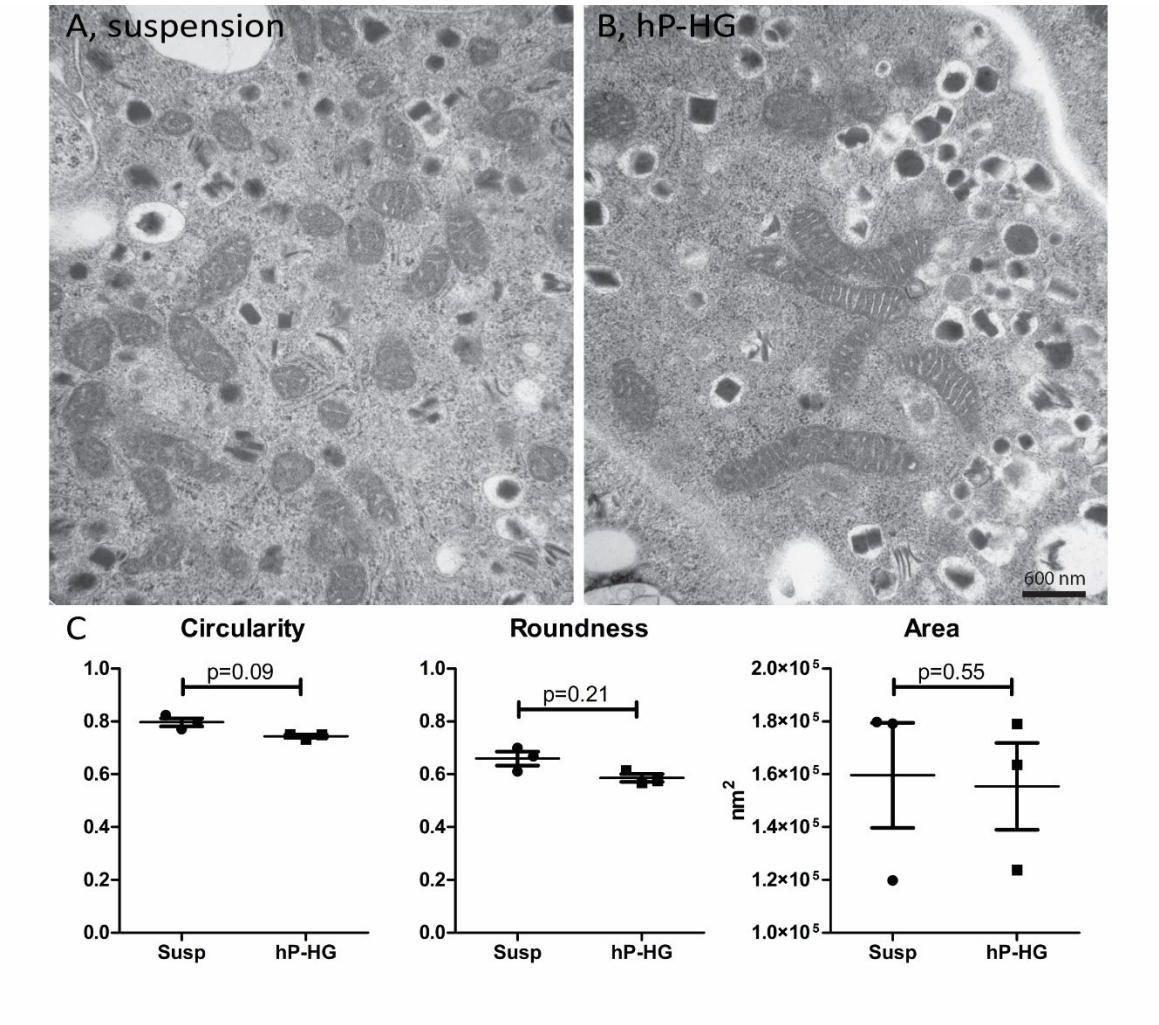

Chapter 5 Supplemental Figure 5: Human islet mitochondria quantifiable phenotypes

TEM images taken at 25000x were used to quantify mitochondrial phenotypes in islets cultured in suspension **(A)** or hP-HG **(B)** for two days. N=3 islet donors. Scale = 600 nm. **(C)** The circularity (unitless), roundness (unitless), and area (nm^2) of individual mitochondria from islets cultured in suspension or hP-HG for two days were found to not be statistically different. 98-163 mitochondria were measured per donor for each treatment, N=3 donors.

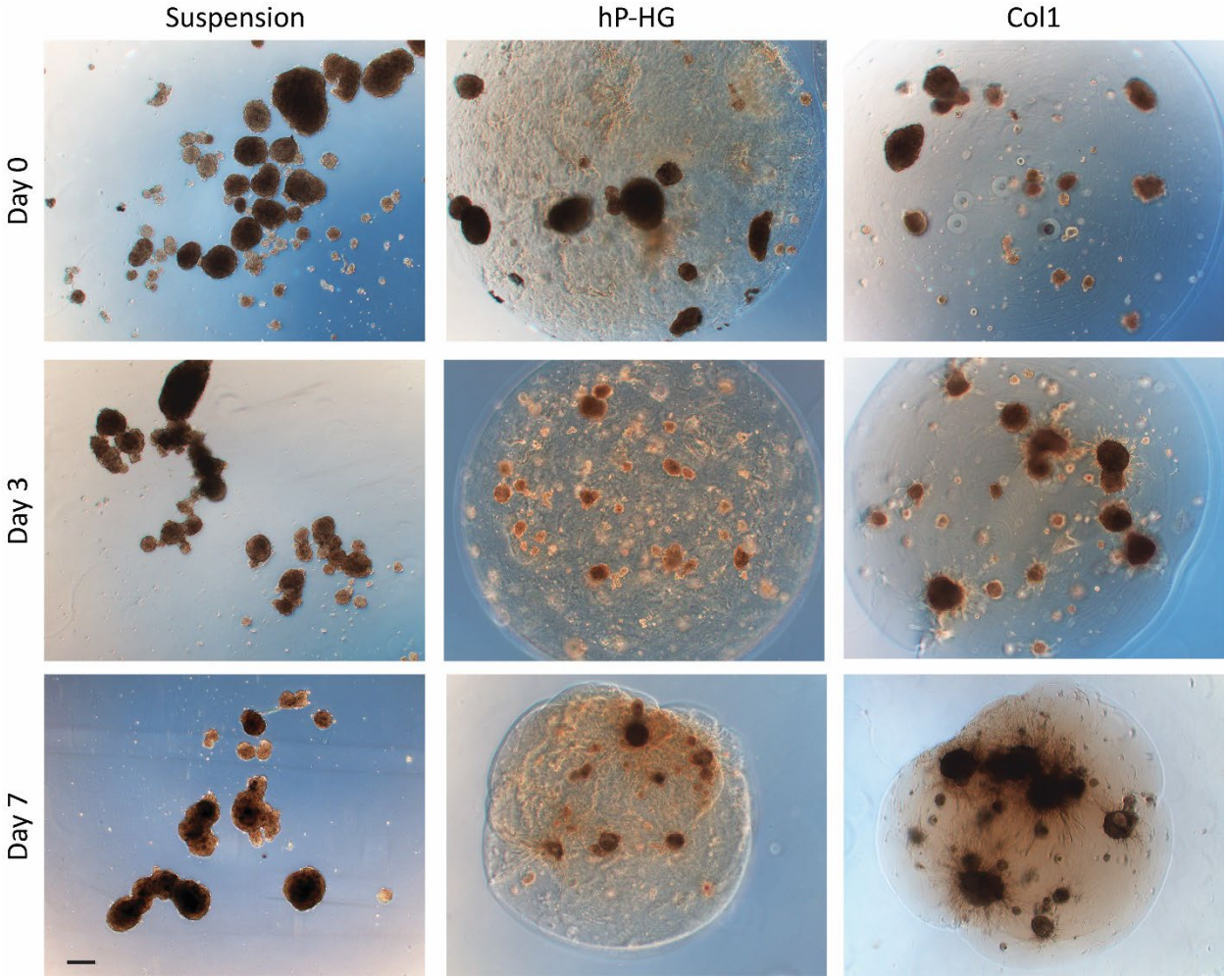

Chapter 5 Supplemental Figure 6: Human islet survival and growth over 7 days

Representative bright field images of human islets cultured in suspension (left column), hP-HG (middle column), and Col1 hydrogel (right column) on day 0, the day the islets were embedded, 3 days after embedding, and 7 days after embedding. Scale = 200 microns.

Chapter 5 Supplemental Figure 7: Human islet architecture

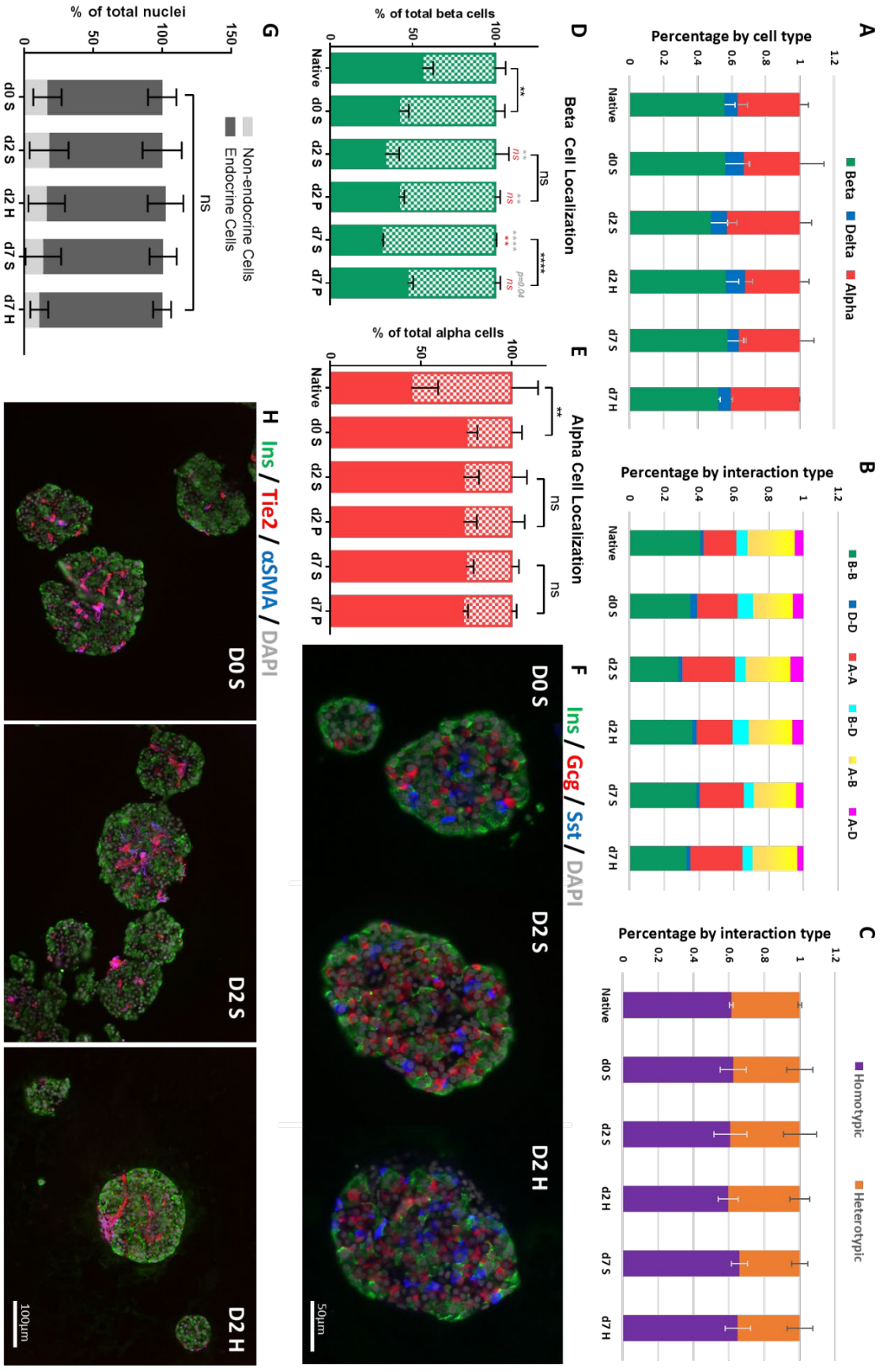

Chapter 5 Supplemental Figure 7: Human islet architecture

Quantification of human islet architecture measuring the total numbers of alpha, beta and delta cells **(A)**, and the interactions between endocrine cell types among the 5 conditions **(B)** and simplified into homotypic and heterotypic interactions **(C)**. Quantification of the core:mantle arrangement of beta **(D)** and alpha **(E)** cells as a percentage of the total same cell type (core=filled bars, mantle=checkered bars). N=5 islet donors. Statistical comparisons indicated in italics and gray are compared to native islets and in italics and red are compared to "Day 0" islets. (ns = not significant, * $p<0.05$, ** $p<0.01$, *** $p<0.001$, **** $p<0.0001$) **(F)** Representative images of isolated islets in day 0 and day 2 in suspension (S) or hydrogel (H) culture, stained for insulin (green), glucagon (red), somatostatin (blue) and DAPI (gray), scale = 50 microns. **(G)** Counts for endocrine (dark gray) and non-endocrine (light gray) cells under each condition and time point, as a percentage of total nuclei counted. **(H)** Representative images of isolated islets in day 0 and day 2 in suspension (S) or hydrogel (H) culture, stained for insulin (green), Tie2 (red), αSMA (blue) and DAPI (gray), scale = 100 microns.

(Previous Page)

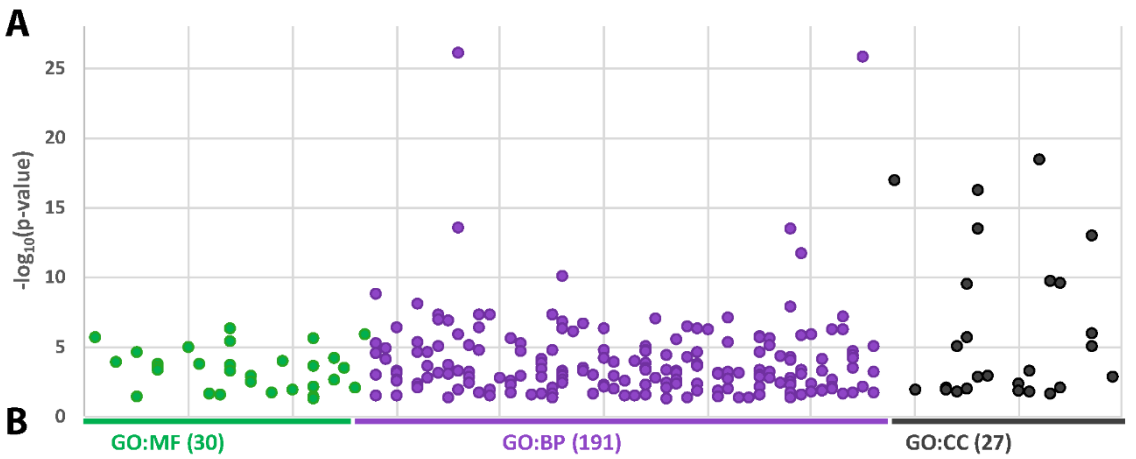

Top 10 GO terms in each subcategory

Molecular Function (MF)	(Biological Process) BP	Cellular Component (CC)
signaling receptor binding (151)	cell adhesion (192)	extracellular space (323)
signaling receptor activator activity (62)	biological adhesion (192)	extracellular matrix (88)
receptor ligand activity (61)	extracellular matrix organization (68)	extracellular region (381)
receptor regulator activity (65)	extracellular structure organization (68)	collagen-containing ecm (69)
metallopeptidase activity (32)	response to external stimulus (264)	vesicle (328)
cytokine activity (35)	regulation of cell adhesion (94)	extracellular exosome (197)
serine-type endopeptidase activity (29)	cell-cell adhesion (103)	extracellular vesicle (198)
molecular function regulator (156)	regulation of cell component movement (122)	extracellular organelle (198)
serine-type peptidase activity (30)	response to wounding (87)	cell periphery (407)
metalloendopeptidase activity (21)	inflammatory response (92)	plasma membrane (398)

Chapter 5 Supplemental Figure 8: Extracellular signaling-related pathways are significantly influenced by hP-HG culture

(A) Plots showing the three aspects of GO analysis: Molecular Function (MF), Biological Process (BP) and Cellular Component (CC). All pathways found to be significantly altered between suspension and hP-HG treatments are plotted, with the -$\log_{10}$(p-value) representing significance on the y-axis. Total number of gene sets identified in each aspect are in parentheses. (N=3 islets donors, each used for both treatments)

(B) List of the top 10 terms identified in each aspect, with the number of altered differentially expressed genes (DEGs) in that pathway in parentheses to the right.

Supplemental References:

1. Raudvere, U., et al. g:Profiler: a web server for functional enrichment analysis and conversions of gene lists (2019 update). Nucleic Acids Res 47, W191-W198 (2019).

Chapter 6

Islet vascularized ECM gel (IVEG) construct for islet culture and transplantation

Chapter 6 Graphical Abstract

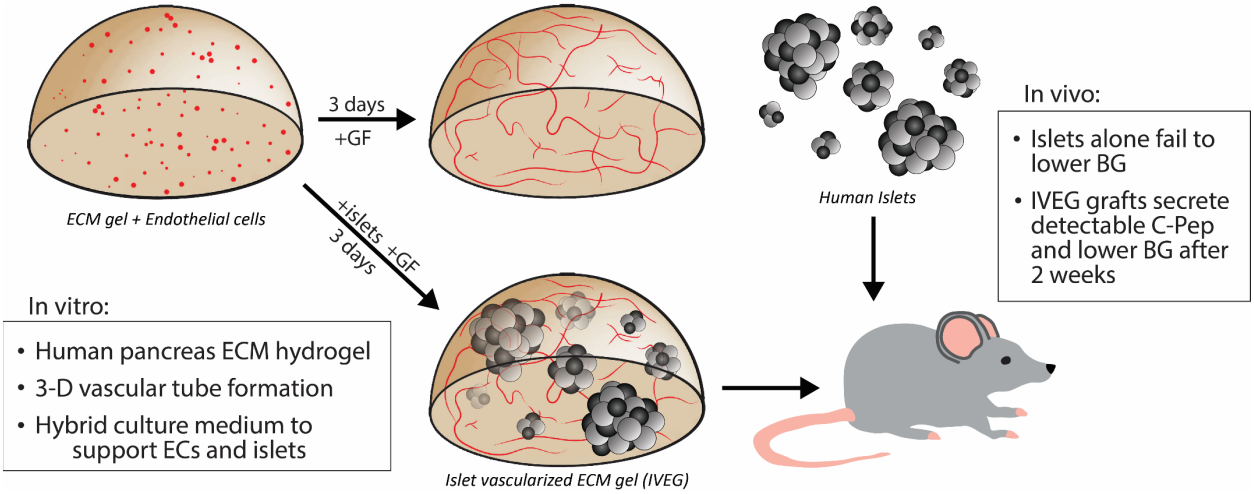

Daniel Tremmel designed the study under the guidance of Sara Dutton Sackett and Jon Odorico. Daniel Tremmel, Vansh Jain, Sakar Gupta, Anna Mikat, and Sam Mitchell performed the experiments and analyzed the data. Daniel Tremmel, Sam Mitchell and Austin Feeney processed and banked human tissues. Daniel Tremmel prepared all figures and wrote the manuscript with guidance from Sara Dutton Sackett and Jon Odorico.

Abstract

The endocrine cells of the pancreas, organized into islets of Langerhans, require an intimate relationship with the surrounding vasculature for both cell survival and to perform endocrine function. Islet-endothelial cell interactions have been studied during normal human development, *ex vivo*, and after transplantation and it is well established that islet re-vascularization is an essential component of successful islet transplantation. While many methods have been established to improve vascularization of islets post-transplantation, we have developed a strategy of pre-vascularizing islets within droplets of pancreas-derived ECM *in vitro*. Here, we report a 3-day protocol for 3-D endothelial tube formation in pancreas ECM hydrogel, which can be combined in culture with human islets without negatively affecting islet survival and function. When transplanted subcutaneously, these islet vascularized ECM gel (IVEG) constructs lead to detectable serum C-pep levels and a reduction in blood glucose, while islets transplanted alone fail to function. IVEG constructs provide both a model for recreating 3-D islet-EC interactions in vitro, as well as a mechanism for improving the engraftment of transplanted islets.

Introduction

The endocrine cells of the pancreas secrete hormones that regulate blood glucose homeostasis. These cells reside within the islets of Langerhans, micro-organs surrounded by the exocrine, or acinar, compartment of the pancreas. Islets comprise only 1-2% of the volume of the pancreas, but utilize 10-15% of blood flow to the organ [1]. Islets are surrounded and infiltrated by a dense network of capillaries, providing blood flow as well as direct and indirect interactions between endocrine and endothelial cells [2, 3]. Within the fetal human pancreas, endocrine cells

begin to align with $CD34^+$ endothelial cells by 10 gestational weeks, and vasculature begins to penetrate the islets by 14 weeks [4]. Vasculature has been demonstrated to stimulate early pancreas bud formation, also inducing expression of transcription factors associated with pancreas fate. Later, the surrounding vasculature constrains the expansive branching of the progenitor population to direct properly morphology, differentiation, and growth [5-11]. An array of biological molecules have been found to participate in crosstalk between islet endocrine and endothelial cells including secreted factors, connexins, extracellular matrix (ECM) proteins and receptors, and other soluble factors [12-18]. In adults, the capillary bed supports the maintenance of islet function and survival [5], and in rodent models has been found to contribute to adult beta cell proliferation [19]. Islet vasculature has been implicated in the progression of type 2 diabetes (T2D), in which islet capillaries become inflamed, thickened and dilated, with some studies finding vascular phenotypes to precede endocrine dysfunction [12, 15]. Islet endothelial cells may also have a distinct identity, such as expressing the glomerular barrier protein nephrin [20, 21], reflecting specialized function and physiology.

Clinically, islet health and function are of interest as diabetes is rapidly expanding in prevalence, with over 10% of the United States population diagnosed, and over 30% with prediabetes conditions. Cell replacement therapies to treat diabetes include whole pancreas and islet transplantation, with significant effort in recent years being made toward utilizing stem cell-derived beta cells as a clinical treatment. Islet transplantation is less invasive than pancreas transplantation, but has not been as successful in sustaining long-term normoglycemia. One of the fundamental reasons islet transplantation has failed to provide long-term treatment is due to the damage islets endure through the process of isolating them from the pancreas, culturing

them for purification, and transplanting them through the portal vein, into the liver. Islet isolation causes complete severance of the islet vasculature, and endothelial cells that are retained with the islets after isolation lose their architecture in culture (Supplemental Fig. 1). Islets revascularize slowly after transplantation, but may have reduced vascular density and oxygen tension compared to native islets [22, 23]. This process causes significant islet death, further reducing the efficacy of the treatment [24], although surviving resident islet endothelial cells have been found to contribute to the re-vascularization of the islet graft [25, 26].

To support islet survival during transplantation, many studies have focused on alternative strategies to improve the vascularization of the islet graft. These strategies involve alternative transplant sites to the portal vein or the kidney capsule, the latter of which is routinely used in rodent studies, but is not translatable to human therapy. Alternative sites include the omentum, a vascularized subcutaneous space, intramuscular space, and others, with the major focus being on revascularization of the graft [27-31]. Other strategies to improve vascularization have involved combining endothelial cells or mesenchymal stem cells with islets before or during the transplant procedure [32-38], co-transplanting with adipose-derived microvessels [39] or using vasculogenic biomaterials or soluble factors to improve vascularization of the graft [27, 40, 41].

Most studies establishing the role of endothelial cells in islet development and survival have been performed in animal models, particularly mice and rats. Significant differences between rodent and human islets have been established, including the arrangement of the endocrine cells [42], the basement membrane structure [43], the degree of vascularization [2], the extent of innervation [44], as well as many differences in the markers of differentiation and maturation of endocrine cells [45, 46]. While *in vivo* study of endothelial-islet relationships is

ideal for understanding the interplay between cell types, the differences among species in islet structure and biology prevent animal studies from translating directly to make conclusions about human islet biology. Furthermore, many previous studies have incorporated endothelial cells into culture with islets in a structural way that does not resemble *in vivo* biology. Islets have been coated with ECs, or dissociated and reaggregated with ECs, without enabling EC tube-like structures to form *in vitro* [34, 36, 47-50]. In adherent 2-D culture, cell behavior can be dramatically altered compared to native cells, therefore recapitulating the 3-D environment in culture is as important as providing the appropriate chemical cues to cells [51-53]. Few studies have successfully cultured ECs in a 3-D environment with pancreatic endocrine cells, although several recent reports have made progress on this front [33, 47, 49], but the scaffolding used for 3-D culture in these reports is not a pancreas-like biomaterial.

We have previously developed a human pancreas ECM hydrogel (hP-HG) for use in studies of pancreas-specific ECM in human islet development and function [54] [Chapter 5]. Due to the importance of ECM in both endothelial tube formation [55, 56] and in islet health and function [57, 58], we are interested in recreating the 3-D islet niche, *in vitro*, with pancreatic ECM and other cell types. Here we report a protocol for hP-HG 3-D culture system for the co-culture of human islets with human umbilical vein endothelial cells (HUVECs). This platform enables the 3-D construction of endothelial tubes within a pancreas-specific hydrogel, while supporting the survival and function of human islets. Expansion of this culture system to stem cell-derived islets or fetal islets may enable further study of the developmental interplay between endothelial cells and islets in a human system.

Results

3-D endothelial tube formation within pancreas ECM hydrogel

To generate 3-D endothelial cell tubes in human pancreatic ECM hydrogel (hP-HG), human umbilical vein endothelial cells (HUVECs) were seeded into the liquid gel at a density of $0.3x10^5$ cells/10 µL of hydrogel, plated into 10 µL droplets and warmed to 37 °C to form solid gel. Gels cultured in EC medium without supplementation with additional growth factors (-GF) did not form tubes within the gel (Fig 1A-B). Gel and medium were supplemented with growth factors bFGF, SDF1α, and VEGF ("+GF") formed endothelial cell tubes over a period of 3 days (Fig 1C-D). To quantify the difference in tube formation under the two conditions, gels were stained for F-actin (phalloidin, red), whole-mount imaged and analyzed using Angiotool to determine the degree of vessel formation, vessel length and junction density; the +GF treatment was found to

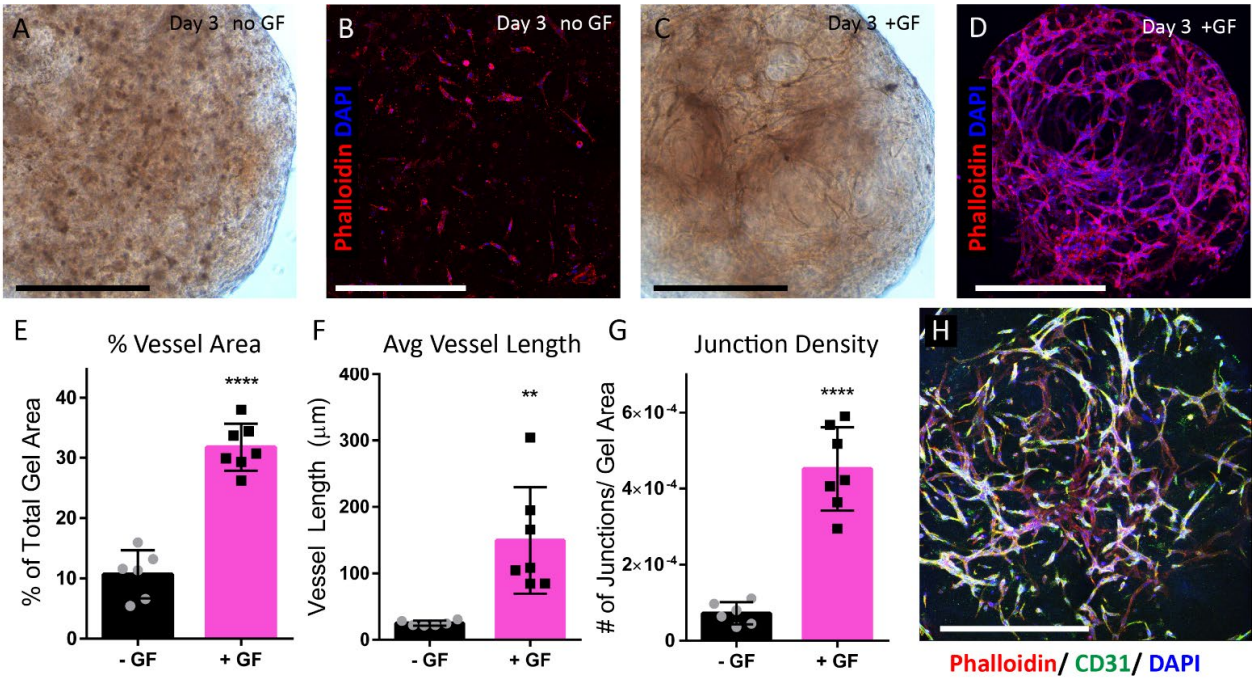

Figure 1: 3-D endothelial tube formation within pancreas ECM hydrogel

Human umbilical vein endothelial cells (HUVECs) embedded within 10 uL droplets of hP-HG and cultured with added growth factors (+GF) for 3 days, form an extensive network of tubes. Bright field images (**A,C**) and phalloidin-stained max-intensity projection images (phalloidin=red, DAPI=blue) (**B, D**) reveal differences in tube formation between gels cultured without added growth factors (-GF) and with added growth factors (+GF). Vessel area (**E**), length (**F**), and junction density (**G**) were quantified by Angiotool analysis of Phalloidin images for both treatments. CD31 (green) was co-stained with phalloidin (red) and DAPI (blue) to indicate maintenance of endothelial cell identity during culture (**H**).

All scale bars = 500 microns. (** p<0.01, **** p<0.0001) **(Next page)**

have significantly higher values by all measures (Fig 1E-G). To assess retention of endothelial cell identity over the culture period, gels were co-stained for CD31 (Fig 1H, green).

Combinatorial effects of media type on HUVEC and INS1 in 2-D culture

Having established a protocol for the induction of endothelial tube formation within hP-HG, we aimed to determine which media would be most permissive for the co-culture of ECs with beta cells or human islets. HUVECs are commonly cultured in the endothelial medium EGM2 (E). In this study we chose to use the rat insulinoma cell line INS1 832/13 and the medium developed to maintain the cell line, “INS1” medium (I) to test beta cell growth in response to the different media. These two media were combined in two different ways, mixed 50:50 (IE mix), or combined by adding the EGM2 supplements at full concentration to the INS1 medium (IE hybrid). To determine how these various media affected EC survival, HUVECs were grown in planar culture over a 3-day period in each medium and assessed for growth with an MTS assay. Interestingly, HUVECs grew more rapidly in the INS1, mixed and hybrid media, than in the EGM2 medium (Fig 2A), and did not have noticeable changes in cell morphology in the various media (Supplemental Fig. 2). The same experiment was performed with INS1 cells in planar culture, in which EGM2 was found to have a detrimental effect on INS1 cell growth, while the mixed and hybrid media

maintained relatively constant cell survival, and the INS1 medium had the highest rate of growth over the 3-day period (Fig 2B). After 3 days, INS1 cells grew confluent in INS1 media, IE hybrid and IE mix media (Fig. 2C-F). The morphology of the INS1 cells after the 3-day culture in EGM2 reflected the growth curves, appearing less confluent with a rounded morphology (Fig 2G).

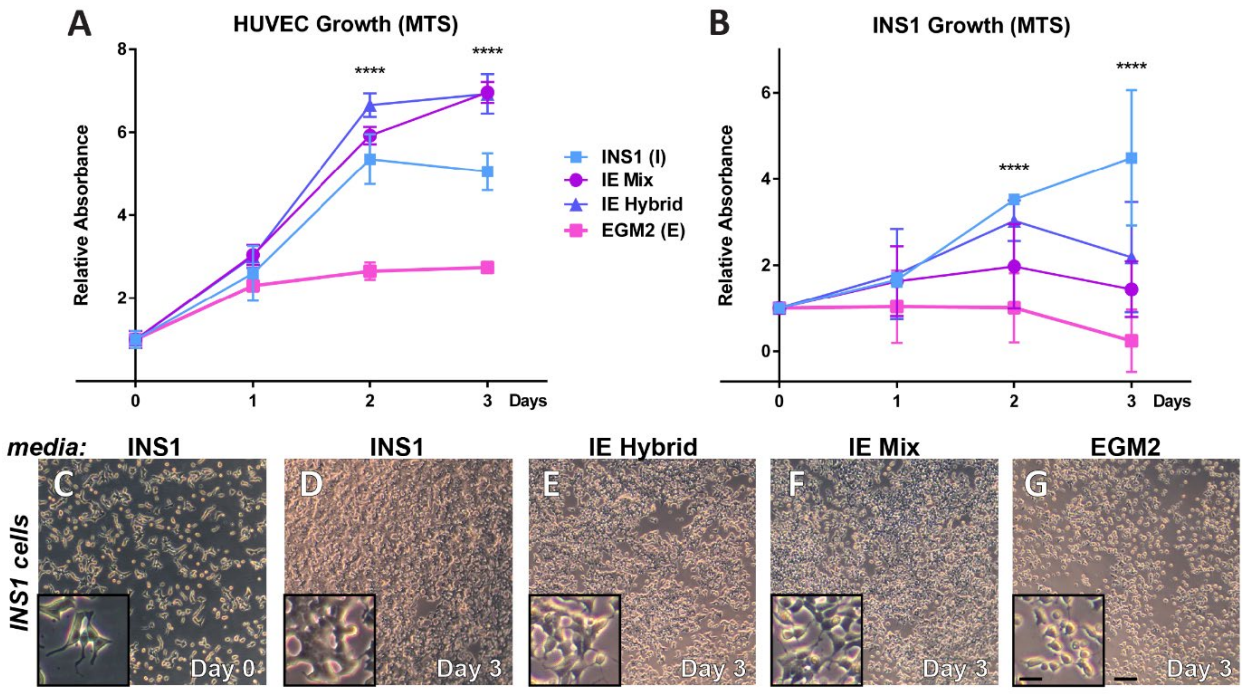

Figure 2: Combinatorial effects of media type on HUVEC and INS1 in 2-D culture

Growth curves for HUVECs (**A**) and INS1 cells (**B**) each cultured for 3 days in endothelial medium (EGM2), INS1 medium, IE hybrid, or IE mix media. Bright field images of INS1 cells taken at 10x resolution at Day 0 (**C**) and in the four different media on Day 3 (**D-G**), insets are digitally enlarged 4x.

Full images: scale bar = 100 microns; insets: scale bar = 25 microns.

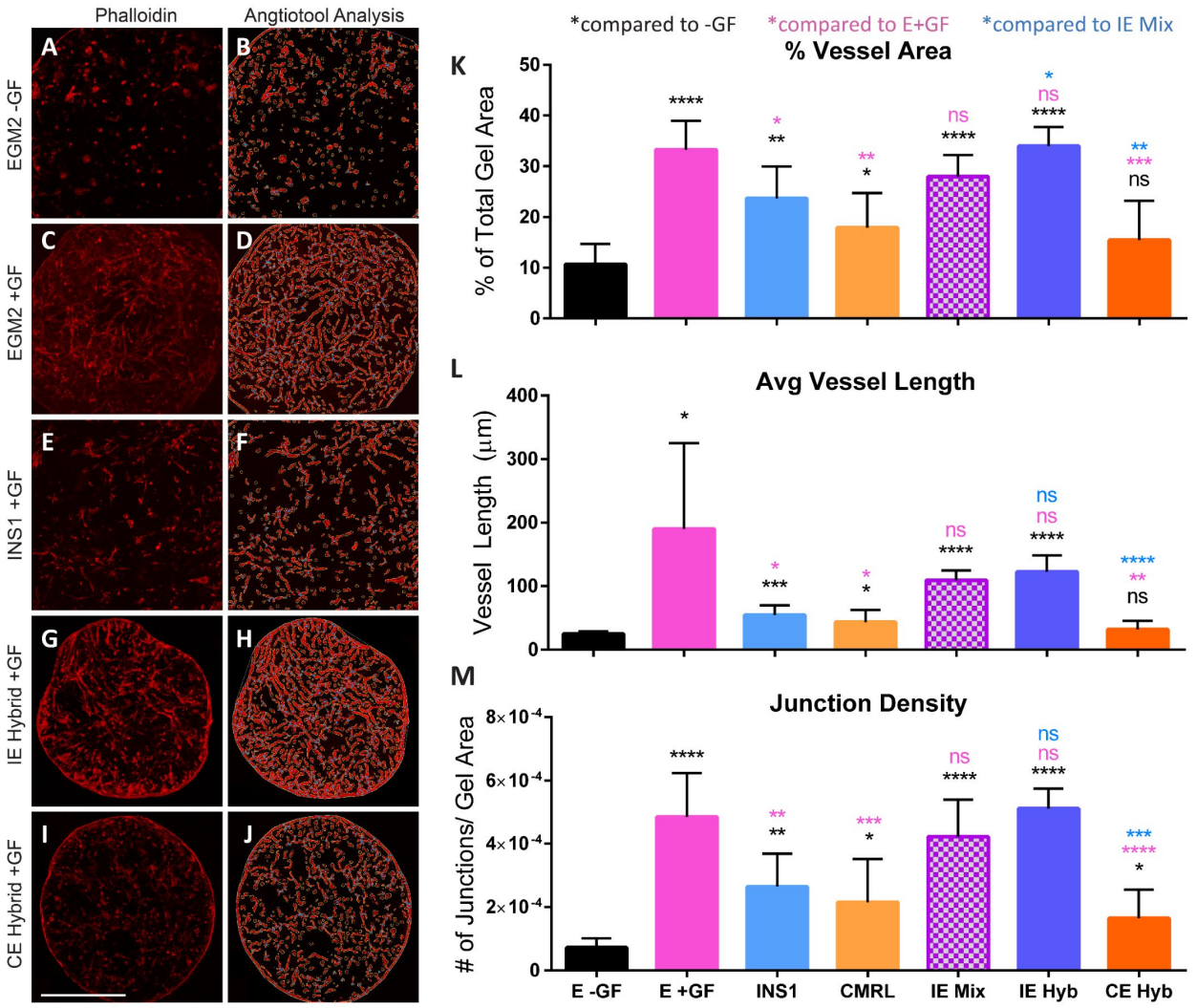

Figure 3: Combinatorial effects of media type on HUVEC tube formation in 3-D culture

Max-intensity projection images of phalloidin staining (**A,C,E,G,I**) and the Angiotool result image (**B,D,F,H,J**) for representative gels cultured in each medium. EGM2-GF is the negative control with minimal tube formation (**A,B**). Vessel area (**K**), length (**L**), and junction density (**M**) were quantified by Angiotool analysis of Phalloidin images for all seven media types. Statistics are represented with asterisks, relative to E-GF (in black), relative to E+GF (in pink) and relative to IE Mix (in blue).

Scale bar = 500 microns. (* p<0.05, ** p<0.01, *** p<0.001, **** p<0.0001, ns = not significant)

Combinatorial effects of media type on HUVEC tube formation in 3-D culture

Different media were not found to have a detrimental effect on HUVEC growth in planar culture, so we aimed to assess whether or not the various media had an effect on the ability of the ECs to form tubes. ECs were seeded into 10 µL hP-HG droplets with added growth factors to assess tube formation after 3 days of culture in each medium. We also assessed tube formation in the islet medium CMRL (C), including hybrid versions of CMRL and EGM2 (CE Hyb), as described in the previous experiment. As previously observed, EGM2 without added GFs (E-GF) (Fig. 3A-B) had little tube formation, while the EGM2+GF treatment (E+GF) induced tube formation (Fig. 3C-D). In various other media, tube formation had variable success in the presence of the added GF cocktail (Fig. 3E-J). All treatments were quantified with Angiotool for vessel area, average vessel length, and junction density (Fig. 3K-M). INS1 medium and CMRL had relatively poor tube formation. While the IE Mix and Hybrid media had improved tube formation, CMRL Hybrid medium did not support successful tube formation. These results indicate that although beta cell and islet medium does not inhibit the growth of ECs in planar culture, it does inhibit the tube-forming ability of the cells if other endothelial factors are not added to the medium as a hybrid or a mix. We conclude that straight EGM2 medium or IE hybrid medium have comparable capacity for tube formation in hP-HG.

Islet vascularized ECM gel (IVEG) constructs maintain survival and function

Islet survival and function in culture declines rapidly after isolation from the pancreas. We recently demonstrated that islets cultured in hP-HG had an improved stimulation index in static glucose stimulated insulin secretion (GSIS) and improved survival over 7 days of culture [Chapter 5]. To assess whether culture media which support EC tube formation have detrimental effects

on islet survival and function, we first cultured islets in suspension in select media. Islets were cultured in standard CMRL and in the IE Hybrid medium, both with and without the added GF cocktail for EC tube formation. Islets cultured in CMRL alone over 3 days had the poorest survival, comparable to previous studies [58], while CMRL+GF, IE Hyb, and IE Hyb+GF all had higher levels of survival, indicating that neither the GF cocktail or the IE medium has a detrimental effect on islet survival in short-term culture (Fig. 4A-B). Next, islets were combined with HUVECs within droplets of hP-HG to form islet vascularized ECM gel (IVEG) constructs. Over 3 days of culture, endothelial cell tubes formed throughout the gel around the islets (Tie2, red) (Fig. 4D) (Supplemental Videos 1 and 2). To assess how this culture period affected islet function, IVEG constructs were put through a static glucose stimulated insulin secretion (GSIS) assay and the stimulation index (SI) from low glucose to high glucose was compared to various controls. Islets in suspension culture in either CMRL or IE Hyb+GF had similar SIs (CMRL=2.07, IE Hyb+GF=1.69). Consistent with previous studies, islets cultured within hP-HG in either media and in co-culture with ECs (IVEG) had a significantly increased SIs, with no negative effect of the hybrid media, GF cocktail, or ECs (CMRL=7.64, IE Hyb+GF=9.42, IVEG=10.00) (Fig. 4C). These results indicate that islets can be co-cultured with ECs in an environment supportive of tube formation, with improved islet survival and function compared to standard islet suspension culture after 3 days. IVEG constructs maintained insulin-positive staining (Fig. 4D-F, green) and maintained a hemispherical shape in free-floating culture (Fig. 4F).

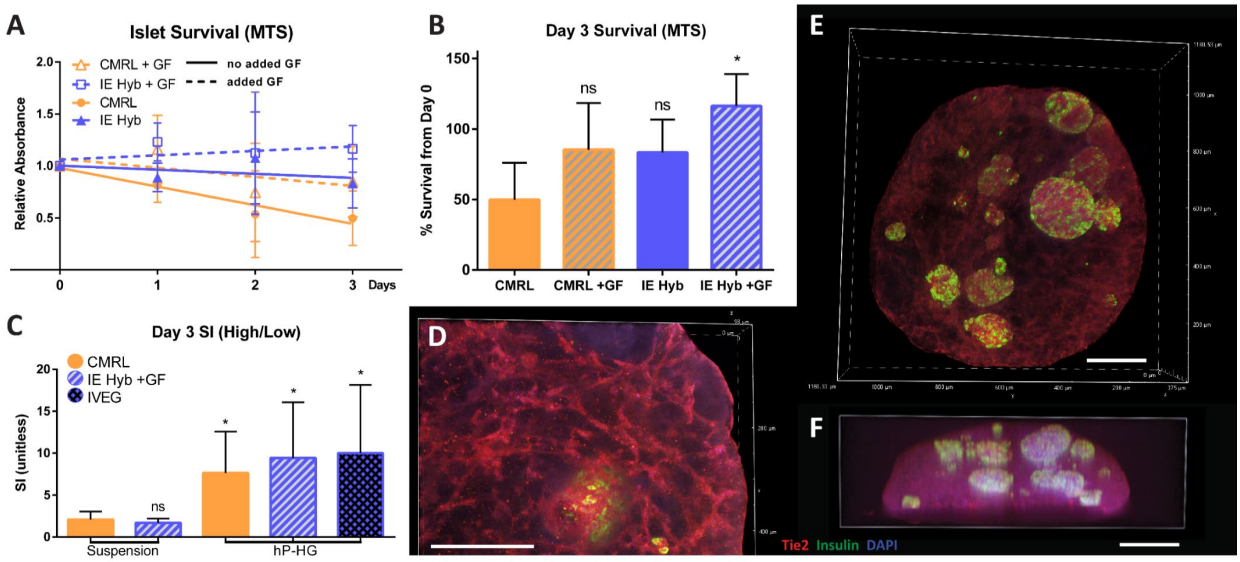

Figure 4: Islet vascularized ECM gel (IVEG) constructs maintain survival and function

Islets cultured in standard islet medium (CMRL) or IE Hybrid medium with (+GF) or without (-GF) added growth factors were assessed for survival over 3 days (**A**). **B**) Bar graphs show the differences in survival after 3 days, statistical analyses presented are relative to the CMRL control.

Islets stimulation index (SI) in a static GSIS assay was assessed in suspension and embedded in hP-HG (x-axis) and in CMRL or IE Hyb+GF, and finally as composite with islets + HUVECs embedded in hP-HG and cultured in IE Hyb+GF (IVEG) (**C**). Statistical analyses presented are relative to suspension culture in CMRL.

After 3 days of culture, IVEG constructs maintained beta cell identity (insulin, green) and formed a network of endothelial tubes (Tie2, red) (**D-F**). The free-floating gels maintained a hemispherical shape throughout culture (**F**). To view confocal videos, see Supplemental Videos 1 and 2.

A scale bars = 200 microns. (* $p<0.05$, ns = not significant)

Islet vascularized ECM gel (IVEG) support improved engraftment

Having successfully generated IVEG constructs in culture, we aimed to assess whether or not pre-vascularization *in vitro* could support improved transplantation outcomes. Diabetic NSG RIP-DTR mice were transplanted with a sub-therapeutic dose of 1000 IEQ of human islets subcutaneously, either as islets alone, on day 0 of culture, or as islets in an IVEG construct, after 3 days of IVEG culture. Weekly, serum human C-peptide levels (Fig. 5A) and fasted blood glucose

levels (Fig. 5B) were measured. After 12 weeks, a subset of mice were assessed with an intraperitoneal glucose tolerance test (IP-GTT) to assess transplanted islet function (Fig. 5C-F). Mice transplanted with IVEG had increased detectable C-Pep after 4 weeks and significantly reduced fasted blood glucose by 3 weeks post-transplant. In the IP-GTT, the IVEG cohort performed similarly to mice that had never been diabetic, while the cohort transplanted with islets alone performed more similarly to diabetic, untreated mice. The IVEG cohort has an improved area under the curve (AUC) and stimulation of human C-Pep in the serum following glucose injection.

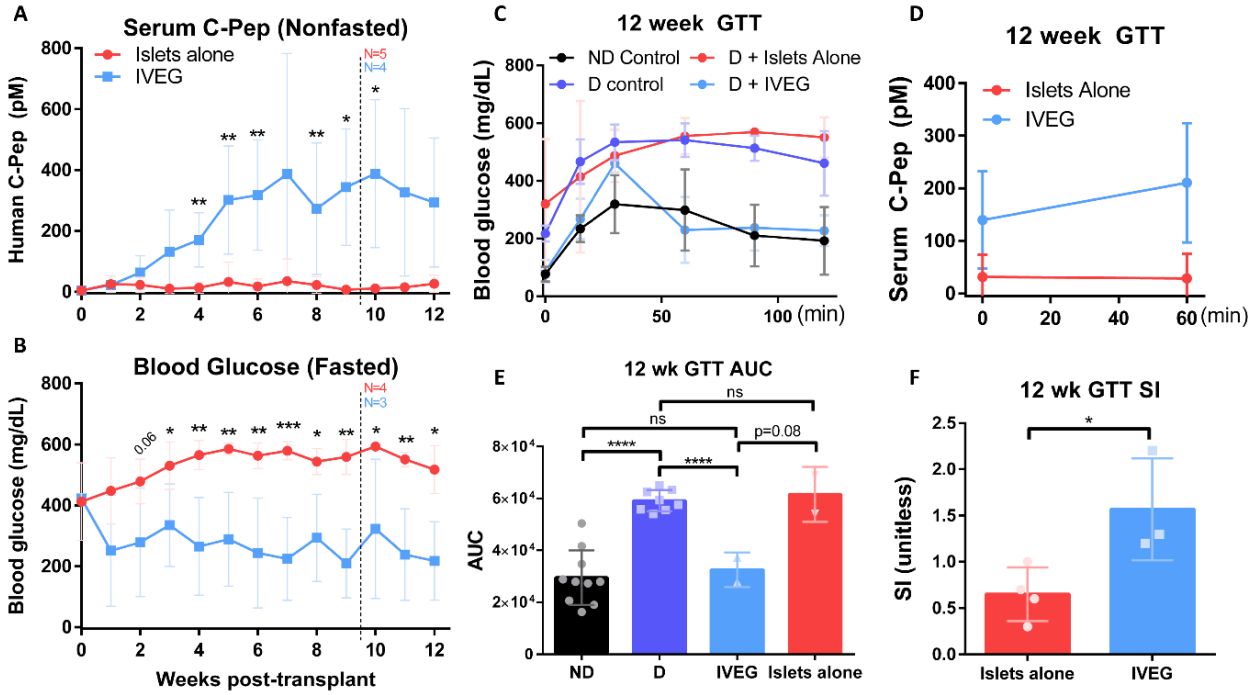

Figure 5: Islet vascularized ECM gel (IVEG) constructs support improved engraftment

1000 IEQ of human islets transplanted in IVEG constructs (blue) have improved transplant outcomes compared to 1000 IEQ transplanted alone (red). The IVEG cohort has significantly higher detectable serum C-Pep after 4 weeks **(A)** and significantly reduced fasted blood glucose after 3 weeks **(B)** compared to islets transplanted alone. After 12 weeks *in vivo*, the IVEG cohort performed better in an IP-GTT assay, having a blood glucose curve that was more similar to non-diabetic mice **(C)**, showing stimulated C-Pep secretion after glucose injection **(D)** and having an area under the curve (AUC) **(E)** and GTT stimulation index (SI) **(F)** that outperformed islets alone.

The maximum reading for the glucometer used is 600 mg/dL.

Discussion

Significant work has been done in the field of tissue engineering to create vascularized scaffolds for *in vitro* and *in vivo* studies [59]. The ubiquity of both ECM and vasculature throughout the body makes this work important and relevant to almost all aspects of biology [60, 61], and opens up opportunities to study tissue-specific effects of the vasculature *in vitro*, as well as to improve the quality of transplantable engineered tissues [62]. The progression of angiogenesis assays from *in vivo* models [63, 64], to 2-D *in vitro* models [65, 66], to 3-D *in vitro* models [67-69] has enabled the study of these processes on a new level with enhanced control. Our study has combined pancreatic ECM with islets and EC-derived vascular networks, in a simple construct that recreates certain elements of the islet niche, using human-derived materials and cells.

First, we establish a protocol to spontaneously generate endothelial tube networks within droplets of ECM hydrogel. This strategy recapitulates a tissue environment at several levels. The ECM hydrogel can be tailored to different tissues, or could be constructed using a defined ECM mixture. We have generated hydrogels from pancreas, kidney [Chapter 5], and spleen (unpublished), and many organs and tissues have now been decellularized for this purpose. The endothelial tubes form lumens with apical and basal polarity, which recreates the endothelial architecture better than 2-D culture, or 3-D co-aggregated clusters that do not form endothelial tubes. Furthermore, the vascular networks deposit new basement membrane along the tubes (Supplemental Fig. 3), adding another layer of complexity to the engineered microenvironment. When human islets are isolated from the pancreas, the ECM is almost entirely destroyed [70], and the endothelial structures are lost (Supplemental Fig. 1)[58]. Therefore, the culture of hP-HG

and ECs with isolated islets could restore many of the elements that are damaged during islet isolation and culture.

Next, to accommodate multiple cell types in co-culture together (i.e. endothelial cells and beta cells or islets), we explore how different media affect the growth and function of endothelial cells and beta cells. We find that the rat insulinoma cell line, INS1, has limited growth when cultured in EC medium, while HUVECs do not have a limited growth rate when cultured in the INS1 medium. However, HUVEC tube formation was significantly reduced in INS1 medium, and also in the islet medium CMRL. Therefore, we developed a hybrid medium that supported both cell types. The hybrid medium, composed of the INS1 medium as a base with all added growth factors from EGM2 at full concentration, was able to support HUVEC tube formation and islet survival and function at equal or better levels as each cell type in their standard medium. These principles for combining media to support multiple cell types simultaneously will be useful for future engineered islet constructs.

When HUVECs and islets were embedded together in hP-HG and co-cultured in hybrid medium, HUVEC tubes are formed throughout the gels and around the islets. In co-culture, we previously found that hP-HG embedded islets had a significant improvement in GSIS function [58]. We observed a similar trend in this study with improved islet function in hP-HG constructs and no deleterious effect on islet function when islets were cultured in hybrid medium or co-cultured with HUVEC vascular networks. Although a beneficial effect of this co-culture may be expected, it is notable that other endothelial cells sources may be necessary to better explore the direct interactions islets and ECs have with one another. Studies of tissue-specific EC biology have found that venous and arterial ECs have relatively similar profiles throughout the body,

while capillaries of different organs are the main EC structure that display significant endothelial heterogeneity [71, 72]. The recent establishment of islet-derived endothelial cell lines [20] creates an opportunity to study tissue-specific markers and traits of ECs within the islet niche. Endothelial cells are influenced by their microenvironments [73]; whether pancreas-specific ECM or EC interactions with beta cells and other islet cell types might stimulate morphologic and gene expression changes in primary or stem cell-derived ECs (SC-ECs) has not yet been studied. These are questions that could be studied in future applications of this work.

Recent work by Aghazadeh et al. establishes that the addition of microvessels to islets transplanted in the SQ space significantly improves the function and survival of the islet graft [39]. For larger-scale use, microvessels could be frozen and banked in bulk, could theoretically be isolated from a patient's own tissues, or collected from the same donor that islets are isolated from. However, many approaches in the islet transplantation and stem cell-derived islet fields envision utilizing methods to reduce or avoid immunosuppression regimens for these future therapies [74-76]. One approach to achieve this involves genetically engineering cells to reduce detection by the immune system – if this were the future of SCβC transplantation, a parallel method of vascularization would have to be equally immune-concealed. In this sense, growing vasculature around the islets in culture from stem cell-derived endothelial cells with the same immune-evasive genetic modifications as the SCβCs could be a useful approach. Recent progress in the generation of stem cell-derived endothelial cells could support this goal [77].

Although vascularization of transplanted islets and SCβCs is an important focus of research to translate these therapies to the clinic, there are other roles that our IVEG model can play in current islet biology research. Major breakthroughs relating to mouse islet development

and function have hit barriers in translation into the human islet and SCβC field due to significant biological differences between rodent and human islets. One reason may be because human islets are largely studied ex vivo, after isolation, and it is difficult to recapitulate the complexity of the human islet environment *in vitro* in order to study the various interactions at work during development in the same way we study these interactions *in vivo* with rodents. With the IVEG model, it is possible to recreate various levels of the islet microenvironment and in combination with SCβCs, SC-ECs and other cell types, one could model the developing human pancreas and study interactions and the roles of genes and growth factors at various stages within the larger context. Our study is just one of many that aim to incorporate these elements, but the simplicity of these constructs and the self-formation of the tubes makes this model more accessible than those that require 3-D printed scaffolds and perfused culture platforms.

In summary, we present protocols for culturing endothelial tubes within pancreas ECM hydrogel, with HUVECs alone and in co-culture with primary human islets. In vitro, these composites support the health and function of islets over the 3 day period it takes to form the vascular tubes. After 3 days, the composites were transplanted subcutaneously at a sub-therapeutic dose of 1000 IEQ into diabetic mice and led to reduced blood glucose levels, significant levels of detectable human C-Pep in the serum, and performance in a 12-week GTT assay that resembled non-diabetic mice. These *in vivo* results significantly outperformed the same dose of islets transplanted alone, which did not lead to changes in blood glucose, detectable human C-Pep or response to glucose injection in the GTT. We therefore present a protocol for generating a vascularized islet microenvironment model with promising *in vitro* and *in vivo* applications.

Methods

Cell Culture

HUVECs (Sigma, 200P-05N) in a single cell suspension were pelleted and combined with hP-HG at a density of $0.3x10^5$ cells/10 µL of hydrogel with added bFGF, VEGF, and SDF1α each at a concentration of 200 ng/mL. The mixture was pipetted into 5 µL droplets in the bottom of an untreated petri dish, inverted, and incubated at 37 ^oC and 5% CO_2 for 30 minutes. The polymerized droplets were moved into 24-well ULA plates (Corning, 3473) for culture for 3 days in appropriate medium. For tube formation, media was supplemented with an additional 200 ng/mL of bFGF, VEGF, and SDF1α ("+GF"). After 3 days, the gels were fixed with 4% PFA for immunofluorescent staining and imaging.

Culture Media

HUVECs were cultured in EGM-2 medium (Lonza, #CC-3162) supplemented as instructed by the supplier. Human islets were cultured in supplemented CMRL 1066 (Cellgro, #99-603-CV) with added 5% fetal bovine serum (FBS) and 1% penicillin/streptomycin (P/S, ThermoFisher).

INS1 medium: RPMI 1640 is supplemented with 10% FBS, 1% P/S, 2mM glutamine, 10mM HEPES, 1mM sodium pyruvate, and 55 uM β-mercaptoethanol.

INS1-EGM2 "mixed" medium ("IE Mix"): INS1 medium and EGM-2 medium were made as described and combined together at a ratio of 50:50.

INS1-EGM2 "hybrid" medium ("IE Hyb"): 500 mL of INS1 medium was made as described. Growth factor additives (hydrocortisone, bFGF, VEGF, IGF, ascorbic acid, EGF, heparin, and gentamicin sulfate-amphotericin) from the EGM-2 kit were added to the INS1 medium at full

concentration. FBS from the EGM-2 kit was not added to the hybrid medium, because INS1 medium already has 10% FBS.

INS1-CMRL "hybrid" medium ("CE Hyb"): 500 mL of supplemented CMRL medium was made as described, with 5% FBS and 1% P/S. Growth factor additives (hydrocortisone, bFGF, VEGF, IGF, ascorbic acid, EGF, heparin, and GA-1000) from the EGM-2 kit were added to the INS1 medium at full concentration. FBS from the EGM-2 kit was not added to the hybrid medium, because the CMRL already has 5% FBS.

Islet Culture and GSIS

Human islets were received through the Integrated Islet Distribution Program (IIDP). Within 24 hours of receipt, islets were counted and used for experiments. For GSIS assays, 100 IEQ were plated in 500 uL of the treatment medium in 24-well ULA plates (Corning) and cultured for 3 days.

Static GSIS Assays were performed in series, as previously described [Chapter 5]. Briefly, islets were moved from low glucose (2.8 mM) to high glucose (28 mM) to low glucose (2.8 mM) to a depolarization solution (30 mM KCl, 2.8 mM glucose). All solutions for GSIS were made in Krebs buffer (25 mM HEPES, 115 mM NaCl, 24 mM $NaHCO_3$, 5 mM KCl, 1 mM $MgCl_2$, 2.5 mM $CaCl_2$, 1% BSA). C-peptide content in supernatants collected from each step of the GSIS were determined with an ultra-sensitive human C-peptide ELISA (Mercodia, Uppsala, Sweden). Stimulation index (SI) was calculated by dividing the average secreted C-Peptide concentration under high glucose by the average C-Peptide secreted under the first low glucose period.

MTS Assay

For plated cells: $1.0x10^4$ INS1 832/13 cells per well or $2.0x10^3$ HUVEC cells per well were plated into 96-well plates in various media and cultured for 3 days. On days 0, 1, 2 and 3, the media was removed and replaced with 150 uL of media spiked with CellTiter-96 reagent (Promega, G3582). The plates were incubated shaking, with open caps for 3 hours, at 5% CO_2 and 37°C.

For islets: 100 IEQ of human islets were plated per well of 24-well ULA plates (Corning, 3473). On days 0, 1, 2 and 3, the cells were transferred to 1.5 mL Eppendorf tubes with 300 uL of MCDB basal medium spiked with CellTiter-96 reagent (Promega, G3582). The tubes were incubated shaking, with open caps for 3 hours, at 5% CO_2 and 37°C.

After incubation, the absorbance of the supernatant was measured on a spectrophotometer at 490 nm (FlexStation 3, Molecular Devices), normalized to a blank. Each treatment was tested in technical replicate for each condition and time point. A survival curve was generated for each condition tested. (N=3 islet donors per group).

Immunofluorescent Staining and 3-D Tube Formation Analysis

Gels were fixed overnight with 4% PFA in 1x PBS at 4˚C. Whole hydrogel constructs were permeabilized with 1x PBS, 1% BSA, 0.1% Triton-X for 30 minutes. For measurement of HUVEC 3-D tube formation, gels were stained with 286 nM DAPI for 5 minutes, followed by BODIPY 558/568 Phalloidin (1:100) (ThermoFisher, B3475) for 15 minutes. Gels were washed with 1x PBS and mounted for imaging with a Nikon A1RS HD confocal microscope. Z-stack images were taken

at intervals of 7.5 microns over approximately 150 micron depth (20 or more z-steps per sample); maximum-intensity projections were created from each z-stack in NIS Elements version 5.20.01. Vascular networks were quantified using the NIH AngioTool program [78]. Maximum intensity z-stacks were analyzed for vessel % area, vessel length and junction density.

Whole Gel Clearing and Confocal Microscopy

For whole imaging of IVEG constructs, a tissue clearing protocol was used. Whole gels were permeabilized for two hours in PBT (1x PBS, 3% BSA, 0.2% Triton-X) and then blocked for 35 minutes (1x PBS, 10% BSA, 5% DMSO) at room temperature. Gels were incubated with conjugated primary antibodies diluted in 1xPBS/1%BSA for 5 days at 4˚C, in the dark. Antibodies were conjugated using Biotium Mix-N-Stain CF conjugation kits (Biotium #92233) with fluorophores of 488 nm (used for insulin) and 568 nm (used for Tie2). Primary antibodies used were mouse anti-insulin (MilliporeSigma, #I2018, used at 1:500 after conjugation) and rabbit anti-Tie2 (Abcam, #ab221154, used at 1:500 after conjugation). Dilution after conjugation varies batch to batch. Following incubation with antibodies, gels were washed 3 times in 1x PBS with 0.05% Triton-X (PBS-T), stained with DAPI (14.3 mM DAPI in 1x PBS) for 7 minutes, and then washed 3 times with 1x PBS. Gels were dehydrated sequentially with 33% methanol (30 min), 66% methanol (30 min), and 100% methanol (1 hour). Dehydrated gels were cleared on-slide in BABB (1:2 solution of Benzyl Alcohol: Benzyl Benzoate); silicone adapters were placed on the slides to from a well and filled with BABB, gels were added to the center of the well and a cover slip over the top to seal the well. Gels become clear rapidly and should be imaged immediately for best images, but can be placed at 4˚C and imaged for several days. Whole gels were imaged

using a Nikon A1RS HD confocal microscope and imaged and videos prepared with NIS Elements version 5.20.01.

Islet Transplantation and In Vivo Assays

On day 0 of culture, 1000 IEQ of fresh human islets were counted and transplanted into the abdominal subcutaneous space. After 3 days of IVEG co-culture, 20 IVEG gels (50 IEQ per gel for a total of 1000 IEQ) were transplanted in the same manner. In all treatment groups islets were transplanted in the center of a silicone ring to identify the graft at the time of retrieval.

Fasted blood glucose was measure before and after transplantation using a Contour Next EZ (Ascensia) glucometer and following a 6-hour fast. 100 µL of blood was collected once per week before and after transplantation, in a non-fasted state to measure serum C-Pep, using an ultra-sensitive human C-peptide ELISA kit (Mercodia, Uppsala, Sweden). After 12 weeks, mice were fasted overnight prior to the glucose tolerance test (GTT). A 30% D-glucose solution was injected intra-peritoneally at a dose of 2 g/kg to initiate the GTT at time 0. Blood glucose was measured at time 0’ (before injection), 15’, 30’, 60’, and 120’ thereafter. Blood was collected at time 0’ (before injection) and at 60’ post-injection to determine serum C-Pep.

Acknowledgements

We would like to offer a special thanks to the donor families who donated tissues, without which this study would not be possible. We acknowledge the support of the Integrated Islet Distribution Program (IIDP) (National Institutes of Health Grant 2UC4DK098085), National Institutes of Health and members of the Fernandez lab for generating islets and providing access to islet donor data. We would like to thank the University of Wisconsin Optical Imaging Core and Lance Rodenkirch for technical assistance on the confocal microscope.

References

1. Jansson, L. and C. Hellerstrom, *Stimulation by glucose of the blood flow to the pancreatic islets of the rat.* Diabetologia, 1983. **25**(1): p. 45-50.
2. Brissova, M., et al., *Human Islets Have Fewer Blood Vessels than Mouse Islets and the Density of Islet Vascular Structures Is Increased in Type 2 Diabetes.* J Histochem Cytochem, 2015. **63**(8): p. 637-45.
3. Henderson, J.R. and M.C. Moss, *A morphometric study of the endocrine and exocrine capillaries of the pancreas.* Q J Exp Physiol, 1985. **70**(3): p. 347-56.
4. Piper, K., et al., *Beta cell differentiation during early human pancreas development.* J Endocrinol, 2004. **181**(1): p. 11-23.
5. Cleaver, O. and Y. Dor, *Vascular instruction of pancreas development.* Development, 2012. **139**(16): p. 2833-43.
6. Edsbagge, J., et al., *Vascular function and sphingosine-1-phosphate regulate development of the dorsal pancreatic mesenchyme.* Development, 2005. **132**(5): p. 1085-92.
7. Jacquemin, P., et al., *An endothelial-mesenchymal relay pathway regulates early phases of pancreas development.* Dev Biol, 2006. **290**(1): p. 189-99.
8. Lammert, E., et al., *Role of VEGF-A in Vascularization of Pancreatic Islets.* Current Biology, 2003. **13**(12): p. 1070-1074.
9. Yoshitomi, H. and K.S. Zaret, *Endothelial cell interactions initiate dorsal pancreas development by selectively inducing the transcription factor Ptf1a.* Development, 2004. **131**(4): p. 807-17.
10. Reinert, R.B., et al., *Vascular endothelial growth factor-a and islet vascularization are necessary in developing, but not adult, pancreatic islets.* Diabetes, 2013. **62**(12): p. 4154-64.
11. Lammert, E., O. Cleaver, and D. Melton, *Induction of pancreatic differentiation by signals from blood vessels.* Science, 2001. **294**(5542): p. 564-7.
12. Hogan, M.F. and R.L. Hull, *The islet endothelial cell: a novel contributor to beta cell secretory dysfunction in diabetes.* Diabetologia, 2017. **60**(6): p. 952-959.
13. Johansson, A., et al., *Endothelial cell signalling supports pancreatic beta cell function in the rat.* Diabetologia, 2009. **52**(11): p. 2385-94.
14. Nikolova, G., et al., *The vascular basement membrane: a niche for insulin gene expression and Beta cell proliferation.* Dev Cell, 2006. **10**(3): p. 397-405.
15. Peiris, H., et al., *The beta-cell/EC axis: how do islet cells talk to each other?* Diabetes, 2014. **63**(1): p. 3-11.
16. Narayanan, S., et al., *Intra-islet endothelial cell and beta-cell crosstalk: Implication for islet cell transplantation.* World J Transplant, 2017. **7**(2): p. 117-128.

17. Olerud, J., et al., *Thrombospondin-1: an islet endothelial cell signal of importance for beta-cell function.* Diabetes, 2011. **60**(7): p. 1946-54.

18. Spelios, M.G., et al., *Islet Endothelial Cells Induce Glycosylation and Increase Cell-surface Expression of Integrin beta1 in beta Cells.* J Biol Chem, 2015. **290**(24): p. 15250-9.

19. Johansson, M., et al., *Islet endothelial cells and pancreatic beta-cell proliferation: studies in vitro and during pregnancy in adult rats.* Endocrinology, 2006. **147**(5): p. 2315-24.

20. Sordi, V., et al., *Establishment, characterization and long-term culture of human endocrine pancreas-derived microvascular endothelial cells.* Cytotherapy, 2017. **19**(1): p. 141-152.

21. Zanone, M.M., et al., *Expression of nephrin by human pancreatic islet endothelial cells.* Diabetologia, 2005. **48**(9): p. 1789-97.

22. Henriksnas, J., et al., *Markedly decreased blood perfusion of pancreatic islets transplanted intraportally into the liver: disruption of islet integrity necessary for islet revascularization.* Diabetes, 2012. **61**(3): p. 665-73.

23. Mattsson, G., L. Jansson, and P.O. Carlsson, *Decreased vascular density in mouse pancreatic islets after transplantation.* Diabetes, 2002. **51**(5): p. 1362-6.

24. Liljeback, H., et al., *Extensive Loss of Islet Mass Beyond the First Day After Intraportal Human Islet Transplantation in a Mouse Model.* Cell Transplant, 2016. **25**(3): p. 481-9.

25. Brissova, M., et al., *Intraislet endothelial cells contribute to revascularization of transplanted pancreatic islets.* Diabetes, 2004. **53**(5): p. 1318-25.

26. Nyqvist, D., et al., *Donor islet endothelial cells participate in formation of functional vessels within pancreatic islet grafts.* Diabetes, 2005. **54**(8): p. 2287-93.

27. Komatsu, H., et al., *Posttransplant oxygen inhalation improves the outcome of subcutaneous islet transplantation: A promising clinical alternative to the conventional intrahepatic site.* Am J Transplant, 2017: p. Apr;18(4): 832-842.

28. Merani, S., et al., *Optimal implantation site for pancreatic islet transplantation.* Br J Surg, 2008. **95**(12): p. 1449-61.

29. Pepper, A.R., et al., *A prevascularized subcutaneous device-less site for islet and cellular transplantation.* Nat Biotechnol, 2015. **33**(5): p. 518-23.

30. Pepper, A.R., et al., *Revascularization of transplanted pancreatic islets and role of the transplantation site.* Clin Dev Immunol, 2013. **2013**: p. 352315.

31. Luan, N.M. and H. Iwata, *Long-term allogeneic islet graft survival in prevascularized subcutaneous sites without immunosuppressive treatment.* Am J Transplant, 2014. **14**(7): p. 1533-42.

32. Bowers, D.T., et al., *Engineering the vasculature for islet transplantation.* Acta Biomater, 2019. **95**: p. 131-151.

33. Citro, A., et al., *Biofabrication of a vascularized islet organ for type 1 diabetes.* Biomaterials, 2019. **199**: p. 40-51.

34. Johansson, U., et al., *Formation of composite endothelial cell-mesenchymal stem cell islets: a novel approach to promote islet revascularization.* Diabetes, 2008. **57**(9): p. 2393-401.

35. Kaufman-Francis, K., et al., *Engineered vascular beds provide key signals to pancreatic hormone-producing cells.* PLoS One, 2012. **7**(7): p. e40741.

36. Takahashi, Y., et al., *Self-Condensation Culture Enables Vascularization of Tissue Fragments for Efficient Therapeutic Transplantation.* Cell Rep, 2018. **23**(6): p. 1620-1629.

37. Grapensparr, L., G. Christoffersson, and P.O. Carlsson, *Bioengineering with Endothelial Progenitor Cells Improves the Vascular Engraftment of Transplanted Human Islets.* Cell Transplant, 2018. **27**(6): p. 948-956.

38. Vlahos, A.E., N. Cober, and M.V. Sefton, *Modular tissue engineering for the vascularization of subcutaneously transplanted pancreatic islets.* Proc Natl Acad Sci U S A, 2017. **114**(35): p. 9337-9342.

39. Aghazadeh, Y., et al., *Microvessels support engraftment and functionality of human islets and hESC-derived pancreatic progenitors in diabetes models.* Cell Stem Cell, 2021. **28**(11): p. 1936-1949 e8.

40. Uzunalli, G., et al., *Improving pancreatic islet in vitro functionality and transplantation efficiency by using heparin mimetic peptide nanofiber gels.* Acta Biomater, 2015. **22**: p. 8-18.

41. Weaver, J.D., et al., *Vasculogenic hydrogel enhances islet survival, engraftment, and function in leading extrahepatic sites.* Sci Adv, 2017. **3**(6): p. e1700184.

42. Arrojo e Drigo, R., et al., *New insights into the architecture of the islet of Langerhans: a focused cross-species assessment.* Diabetologia, 2015. **58**(10): p. 2218-28.

43. Otonkoski, T., et al., *Unique basement membrane structure of human pancreatic islets: implications for beta-cell growth and differentiation.* Diabetes Obes Metab, 2008. **10 Suppl 4**: p. 119-27.

44. Rodriguez-Diaz, R., et al., *Innervation patterns of autonomic axons in the human endocrine pancreas.* Cell Metab, 2011. **14**(1): p. 45-54.

45. Arda, H.E., et al., *Age-Dependent Pancreatic Gene Regulation Reveals Mechanisms Governing Human beta Cell Function.* Cell Metab, 2016. **23**(5): p. 909-20.

46. Benner, C., et al., *The transcriptional landscape of mouse beta cells compared to human beta cells reveals notable species differences in long non-coding RNA and protein-coding gene expression.* BMC Genomics, 2014. **15**: p. 620.

47. Augsornworawat, P., et al., *A hydrogel platform for in vitro three dimensional assembly of human stem cell-derived islet cells and endothelial cells.* Acta Biomater, 2019. **97**: p. 272-280.

48. Wassmer, C.H., et al., *Bio-Engineering of Pre-Vascularized Islet Organoids for the Treatment of Type 1 Diabetes.* Transpl Int, 2021. **35**: p. 10214.

49. Talavera-Adame, D., et al., *Effective endothelial cell and human pluripotent stem cell interactions generate functional insulin-producing beta cells.* Diabetologia, 2016. **59**(11): p. 2378-2386.

50. Skrzypek, K., et al., *Endothelial and beta cell composite aggregates for improved function of a bioartificial pancreas encapsulation device.* Int J Artif Organs, 2018. **41**(3): p. 152-159.

51. Bakhti, M., A. Bottcher, and H. Lickert, *Modelling the endocrine pancreas in health and disease.* Nat Rev Endocrinol, 2019. **15**(3): p. 155-171.

52. Kirkpatrick, C.J., S. Fuchs, and R.E. Unger, *Co-culture systems for vascularization--learning from nature.* Adv Drug Deliv Rev, 2011. **63**(4-5): p. 291-9.

53. Yamada, K.M. and K. Clark, *Cell biology: survival in three dimensions.* Nature, 2002. **419**(6909): p. 790-1.

54. Sackett, S.D., et al., *Extracellular matrix scaffold and hydrogel derived from decellularized and delipidized human pancreas.* Sci Rep, 2018. **8**(1): p. 10452.

55. Berthod, F., et al., *Extracellular matrix deposition by fibroblasts is necessary to promote capillary-like tube formation in vitro.* J Cell Physiol, 2006. **207**(2): p. 491-8.

56. Newman, A.C., et al., *The requirement for fibroblasts in angiogenesis: fibroblast-derived matrix proteins are essential for endothelial cell lumen formation.* Mol Biol Cell, 2011. **22**(20): p. 3791-800.

57. Stendahl, J.C., D.B. Kaufman, and S.I. Stupp, *Extracellular matrix in pancreatic islets: relevance to scaffold design and transplantation.* Cell Transplant, 2009. **18**(1): p. 1-12.

58. Tremmel, D.M., et al., *A human pancreatic ECM hydrogel optimized for 3-D modeling of the islet microenvironment.* Scientific Reports, 2022. **12**(1).

59. Blinder, Y.J., D.J. Mooney, and S. Levenberg, *Engineering approaches for inducing blood vessel formation.* Current Opinion in Chemical Engineering, 2014. **3**: p. 56-61.

60. Kular, J.K., S. Basu, and R.I. Sharma, *The extracellular matrix: Structure, composition, age-related differences, tools for analysis and applications for tissue engineering.* J Tissue Eng, 2014. **5**: p. 2041731414557112.

61. Weis, S.M. and D.A. Cheresh, *Tumor angiogenesis: molecular pathways and therapeutic targets.* Nat Med, 2011. **17**(11): p. 1359-70.

62. Du, P., et al., *Human lung fibroblast-derived matrix facilitates vascular morphogenesis in 3D environment and enhances skin wound healing.* Acta Biomater, 2017. **54**: p. 333-344.

63. Akhtar, N., E.B. Dickerson, and R. Auerbach, *The sponge/Matrigel angiogenesis assay.* Angiogenesis, 2002. **5**(1-2): p. 75-80.

64. Passaniti, A., et al., *A simple, quantitative method for assessing angiogenesis and antiangiogenic agents using reconstituted basement membrane, heparin, and fibroblast growth factor.* Lab Invest, 1992. **67**(4): p. 519-28.

65. Arnaoutova, I. and H.K. Kleinman, *In vitro angiogenesis: endothelial cell tube formation on gelled basement membrane extract.* Nat Protoc, 2010. **5**(4): p. 628-35.

66. DeCicco-Skinner, K.L., et al., *Endothelial cell tube formation assay for the in vitro study of angiogenesis.* J Vis Exp, 2014(91): p. e51312.

67. Auler, M., et al., *Mimicking Angiogenesis in vitro: Three-dimensional Co-culture of Vascular Endothelial Cells and Perivascular Cells in Collagen Type I Gels.* Bio Protoc, 2017. **7**(8): p. e2247.

68. Kim, S., et al., *Engineering of functional, perfusable 3D microvascular networks on a chip.* Lab Chip, 2013. **13**(8): p. 1489-500.

69. Stratman, A.N., et al., *Pericyte recruitment during vasculogenic tube assembly stimulates endothelial basement membrane matrix formation.* Blood, 2009. **114**(24): p. 5091-101.

70. Cross, S.E., et al., *Key Matrix Proteins Within the Pancreatic Islet Basement Membrane Are Differentially Digested During Human Islet Isolation.* Am J Transplant, 2017. **17**(2): p. 451-461.

71. Nguyen, J., Y.Y. Lin, and S. Gerecht, *The next generation of endothelial differentiation: Tissue-specific ECs.* Cell Stem Cell, 2021. **28**(7): p. 1188-1204.

72. Paik, D.T., et al., *Single-Cell RNA Sequencing Unveils Unique Transcriptomic Signatures of Organ-Specific Endothelial Cells.* Circulation, 2020. **142**(19): p. 1848-1862.

73. Gifre-Renom, L., et al., *Organ-Specific Endothelial Cell Differentiation and Impact of Microenvironmental Cues on Endothelial Heterogeneity.* Int J Mol Sci, 2022. **23**(3).

74. Lu, P., et al., *Generating hypoimmunogenic human embryonic stem cells by the disruption of beta 2-microglobulin.* Stem Cell Rev Rep, 2013. **9**(6): p. 806-13.

75. Riolobos, L., et al., *HLA engineering of human pluripotent stem cells.* Mol Ther, 2013. **21**(6): p. 1232-41.

76. Sackett, S.D., et al., *Modulation of human allogeneic and syngeneic pluripotent stem cells and immunological implications for transplantation.* Transplant Rev (Orlando), 2016. **30**(2): p. 61-70.

77. Wang, K., et al., *Robust differentiation of human pluripotent stem cells into endothelial cells via temporal modulation of ETV2 with modified mRNA.* Sci Adv, 2020. **6**(30): p. eaba7606.

78. Zudaire, E., et al., *A computational tool for quantitative analysis of vascular networks.* PLoS One, 2011. **6**(11): p. e27385.

Supplemental Materials:

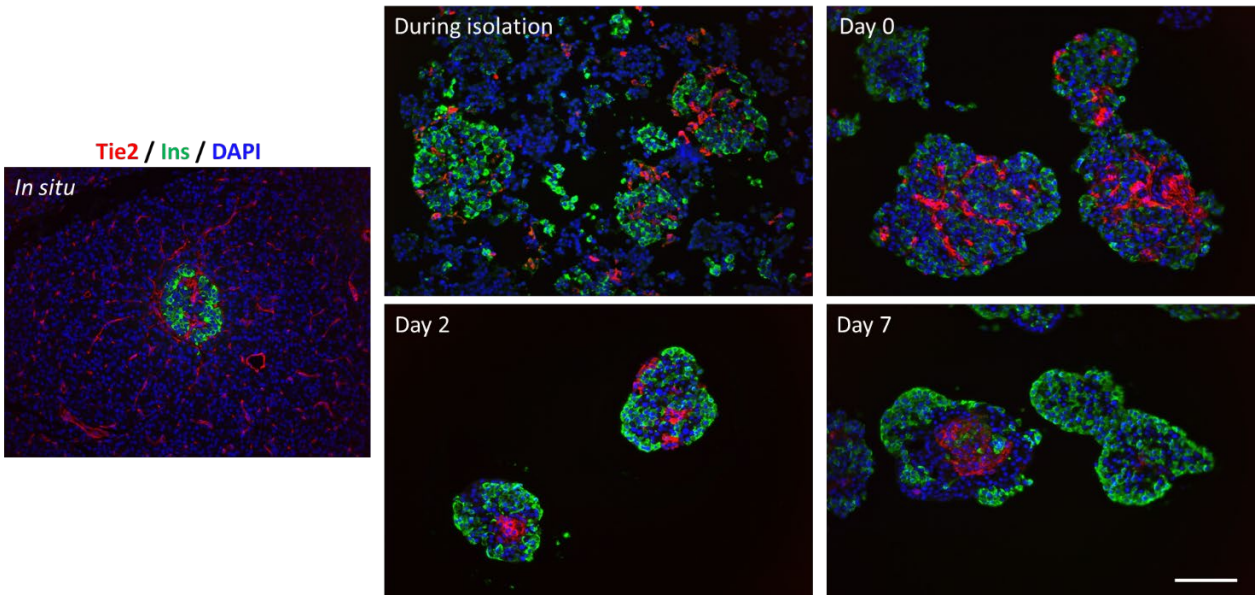

Chapter 6 Supplemental Figure 1: Islet endothelial cells rearrange after transplantation and in culture.

Islets stained for Tie2 (to mark endothelial cells) (red), insulin (green) and DAPI (blue). The arrangement of islet endothelial cells is not immediately altered at the time of isolation, or the beginning of culture (Day 0) but is altered over time in suspension culture (e.g. Day 2, Day 7). All images taken from islets from the same donor. The same pattern of endothelial cell rearrangement was observed in 5 donors assessed at each of the same time points. Scale bar = 100 microns.

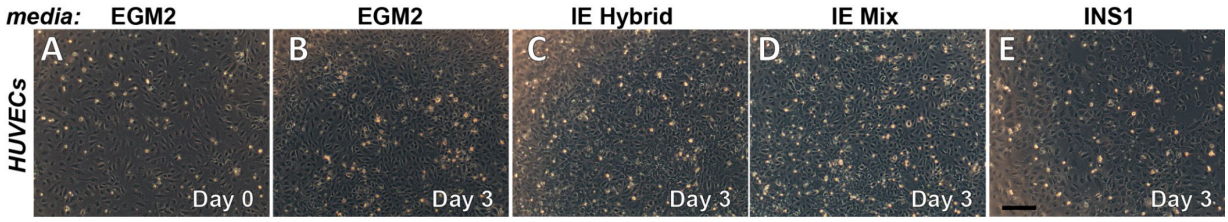

Chapter 6 Supplemental Figure 2: HUVECs in adherent culture (**A**) HUVECs on Day 0 or Day 3 (**B-E**) in various media have similar morphology and confluence. Scale = 200 microns.

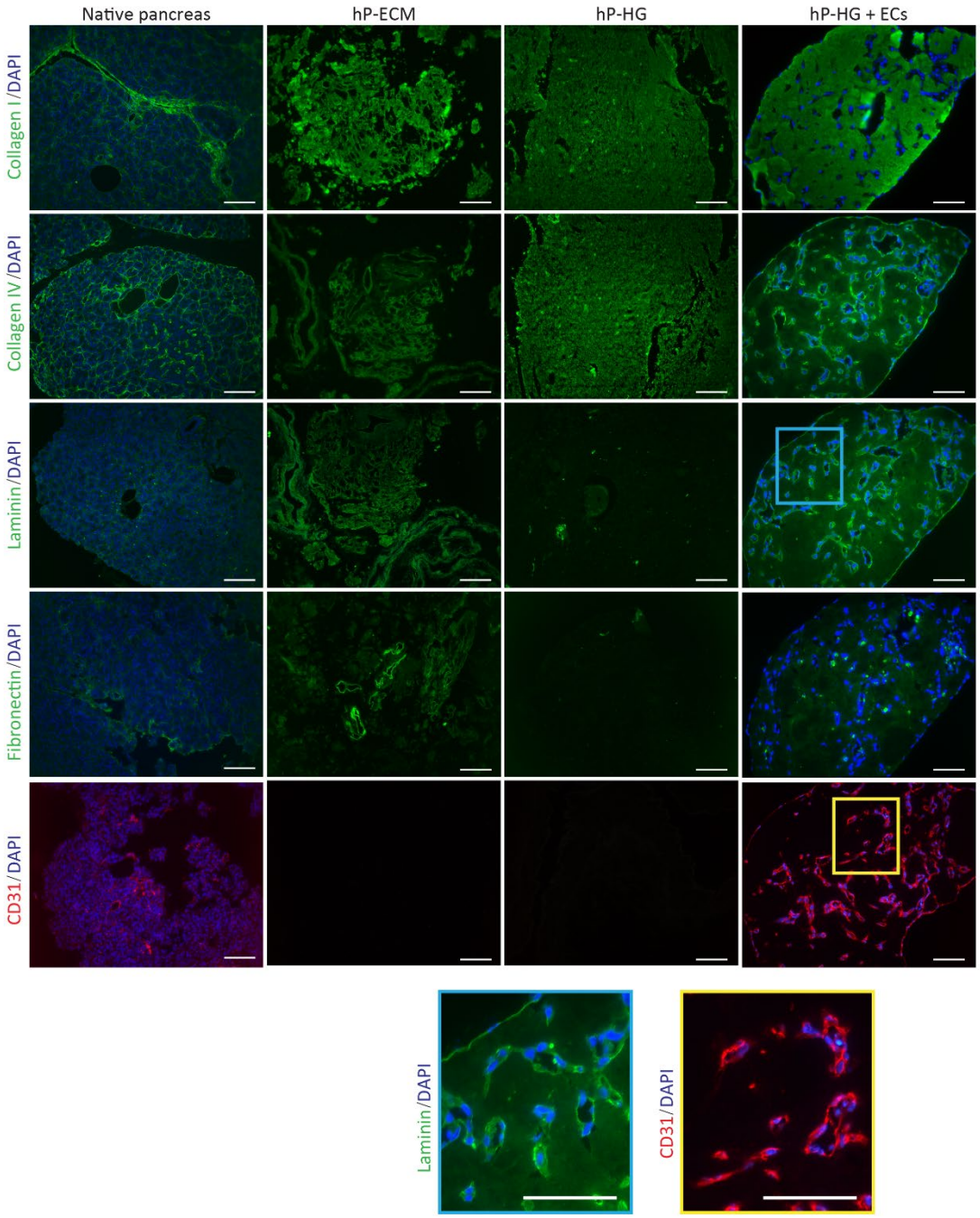

Chapter 6 Supplemental Figure 3: ECM deposition by ECs cultured in hP-HG restores lost basement membrane proteins. ECM proteins Collagen I, Collagen IV, Laminins (pan-laminin), and Fibronectin are present in the native pancreas and decellularized ECM, but only Collagen I and Iv are robustly detected in hP-HG. EC culture and tube formation in hP-HG after 3 days of culture deposits these ECM proteins in basement membrane structures formed around the tubes. Cross-sections of the tubes also reveals many lumen-like structures at the center of the tubes (see insets). CD31 staining indicates presence of ECs in native tissue and hP-HG + EC co-culture, and removal of ECs in the acellular hP-ECM and hP-HG.

All scale bars = 100 microns.

Chapter 6 Supplemental Video 1: IVEG construct stained for insulin (green) and Tie2 (red). Z-stack image collected following tissues clearing. Video prepared using NIS Elements. The dimension of the box in the video are: y-axis = 1180.5 microns, x-axis = 1075 microns, z-axis = 375 microns. Scaling provided in the video.

Chapter 6 Supplemental Video 2: IVEG construct stained for insulin (green) and Tie2 (red). Z-stack image collected following tissues clearing. Video prepared using NIS Elements. The dimension of the box in the video are: y-axis = 637.9 microns, x-axis = 637.9 microns, z-axis = 98 microns.

Supplemental Methods

Immunohistochemistry

For staining of tissue sections, samples were fixed in 4% PFA, paraffin embedded, and 5 micron sections were cut for staining. Sections were deparaffinized using xylene and rehydrated. Antigen retrieval was performed by treatment with 10mM Citrate Buffer, pH6.0 for 2 hours in an 80˚C water bath. Slides were blocked with 10% BSA/1x PBS for 1 h at room temperature, incubated with primary antibodies overnight at 4˚C, washed, incubated with secondary antibodies for 40 min at room temperature. Nuclei were stained with DAPI. All antibodies used are included in Supplemental Table 1.

Chapter 6 Supplemental Table 1:

Antibodies used in this study

Target	Species	Dilution	Product
CD31	Mouse	1:50	sc-376764 (Santa Cruz)
Col1	Rabbit	1:500	ab34710 (Abcam)
Col6	Rabbit	1:200	17023-1-AP (Proteintech)
Fibronectin	Rabbit	1:200	ab2413 (Abcam)
Ins	Mouse	1:5000	I2018 (Sigma)
Ins	Guinea Pig	1:2000	I8510 (Sigma)
Laminins	Rabbit	1:200	L9393 (Sigma Aldrich)
Tie2	Rabbit	1:4000	ab221154 (Abcam)

Target	Color	Dilution	Product
Anti-Mouse	488	1:800	A11001 (Life Technologies)
Anti-Mouse	568	1:800	A11031 (Life Technologies)
Anti-Mouse	647	1:800	A21235 (Life Technologies)
Anti-Rabbit	488	1:800	A21206 (Life Technologies)
Anti-Rabbit	568	1:800	A11011 (Life Technologies)
Anti-Guinea Pig	488	1:800	A11073 (Life Technologies)

Chapter 7

Validating phenotypic beta cell maturation markers in human pancreas development

Chapter 7 Graphical Abstract

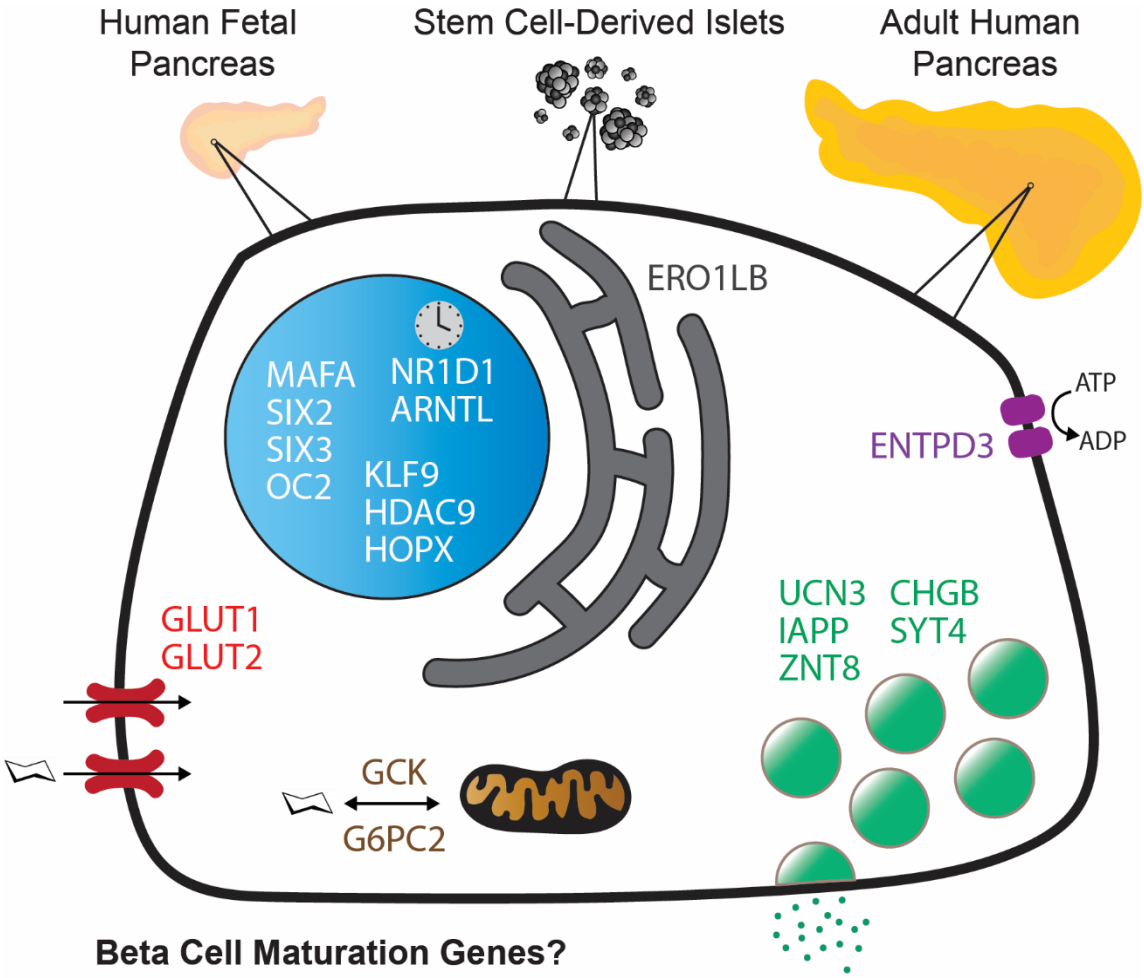

Daniel Tremmel designed the study under the guidance of Sara Dutton Sackett and Jon Odorico. Daniel Tremmel, Anna Mikat, Sakar Gupta, Andrew Curran and Jenna Menadue performed the experiments and analyzed the data. Daniel Tremmel and Sam Mitchell processed and banked human tissues. Daniel Tremmel prepared all figures and wrote the manuscript with guidance from Sara Dutton Sackett and Jon Odorico.

Abstract

The identification of markers for human pancreatic beta cell maturation could stimulate a better understanding of normal human islet development, be informative for improving stem cell-derived islets like cluster (SC-ILC) differentiation, and facilitate the sorting of more mature beta cells from the pool of differentiated cells. While several candidate factors to mark beta cell maturation have been identified, much of the data supporting these markers come from animal models or SC-ILC culture. One such marker is Urocortin-3 (Ucn3). In this study, we provide evidence that Ucn3 is expressed in human fetal islets well before the acquisition of functional maturation. When SC-ILCs expressing significant levels of Ucn3 were generated, the cells did not exhibit GSIS, indicating that Ucn3 expression is not correlated with functional maturation in these cells. We utilize our tissue bank and SC-ILC resources to test an array of other candidate maturation markers, and identify NTPDase3, G6PC2, IAPP, MAFA, SIX2, and SIX3 as markers with expression patterns that correlate developmentally with the onset of functional maturation in human islets.

Introduction

The pancreas is an essential organ composed of exocrine and endocrine cell types. The clusters of endocrine cells, called islets of Langerhans, contain alpha, beta and delta cells, which control blood glucose through the secretion of glucagon, insulin and somatostatin, respectively. Loss of beta cell mass causes diabetes, either due to autoimmune infiltration (Type 1 Diabetes, T1D) or due to stress and damage to the beta cells (Type 2 Diabetes, T2D). Due to a near-inability for mature human beta cells to proliferate [1], beta cell loss is irreversible and is treated clinically with exogenous insulin treatment, or beta cell replacement, including either pancreas or islet

transplantation. Exogenous insulin administration is an effective short-term treatment yet is imperfect because, unlike endogenous beta cells, it is unable to continuously monitor and prevent hyper- and hypoglycemic episodes. Other treatments which achieve appropriate glycemic control, such as total pancreas and islet of Langerhans transplantation, provide a sustainable allogeneic replacement for the patient's lost or dysfunctional beta cells. However, a shortage of donor organs, invasiveness of the surgery, inadequate long-term function, and the need for prolonged immunosuppression therapy have made transplantation largely unavailable to a majority of the affected population [2].

As an alternative to transplantation from deceased organ donors, many research groups are focusing efforts towards using hPSCs, which have the potential to differentiate into insulin-secreting beta cells. *In vitro* differentiation protocols produce "beta-like" cells that express many beta cell genes and can secrete insulin in response to glucose, but based on a combination of analyses including gene expression, metabolic profiles, total insulin content and insulin secretion in response to a variety of stimuli, these cells do not fully resemble primary mature beta cells [3]. Stem cell-derived islet-like clusters (SC-ILCs) have been shown to further mature following transplantation into mice [4-6]. However, there are also populations of off-target cells (e.g. ductal, acinar, enterochromaffin-like, mesenchymal, and other non-endocrine cells) present in SC-ILCs [4, 7, 8]which are undesirable to co-transplant with the endocrine cells due to added variables and uncertainty as to how those cells may affect transplant outcomes. In recent clinical trials conducted by ViaCyte in which stem cell-derived pancreas progenitor cells were transplanted into diabetic patients, the transplanted cells differentiated into a variety of off-target cell types and did not produce sufficient detectable insulin [9]. For application in a clinical

setting, SC-ILCs ideally should have rapid and full function, similar to endogenous mature beta cells. Mature function is necessary for adequate regulation of blood sugar homeostasis; unregulated over-secretion of insulin can lead to hypoglycemia while under-secretion by immature cells during levels of high blood glucose can result in sustained hyperglycemia. To date, no differentiation protocol has generated fully functionally mature beta cells that show levels of total insulin content, glucose-stimulated insulin secretion (GSIS), and gene expression profiles comparable to adult human islets [3], but the field is continuously moving closer to this goal [5]. Therefore, to pursue the clinical use of SC-ILCs, achieving functional maturation *in vitro* and prior to transplantation is a high priority. The identification of phenotypic markers of beta cell maturity will help to facilitate the characterization of the most effective differentiation protocols.

Compared to adult islets, fetal human islets are less responsive to high glucose concentrations, but do respond to other signals including amino acids [10]. Beta cell functional maturation occurs postnatally, which involves the acquisition and gradual enhancement of GSIS until puberty [11, 12]. Additional metabolic, epigenetic, and gene expression differences from immature to mature adult beta cells can be identified with cell markers, however they are still not fully understood [13, 14]. Stepwise protocols to generate SC-ILCs use the expression of genes and phenotypic markers at each stage as checkpoints for confirming developmental progress and specification. Understanding these gene expression profiles for normal beta cell development has been key to recapitulating those developmental stages *in vitro*. For instance, the discovery that *PDX1* and *NKX6.1* expression must precede *NGN3* induction in order to successfully produce endocrine progenitors has allowed for the generation of more highly enriched endocrine cell and beta cell populations at the end of the differentiation protocol [15]. The identification of similar

markers at the transition from immature to mature beta cells would provide an efficient way to isolate and purify functionally mature SC-ILCs from heterogeneous populations, and advance our understanding of the biology underlying maturation.

One example of a gene thought to mark beta cell maturation is Urocortin-3 (Ucn3), a peptide hormone that was first identified in pancreatic beta cells in 2003 [16], and found to be stimulated by insulin secretagogues in mice and rats [16, 17]. Ucn3 was later identified as a marker of beta cell functional maturation in mice, and found to be expressed only in mouse beta cells postnatally [18]. In primate and human islets, however, Ucn3 is expressed in both alpha and beta cells [19], and has been described as being a marker of human beta cell maturation despite evidence that Ucn3 may be expressed in prenatally [20, 21]. Nevertheless, Ucn3 has commonly been used as a tool for monitoring beta cell maturation in SC-ILCs. None of the leading protocols in the SC-ILC field have described significant Ucn3 expression in stem cell-derived beta or alpha cells [5, 6, 22, 23], although some have observed expression of Ucn3 following transplantation of the cells and subsequent maturation *in vivo* [5, 21]. Ucn3 is secreted along with insulin, packaged within the same secretory vesicles [24], and is active in a feedback mechanism in which it binds corticotropin releasing hormone receptor 2 (CRFR2) on delta cells to stimulate somatostatin secretion, which inhibits alpha and beta cell function [24]. Loss of Ucn3 has also been associated with the progression of type 2 diabetes in mice [25] and in humans [24]. Ucn3 KO mice were recently generated and reported to have no deficit in beta cell maturation or function, deeming Ucn3 a marker, but not a driver of maturation [26].

Many other maturation markers have been postulated through studies of mouse development, in human diabetes, or with human SC-ILCs, but lack corresponding evaluation

comparing mature vs. immature fetal human tissues [8, 14, 27]. Arda *et al.* provided an important resource with their 2016 publication assessing single-cell human beta cell transcriptomes, identifying several genes that significantly change expression postnatally [11]. Interestingly, this study did not identify *UCN3* as a gene of interest. *MAFA*, *SIX2*, *SIX3* and several other genes were identified to have moderate, but significant, increases in expression between juvenile and adult human beta cells. The Arda *et al.* study has been cited to justify low expression of genes such as *MAFA* in stem cell-derived islets to be similar to neonatal beta cells, but the relative expression profiles are not comparable. *MAFA* expression from juvenile to adult beta cells was found to have approximately a two-fold increase, while primary islets have at least 10-fold higher *MAFA* expression than SC-ILCs [3, 6, 23]). The more recent differentiation protocol described by Balboa *et al.*, with extensive characterization of SC-ILC function and metabolism, also found that *MAFA* and *UCN3* are not highly expressed *in vitro*, but do increase in expression to levels comparable to primary islets weeks after transplantation [5].

Here we report two SC-ILC differentiation protocols, one which generates alpha and beta cells that express *UCN3* at levels comparable to native adult islets, but still lacks function comparable to primary islets. We explore the expression profiles of *UCN3* in SC-ILCs as well as in primary human fetal pancreas and adult islets to establish that *UCN3* expression does not correlate with functional maturation in human islets. We then explore the expression profiles of other candidate beta cell maturation markers in human fetal and adult tissues to help evaluate the relevance of these genes and proteins in normal human islet development.

Results

Two protocols developed in our lab, at a time before dynamic insulin secretion was robustly achieved in SC-ILCs, are outlined in Figure 1A and detailed fully in Supplemental Tables 1-3. These protocols are derived from Xu *et al.* (2011) [28] with modifications inspired by Rezania *et al.* (2014) [29], Pagliuca *et al.* (2014) [30], Nostro *et al.* (2015) [15] and Zhu *et al.* (2016) [31]. Although both protocols, Protocol A and Protocol B, have low glucose-responsive function, we find that major gene expression differences between these two protocols warrant the use of these SC-ILCs for further study. To complement these protocols, our study utilizes adult human pancreas tissue, isolated adult human islets (AHI) and human fetal pancreas (HFP) tissues to investigate candidate human beta cell maturation markers (Fig. 1B).

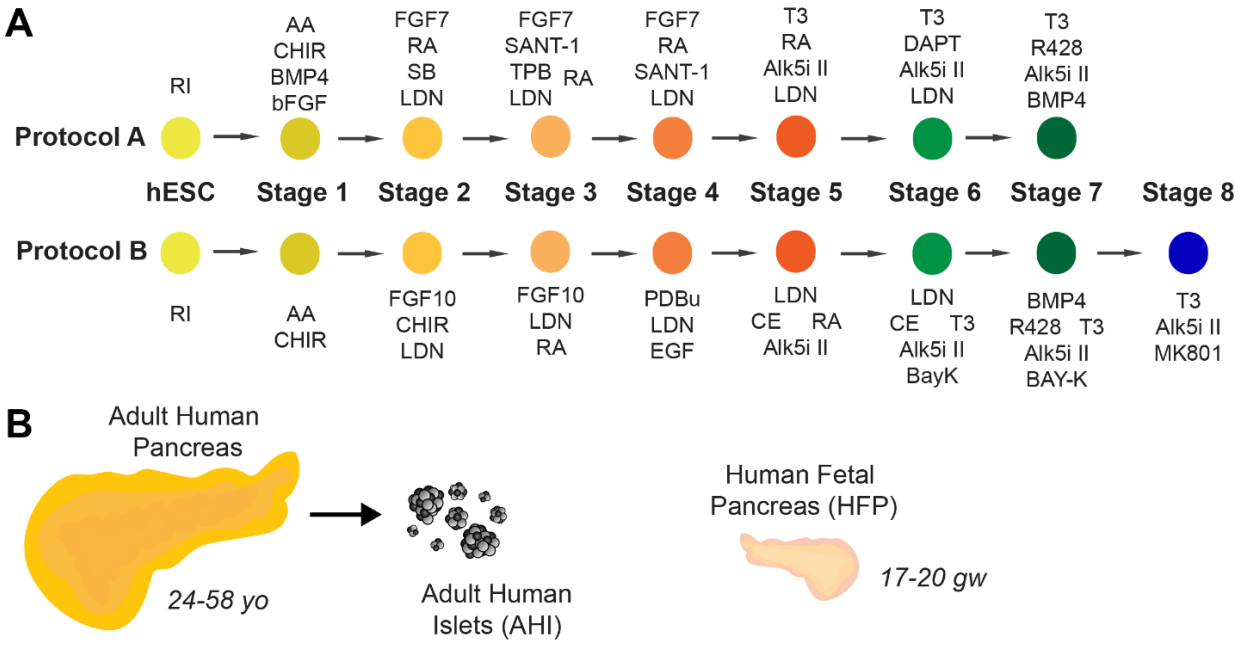

Figure 1: Resources used in this study.

A) Schematic diagrams for two SC-ILC differentiation protocols, Protocol A ("A") and Protocol B ("B"). Full details of these protocols are detailed in Supplemental Tables 1-3.

B) Adult human pancreas tissue (age range 24-58 years old), isolated adult human islets ("AHI") and human fetal pancreas ("HFP") (age range 17-20 gestational weeks) are used in this study for assessment of gene expression, protein localization, and function.

Ucn3 expression in SC-ILCs does not correlate with improved function

H1 stem cells were differentiated to the end of Protocol A (Pro A, end Stage 7, day 28) and Protocol B (Pro B, end Stage 8, day 28) to assess gene expression, protein localization and SC-ILC function. Ucn3, Ins, and Gcg were co-stained to reveal that Pro A has almost no detectable Ucn3, while Pro B has detectable Ucn3 in both Ins^+ and Gcg^+ cells, similar to *in situ* adult human islets (Fig. 2A). Co-localization of Ucn3 with either insulin (Fig. 2B) or glucagon (Fig. 2C) was quantified to find that in Pro B, Ucn3 is expressed in alpha cells at a similar level as in adult pancreas, while Ucn3 is expressed in beta cells at a reduced level compared to adult pancreas, but a significantly higher level than in Pro A. Relative *UCN3* gene expression in Pro B was insignificantly different from AHI, while Protocol A had low *UCN3* gene expression and was significantly lower than both Protocol B and AHI (Fig. 2D). Despite Pro B expressing substantially improved *UCN3* levels, the functional performance of Pro A and B in a static GSIS assay were not distinguishable from one another (A, SI = 1.3; B, SI=1.2), and both performed poorly compared to isolated AHI (SI=2.2) (Fig. 2E-F). Despite having poor insulin secretion in response to glucose, the cells were responsive to potassium stimulation (Fig. 2G).

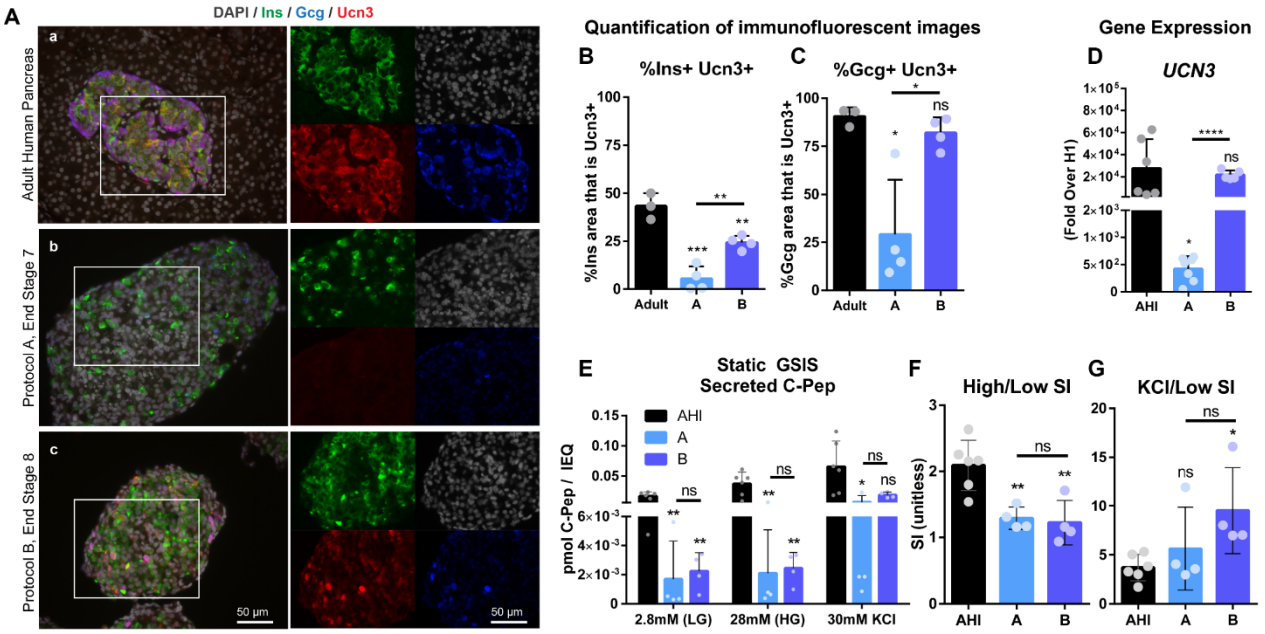

Figure 2: Ucn3 expression in SC-ILCs does not correlate with improved function.

A) Immunostaining for insulin (green), glucagon (blue) and Ucn3 (red) in adult human pancreas (a), and end-stage cells collected after differentiation using Protocols A (b) and B (c). Images of individual channels are the same magnification as the merged images. Scale bars are 50 microns.

B) Quantification of co-localization of Ucn3 with insulin in adult human pancreas, Pro A or Pro B. **C)** Quantification of co-localization of Ucn3 with glucagon in adult human pancreas, Pro A or Pro B. **D)** Gene expression of *UCN3* normalized to beta-actin, relative to undifferentiated cells (H1) in adult human pancreas, Pro A or Pro B.

E) Static GSIS assay to assess insulin secretion in response to low glucose (LG, 2.8 mM), high glucose (HG, 28 mM) and KCl (30 mM) measured by the concentration of human C-Pep in the supernatant (pmol C-Pep/IEQ). **F)** Glucose-mediated stimulation index (SI) (C-pep secreted under high glucose / C-pep secreted under low glucose) calculated from the static GSIS assay. **G)** Potassium-mediated SI (C-pep secreted under KCl / C-pep secreted under low glucose) calculated from the static GSIS assay.

Ucn3 is highly expressed in human fetal islets, long before attainment of functional maturation

To further explore the relevance of Ucn3 as a maturation marker in human islets, HFP was compared to adult pancreas tissue and AHI to assess gene expression, protein localization and function. Co-staining of HFP tissues with Ucn3, Ins, and Gcg revealed that Ucn3 is strongly expressed in both Ins^+ and Gcg^+ cells at early fetal stages (17-20 gestational weeks) (Fig. 3A). Quantification of co-localization of Ucn3 with Ins (Fig. 3B) and Gcg (Fig. 3C) indicates that most

Gcg^+ area co-expresses Ucn3 at both developmental time points, while an even higher Ins^+Ucn3^+ area was found in HFP compared to adult pancreas.

To assess gene expression of *UCN3* in HFP compared to AHI and SC-ILCs, *UCN3* and Chromogranin A (*CHGA*) gene expression was measured. HFP contains developing mesenchymal, exocrine, duct and endocrine tissue, while isolated adult islets are primarily endocrine cells, therefore the gene expression levels in these samples required normalization for comparison. *CHGA* was selected for normalization because it is expressed at high levels in both alpha and beta cells (see Fig. 6E), its expression precedes that of hormones in endocrine cell development, and it is not lost with de-differentiation in beta cell failure. For these reasons, we felt that *CHGA* rather than a gene like *INS* was better for normalization, because insulin expression itself is lower in immature cells and is lost in de-differentiated states [32-34]. Thus, the ratio of *UCN3*/*CHGA* was used to normalize to the fraction of RNA derived from the endocrine cells only. The ratio of *UCN3*/*CHGA* was not significantly different between AHI and HFP (Fig. 3D). Although it has been well established that prenatal human islets lack mature function, we assessed function in HFP compared to AHI using a static GSIS assay. Not surprisingly, HFP had significantly reduced C-Pep secretion at all stages of the GSIS compared to AHI (Fig. 3E). To normalize the number of islets loaded into each GSIS replicate and because the fetal islets could not be accurately counted, GSIS results are presented as a percentage of the total insulin content of each sample. HFP had a stimulation index (SI), as defined by insulin secreted in high (28 mM) glucose over insulin secreted in low (2.8 mM) glucose, of 1.1 (Fig. 3F), reflecting no stimulation, while C-Pep secretion was stimulated by potassium (Fig. 3G).

Ucn3 is expressed in polyhormonal cells in both primary fetal pancreas and SC-ILCs

Polyhormonal cells that co-express multiple endocrine hormones, such as insulin and glucagon, are known to be an immature cell type in the developing pancreas [15, 35]. Although rare in HFP at gestational week 17 and older, we identified $Ins^{+}Gcg^{+}$ cells that also co-expressed $Ucn3^{+}$ (Fig. 4A). Polyhormonal cells are also generated by some SC-ILC differentiation protocols, and are considered to be an undesirable immature cell type. $Ins^{+}Gcg^{+}Ucn3^{+}$ cells were also found in Protocol B (Fig. 4B). The existence of $Ins^{+}Gcg^{+}Ucn3^{+}$ in both normal human fetal pancreas and SC-ILCs is therefore a striking example of how Ucn3 is present well before beta cell maturation occurs.

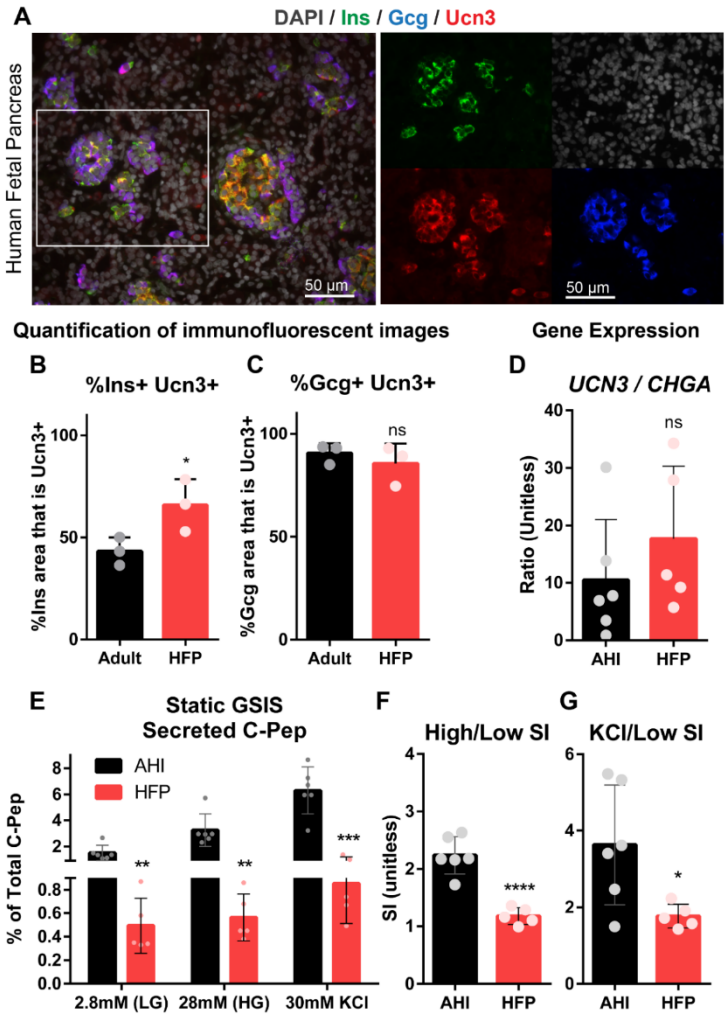

Figure 3: Ucn3 is highly expressed in human fetal islets, long before attainment of functional maturation.

A) Immunostaining for insulin (green), glucagon (blue) and Ucn3 (red) in human fetal pancreas (HFP).

B) Quantification of co-localization of Ucn3 with insulin in adult human pancreas and HFP. **C)** Quantification of co-localization of Ucn3 with glucagon in adult human pancreas and HFP. **D)** Gene expression of *UCN3* normalized to *CHGA* in adult human islets (AHI) and HFP.

E) Static GSIS assay to assess insulin secretion in response to low glucose (LG, 2.8 mM), high glucose (HG, 28 mM) and KCl (30 mM) measured by the concentration of human C-Pep in the supernatant as a percentage of total C-Pep content. **F)** Glucose-mediated stimulation index (SI) (C-pep secreted under high glucose / C-pep secreted under low glucose) calculated from the static GSIS assay. **G)** Potassium-mediated SI (C-pep secreted under KCl / C-pep secreted under low glucose) calculated from the static GSIS assay.

(Previous Page)

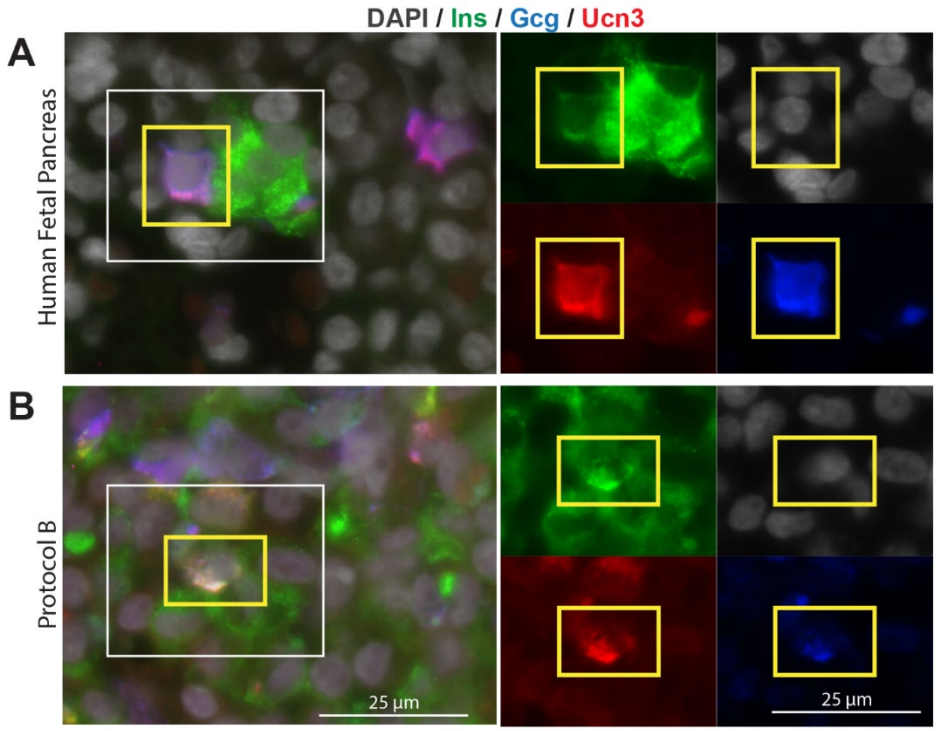

Figure 4: Ucn3 is expressed in polyhormonal cells in both primary fetal pancreas and SC-ILCs.

A) In normal human fetal pancreas (HFP), polyhormonal (Ins^+Gcg^+) cells are considered to be immature and can be found to already express Ucn3. **B)** In SC-ILCs derived with Protocol B, $Ucn3^+Ins^+Gcg^+$ triple-positive cells can also be found. Images of individual channels are the same magnification as the merged images. Scale bars are 25 microns.

Gene expression of candidate maturation markers in AHI, HFP and SC-ILCs

Having established the abundant expression of Ucn3 prior to islet functional maturation in human tissues, we employed the same resources and methods to interrogate other candidate maturation markers. Due to the practical application of quantitative real-time PCR (QPCR) in assessing expression of maultiple genes across large numbers of samples, we used QPCR is often used to evaluate SC-ILC differentiations both at the end stage and at distinct stages throughout the protocols. The expression levels of an array of candidate maturation marker genes were measured with QPCR in human fetal pancreas (HFP), adult human islets (AHI), and protocols A and B (Fig. 5). For all genes, *CHGA* was used for normalization. Genes encoding glucose transporters Glut1 and Glut2 (*SLC2A1* and *SLC2A2*, respectively) are presented as a ratio relative to one another; more detailed gene expression data for these two genes is included in Supplemental Fig 1.

The results indicate that several genes (e.g. *ARNTL*, *ERO1LB*, *HOPX*, *SLC30A8*) did not have increased expression from fetal to adult islets, and therefore may not correlate with maturation. In contrast, many genes (e.g. *CHGB*, *FAM159B*, *IAPP*, *MAFA*, *SIX2*, *SIX3*, *SYT4*) did have significant differences between fetal it islets that suggests increased expression with maturation. Interestingly, most genes assessed in our study had low expression in SC-ILCs relative to adult islets, but some genes had expression in SC-ILCs that was similar to HFP (e.g. *G6PC2*, *SIX2*, *SIX3*) while others were significantly lower in SC-ILCs compared to HFP (e.g. *CHGB*, *FAM159B*, *IAPP*, *MAFA*, *SYT4*).

Specificity of beta cell maturation markers in human development

To further validate the gene expression data, proteins of interest were assessed with immunofluroescent (IF) staining on human fetal and adult pancreas sections (Fig. 6). Where possible, antibodies used for this study were matched to those used in the previous studies that had established the protein as a maturation markers. Each candidate marker (red) was co-stained with insulin (green). When possible, accounting for antibody species and cross-reactivity, some markers were also co-stained with glucagon (blue). Images were used to quantify protein localization and expression differences between fetal and adult beta cells, and specificity of the maturation marker expression in islets compared to other pancreatic cells types, such as the exocrine or ductal cells (Supplemental Fig. 2).

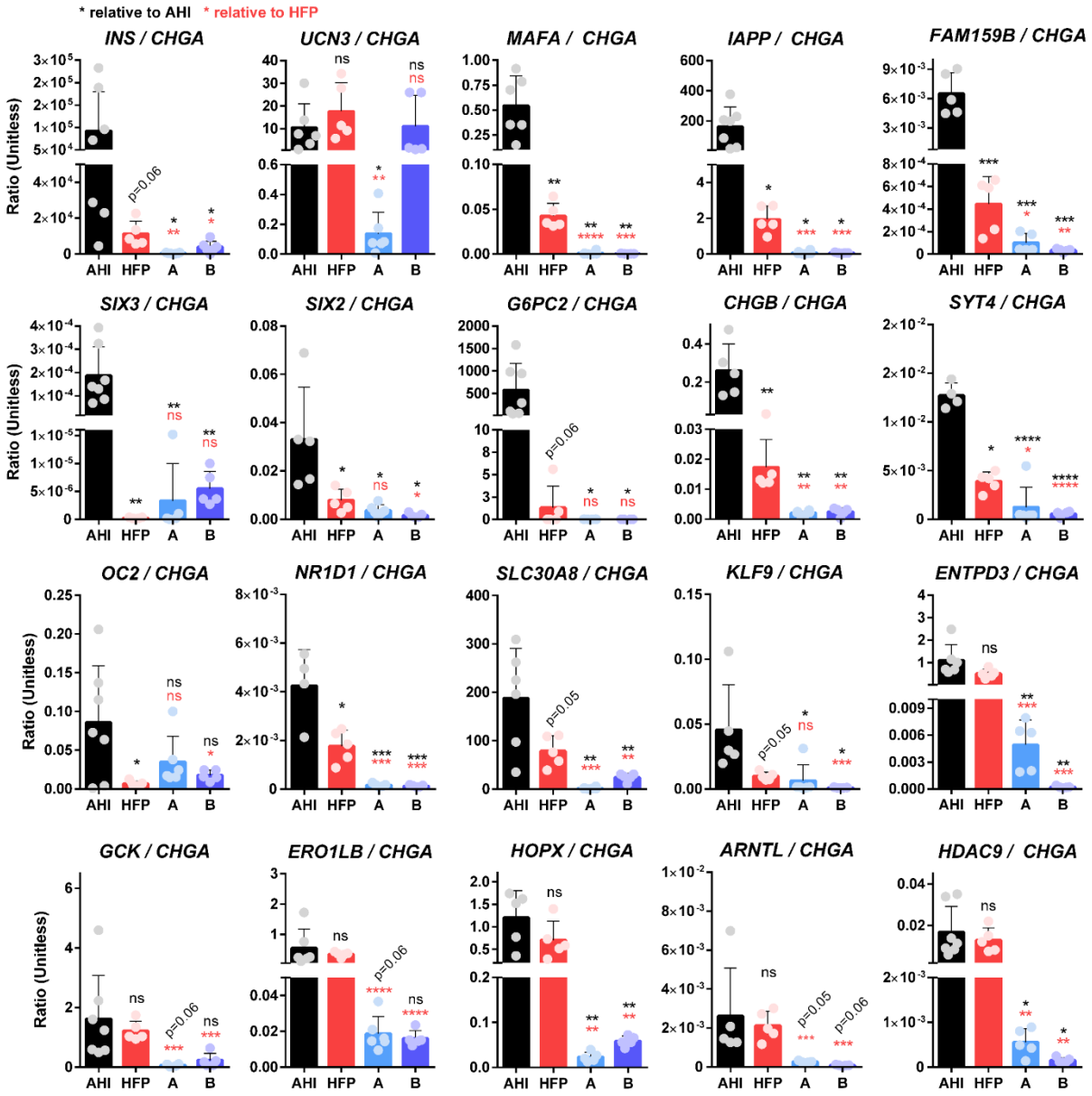

Figure 5: Gene expression of candidate maturation markers in AHI, HFP and SC-ILCs.

QPCR-based analysis of gene expression of several candidate maturation markers in adult human islets ("AHI"), human fetal pancreas ("HFP") and Protocols A ("A") and B ("B"). All genes were normalized to beta-actin within the same sample, then normalized to undifferentiated H1 cells and presented as a ratio of gene expression over *CHGA* to normalize for differences in endocrine mass between the various samples. Statistics relative to AHI are represented in black font, and relative to HFP are represented in red font.

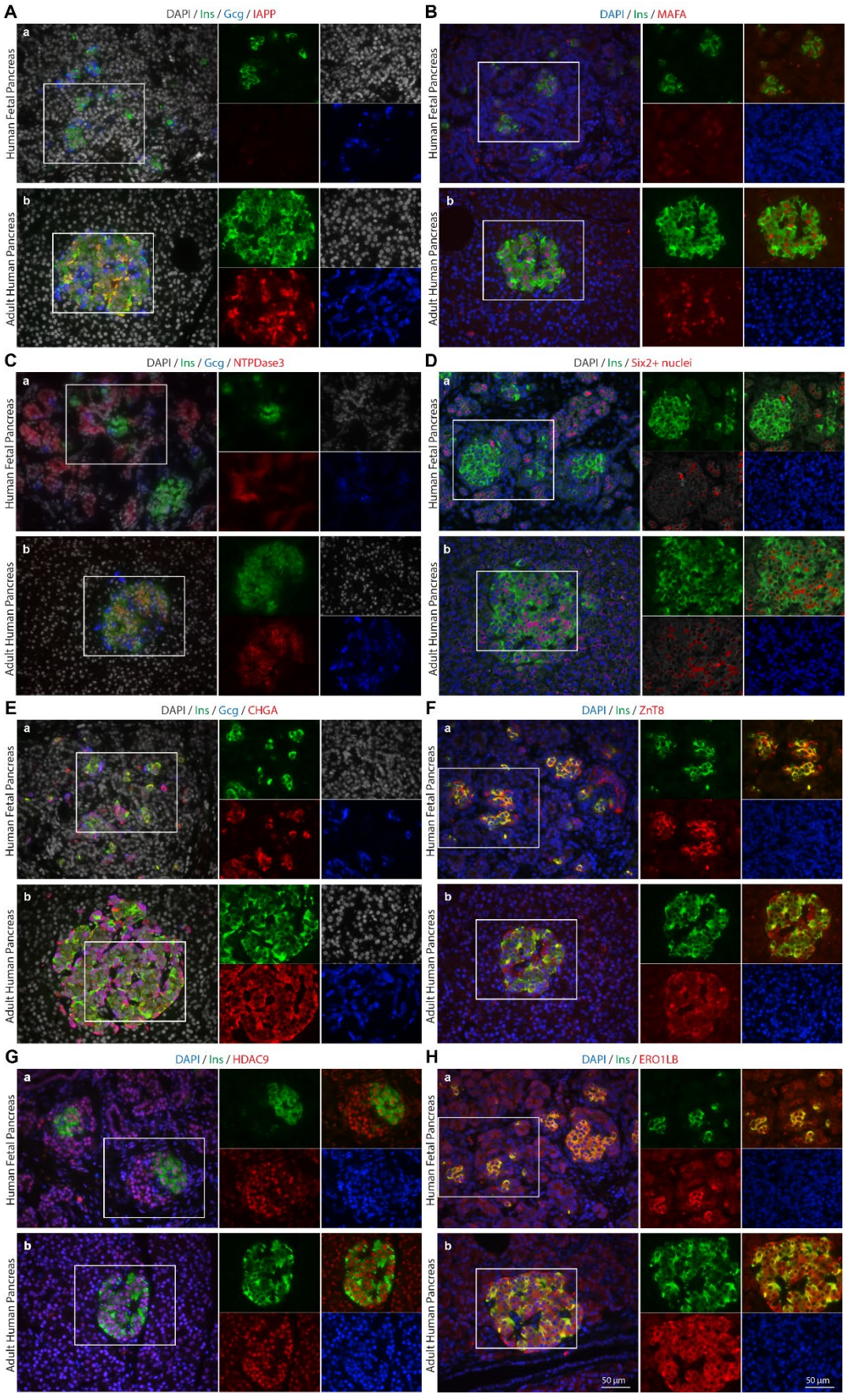
A
DAPI / Ins / Gcg / IAPP
B
DAPI / Ins / MAFA
C
DAPI / Ins / Gcg / NTPDase3
D
DAPI / Ins / Six2+ nuclei
E
DAPI / Ins / Gcg / CHGA
F
DAPI / Ins / ZnT8
G
DAPI / Ins / HDAC9
H
DAPI / Ins / ERO1LB
Human Fetal Pancreas
Adult Human Pancreas
a
b
50 µm

Figure 6: Markers that correlate with beta cell maturation in human development

Immunofluorescent staining of candidate human beta cell maturation markers reveals significant increase in beta cell-specific expression of the markers IAPP **(A)**, MAFA **(B)**, NTPDase3 **(C)**, Six2 **(D)**, CHGA **(E)**, ZnT8 **(F)**, HDAC9 **(G)**, ERO1LB **(H)** from fetal to adult stages. Each candidate maturation marker is indicated in red and insulin is indicated in green. Individual channel images are the same magnification as the larger merged images. Scale bars = 50 microns. **(Previous page)**

Discussion

Our study establishes that, while *UCN3* has been a useful beta cell maturation marker in mouse development, this principle does not translate to human beta cells. *UCN3* is highly expressed in fetal human pancreas, in both alpha and beta cells, and can be expressed in immature polyhormonal cells. We also report that high levels of *UCN3* expression in SC-ILCs does not correlate with an improvement in GSIS function as seen in Protocol B of this study. Together, these data suggest that *UCN3* may not be useful to identify a more mature population of SC-ILCs, but intriguingly also reveals that *UCN3* expression is abnormally delayed in almost every published SC-ILC differentiation protocol, where SC-ILCs resemble fetal-like beta cells in some ways but *UCN3* expression remains nearly undetectable [5, 6, 22]. Our data showing Ucn3 gene and protein expression in human fetal islets corroborates previous data sets that have also indicated that *UCN3* is expressed in human fetal islets [20, 21]; nonetheless Ucn3 has been touted as a maturation marker in many studies and reviews [14].

We similarly find that *MAFA* expression, which has been notoriously absent in SC-ILC protocols, is present in early fetal beta cells, and has ten-fold increased expression from fetal to adult stages (Fig. 6B). While previous studies found that *MAFA* expression increases two-fold during postnatal maturation from human neonatal to adult beta cells [11], SC-ILC *MAFA* expression in our study and other published protocols appears to be significantly lower than that

of human fetal islets (Fig. 5, Supplemental Fig. 3). This suggests that very low *MAFA* expression at the final stage of *in vitro* differentiation and the subsequent increase in *MAFA* expression after transplantation is not comparable to postnatal maturation as suggested in several previous reports; low *MAFA* expression in culture may indeed be indicative of immature beta cells.

In addition to *MAFA*, the genes *SIX2*, *SIX3*, and *ONECUT2* (*OC2*) were identified by Arda *et al.* to exhibit significantly increased expression as human beta cells transition from neonatal to adult stages [11]. *SIX2* and *SIX3* in particular have also been identified affect GSIS function in SC-ILCs and primary human islets [5, 36, 37]. Balboa *et el.* found that while *SIX2* expression was present during *in vitro* SC-ILC differentiation, *SIX3* was not expressed even weeks following transplantation [5]. *OC2* is expressed in pancreas progenitor cells and involved in regulation of *NGN3* [38], but was found to be expressed again later in mature beta cells [11]. OC2 expression has been shown to be regulated by microRNAs and reduced OC2 coincides with defective insulin secretion [39]. In our study, we find that the relative expression of *OC2*, *SIX2* and *SIX3* genes are significantly lower in fetal compared to adult pancreas, which supports the notion that they represent potential maturity markers.

Our data substantiates previous findings about ectonucleoside triphosphate diphosphohydrolase-3 (NTPDase3, encoded by the gene *ENTPD3*) as a beta cell-specific marker in human development (Fig. 6C) [40]. *ENTPD3* has also been shown to mark a functionally mature subset of SC-ILCs and is useful for selecting that subset from the total population of differentiated cells [41]. Changes in glucose-sensitive purine synthesis and metabolic ATP trafficking that occur with beta cell maturation in postnatal islets could have a connection to NTPDase3 function, providing a possible mechanistic role for this gene during functional maturation [14, 42]. This

suggests that NTPDase3 may be both a genuine beta cell maturation marker in normal human development, and directly play a role in beta cell function. However, NTPDase3 is expressed in fetal and neonatal acinar, while absent in fetal and neonatal islets – this expression shifts to exclusively beta cell-specific in adulthood [40] (Fig. 6C). These expression patterns are important for the use of this marker to sort mature cells from native tissues or differentiated SC-ILCs.

IAPP is stored in the same vesicles as, and co-secreted with, insulin. Upon glucose stimulation, serum IAPP concentrations mirror of that insulin, and IAPP has putative function at distant sites as well as locally at the islet, in inhibiting both insulin and glucagon secretion [43]. IAPP in humans can form pathologic amylin deposits associated with the progression of T2D [44], however mouse IAPP is not capable of forming these plaques – another example of differences in these proteins between mouse and human islet biology. Due to the role IAPP has in feedback inhibition of islet endocrine function, and because IAPP has been found to increase in beta cell differentiation along a pseudo-time scale [8], IAPP has been suggested as a marker of beta cell maturation. Our results reveal that indeed, IAPP expression significantly increases from human fetal to adult islets (Fig. 6A) and is critically deficient in our SC-ILCs which lack function, pointing to IAPP as a potential reliable marker of maturation.

The same secretory vesicles require Zn^{2+} for proper formation, maturation, and function, which relies on the islet-specific zinc transporter, ZnT8 encoded by the gene *SLC30A8* [45]. In humans, several ZnT8 SNPs have been associated with altered T2D risk in GWAS studies [46]. Our results indicate that ZnT8 is expressed at about equal levels in fetal and adult human islets (Fig. 6F). Interestingly, Zn^{2+} transport plays a role in the stability and solubility of IAPP, where ZnT8 dysfunction can lead to IAPP amyloid deposition [44]. It is possible that ZnT8 expression precedes

IAPP expression in order to provide the appropriate environment for healthy IAPP function, and this may an important consideration for supporting healthy function of SC-ILCs.

Other proposed markers of beta cell maturation have direct roles in glucose sensing and metabolism. Glut1 and Glut2 (transcribed from *SLC2A1* and *SLC2A2*, respectively) have an essential role in glucose transport into islet cells, and have established differences in expression between human and rodent islets [47]. Glucokinase (*GCK*) plays a central role in glucose processing prior to glycolysis and is considered a key factor in islet glucose sensing [48]. Glucose-6-phosphatase catalytic subunit 2 (*G6PC2*) is a negative inhibitor of GSIS and has been found to have reduced levels in T2D samples compared to nondiabetic islets, and increased expression in SC-ILCs with improved function, implicating this gene in maturation [14, 49]. In our study, we find that the relative levels of *SLC2A1*, *SLC2A2*, and *GCK* do not change between fetal and adult islets, while *G6PC2* expression is significantly increased from fetal to adult.

The histone deacetylase HDAC9 was identified in mice as part of a group of HDACs that control beta and delta cell mass; HDAC9 is enriched in mouse beta cells and mediates activation of metabolic genes in response to fasting, suggesting it may play a role in beta cell functional maturation [50, 51]. In contrast to these findings in mice, we find that *HDAC9* expression is not significantly different between fetal and adult human islets, although it is relatively deficient in SC-ILCs. HDAC9 protein localizes to the beta cell nuclei in higher abundance than in other pancreatic cell types, but does not correlate with beta cell maturation (Fig. 6G).

ERO1LB is an endoplasmic reticulum disulfide oxidase that supports protein processing and folding in the ER and may be involved in ER stress response. High basal levels of ERO1LB in

pancreatic islets and the fact that reduced ERO1LB activity compromises folding of proinsulin and promotes glucose intolerance has resulted in interest in the role ERO1LB has in beta cell health and maturation [26, 27]. We find that *ERO1LB* indeed has high expression in human pancreatic islets, but that this expression both at the gene and protein level, does not change between fetal and adult stages of development (Fig. 6H).

In recent years, significant improvements in SC-islet *in vitro* function have been achieved [5, 6, 22]. Despite this progress, it is clear that expression of certain key genes (e.g. MAFA, Six2, Six3) *in vitro* is deficient compared to primary human islets, and that after transplantation the cells undergo changes, which include improved beta cell maturation [4, 5, 52], but also includes subpopulations of end-stage cells differentiating into off-target cell types [4]. Cell sorting prior to transplantation to purify cells using a variety of different markers has been shown to improve graft outcomes – avoiding the risk of teratoma formation, leading to a decreased population of off-target cell types and a more pure and functional population of pancreatic endocrine cells [6, 8, 53, 54]. Cell sorting is relatively inefficient, requiring a large number of cells and only isolating a fraction of the total targeted population, and is stressful and damaging to the recovered cells. The fact that end-stage SC-islets require purification prior to transplantation [6, 8], and the fact that significant biological changes occur in the cells following transplantation [4] suggest that SC-islet differentiation protocols may require further improvements in order to achieve the safe, stable, and functional differentiated *in vitro* product that is desirable for clinical application. A better understanding of phenotypic gene expression profiles that mark a stable, mature beta cell will guide this process.

In summary, understanding the normal expression profiles of potential maturation markers in human islets is essential to generating functional and safe SC-ILCs. While certain markers that we have identified do not have significant differences in expression between fetal and adult islets (Ero1LB, HDAC9, GCK, Glut1, Glut2, Ucn3, ZnT8), it is notable that the expression of many of these markers remain deficient in the SC-ILCs derived by these two differentiation protocols, and therefor merit further attention to ensure proper expression is achieved in future protocols. Markers that are significantly different between adult and fetal islets (G6PC2, IAPP, MafA, OC2, SIX2, SIX3), may have further application to help improve identification of mature beta cells and possibly to unravel roles these genes play in the onset of maturation. Furthermore, many of these markers have been found to change in expression with the progression of diabetes, and thus, a better understanding of the roles of these maturation-associated genes in normal islet function may inform future therapies to prevent or treat diabetes.

Methods

Tissue procurement and ethics

Human fetal pancreas tissue was obtained from secondary sources (Advanced Biosystems Resources, Inc.) under approved Material Transfer Agreements and with protocols approved by the University of Wisconsin's Institutional Animal Care and Use Committee (IACUC) and Institutional Review Board (IRB) (IRB Study #2013-141). ABR, Inc. obtains consent in accordance with Uniform Anatomical Gift Act (UAGA) and National Organ Transplant Act (NOTA) guidelines. ABR, Inc. warrants that appropriate consent for tissue donation is obtained and adequate records of such consents are maintained. In addition, that tissues are obtained with local, state, and federal laws and regulations governing the procurement of human tissue. Within 24 hours of recovery, the organs were received and cleaned of surrounding connective tissue. Small pieces of tissue were removed and fixed with 4% PFA for paraffin embedding, or equilibrated in 30% sucrose and OCT-embedded. Other pieces were immediately lysed in TRIzol (ThermoFisher, 15596026) for RNA extraction. Two small pieces of tissue (ranging from 5-10 mg in weight) from each donor were also immediately washed and used for functional studies (GSIS).

Adult human pancreas tissue was procured by the University of Wisconsin Organ and Tissue Donation Services from donors with no indication of diabetes or pancreatitis, with consent obtained for research from next of kin and authorization by the University of Wisconsin-Madison Health Sciences Institutional Review Board (IRB granted an exempt from protocol approval for studies on post-natal tissue because research on deceased donors is not considered human subjects research). IRB oversight of the project is not required because it does not involve human subjects as recognized by 45 CFR 46.102(f) which defines a 'human subject' as "a living individual

about whom an investigator (whether professional or student) conducting research obtains (1) data through intervention or interaction with the individual, or (2) identifiable private information." Following organ harvest, pancreata were allocated for research if deemed unfit for transplantation due to vascular damage during organ recovery, no suitable recipient, and non-ideal age or BMI. The organs were received within 24 hours of recovery and trimmed of extra-pancreatic connective tissues, including duodenum, large arteries and veins. The parenchyma was cut into 1 cm^3 cubes and fixed with 4% PFA for paraffin embedding, or equilibrated in 30% sucrose and OCT-embedded.

All donor tissues used are summarized in Supplemental Table 4.

Human Islets

Human islets were received through the Integrated Islet Distribution Program (IIDP) and experiments were performed within 48 hours of receipt. Islets used for QPCR were lysed with TRIzol (ThermoFisher, 15596026) for gene expression analysis.

All human islets used in this study are summarized in Supplemental Table 4.

Cell Culture and Differentiation

H1 cells were differentiated toward a pancreatic endocrine fate using protocols based on Xu et al. (2011) [28], Rezania *et al.* (2014) [29], Pagliuca *et al.* (2014) [30], Nostro *et al.* (2015) [15] and Zhu *et al.* (2016) [31]. Media components for each stage of differentiation for both Protocol A and Protocol B are included in detail in Supplemental Tables 1-3. To initiate the differentiation,

H1 colonies were treated with ROCK-Inhibitor for 4 h (Y-27632) and plated as single cells onto Matrigel-coated 6-well Transwell plates (Corning, 3450) at a density of $1.5x10^5$ cells per cm^2 surface area. Standard E8 medium (ThermoFisher, A1517001) was added to both sides of the Transwell to expand the cells before differentiation was initiated (1-2 days). When the cells covered the Transwell membranes at near 100% confluence, Stage 1 was initiated, this was considered “Day 0”. Full medium changes were made every day thereafter until the end of Stage 4, in accordance with Supplemental Tables 1 and 2. At the end of Stage 4, cells were transferred into suspension culture. During Stage 5, media was changed 50% each day. In Stages 6, 7 and 8, media was fully changed every other day, as indicated in Supplemental Tables 1-3.

Glucose Stimulated Insulin Secretion (GSIS)

Static GSIS Assays were performed in series, in 24-well plates with cell filter inserts (MilliporeSigma, St. Louis, MO). Cells were added to the filters and moved from low glucose (2.8 mM) to high glucose (28 mM) to low glucose (2.8 mM) to a depolarization solution (30 mM KCl, 2.8 mM glucose). All solutions for GSIS were made in Krebs buffer (25 mM HEPES, 115 mM NaCl, 24 mM NaHCO3, 5 mM KCl, 1 mM MgCl2, 2.5 mM CaCl2, 1% BSA). The supernatant was collected following 1 hour in each step of the GSIS for secreted C-pep measurement. For human islets, 100 IEQ were used per well. For differentiated SC-ILCs, 500 IEQ were used per well. Supernatants collected from each treatment were frozen in aliquots.

For HFP tissue and primary islets, following GSIS, cells were lysed in 1 mL of lysis buffer (20 mM Tris-HCl, pH 7.5, 150 mM NaCl, 1 mM EDTA, 1% Triton) and homogenized with a PowerGen 500 homogenizer (ThermoFisher, Waltham, MA); these lysates were used to measure

total C-peptide content. C-peptide content for all lysates and supernatants were determined with an ultra-sensitive human C-pep ELISA (Mercodia, Uppsala, Sweden). Stimulation index (SI) for the static GSIS was calculated by dividing the average secreted C-Peptide concentration under high glucose by the average C-Peptide secreted under the first low glucose period.

Immunofluorescent (IF) Staining

For most antibodies, formalin-fixed paraffin embedded (FFPE) sections were used. 5 micron paraffin sections were deparaffinized using xylene and rehydrated. Antigen retrieval was performed by treatment with 10mM Citrate Buffer, pH6.0 for 2 hours in an 80˚C water bath. Slides were blocked with 10% BSA/1x PBS for 1 h at room temperature, incubated with primary antibodies overnight at 4˚C, washed, incubated with secondary antibodies for 40 min at room temperature.

For antibodies that did not react with FFPE sections (NTPDase3), frozen sections were used. 5 micron sections were cut from unfixed OCT-embedded tissues, warmed to room temperature for 15 minutes and fixed in 4% PFA for 15 minutes. Slides were washed, blocked and stained following the same protocol as FFPE sections.

The antibodies and dilutions used are listed in Supplemental Table 5. Nuclei were counterstained with 40-6-diamidino-2-phenylindole (DAPI). Images were generated with a Zeiss Axiovert 200M microscope.

QPCR

All samples were lysed in TRIzol (ThermoFisher, 15596026) and RNA was extracted using the QIAprep Spin Miniprep kit (QIAGEN, 27104). cDNA was prepared from extracted RNA using the Omniscript RT kit (QIAGEN, 205113). Quantitative Real-Time Polymerase Chain Reaction (QPCR) was performed using the TaqMan Real-Time PCR Master Mix (ThermoFisher, 4304437) and Taqman Gene Expression Assay Primers (ThermoFisher) listed in Supplemental Table 6.

Image Quantification

Images were quantified using ImageJ. For co-localization measurements, the JACoP plugin [55] was used and Mander's coefficients quantified. For proteins that localize to the nucleus, total nuclei were counted using Measure Particles in ImageJ on the binary DAPI channel and individual nuclei were counted in Ins^+ or Ins^- cells to determine the percentage of positive cells for each group. For SIX2, to clean up non-specific signal in the images for quantification, merged images were generated between the DAPI and SIX2 channels to establish the "SIX2+ nuclei" overlap. The merged image clearly revealed localization of SIX2 to the nuclei of the adult islets only and absence in the fetal tissues, in correlation with previous studies using the same antibody [11].

Acknowledgments

We would like to offer a special thanks to the donor families who donated tissues, without which this study would not be possible. We acknowledge the support of the Integrated Islet Distribution Program (IIDP) (National Institutes of Health Grant 2UC4DK098085), National Institutes of Health and members of the Fernandez lab for generating islets and providing access to islet donor data. We would like to thank the University of Wisconsin Optical Imaging Core and Lance Rodenkirch for technical assistance on the confocal microscope. We thank the Department of Surgery Histology Core, Sierra Raglin and Becky Lyons for help processing and cutting tissue blocks.

References:

1. Wang, P., et al., *Diabetes mellitus--advances and challenges in human beta-cell proliferation.* Nat Rev Endocrinol, 2015. **11**(4): p. 201-12.
2. Salinno, C., et al., *beta-Cell Maturation and Identity in Health and Disease.* Int J Mol Sci, 2019. **20**(21).
3. Tremmel, D.M., et al., *Mimicking nature-made beta cells: recent advances towards stem cell-derived islets.* Curr Opin Organ Transplant, 2019. **24**(5): p. 574-581.
4. Augsornworawat, P., et al., *Single-Cell Transcriptome Profiling Reveals beta Cell Maturation in Stem Cell-Derived Islets after Transplantation.* Cell Rep, 2020. **32**(8): p. 108067.
5. Balboa, D., et al., *Functional, metabolic and transcriptional maturation of human pancreatic islets derived from stem cells.* Nat Biotechnol, 2022.
6. Nair, G.G., et al., *Recapitulating endocrine cell clustering in culture promotes maturation of human stem-cell-derived beta cells.* Nat Cell Biol, 2019. **21**(2): p. 263-274.
7. Schulz, T.C., et al., *A scalable system for production of functional pancreatic progenitors from human embryonic stem cells.* PLoS One, 2012. **7**(5): p. e37004.
8. Veres, A., et al., *Charting cellular identity during human in vitro beta-cell differentiation.* Nature, 2019. **569**(7756): p. 368-373.
9. Shapiro, A.M.J., et al., *Insulin expression and C-peptide in type 1 diabetes subjects implanted with stem cell-derived pancreatic endoderm cells in an encapsulation device.* Cell Rep Med, 2021. **2**(12): p. 100466.
10. Helman, A., et al., *A Nutrient-Sensing Transition at Birth Triggers Glucose-Responsive Insulin Secretion.* Cell Metab, 2020. **31**(5): p. 1004-1016 e5.
11. Arda, H.E., et al., *Age-Dependent Pancreatic Gene Regulation Reveals Mechanisms Governing Human beta Cell Function.* Cell Metab, 2016. **23**(5): p. 909-20.
12. Otonkoski, T., et al., *Maturation of insulin response to glucose during human fetal and neonatal development. Studies with perifusion of pancreatic isletlike cell clusters.* Diabetes, 1988. **37**(3): p. 286-91.
13. Aye, T., et al., *Identification of markers for newly formed beta-cells in the perinatal period: a time of recognized beta-cell immaturity.* J Histochem Cytochem, 2010. **58**(4): p. 369-76.
14. Barsby, T. and T. Otonkoski, *Maturation of beta cells: lessons from in vivo and in vitro models.* Diabetologia, 2022.
15. Nostro, M.C., et al., *Efficient generation of NKX6-1+ pancreatic progenitors from multiple human pluripotent stem cell lines.* Stem Cell Reports, 2015. **4**(4): p. 591-604.
16. Li, C., et al., *Urocortin III is expressed in pancreatic beta-cells and stimulates insulin and glucagon secretion.* Endocrinology, 2003. **144**(7): p. 3216-24.

17. Li, C., et al., *Urocortin 3 regulates glucose-stimulated insulin secretion and energy homeostasis.* Proc Natl Acad Sci U S A, 2007. **104**(10): p. 4206-11.

18. Blum, B., et al., *Functional beta-cell maturation is marked by an increased glucose threshold and by expression of urocortin 3.* Nat Biotechnol, 2012. **30**(3): p. 261-4.

19. van der Meulen, T., et al., *Urocortin 3 marks mature human primary and embryonic stem cell-derived pancreatic alpha and beta cells.* PLoS One, 2012. **7**(12): p. e52181.

20. Hrvatin, S., et al., *Differentiated human stem cells resemble fetal, not adult, beta cells.* Proc Natl Acad Sci U S A, 2014. **111**(8): p. 3038-43.

21. van der Meulen, T. and M.O. Huising, *Maturation of stem cell-derived beta-cells guided by the expression of urocortin 3.* Rev Diabet Stud, 2014. **11**(1): p. 115-32.

22. Hogrebe, N.J., et al., *Targeting the cytoskeleton to direct pancreatic differentiation of human pluripotent stem cells.* Nat Biotechnol, 2020. **38**(4): p. 460-470.

23. Velazco-Cruz, L., et al., *Acquisition of Dynamic Function in Human Stem Cell-Derived beta Cells.* Stem Cell Reports, 2019. **12**(2): p. 351-365.

24. van der Meulen, T., et al., *Urocortin3 mediates somatostatin-dependent negative feedback control of insulin secretion.* Nat Med, 2015. **21**(7): p. 769-76.

25. Blum, B., et al., *Reversal of beta cell de-differentiation by a small molecule inhibitor of the TGFbeta pathway.* Elife, 2014. **3**: p. e02809.

26. Huang, J.L., et al., *Genetic deletion of Urocortin 3 does not prevent functional maturation of beta cells.* J Endocrinol, 2020. **246**(1): p. 69-78.

27. Zito, E., et al., *ERO1-beta, a pancreas-specific disulfide oxidase, promotes insulin biogenesis and glucose homeostasis.* J Cell Biol, 2010. **188**(6): p. 821-32.

28. Xu, X., V.L. Browning, and J.S. Odorico, *Activin, BMP and FGF pathways cooperate to promote endoderm and pancreatic lineage cell differentiation from human embryonic stem cells.* Mech Dev, 2011. **128**(7-10): p. 412-27.

29. Rezania, A., et al., *Reversal of diabetes with insulin-producing cells derived in vitro from human pluripotent stem cells.* Nat Biotechnol, 2014. **32**(11): p. 1121-33.

30. Pagliuca, F.W., et al., *Generation of functional human pancreatic beta cells in vitro.* Cell, 2014. **159**(2): p. 428-39.

31. Zhu, S., et al., *Human pancreatic beta-like cells converted from fibroblasts.* Nat Commun, 2016. **7**: p. 10080.

32. Moin, A.S.M., et al., *Characterization of Non-hormone Expressing Endocrine Cells in Fetal and Infant Human Pancreas.* Front Endocrinol (Lausanne), 2018. **9**: p. 791.

33. Ramond, C., et al., *Understanding human fetal pancreas development using subpopulation sorting, RNA sequencing and single-cell profiling.* Development, 2018. **145**(16).

34. Talchai, C., et al., *Pancreatic beta cell dedifferentiation as a mechanism of diabetic beta cell failure.* Cell, 2012. **150**(6): p. 1223-34.

35. Teitelman, G., et al., *Precursor cells of mouse endocrine pancreas coexpress insulin, glucagon and the neuronal proteins tyrosine hydroxylase and neuropeptide Y, but not pancreatic polypeptide.* Development, 1993. **118**(4): p. 1031-9.

36. Velazco-Cruz, L., et al., *SIX2 Regulates Human beta Cell Differentiation from Stem Cells and Functional Maturation In Vitro.* Cell Rep, 2020. **31**(8): p. 107687.

37. Bevacqua, R.J., et al., *SIX2 and SIX3 coordinately regulate functional maturity and fate of human pancreatic beta cells.* Genes Dev, 2021. **35**(3-4): p. 234-249.

38. Vanhorenbeeck, V., et al., *Role of the Onecut transcription factors in pancreas morphogenesis and in pancreatic and enteric endocrine differentiation.* Dev Biol, 2007. **305**(2): p. 685-94.

39. Roggli, E., et al., *Changes in microRNA expression contribute to pancreatic beta-cell dysfunction in prediabetic NOD mice.* Diabetes, 2012. **61**(7): p. 1742-51.

40. Saunders, D.C., et al., *Ectonucleoside Triphosphate Diphosphohydrolase-3 Antibody Targets Adult Human Pancreatic beta Cells for In Vitro and In Vivo Analysis.* Cell Metab, 2019. **29**(3): p. 745-754 e4.

41. Docherty, F.M., et al., *ENTPD3 Marks Mature Stem Cell-Derived beta-Cells Formed by Self-Aggregation In Vitro.* Diabetes, 2021. **70**(11): p. 2554-2567.

42. Bartley, C., et al., *Chronic fructose renders pancreatic beta-cells hyper-responsive to glucose-stimulated insulin secretion through extracellular ATP signaling.* Am J Physiol Endocrinol Metab, 2019. **317**(1): p. E25-E41.

43. Westermark, P., A. Andersson, and G.T. Westermark, *Islet amyloid polypeptide, islet amyloid, and diabetes mellitus.* Physiol Rev, 2011. **91**(3): p. 795-826.

44. Xu, J., et al., *Pancreatic beta cell-selective zinc transporter 8 insufficiency accelerates diabetes associated with islet amyloidosis.* JCI Insight, 2021. **6**(10).

45. Wijesekara, N., F. Chimienti, and M.B. Wheeler, *Zinc, a regulator of islet function and glucose homeostasis.* Diabetes Obes Metab, 2009. **11 Suppl 4**: p. 202-14.

46. Davidson, H.W., J.M. Wenzlau, and R.M. O'Brien, *Zinc transporter 8 (ZnT8) and beta cell function.* Trends Endocrinol Metab, 2014. **25**(8): p. 415-24.

47. Berger, C. and D. Zdzieblo, *Glucose transporters in pancreatic islets.* Pflugers Arch, 2020. **472**(9): p. 1249-1272.

48. Matschinsky, F.M. and D.F. Wilson, *The Central Role of Glucokinase in Glucose Homeostasis: A Perspective 50 Years After Demonstrating the Presence of the Enzyme in Islets of Langerhans.* Front Physiol, 2019. **10**: p. 148.

49. Pound, L.D., et al., *G6PC2: a negative regulator of basal glucose-stimulated insulin secretion.* Diabetes, 2013. **62**(5): p. 1547-56.

50. Dorrell, C., et al., *Transcriptomes of the major human pancreatic cell types.* Diabetologia, 2011. **54**(11): p. 2832-44.

51. Wong, R.H., et al., *A role of DNA-PK for the metabolic gene regulation in response to insulin.* Cell, 2009. **136**(6): p. 1056-72.

52. Maxwell, K.G., et al., *Differential Function and Maturation of Human Stem Cell-Derived Islets After Transplantation.* Stem Cells Transl Med, 2022. **11**(3): p. 322-331.

53. Aghazadeh, Y., et al., *GP2-enriched pancreatic progenitors give rise to functional beta cells in vivo and eliminate the risk of teratoma formation.* Stem Cell Reports, 2022. **17**(4): p. 964-978.

54. Parent, A.V., et al., *Development of a scalable method to isolate subsets of stem cell-derived pancreatic islet cells.* Stem Cell Reports, 2022. **17**(4): p. 979-992.

55. Bolte, S. and F.P. Cordelieres, *A guided tour into subcellular colocalization analysis in light microscopy.* J Microsc, 2006. **224**(Pt 3): p. 213-32.

Chapter 7 Supplemental Information

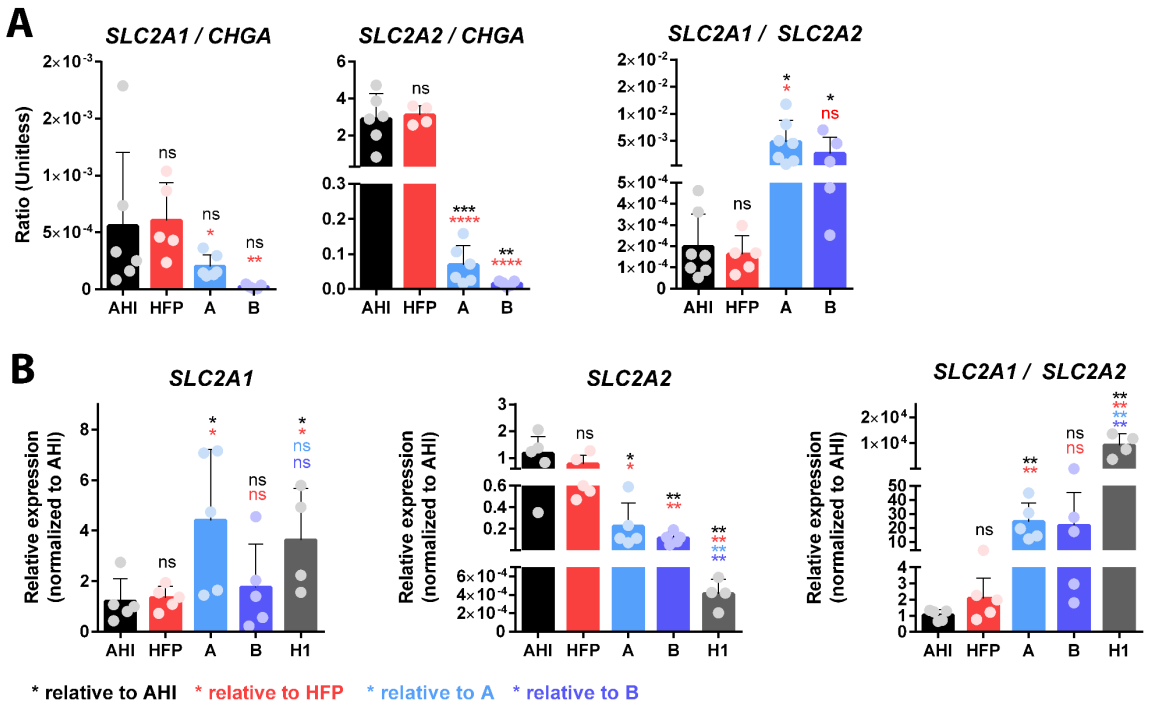

Chapter 7 Supplemental Fig. 1 Expression of glucose transporters Glut1 and Glut2

QPCR-based analysis of gene expression of glucose transporters SLC2A1 (Glut1) and SLC2A2 (Glut2) in adult human islets ("AHI"), human fetal pancreas ("HFP") and Protocols A ("A") and B ("B"). **A)** Gene expression was normalized to beta-actin within the same sample, then normalized to undifferentiated H1 cells and presented as a ratio of gene expression over *CHGA* to normalize for differences in endocrine mass between the various samples. **B)** Gene expression was normalized to beta-actin within the same sample, then normalized to AHI. Statistics relative to AHI are represented in black font, relative to HFP are represented in red font, relative to Protocol A are represented in light blue font, and relative to Protocol B are represented in purple font.

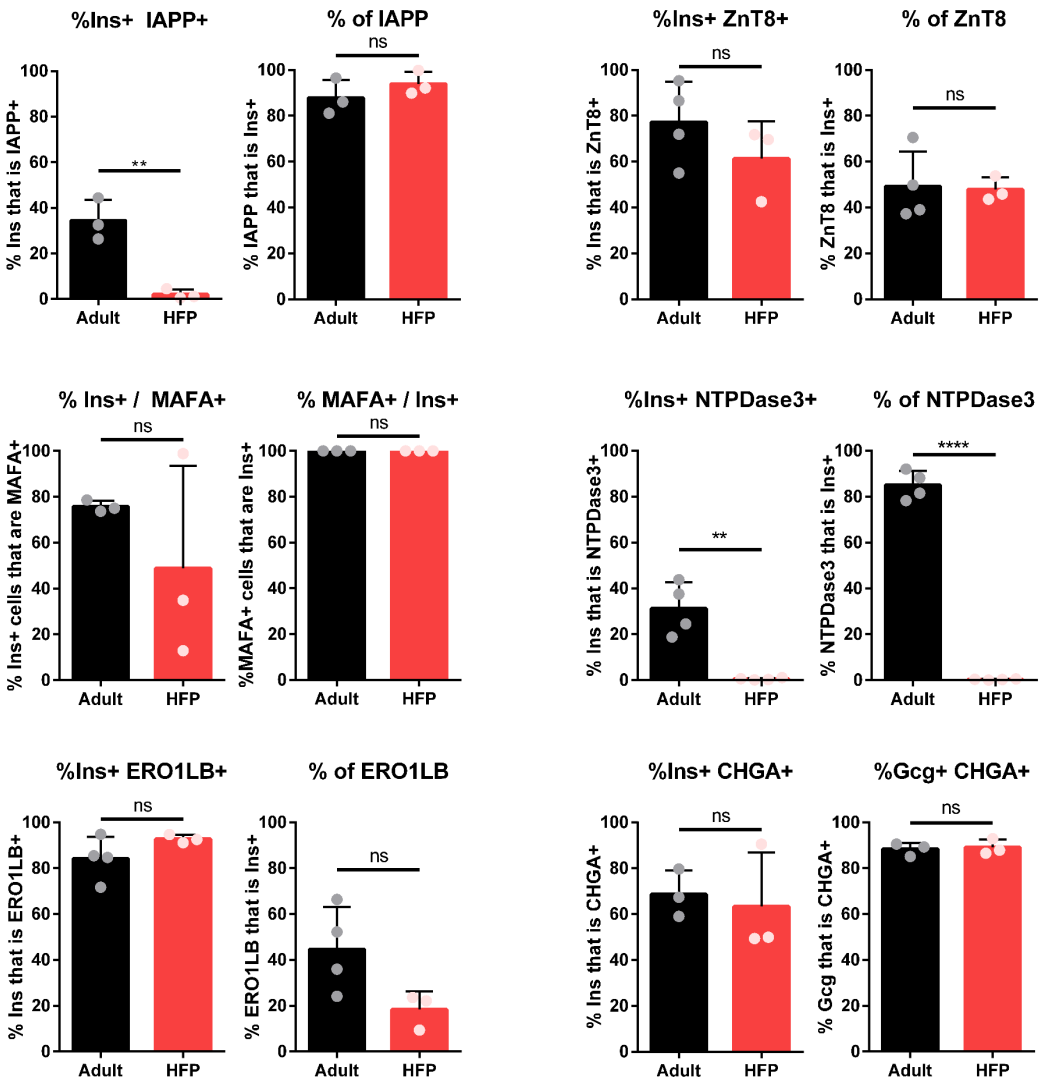

Chapter 7 Supplemental Fig. 2 Quantification of marker localization and beta cell specificity in development.

Immunofluorescent staining of candidate human beta cell maturation markers were quantified to determine co-expression. The percentage insulin co-localized with each marker (%Ins+ *Marker*+) reflects the presence of each marker in adult or fetal beta cells. The percentage of each marker that co-localizes with insulin (%*Marker*) reflects the specificity of the marker to beta cells.

Because MAFA is a nuclear marker and does not co-localize with insulin, MAFA is quantified as the percentage of Ins+ nuclei that are also MAFA+ (left) and the percentage of MAFA+ nuclei that are also Ins+ (right).

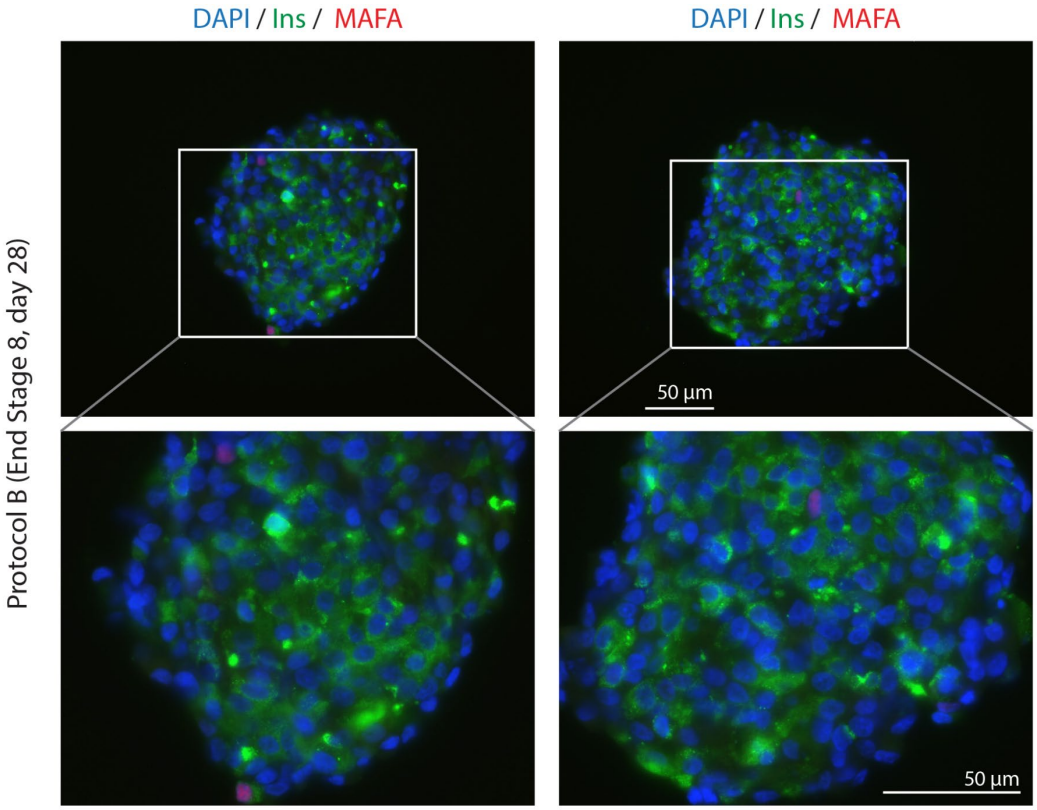

Chapter 7 Supplemental Fig. 3 MAFA expression is low in Protocol B SC-ILCs.

In an effort to validate the accuracy of the MAFA antibody and the findings that MAFA is expressed in human fetal islets, Protocol B SC-ILCs were stained for MAFA (red), demonstrating very low MAFA protein expression which correlates with gene espression data for these cells.

Chapter 7 Supplemental Table 1: Protocol A

	Stage	Day	Media	Supplement											
Adherant	S0 (2d)	d-2	seeded 750,000 cells/well of a 6-well Transwell plate (Corning, 3450)												
		d-1													
	S1 (3d)	d0	Begin differentiation when cells reach ~90% confluency												
		d0	*Basal A1*	**CHIR-99021** 2uM	**Activin A** 100ng/ml	**bFGF** 0.1 ug/ml	**BMP4** 0.01ug/ml								
		d1	*Basal A1*	**CHIR-99021** 0.2uM	**Activin A** 100ng/ml	**bFGF** 0.1 ug/ml	**BMP4** 0.01ug/ml								
		d2	*Basal A1*		**Activin A** 100ng/ml	**bFGF** 0.1 ug/ml	**BMP4** 0.01ug/ml								
	S2 (2d)	d3	*Basal A1*	**Vitamin C** 0.25mM	**FGF7** 50ng/ml	**RA** 0.5uM	**LDN** 100ng/ml	**SB-431542** 2.5mM							
		d4	*Basal A1*	**Vitamin C** 0.25mM	**FGF7** 50ng/ml	**RA** 0.5uM	**LDN** 100ng/ml	-							
	S3 (3d)	d5 - 7	*Basal A2*	**Vitamin C** 0.25mM	**FGF7** 50ng/ml	**RA** 1.0uM	**LDN** 200ng/ml	**Sant-1** 0.25uM	**TPB** 0.2uM	**ITS-X** 0.5 x					
	S4 (3d)	d8 - 10	*Basal A2*	**Vitamin C** 0.25mM	**FGF7** 2ng/ml	**RA** 0.1uM	**LDN** 100ng/ml	**Forskolin** 10uM	**SANT-1** 0.25 uM	**ITS-X** 0.5 x					
Suspension	S5 (3d)	On day 11: S4 cells are treated with 10um Y-27632 for 4 hours, rinsed with PBS -/- and treated with versene for 3-5 mins. Keep cells in clusters, making sure they are not too small. Spin 300xg for spin. Gently resuspend pellet in stage 5 medium - keeping attention to size of clusters, try to keep ~100um. Plate cells into ultra-low attachment plates or T25s													
	S6 (7d)	d11 - 13 *50% change each day*	*Basal A3*	**Nico** 10mM	**ITS-X** 0.5 x	**Alk5i II** 0.01mM	**Heparin** 10ug/ml	**T3** 1.0uM	**LDN** 100ng/ml	**Forskolin** 10uM	**Exendin-4** 0.01uM	**RA** 0.025 uM			
		d14 - 20 *Feed every other day*	*Basal A3*	**Nico** 10mM	**ITS-X** 0.5 x	**Alk5i II** 0.01mM	**Heparin** 10ug/ml	**T3** 1.0uM	**LDN** 100ng/ml	**Forskolin** 10uM	**Exendin-4** 0.01uM	**DAPT** 1 uM			
	S7 (7d)	d21 - 27 *Feed every other day*	*Basal A3*	**Nico** 10mM	**ITS-X** 0.5 x	**Alk5i II** 0.01mM	**Heparin** 10ug/ml	**T3** 1.0uM	**BMP4** 0.01ug/ml	**NAC** 1mM	**Trolox** 10uM	**R428** 2uM			

Chapter 7 Supplemental Table 2: Protocol B

	Stage	Day	Media		Supplement														
Adherant	S0 (2d)	**d-2**	seeded 750,000 cells/well of a 6-well Transwell plate (Corning, 3450)																
		d-1																	
	S1 (3d)	**d0**	Begin differentiation when cells reach ~90% confluency																
		d0	***Basal B1***		**CHIR-99021** 2uM		**Activin A** 100ng/ml												
		d1	***Basal B1***				**Activin A** 100ng/ml		**bFGF** 0.005 ug/ml										
		d2	***Basal B1***				**Activin A** 100ng/ml		**bFGF** 0.005 ug/ml										
	S2 (3d)	**d3 - 5**	***Basal B2***		**Vitamin C** 0.50mM		**FGF10** 50ng/ml		**CHIR-99021** 2uM		**LDN** 100ng/ml								
	S3 (2d)	**d6 - 7**	***Basal B3***		**Vitamin C** 0.285mM		**FGF10** 50ng/ml		**RA** 2.0uM		**LDN** 100ng/ml		**B27 (-VitA)** 1%						
	S4 (3d)	**d8 - 10**	***Basal B3***		**Vitamin C** 0.285mM		**EGF** 100ng/ml		**PDBu** 0.03uM		**LDN** 100ng/ml		**B27** 1%		**Nico** 10mM				
	S5 (3d)	On day 11: S4 cells are treated with 10um Y-27632 for 4 hours, rinsed with PBS -/- and treated with versene for 3-5 mins. Keep cells in clusters, making sure they are not too small. Spin 300xg for spin. Gently resuspend pellet in stage 5 medium - keeping attention to size of clusters, try to keep ~100um. Plate cells into ultra-low attachment plates or T25s																	
Suspension		**d11 - 13** *50% change each day*	***Basal B4***		**Vitamin C** 0.25mM		**LDN** 100ng/ml		**Alk5i II** 0.01mM		**Heparin** 10ug/ml		**Comp E** 1.0uM		**Nico** 10mM		**Forskolin** 10uM	**Exendin-4** 0.01uM	**RA** 0.025 uM
	S6 (4d)	**d14 - 17** *Feed every other day*	***Basal B4***		**Vitamin C** 0.25mM		**LDN** 100ng/ml		**Alk5i II** 0.01mM		**Heparin** 10ug/ml		**Comp E** 1.0uM		**Nico** 10mM		**T3** 1.0uM	**$ZnSO_4$** 10uM	**BayK** 2uM
	S7 (7d)	**d18 - 21** *Feed every other day*	***Basal B4***		**Vitamin C** 0.25mM		**BMP4** 0.01ug/ml		**Alk5i II** 0.01mM		**Heparin** 10ug/ml		**R428** 2uM		**NAC** 1.0mM		**T3** 1.0uM	**$ZnSO_4$** 10uM	**BayK** 2uM	**Trolox** 10uM
	S8 (7d)	**d21 - 27** *Feed every other day*	***Basal B5***		**MK-801** 10uM		**T3** 1.0uM		**Alk5i II** 0.01mM										

Chapter 7 Supplemental Table 3: Basal Media

Basal Media:							
Basal A1	MCDB131	**Glutamax** 1 x	**BSA** 0.5%	**$NaHC0_3$** 1.5 g/L	**Glucose** 10mM		
Basal A2	MCDB131	**Glutamax** 1 x	**BSA** 2%	**$NaHC0_3$** 2.5 g/L	**Glucose** 10mM		
Basal A3	MCDB131	**Glutamax** 1 x	**BSA** 2%	**$NaHC0_3$** 1.5 g/L	**Glucose** 20mM	**P/S** 1 x	
Basal B1	RPMI						
Basal B2	IMDM: Ham's F12 75:25	**P/S** 1 x	**Glutamax** 1 x	**BSA** 0.05%	**N2** 0.5 x	**B27** 0.5 x	**MTG** 0.45mM
Basal B3	DMEM	**P/S** 1 x					
Basal B4	MCDB131	**P/S** 1 x	**Glutamax** 1 x	**BSA** 2%	**$NaHC0_3$** 1.5 g/L	**Glucose** 20mM	**ITS-X** 0.5X
Basal B5	CRML supplemented	**P/S** 1 x	**AB Serum** 5%				

Chapter 7 Supplemental Table 4: Donor Tissues

Isolated Adult Human islets

Islet Source	Islet RRID	Age	Sex	BMI	Islet Purity	Islet Viability	Cause of Death
IIDP	SAMN08768974	28 years	Male	29.2	85%	98%	Head trauma
IIDP	SAMN08768991	51 years	Male	29	80%	95%	Head trauma
IIDP	SAMN08769201	24 years	Male	34.8	95%	97%	Head trauma
IIDP	SAMN08769390	33 years	Female	34.2	95%	98%	Stroke
IIDP	SAMN08769826	30 years	Male	56.8	95%	98%	Anoxia
IIDP	SAMN12670838	40 years	Male	30.7	90%	90%	Head trauma
Internal	UWHI325R	46 years	Male	39.5	80%	98%	Cardiac Arrest

Adult Human Pancreas

Donor	Age	Sex
Donor 52	61 years	Female
Donor 64	22 years	Male
Donor 66	38 years	Male
Donor 68	57 years	Female
Donor 84	46 years	Male
Donor 92	42 years	Male
Donor 93	24 years	Female
Donor 98	35 years	Male

Human Fetal Pancreas

Donor	Age	Sex
HFP 85	18 gw	Male
HFP 88	18 gw	Unk
HFP 92	19 gw	Unk
HFP 99	17 gw	Female
HFP 102	18 gw	Male

Chapter 7 Supplemental Table 5: Antibodies used for IF

Antibodies used for IF

Target	Species	Dilution	Product
CHGA	Rabbit	1:400	23342-1-AP (Proteintech)
ERO1LB	Rabbit	1:50	ab230540 (Abcam)
Gcg	Mouse	1:1000	G2654 (Sigma)
Gcg	Rabbit	1:2000	ab92517 (Abcam)
HDAC9	Rabbit	1:100	MA5-33151 (ThermoFisher)
IAPP	Rabbit	1:1000	ab254259 (Abcam)
Ins	Mouse	1:5000	I2018 (Sigma)
Ins	Guinea Pig	1:2000	I8510 (Sigma)
MAFA	Rabbit	1:200	BLR067G (Bethyl)
NTPDase3	Mouse	1:50	hN3-B3s
SIX2	Rabbit	1:500	11562-1-AP (Proteintech)
Ucn3	Rabbit	1:2000	#7218 (from Salk)
ZNT8	Rabbit	1:2000	ab244550 (Abcam)

Target	Color	Dilution	Product
Anti-Mouse	488	1:800	A11001 (Life Technologies)
Anti-Mouse	568	1:800	A11031 (Life Technologies)
Anti-Mouse	647	1:800	A21235 (Life Technologies)
Anti-Rabbit	488	1:800	A21206 (Life Technologies)
Anti-Rabbit	568	1:800	A11011 (Life Technologies)
Anti-Guinea Pig	488	1:800	A11073 (Life Technologies)

Chapter 7 Supplemental Table 6: Primers used for QPCR

Primers used for QPCR

Gene	Product Number
ARNTL	Hs00154147_m1
CHGA	Hs00154441_m1
CHGB	Hs01084631_m1
ENTPD3	Hs00154325_m1
ERO1LB	Hs00219877_m1
FAM159B	Hs00971129_m1
G6PC2	Hs01549772_m1
GCK	Hs01564555_m1
HDAC9	Hs01081558_m1
HOPX	Hs05028646_s1
IAPP	Hs00169095_m1
INS	Hs02741908_m1
KLF9	Hs00230918_m1
MAFA	Hs01651425_s1
NR1D1	Hs00253876_m1
OC2	Hs00191477_m1
SIX2	Hs00232731_m1
SIX3	Hs00193667_m1
SYT4	Hs01086433_m1
SLC2A1	Hs00892681_m1
SLC2A2	Hs01096908_m1
SLC30A8	Hs00545183_m1
UCN3	Hs00846499_s1

Chapter 8: Conclusions and Final Directions

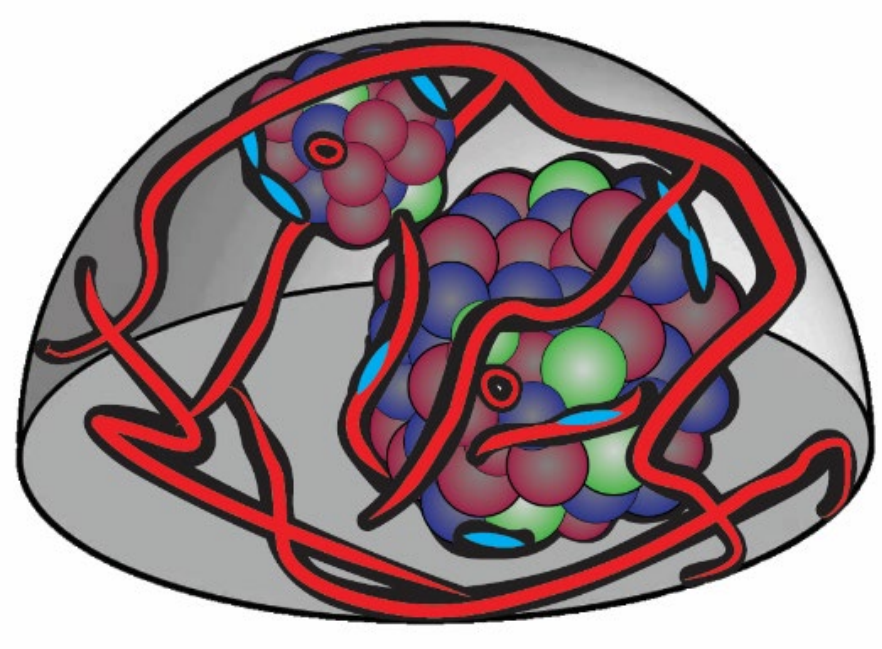

Daniel Tremmel wrote the chapter and made the figures.

Pancreatic islets are essential micro-organs and islet dysfunction causes life-threatening diabetes. Human islets have been difficult to directly study because they are embedded within and throughout the pancreas, surrounded by exocrine and ductal tissue, and in order to isolate the cells from the rest of the organ, a harsh mechanical and enzymatic digestion process must be used, which damages the islets, reducing their survival time after isolation. Furthermore, major differences exist between islet development of various animal species, meaning that fundamental work on islet development in rodent models does not always translate to human islet biology [1]. Isolated islets from deceased human donors can be transplanted as a diabetes therapy, but because of limited supply there is significant invested interest in developing stem cell-derived islets (SC-islets) as a renewable and customizable source of insulin-producing cells for transplantation. Much more needs to be understood about the unique aspects of human islet biology and function to improve these treatment options.

Digestion during islet isolation has been shown to significantly damage the native islet extracellular matrix (ECM) [2], leading to anoikis-mediated apoptosis, a major cause of islet attrition in culture [3, 4]. Both isolated islets and SC-islets exhibit improvements in islet health and function after they are transplanted into an *in vivo* environment [5-7], which presents the islets with a variety of supportive signals that are not present in culture including ECM signaling, interactions with different cell types present in the pancreas, circadian rhythms, and connection to blood flow which provides oxygen and glucose stimulation at physiologic levels and feeding patterns. Most importantly, significant inadequacies in SC-islet maturation, including deficits in *in vitro* function and expression of key beta cell genes, have only been overcome thus far

following transplantation [5, 6]. Together, these observations have led our lab to investigate how the human islet microenvironment affects islet identity, health and function.

In this thesis I have presented several studies that assess the composition and localization of ECM proteins in the human pancreas as a whole, and specifically within the islets (Chapter 2, Chapter 3). I have established a protocol to decellularize the human pancreas and create a stable and durable natural ECM hydrogel (hP-HG) (Chapter 3, 5), which is useful for testing the effect that ECM co-culture has on human islet survival, health and function (Chapter 5) and for incorporating into SC-islet differentiation protocols to test the effect ECM has on developing islets (Chapter 4). Isolated islets are cultured in suspension, which has presented difficulties to co-culture of islets with other cell types to study the cell-cell interactions that are present *in vivo*. The hP-HG scaffold presents cues from the ECM component of the human islet microenvironment and facilitates the inclusion of other cell types in 3-D composite culture and resembles the cell architecture *in vivo*. Therefore, we derived a protocol to co-culture endothelial cells with islets in the hP-HG in an attempt to model these interactions *in vitro* and pre-vascularize the islets before transplantation (Chapter 6). Finally, in an effort to utilize the tissue resources available in our lab, I have characterized the functional profiles and expression patterns of potential maturation markers in fetal human pancreas, adult human pancreas and SC-ILCs, in order to better establish expected gene expression profiles in SC-ILCs as the differentiation protocols get closer to generating cells that resemble primary human islets (Chapter 7).

ECM is an essential part of the tissue environment and influences cell behavior directly by binding cell surface receptors, such as integrins, through regulation of growth factor diffusion and presentation, and through mechanical stimulation [8]. For decades, ECM has been shown to

have an important role in the health of isolated islets, and aspects of the ECM composition of the pancreas and islets of many species had been characterized through the use of immunostaining and other limited targeted approaches (reviewed in [9-11]). However, previous studies that have supported islets with ECM used purified ECM components that were only putatively comparable to the native islet ECM. As *in vitro* islet culture moves from 2-D adherent methods toward more complex customized 3-D systems that better resemble the native cell environment [12], a more complete understanding of the pancreas matrisome is necessary to appropriately engineer these models. The majority of prior islet ECM studies combined data from different species to make conclusions about the human islet matrisome [9-11, 13], but few previous studies have directly, comprehensively, and quantitatively measured expression of ECM proteins in the human pancreas and islets.

Our mass-spectrometry based study (Chapter 2) identified 185 ECM proteins in the human pancreas throughout development and quantified 117 of these at each distinct stage we studied (fetal, juvenile, young adult, older adult). This is among the first published comprehensive proteomic data sets for the human pancreas matrisome, and to date the only published study that assesses changes in human pancreas ECM throughout the entire developmental lifespan. This establishes a useful database for the field of islet tissue engineering going forward in a variety of ways. First, it provides guidance and context for how ECM components should be incorporated into tissue-engineered islet constructs, including relative ECM protein ratios for all 117 matrisome proteins quantified in our study. This will help fine-tune studies that aim to use defined ECM scaffolds made from different ratios of purified ECM proteins to support islets or SC-islets in culture or transplantation.

Second, our study provides data on the relative abundance of different ECM proteins in the islet and acinar compartments of the pancreas. Although our mass spec data is biased toward detecting acinar ECM (based on the high percentage of the pancreas that is exocrine tissue), the IF staining for 16 of the most abundant structural ECM proteins shows that most ECM components detected in the pancreas are present in both the islets and acinar. This has significant implications in our studies with decellularized pancreatic ECM, because again this material is mainly composed of acinar ECM – but we have established that the major structural components of the islet and acinar ECM are very similar. Furthermore, the ECM proteins lost during decellularization, or that have significant enrichment in islets compared to the acinar, could be custom-added to the hP-HG to create a more islet-like hydrogel.

While the quantitative measurement of the pancreas ECM throughout development is an important achievement, there is much more that can be done in this area, and a more in-depth analysis of the human islet-specific matrisome is underway. Continuing to work closely with Dr. Lingjun Li's group, we aim to quantify the human islet matrisome more precisely using two methods. Future work will use laser-capture microdissection to isolate only the islets from sections of human pancreas, and use the protein extracted from those samples to identify islet ECM in a more high-throughput method than our previous immunostaining technique. The same approach could be used to isolate the acinar tissue and quantify the exocrine ECM. This method will generate a list of ECM proteins in islets or acinar regions with relative quantitation, which could be compared to that of the whole pancreas to make more conclusive observations about islet-enriched ECM. However, this method will not be helpful for further specifying the localization of ECM components within the islets. Mass spectrometry imaging (MSI) will be used

on human pancreas tissue sections to quantitatively and spatially map the distribution of ECM and other islet proteins within the tissue. These combined studies are important next steps in understanding the islet matrisome so that it can be appropriately modeled or recapitulated for future *in vitro* and *in vivo* studies using human islets or SC-islets.

Prior to our study, several studies have indicated that differences in islet ECM between younger and older adult pancreas donors has affected the efficiency of islet isolation between these populations, with young adult donors being more difficult to isolate pure, high quality islets from [14-16]. Interestingly, in our study we found that at the whole-proteome level, there were no differences in the relative abundance of any ECM proteins between younger and older adults. However, we found that some ECM proteins accumulated in and around the islets in older adulthood compared to younger adults. ECM proteins that may be enriched in/around older adult islets compared to younger adults include collagen 1, collagen 5, collagen 12 and both laminin α4 and α5. Intriguingly, collagen 6 is highly enriched around both young and older adult human islets – this suggests that potentially, the ratio of collagen 6 to other ECM proteins may be different under different donor conditions, such as age. This could have a potential effect on islet isolation efficiency, because the collagenase blends typically used in human islet isolation are less effective at digesting collagen 6 compared to collagens 1-5, and therefore these data would correlate with lower digestion efficiency of islets surrounded by an ECM membrane that is more highly enriched in collagen 6 [17, 18]. Of course, future studies that quantify the human islet-specific matrisome more thoroughly may help to conclusively identify how these ECM protein ratios may change with older age, and potentially other donor variables, and whether or not these changes coincide with differences in islet health, function or isolation efficiency.

After our pancreas proteomics report was published [19], one other study has utilized broad proteomic approaches to characterize the human pancreas matrisome [20]. Rather than focusing on human pancreas development, this study highlights how decellularization and solubilization of human pancreatic ECM affects the protein composition. Combining mass spectrometry and multiplex ELISA-based assays, they identify a total of 314 matrisome proteins among all of their pancreas donors and samples. Most importantly, this study demonstrates how decellularization biases the ECM proteins extracted from a tissues, generally towards having high collagen preservation and lower retention of other ECM components. The protein composition is further affected by the digestion and solubilization of the ECM to create a gel. Together, our Li and Tremmel et al. study [19]and that of Asthana et al. [20] provide a strong framework for reconstructing the natural ECM composition of the human pancreas in future tissue engineering applications.

The next portion of this thesis was dedicated to establishing protocols to decellularize the human pancreas, create a hydrogel from human pancreatic ECM and optimize the hydrogel material for stable use in culture and transplantation studies with islets and cells. Although many studies had previously worked on decellularizing the pancreas of different species [21], prior to the publication of our study, only one group had reported decellularization of the human pancreas [22], and none had successfully created a hydrogel material. Due to the difficultly of culturing islets in whole perfusion-decellularized pancreas or cryosections of decellularized pancreas pieces, our goal was to create a hydrogel that could very easily be incorporated into tissue engineering, cell culture and transplantation platforms.

We report two main protocols that have led to the formation of a stable decellularized human pancreas ECM hydrogel (hP-HG). First, we show that human pancreas tissue has high levels of parenchymal fat which is not easily removed during decellularization of cubes of tissue as had been previously reported for some human tissues. The premise of this method is to decellularize intact pieces of pancreas to use as scaffolds that retain the native ECM architecture. These decellularized pieces can be frozen and cryosectioned into slices of decellularized ECM which could be amenable to cell culture studies. When cut into 1 cm^3 cubes and treated with various detergents, there were trapped lipids in the center of the cubes. Because our ultimate goal was to create a hydrogel from the ECM, the tissue architecture was dispensable for our subsequent studies, and therefore we homogenized the tissue to release some of the trapped lipid and improve gelation of the decellularized ECM (Chapter 3). However, the pancreata that are donated for use in research are often rejected for transplantation due to high fat content of the pancreas. We find that in a cohort of over 100 pancreata we received for research, there is a broad range of lipid content, and that the homogenization protocol only worked on a subset of them. To optimize the protocol to work for the majority of the donated pancreata, we added an organic solvent delipidization step, which essentially removed all remaining lipids after homogenization. We found that this method led to the highest performing hydrogels based on rheological measurements and practical properties, like the stability of the gels in media during culture and the ability to pick up and transfer the hydrogel constructs for experiments and transplantation (Chapter 5).

In our first study using hP-HG (Chapter 3), we demonstrated that the hydrogel was highly compatible with cultured cells and tolerated by a host immune system post-transplantation.

Undifferentiated stem cells proliferated when embedded within hP-HG, and cells differentiated toward a pancreatic fate maintained their gene expression and level of proliferation, and did not have increased apoptosis in the gel. We also demonstrated that hP-HG could be utilized for cell culture in two different ways – either as an ECM coating on a plastic well in 2-D culture, or with cells embedded in 3-D within the hydrogel, generally molded into a Transwell plate with media on the top and bottom chamber surrounding the gel. When acellular hP-HG was transplanted into humanized mice, there was little evidence of human immune cells infiltrating the grafts, whereas allogeneic human tissue transplanted into the same mice were heavily infiltrated by human T-cells, indicating rejection. The only cells we identified within the transplanted hP-HG were mouse macrophages, which may infiltrate the transplanted materials as part of routine tissue surveillance. We did not detect noticeable fibrosis around the hP-HG grafts. Together, these initial studies provided evidence that the hP-HG material we produced may be useful in both *in vitro* culture studies and in transplantation studies, which were the two major applications for which we had interest in developing this material.

Our next goal was to assess how hP-HG could be incorporated in SC-islet differentiation protocols (Chapter 4). Leading protocols used around that time had two phases of culture, starting the cells in adherent culture and moving into 3-D suspension culture at later stages of the differentiation. To test hP-HG in the context of these protocols, we replaced the standard Matrigel coating in the first (adherent) stages of differentiation, with an hP-HG-coating. This did not result in a beneficial effect on cell gene expression, likely because the adult pancreatic ECM is developmentally incongruous at these early stages of differentiation. Instead, when the cells were moved into suspension after the pancreatic progenitor 1 (PP1) stage of differentiation, we

embedded cells within droplets of hP-HG and cultured them throughout the remainder of the protocol in this 3-D ECM environment. This 3-D implementation of hP-HG in the differentiation protocol has more promising results, including improved gene expression, better co-localization of β cell markers and higher insulin-positive cell area. However, SC-islets generated with these older differentiation protocols had poor function, and in this study the hP-HG environment did not rescue this deficit in glucose-responsive insulin secretion.

To address these deficiencies in SC-islet differentiation, several labs in the subsequent years developed protocols which have attained significant improvements in SC-islet function [6, 23-25]. While these protocols have achieved success in producing β-like cells with gene expression profiles more similar to primary β cells and improved glucose-responsive function, there remain significant differences between primary islets and SC-islets. SC-islet expression of several key genes (e.g. MAFA, Ucn3) are extremely low, total insulin content is lower than primary islets, and the amount of secreted insulin in response to glucose in many cases is also significantly lower [26]. SC-islets have been shown to undergo significant changes in gene expression and function after transplantation, however [5-7]. The underlying mechanism of this *in vivo*-maturation is unknown, but is potentially due to several different microenvironmental factors, among them the possibility that ECM plays an active role in this process. For the purposes of having a high safety profile for transplanting cells into patients and in order to have robust and accurate insulin secretion as soon as possible after transplantation, it is widely held that it would be ideal for SC-islets to be fully matured *in vitro*, prior to transplantation. Therefore, future studies combining hP-HG with more modern SC-islet differentiation protocols will be important to understand what role ECM may play in SC-islet maturation. hP-HG droplets also create a 3-D

microenvironment that is amenable to the addition of other factors that may improve SC-islet maturation, such as the inclusion of other cell types in a physiologically relevant 3-D construct (Chapter 7), which could facilitate better tissue-engineered models for *in vitro* studies.

We aimed to generate an improved decellularization protocol to create an hP-HG material that would perform better in culture and could be handled more easily without falling apart. We also intended to co-culture hP-HG with primary human islets before doing additional SC-islet studies, in order to optimize our co-culture protocols for better assessment of cell function and health in the hydrogel constructs and to assess effectiveness with a demonstrably insulin-secreting product. Therefore, upon development of the "optimized" hP-HG material, we combined the hP-HG with primary human islets to assess survival and function in culture (Chapter 5). In order to assess whether the unique tissue-specific ECM composition of hP-HG had a role in islet function, islets were co-culture in suspension (no ECM), ow with hP-HG (pancreas-specific complex ECM mixture), human kidney ECM hydrogel (hK-HG) (non-pancreas-specific complex ECM mixture) purified collagen 1 (simple non-specific ECM composition), or alginate (non-ECM hydrogel). Interestingly, islets consistently had the highest function in hP-HG compared to all other co-culture methods. Culture of islets in hP-HG reduced basal insulin secretion in cultured islets compared to suspension culture, but did not significantly change the stimulated insulin secretion. In hK-HG or Col1 gels, islets showed a significant reduction in both basal and stimulated insulin secretion, suggesting these ECM compositions inhibited insulin secretion. Alginate did not affect the insulin secretion of the islets compared to suspension culture, both had relatively low stimulation and very high levels of basal insulin secretion. This study provides evidence that the tissue-specific ECM composition of the pancreas plays a role in islet insulin secretion.

In our studies, all ECM hydrogels were prepared with a high protein concentration of 10 mg/mL. Digested ECM forms a gel based on the natural formation of collagen fibrils at neutral pH and physiologic temperature, but because the ECM protein composition of the various hydrogels are not the same, the physical properties of gels at the same total protein content are different. Therefore, future studies should assess how the stiffness of a gel environment affects islet insulin secretion. These assays are complex – in order to control both the gel stiffness and ECM protein composition, synthetic crosslinking agents would need to be used at empirically-determined concentrations to match gel stiffness across the different hydrogel materials and at different ECM concentrations. After establishing a methodology to synthesize hydrogels from tissue-specific ECM derived from different organs or composed of defined ECM components, islets could be cultured within the different substrates at the same stiffness, or in the same substrates at different stiffness, to parse out the contribution that stiffness or ECM protein signaling play in the functional changes islets undergo when embedded in hydrogel. Recent studies of islets and SC-islets cultured in 3-D ECM platforms have also revealed high levels of β cell polarization mediated by adherence to basement membrane, which is thought to direct insulin secretion toward the vasculature [27, 28]. In our study, we found that changes in gene expression related to ECM-mediated signaling are among the top pathways altered in islets when comparing suspension and hP-HG culture, indicating that islets are experiencing more than just mechanical stimulation in hP-HG culture. Ultimately, dissecting the mechanical and biochemical roles that ECM has in islet function would be beneficial to better understand and control for the different variables that the islets are responding to within these environments.

To further explore the effect that hP-HG has on human islets, survival, mitochondrial respiration, and islet architecture were assessed in islets cultured in both suspension and hP-HG. We found that islets had significantly improved survival in hP-HG compared to suspension. Islets also had improved mitochondrial respiration in hP-HG compared to suspension. As mitochondrial metabolism plays a central role in β cell glucose-sensitive insulin secretion, improved mitochondrial function could be one mechanism through which islets perform better GSIS in hP-HG co-culture. It would be interesting to see if mitochondrial respiration was altered in human islets cultured in hK-HG and Col1, which both have suppressed insulin secretion overall, but these studies have not yet been performed.

Consistent with recent findings from several other groups [29, 30], we found that islet architecture – the arrangement of the various different cell types in the islet clusters – was significantly altered after islet isolation. However, the arrangement of the endocrine cells in cultured islets remained stable after isolation when cultured in hP-HG, while in suspension there continued to be movement of the islets β cells toward the islet mantle. The resident endothelial cells and vascular mural cells also had a dramatically different localization in suspension, where both cell types moved toward the core of the islets, and in hP-HG where these supportive cells had a tendency to move toward the periphery of the islet at the interface with the hydrogel. Although the arrangement of α and β cells in islets cultured in hP-HG over 7 days was not restored to a state completely similar to native islets, we do find that embedding in hP-HG “freezes” the arrangement of these cells relative to the day they are embedded. It appears that islets do not undergo much of an architecture change on the day of isolation (unpublished), so if islets were embedded soon after isolation, the arrangement of α and β cells may retain better architecture.

This study has not yet been performed, and is limited by the time it takes to purify and transport isolated islets between the isolation center and the lab.

It is interesting how diverse islet architecture is across various species, and yet so well conserved from individual to individual within each species. The differences between mouse and human islets are well known in the field and have been discussed throughout this thesis, but other species also have distinct islet architecture. For example, horses and cats, which are very distantly related, both have a β cell mantle and α cell core arrangement, while other more closely-related species to the cat, like the hyena, have a very distinct α cell mantle and β cell core [31, 32]. The mechanisms through which islet architecture is established are not well understood, and while the alteration of several pathways have been found to affect islet architecture in mice, it is still not clear if these same mechanisms play a role in human islet architecture or what role the architecture has in islet function [32]. The resources are now available to study the driving mechanisms of human islet architecture – aided by the recent findings that human islets rearrange after isolation (Chapter 5, [29, 30]) and the development of pseudo-islet culture systems in which islets are dissociated and reaggregated with potential to manipulate gene expression during the process. One study identified similar cell arrangement in isolated human islets and re-aggregated pseudoislets, indicating that even after dissociation and reaggregation, there is a tendency for the cells to form an α cell core and β cell mantle [30]. It would be useful to study which cell-cell and cell-ECM signals are affecting the self-organization of these cells in culture, this could be tested by altering the ratio of the different endocrine cells present or by embedding the cells in hP-HG or other ECM environments to study how the different cells respond to the ECM cues. Upon identifying the cell-cell and cell-ECM interaction profiles,

proteomics or single-cell RNA sequencing could be used to identify pathways involved in these processes, and gene editing or gene expression vectors could be used during pseudoislet formation to alter those pathways and test the effect the alterations may have on the self-assembly of the cells in those contexts.

Interestingly, in our study we found an altered arrangement of the endothelial and vascular mural cells in isolated islets depending on whether the islets were cultured in suspension (S) or in hP-HG (P): this observation gives us hints to whether these cells are important for guiding islet architecture. At day 7 of culture, the $Tie2^+$ and αSMA^+ cells have completely inverted localization patterns in the two different treatments (S and P). Furthermore, these cell types deposit ECM within the isolated islets, and the ECM localization traces with the endothelial and mural cells over time in culture (Appendix Chapter 2). Therefore in suspension (S), the supportive cell types ($Tie2^+$ and αSMA^+) and the newly synthesized ECM are at the core of most islets, and mainly in contact with the α cells, which are also primarily located in the core. In the hP-HG treatment (P), the hydrogel environment drives most of the support cells toward the mantle of the islets, where they deposit more ECM. In hP-HG, primarily β cells, but also some α and δ cells are in close proximity to the mantle. This seems to indicate that direct contact between the endocrine cells and either the ECM or the endothelial and mural cells is not a major driver of the cell rearrangement in culture. Another perspective may be that the mechanical force of the hydrogel affects the migration of the $Tie2^+$ and αSMA^+ cells, but not the endocrine cells. To explore the role that the physical properties of the hydrogel have on the islets, gel stiffness could be modified at a constant ECM concentration to measure how the islet architecture changes in the various mechanical environments. These studies could also be performed with pseudoislets

of different endocrine compositions (natural α to β cell ratio, or altered ratios), or of altered non-endocrine cell:endocrine cell ratios in the pseudoislets, to better understand which cell type may be driving such a response to stiffness. If these studies were successful, they could also enable future work to understand how the arrangement of the cells affects their function in culture.

The improvement of islet GSIS in hP-HG raises questions about how much islet function may be affected by the harsh isolation treatment and culture conditions that do not resemble the native islet milieu. If there are dramatic effects on islet function following isolation, it would jeopardize the ability of studies on isolated islets to translate to *bona fide* human islet function *in vivo,* and it would complicate our understanding of islet function as it translates to assessing maturity of SC-islets. Indeed, other than studies using ECM, several groups have reconstituted other elements of *in vivo* islet environment and found similar changes in isolated islet function. In 2020, Alvarez-Dominguez *et al.* found that circadian entrainment of human islets in culture dramatically improved the stimulation index – not through an increase in stimulated insulin secretion, but through a significant reduction in basal insulin secretion [33]. Similarly, studies that have cultured isolated human islets in perfusion culture systems to mimic blood flow have found improved islet function and gene expression in this environment [34]. Combining multiple elements of the *in vivo* environment may have a synergistic effect on islet health and function and may be able to positively influence the differentiation of SC-islets. If modifications to islet environment in culture (i.e. ECM, circadian entrainment, perfusion) do help to preserve or re-establish aspects of islet biology that are more similar to the native islets *in vivo*, then it will be important for these elements to be integrated into most future islet studies in order to make accurate conclusions about human islet function.

In the next step in my effort to re-engineer the islet niche *in vitro*, we developed a protocol for forming endothelial tubes throughout the hP-HG droplets in order to bring together the islet endocrine cells, the vasculature, and the ECM in one co-culture system. This system utilized human umbilical vein endothelial cells (HUVECs) to form a network of aligned endothelial tubes in culture, which could be co-cultured with islets to study the microenvironment *in vitro*, or transplanted to support islet engraftment *in vivo*. We conceptualized this study based on our observations that when we transplanted single cell endothelial cells with human islets or SC-islets, we were consistently unable to identify the ECs in the graft after a very short time *in vivo* – the cells were either leaving the transplant site, or dying. Therefore, we postulated that pre-forming tubes *in vitro* may help to keep the endothelial cells at the transplant site in order to support the graft. Indeed, since we began this work, several studies have shown that single-cell endothelial cells form unstable vasculature upon transplantation that is quickly replaced by host cells and not as effective at supporting the survival of the islet graft [35-37].

Several other methods of supporting islet engraftment have been reported, and many have successfully improved islet survival and function after transplantation into hypoxic sites, such as the subcutaneous (SQ) space (reviewed in Introduction Figure 6) [35, 38-45]. None of these previous methods, however, have formed endothelial tube structures around the islets *in vitro* in a transplantable construct. Other studies using perfusion culture systems have successfully combined endothelialized tubes and islets within the system, but none of these studies have used their platform as a method of pre-vascularizing the islets prior to transplantation. Future directions in this field could be to combine these techniques to create a perfused vascular support system for islets that improves islet survival in culture and can be

transplanted with pre-formed vessels to accelerate the islet engraftment as well. For work aiming to study these cell-environment interactions *in vitro*, it may be important to consider the source of endothelial cells used in the culture system. Despite being commercially available and having the potential to undergo robust tube formation, HUVECs are a venous cell type that do not resemble the vasculature of islets. Islets are permeated with capillaries, the smallest vascular structures that can have different physiological properties (i.e. continuous vs. fenestrated capillaries), and have unique gene expression profiles from tissue to tissue [46-48]. Future work using endothelial cells for *in vitro* modeling should strive to use endothelial cells that resemble the islet capillary network in order to properly recapitulate the islet-endothelial signaling that happens *in vivo*. It is important to note that little has been published about islet-specific endothelial cells [49, 50], so studies determining what makes these endothelial cells unique are also a priority for the field, with a specific focus on human islet endothelial cells.

Figure 1. A closer look at the ECM of human pancreas vasculature in development.
ECM proteins (COL3A1, COL4A1, COL5A1, COL6A1, LAMA4, LAMA5) (green) co-stained with Insulin (red) in human fetal pancreas and human adult pancreas. All scale bars = 100 microns.
(Next page)

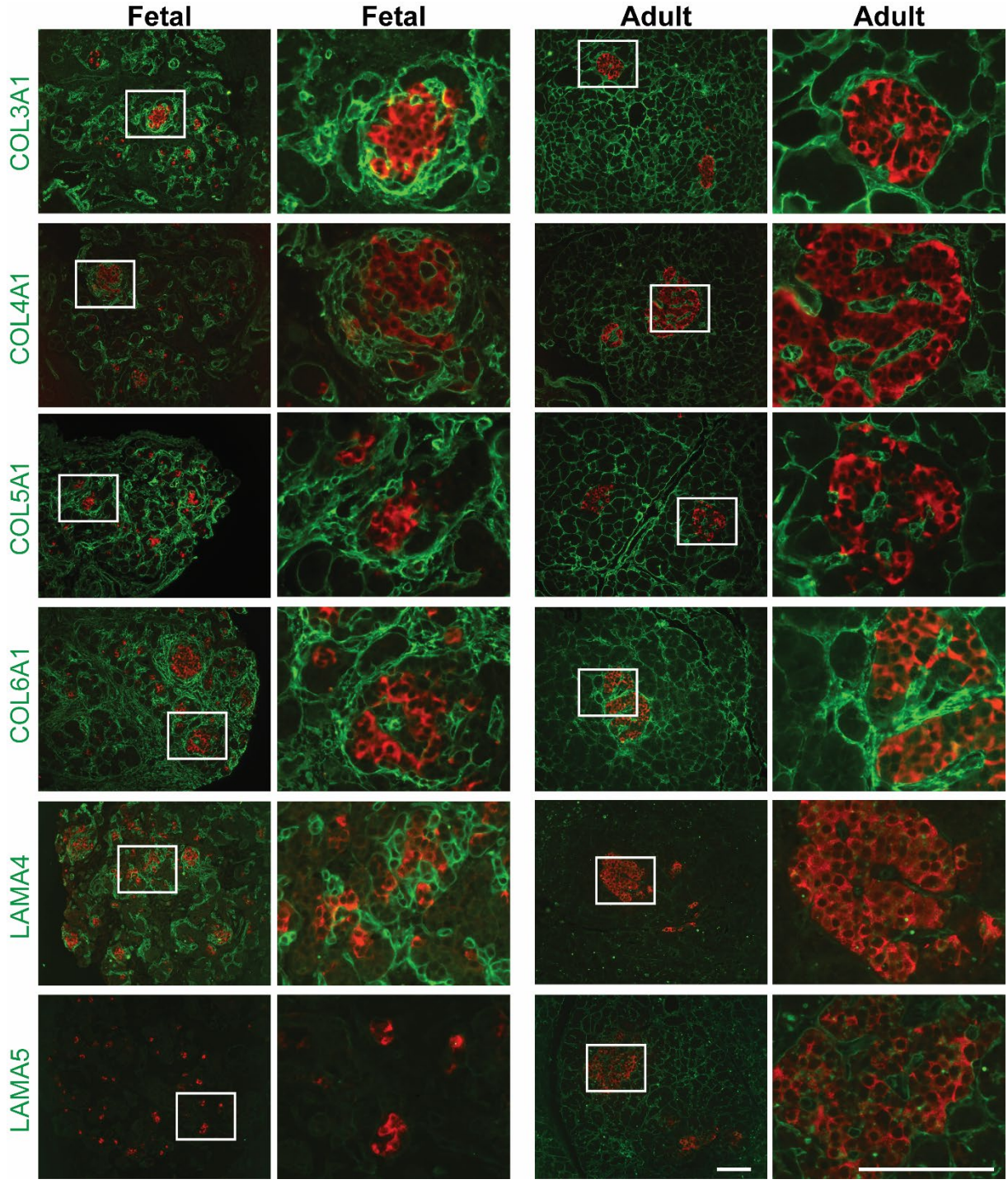

In Chapter 2, we inferred the localization of certain ECM proteins in the developing pancreas based on the histology of the ECM staining, but there is room for deeper exploration

into how the ECM localization changes in the pancreas during development. For example, we observed differences in the total abundance of laminins in the pancreas, in which laminins α1 and α4 are more abundant in the fetal tissue, and laminin α5 is more abundant in adult tissue. Looking more closely at the immunostaining (Figure 1), laminin α4 is highly enriched in the fetal vasculature, and faint in the adult vasculature, while laminin α5 is absent in the fetal vasculature but present in the adult vasculature and the ECM surrounding the acinar clusters. The expression of collagens is consistent in the vasculature throughout development, with collagens 3, 4, 5, and 6 being abundant in both the fetal and adult islet vessels. However, in the fetal pancreas, the localization of laminin α4 and collagens 3 and 4 appears to be only within the vascular basement membrane, while in the adult pancreas collagens 1, 3, 4, 5 6 and laminin α5 localize to ECM interfaces throughout the acinar compartment in addition to the islet blood vessels. Many of the ECM proteins we identify within the islet vasculature, especially collagens 1, 3, 5 and 6, are not generally discussed as part of the vascular basement membrane. There is a clear intimate connection between ECM, vasculature and developing islets. This might mean that the blood vessels are the main source of these ECM proteins in the developing pancreas, and endothelial-derived ECM could be leveraged in engineered microenvironments to model both endothelial and ECM signals. Stem cell-derived endocrine progenitors could be co-cultured with or without endothelial cells in the absence of an ECM scaffold, the endothelial-derived ECM composition could be assessed in the constructs and one could study how the ECM and endothelium together contribute to the fate of endocrine cells. Islet-derived endothelial cells may be required to properly express the ECM proteins enriched around the islet vasculature, but a better understanding of the islet endothelial cell is needed.

We did not co-stain ECM proteins with markers of vasculature in our developmental study, and this may be an important future step in order to make more conclusive assessments of ECM localization throughout development. Further, several studies have identified that human islets have a double layer basement membrane between the endocrine cells and the vasculature, and that the two sides of this structure may be composed of different ECM proteins [51]. It would be informative to further assess which of our identified ECM proteins are expressed on which side of this basement membrane structure, and therefore infer which ECM proteins may bind to the endocrine cells compared to the vascular cells.

The final chapter of this thesis explores β cell maturation marker expression in human development. These maturation markers have been primarily been studied in mouse islet development, but clues over the years have indicated that the expression patterns of some of these markers may be significantly different in human islets. This is not a novel concept in the field of islet biology. For example, is has been widely reported that there are differences in islet glucose transporters, Glut1 and Glut2, with Glut2 being the primary transporter in mice and Glut1 being the primary transporter in human β cells; this could be a driver of differences in the euglycemic set point between the two species [52]. Similarly, while the maturation marker MAFA is widely considered a *bona fide* maturation marker in both mouse and human, the homolog MAFB is expressed in mouse fetal α and β cells but postnatally only in mature α cells –in human MAFB is highly expressed postnatally in α, β, and δ cells [53]. While these differences in gene expression have been previously established, the expected expression profiles of other β cell genes continue to be modeled based on mouse developmental studies, and compared to expression patterns in human SC-islets without strong evidence from primary human tissues. For

these reasons, our data describing the expression of some candidate maturation markers in SC-islets, human fetal pancreas and human adult pancreas will be useful to help establish new goals for SC-islets *in vitro*, through which better maturation and function may be achievable. *MAFA* and *UCN3* are both expressed at much lower levels in SC-islets than primary adult human islets, and have been commonly considered markers of postnatal maturation in human β cells. However, our work identifies *UCN3* as one β cell gene with dissimilar expression in mouse and human development, such that *UCN3* may mark mature β cells in mice, but not in humans. We also find that *MAFA* expression in fetal islets is significantly higher than that of SC-islets, which indicates that SC-islets may be less mature than some publications have suggested. We also present evidence that *IAPP*, *ENTPD3*, *SIX2*, *SIX3*, *G6PC2*, and *OC2* increase significantly in expression from fetal to adult human islets, but of these only *IAPP* and *ENTPD3* are also expressed at lower levels in our SC-islets than in fetal islets.

New β cell markers are continuously being identified in mouse studies and keeping up with how they translate to human islet biology is important; other markers we have not yet explored that may increase in β cell expression from fetal to adult stages could include *SYT4* (synaptotagmin-4) [54], or circadian rhythm-induced genes like *ARNTL* (*BMAL1*) [55] and *NR1D1*, among others [7]. These expression profiles help to sort out which genes remain significantly deficient in differentiated SC-islets compared to normal human development. The next steps toward generating more mature β cells *in vitro* is to investigate ways of inducing expression of these genes, which may be indicative of a stronger commitment to the β cell fate and may also correlate with better SC-islet function – both are important factors for safely transplanting these cells into patients with diabetes. Furthermore, although the expression of one gene may never

be sufficient to distinguish a functionally mature population of β cells, defining a subset of genes and expression profiles that correlate with maturation will be helpful to establish a new target for producing higher quality SC-islets.

Final Conclusions

Together, the work I have reported in this thesis establishes a foundation for recreating the islet extracellular environment in culture. The relative profiles of ECM proteins in the pancreas will inform future work to supplement the hP-HG scaffold to be enriched with islet-like ECM components. Our established protocols for co-culturing islets and endothelial cells within hP-HG and the formation of vascular networks within the hP-HG constructs will facilitate future studies of islet-EC interactions and may enhance the survival of islets after transplantation. This optimized co-culture platform can also be used with modern SC-islet differentiation protocols to assess whether elements of the *in vivo* environment can be used to stimulate maturation *in vitro* in a similar way to the maturation of these cells after transplantation, or could accelerate maturation *in vivo*. Our description of β cell maturation marker expression during normal human development (fetal and adult human islets) will help inform the use of these markers in future SC-islet studies. Overall, the ability to model multiple elements of the islet environment in culture *ex vivo* will lead to a more complete understanding of human islet health and function thereby promoting improved β cell transplantation strategies (Figure 2).

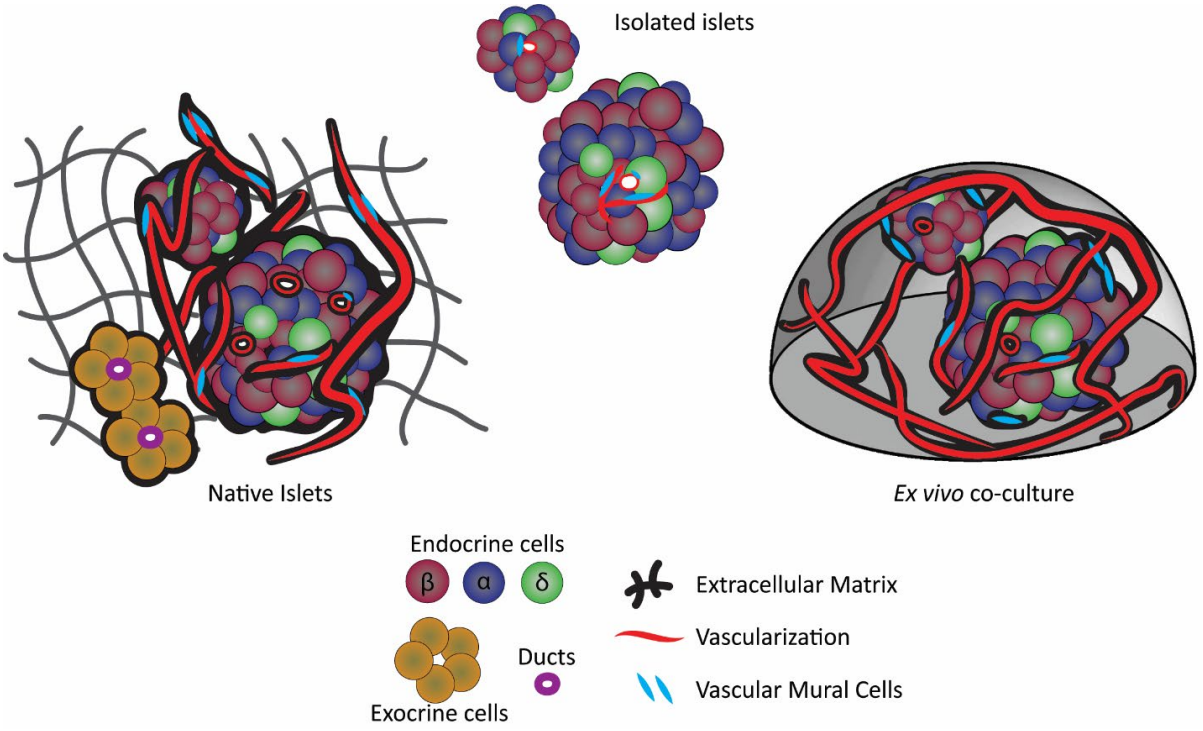

Figure 2. Reconstructing the Islet Extracellular Niche
Co-culture of human islets with ECM hydrogel and endothelial cells *ex vivo* recapitulates various elements of the native islet microenvironment that are lost after isolation and in suspension culture.

References

1. Nair, G. and M. Hebrok, *Islet formation in mice and men: lessons for the generation of functional insulin-producing beta-cells from human pluripotent stem cells.* Curr Opin Genet Dev, 2015. **32**: p. 171-80.
2. Cross, S.E., et al., *Key Matrix Proteins Within the Pancreatic Islet Basement Membrane Are Differentially Digested During Human Islet Isolation.* Am J Transplant, 2017. **17**(2): p. 451-461.
3. Thomas, F., et al., *A tripartite anoikis-like mechanism causes early isolated islet apoptosis.* Surgery, 2001. **130**(2): p. 333-8.
4. Thomas, F.T., et al., *Anoikis, extracellular matrix, and apoptosis factors in isolated cell transplantation.* Surgery, 1999. **126**(2): p. 299-304.
5. Augsornworawat, P., et al., *Single-Cell Transcriptome Profiling Reveals beta Cell Maturation in Stem Cell-Derived Islets after Transplantation.* Cell Rep, 2020. **32**(8): p. 108067.
6. Balboa, D., et al., *Functional, metabolic and transcriptional maturation of human pancreatic islets derived from stem cells.* Nat Biotechnol, 2022.
7. Barsby, T. and T. Otonkoski, *Maturation of beta cells: lessons from in vivo and in vitro models.* Diabetologia, 2022.
8. Frantz, C., K.M. Stewart, and V.M. Weaver, *The extracellular matrix at a glance.* J Cell Sci, 2010. **123**(Pt 24): p. 4195-200.
9. Aamodt, K.I. and A.C. Powers, *Signals in the pancreatic islet microenvironment influence beta-cell proliferation.* Diabetes Obes Metab, 2017. **19 Suppl 1**: p. 124-136.
10. Llacua, L.A., M.M. Faas, and P. de Vos, *Extracellular matrix molecules and their potential contribution to the function of transplanted pancreatic islets.* Diabetologia, 2018. **61**(6): p. 1261-1272.
11. Stendahl, J.C., D.B. Kaufman, and S.I. Stupp, *Extracellular matrix in pancreatic islets: relevance to scaffold design and transplantation.* Cell Transplant, 2009. **18**(1): p. 1-12.
12. Yamada, K.M. and K. Clark, *Cell biology: survival in three dimensions.* Nature, 2002. **419**(6909): p. 790-1.
13. Townsend, S.E. and M. Gannon, *Extracellular Matrix-Associated Factors Play Critical Roles in Regulating Pancreatic beta-Cell Proliferation and Survival.* Endocrinology, 2019. **160**(8): p. 1885-1894.
14. Meier, R.P.H., et al., *Pancreas collagen digestion during islet of Langerhans isolation-a prospective study.* Transpl Int, 2020. **33**(11): p. 1516-1528.
15. Spiers, R.M., et al., *Development of a Simple In Vitro Assay to Assess Digestion of the Extracellular Matrix of the Human Pancreas by Collagenase Enzyme Blends.* Cell Transplant, 2018. **27**(7): p. 1039-1046.

16. Spiers, R.M., et al., *Donor age significantly influences the Raman spectroscopic biomolecular fingerprint of human pancreatic extracellular matrix proteins following collagenase-based digestion.* Acta Biomater, 2019. **99**: p. 269-283.

17. Heller-Harrison, R.A. and W.G. Carter, *Pepsin-generated type VI collagen is a degradation product of GP140.* J Biol Chem, 1984. **259**(11): p. 6858-64.

18. Hughes, S.J., et al., *Characterisation of collagen VI within the islet-exocrine interface of the human pancreas: implications for clinical islet isolation?* Transplantation, 2006. **81**(3): p. 423-6.

19. Tremmel, D.M., et al., *A human pancreatic ECM hydrogel optimized for 3-D modeling of the islet microenvironment.* Scientific Reports, 2022. **12**(1).

20. Asthana, A., et al., *Comprehensive characterization of the human pancreatic proteome for bioengineering applications.* Biomaterials, 2021. **270**: p. 120613.

21. Tremmel, D.M. and J.S. Odorico, *Rebuilding a better home for transplanted islets.* Organogenesis, 2018. **14**(4): p. 163-168.

22. Peloso, A., et al., *The Human Pancreas as a Source of Protolerogenic Extracellular Matrix Scaffold for a New-generation Bioartificial Endocrine Pancreas.* Ann Surg, 2016. **264**(1): p. 169-79.

23. Hogrebe, N.J., et al., *Targeting the cytoskeleton to direct pancreatic differentiation of human pluripotent stem cells.* Nat Biotechnol, 2020. **38**(4): p. 460-470.

24. Nair, G.G., et al., *Recapitulating endocrine cell clustering in culture promotes maturation of human stem-cell-derived beta cells.* Nat Cell Biol, 2019. **21**(2): p. 263-274.

25. Velazco-Cruz, L., et al., *Acquisition of Dynamic Function in Human Stem Cell-Derived beta Cells.* Stem Cell Reports, 2019. **12**(2): p. 351-365.

26. Tremmel, D.M., et al., *Mimicking nature-made beta cells: recent advances towards stem cell-derived islets.* Curr Opin Organ Transplant, 2019. **24**(5): p. 574-581.

27. Gan, W.J., et al., *Cell polarity defines three distinct domains in pancreatic beta-cells.* J Cell Sci, 2017. **130**(1): p. 143-151.

28. Singh, R., et al., *Enhanced structure and function of human pluripotent stem cell-derived beta-cells cultured on extracellular matrix.* Stem Cells Transl Med, 2020.

29. Lavallard, V., et al., *Cell rearrangement in transplanted human islets.* FASEB J, 2016. **30**(2): p. 748-60.

30. Walker, J.T., et al., *Integrated human pseudoislet system and microfluidic platform demonstrate differences in GPCR signaling in islet cells.* JCI Insight, 2020. **5**(10).

31. Kim, A., et al., *Islet architecture: A comparative study.* Islets, 2009. **1**(2): p. 129-36.

32. Adams, M.T. and B. Blum, *Determinants and dynamics of pancreatic islet architecture.* Islets, 2022. **14**(1): p. 82-100.

33. Alvarez-Dominguez, J.R., et al., *Circadian Entrainment Triggers Maturation of Human In Vitro Islets.* Cell Stem Cell, 2020. **26**(1): p. 108-122 e10.

34. Jun, Y., et al., *In vivo-mimicking microfluidic perfusion culture of pancreatic islet spheroids.* Sci Adv, 2019. **5**(11): p. eaax4520.

35. Aghazadeh, Y., et al., *Microvessels support engraftment and functionality of human islets and hESC-derived pancreatic progenitors in diabetes models.* Cell Stem Cell, 2021. **28**(11): p. 1936-1949 e8.

36. Ben-Shaul, S., et al., *Mature vessel networks in engineered tissue promote graft-host anastomosis and prevent graft thrombosis.* Proc Natl Acad Sci U S A, 2019. **116**(8): p. 2955-2960.

37. Lin, R.Z., et al., *Host non-inflammatory neutrophils mediate the engraftment of bioengineered vascular networks.* Nat Biomed Eng, 2017. **1**.

38. Bowers, D.T., et al., *Engineering the vasculature for islet transplantation.* Acta Biomater, 2019. **95**: p. 131-151.

39. Citro, A., et al., *Biofabrication of a vascularized islet organ for type 1 diabetes.* Biomaterials, 2019. **199**: p. 40-51.

40. Kaufman-Francis, K., et al., *Engineered vascular beds provide key signals to pancreatic hormone-producing cells.* PLoS One, 2012. **7**(7): p. e40741.

41. Takahashi, Y., et al., *Self-Condensation Culture Enables Vascularization of Tissue Fragments for Efficient Therapeutic Transplantation.* Cell Rep, 2018. **23**(6): p. 1620-1629.

42. Vlahos, A.E., N. Cober, and M.V. Sefton, *Modular tissue engineering for the vascularization of subcutaneously transplanted pancreatic islets.* Proc Natl Acad Sci U S A, 2017. **114**(35): p. 9337-9342.

43. Uzunalli, G., et al., *Improving pancreatic islet in vitro functionality and transplantation efficiency by using heparin mimetic peptide nanofiber gels.* Acta Biomater, 2015. **22**: p. 8-18.

44. Weaver, J.D., et al., *Vasculogenic hydrogel enhances islet survival, engraftment, and function in leading extrahepatic sites.* Sci Adv, 2017. **3**(6): p. e1700184.

45. Komatsu, H., et al., *Posttransplant oxygen inhalation improves the outcome of subcutaneous islet transplantation: A promising clinical alternative to the conventional intrahepatic site.* Am J Transplant, 2017: p. Apr;18(4): 832-842.

46. Gifre-Renom, L., et al., *Organ-Specific Endothelial Cell Differentiation and Impact of Microenvironmental Cues on Endothelial Heterogeneity.* Int J Mol Sci, 2022. **23**(3).

47. Nguyen, J., Y.Y. Lin, and S. Gerecht, *The next generation of endothelial differentiation: Tissue-specific ECs.* Cell Stem Cell, 2021. **28**(7): p. 1188-1204.

48. Paik, D.T., et al., *Single-Cell RNA Sequencing Unveils Unique Transcriptomic Signatures of Organ-Specific Endothelial Cells.* Circulation, 2020. **142**(19): p. 1848-1862.

49. Sordi, V., et al., *Establishment, characterization and long-term culture of human endocrine pancreas-derived microvascular endothelial cells.* Cytotherapy, 2017. **19**(1): p. 141-152.

50. Zanone, M.M., et al., *Expression of nephrin by human pancreatic islet endothelial cells.* Diabetologia, 2005. **48**(9): p. 1789-97.

51. Virtanen, I., et al., *Blood vessels of human islets of Langerhans are surrounded by a double basement membrane.* Diabetologia, 2008. **51**(7): p. 1181-91.

52. Berger, C. and D. Zdzieblo, *Glucose transporters in pancreatic islets.* Pflugers Arch, 2020. **472**(9): p. 1249-1272.

53. Russell, R., et al., *Loss of the transcription factor MAFB limits beta-cell derivation from human PSCs.* Nat Commun, 2020. **11**(1): p. 2742.

54. Huang, C., et al., *Synaptotagmin 4 Regulates Pancreatic beta Cell Maturation by Modulating the Ca(2+) Sensitivity of Insulin Secretion Vesicles.* Dev Cell, 2018. **45**(3): p. 347-361 e5.

55. Rakshit, K., et al., *Postnatal Ontogenesis of the Islet Circadian Clock Plays a Contributory Role in beta-Cell Maturation Process.* Diabetes, 2018. **67**(5): p. 911-922.

Appendix Chapter 1

Hypertension, but not BMI, is predictive of increased pancreatic lipid content and islet dysfunction

This chapter was adapted from the paper published as: Tremmel DM* and Feeney AK*, Mitchell SA, Chlebeck PJ, Raglin S, Fernandez LA, Odorico JS, Sackett SD. Hypertension, but not body mass index, is predictive of increased pancreatic lipid content and islet dysfunction. Am J Transplant. 2020;20:1105–1115. doi: 10.1111/ajt.15698. (*Co-first authors) PMID: 31715064

Daniel Tremmel and Austin Feeney conceived and designed the study under the guidance of Sara Dutton Sackett and Jon Odorico. Daniel Tremmel and Austin Feeney performed the experiments with the assistance of Sierra Raglin, Peter Chlebeck, and Sam Mitchell. Daniel Tremmel and Austin Feeney prepared figures and wrote the manuscript. Jon Odorico, Sara Dutton Sackett and Luis Fernandez edited the manuscript.

Abstract

Pancreatic steatosis is thought to be a negative risk factor for pancreas transplantation outcomes. Despite considering donor body mass index (BMI) and the visualization of intercalated fat as indicators of donor pancreas lipid content, transplant surgeons do not use a quantitative method to directly measure steatosis when deciding to transplant a pancreas. In this study, we utilized non-diabetic human pancreata donated for research to measure the pancreatic and islet-specific lipid content in order to determine which clinical markers correlate best with lipid content. Interestingly, we found that BMI and age correlate with increased pancreatic lipid content (Panc-LC) in men, but not women. Our findings further suggest that total Panc-LC correlates with an increase in islet lipid content (Islet-LC) for both men and women. We noted that pancreata donated from individuals with a history of hypertension have increased Panc-LC independent of donor BMI or sex. Moreover, we identify hypertension as a risk factor for reduced islet function following islet isolation. Together, our findings emphasize differences in pancreas graft quality related to pancreatic and islet lipid content, which may not be predicted by assessing BMI alone, but may be influenced by a donor history of hypertension.

Abbreviations:

BMI	Body Mass Index
Panc-LC	Pancreas Lipid Content
Islet-LC	Islet Lipid Content
MRI	Magnetic Resonance Imaging
MRS	Magnetic Resonance Spectroscopy
CT	Computerized Tomography
GSIS	Glucose Stimulated Insulin Secretion
SI	Stimulation Index
IIDP	Integrated Islet Distribution Program
ORO	Oil Red O
PDRI	Pancreatic Risk Donor Index
UNOS	United Network for Organ Sharing
CIT	Cold Ischemia Time
GAD	Gastrointestinal Disease
HLD	Hyperlipidemia
HTN	Hypertension
CAD	Coronary Artery Disease

Introduction

In 2014, the global burden of diabetes was estimated at 422 million individuals, almost quadrupling from 1980 [1]. In 2015, it was estimated that 711 million individuals were obese [2] and it is well accepted that obesity is a significant risk factor for diabetes [3]. Injectable insulin and numerous oral medications are commonly used to treat diabetes [4]; however, these treatments do not perfectly mimic or correct endogenous insulin secretion. Pancreas or islet transplantation remain the only clinically available treatments capable of replacing lost or dysfunctional beta cells, and restoring euglycemia without the need for exogenous insulin [5].

Over the past 10 years, the number of annual pancreas transplants have decreased, and currently, only ~10% of all deceased donors provide a suitable quality pancreas for transplantation. Approximately 25% of pancreata recovered for intended transplant are discarded [6]. These discarded organs represent potential life-saving treatments for thousands

of recipients on the waiting list, but are not used due to a variety of criteria, including donor age, BMI and damage to the organ. Statistically, discard rates steadily rise as donor age and BMI increase, with discard rates of over 80% from donors with a BMI >35 kg/m^2 and 72% of donors above age 50 [6]. Though the reasons for organ discard are myriad, major concerns arise related to steatosis-associated inflammation and ischemia-reperfusion injury, leading to subsequent thrombosis and graft failure [7-9]. The ability, however, to definitively determine whether a graft is suitable for transplantation and to directly quantify the degree of steatosis in pancreata prior to transplantation is highly subjective. Thus, assessment based on visualization, and unclear relationships between BMI and pancreatic steatosis may result in the unnecessary discard of otherwise healthy organs [8]. To better utilize donor pancreata and reduce discard rates, an improved understanding of how donor selection criteria, such as age and BMI, as well as other donor parameters, actually correlate with steatosis of the pancreas would be beneficial. Furthermore, identifying better demographic correlates for pancreatic steatosis, and understanding how lipid infiltration into the pancreas impacts the endocrine function of the organ, may aid in these decisions.

To this end, several studies have attempted to characterize pancreatic steatosis in humans using histopathology [10, 11] and in vivo imaging techniques, including magnetic resonance imaging (MRI) [12-20], magnetic resonance spectroscopy (MRS) [21-24], ultrasonography [25-33], computerized tomography (CT) [34-36], as well as combinations of these [37, 38]. Although MRI and MRS remain the most sensitive imaging options for estimating donor pancreas fat content in vivo, these techniques are time-consuming and impractical to incorporate into the donor workflow [8]. Furthermore, ultrasonography does not have the ability

to discern steatosis from fibrosis, which precludes its use for accurately characterizing pancreas fat [8, 39]. Finally, CT imaging for pancreatic steatosis lacks sufficient specificity and sensitivity [8, 40].

Given the extensive variety of techniques and study populations, data on the potential clinical factors associated with pancreatic steatosis are conflicting. MRI, MRS, ultrasonography, and CT studies of live patients have correlated different clinical parameters with increased pancreas fat infiltration, including diabetes [16, 21, 23, 24, 30, 32, 36], BMI/obesity [12, 14, 16, 18, 21, 24, 25, 27, 29, 31-35], heavy alcohol use [25], metabolic syndrome [28, 31, 33], increased age [14, 15, 24, 26, 29, 32, 35, 37], hypertension [26, 29, 33], visceral adipose tissue [12, 14, 18, 26, 28], race/ethnicity [14, 22], waist circumference [12, 18], male sex [18, 26, 29], dyslipidemia [14, 20, 29, 31, 33], and hyperglycemia [29, 33]. In particular, BMI, a commonly used marker for evaluating pancreata suitable for transplant, has had mixed results regarding its relationship with pancreas fat quantified by imaging. Several studies have suggested that high BMI or obese subjects have higher pancreas fat content [12, 14, 21, 24, 25, 31-33], however, other studies have reported no association between BMI and pancreas fat [23] and others have reported sex-specific findings in which increased BMI and pancreas fat have a stronger relationship in men [18, 20].

It is also important to whether pancreatic steatosis impacts islet function. Unfortunately, the studies of pancreatic steatosis that have simultaneously evaluated islet function, present findings that are inconsistent [12, 14, 16, 20, 22-24, 37]. In a study employing MRS and standard oral glucose tolerance tests, increased pancreas fat content as assessed by imaging was suggested to be associated with a decline in beta cell function in non-diabetic Caucasian males; the authors suggested it may correlate with the onset of type 2 diabetes [23]. In another study,

pancreatic fat, measured by MRS, was found to be predictive of beta cell dysfunction, as assessed by insulin secretion and insulin sensitivity in a multiethnic sample of men and women [22]. However, several other studies have reported no association between pancreatic fat and islet function [14, 20, 24, 37].

Animal and cell culture studies have the ability to examine the effect of lipids on islet function on a more mechanistic level, albeit with less clinical relevance. Studies of minipigs and mice have shown that a high-fat diet promotes enlarged islets, beta cell damage through oxidative stress, insulin resistance, and increased pancreatic steatosis [41-43]. Mouse islets cultured in media with elevated fatty acid levels resulted in increased intracellular triglyceride storage, as evidenced by Oil Red O (ORO)-positive staining, coincident with morphological changes in the islets and reduced glucose-stimulated insulin secretion (GSIS) performance [44]. Moreover, a study of isolated human islets co-cultured with pancreatic adipocytes showed that adipocyte-secreted cytokines (IL-6, IL-8, and MCP-1) impair GSIS through inflammation of the islet milieu [45].

Given the contradictory findings regarding pancreatic fat content in human imaging studies, we sought to quantify human pancreatic lipid content (Panc-LC) using a protocol to extract lipids directly from donor tissue. Furthermore, because animal and cell culture studies have suggested that lipids disrupt islet function, and modern imaging studies have not yet explored islet-specific steatosis, we histologically quantified islet lipid content (Islet-LC). We correlated these data with islet stimulation indices (SI) following isolation to investigate how a variety of clinical donor parameters, correlate with islet function. We hypothesized that BMI is

not an accurate predictor of Panc-LC and Islet-LC, and evaluated whether other clinical parameters correlate with increased pancreatic and islet steatosis.

Materials and Methods

Pancreas Procurement and Donor Demographics

Donated non-diabetic human pancreata (n = 51, age 16-80 years) were procured for transplantation or research. Following organ recovery, the pancreas was allocated for research if deemed unfit for transplantation due to vascular damage, no suitable recipient, non-ideal age or BMI, and other circumstances. Pancreata were obtained through University of Wisconsin Organ and Tissue Donation services with consent obtained for research from next of kin. The use of human pancreata for research was approved by the University of Wisconsin-Madison Health Sciences Institutional Review Board. Organs were received within 24 hours of procurement and processed to remove extra-pancreatic adipose and vascular tissue.

Pancreatic donor risk index (PDRI) was calculated for all donors excluding the terms for pancreas preservation time and the adjustment for pancreas-after-kidney transplant from the equation [46]. Pancreatic lipid content was determined using the methodology below. Donor clinical parameters, including age, BMI, sex, ethnicity, HbA1c, amylase, lipase, creatinine, cause of death, cold ischemia time (CIT), and health history were excerpted from the United Network for Organ Sharing (UNOS) donor chart and recorded. Elements of our search included the examination of smoking, drug, and alcohol abuse as well as any well-documented history of chronic medical conditions including gastrointestinal disease (GAD), hyperlipidemia (HLD), hypertension (HTN) and coronary artery disease (CAD). All donors had already been selected with

no history or symptoms of pre-diabetes, T1DM, T2DM, or pancreatitis. All parameters were separately assessed for correlation with Panc-LC for all donors with a recorded history for that parameter.

Lipid Extraction and Quantification

Tissue samples were collected from the central parenchyma of the neck of the pancreas, to avoid collecting any extra-pancreatic adipose tissue from the surface of the organ. Pancreatic lipid content (Panc-LC) was quantified using a version of Folch lipid extraction as previously described [47]. This modified Folch method was not significantly different for lipid quantification than the standard Folch Method, which uses 2:1 chloroform:methanol for lipid extraction (Fig. S1A,C) [48]. Pure adipose tissue was used as a positive control, and contained >90% lipid by dry weight (Fig. S1B).

Histology and Image Quantification

Fresh pancreas samples were treated with 30% sucrose overnight, embedded in OCT and stored at -80°C. For staining (adapted from Koopman et al.), samples were cut into 10 μm sections and fixed in 3.7% formaldehyde for 1 hour. Sections were permeabilized with 0.5% Triton X-100/PBS for 5 minutes, and stained with insulin primary (Sigma I2018, 1:10,000) and secondary (Abcam ab150117, 1:2,000) antibodies in 1% BSA for 30 minutes. Following rinses with 1x PBS, the ORO working solution was applied for 30 minutes. The sections were then stained with DAPI (ThermoFisher, D1306) in 1% BSA for 1 minute [49]. Samples were imaged using a Zeiss Axiovert 200M microscope and an Olympus BX51TF microscope. Image quantification for Islet-LC was performed in ImageJ by tracing the Ins+ area and measuring the ORO-positive area within the islet. Acinar lipid content quantification was performed by tracing the Ins-negative area,

immediately surrounding islets. Islet-LC was measured for 19-38 islets per donor. Acinar lipid content was measured on 7-15 images per donor.

Islet Isolation and GSIS

Human pancreata from non-diabetic donors were recovered for research following confirmed donation consent and consent for research use of organs. Islets were isolated using a previously described method (Hanson, et al.) and cultured in CMRL 1066 Supplemented (Corning) with 2.5% human serum albumin at 37°C in a 5% CO_2 incubator for 24 to 36 hours [50].

Islets were assayed in vitro for response to glucose stimulation according to a previously published protocol.[51] Briefly, triplicate islet samples were incubated 1 hour in media containing 2.8mM glucose and a sample of supernatant was collected. The same islets were then incubated 1 hour in media containing 28mM glucose and a sample of supernatant was collected. The insulin concentration of supernatant samples was measured using a Human Insulin ELISA kit (Mercodia). The SI is calculated as the ratio of insulin concentrations from the 28mM glucose incubation supernatants to the corresponding 2.8 mM glucose incubation supernatants.

Statistical Analyses

Statistical analyses were performed using Prism 6 for Windows (GraphPad Software, Inc.). For pairwise comparisons, independent unpaired two-sample t-tests were performed except when population proportions were compared. In these instances, a Chi-square test of independence was performed. All correlations were assessed using Pearson's Correlation and R2 and p-values were reported. A p-value < 0.05 was considered significant, and Prism's suggested significance classification scheme was followed (**$p< 0.01$) and (* $p < 0.05$).

Results

Pancreas donor demographics and graft quality

The donor demographics of 51 non-diabetic human pancreata recovered for Panc-LC analysis are described (Table 1). The average age was 47.9 years, the average BMI was 27.2, 84.3% were Caucasian, 56.9% were men. The donors exhibited a wide range of Panc-LC, ranging from 4.7% to 70.2% with an average of 27.7%. Comparing men and women, only PDRI and the prevalence of CAD were significantly different, both being increased in women compared to men. Notably, mean creatinine and HbA1c are within normal ranges, suggesting normal kidney function and glucose homeostasis in this cohort of non-diabetic donors.

Pancreas lipid content is correlated with BMI and age in men but not women

To evaluate if BMI and age correlate with Panc-LC, we quantified Panc-LC using lipid extraction. Upon examination of population-level trends for all donors, there was no significant correlation between BMI and age ($p=0.085$), which indicated that these variables should be investigated separately for their relationship with Panc-LC (Fig. 1A). Furthermore, there was no significant correlation between age and Panc-LC for all donors ($p=0.054$) (Fig. 1B). Even without statistical significance, these relatively low p-values represent modest evidence that these variable pairs may be related. However, there was a significant correlation when comparing BMI and Panc-LC for all donors ($p=0.019$) (Fig. 1C). However, when we separated donors according to sex, we observed that age versus Panc-LC ($p=0.024$), and BMI versus Panc-LC ($p=0.010$) were both significantly correlated in men (Fig. 2A-B) but were not significantly correlated in women ($p=0.647$ and $p=0.397$, respectively) (Fig. 2 C-D).

Table 1. Pancreas Donor Demographics

	All Donors		Men		Women		P-value	
N-value	51		29		22		-	-
Age (years)	47.86	± 14.85	44.97	± 14.24	51.68	± 15.10	0.148	(ns)
BMI (kg/m2)	27.16	± 6.01	27.38	± 5.02	26.88	± 7.23	0.605	(ns)
Race (% Caucasian)	92.16	(N= 47)	93.10	(N= 27)	90.91	(N= 20)	0.936	(ns)
CIT (hours)	11.94	± 6.90	12.84	± 7.75	10.78	± 5.61	0.215	(ns)
PDRI	2.07	± 1.08	1.73	± 0.96	2.51	± 1.09	0.023	*
% Smoker	64.71	(N= 33)	58.62	(N= 17)	72.73	(N= 16)	0.535	(ns)
% Heavy Alcohol Use	27.45	(N= 14)	20.69	(N= 6)	36.36	(N= 8)	0.290	(ns)
% HTN	43.14	(N= 22)	44.83	(N= 13)	40.91	(N= 9)	0.833	(ns)
% HTN (>5 years)	25.49	(N= 13)	27.59	(N= 8)	22.73	(N= 5)	0.734	(ns)
% CAD	5.88	(N= 3)	0.00	(N= 0)	13.64	(N= 3)	0.047	*
% HLD	11.76	(N= 6)	10.34	(N= 3)	13.64	(N= 3)	0.734	(ns)
% GAD	15.69	(N= 8)	17.24	(N= 5)	13.64	(N= 3)	0.747	(ns)
Death Cause (% Trauma)	23.53	(N= 12)	27.59	(N= 8)	18.18	(N= 4)	0.493	(ns)
% DBD	82.35	(N= 42)	79.31	(N= 23)	86.36	(N= 19)	0.783	(ns)
Creatinine (mg/dL)	1.05	± 0.69	1.04	± 0.50	1.07	± 0.89	0.786	(ns)
HbA1C (%) (n=28)	5.33	± 0.46	5.27	± 0.12	5.35	± 0.09	0.657	(ns)
Amylase (u/L) (n=44)	81.12	± 91.68	65.77	± 59.24	104.59	± 124.95	0.356	(ns)
Lipase (u/L) (n=44)	57.21	± 93.60	48.62	± 84.26	71.19	± 108.53	0.372	(ns)
Pancreatic Lipid Content (%)	27.72	± 14.62	28.48	± 15.38	26.80	± 13.93	0.656	(ns)

Table 1. Correlation of pancreatic donor demographics and graft quality.
Graft quality is expressed by PDRI and pancreatic lipid content, which was determined using the Folch method. Values are reported with ± 1SD or the number of patients (N) for population proportion data. Abbreviations: CIT=Cold Ischemia Time, HTN=Hypertension, CAD=Coronary Artery Disease, HLD=Hyperlipidemia, GAD=Gastrointestinal Disease, PDRI=pancreatic donor risk index, DBD=Donor After Brain Death. *Indicates p-value<0.05. ns indicates not significant (p-value>0.05).

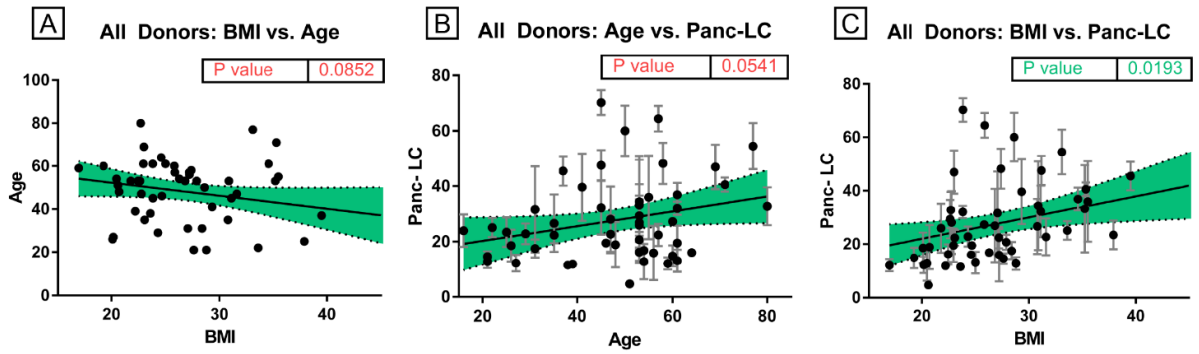

Figure 1. Pancreas lipid content is correlated with BMI but not age for all donors.
A-C) Correlations including BMI, Age, and Panc-LC in all pancreatic donors (men and women combined) indicate a significant correlation for BMI and Panc-LC. The 95% confidence interval is shaded around the line of best fit. The p-values were determined using a Pearson correlation. Donor BMI and Age are extracted from the donor chart in the UNOS system. Error bars indicate ± 1 SD among technical replicates for Panc-LC. N=51 donor pancreata.

Pancreas lipid content is correlated with increased islet lipid content

To assess whether Panc-LC may have implications for pancreas quality and endocrine function, we assessed islet quality within a subset of donor organs. When pancreas sections were co-stained for insulin, to identify islets, and ORO, to stain lipids, there were distinct differences in the lipid localization among the islet and acinar compartments. Specifically, there were high concentrations of lipid droplets found within the islets of high lipid content pancreata, but not in lower Panc-LC organs (Fig. 3). To further investigate how lipid distribution varied among pancreas donors, we quantified the ORO staining content within the islet and acinar compartments. Islet-LC was found to strongly correlate with total Panc-LC ($p=0.007$) (Fig. 4A) and this was the case regardless of sex (Fig. S2A-B). Furthermore, the ratio of lipids in the islet compared to acinar regions (Isl/Ac) also increased with total Panc-LC ($p=0.0004$) (Fig. 4B). This indicates that high lipid content pancreata contain islets that have significant lipid deposits compared to lower lipid content pancreata. This is visibly distinguishable upon direct histological comparison (Fig. 3).

Donor hypertension is predictive of increased pancreas and islet lipid content and islet dysfunction

A population of donors within the same moderate BMI range were found to have a broad range for total Panc-LC, with a subpopulation that contained significantly higher than average lipid content, and a different subpopulation that exhibited significantly below average lipid content (Fig. 5A). To identify additional donor metrics that may correlate with this striking difference in Panc-LC for this BMI-matched subset of donors, we examined the medical histories available through the UNOS system. We failed to uncover any trends based on smoking, alcohol or drug abuse, or GAD, among the two groups (data not shown). In contrast, within the two subsets of donors, we found that 7 of 8 donors in the above average Panc-LC group had a history

of HTN, while no donors in the below average group had a history of HTN. There was also an increased presence of CAD and HLD in the high Panc-LC group, but the overall prevalence of these diseases in our donor population was too low to further investigate.

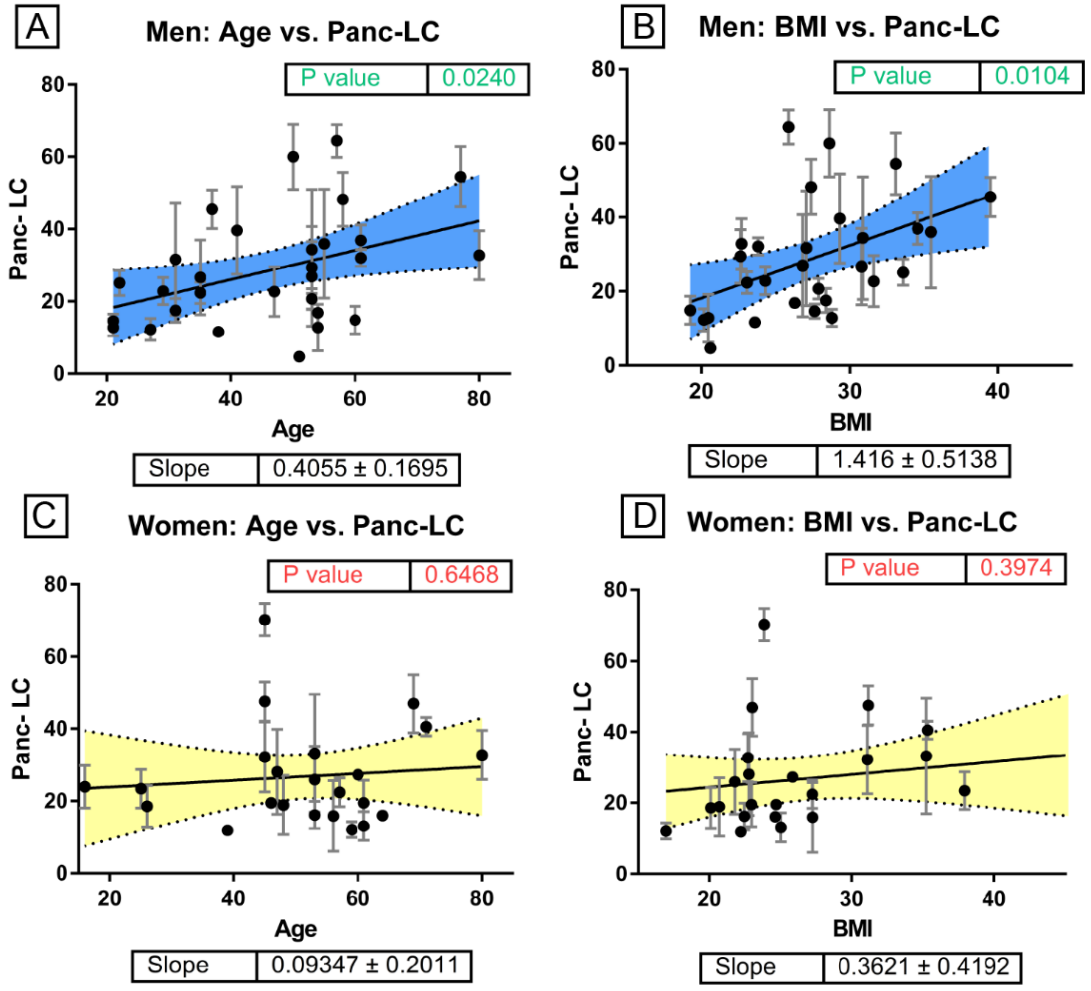

Figure 2. Pancreas lipid content is correlated with BMI and age in men only.
A-D) Correlations including BMI, Age, and Panc-LC in sex-stratified donor populations as labeled above indicate significant correlations for men. The 95% confidence interval is shaded around the line of best fit. The p-values were determined using a Pearson correlation. Error bars indicate ± 1 SD among technical replicates for Panc-LC. Donor BMI and Age are extracted from the UNOS system. N=29 men; N=22 women donor pancreata.

Figure 3:

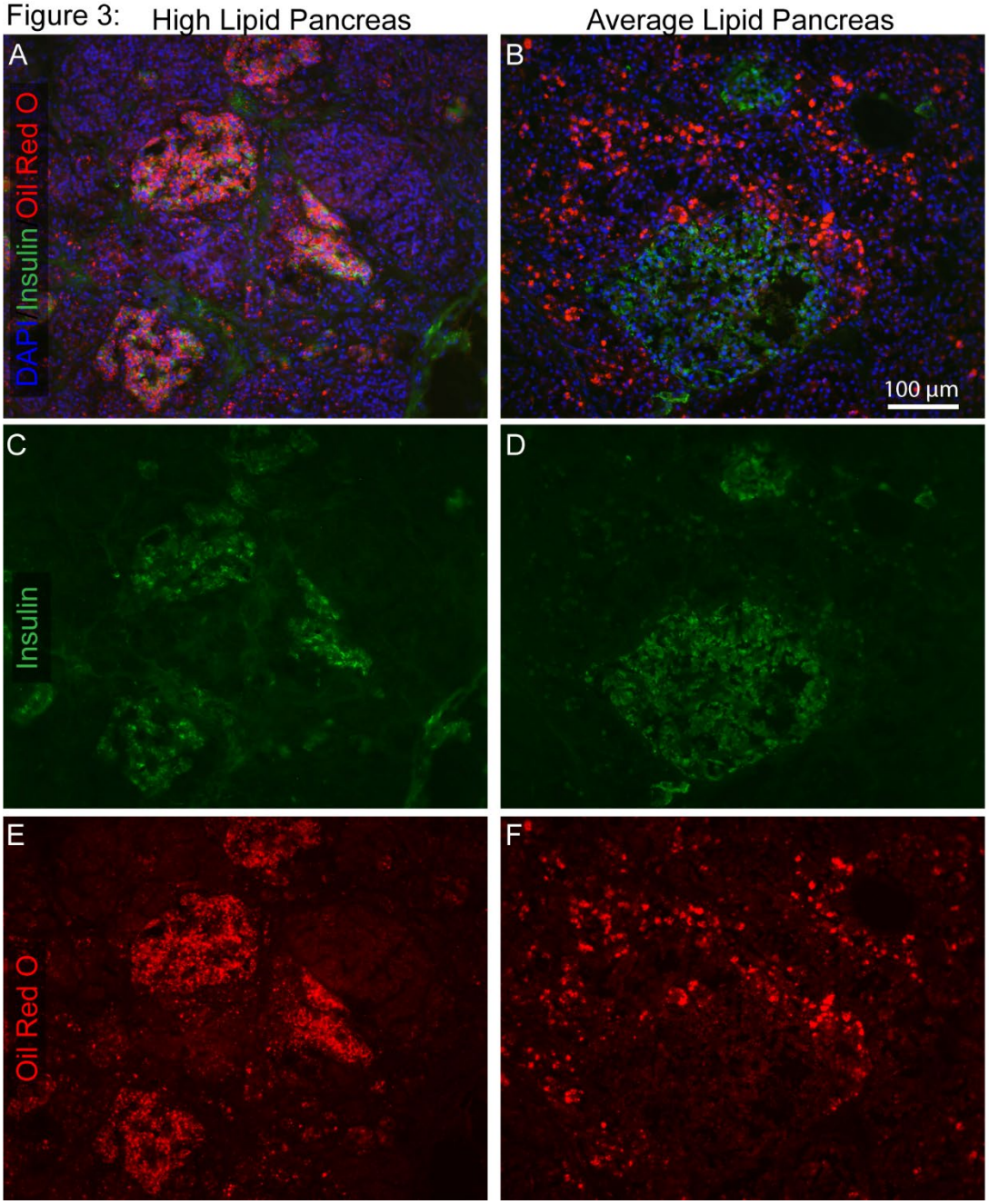

Figure 3. Islets from steatotic donors (high lipid pancreata) are enriched for lipids within islets. A-F) Sections from a high lipid pancreas (70.2% Panc-LC) and an average lipid pancreas (26.0% Panc-LC) were embedded in OCT were stained for insulin (green), ORO (red), and DAPI (blue) and imaged at 20X magnification. **A)** Representative merged image showing ORO-positive tissue overlapping with insulin-positive tissue in a pancreas with high Panc-LC. **B)** Representative merged image depicting ORO-positive tissue separate from insulin-positive tissue (localized to the acinar) in a pancreas with average Panc-LC. **C-D)** Insulin channel showing the localization of islets in both pancreata. **E-F)** ORO channel showing the localization of lipids in both pancreata. Scale bar in B = 100µm.

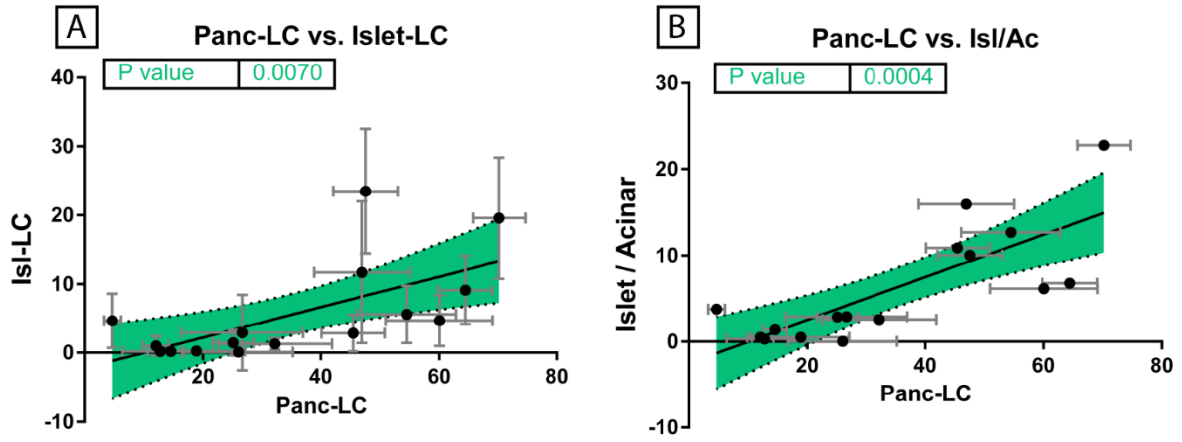

Figure 4. Panc-LC is significantly correlated with Islet-LC and the Isl/Ac lipid ratio.
A-B) Correlations including Panc-LC, Islet-LC, and an Isl/Ac lipid ratio for a subset of donors. Islet-LC tends to appear in high Panc-LC pancreata. The 95% confidence interval is shaded around the line of best fit, and the p-values were determined using a Pearson correlation. Error bars represent ± 1SD.

To examine the correlation of HTN with Panc-LC, donors were categorized into three groups: donors with no history of HTN (N=26), donors with >1-year (N=16) and >5-year histories of HTN (N=13) (Fig. 5B-D). Donors with unclear history or less than a 1-year duration were excluded to prevent potential confounding. When comparing the three groups, we found that the average BMI was indistinguishable (p=0.991) (Fig. 5B), but there were significant differences with regard to Panc-LC (p=0.002) (Fig. 5C) and Islet-LC (p=0.014) (Fig. 5D) for both HTN groups, compared to the non-HTN group. We also observed this correlation for both men and women when analyzed separately, although women had significance only with >5 years of HTN duration. (Fig. S3).

Using this information, we performed a retrospective study of isolated islets from 95 pancreata donated for research purposes, assessing the stimulation index (SI) during static GSIS. These organs were donated for islet isolation and distributed through the Integrated Islet Distribution Program (IIDP), and therefore were by necessity different donors from the pool used

to study Panc-LC. Donor history of HTN was collected using UNOS records, and donors were categorized into three groups based on this history: no HTN, >1-year HTN, and >5-years of HTN history. Again, donors with unclear records of HTN were excluded from the dataset. The results indicate that donors with a 5-year or longer documented history of HTN had a significantly lower average SI (SI=1.90, N=14) (p=0.016), compared to donors with no history of HTN (SI=3.14, N=58). The group of donors with a 1-year or greater history of HTN was lower than the control group, but was not significantly different (SI=2.46, N=34) (p=0.062) (Fig. 6C). Furthermore, the SI showed no correlation with donor BMI (p=0.670) (Fig. 6A), and the islet SI was not significantly different between discrete groups of donors with BMI <30 and obese donors with BMI >35 (p=0.811) (Fig. 6B).

Figure 5:

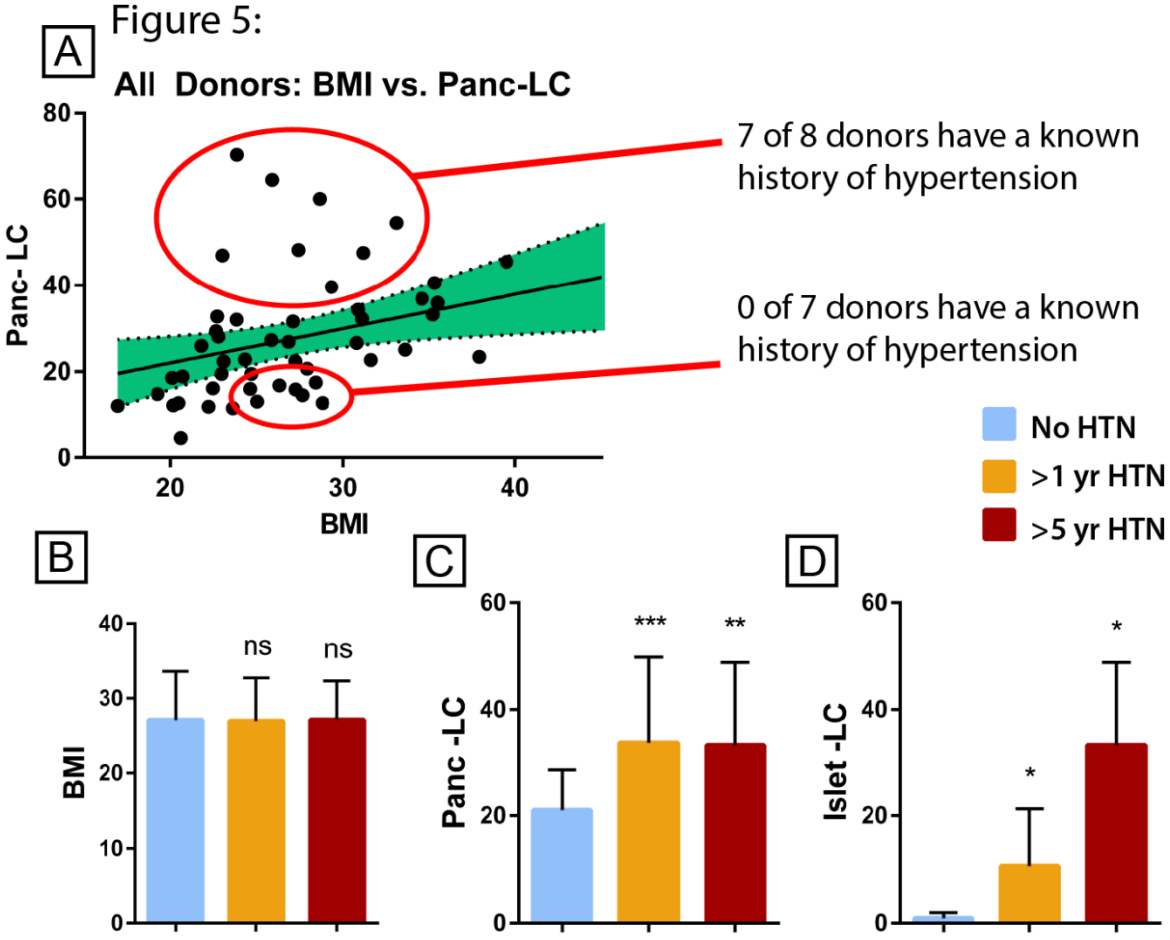

Figure 5. Donor history of hypertension is predictive of increased pancreas and islet lipid content independent from changes in BMI. **A)** Correlation plots for Panc-LC and BMI indicate two distinct populations of donors with differences in Panc-LC independent of BMI. Donors were divided into groups with no history of HTN (N=26) and history of HTN (>1 yr, N=16) (>5 yr, N=13) **B)** Average BMI and **C)** Panc-LC for the three groups. **D)** Average Islet-LC in No HTN (N=7) and HTN (>1 yr, N=6) (>5 yr, N=5) groups. Error bars indicate ± 1SD, (* p<0.05, ** p<0.01, *** p<0.001). **(Previous Page)**

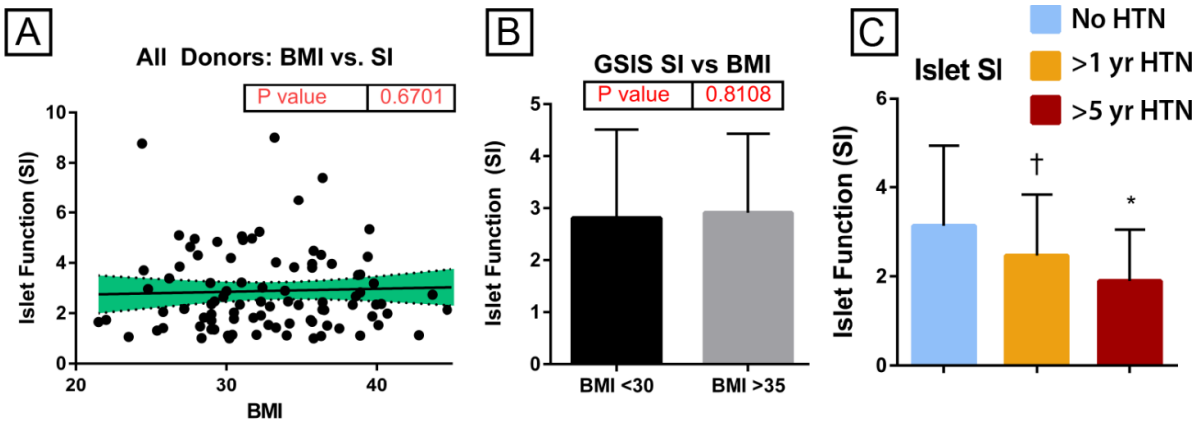

Figure 6. Donor history of hypertension, but not BMI, is predictive of islet dysfunction.
A) Among all islet donors, there is no significant correlation between islet function (SI) and BMI (N=95). **B)** Donors with BMI <30 (N=29) and BMI >35 (N=35) have indistinguishable islet function by GSIS. **C)** Donors were divided into groups with no history of HTN (N=58) and history of HTN (>1 yr, N=34) (>5 yr, N=14). Donors with >5 years of documented hypertension had significantly lower SI following islet isolation. Error bars indicate ± 1SD, († not significant, p=0.062), (*p<0.05).

Discussion

Steatosis is considered a critical factor for determining the suitability of donor pancreata for transplantation, but many pancreata from high BMI donors can be successfully transplanted. Given the need to be good stewards of precious donated organ resources and the rising prevalence of diabetes worldwide, it is imperative that available pancreata are maximally utilized. To date, BMI and surgeon qualitative estimates of fat content serve as surrogates for

pancreatic fat infiltration, yet neither precisely measures quantitative intracellular fat content. Biopsy-based methods for quantifying lipid content could more precisely determine degree of fat infiltration or replacement; however, the fear of biopsy related complications, such as pseudocysts and enzyme leaks after transplantation has prevented adoption of back table biopsies into routine clinical practice. Furthermore, understanding how the measured lipid content correlates with other associated donor parameters could improve our ability to discern lesser quality pancreata based on non-invasive clinical parameters to determine whether or not the pancreas should be transplanted. To our knowledge, we are the first to directly quantify the lipid content of human pancreata, in order to better understand the clinical correlates and functional impact of lipid accumulation in deceased donor pancreata.

Our current data demonstrate that BMI and Panc-LC are correlated when considering the entire population of 51 pancreata. However, upon further investigation, BMI and Panc-LC were found to be significantly correlated for men, but not women. This finding could reflect sex-related differences in systemic fat distribution, as has been postulated by a variety of studies [52]. Such an observation could be useful clinically, for example, to broaden the BMI threshold for accepting female pancreata for transplantation while restricting the threshold for male pancreata. While our study lacks transplant graft survival outcomes data, and the aforementioned recommendation is tentative, it does align with a current pre-determined pancreas acceptance policy at the University of Wisconsin. Similarly, age is significantly correlated with Panc-LC for men, but not women. These sex-specific differences may be one reason that various population-level studies, including both men and women, have only found modest trends relating Panc-LC with other variables. Taken together these data suggest that BMI and age play a sex-specific role

in pancreatic steatosis, which has been reported in only a few prior imaging studies [18, 20, 26, 29]. Additionally, we found a significant correlation between Panc-LC and Islet-LC for both men and women (Fig. S2A-B), which has not previously been reported to our knowledge and highlights how Panc-LC may correlate with beta cell dysfunction. Moreover, Panc-LC is significantly correlated with the ratio of islet to acinar lipids (Isl/Ac), which suggests that as the pancreas becomes progressively steatotic, islets become intracellularly enriched with lipids.

Others have previously reported that hypertension [26, 29, 33] and dyslipidemia [14, 20, 29, 31, 33] are associated with increased pancreatic steatosis as assessed by imaging by MR and ultrasound. In our study, we also identified hypertension as a potential risk for increased Panc-LC. We found that donors with and without a history of HTN did not differ in BMI overall, but both Panc-LC and Islet-LC were significantly higher for donors with a 5-year or longer history of HTN, regardless of sex. These data indicate that a history of HTN contributes to an increase in Panc-LC and Islet-LC independently from either BMI or sex. We also made an effort to correlate HLD and CAD as potential risk factors for increased Panc-LC, but our donor population had too few donors with these conditions to make firm conclusions. We speculate that high Panc-LC and long standing HTN may be markers of metabolic syndrome. Interestingly, we also found that in many long duration HTN donors with high Panc-LC, lipids were concentrated within the islets, in addition to steatotic deposits throughout the pancreas, while the lipid content of the peri-islet acinar tissue varied little among all donors. This is different than what was previously observed in a mouse study, where both islets and acinar cells accumulated lipids equally as the pancreas became steatotic over time during exposure to a high fat diet [53]. The differential accumulation

of fat in islets vs. acinar tissue of the human pancreas has important implications in the field of pancreas and islet transplantation.

Some studies have found that donor BMI has minimal impact on pancreas transplant outcomes, whereas others have suggested high BMI is associated with increased risk of technical failure. Humar et al. found that BMI may have a stronger impact on the technical success of the transplant, and minimal impact on the longer term glycemic outcomes following a successful surgery [54]. Alhamad et al. similarly found that mildly obese donors (BMI=30-35 kg/m^2) had similar allograft failure rates as pancreata from donors with a BMI from 20-30 kg/m^2, but donors above 35 kg/m^2 were associated with increased graft failure [55]. Finger et al. also showed that if a donor possesses one risk factor for technical failure, such as high BMI alone, grafts experience nearly equal technical successes to ideal grafts without any risk factors and normal BMI [56]. On the other hand, Axelrod et al. showed that a high BMI, older age and other factors contribute to lower 1 year graft survival rates [46].

Our study suggests that HTN, but not BMI, is associated with decreased in vitro functional performance of isolated islets. It would be highly speculative to suggest that HTN would be associated with higher technical failure rates or worse glycemic control in the long-term. In support of this hypothesis however, a recent study analyzing a database of ~25,000 pancreas transplants found that a donor history of HTN had an independent, negative impact on overall recipient and graft survival [57]. Borrowing from kidney transplant research, the authors postulated that the negative effect of HTN on pancreas graft function could occur through vascular damage, which results in poor organ blood supply [57]. However, based on our findings, we additionally propose that HTN, which correlates with increased Panc-LC and Islet-LC and

reduced islet function, could thereby contribute to inferior long-term pancreas graft glycemic outcomes as a result of increased lipid peroxidation or lipotoxicity and/or greater sensitivity to ischemia-reperfusion injury. Several animal and cell culture studies have identified that intracellular lipid storage within islets causes a marked reduction in islet function [41-45]. Thus, because hypertension is associated with an increase in Panc-LC and Islet-LC independently from sex, it may represent a more useful marker than BMI for pancreas and islet steatosis, and possibly graft function post-transplantation.

Our direct method of measuring Panc-LC may have advantages over the variety of imaging studies that have resulted in inconsistent findings related to pancreatic steatosis. Imaging may not be the most translatable technique for organ donation, but organ biopsies are routinely used to assess donated livers and kidneys prior to transplant. Because hepatic steatosis is a transplantation concern, crudely estimating the degree of hepatic steatosis of the liver by biopsy has become common practice. We collected biopsies of pancreata for ORO staining (Fig. S4) and lipid extraction (Fig. S5) to demonstrate that clinical biopsies may be useful in pre-transplant donor selection. We found that the lipid content values obtained from biopsies were consistent with those obtained from larger pieces of tissue (Fig. S5), but the lipid extraction takes several days and is therefore not a translatable method to apply to organ donation and transplantation practices. On the other hand, pancreas graft biopsies could potentially be obtained at the time of recovery and immediately processed to estimate the degree of steatosis of the acinar and islet regions [58-60]. Additionally, ORO staining could be accomplished in a timely fashion in parallel. Although performing pancreas graft biopsies is not common, several studies indicate they are associated with very low complication rates [61-63].

In conclusion, by directly quantifying the pancreatic lipid content, our study demonstrates that men and women may have differential lipid accumulation profiles in the pancreas based on age and BMI. We found that men are at higher risk to have increased Panc-LC with increased age and BMI, but this trend was not found for women. For both sexes, very high Panc-LC was associated with an increased lipid enrichment specifically in islets, which could be an indication of poor islet health and function and increased potential for damage after an ischemia-reperfusion injury. Both total Panc-LC and Islet-LC were found to be significantly increased in a population of donors with histories of HTN, and in islets isolated from donors with a history of HTN, GSIS function was reduced. Moving forward, further investigation into improving the identification of steatotic pancreata prior to transplantation is necessary to better utilize available donor organs. It is also important to understand how islet function may be affected in donors and patients with high Panc-LC and Islet-LC and whether these factors impact pancreas transplant outcomes.

Acknowledgements

This study was supported in part through grants from the National Institutes of Health R21AI126419-02. We would like to thank Carrie Sparks and the UW Organ and Tissue Donation (OTD) services for their help regarding donor medical histories. We would like to acknowledge the support of the Integrated Islet Distribution Program (IIDP) and members of the Fernandez lab for generating islets and providing access to islet donor data, as well as Sierra Raglin, Vansh Jain, and Nicholas Quirini in the Department of Surgery Histology Core for their excellent skills with tissue processing and immunohistochemistry. Additionally, we would like to offer a special thanks to the donor families who donated tissues for this research.

References:

1. Roglic, G. and World Health Organization, Global report on diabetes. 2016, Geneva, Switzerland: World Health Organization. 86 pages.
2. Collaborators, G.B.D.O., et al., Health Effects of Overweight and Obesity in 195 Countries over 25 Years. N Engl J Med, 2017. 377(1): p. 13-27.
3. Collaborators, G.B.D.R.F., et al., Global, regional, and national comparative risk assessment of 79 behavioural, environmental and occupational, and metabolic risks or clusters of risks in 188 countries, 1990-2013: a systematic analysis for the Global Burden of Disease Study 2013. Lancet, 2015. 386(10010): p. 2287-323.
4. Marin-Penalver, J.J., et al., Update on the treatment of type 2 diabetes mellitus. World J Diabetes, 2016. 7(17): p. 354-95.
5. Gruessner, R.W., D.E. Sutherland, and A.C. Gruessner, Mortality assessment for pancreas transplants. Am J Transplant, 2004. 4(12): p. 2018-26.
6. Kandaswamy, R., et al., OPTN/SRTR 2017 Annual Data Report: Pancreas. Am J Transplant, 2019. 19 Suppl 2: p. 124-183.
7. Chu, M.J., et al., The impact of hepatic steatosis on hepatic ischemia-reperfusion injury in experimental studies: a systematic review. Biomed Res Int, 2013. 2013: p. 192029.
8. Dholakia, S., et al., Significance of steatosis in pancreatic transplantation. Transplant Rev (Orlando), 2017. 31(4): p. 225-231.
9. Giorgakis, E., et al., Solid pancreas transplant: Pushing forward. World J Transplant, 2018. 8(7): p. 237-251.
10. Nacif, L.S., et al., Liver biopsy may facilitate pancreatic graft evaluation: Positive association between liver steatosis and pancreatic graft adipose infiltration. Clinics (Sao Paulo), 2018. 73: p. e49.
11. van Geenen, E.J., et al., Nonalcoholic fatty liver disease is related to nonalcoholic fatty pancreas disease. Pancreas, 2010. 39(8): p. 1185-90.
12. Heni, M., et al., Pancreatic fat is negatively associated with insulin secretion in individuals with impaired fasting glucose and/or impaired glucose tolerance: a nuclear magnetic resonance study. Diabetes Metab Res Rev, 2010. 26(3): p. 200-5.
13. Kim, H.J., et al., Focal fatty replacement of the pancreas: usefulness of chemical shift MRI. AJR Am J Roentgenol, 2007. 188(2): p. 429-32.
14. Le, K.A., et al., Ethnic differences in pancreatic fat accumulation and its relationship with other fat depots and inflammatory markers. Diabetes Care, 2011. 34(2): p. 485-90.
15. Li, J., et al., Noninvasive quantification of pancreatic fat in healthy male population using chemical shift magnetic resonance imaging: effect of aging on pancreatic fat content. Pancreas, 2011. 40(2): p. 295-9.

16. Macauley, M., et al., Altered volume, morphology and composition of the pancreas in type 2 diabetes. PLoS One, 2015. 10(5): p. e0126825.

17. Patel, N.S., et al., Association between novel MRI-estimated pancreatic fat and liver histology-determined steatosis and fibrosis in non-alcoholic fatty liver disease. Aliment Pharmacol Ther, 2013. 37(6): p. 630-9.

18. Rossi, A.P., et al., Predictors of ectopic fat accumulation in liver and pancreas in obese men and women. Obesity (Silver Spring), 2011. 19(9): p. 1747-54.

19. Sijens, P.E., et al., MRI-determined fat content of human liver, pancreas and kidney. World J Gastroenterol, 2010. 16(16): p. 1993-8.

20. Wong, V.W., et al., Fatty pancreas, insulin resistance, and beta-cell function: a population study using fat-water magnetic resonance imaging. Am J Gastroenterol, 2014. 109(4): p. 589-97.

21. Lingvay, I., et al., Noninvasive quantification of pancreatic fat in humans. J Clin Endocrinol Metab, 2009. 94(10): p. 4070-6.

22. Szczepaniak, L.S., et al., Pancreatic steatosis and its relationship to beta-cell dysfunction in humans: racial and ethnic variations. Diabetes Care, 2012. 35(11): p. 2377-83.

23. Tushuizen, M.E., et al., Pancreatic fat content and beta-cell function in men with and without type 2 diabetes. Diabetes Care, 2007. 30(11): p. 2916-21.

24. van der Zijl, N.J., et al., Ectopic fat storage in the pancreas, liver, and abdominal fat depots: impact on beta-cell function in individuals with impaired glucose metabolism. J Clin Endocrinol Metab, 2011. 96(2): p. 459-67.

25. Al-Haddad, M., et al., Risk factors for hyperechogenic pancreas on endoscopic ultrasound: a case-control study. Pancreas, 2009. 38(6): p. 672-5.

26. Choi, C.W., et al., Associated factors for a hyperechogenic pancreas on endoscopic ultrasound. World J Gastroenterol, 2010. 16(34): p. 4329-34.

27. Della Corte, C., et al., Nonalcoholic fatty pancreas disease and Nonalcoholic fatty liver disease: more than ectopic fat. Clin Endocrinol (Oxf), 2015. 83(5): p. 656-62.

28. Lee, J.S., et al., Clinical implications of fatty pancreas: correlations between fatty pancreas and metabolic syndrome. World J Gastroenterol, 2009. 15(15): p. 1869-75.

29. Lesmana, C.R., et al., Prevalence of Non-Alcoholic Fatty Pancreas Disease (NAFPD) and its risk factors among adult medical check-up patients in a private hospital: a large cross sectional study. BMC Gastroenterol, 2015. 15: p. 174.

30. Ou, H.Y., et al., The association between nonalcoholic fatty pancreas disease and diabetes. PLoS One, 2013. 8(5): p. e62561.

31. Sepe, P.S., et al., A prospective evaluation of fatty pancreas by using EUS. Gastrointest Endosc, 2011. 73(5): p. 987-93.

32. Wang, C.Y., et al., Enigmatic ectopic fat: prevalence of nonalcoholic fatty pancreas disease and its associated factors in a Chinese population. J Am Heart Assoc, 2014. 3(1): p. e000297.

33. Wu, W.C. and C.Y. Wang, Association between non-alcoholic fatty pancreatic disease (NAFPD) and the metabolic syndrome: case-control retrospective study. Cardiovasc Diabetol, 2013. 12: p. 77.

34. Pham, Y.H., et al., Prevalence of Pancreatic Steatosis at a Pediatric Tertiary Care Center. South Med J, 2016. 109(3): p. 196-8.

35. Saisho, Y., et al., Pancreas volumes in humans from birth to age one hundred taking into account sex, obesity, and presence of type-2 diabetes. Clin Anat, 2007. 20(8): p. 933-42.

36. Yamazaki, H., et al., Lack of Independent Association Between Fatty Pancreas and Incidence of Type 2 Diabetes: 5-Year Japanese Cohort Study. Diabetes Care, 2016. 39(10): p. 1677-83.

37. Begovatz, P., et al., Pancreatic adipose tissue infiltration, parenchymal steatosis and beta cell function in humans. Diabetologia, 2015. 58(7): p. 1646-55.

38. Hu, H.H., et al., Comparison of fat-water MRI and single-voxel MRS in the assessment of hepatic and pancreatic fat fractions in humans. Obesity (Silver Spring), 2010. 18(4): p. 841-7.

39. Yang, D.M., et al., Sonographic appearance of focal fatty infiltration of the pancreas. J Clin Ultrasound, 2010. 38(1): p. 45-7.

40. Katz, D.S., et al., Using CT to reveal fat-containing abnormalities of the pancreas. AJR Am J Roentgenol, 1999. 172(2): p. 393-6.

41. Zhao, Z.Z., et al., Long-term High-fat High-sucrose Diet Promotes Enlarged Islets and beta-Cell Damage by Oxidative Stress in Bama Minipigs. Pancreas, 2015. 44(6): p. 888-95.

42. Fernandes-Santos, C., et al., Rosiglitazone aggravates nonalcoholic Fatty pancreatic disease in C57BL/6 mice fed high-fat and high-sucrose diet. Pancreas, 2009. 38(3): p. e80-6.

43. Fraulob, J.C., et al., A Mouse Model of Metabolic Syndrome: Insulin Resistance, Fatty Liver and Non-Alcoholic Fatty Pancreas Disease (NAFPD) in C57BL/6 Mice Fed a High Fat Diet. J Clin Biochem Nutr, 2010. 46(3): p. 212-23.

44. Pinnick, K., et al., Reversibility of metabolic and morphological changes associated with chronic exposure of pancreatic islet beta-cells to fatty acids. J Cell Biochem, 2010. 109(4): p. 683-92.

45. Gerst, F., et al., Metabolic crosstalk between fatty pancreas and fatty liver: effects on local inflammation and insulin secretion. Diabetologia, 2017. 60(11): p. 2240-2251.

46. Axelrod, D.A., et al., Systematic evaluation of pancreas allograft quality, outcomes and geographic variation in utilization. Am J Transplant, 2010. 10(4): p. 837-45.

47. Sackett, S.D., et al., Extracellular matrix scaffold and hydrogel derived from decellularized and delipidized human pancreas. Sci Rep, 2018. 8(1): p. 10452.

48. Folch, J., M. Lees, and G.H. Sloane Stanley, A simple method for the isolation and purification of total lipides from animal tissues. J Biol Chem, 1957. 226(1): p. 497-509.

49. Koopman, R., G. Schaart, and M.K. Hesselink, Optimisation of oil red O staining permits combination with immunofluorescence and automated quantification of lipids. Histochem Cell Biol, 2001. 116(1): p. 63-8.

50. Hanson, M.S., et al., A simplified approach to human islet quality assessment. Transplantation, 2010. 89(10): p. 1178-88.

51. Committee, N.C.C.C.M.C.M. and N.C. Consortium, Functional assessment of purified human pancreatic islets: glucose stimulated insulin release by ELISA: A Standard Operating Procedure of the NIH Clinical Islet Transplantation Consortium. CellR4 Repair Replace Regen Reprogram, 2014. 2(2).

52. Palmer, B.F. and D.J. Clegg, The sexual dimorphism of obesity. Mol Cell Endocrinol, 2015. 402: p. 113-9.

53. Lee, Y., et al., Pancreatic steatosis: harbinger of type 2 diabetes in obese rodents. Int J Obes (Lond), 2010. 34(2): p. 396-400.

54. Humar, A., et al., The impact of donor obesity on outcomes after cadaver pancreas transplants. Am J Transplant, 2004. 4(4): p. 605-10.

55. Alhamad, T., et al., Selected Mildly Obese Donors Can Be Used Safely in Simultaneous Pancreas and Kidney Transplantation. Transplantation, 2017. 101(6): p. 1159-1166.

56. Finger, E.B., et al., A composite risk model for predicting technical failure in pancreas transplantation. Am J Transplant, 2013. 13(7): p. 1840-9.

57. Hu, Z.H., et al., Pancreas grafts for transplantation from donors with hypertension: an analysis of the scientific registry of transplant recipients database. BMC Gastroenterol, 2018. 18(1): p. 141.

58. Geramizadeh, B. and S.A. Malek-Hosseini, Role of Histopathologist in Liver Transplantation. Int J Organ Transplant Med, 2017. 8(1): p. 1-6.

59. Heller, B. and S. Peters, Assessment of liver transplant donor biopsies for steatosis using frozen section: accuracy and possible impact on transplantation. J Clin Med Res, 2011. 3(4): p. 191-4.

60. Markin, R.S., et al., Frozen section evaluation of donor livers before transplantation. Transplantation, 1993. 56(6): p. 1403-9.

61. Niederhaus, S.V., et al., Acute cellular and antibody-mediated rejection of the pancreas allograft: incidence, risk factors and outcomes. Am J Transplant, 2013. 13(11): p. 2945-55.

62. Redfield, R.R., D.B. Kaufman, and J.S. Odorico, Diagnosis and Treatment of Pancreas Rejection. Curr Transplant Rep, 2015. 2(2): p. 169-175.

63. Uva, P.D., et al., Laparoscopic Biopsies in Pancreas Transplantation. Am J Transplant, 2017. 17(8): p. 2173-2177.

Supplemental Information

Methods

Pancreas Processing and Donor Demographics

Human pancreata were trimmed of surrounding fat and vessels, and biopsies were taken before the remaining parenchyma was sectioned into approximately 1cm^3 pieces. Pieces from the neck of the pancreas were collected for histology and lipid content studies.

Heavy alcohol usage was defined as >2 drinks per day for both men and women. The racial or ethnic categorizations used in documentation by the UW Health Organ Procurement Organization (OPO) include the following: White, Hispanic/Latino, Black/African American, Asian, and American Indian/Alaska Native. Smoking abuse was determined by the OPO from the patient medical history. Gastrointestinal diseases recorded in this population include the following: heartburn, GERD, erosive esophagitis, barrett's esophagus, esophageal dysplasia, and chronic or acute ulcers.

Lipid Extraction and Quantification

Briefly, 20-40 mg of lyophilized tissue was weighed and 2 ml of 1:3 (v:v) chloroform:methanol solution was added to each sample. Tissue was broken up in solution and placed on the shaker (RT, 1 hour). The samples were centrifuged (4300 rpm, 5 minutes) and the supernatant decanted into a new tube where it was combined vigorously with 1 ml of 0.9% NaCl and 2.5 ml of chloroform to bring the chloroform:methanol ratio to 2:1 (v:v). Samples were centrifuged (2000 rpm, 5 minutes) and the upper phase (aqueous phase) was discarded before washing the lower phase (lipid phase) gently with 1 ml of 50% methanol. The lower phase was

air dried in a fume hood for 7 days and the dry lipid material was weighed to determine the lipid content of the tissue sample. Each donor was measured using 3-4 technical replicates.

Pancreas Biopsies

Pancreas biopsies were taken following the removal of the extra-pancreatic adipose and vascular tissue from the organ, using a Tru-Core II URO biopsy gun (Argon Medical Devices) with an 18G needle. For lipid quantification, 15-20 biopsies were taken from each donor such that one technical replicate of modified Folch lipid extraction could be performed to compare to three technical replicates from the normal dissection process. For histology, 3-5 biopsies were embedded fresh in OCT, sectioned, stained with ORO (red), and counterstained with hematoxylin (blue).

Supplemental Figures:

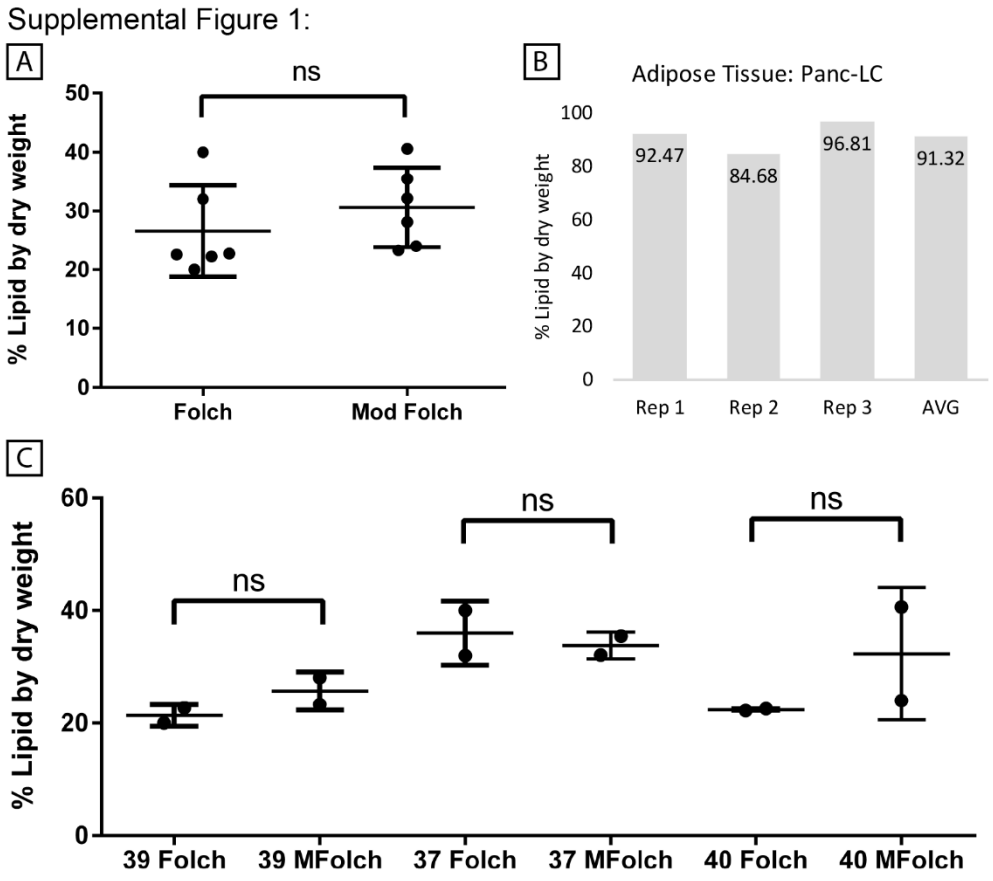

Supplemental Figure 1. Verification of the modified Folch method (Mod Folch) used in this study. A) Three pancreas donors were used for lipid extraction via the Folch Method (1:3 chloroform:methanol v/v used during extraction) and the Mod Folch method (2:1 v/v chloroform:methanol used during extraction) in duplicate. **B)** Pure visceral adipose tissue (Adipose Tissue) as determined by visual inspection was removed from one donor pancreas and the lipids were quantified in triplicate (as shown Reps 1-3). The average (AVG) lipid content for pure adipose tissue was 91.32%. **C)** The Folch and Mod Folch method lipid quantification of pancreatic grafts displayed separately for 3 donors (data is the same as in A). Error bars represent ± 1SD.

Supplemental Figure 2:

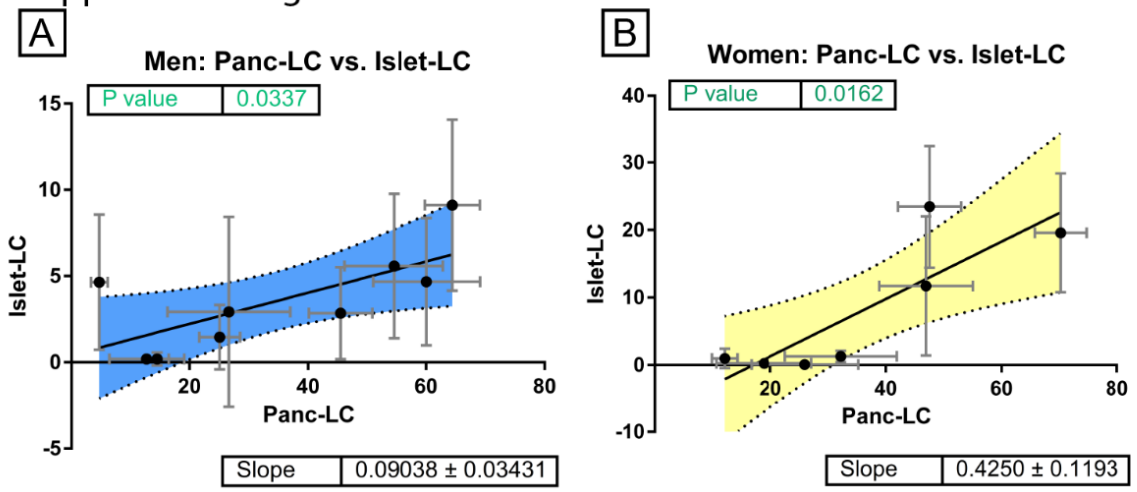

Supplemental Figure 2. Panc-LC is significantly correlated with Islet-LC in men and women. A-B) Correlations including Panc-LC and Islet-LC for a subset of donors. The 95% confidence interval is shaded around the line of best fit. The p-values were determined using a Pearson correlation. Error bars indicate ± 1 SD for Panc-LC and Islet-LC. N=9 men; N=8 women.

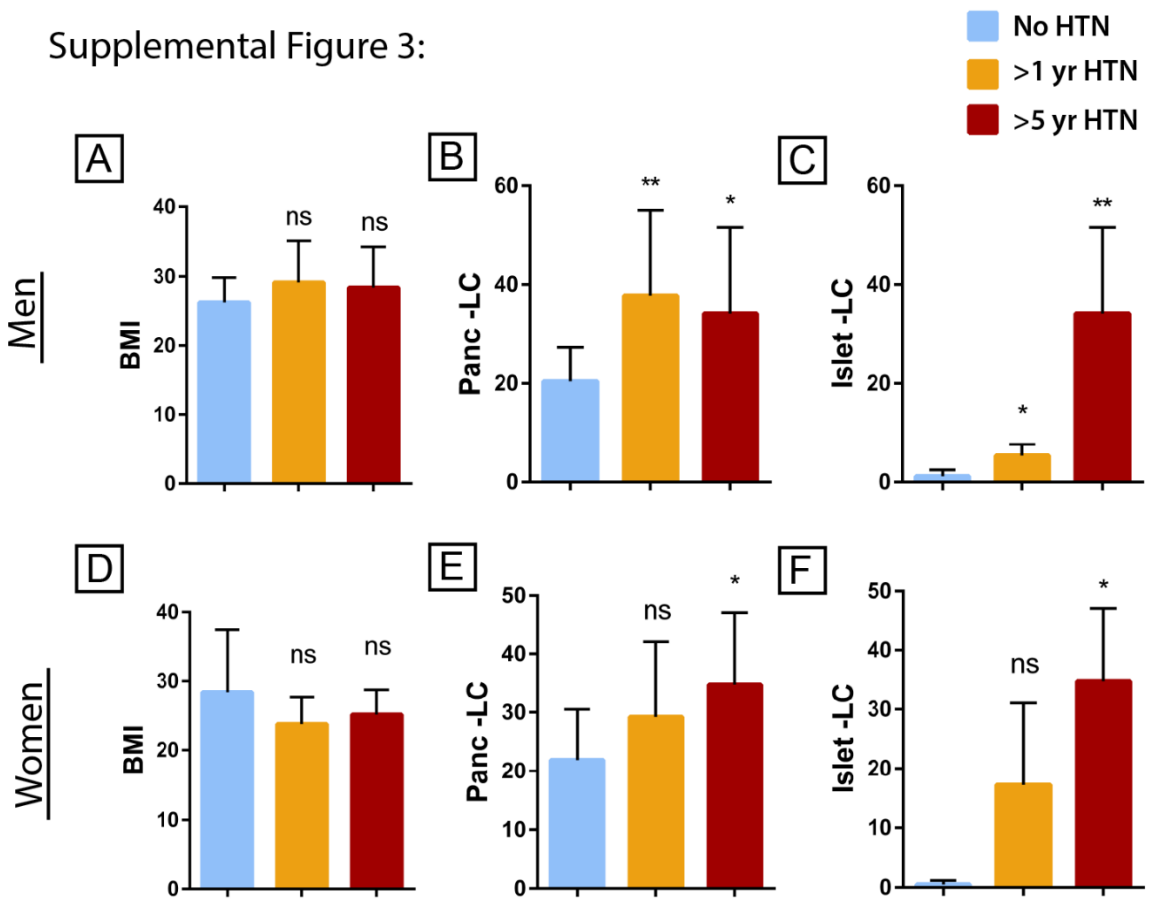

Supplemental Figure 3: Panc-LC and Islet-LC increase with HTN history in both men and women. HTN history in men **(A-C)** and women **(D-F)** were analyzed separately for trends in BMI **(A,D)**, Panc-LC **(B,E)** and Islet-LC **(C,F)**. BMI and Panc-LC: N=28 men; N=19 women. Islet-LC: N=8 men, N=7 women.

Supplemental Figure 4:

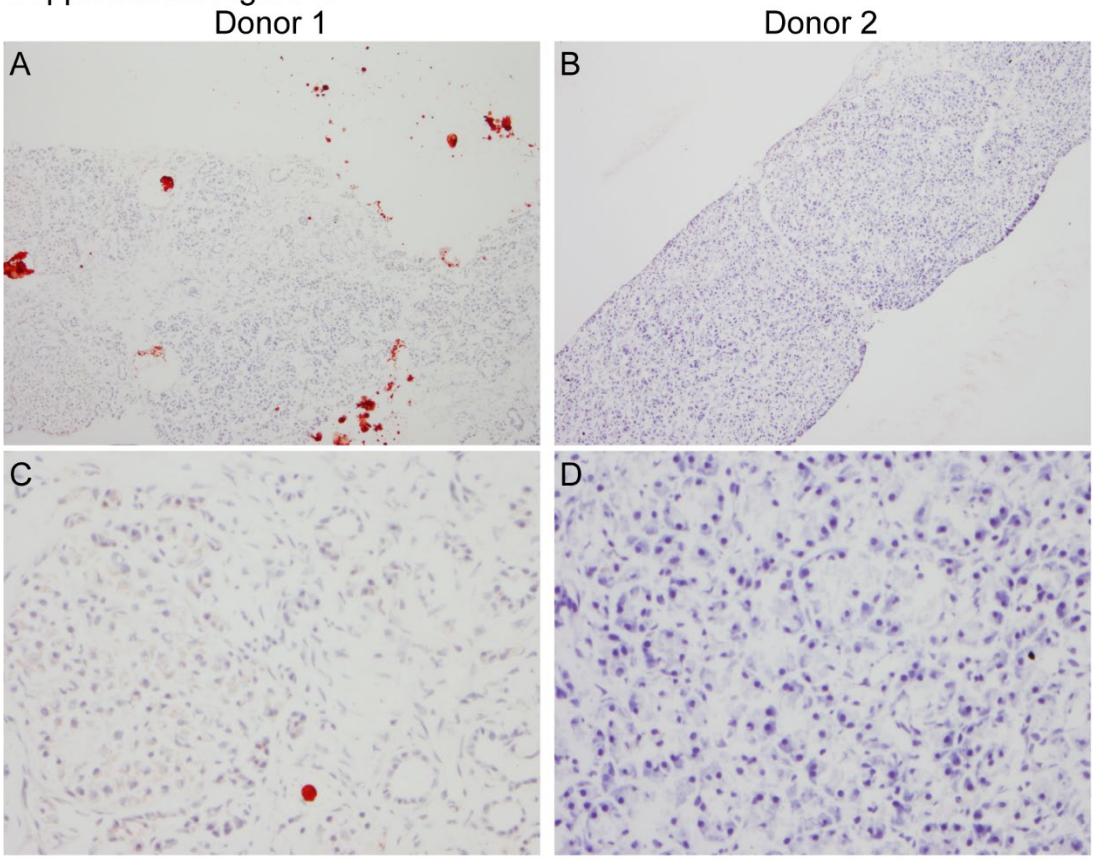

Supplemental Figure 4: Pancreas biopsies can be used for Oil Red O staining. A-B) Representative images showing ORO-positive tissue from biopsies from two pancreas donors. Images are 10X magnification. C-D) Representative images from the same donors at 40X magnification.

Supplemental Figure 5:

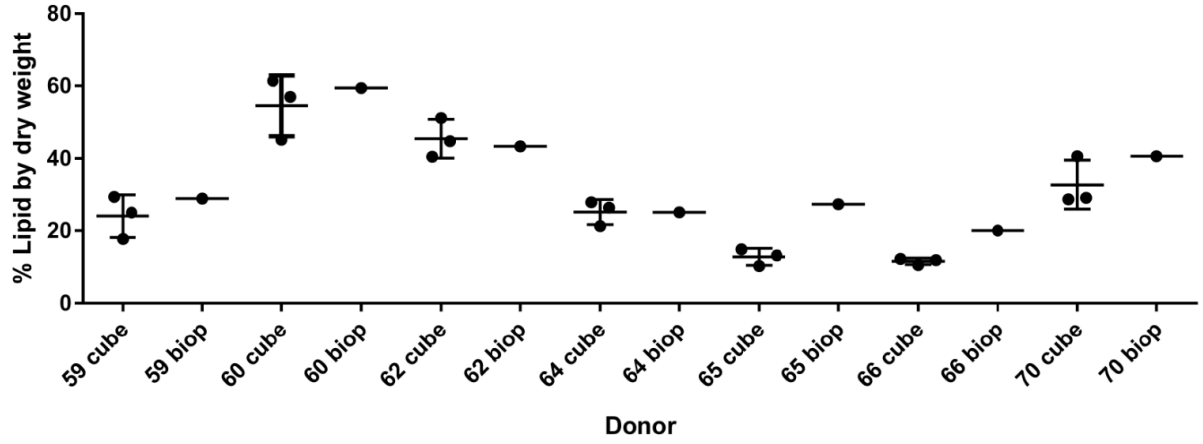

Supplemental Figure 5: Biopsies can be used for lipid content quantification. From 7 distinct donors (Donor #59, 60, 62, 64, 65, 66, 70), lipids were extracts from both 18 gauge needle core pancreas biopsies (biop) and 1 cm^3 pancreas cubes dissected from the parenchyma of the neck of the gland (cube). Lipid content determined from the biopsies was similar to that obtained from the 1 cm^3 cube. Biopsies were taken from donors such that one technical replicate of modified Folch lipid extraction could be performed to compare to three technical replicates from the cube dissection process.

Appendix Chapter 2

The expression patterns of select islet ECM proteins *in situ* and in culture

Daniel Tremmel designed the study under the guidance of Sara Dutton Sackett and Jon Odorico. Daniel Tremmel and Sakar Gupta performed the experiments and analyzed the data. Daniel Tremmel and Sam Mitchell processed and banked human tissues. Daniel Tremmel prepared all figures and wrote the chapter.

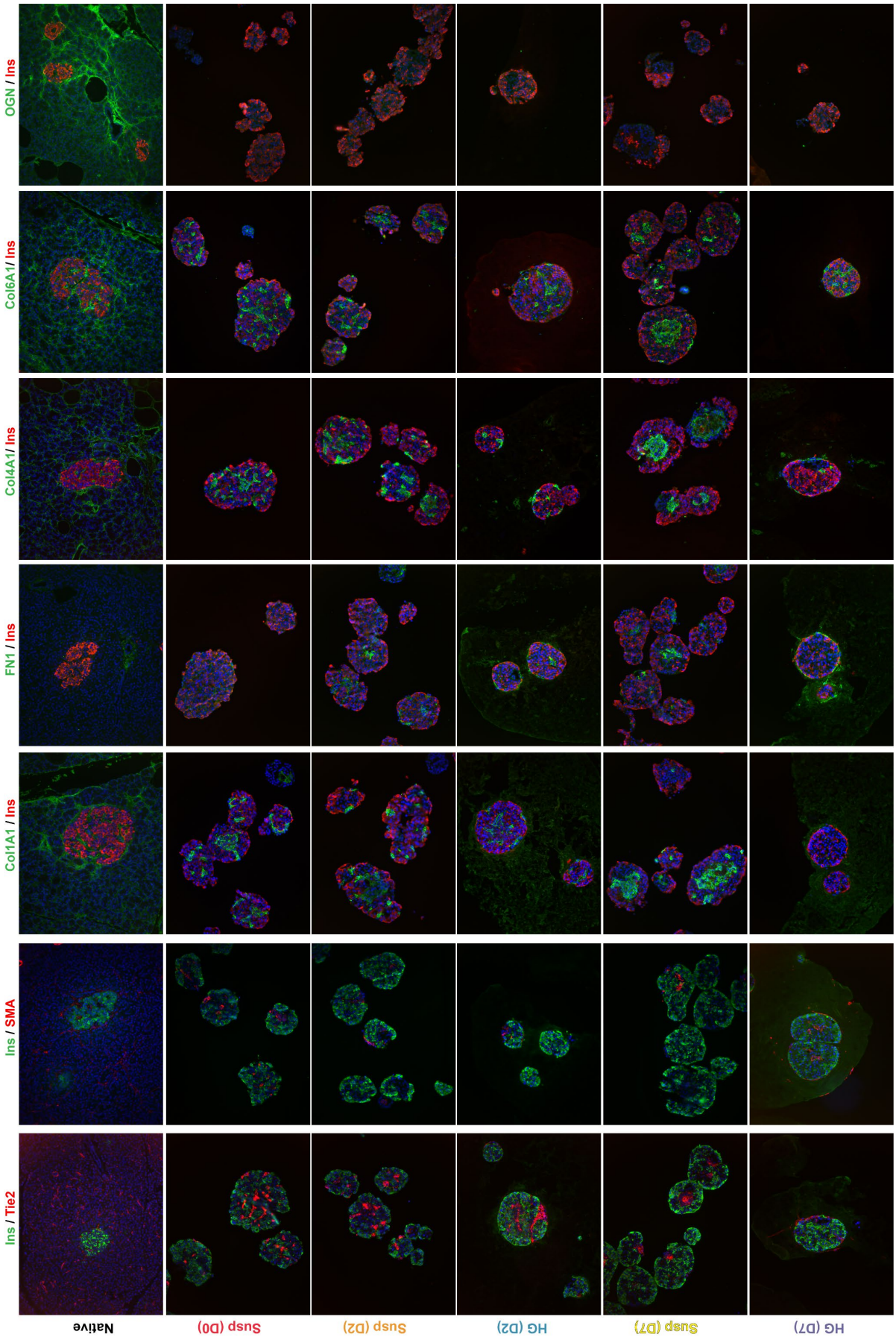
Ins / Tie2
Ins / SMA
Col1A1 / Ins
FN1 / Ins
Col4A1 / Ins
Col6A1 / Ins
OGN / Ins
Native
Susp (D0)
Susp (D2)
HG (D2)
Susp (D7)
HG (D7)

Appendix Chapter 2 Figure 1

ECM expression and localization in native, isolated, and cultured islets.

Islets *in situ*, freshly isolated (day 0) and cultured for 2 or 7 days in suspension (Susp) or hP-HG (HG) were fixed, paraffin embedded, sectioned and stained for insulin (Ins), Tie2, αSMA, collagen 1 α1 (COL1A1), collagen 4 α1 (COL4A1), collagen 6 α1 (COL6A1), and fibronectin (FN1). and osteoglycin (OGN). Higher resolution images are included in Appendix Chapter 2 Fig. 4.

(Previous page)

Appendix Chapter 2 Figure 2

Quantification of ECM expression and localization in native, isolated, and cultured islets.

Islets *in situ*, freshly isolated (day 0) and cultured for 2 or 7 days in suspension (S) or hP-HG (H) were fixed, paraffin embedded, sectioned and stained for collagen 1 (Col1), collagen 4 (Col4), collagen 6 (Col6), fibronectin (FN). The ECM content as a of total islet area (%Area), ECM as a percentage of the islet perimeter (%Perimeter), and the percentage of total ECM that localized to the perimeter (%p-ECM/t-ECM) was quantified as detailed in Appendix Chapter 2 Supplemental Fig. 5. Statistical comparisons are relative to the native islets for each group.

(Next page)

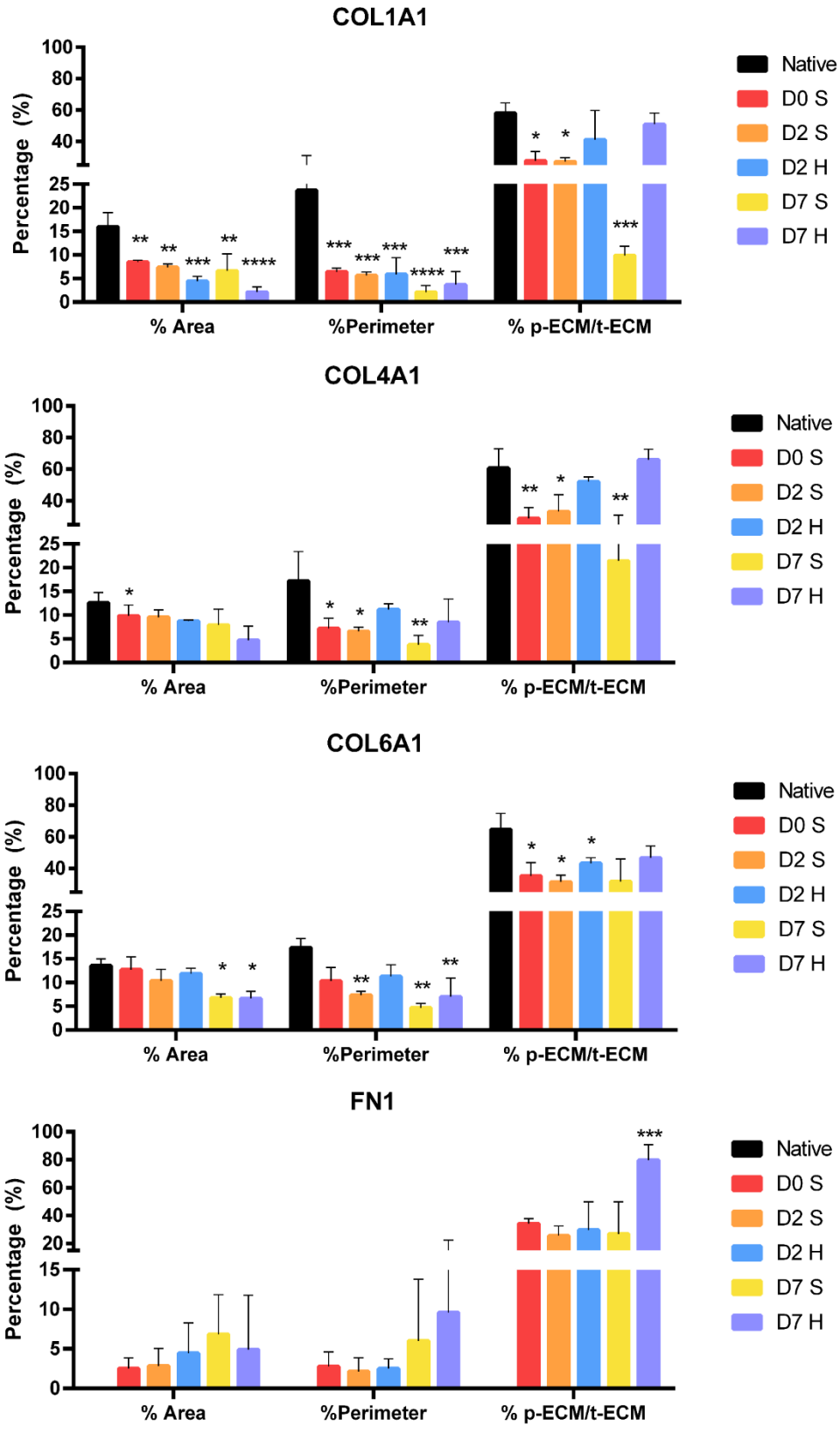
COL1A1
Percentage (%)
100
80
60
40
25
20
15
10
5
0
% Area
%Perimeter
% p-ECM/t-ECM
Native
D0 S
D2 S
D2 H
D7 S
D7 H
COL4A1
COL6A1
FN1

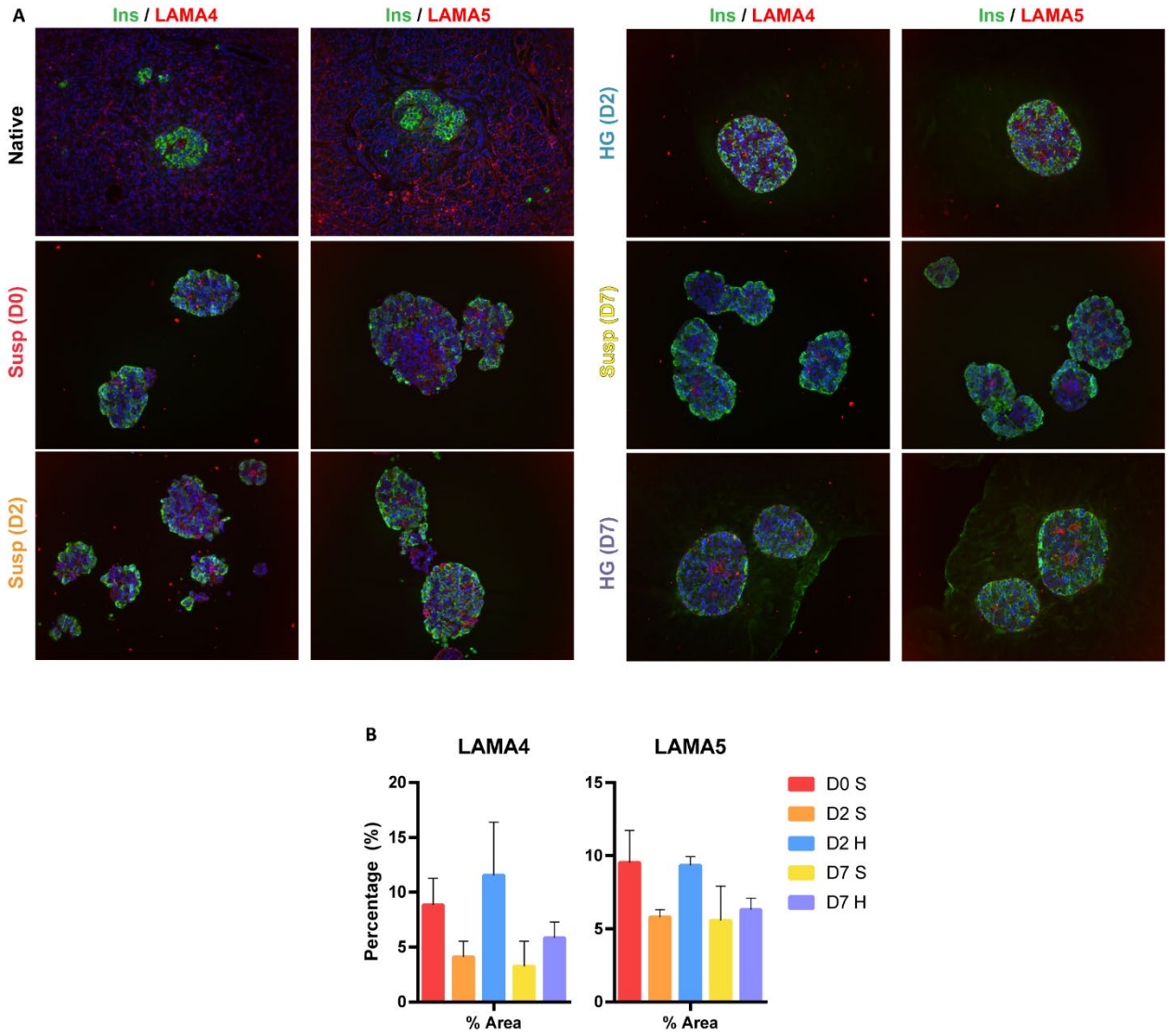

Appendix Chapter 2 Figure 3

Laminin expression in native, isolated, and cultured islets.

A) Islets *in situ*, freshly isolated (day 0) and cultured for 2 or 7 days in suspension (Susp) or hP-HG (HG) were fixed, paraffin embedded, sectioned and stained for insulin (Ins), Laminin A4 (LAMA4) and Laminin A5 (LAMA5).

B) Quantification of total LAMA4 and LAMA5-positive area in islets after isolation on day 0, 2, and 7 in either suspension (S) or hP-HG (H).

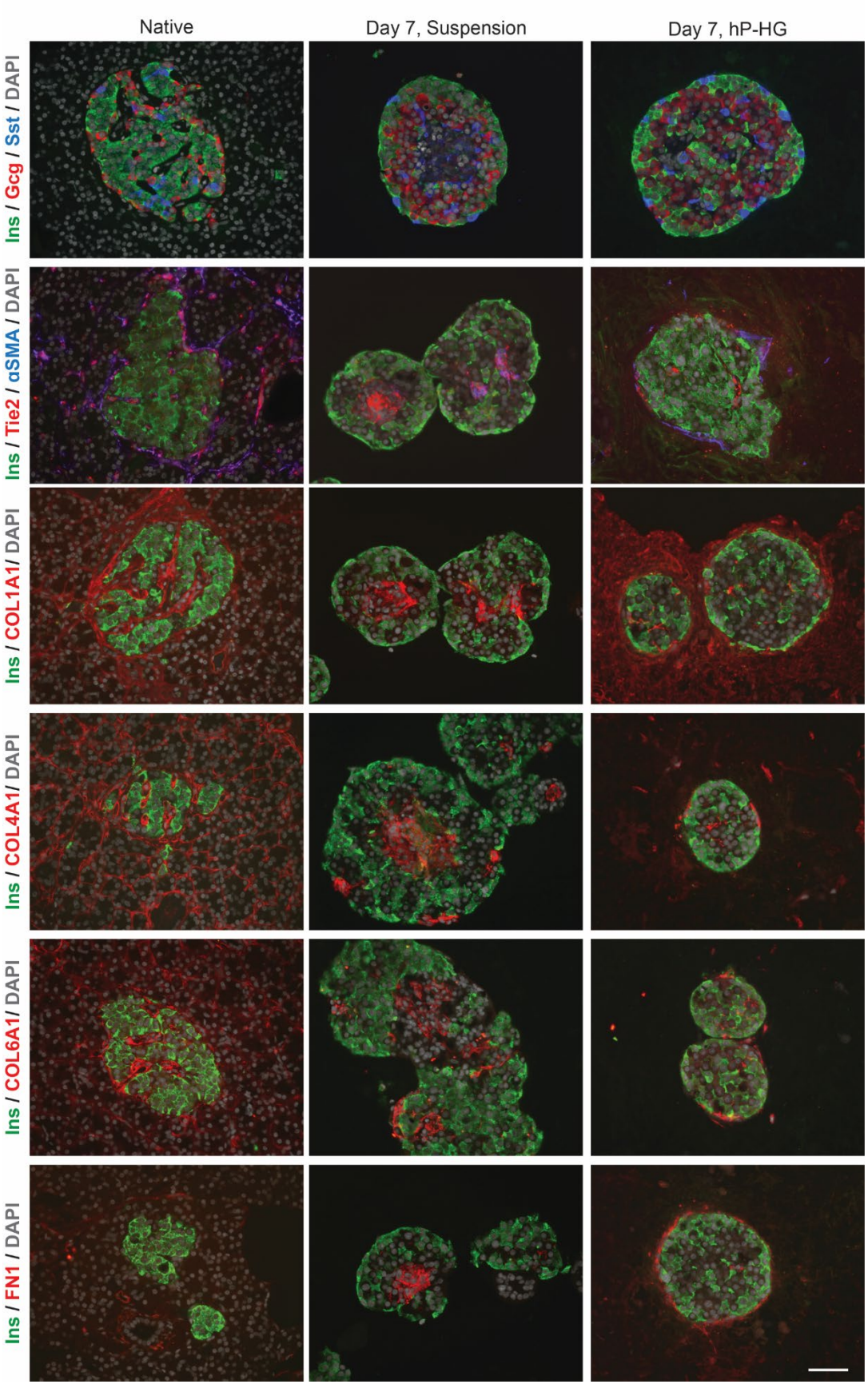
Native
Day 7, Suspension
Day 7, hP-HG
Ins / Gcg / Sst / DAPI
Ins / Tie2 / αSMA / DAPI
Ins / COL1A1/ DAPI
Ins / COL4A1/ DAPI
Ins / COL6A1/ DAPI
Ins / FN1 / DAPI

Appendix Chapter 2 Figure 4

ECM expression and localization in native and isolated/cultured islets (40x images).

Islets *in situ*, and cultured for 7 days in suspension or hP-HG were fixed, paraffin embedded, sectioned and stained for insulin (Ins), glucagon (Gcg), somatostatin (Sst), Tie2, αSMA, collagen 1 α1 (COL1A1), collagen 4 α1 (COL4A1), collagen 6 α1 (COL6A1), and fibronectin (FN1). Nuclei are stained with DAPI (gray).

Scale = 100 microns.

(Previous page)

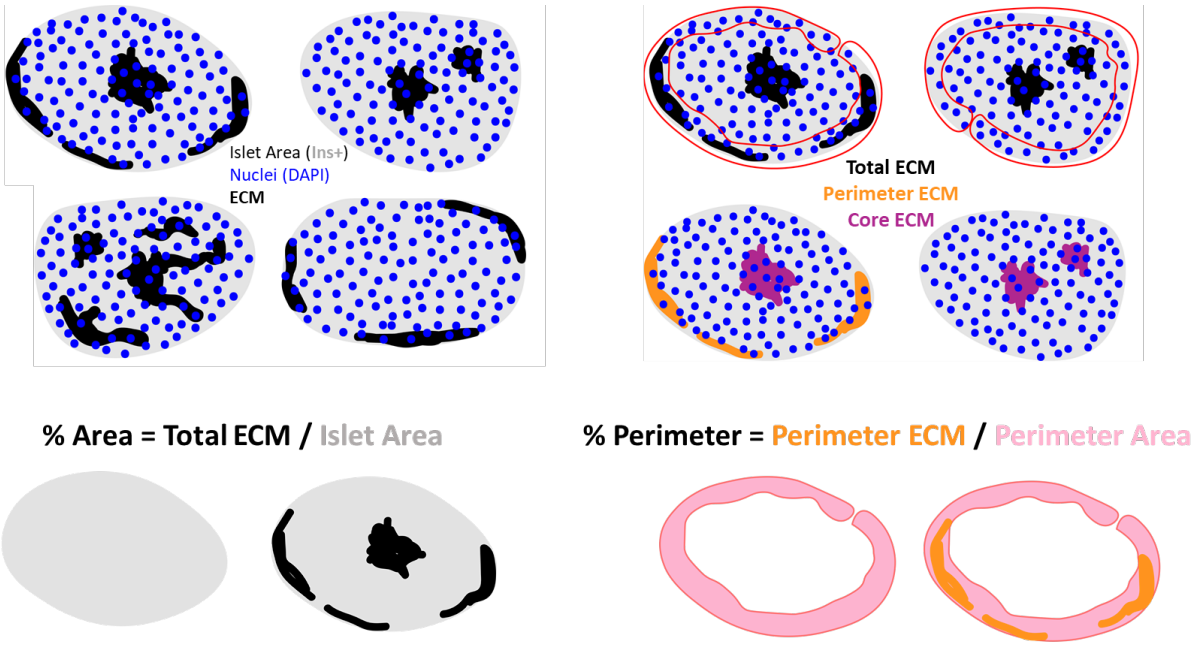

Appendix Chapter 2 Figure 5

Method for quantifying ECM expression and localization.

To describe changes in ECM content and localization the %Area, %Perimeter and %P-ECM/t-ECM were calculated by measuring the total islet area, total ECM area (t-ECM), perimeter area and perimeter ECM (P-ECM) area, and each were calculated as described in the figure. The perimeter was defined as one cell width at the outer edge of each islet, and islet area was defined by insulin-positive area.

Discussion

ECM proteins that we previously identified as having high abundance or interesting changes in expression during pancreas development were selected for staining in cultured islets. We questioned whether ECM content and localization in cultured islets may have difference based on our previous findings that islet architecture changed after islet isolation and during culture, and was affected by the ECM environment of the islets. Therefore, we cultured islets for 0, 2 and 7 days in suspension or in hP-HG, and used formalin-fixed paraffin embedded (FFPE) sections to perform staining of specific ECM components. ECM localization was quantified in the entire islet and in the perimeter (mantle) of the islets, demonstrated in Figure 5.

We find that like the localization of non-endocrine cells (Tie2, αSMA) the ECM expression and localization is affected by islets culture conditions and time. In suspension, collagens and fibronectin have a higher tendency to be deposited in the center of the islets over longer-term culture (7 days) (Figure 1, 2, 4). LAMA4 and LAMA5 were also stained in the isolated islets but no significant differences were found in total percent-positive area among the cultured islet groups. Interestingly, osteoglycin (OGN) is highly expressed in the pancreas and islets, but is lost with isolation and is not regenerated during culture. This may mean that OGN is made by a source outside of the islets but accumulates in and around them *in situ*. If OGN is important to islet function, then providing OGN in culture may have potential to better support islets after isolation. Conversely, fibronectin (FN1) is not abundant in islets *in situ*, but is expressed in the islets after isolation. This may be due to the wounding or stress response that the non-endocrine cells of the islets undergo during isolation, and fibronectin itself may not be a normal component of the islet microenvironment.

Methods

Cell Culture

Human islets were received through the Integrated Islet Distribution Program (IIDP) and experiments were initiated within 24 hours of receipt. On day 0, islets were counted and plated in suspension or in hydrogel co-culture. Islets were combined with hP-HG (8 mg/mL) at a density of 100 IEQ/10µL of hydrogel. The mixture was pipetted into 5 µL droplets in the bottom of an untreated petri dish, inverted, and incubated at 37^{o}C and 5% CO_2 for 30 minutes. The polymerized droplets were moved into 24-well ULA plates (Corning, Corning, NY) for culture for 1-7 days in PIM(R) medium (Prodo Labs, Aliso Viejo, CA).

Histology and Immunofluorescent Staining

Samples were fixed in 4% paraformaldehyde (PFA), paraffin embedded, and sectioned (5 µm) for immunofluorescent staining. Slides were deparaffinized using xylene and rehydrated. Antigen retrieval was performed by incubation in 10 mM Citrate Buffer, pH 6.0 for 2.5 hours at 80°C. Slides were blocked with 10% BSA/PBS for 40 minutes at RT, incubated with primary antibodies overnight at 4^{o}C, washed, incubated with secondary antibody incubation for 40 minutes at RT and cover slipped. All antibodies and dilutions are listed in Table 1. Nuclei were labeled with 40–6-diamidino-2-phenylindole (DAPI) (Life Technologies, Carlsbad, CA). Images were generated with a Zeiss Axiovert 200 M microscope or a Nikon A1R confocal microscope.

Image Quantification

Images were converted to binary using ImageJ. Islet area was traced based on the insulin staining and quantified in the binary image corresponding to each marker of interest. Perimeter

was defined by tracing to area of the outermost layer of cells of each islet, guided by the DAPI and insulin channels. The total area of each islet, perimeter area of each islet, % of islet are and % of islet perimeter area that was positive for each marker were measured and used to calculate the %Area, %Perimeter and %p-ECM/t-ECM as described in Figure 5.

Table 1: Antibodies used in this study

Target	Species	Dilution	Product
Col1A1	Rabbit	1:500	ab34710 (Abcam)
Col4A1	Rabbit	1:1000	ab6586 (Abcam)
Col6A1	Rabbit	1:200	17023-1-AP (Proteintech)
Fibronectin	Rabbit	1:200	ab2413 (Abcam)
Gcg	Rabbit	1:2000	ab92517 (Abcam)
Ins	Mouse	1:5000	I2018 (Sigma)
Ins	Guinea Pig	1:2000	I8510 (Sigma)
LAMA4	Mouse	1:200	ab242198 (Abcam)
LAMA5	Mouse	1:100	ab77175 (Abcam)
OGN	Rabbit	1:50	12755-1-AP (Proteintech)
Tie2	Rabbit	1:4000	ab221154 (Abcam)
αSMA	Mouse	1:50000	A2547 (Sigma)
Sst	Mouse	1:100	sc-74556 (Santa Cruz)

Target	Color	Dilution	Product
Anti-Mouse	488	1:800	A11001 (Life Technologies)
Anti-Mouse	568	1:800	A11031 (Life Technologies)
Anti-Mouse	647	1:800	A21235 (Life Technologies)
Anti-Rabbit	488	1:800	A21206 (Life Technologies)
Anti-Rabbit	568	1:800	A11011 (Life Technologies)
Anti-Guinea Pig	488	1:800	A11073 (Life Technologies)

Appendix Chapter 3

Human Pancreas and Islet ECM Atlas

Daniel Tremmel prepared the tables and text in this chapter.

Table 1

Antibodies used for Pancreas and Islet ECM staining

Staining information						
ECM protein	Antibody	Product	Dilution	Froz	FFPE	Other notes
Col12A1	Rb αCollagen 12	PA5-38890	1:100	ND	Y	
Col14A1	Rb αCollagen 14	PA5-54886	1:150	ND	Y	
Col16A1	Rb αCollagen 16	SAB4500398	1:100	ND	Y	
Col1A1	Rb αCollagen 1	ab34710	1:500	ND	Y	
Col2A1	Rb αCollagen 2	ab34712	1:200	ND	Y	
Col3A1	Rb αCol3	ab6310	1:100	ND	Y	Works on denatured ECM (hydrogel)
Col3A1	Rb αCol3A1	ab7778	1:500	ND	Y	3D protein structure only (not with hydrogel)
Col4A1	Rb αCollagen 4	ab6586	1:1000	ND	Y	
Col5A1	Rb αCol5A1	ab7046	1:100	ND	Y	
Col6A1	Rb αCol6	ab6588	1:200	ND	Y	Works on denatured ECM (hydrogel)
Col6A1	Rb αCol6A1	17023-1-AP	1:200	ND	Y	Doesn't work on hydrogel
DCN	Rb αDecorin	14667-1-AP	1:100	ND	Y	
ELN	Rb αElastin	15257-1-AP	1:500	ND	Y	
EMILIN1	Ms αEMILIN1	60047-1-Ig	1:100	ND	Y	
EMILIN2	Rb αEMILIN2	24779-1-AP	1:200	ND	Y	
Fibrillin-1	Rb αFBN1	PA5-82743	1:500	ND	Y	
Fibrillin2	Rb αFBN2	20252-1-AP	1:200	ND	Y	
FN1	Rb αFibronectin	ab2413	1:200	ND	Y	
FN1	Rb αFibronectin	ab268020	1:500	ND	Y	
HSPG2	Ms αPerlecan	sc-377219	1:300	Y	N	Does not work on FFPE
LamA4	Ms αLaminin alpha-4	ab242198	1:200	ND	Y	
LamA5	Ms αLaminin alpha-5	ab77175	1:100	ND	Y	
OGN	Rb αOsteoglycin	12755-1-AP	1:50	ND	Y	
Periostin	Rb αPOSTN	19899-1-AP	1:200	ND	Y	

Table 2

Abundance and localization of ECM proteins in the pancreas and islets

	Pancreas Expression (Histology)			Enrichment		
Protein	Fetal	Adult	Isolated islets	Acinar	Islet	Other notes
Col12A1	+	+	N/A	++	0 (adult only)	
Col14A1	+ (mesenchyme)	-	N/A	+ (fetal only)	Not present	
Col16A1	+ (acinar)	+ (acinar)	N/A	++	Not present	
Col1A1	+++	+++	+	0	0	
Col2A1	+++	+	N/A	0	0	
Col3A1	+++	+++	+	0	0	
Col4A1	++	+++	+	0	+ (fetal only)	
Col5A1	+++	+++	N/A	0	+ (adult only)	
Col6A1	+++	+++	+	0	0 (adult only)	
DCN	++	++	N/A	0	0	
ELN	N/A	+	N/A	NP	NP	
EMILIN1	+++	+	N/A	0 (fetal only)	++	Appears to be intracellular
EMILIN2	++	+	N/A	NP	NP	
Fibrillin-1	+	+	N/A	N/A	N/A	
Fibrillin2	+ (islets)	+ (islets)	N/A	NP	++	Appears to be intracellular
FN1	++	-	++	0	+ (fetal only)	
HSPG2	N/A	++	N/A	N/A	N/A	
LamA4	++	++	+	0	+	
LamA5	+	++	+	+	0 (adult only)	
OGN	++	++	-	+ (fetal only)	+ (adult only)	
Periostin	+ (mesenchyme)	-	N/A	+ (fetal only)	NP	

Histology

- **- -** Not present at all
- **-** Only present in vessels, ducts and connective tissue
- **+** Present in limited pancreas ECM structures
- **++** Present in multiple pancreas ECM structures
- **+++** Present in most pancreas ECM structures

Enrichment (Ratio of expression between islet and acinar)

- **NP** Not present
- **0** Evenly distributed, Ratio between 0.5-1.5
- **+** Slightly enriched, Ratio 1.5-2.0
- **++** Enriched, Ratio 2.0+

ECM structures: Major/minor vessels and ducts, acinar membrane, islet membrane, intracellular
N/A: Not available / not determined

Discussion

The tables in this section were prepared as a way of summarizing the expression and localization of ECM proteins in the human pancreas, islets and in isolated islets as described in the chapters of this thesis. Antibodies used to detect ECM proteins in the native tissues did not always detect the proteins in ECM hydrogels, this is due to differences in the ability of antibodies to bind to proteins based on the protein folding. Thus, notes are also made in these tables about antibodies that did or did not work on hP-HG.

Trends in ECM expression have been detected in this study in a variety of contexts and using different methodologies. In order to fully appreciate changes in ECM expression throughout development alongside ECM localization in the different compartments of the

pancreas and also compare to ECM expression in isolated islets, these tables roughly estimate the findings of the various studies in this thesis.

As an example of the practicality of this table, there are two notable trends that I have identified in my work that were not fully discussed in any chapter of the main body of this thesis. First, fibronectin, which has been cited in many reviews to be a main component of the human pancreas ECM [1-3], was not found to be a major constituent of either the human acinar tissue or islets. In developmental (Chapter 2), we found that fibronectin was present throughout the fetal pancreas, but in the adult human pancreas, it was only detected around vessel and ducts, and at the intersections of the pancreas lobes, but rarely in or near the islets. In isolated islets, however, fibronectin is abundantly detected (appendix Chapter 2). This may be the result of the damage caused by the isolation process, and the repair mechanisms triggered by the supportive cells that are co-isolated with the islets. This could be an important discovery about the role of fibronectin in islet ECM.

Second, osteoglycin (OGN) was one of the ECM proteins that was found to be more abundant in and around the adult islets compared to the juvenile and fetal islets in development (Chapter 2). In fact, we detected OGN in the pancreas at high levels throughout development. However OGN is not detected in isolated islets and is not deposited over time in culture either in suspension or in hP-HG (Appendix Chapter 2). This indicates that the cells isolated with the islets (endocrine, exocrine and supportive cells like endothelial cells or fibroblasts) do not produce OGN in culture the way other ECM proteins are expressed. This could suggest that the source of islet OGN the may be extra-pancreatic, and could be deposited in the pancreas through the blood stream. OGN is thought to have important roles in bone function and may also affect

cardiovascular and metabolic functions [4]. One study has previously found that OGN knockout mice had deficiencies in blood glucose regulation, making a connection of OGN to pancreas function as well [5]. OGN also appears to be highly expressed in the parathyroid [6], which is interesting because parathyroid and islet co-transplantation has been shown to highly improve islet engraftment and function [7]. Because OGN is secreted into circulation, this may be a mechanism through which OGN is deposited in the pancreas, but further work is required to explore the role and source of OGN in the pancreas and islets.

Of course, our mass spectrometry-based study identified 185 ECM and ECM-related proteins present in the pancreas throughout development and this table represents only a small subset of those proteins. This highlights how much more work needs to be done to understand the composition and dynamics of the human islet matrisome, both during development and after isolation.

References

1. Aamodt, K.I. and A.C. Powers, *Signals in the pancreatic islet microenvironment influence beta-cell proliferation.* Diabetes Obes Metab, 2017. **19 Suppl 1**: p. 124-136.
2. Llacua, L.A., M.M. Faas, and P. de Vos, *Extracellular matrix molecules and their potential contribution to the function of transplanted pancreatic islets.* Diabetologia, 2018. **61**(6): p. 1261-1272.
3. Stendahl, J.C., D.B. Kaufman, and S.I. Stupp, *Extracellular matrix in pancreatic islets: relevance to scaffold design and transplantation.* Cell Transplant, 2009. **18**(1): p. 1-12.
4. Starup-Linde, J., R. Viggers, and A. Handberg, *Osteoglycin and Bone-a Systematic Review.* Curr Osteoporos Rep, 2019. **17**(5): p. 250-255.
5. Lee, N.J., et al., *Osteoglycin, a novel coordinator of bone and glucose homeostasis.* Mol Metab, 2018. **13**: p. 30-44.
6. Adam, M.A., B.R. Untch, and J.A. Olson, Jr., *Parathyroid carcinoma: current understanding and new insights into gene expression and intraoperative parathyroid hormone kinetics.* Oncologist, 2010. **15**(1): p. 61-72.
7. Faleo, G., et al., *Co-Transplant of Parathyroid Gland and Stem Cell-Derived Insulin-Producing Cells Enhances Graft Survival through Release of Pro-Angiogenic and Pro-Survival Factors.* Transplantation, 2018. **102**: p. S350-S350.